Variations actuelles du niveau de la mer

Habib Boubacar Dieng

Université Fédérale
Toulouse Midi-Pyrénées

THÈSE

En vue de l'obtention du

DOCTORAT DE L'UNIVERSITÉ DE TOULOUSE

Délivré par :

Université Toulouse 3 Paul Sabatier (UT3 Paul Sabatier)

Présentée et soutenue par :
Habib Boubacar DIENG

le 10 Janvier 2017

Titre :

Variations Actuelles du Niveau de la Mer

École doctorale et discipline ou spécialité :
ED SDU2E : Océan, Atmosphère, Climat

Unité de recherche :
LEGOS UMR 5566

Directeur/trice(s) de Thèse :
Directrice de thèse : Anny Cazenave
Co-directeur de thèse : Benoît Meyssignac

Jury :
Isabelle Dadou, Professeur des universités, UPS – LEGOS (Présidente du jury)
Guy Wöppelmann, Professeur des universités, UR – LIENSS (Rapporteur)
Bamol Ali Sow, Professeur associé, UASZ – LOSEC (Rapporteur)
Jérôme Benveniste, Senior Scientist, ESA/ESRIN (Examinateur)
Frédérique Seyler, Directrice de recherche IRD, ESPACE-DEV (Examinatrice)
Alexandre Ganachaud, Directeur de recherche, LEGOS (Examinateur)
Anny Cazenave, Directrice de recherche, LEGOS (Directrice de thèse)
Benoît Meyssignac, Chargé de recherche CNES, LEGOS (Co-directeur de thèse)

Remerciements

Je tiens particulièrement à remercier ma directrice de thèse Anny Cazenave pour tout ce qu'elle a fait pour moi durant ces 3 années passées au LEGOS et pour m'avoir fait confiance en me confiant un sujet de thèse vraiment passionnant. J'ai beaucoup appris à ses côtés. Elle m'a fait partager sa large culture générale et sa passion pour la géophysique et le climat et la science en générale. Merci pour tous ces voyages d'étude un peu partout dans le monde y compris quelques missions scientifiques au Sénégal, ce qui m'a donnée quelques occasions de revoir ma famille. Si seulement je pouvais trouver un mot plus grand que MERCI... Sincèrement je suis très reconnaissant et très honoré d'être sous sa direction durant ma thèse.

Je voudrais aussi remercier Benoît Meyssignac d'avoir co-encadré ma thèse et pour tout ses précieux conseils, discussions très techniques et soutien permanent. Merci aussi à Olivier Henry pour ses aides permanentes au traitement des données altimétriques durant ma première année de thèse.

Je tiens à remercier tous les chercheurs avec qui j'ai travaillé, discuté et échangé dans le cadre du projet niveau de la mer CCI "*Climate Change Initiative*" de l'ESA qui a financé ma thèse. Merci en particulier aux chercheurs du CLS (Michael Ablain, Jean-François Legeais, ...), Karina von Schucmann, Nicolas Champollion, Fenoglio-Marc Luciana, Don Chambers, Yoshihide Wada, Ernest Schrama, Magdalena Balmaseda, etc.

Merci à tous les collègues et amis que j'ai côtoyés durant ces 3 années : Elodie, Alejandro, Angélique, Alice, Mesmin, Michel, Nadine, Martine, Agathe, Brigitte, ...

Je veux également remercier Guy Wöppelmann et Bamol Ali Sow qui ont accepté le rôle fastidieux de rapporteur, ainsi que tous les autres membres du jury : Isabelle Dadou, Jérôme Benveniste, Frédérique Seyler et Alexandre Ganachaud, directeur du LEGOS.

Mes remerciements vont également à ma famille, en particulier à ma mère, ma femme Mame Faye et mon fils Boubacar qui a vu le jour durant ma 2éme année de thèse. Mame, je te remercie vivement pour ta patience en étant au Sénégal loin de moi, pour ton aide et tes encouragements et pour ton soutien permanent... Je te serai reconnaissant pour toujours. Je remercie aussi mes frères et sœurs du Sénégal et mes amis ici en France pour leurs soutiens.

Enfin, au moment de terminer ce manuscrit, mes pensées vont à mon père qui m'a appris la Vie et qui a beaucoup contribué à ma formation intellectuelle et spirituelle. Je prie fort pour toi, que Dieu vous accueille dans son paradis éternel. Un grand merci à Mawlana BAYE...

Variations Actuelles du Niveau de la Mer

Auteur : Habib Boubacar Dieng.
Directrice/co-directeur de thèse : Anny Cazenave et Benoît Meyssignac.
Discipline : Océanographie Spatiale.
Lieu et date de soutenance : Observatoire Midi-Pyrénées, le 10 Janvier 2017.
Laboratoire : LEGOS, UMR 5566 CNRS/CNES/IRD/UPS, OMP, Toulouse/France.

Résumé : Depuis le début des années 1990 on suit l'évolution globale du niveau de la mer grâce aux satellites altimétriques. Ils observent une hausse du niveau moyen global de la mer (GMSL) de 3.4 ± 0.4 mm/an sur la période 1993-2016 (ce qui représente le double de ce qui a été observé au cours du 20ème siècle par les marégraphes, hausse à 1.7 mm/an entre 1900 et 1990). Le GMSL présente aussi des fluctuations interannuelles qui peuvent atteindre quelques millimètres, surtout pendant les épisodes ENSO. Cette hausse n'est pas régionalement uniforme : elle a été 3 fois plus rapide que la hausse moyenne globale dans certaines zones entre 1993 et 2016. Au cours du 21ème siècle, on s'attend à une hausse accrue du GMSL pouvant aller jusqu'à 1 m à l'horizon 2100, avec une forte variabilité régionale. Il est donc important de comprendre l'évolution actuelle du niveau des océans qui constitue une menace sérieuse pour de nombreuses régions côtières basses souvent très peuplées. Cette thèse s'inscrit dans le contexte du projet niveau de la mer CCI (Climate Change Initiative) de l'Agence Spatiale Européenne (ESA) ayant pour objectif de fournir de meilleurs produits du niveau de la mer combinant les missions Topex/Poseidon, Jason-1/2, ERS-1/2 et Envisat.

L'objectif premier de cette thèse est de valider ces produits SL_CCI du niveau de la mer en utilisant différentes approches, en particulier par l'étude du bilan (comparaison du GMSL observé avec la somme des différentes contributions : composante stérique, fonte des glaces continentales et transferts d'eau depuis les terres émergées). Un autre objectif est d'estimer les composantes du niveau de la mer mal connues, et tout particulièrement le contenu thermique de l'océan profond non mesurable par le système Argo, et la contribution du stock d'eau sur les continents. Ces travaux ont montré que la contribution de l'océan profond en dessous de 2000m est faible sur la période 2005-2013 et contenue dans la barre d'incertitudes des données (erreurs qui proviennent essentiellement, *(1)* des produits niveau de la mer altimétriques et des lacunes de la couverture géographique des données Argo dans la région Indonésienne pour la tendance et *(2)* des produits GRACE et Argo pour la variabilité interannuelle). Nos résultats et la méthode utilisée montrent que le niveau de la mer et ses composantes sont encore entachés d'erreurs importantes.

Dans la deuxième partie, nous avons analysé l'influence du phénomène ENSO (El Niño et La Niña) sur les variations interannuelles du GMSL. Nous montrons que lors des évènements La Niña comme celui de 2010-2011, le déficit de précipitations sur l'océan (et l'excès sur les continents) conduit à une baisse temporaire de la masse de l'océan global et donc du niveau de la mer. C'est essentiellement la variation de masse de l'océan qui explique la variabilité interannuelle du niveau de la mer lors des évènements ENSO, et le déficit (La Niña) ou excès (El Niño) de masse se trouve confiné dans l'océan Pacifique tropical Nord.

Pour finir, nous analysons l'évolution de la température moyenne de l'air et de l'océan en surface sur la période du "hiatus" (2003-2013). Nous montrons que ce hiatus, c'est à dire le ralentissement récent de la hausse de la température moyenne globale de la Terre est un phénomène quasi global, même si le Pacifique tropical Est s'est fortement refroidi. Cette "supposée" pause récente s'explique par la variabilité naturelle interne du climat. La Terre est toujours en état de déséquilibre énergétique dû à l'accumulation de gaz à effet de serre. Nous mettons en évidence le rôle de la variabilité naturelle à court terme sur les changements à plus long terme associés au réchauffement climatique anthropique.

Mots clés : niveau moyen global de la mer, niveau stérique, masse océan, bilan niveau de la mer, contenu thermique, océan profond, variabilité interannuelle, ENSO, variabilité régionale, changement climatique, altimétrie spatiale, Argo, GRACE, variabilité naturelle et interne, température de surface.

Present day Sea Level Variations

Author : Habib Boubacar Dieng
Ph.D. Director/co-director : Anny Cazenave and Benoît Meyssignac
Discipline : Space Oceanography
Place and date of defense : Observatoire Midi-Pyrénées, the 10th January 2017.
Laboratory : LEGOS, UMR 5566 CNRS/CNES/IRD/UPS, OMP, 14 avenue Edouard Belin, 31400 Toulouse, France.

Summary : Since the early 1990s sea level is routinely measured using high-precision altimeter satellites. These observe a rise in global mean sea level (GMSL) of 3.4 ± 0.4 mm/yr over the 1993-2016 period (which is twice what has been observed during the 20th century by the tide gauges, with a rise of 1.7 +/- 0.3 mm/yr). The interannual variability in the GMSL can reach several millimeters, especially during ENSO events. The rate of sea level rise is not regionally uniform. During the altimetry era, it was three times faster than the global mean in some areas. During the 21st century, we expect a greater rise of the GMSL than today, up to 1 m in 2100, with strong regional variability. It is therefore important to understand the current evolution of the sea level, since it represents a serious threat to many low coastal areas, often densely populated of the planet. My thesis research deals with the Sea Level CCI (Climate Change Initiative) project of the European Space Agency (ESA) which objective is to provide improved sea level products combining several altimetry missions, including Topex/Poseidon, Jason-1/2, ERS-1/2 and Envisat.

The primary objective of my thesis was to validate the CCI sea level products using different approaches, in particular the sea level budget approach. It consists of comparing the observed GMSL with the sum of different contributions : the steric component, melting of continental ice and transfers of water between the land surface and oceans. Another objective was to estimate the poorly known components to sea level rise, in particular the heat content of the deep ocean not measurable by Argo, and the contribution of water storage on the land. My work has shown that the contribution of the deep ocean below 2000m to the rising sea level is small over the 2005-2013 periods and not significant compared to the data uncertainties. The main uncertainties come from: *(1)* –in terms of trend- the altimetry sea level products and gaps in the geographical coverage of Argo data in the Indonesian region, and *(2)* –in terms of interannual variability- the GRACE and Argo products. My results and the method used show that the sea level and its components are still affected by important errors.

In the second part, I analyzed the influence of ENSO (El Niño and La Niña) on the interannual variations of the GMSL. I showed that during La Niña events, like that of 2010-2011, the rainfall deficit over the ocean (and excess over the continents) leads to a temporary decrease in the global ocean mass and therefore in the GMSL. This is essentially the ocean mass variation that explains the interannual variability of the GMSL during ENSO events. Furthermore, the deficit (La Niña) or excess (El Niño) ocean mass is confined in the north tropical Pacific Ocean.

Finally, I analyzed the evolution of the average temperature of air and ocean surface over the period of the "hiatus" (2003-2013). I showed that this hiatus, i.e. the recent slowdown in the rise of the global mean Earth's temperature is an almost global phenomenon, though cooling of the tropical eastern Pacific has slightly contributed. This recent pause is attributable to natural internal climate variability. The Earth is indeed still in a state of energetic imbalance due to the accumulation of greenhouse gases. I highlighted the role of the natural variability that is superimposed to the anthropogenic global warming.

Keywords : global mean sea level, steric sea level, ocean mass, sea level budget, thermal expansion, depth ocean, interannual variability, ENSO, regional sea level, climate change, satellite altimetry, Argo, GRACE, natural and intern climate variability, surface temperature, "hiatus", "pause".

Table des matières

Introduction

L’océan stocke la chaleur accumulée dans le système Terre en réponse aux gaz à effet de serre émis par les activités humaines, bien plus que les continents et l’atmosphère (actuellement près de 93%) (*MEEHL et al.* 2007 ; *Bindoff et al.* 2007 ; *Church et al.* 2013). La grande inertie thermique de l'océan est une des raisons principales de sa grande influence sur le climat. Une des conséquences de ce phénomène est la hausse du niveau moyen global des océans, un des indicateurs les plus importants du changement climatique (*Solomon et al.* 2007; *Church et al.* 2013). Les variations du niveau de la mer au cours du dernier siècle sont principalement causées par l’expansion thermique de l'océan, la fonte des glaces continentales (glaciers de montagne et calottes polaires) et les échanges d'eau avec les terres émergées et l'atmosphère. Ces phénomènes résultent du réchauffement d'origine humaine, mais aussi de la variabilité naturelle et interne du système climatique (*Church et al.* 2013).

A la fin de la déglaciation (associée au dernier cycle glaciaire) il y a environ 3000 ans le niveau de la mer s’est stabilisé, avec une hausse ne dépassant pas 0.5 mm/an *(Masson-Delmotte et al.* 2013). Avec les observations marégraphiques disponibles depuis ~200 ans, on observe que le niveau de la mer a recommencé à monter au cours du 20ème siècle avec une vitesse de 1.7 mm/an, ce qui représente un rythme 3 à 4 fois plus élevé que ce qui a été estimé durant les 2 derniers millénaires (*Kemp et al.* 2011 ; *Church et White* 2011). Depuis le début des années 1990, la vitesse d’élévation du niveau de la mer enregistré par les satellites altimétriques Topex/Poseidon et ses successeurs (Jason-1, 2, 3, Envisat, etc) a doublée (en comparaison à ce qui a été observé au cours du 20éme siècle), atteignant aujourd’hui 3.4 mm/an en moyenne globale (*Ablain et al.*2016; *Chambers et al.* 2016). Tout suggère que la hausse actuelle du niveau moyen global de la mer est liée au réchauffement climatique anthropique affectant la planète depuis quelques décennies (*Church et al.* 2013). La hausse du niveau de la mer n’est pas régionalement uniforme (principalement à cause de la répartition non uniforme de la chaleur dans l’océan). Dans certaines zones, cette hausse a été 3 fois plus rapide que la hausse moyenne globale (*Meyssignac et al.*

2012; *Ablain et al.* 2015). De plus le niveau moyen global de la mer présente des fluctuations interannuelles qui peuvent atteindre quelques millimètres surtout pendant les épisodes ENSO (El Nino Southern Oscillation) (*Boening et al.* 2012; *Cazenave et al.* 2014).
On s'attend à une hausse accrue du niveau de la mer au cours du 21ème siècle, à cause de l'expansion thermique des océans qui se poursuivra, et surtout à cause de la fonte des glaces continentales (dernier rapport du GIEC, AR5, *Church et al.* 2013). En utilisant des modèles de climat, plusieurs articles récents proposent une hausse du niveau moyen global de la mer de l'ordre de 0.5 m à 1 m à l'horizon 2100, avec une forte variabilité régionale (*Church et al.* 2013). Cependant, cette estimation présente des incertitudes importantes en raison d'une méconnaissance des émissions futures des gaz à effet de serre et de la réponse du climat à ce forçage.

La hausse actuelle du niveau de la mer constitue une menace sérieuse pour de nombreuses régions côtières basses souvent très peuplées de la planète (*Parry et al.* 2007; *Nicholls and Cazenave,* 2010 ; *Nicholls et al.* 2011b ; *Mondal and Tatem,* 2012). Cette hausse peut se combiner avec d'autres facteurs non climatiques (par exemple, l'enfoncement du sol lié au pompage d'eau et des hydrocarbures, etc.), ce qui rend ces régions encore plus vulnérables (*Nicholls and Cazenave,* 2010). Les conséquences de la hausse du niveau de la mer pourraient être : *(1)* la perte d'une grande superficie des littoraux qui déplaceront des centaines de millions de personnes à l'intérieur des terres, *(2)* une perte économique considérable et *(3)* une augmentation des zones inondables impliquant une salinisation des terres agricoles ainsi que des aquifères, avec des conséquences néfastes sur les ressources en eau (*MEEHL et al.* 2007 ; *Nicholls and Cazenave,* 2010). En effet, plusieurs centaines de millions de personnes (attirées par les activités économiques comme la pêche, le transport maritime, les terres fertiles et l'emploi concentrées sur les grandes métropoles côtières) vivent à moins de 100 km des côtes continentales et sur les îles (*MEEHL et al.* 2007 ; *McGranahan et al.* 2007 ; *Nicholls et al.* 2008, 2011a). D'après *McGranahan et al.* (2007) 13% de la population mondiale (soit ~780 millions de personnes) vit à moins de 10 m au dessus du niveau de la mer (région couvrant moins de 2% de la superficie terrestre totale). Ce nombre qui ne cesse de croître constitue un risque réel, forçant jusqu'à 187 millions de personnes (soit ~2.4% de la population mondiale) au cours de ce siècle à des migrations (*Nicholls et al.* 2011b).

Il est donc important de comprendre l'évolution du niveau des océans, non seulement pour la compréhension du climat mais aussi pour anticiper les conséquences socio-économiques de la hausse du niveau de la mer dans les régions côtières et les îles. Pour cela, il est nécessaire de disposer de plusieurs systèmes d'observation de grande précision, indépendants et opérants simultanément (satellites altimétriques, satellites de gravimétrie spatiale GRACE et flotteurs automatiques Argo) pour estimer le niveau de la mer et ses diverses composantes. Différents

centres de traitement de données altimétriques dans le monde (CLS/AVISO, Colorado University, NOAA, NASA/GSFC et CSIRO) fournissent régulièrement des séries temporelles du niveau de la mer sur des grilles ou en moyenne globale, sur la période altimétrique (de 1993 à aujourd'hui). Chaque groupe a mis en place sa propre approche pour le traitement des données et différentes stratégies ont été développées. Ma thèse s'inscrit dans le contexte du projet CCI (Climate Change Initiative) de l'Agence Spatiale Européenne (ESA) qui a pour objectif de fournir de meilleurs produits du niveau de la mer (série temporelle du niveau moyen global de la mer et séries temporelles de grilles en 2-D) combinant les missions Topex/Poseidon, Jason-1/2, ERS-1/2 et Envisat. L'objectif principal de ma thèse est de valider ces produits CCI du niveau de la mer en utilisant différentes approches, en particulier par l'étude du bilan tout en estimant les composantes du niveau de la mer mal connues.

Ce manuscrit s'articule autour de 4 chapitres, avec 9 articles scientifiques insérés.

Le premier chapitre est une introduction sur les connaissances récentes des évolutions passées et actuelles du niveau de la mer, des temps géologiques à l'altimétrie spatiale en passant par le dernier interglaciaire et les périodes pré et postindustrielles. Nous décrivons aussi les différentes techniques utilisées pour estimer les variations du niveau de la mer et ses différentes contributions, dans le passé et le présent.

Le deuxième chapitre porte sur l'étude de bilan du niveau moyen global de la mer au cours des 2 dernières décennies. Une première partie de mon travail a consisté à faire une inter-comparaison de tous les produits du niveau de la mer disponibles au niveau international (CCI, AVISO, Colorado University, NOAA, GSFC et CSIRO). Ensuite, nous avons estimé les différentes contributions aux variations du niveau de la mer depuis le début des années 2000 en utilisant une diversité de produits GRACE et Argo. Enfin, nous avons étudié le bilan du niveau moyen global de la mer (qui consiste à comparer le niveau moyen global de la mer observé à la somme des différentes contributions climatiques) en terme de tendance et de variabilité interannuelle sur deux périodes : période Argo/GRACE (2003 - 2012/13) et période altimétrique (1993-2014). Nous avons ainsi quantifié les contributions manquantes, et tout particulièrement celle due au réchauffement de l'océan profond (en dessous de 2000m de profondeur) mais aussi la contribution totale des eaux continentales à la hausse du niveau de la mer, ainsi que les erreurs résiduelles.

Dans le chapitre 3, après avoir décrit le phénomène ENSO (El Niño et La Niña), nous avons analysé la variabilité interannuelle du niveau moyen global de la mer en lien avec les modifications du cycle global de l'eau causées par les événements ENSO. Ce chapitre porte sur

l'influence de El Niño et de La Niña (principalement le El Niño de 1997/1998 et la La Niña de 2010/2011) sur la variabilité interannuelle du niveau moyen global de la mer.

Dans le chapitre 4, une première partie de mon travail consiste à analyser l'évolution de la température de surface de la Terre au niveau des continents et des océans, en lien avec la "pause" ou "hiatus" des années 2000. Nous avons ensuite étudié l'évolution du contenu thermique des océans et le bilan énergétique du système climatique au cours des dernières décennies. Enfin, nous avons identifié les causes du ralentissement de la vitesse de hausse du niveau moyen global de la mer sur la période 2003-2011, et estimé l'impact de la variabilité naturelle du climat sur l'estimation de la tendance du niveau moyen global de la mer.

Chapitre 1

Les variations passées et actuelles du niveau de la mer

Dans ce chapitre nous présentons les évolutions du niveau de la mer des temps géologiques à l'ère de l'altimétrie spatiale. Ce chapitre résume les connaissances actuelles des évolutions passées et actuelles du niveau de la mer. Ce chapitre n'illustrera pas de résultats issus de notre thèse.

1.1 Les variations passées du niveau de la mer

Les variations passées (avant la période des mesures instrumentales) du niveau de la mer sont estimées de manière indirecte, à partir d'informations issues d'archives sur les fossiles (récifs coralliens, débris de plages émergées), les sédiments (sédiments marins) et les fouilles archéologiques (structures portuaires). La combinaison des trois sources d'informations est utilisée pour reconstruire les variations passées du niveau de la mer sur plusieurs dizaines de millions d'années (*Masson-Delmotte et al.* 2013) :

(1) la mesure du rapport isotopique de l'oxygène (rapport $^{18}O/^{16}O$) contenu dans les sédiments marins. Cela permet d'estimer le volume des glaces continentales, donc les variations de masse de l'océan. Les variations du volume des glaces continentales modifient la composition isotopique de l'eau de mer, donc la composition isotopique de la calcite d'espèces marines contenues dans les carottes de sédiments marins (*Siddall et al.* 2006 ; *Rohling et al.* 2007). Cette méthode permet d'estimer les variations du volume d'eau des océans jusqu'à 80 millions d'années dans le passé,

après correction des effets des variations de température de l'océan (*Cramer et al.* 2009; *Masson-Delmotte et al.* 2013).

(2) La stratigraphie séquentielle permet d'estimer les dépôts sédimentaires qui se produisent sur les marges continentales lors des fluctuations successives du niveau de la mer. Ces marges continentales enregistrent ainsi les variations des lignes de rivage, donc du niveau de la mer relatives sur les dernières centaines de millions d'années (*Vail et al.* 1977; *Haq and Al-Qahtani,* 2005; *Haq and Schutter,* 2008).

(3) La datation des récifs coralliens fournit des enregistrements du niveau de la mer sur des échelles de plusieurs centaines de milliers d'années avec une précision de ±5 m (*Bard et al.* 1991, 2010).

1.1.1 Des temps géologiques au dernier interglaciaire (-125 000 ans)

La vitesse du niveau de la mer, sur des échelles de temps géologiques (plusieurs dizaines à plusieurs centaines de millions d'années) est particulièrement lente (avec une hausse de 0.01 mm/an). Le niveau de la mer présente de fortes variabilités, par fois supérieures à 100m. Ces variations sont principalement causées par les mouvements de la croûte terrestre (collision des continents, production de plancher océanique au niveau des dorsales océaniques) entraînant des changements de forme des bassins océaniques (*Vail et al.* 1977 ; *Rowley,* 2002 ; *Cogné and Humler,* 2004 ; *Miller et al.* 2005 ; *Müller et al.* 2008 ; *Kopp et al.* 2009, 2013 ; *Raymo et al.* 2011 ; *Dutton and Lambeck,* 2012 ; *Lambeck et al.* 2012 ; *Raymo and Mitrovica,* 2012).

Durant la période chaude du Pliocène moyen (il ya 3 à 3.3 millions d'années), le niveau de la mer était plus élevé qu'aujourd'hui d'environ 10 à 20m (*Masson-Delmotte et al.* 2013). Cela est principalement causé par une absence quasi totale de glace au Groenland (contribuant à environ 7m à la hausse du niveau de la mer) et en Antarctique de l'Ouest (plus quelques zones côtières de l'Antarctique de l'Est ; contribuant à ~7m à la hausse du niveau de la mer) (*Naish et al.* 2009 ; *Kopp et al.* 2009, 2013 ; *Passchier,* 2011 ; *Thompson et al.* 2011 ; *Masson-Delmotte et al.* 2013).

Au cours du dernier million d'années, les variations du niveau de la mer ont été dominées par celles du volume d'eau des océans causées par la dynamique (formation et fonte) des calottes de glace continentales. Le niveau de la mer sur cette période, présente des variations rapides (pouvant atteindre jusqu'à 40 mm/an sur quelques siècles) (*Bard et al.* 2010; *Deschamps et al.* 2012) et de fortes amplitudes (*Rohling et al.* 2009 ; *Dutton et al.* 2009 ; *Miller et al.* 2011). Cette période est marquée par une succession de glaciations (périodes froides d'une durée d'environ 100 000 ans en lien avec les variations de l'excentricité de la Terre autour du Soleil) et la formation

des calottes de glace au nord de l'Europe et de l'Amérique. Cela entraîne une baisse du niveau de la mer de plus de 100 m (*Raymo and Mitrovica*, 2012 ; *Lambeck et al.* 2010). Ces glaciations sont interrompues par des périodes interglaciaires (chaudes). Durant ces périodes interglaciaires (la dernière date de -125 000 ans), les calottes de glaces continentales fondent complètement (à l'exception du Groenland et de l'Antarctique) et le niveau de la mer est proche de l'état actuel (*Masson-Delmotte et al.* 2013).

1.1.2 De la dernière glaciation (-20 000 ans) au dernier millénaire

Le dernier maximum glaciaire il y a 20 000 ans, a été suivi par une période de fonte des grandes calottes de glace qui recouvraient le nord de l'Amérique et de l'Europe, causant une remontée du niveau de la mer de ~130 m en moyenne pendant environ 13 000 ans (jusqu'en environ -7000 ans), soit une hausse de 10 mm/an *(Lambeck et al.* 2002; *Masson-Delmotte et al.* 2013). Sur la période allant de -7000 à -3000 ans, le niveau de la mer a augmenté moins vite (de 2 à 3m) (*Masson-Delmotte et al.* 2013), avec des fluctuations de moins de 25 cm sur quelques siècles (*Woodroffe et al.* 2012), puis s'est stabilisé il y a environ 2000 à 3000 ans (*Milne et al.* 2008 ; *Lambeck et al.* 2010 ; *Masson-Delmotte et al.* 2013). Au cours des 2000 dernières années avant le début de l'ère industrielle (au milieu du 18éme siècle), l'analyse des sites archéologiques (*Lambeck et al.* 2004) et la datation des microfossiles de marais maritimes (*Miller et al.* 2009 ; *Kemp et al.* 2011) montrent que le niveau de la mer global n'a pas connu de fortes variations (la tendance ne dépasse pas les 0.5 à 0.7 mm/an) *(Masson-Delmotte et al.* 2013).

1.2 Les variations du niveau de la mer : post-industrielle à nos jours

Les mesures instrumentales du niveau de la mer ont commencé au début de l'ère industrielle (il y a un peu plus de 2 siècles) à l'aide de marégraphes, et depuis le début des années 1990 avec les satellites altimétriques de grande précision.

1.2.1 Les marégraphes (~1750 - présent)

Pour faciliter l'accès des gros navires sur les ports, les premiers marégraphes ont été installés dans certains ports d'Europe du Nord-Ouest au cours du 18^{éme} siècle, afin de mesurer le marnage causé par les marées (*Wöppelmann et al.* 2006, 2008, 2014a ; *Mitchum et al.* 2010). Depuis le début du 19^{éme} siècle, le nombre de marégraphes a augmenté dans les ports d'Europe du Nord-Ouest, mais aussi d'Amérique du Nord. Les mesures marégraphiques ont commencé seulement à la fin du 19ème siècle dans l'Hémisphère Sud (*Church et al.* 2013 ; *Wöppelmann et al.* 2014b).

Au cours du 20^{éme} siècle le réseau de marégraphes s'est élargi le long de certaines côtes continentales et sur quelques îles, mais avec une répartition géographique non homogène, largement dominée par l'Hémisphère Nord (*Wöppelmann et al.* 2007, 2014b ; *Holgate,* 2007 ; *Ray and Douglas,* 2011 ; *Church et al.* 2013). De plus, la couverture temporelle de la majorité des séries marégraphiques fait défaut. Cela est lié à des absences de données de plusieurs années de mesures (*Wöppelmann et al.* 2006, 2014b ; *Jevrejeva et al*. 2006, 2008; *Church and White*, 2006, 2011). Une autre difficulté vient du fait que les marégraphes fournissent une mesure relative du niveau de la mer par rapport à une référence locale (car en plus du changement de niveau de la mer et de sa variabilité, ils enregistrent aussi les mouvements verticaux de la croûte terrestre) (*Wöppelmann et al.* 2007, 2013 ; *Wöppelmann and Marcos,* 2016 ; *Hamlington et al.* 2016). Ces mouvements verticaux sont soit induits par la tectonique des plaques, le rebond postglaciaire (GIA -Glacial Isostatic Adjustment-), l'affaissement du sol dans les deltas de grands fleuves sous l'effet du poids des sédiments fluviaux, ou encore par les activités humaines (l'extraction des eaux souterraines et des hydrocarbures entraînant l'enfoncement des sols) (*Wöppelmann et al.* 2007, 2009 ; *Santamaria et al.* 2014 ; *Wöppelmann and Marcos,* 2016 ; *Hamlington et al.* 2016 ; *Spada,* 2016).

L'analyse des quelques longues séries marégraphiques de qualité (en tenant compte de la couverture inhomogène dans l'espace et dans le temps des données de marégraphes et en corrigeant les mouvements verticaux de la croûte terrestre) indique qu'au cours du 20ème siècle, le niveau moyen global de la mer (GMSL -global mean sea level- en anglais) s'est élevé à une vitesse moyenne de 1.7 mm/an (*Church and White,* 2006, 2011 ; *Collilieux and Wöppelmann,* 2011 ; *Wöppelmann and Marcos,* 2012 ; *Marcos et al.* 2013 ; *Church et al.* 2013 ; *Wöppelmann et al.* 2014b ; *Hamlington et al.* 2016). Cela est illustré plus loin par la courbe bleue de la Fig.1.5 montrant l'évolution temporelle du GMSL (avec une tendance de 1.8 ± 0.6 mm/an sur la période 1900-1992) estimée à partir d'une reconstruction des données marégraphiques par *Church and White,* (2011). A noter cependant que quelques articles récents proposent une hausse du niveau de la mer au 20^{e} siècle comprise entre 1.1 mm/an et 1.9 mm/an (*Hay et al.* 2013 ; *Jevrejeva et al.* 2014 ; *Hamlington et al.* 2016).

1.2.2 L'altimétrie spatiale (~1990 - présent)

Depuis le début des années 1990, les satellites altimétriques de très haute précision (Topex/Poseidon (1992-2006); Jason-1 (2001-2013); Jason-2 (2008-); ERS-1 (1991-2000); ERS-2 (1995-2011); Envisat (2002-2012); CryoSat-2 (2010-); SARAL/AltiKa (2013-); et depuis début 2016, Jason-3 et Sentinel-3) offrent une nouvelle méthode pour mesurer avec une précision

remarquable l'évolution du niveau moyen des mers sur l'ensemble du domaine océanique. Bien que l'altimétrie spatiale ait été développée dès le milieu des années 1970, il a fallu attendre la mission altimétrique Topex/Poseidon, lancée en août 1992 et développée conjointement par la NASA (USA) et le Centre National d'Etudes Spatiales (CNES ; France), pour atteindre la précision requise permettant de mesurer les variations globales et régionales du niveau de la mer et d'étudier la dynamique océanique aux échelles de temps mensuelles à multi-décennales (*Fu and Cazenave*, 2001). Cela est illustré par la Fig.1.1 qui montre l'évolution de la précision des orbites des satellites altimétriques depuis le lancement de GEOS-3 en avril 1975. La Fig.1.2 montre les différentes missions d'altimétrie spatiale depuis 1991 et celles prévues d'ici 2022 (source : *Dibarboure and Morrow*, 2016).

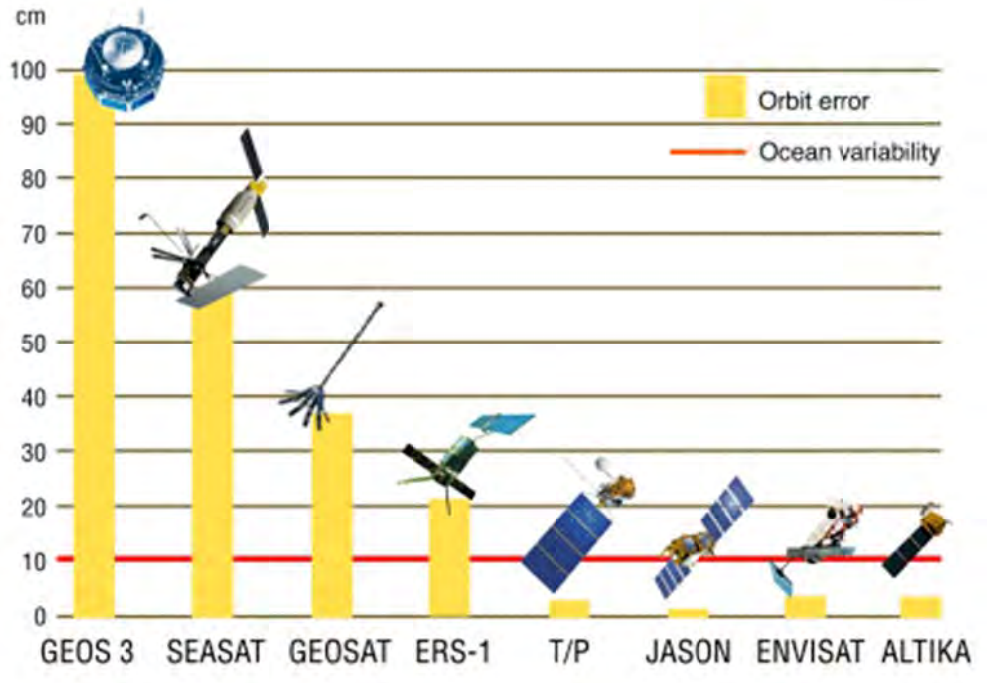

Fig.1.1 : L'évolution de la précision des orbites des satellites altimétriques. Source : CNES/AVISO.

Les satellites altimétriques Topex/Poséidon, Jason-1, 2 et 3 effectuent leurs mesures sur la bande de latitudes 66°S-66°N avec une couverture complète de la Terre en 10 jours (appelée cycle orbital). Cela est illustré par la Fig.1.3 ci-dessous, montrant la couverture spatiale en 10 jours des traces des satellites Topex-Poséidon, Jason-1, 2 et 3. A chaque cycle orbital, le satellite collecte environ 500 000 mesures, ce qui représente un taux d'acquisition de 95%. Pour les satellites ERS-1/2, Envisat et SARAL/AltiKa, le cycle orbital est de 35 jours avec une inclinaison de 98.5° (correspondant à une couverture spatiale sur la bande de latitudes 81.5°S - 81.5°N). En conséquence leur cycle orbital est plus long, mais le quadrillage de l'océan est plus serré que pour

Topex/Poséidon et Jason, avec une distance inter-traces à l'équateur de 80 km. Une description plus détaillée de ces diverses missions spatiales est renseignée sur la Table 1.1 ci-dessous.

Satellites	Topex/ Poséidon	Jason-1	Jason-2	Envisat	CryoSat-2	SARA/ AltiKa	Jason-3	Sentinel-3
Lancement	10/08/1992	07/12/2001	20/06/2008	01/03/2002	08/04/2010	25/02/2013	17/01/2016	16/02/2016
Fin de mission	18/01/2006	01/07/2013	---	08/06/2012	---	---	---	---
Inclinaison orbite	Non héliosync-hrone 66°	Non héliosync-hrone 66°	Non héliosync-hrone 66°	98.55°	Polaire 92°	Héliosync-hrone 98.55°	Non héliosync-hrone 66.04°	Polaire 98.65°
Couverture spatiale	66°S-66°N	66°S-66°N	66°S-66°N	81.5°S - 81.5°N	88°S - 88°N	81.5°S - 81.5°N	66°S-66°N	88°S - 88°N
Répétitivité	10 jours	10 jours	10 jours	30-35 jours	369 jours Sous-cycle de 30 jours	35 jours	10 jours	27 jours
Altitude	1336 km	1336 km	1336 km	782.4-799.8 km	717 km	800 km	1336 km	814.5 km
Mode	LRM	LRM	LRM	ASAR	SAR	---	LRM	SAR
Bandes altimètre	C, Ku	C, Ku	C, Ku	Ku, S	Ku	Ka (35.75GHz)	C, Ku	Ku, C
Agence	NASA CNES	NASA CNES	NASA CNES EUMETSAT NOAA	ESA	ESA	CNES ISRO	NASA CNES EUMETSAT NOAA	ESA

Table 1.1 : Description des différentes missions d'altimétrie spatiale de haute précision. (Sources : NASA, CNES, AVISO et ESA).

Une valeur du GMSL est obtenue en moyennant les hauteurs de mer mesurées au cours d'un cycle sur l'ensemble du domaine océanique. Cette valeur du GMSL varie d'un cycle à l'autre. On peut ainsi construire une courbe d'évolution du GMSL, comme illustré sur la Fig.1.5 (courbe rouge).

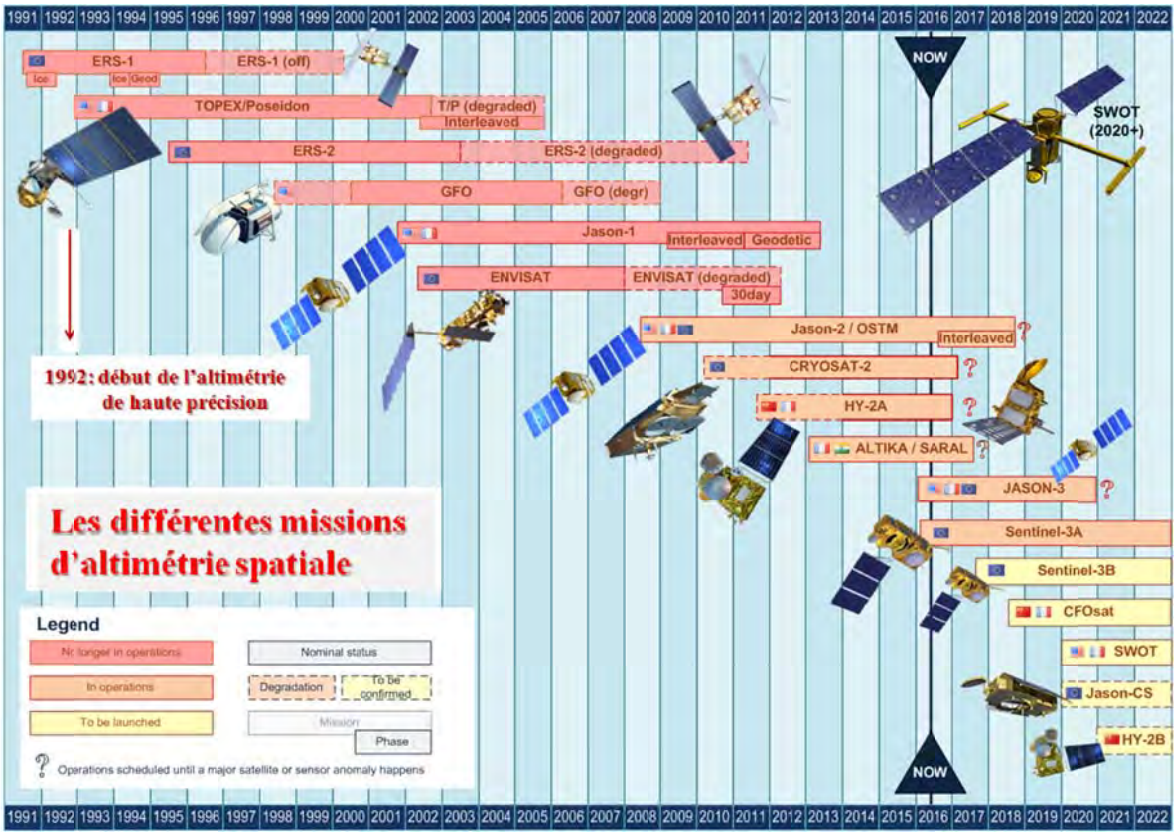

Fig.1.2 : Les différentes missions d'altimétrie spatiale depuis 1991 et celles prévues d'ici 2022. Source: *Dibarboure and Morrow*, 2016.

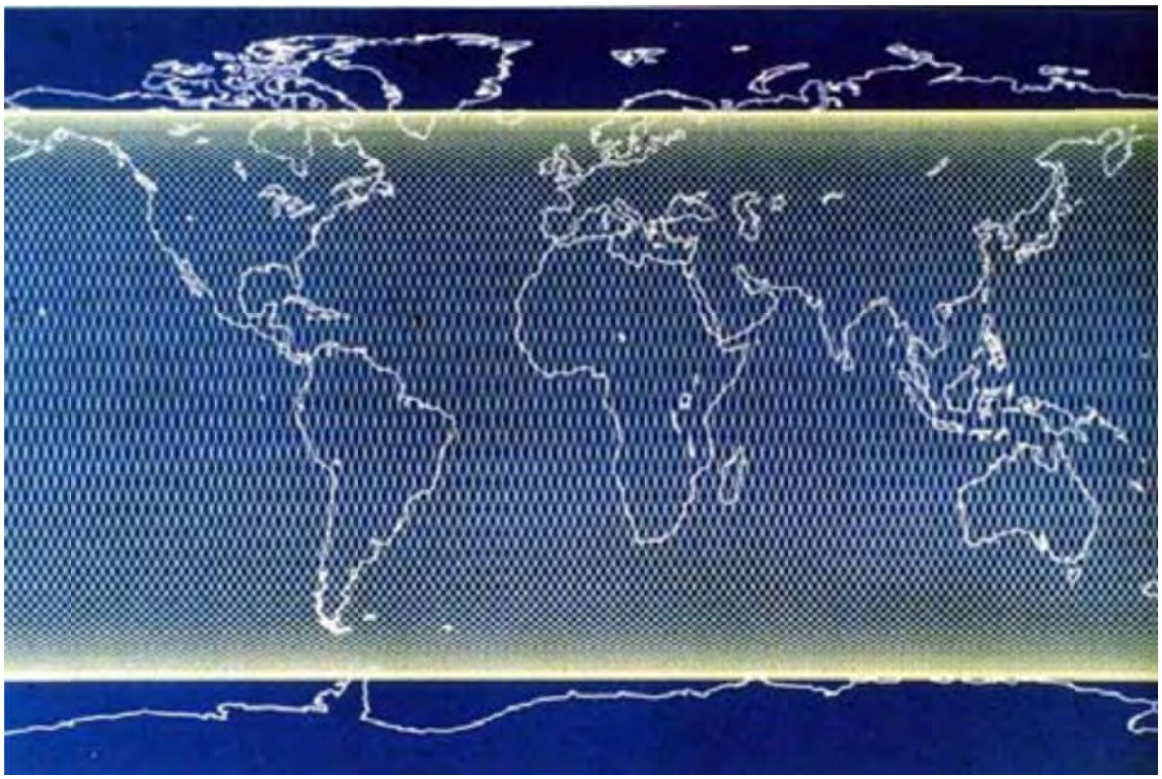

Fig.1.3 : Couverture spatiale et traces des satellites Topex-Poséidon, Jason-1, 2 et 3 au cours d'un cycle orbital de 10 jours. Source : CNES/AVISO.

On peut aussi calculer (à partir du quadrillage de mesures réalisées par le satellite au cours d'un cycle orbital) des grilles de hauteur de mer sur l'ensemble du domaine océanique en interpolant les mesures réalisées le long des traces sur un quadrillage régulier. On peut éventuellement combiner les mesures de plusieurs satellites volant simultanément, pour une meilleure résolution spatiale. Il en résulte ainsi des séries temporelles de hauteur de mer interpolées sur une grille, comme illustré sur la Fig.1.6 (en termes de tendances).

Principe de la mesure altimétrique

Le satellite altimétrique emporte un ensemble d'instruments, dont un radar altimétrique pour la mesure de distance du satellite à la surface de la mer. Le radar émet à la verticale, à intervalles réguliers, une impulsion électromagnétique à très haute fréquence (plus de 1700 impulsions par seconde) en direction de la surface des océans (Fig.1.4). Il reçoit en retour une partie du signal réfléchi par la surface instantanée de la mer (appelée écho radar ou encore "forme d'onde"). L'analyse de l'écho radar permet d'estimer le temps de trajet aller-retour de l'onde radar (noté *temps*), dont on déduit une mesure très précise de la distance entre le satellite et la surface instantanée de la mer. Outre la distance du satellite à la surface de la mer (Hauteur altimétrique *R* ; voir l'équation *1.1*), la forme de l'écho radar permet de calculer d'autres paramètres comme la hauteur des vagues et la vitesse du vent.

$$R = c * temps / 2 \qquad (1.1)$$

c est la vitesse de propagation des ondes électromagnétiques émises par le radar.

Les systèmes de positionnement (encore appelés "mesures de poursuite") des satellites altimétriques de grande précision (comme Topex/Poséidon, Jason-1, 2 et 3, Envisat, SARAL/AltiKa), tels que DORIS (Doppler Orbitography and Radiopositioning Integrated by Satellite), GPS et le Laser fournissent, après un calcul de l'orbite, l'altitude du satellite par rapport à l'ellipsoïde de référence (qui coïncide avec la forme moyenne de la Terre) avec une précision remarquable de quelques cm (*S* altitude du satellite par rapport à l'ellipsoïde). Le calcul d'orbite s'appuie sur des modèles des forces agissant sur le satellite (en particulier celle due au champ de gravité de la Terre, mais aussi l'attraction de la Lune, du Soleil et des autres planètes, le freinage de l'atmosphère, la pression de radiation solaire, les forces de marées terrestres et océaniques, etc.), pour calculer une trajectoire théorique du satellite que l'on recale en permanence en utilisant les mesures de poursuite. Ce processus permet de déduire à tout instant la trajectoire exacte du satellite, donc son altitude par rapport à l'ellipsoïde de référence. La hauteur du niveau de la mer

notée *H* est ainsi déduite par simple différence entre l'orbite du satellite et la hauteur altimétrique, décrite par l'expression suivante:

$$H = S - R \qquad (1.2)$$

Cette hauteur instantanée du niveau de la mer représente les effets combinés du géoïde (surface équipotentielle du champ de gravité de la Terre qui coïncide avec le niveau moyen des océans au repos, en absence de toutes perturbations) et des variations de la topographie dynamique océanique. D'autres phénomènes comme les marées océaniques, les variations de hauteur de mer dues à la charge de l'atmosphère influent aussi sur la valeur de *H*. Le géoïde est donné par une composante permanente due au champ de gravité à grande échelle de la Terre solide (amplitude de l'ordre de 100 m) et une composante temporelle due aux redistributions de masses à la surface et à l'intérieur de la Terre (par exemple, dues au GIA).

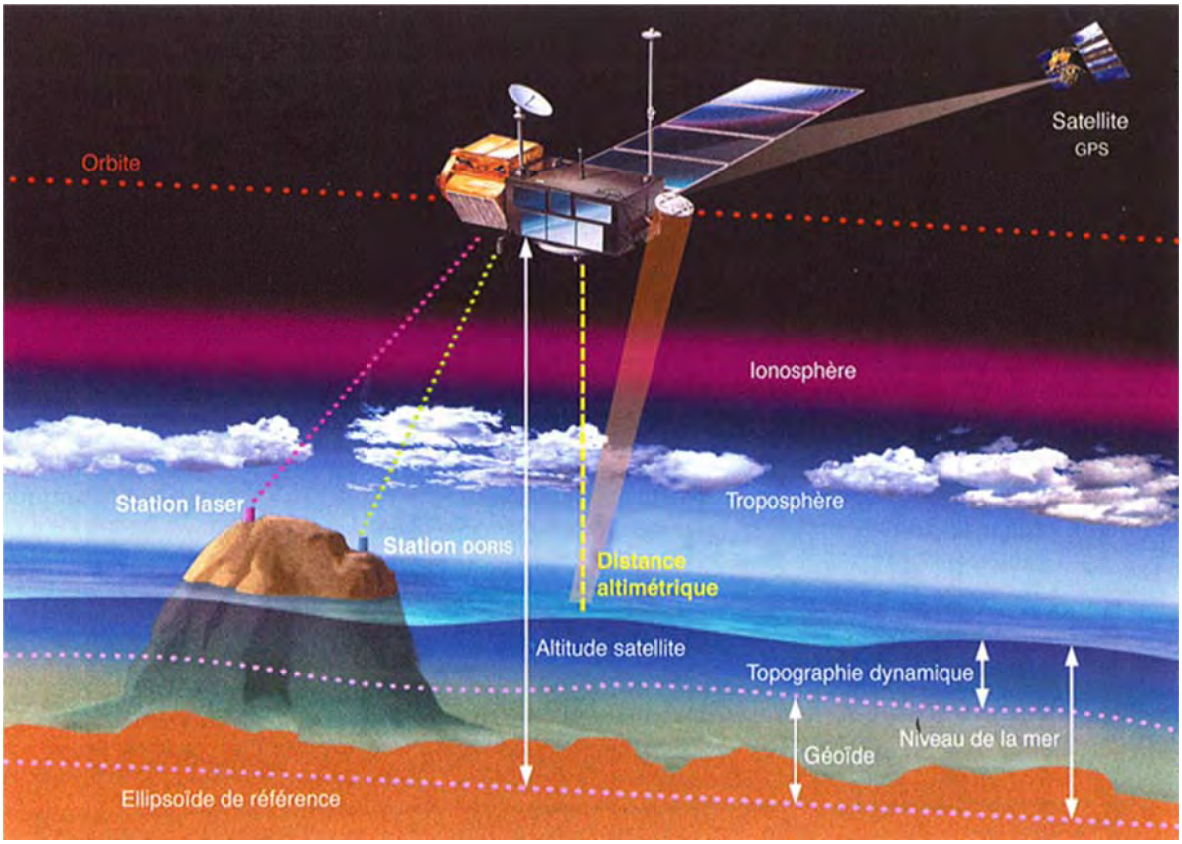

Fig.1.4 : Principe de la mesure du niveau de la mer par altimétrie spatiale. Source : CNES/AVISO.

Incertitudes de la mesure du niveau de la mer par altimétrie

En plus de l'orbite, la hauteur du niveau de la mer doit être corrigée des différents effets : délais de propagation des ondes électromagnétiques pendant leur traversée dans l'atmosphère, liés au taux d'ionisation dans l'ionosphère et à la présence de vapeur d'eau dans la troposphère (ce dernier effet est mesuré par le radiomètre embarqué à bord du satellite), l'état de surface de la mer (dû à la présence de vagues) et certains effets géophysiques (par exemple, les marées terrestres). On estime que la précision de la mesure de la hauteur du niveau de la mer est aujourd'hui de l'ordre de 2 cm (*Ablain et al.* 2015). En termes de tendance, l'incertitude de la mesure du GMSL, basée sur l'évaluation de toutes les sources d'erreurs affectant le système altimétrique, est estimé à ±0.4 mm/an (la même valeur trouvée en faisant un étalonnage externe du GMSL avec des données marégraphiques) (*Ablain et al.* 2009, 2015). Cette incertitude est dominée par les erreurs d'orbite et celle due à la présence de vapeur d'eau dans l'atmosphère (*Ablain et al.* 2009, 2015). Ces valeurs se dégradent en s'approchant des côtes (50 km pour la vapeur d'eau; 10 km pour la mesure de hauteur).

Variation du niveau de la mer altimétrique

L'altimétrie spatiale présente un double avantage pour la mesure du niveau de la mer en comparaison aux marégraphes. D'une part, elle fournit une couverture complète du domaine océanique (voir Fig.1.3) permettant ainsi de suivre réellement l'évolution du GMSL ; d'autre part, la mesure du niveau de la mer est "absolue", c'est-à-dire indépendante des mouvements de la croûte terrestre.

Le GMSL a fortement augmenté sur la période altimétrique en comparaison des décennies antérieures. Depuis 1993, l'altimétrie enregistre une tendance moyenne du GMSL de 3.4 ± 0.4 mm/an (*Ablain et al.*2016 ; *Chambers et al.* 2016), ce qui représente une hausse 2 fois plus élevée que ce qui a été observé au cours du 20^{éme} siècle. Cela est illustré sur la Fig.1.5, montrant l'évolution temporelle du GMSL : en bleu enregistré par les marégraphes entre 1900 et 1992; en rouge basé sur la moyenne des séries temporelles de GMSL des 6 groupes de traitement de produits altimétriques (voir *section 2.1* dans le *chapitre 2* ; *Dieng et al.* 2015a, 2015b) sur la période janvier 1993 - décembre 2015.

En calculant la tendance linéaire sur la période altimétrique, en chaque point de grille, on obtient une carte des tendances du niveau de la mer. Cela est illustré sur la Fig.1.6. Elle montre qu'au cours des deux dernières décennies, la hausse du niveau de la mer n'est pas uniforme, mais que dans certaines régions (comme le Pacifique tropical Ouest) cette hausse a été trois fois plus

rapide que la hausse moyenne globale. Ce non uniformité régionale du niveau de la mer est fortement impacté par les modes de variabilité naturelle interne du système climatique comme *ENSO (El Niño-Southern Oscillation*) (voir *chapitre 3*).

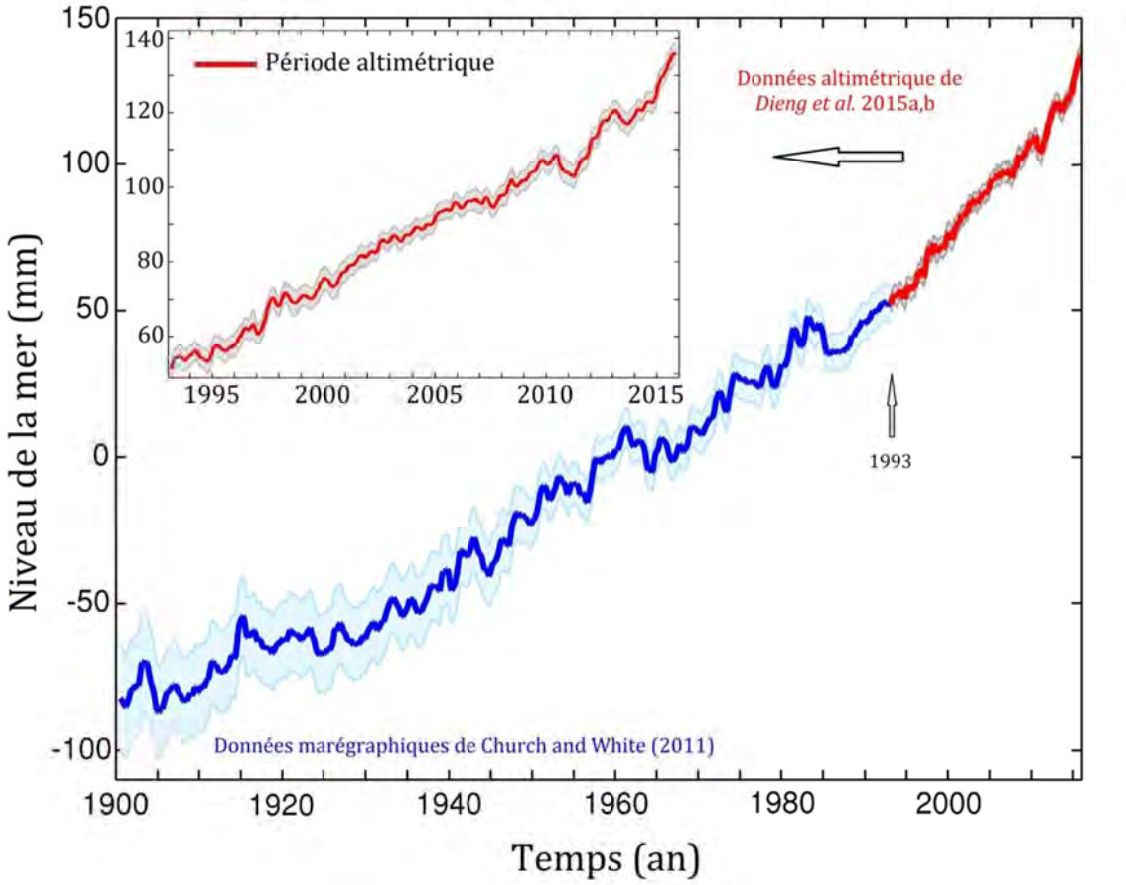

Fig.1.5 : Courbe bleue: série temporelle du niveau moyen global de la mer (GMSL) basé sur la reconstruction par *Church and White* (2011) à partir des données marégraphiques, sur la période 1900-1992. Courbe rouge : moyenne des séries temporelles de GMSL des 6 groupes de traitement de produits altimétriques (voir *section 2.1* dans le *chapitre 2* ; *Dieng et al.* 2015a, 2015b) sur la période janvier 1993 - décembre 2015. La surface bleue-grisée autour de la courbe bleue représente l'erreur à 1-sigma des données marégraphiques. Celle en grisée autour de la courbe rouge représente l'erreur à 1-sigma de la dispersion autour de la moyenne des 6 produits GMSL.

Depuis peu, le CLS (*Collecte Localisation Satellites*), dans le cadre du projet "Sea Level" CCI (Climate Change Initiative) de l'Agence Spatiale (ESA), fournit les incertitudes régionales du niveau de la mer mesuré par altimétrie. Ces incertitudes sont plus marquées dans les régions des gyres subtropicales (*Ablain et al.* 2016). Cela est illustré par la Fig.1.7 montrant les incertitudes de la tendance régionale du niveau de la mer basées sur les données altimétrique du projet "Sea Level" CCI de l'ESA, sur la période janvier 1993 - décembre 2014. Cette figure montre aussi une incertitude non négligeable dans les régions tropicales et le long du courant circumpolaire.

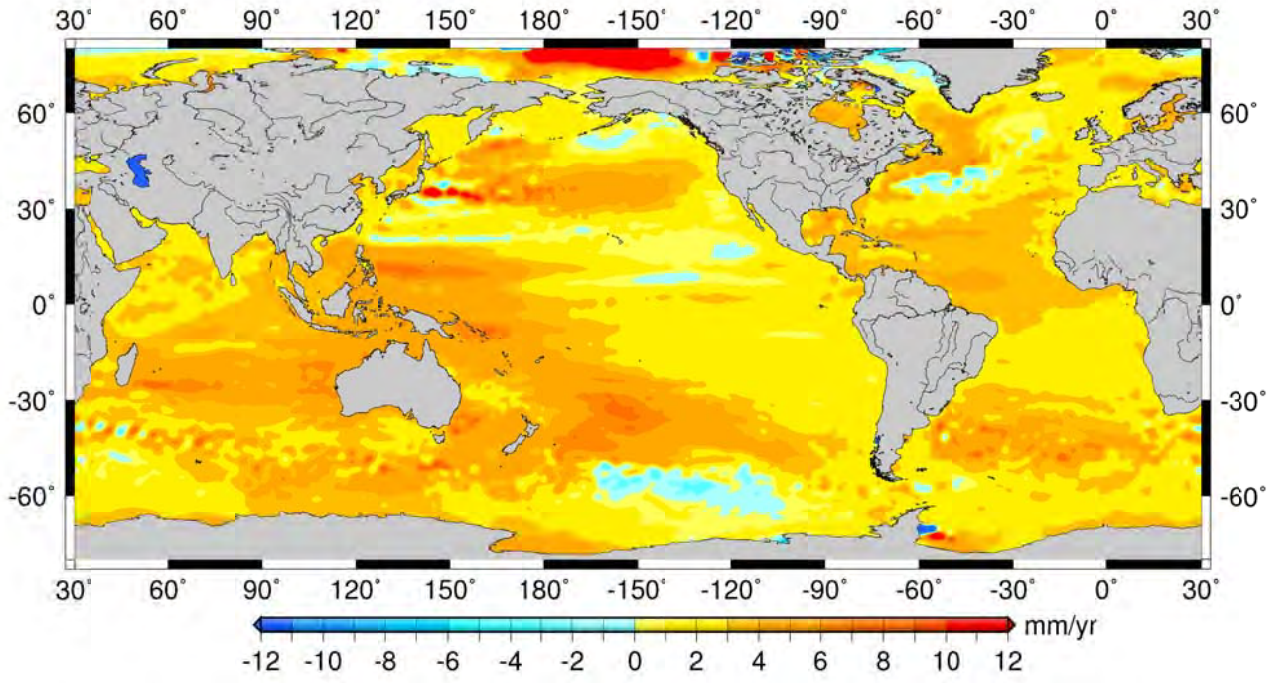

Fig.1.6 : Tendances du niveau de la mer calculées à partir de la combinaison des données altimétriques Topex/Poseidon, Jason-1/2, ERS-1/2 et Envisat sur la période janvier 1993 - décembre 2015.

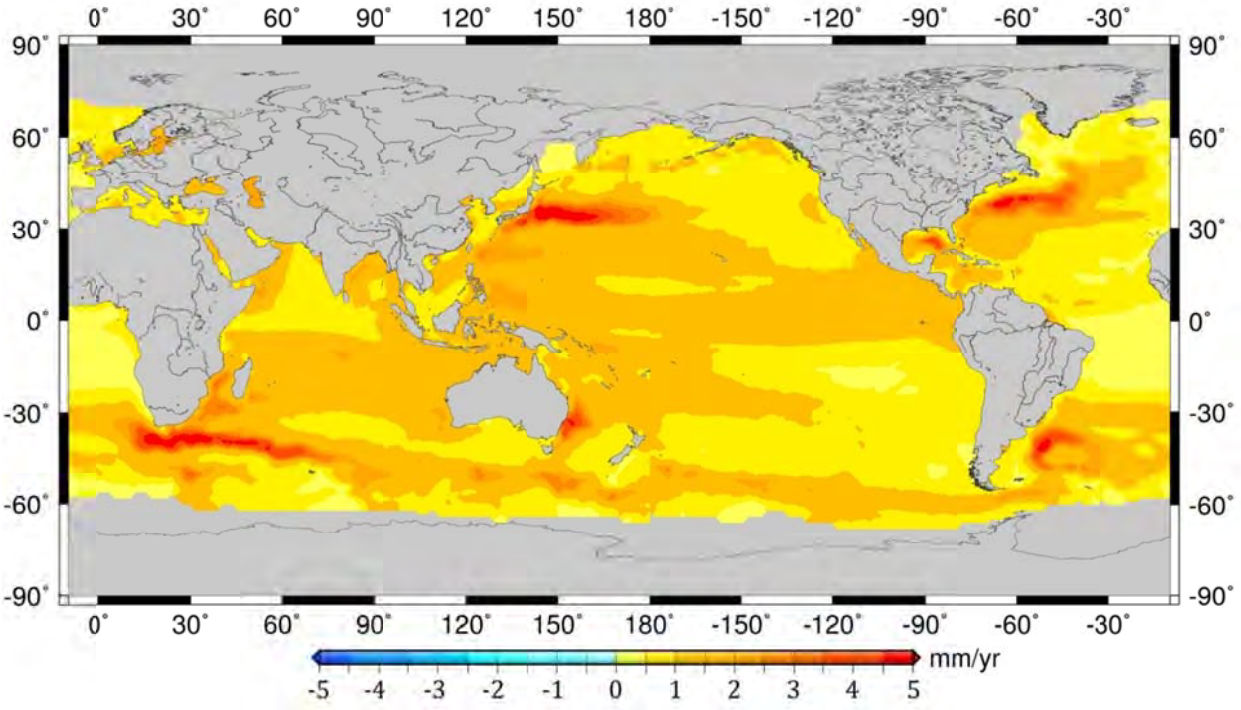

Fig.1.7 : Incertitudes des tendances du niveau de la mer du produit "Sea Level" CCI de l'ESA, calculées à partir de la combinaison des données altimétriques Topex/Poseidon, Jason-1/2, ERS-1/2 et Envisat sur la période janvier 1993 - décembre 2014. (Source : *Ablain et al.* 2016).

Produits niveau de la mer altimétrique

Six différents centres de traitement (AVISO/CLS, University of Colorado -CU-, NOAA, GSFC/NASA, CSIRO et CCI/ESA) des données altimétriques dans le monde fournissent régulièrement des produits niveau de la mer (en global et sur des grilles) sur la période altimétrique. Les séries temporelles de GMSL sont basées sur les satellites altimétriques Topex/Poseidon, Jason-1 et 2 (pour AVISO/CLS, CU, NOAA, GSFC/NASA et CSIRO). Pour les produits grillés, ils sont basés sur la combinaison des satellites Topex/Poseidon, Jason-1 et 2, ERS-1 et 2 et Envisat (pour AVISO/CLS et CCI/ESA). Les séries temporelles de GMSL sont obtenues soit en moyennant directement les données de hauteur de mer le long des traces des satellites à la surface de la mer, soit en calculant d'abord des grilles régulières à partir des données inégalement réparties le long des traces, puis en moyennant les grilles sur l'ensemble du domaine considéré. Ces produits sont disponibles sur internet. Les produits niveau de la mer des différents centres sont décrits dans la *section 2.1,* du *chapitre 2*.

1.3. Les causes des variations actuelles du niveau de la mer (20ème siècle et période altimétrique)

Au cours du dernier siècle, les variations du niveau de la mer ont été principalement causées par des changements de la composante stérique du niveau de la mer (due aux variations de température et de salinité) et des variations de masse de l'océan (dues à la fonte des glaces continentales -Antarctique, Groenland et glaciers de montagnes- et aux échanges d'eau avec les terres émergées et l'atmosphère) (*Leuliette and Willis,* 2011; *Chen et al.* 2013; *Cazenave et al.* 2012b, 2014 ; *Church et al.* 2013). Comme cela a été montré par de nombreux travaux récents, plusieurs de ces phénomènes sont une conséquence directe du réchauffement climatique (*Bindoff et al.* 2007; *Church et al.* 2013). Une autre cause (mineure) de la hausse du niveau de la mer résulte du rebond postglaciaire (GIA) en lien avec la fonte des glaces qui a suivi le dernier maximum glaciaire il ya 20 000 ans (voir *section 1.1.2*).

1.3.1 La hauteur stérique du niveau de la mer

Le terme "hauteur stérique" utilisé par les océanographes, désigne les variations de densité de la colonne d'eau en réponse aux variations de température et de salinité de l'océan. En effet, lorsque la température augmente, l'eau de mer se dilate et le niveau de l'océan s'élève. L'augmentation ou la diminution de la salinité crée une baisse ou une hausse du niveau de la mer. Le calcul de la hauteur stérique d'une colonne d'eau est décrit par l'équation *2.4* (voir *section*

2.2 du *chapitre 2*). Cette hauteur stérique peut être décomposée en deux parties : la hauteur thermostérique (encore appelée expansion thermique de l'océan) due au seul effet des variations de température de l'eau de mer ; et la hauteur halostérique causée par les variations de salinité de l'océan.

Depuis le milieu du 20éme siècle, les mesures de température et de salinité (depuis la surface jusqu'à environ 700 ou 1000m de profondeur) ont été collectées par des navires marchands et de recherche océanographique à l'aide des XBT (Expandable Bathy Thermographers), des CTD (Conductivity-Temperature-Depth) et des MBT (Mechanical BathyThermograph). Ces données ont été complétées par des mesures issues de mouillages et des bouées dérivantes. Depuis le début des années 2000 ces mesures sont réalisées de la surface jusqu'à 2000m de profondeur par les flotteurs profilants autonomes du programme international Argo (*Roemmich et al.* 2015). Les profils de température et de salinité fournis par les navires marchands et de recherche présentent une distribution spatiale non homogène (*Levitus et al.* 2009 ; *Ishii and Kimoto,* 2009). Les mesures ne couvrent pas toutes les saisons et toutes les zones géographiques, en particulier les hautes latitudes inaccessibles en hiver. En plus des lacunes spatio-temporelles, les données XBT présentent des problèmes de biais qui proviennent de l'incertitude sur la profondeur de mesure de la température (*Gouretski and Koltermann,* 2007). En effet les XBT ne mesurent pas la profondeur à laquelle la mesure a été faite. Cette profondeur est déduite de l'équation de la trajectoire du XBT et du temps depuis son immersion dans l'eau. Les lacunes géographiques (principalement dans l'hémisphère Sud) et temporelles des données in-situ de température et de salinité, ainsi que le biais des données XBT, sont la cause d'une forte incertitude sur la contribution globale de la composante stérique du niveau de la mer pour les dernières décennies. Les flotteurs Argo (dont le nombre est estimé actuellement à ~3900; *Roemmich et al.* 2015) fournissent une couverture quasi globale de l'océan (voir Fig.1.8) avec des mesures tous les 10 jours. Cependant, Argo ne fournit pas de données en dessous de 2000m de profondeur. Pour estimer le niveau de la mer stérique en dessous de 2000m de profondeur (voir la *section 2.3* du *chapitre 2*), on peut utiliser des réanalyses océaniques avec une bonne résolution spatiale et temporelle (exemple, *Balmaseda et al.* 2013a).

Les données in-situ (historiques et actuelles) de température et de salinité de l'océan sont disponibles à partir de plusieurs bases de données, comme la WOD (-World Ocean Database-, *Levitus et al.* 2009) et Coriolis (http://www.coriolis.eu.org/). Ces données in-situ sont traitées par divers groupes dans le monde, qui utilisent des méthodes de traitement différentes, par exemple pour le remplissage des lacunes dans la couverture des données, le contrôle de la qualité, le choix de la climatologie, les techniques de maillage mais aussi la correction des biais sur les données

XBT (*Abraham et al.* 2013, 2014). Des informations complémentaires sur les différents produits de température et leur traitement sont disponibles dans la *section 2.2* du *chapitre 2* et dans *Dieng et al.* (2015a, b).

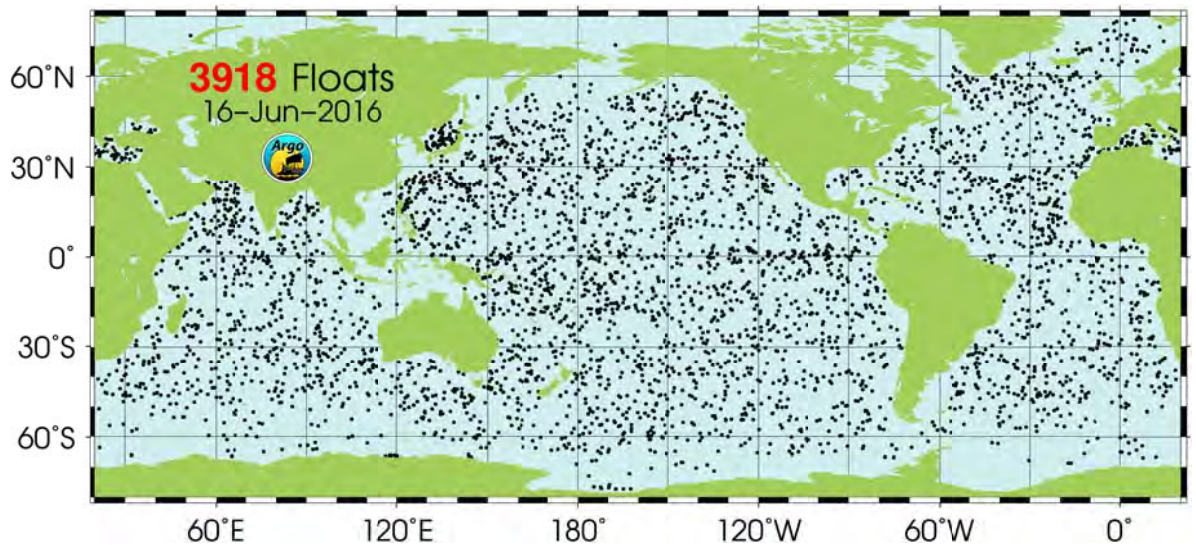

Fig.1.8 : Répartition géographique, au 16 juin 2016, des flotteurs profilants du programme international Argo. Source (http://www.argo.ucsd.edu/).

a. Expansion thermique des océans

En analysant les profils de température dans l'océan depuis le milieu du siècle, les océanographes ont observé un réchauffement global de l'océan depuis le milieu du 20e siècle (*Church et al.* 2013). L'accumulation de chaleur dans le système climatique est stockée principalement dans l'océan (93%, soit 15 à 20 fois plus que l'atmosphère et les terres émergées) (*Bindoff et al.* 2007 ; *Levitus et al.* 2009 ; *Hansen et al.* 2011 ; *Church et al.* 2011, 2013). Au cours de la seconde moitié du 20^{éme} siècle, la dilatation thermique des 700 premiers mètres de l'océan explique ~25% de la tendance du niveau de la mer observée par les marégraphes (*Levitus et al.* 2005, 2012 ; *Antonov et al.* 2005 ; *Ishii et al.* 2006 ; *Bindoff et al.* 2007). Durant les 2 dernières décennies, elle contribue cependant à hauteur de 1.1 mm/an (soit ~34%) à la hausse du GMSL observée par altimétrie spatiale (*Church et al.* 2013 ; *Chambers et al.* 2016). En termes de variabilité interannuelle, l'expansion thermique globale est fortement impactée par les éruptions volcaniques (par exemple, celle du Pinatubo en 1991, la plus marquée durant ces 3 dernières décennies) (*Church et al.* 2005 ; *Gregory et al.* 2004, 2006).

Comme pour le niveau de la mer observé par altimétrie, les observations de température de l'océan montrent que l'expansion thermique de l'océan n'est pas uniforme spatialement (*Meyssignac and Cazenave*, 2012 ; *Church et al.* 2013). La variabilité des tendances régionales de l'expansion thermique de l'océan (illustrés sur la Fig.1.9 basée sur la version v.6.13 des données

de température (entre la surface et 1500m de profondeur) de *Ishii and Kimoto*, 2009) apparaît très similaire à celle des tendances du niveau de la mer altimétrique sur la même période (voir Fig.1.6). Les régions de forte hausse du niveau (exemple, l'Ouest du Pacifique tropical) correspondent aux régions océaniques stockant plus de chaleur, et inversement.

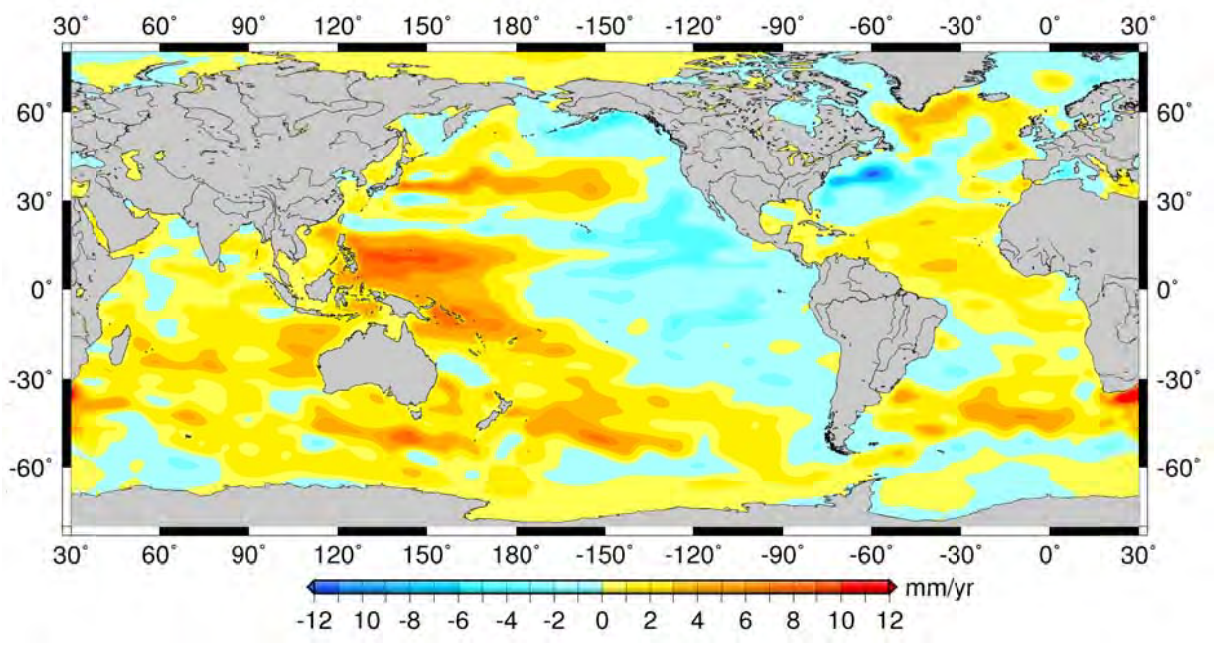

Fig.1.9 : Tendances du niveau de la mer thermostérique calculées à partir des données de température de *Ishii and Kmoto* (2009) version v.6.13, intégrées entre la surface et 1500 m de profondeur, sur la période janvier 1993 - décembre 2012.

b. Le niveau de la mer halostérique

Les variations de salinité de l'océan, ont une contribution négligeable à la hausse du niveau de la mer en global (*Bindoff et al.* 2007 ; *Church et al.* 2013). Néanmoins, la variation globale de la salinité est un très bon indicateur indirect des modifications du cycle hydrologique (dues aux échanges d'eau entre océans, atmosphère et terres émergées : voir *section 1.3.2* suivante) et du volume de la cryosphère (fonte des glaces continentales), entraînant des variations de la masse de l'océan (*Wong et al.* 1999 ; *Antonov et al.* 2002 ; *Curry et al.* 2003 ; *Munk*, 2003 ; *Wadhams and Munk*, 2004 ; *Bindoff et al.* 2007). Contrairement à la température, lorsque la salinité diminue (la densité diminue), l'eau de mer se dilate et le niveau de l'océan s'élève. Au cours de la seconde moitié du 20^{éme} siècle, la contribution halostérique (sur les premiers 700 m) à la hausse du GMSL observée par les marégraphes, est estimée à moins de 3% (soit environ 10% du niveau de la mer stérique global de 0.5 mm/an) (*Antonov et al.* 2002, 2005 ; *Ishii et al.* 2006 ; *Bindoff et al.* 2007). Cette contribution halostérique (diminution de la salinité) suggère une amplification du cycle hydrologique, correspondant à un apport d'eau des continents de ~1.3 mm/an (en équivalent

niveau de la mer -SLE-) (*Antonov et al.* 2002). Selon *Wadhams and Munk,* (2004), la moitié de cette contribution halostérique proviendrait de la fonde des glaces de mer, réduisant ainsi l'apport d'eau des continents à 0.6 mm/an (du même ordre de grandeur que la fonte des glaces continentales sur la même période, *Bindoff et al.* 2007).

En revanche à l'échelle régionale, le niveau de la mer halostérique n'est pas négligeable (*Bindoff et al.* 2007). Les anomalies halostériques peuvent être importantes dans certaines régions (par exemple, l'océan Atlantique, le Golfe du Bengale) (*Stammer et al.* 2013 ; *Church et al.* 2013). Cependant, sur la période altimétrique, le niveau de la mer stérique semblent être principalement d'origine thermostérique, bien que les effets halostériques puissent réduire ou augmenter les changements thermostériques dans certaines régions comme l'océan Atlantique (*Lombard et al.* 2005).

1.3.2 Les variations de masse de l'océan

Les variations de masse de l'océan durant les dernières décennies sont essentiellement causées par la fonte des glaciers continentaux et des calottes polaires (Antarctique et Groenland), ainsi que par échanges d'eau avec les terres émergées et l'atmosphère (*Chen et al.* 2013 ; *Church et al.* 2013 ; *Cazenave et al.* 2014). En effet l'océan, les continents et l'atmosphère échangent en permanence de l'eau via les précipitations, l'évaporation, le ruissellement des rivières et la fonte des glaces.

Au cours des dernières décennies, l'amélioration continue des techniques spatiales et de la modélisation des orbites des satellites ont permis l'observation des variations temporelles du champ de gravité de la Terre (ou de manière équivalente le géoïde) en réponse à la redistribution de masses au sein et entre les différents éléments du système climatique (atmosphère, océans, l'eau terrestre et cryosphère) (*Cazenave and Chen,* 2010). Le champ de gravité terrestre est représenté par une série de coefficients d'harmonique sphérique C_{nm}, S_{nm} de degré n et l'ordre m (voir, *Heiskanen and Moritz,* 1967 ; *Lambeck,* 1990 ; *Cazenave and Chen,* 2010).

$$H(\theta, \emptyset) = R_e \sum_{n=0}^{\infty} \sum_{m=0}^{n} \tilde{P}_{nm} (\cos\theta) \times [C_{nm} \cos(m\emptyset) + S_{nm} \sin(m\emptyset)] \qquad (1.3)$$

H définie comme la hauteur de mer, est le changement de la hauteur du géoïde à la surface moyenne à l'emplacement θ (latitude), φ (longitude). R_e est le rayon moyen de la Terre, et P_{nm} est nommé polynôme de Legendre. Le degré *n* est lié à la longueur d'onde λ (en km) à travers la relation $\lambda = 40000/n$. Au cours des années 1990, il est devenu possible de déterminer les variations temporelles des premiers termes de l'équation *1.3* jusqu'au degré 4. Mais ces quelques termes de grandes longueurs d'onde sont insuffisants pour estimer les variations spatio-temporelles du

géoïde dues aux variations de la masse de l'océan et des glaces continentales (*Cazenave and Chen*, 2010).

Les variations de masse de l'océan global peuvent être estimées de manière indirecte en faisant la somme des contributions de masse "fonte de l'Antarctique, du Groenland et des glaciers de montagne et variations du stock d'eaux continentales" (*Church et al.* 2013). Avec le lancement de la mission de gravimétrie spatiale GRACE (Gravity Recovery And Climate Experiment) en 2002, il est devenu possible pour la première fois de déterminer les redistributions de masse à la surface et à l'intérieur de la Terre avec une résolution spatiale et temporelle remarquable. En effet, GRACE fournit les variations du champ de gravité terrestre jusqu'au degré harmonique sphérique 60, ce qui correspond à une résolution spatiale ~300-400 km (*Tapley et al.* 2004). GRACE permet de mesurer directement, en plus du bilan de masse des calottes polaires, des glaciers de montagne et les variations des stocks d'eau dans les bassins hydrographiques, les variations de masse de l'océan (*Chambers et al.* 2004, 2010 ; *Chambers,* 2006 ; *Cazenave et al.* 2009 ; *Leuliette and Miller,* 2009 ; *Llovel et al.* 2010). Pour plus d'informations sur les données GRACE et leur traitement, voir la *section 2.2.2* dans le *chapitre 2*. La masse de l'océan basée sur GRACE a contribué à hauteur de 1.8 mm/an (soit ~60%) à la hausse du GMSL durant la décennie 2003-2012 (*Leuliette and Willis,* 2011 ; *von Schuckmann and Le Traon,* 2011 ; *Dieng et al.* 2015a ; *Chambers et al.* 2016).

a. La fonte des glaces continentales : glaciers et calottes polaires

Les glaciers continentaux

La perte de masse des glaciers constitue avec l'expansion thermique la contribution essentielle de la hausse du niveau de la mer du 20e siècle (*Church et al.* 2013 ; *Gregory et al.* 2014 ; *Marzeion et al.* 2015, 2016). Cependant, ces estimations présentent de grandes incertitudes à cause du nombre limité de mesures in-situ effectuées et de glaciers étudiés (une centaine sur les ~120000 glaciers sur Terre, *Radic and Hock,* 2010 ; *Cogley,* 2010). Au cours du 20^{éme} siècle la contribution des glaciers à la hausse du niveau de la mer est estimée à 0.54 mm/an en équivalent niveau de la mer (SLE -en anglais-) (*Church et al.* 2013 ; *Marzeion et al.* 2016). En plus des mesures in-situ (principalement sur les grands glaciers du monde, par exemple : Alaska, Patagonie, Himalaya, etc.), les observations des glaciers se sont multipliées dés le début des années 1990 avec les mesures de télédétection (cartographie aéroportée et utilisation des satellites) (*Berthier et al.* 2011). La perte de masse (quasi généralisée) des glaciers de montagne s'est accélérée durant les dernières décennies, phénomène attribué au réchauffement climatique anthropique (*Bindoff et al.* 2007 ; *Marzeion et al.* 2015). En effet, les glaciers, avec leurs

dimensions limitées, sont très sensibles à l'élévation de la température de l'air. Les glaciers ont contribué pour 0.76 mm/an (soit ~25%) à la hausse du GMSL sur la période altimétrique 1993-2010 (*Church et al.* 2013). Chambers et al. (2016) donne la même contribution des glaciers (0.76 ± 0.30 mm/an) sur la période 1992-2013. Pour l'estimation du bilan de masse des glaciers, voir la *section 2.3.3* dans le *chapitre 2*.

Les calottes polaires : Groenland et Antarctique

Avant les années 1990, le bilan de masse des calottes polaires du Groenland et de l'Antarctique était quasi inconnu (*Vaughan et al.* 2013). Avec l'arrivée des satellites d'observation de la Terre (altimétrie, interférométrie radar et depuis 2002, gravimétrie spatiale GRACE) depuis le début des années 1990, il est devenu possible de mesurer les variations de masse de ces calottes polaires (*Vaughan et al.* 2013). GRACE permet d'estimer directement les variations de masse des calottes polaires. L'interférométrie radar permet d'estimer la quantité de glace déversée dans l'océan sous forme d'icebergs, en mesurant les flux vers l'océan des glaciers côtiers des calottes polaires. Ces données combinées aux mesures de bilan de masse en surface (fonte et précipitation), permettent de déduire le bilan de masse total des calottes polaires. Quand à l'altimétrie, elle mesure les variations d'épaisseur des calottes, ce qui permet d'en déduire le bilan de masse.

Les calottes polaires ont contribué pour 0.7 mm/an (~22%) à la hausse du GMSL sur la période 1993-2010 (avec une contribution du Groenland de 0.43 mm/an et de l'Antarctique de 0.27 mm/an) (*Church et al.* 2013). Par contre, cette contribution était de 0.42 mm/an (soit ~14%) sur la période 1993-2003 (avec une contribution du Groenland et de l'Antarctique de 0.21 mm/an chacune) (*Bindoff et al.* 2007). Depuis le début des années 2000, les observations ont montré une accélération de la fonte des calottes polaires, principalement localisée dans les régions périphériques du Groenland et de l'Antarctique ouest devenues instables sous l'effet du réchauffement des eaux océaniques périphériques (*Shepherd et al.* 2012 ; *Marzeion et al.* 2012 ; *Vaughan et al.* 2013). Cela est illustré sur la Fig.1.10, montrant l'évolution du bilan de masse du Groenland et de l'Antarctique (données du projet "Ice Sheets" CCI de l'ESA) d'après GRACE, exprimée en SLE sur la période janvier 2003 - décembre 2014. En SLE, le Groenland a contribué pour ~0.7 mm/an à la hausse du niveau de la mer, l'Antarctique pour ~0.3 mm/an. Cela fait une contribution totale des calottes polaires de ~1 mm/an à la hausse du GMSL sur la période 2003-2014.

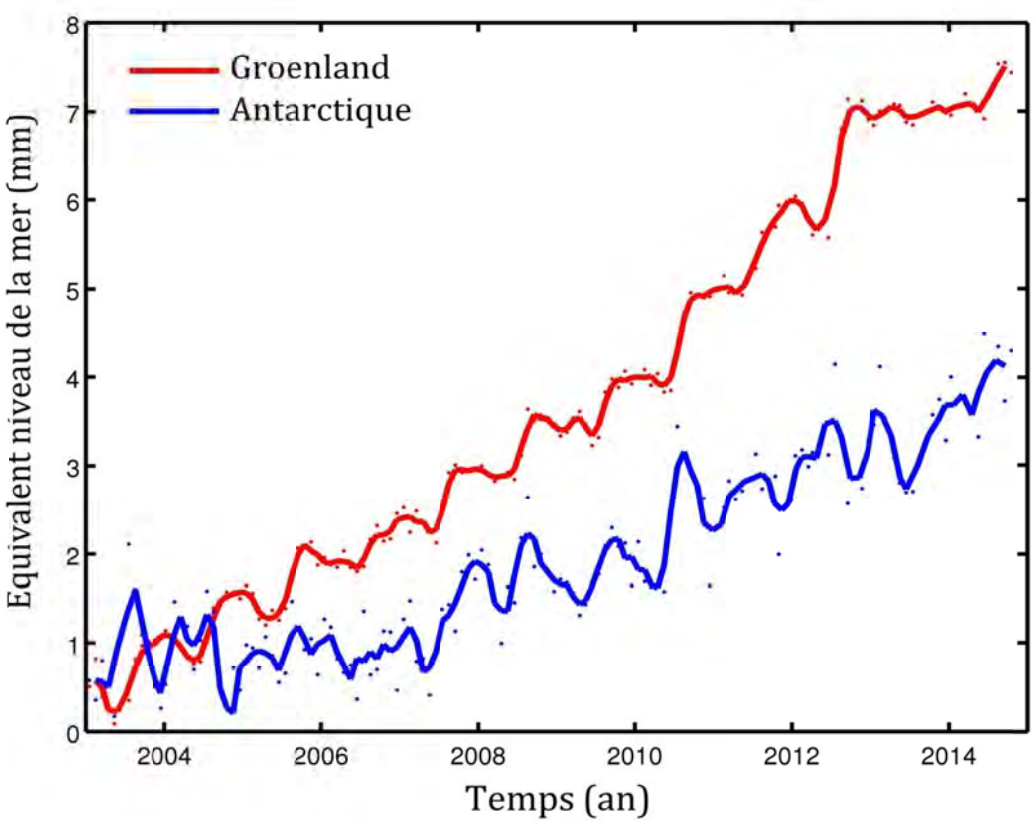

Fig.1.10 : Evolution du bilan de masse du Groenland et de l'Antarctique en SLE, basé sur les données du projet CCI "Ice Sheets" de l'ESA, sur la période janvier 2003 - décembre 2014.

b. Échanges d'eau avec les terres émergées et l'atmosphère

Les continents échangent en permanence de l'eau avec l'atmosphère et les océans, par le biais des précipitations, de l'évaporation, de la transpiration de la végétation, des eaux de ruissellement et de l'écoulement souterrain. Ces échanges d'eau influent de façon importante sur le niveau de la mer (*Boening et al.* 2012 ; *Fasullo et al.* 2013 ; *Cazenave et al.* 2014 ; *Dieng et al.* 2014). Les variations du stock d'eau dans les réservoirs terrestres, en plus de la variabilité naturelle du climat, sont impactées par les activités humaines (par exemple, le pompage de l'eau dans les nappes et la construction de barrages sur les cours d'eau) (*Pokhrel et al.* 2012 ; *Wada et al.* 2012). Le stock d'eau total des continents a contribué pour 0.38 mm/an (soit ~12%) à la hausse du GMSL sur la période 1993-2010 (*Church et al.* 2013). Cette contribution était estimée à -0.11 mm/an et 0.12 mm/an respectivement sur les périodes 1901-1990 et 1971-2010 (*Church et al.* 2013). Cela implique une augmentation des pertes d'eau des continents probablement due aux activités humaines (*Wada et al.* 2012, 2015).

Pour des d'informations détaillées, sur les méthodes d'estimation de la contribution des eaux continentales aux variations du niveau de la mer durant ces dernières décennies, voir la *section 2.3.3* du *chapitre 2*.

1.3.3 Les causes influant la variabilité régionale et locale du niveau de la mer

En plus des variations régionales de la composante stérique et de masse de l'océan, plusieurs facteurs sont responsables de la variabilité régionale du niveau de la mer, par exemple, la pression atmosphérique et les effets statiques (voir définition ci-dessous) (*Stammer et al.* 2013). D'autres phénomènes (par exemples : les effets des vagues, de la houle, des marées océaniques, etc.) peuvent contribuer de manière significative à la variabilité locale du niveau de la mer (*Stammer et al.* 2013).

Les effets statiques correspondent à la déformation de la Terre solide et aux variations de gravité causées par la redistribution de masses passées et actuelles de glaces et d'eau à la surface de la Terre en réponse à la dernière déglaciation et au réchauffement climatique actuel (*Riva et al.* 2010 ; *Tamisiea and Mitrovica,* 2011 ; *Jacob et al.* 2012 ; *Stammer et al.* 2013) :

(1) Le GIA : il contribue différemment à chacune des observations du niveau de la mer (marégraphes, altimétrie et GRACE). Les marégraphes localisés prés des calottes de glace du dernier maximum glaciaire (par exemple, autour de la baie de Hudson, en Patagonie en Antarctique, etc.) sont principalement affectés, montrant une baisse du niveau de la mer (*Tamisiea and Mitrovica,* 2011). Les effets du GIA peuvent entraîner une baisse du niveau de la mer absolue sur une grande échelle (*Tamisiea and Mitrovica,* 2011 ; *Stammer et al.* 2013). En global, le GIA contribue pour environ -0.3 mm/an aux variations du niveau de la mer absolue observées par altimétrie (*Peltier,* 2001, 2009 ; *Peltier and Luthcke,* 2009). En revanche, le GIA a la plus grande contribution aux variations de masse de l'océan mesurées par GRACE. Sa contribution négative à la hausse apparente du niveau de la mer global est estimée à plus de -1 mm/an (par exemple, *Chambers et al.* 2010). Cette valeur a une grande incertitude en raison de sa dépendance sur la viscosité du manteau et l'histoire de la déglaciation (*Tamisiea and Mitrovica,* 2011 ; *Stammer et al.* 2013).

(2) La réponse de la Terre à la fonte actuelle des glaces continentales est différente de celle du GIA car elle fait intervenir seulement la réponse élastique de la croûte et les sources (Groenland, Antarctique, glaciers) ont une localisation différente (et bien connue) (*Tamisiea and Mitrovica,* 2011). La signature régionale dans le niveau de la mer de ce phénomène est actuellement difficile à détecter dans les observations car le signal associé est faible (*Kopp et al.* 2010 ; *Church et al.* 2013). Il deviendra important dans le futur si la fonte des glaces continentales s'accélère (*Slangen et al.* 2011, 2014 ; *Stammer et al.* 2013 ; *Church et al.* 2013).

Chapitre 2

Bilan du niveau de la mer et estimation des contributions manquantes ou mal connues

Le niveau moyen global de la mer (GMSL) a fortement augmenté sur la période altimétrique en comparaison des décennies antérieures. Depuis 1993, l'altimétrie enregistre une tendance moyenne du GMSL de 3.3 ± 0.4 mm/an et des fluctuations interannuelles qui peuvent atteindre quelques millimètres surtout pendant les épisodes ENSO (El Nino Southern Oscillation) (*Ablain et al.* 2016 ; *Chambers et al.* 2016). Sur les deux dernières décennies, la hausse du GMSL est causée par des changements de la composante stérique de l'océan (due aux changements de température et de salinité de l'océan) et par les variations de masse de l'océan (dues à la fonte des glaces continentales -Antarctique, Groenland et des glaciers de montagne-, ainsi qu'aux échanges d'eau avec les terres émergées et l'atmosphère) (*Leuliette and Willis,* 2011 ; *Chen et al.* 2013 ; *Church et al.* 2013 ; *Cazenave et al*. 2014 ; *Dieng et al.* 2014, 2015c).

Dans le dernier rapport (5éme rapport) du groupe d'experts intergouvernemental sur l'évolution du climat (GIEC, -IPCC- en anglais), publié en 2013, la hausse du GMSL sur la période 1993-2010 est estimée à 45% par la fonte des glaces continentales, à 32% par l'expansion thermique de l'océan (l'effet de la salinité reste négligeable en global) et à 12% par les eaux continentales (*Church et al.* 2013). La tendance de la somme de ces contributions vaut 2.8 ± 0.5 mm/an, une valeur légèrement inférieure à la hausse du GMSL observée par les satellites altimétriques de 3.2 ± 0.4 mm/an. Bien que du même ordre de grandeur que les incertitudes associées, cette différence peut également refléter d'autres contributions non prises en compte (par

exemple, l'océan profond, voir ci-dessous). Le rapport du GIEC précédent (4ème rapport, publié en 2007) estimait que l'expansion thermique avait contribué pour ~50% à la hausse du GMSL sur la période 1993-2003 (*Bindoff et al.* 2007). Depuis le début des années 2000, on observe une accélération de la fonte des glaces continentales, en particulier des calottes polaires (*Shepherd et al.* 2012), alors que l'expansion thermique a augmenté moins vite en comparaison de la période 1993-2003 (*Lyman et al.* 2010). La décennie 2000 coïncide avec la période dite de "pause" ou encore "hiatus" (*Held,* 2013), période durant laquelle la température moyenne de la Terre a augmenté 2 fois moins que durant les décennies précédentes. Cette "pause" sera discutée dans la *section 2.3.1* et plus en détail dans le *chapitre 4*.

Certaines contributions à la hausse du GMSL sont mal connues, telle la composante stérique de l'océan profond en raison du manque de mesures de température et de salinité en dessous d'une certaine profondeur (environ 1000 m pour les mesures réalisées à partir des bateaux et 2000 m avec le système Argo mis en place au début des années 2000). Plusieurs publications estiment cependant que la contribution stérique au niveau de la mer de l'océan profond est faible. Par exemple, sur la base des quelques mesures profondes disponibles, *Purkey and Johnson* (2010) l'estiment à environ 0.1 mm/an pour la décennie 1990-2000. Pour *Kouketsu et al.* (2011), cette contribution est estimée à moins de 0.1 mm/an en dessous de 3000m de profondeur. Ces valeurs concordent bien avec les résultats de la réanalyse ORAS4 (*Balmaseda et al.* 2013), à savoir 0.17 mm/an pour la couche 1500-6000m sur la décennie 1993-2003. La propagation de la chaleur stockée dans l'océan vers les grandes profondeurs suggère cependant que sur la dernière décennie, cette contribution pourrait être plus importante.

Dans ce chapitre, nous étudions le bilan du GMSL en terme de tendance et de variabilité interannuelle sur deux périodes : période Argo/GRACE (2003 - 2012/13) et période altimétrique (1993-2014). Cette étude de bilan qui consiste à comparer le GMSL observé avec la somme des différentes contributions climatiques, a pour objectif principal d'estimer les contributions manquantes, et tout particulièrement celle due au réchauffement de l'océan profond (en dessous de 2000m de profondeur) mais aussi la contribution totale des eaux continentales à la hausse du niveau de la mer, ainsi que les erreurs résiduelles.
L'équation de bilan s'écrit :

$$GMSL\ (t) = \Delta M_{ocean}(t) + \Delta H_{Stérique(0\text{-}2000m)}(t) + \Delta H_{Stérique\ (>2000m)}(t) + \mathcal{E}_{Erreurs\ données} \qquad (2.1)$$

$$Résiduel\ (t) = GMSL(t) - \Delta M_{ocean}(t) - \Delta H_{Stérique(0\text{-}2000m)}(t)$$
$$= \Delta H_{Stérique\ (>2000m)}(t) + \mathcal{E}_{Erreurs\ données} \qquad (2.2)$$

avec

$$\Delta M_{Ocean}(t) = -[\Delta M_{Glaciers}(t) + \Delta M_{Groenland}(t) + \Delta M_{Antarctique}(t) + \Delta M_{Atmosphere}(t) + \Delta M_{Eaux\_continents}(t)] \quad (2.3)$$

GMSL(t) représente l'évolution temporelle du niveau moyen global de la mer observé par altimétrie spatiale. Le terme $\Delta M_{ocean}(t)$ décrit la variation au cours du temps de la masse de l'océan, exprimée en équivalent niveau de la mer (SLE). Les termes $\Delta H_{Stérique(0\text{-}2000m)}$ et $\Delta H_{Stérique\ (>2000m)}$ décrivent la contribution stérique globale du niveau de la mer, respectivement des couches 0-2000m et 2000m-fond. Les erreurs de données des termes de l'équation bilan sont représentées par $\mathcal{E}_{Erreurs\ données}$.

Une première partie de ce chapitre consiste en une inter-comparaison de tous les produits du niveau de la mer disponibles au niveau international. On calcule ensuite les différentes contributions climatiques (composante stérique et variation de masse de l'océan) à la hausse du GMSL. Pour chaque composante, nous utilisons plusieurs sources de données produites par divers centres de traitement. Cette approche permet une estimation réaliste de l'incertitude sur les composantes (voir ci-dessous). En particulier, nous discutons les incertitudes des composantes sur la période Argo/GRACE par une méthode statistique.

Outre la contribution de l'océan profond, nous utilisons l'équation de conservation de la masse d'eau (Eq.*2.3* ci-dessus) pour estimer la variation du stock d'eau total sur les continents. En termes de tendance, celle-ci résulte principalement de l'effet des activités humaines sur l'hydrologie (pompage de l'eau dans les nappes et construction de barrages sur les cours d'eau ...). Ce facteur est mal connu et mal (ou pas du tout) modélisé dans les modèles hydrologiques. La différence de cette approche de bilan par rapport aux études antérieures réside dans la diversité des sources de données combinant l'altimétrie, la gravimétrie, les mesures in-situ, des ré-analyses océaniques et atmosphériques et des modèles hydrologiques.

Le bilan du niveau de la mer régional n'est pas traité dans ce chapitre.

2.1 Niveau de la mer altimétrique : inter-comparaison des produits CCI, AVISO, CU, NOAA, GSFC et CSIRO

Depuis le début des années 1990 on suit avec une très grande précision l'évolution globale du niveau moyen de la mer grâce aux satellites altimétriques (Topex/Poseidon, Jason 1 et 2, ERS-1 et 2, Envisat, SARAL/AltiKa, et depuis peu, CryoSat, Jason-3 et Sentinel-3). Différents centres de traitement de données altimétriques dans le monde fournissent régulièrement des séries

temporelles du GMSL sur la période altimétrique. Nous utilisons dans ce travail 6 produits GMSL des 6 centres de traitement de données altimétriques:

1. AVISO (Archiving Validation and Interpretation Satellite Oceanographic Center) traitées par le CLS/CNES (Collecte Localisation Satellites / Centre national d'études spatiales), France
2. Université du Colorado (CU ; -Colorado University-), USA
3. NOAA (National Oceanographic and Atmospheric Administration), USA
4. GSFC (Goddard Space Flight Center) de la NASA (National Aeronautics and Space Administration), USA
5. CSIRO (Commonwealth Scientific and Industrial Research Organization), Australie
6. CCI dans le cadre du projet "Climate Change Initiative" de l'Agence Spatiale Européenne (ESA), Europe.

Le projet CCI (Climate Change Initiative) de l'ESA

Avec l'appui de la convention-cadre des Nations Unies sur les changements climatiques (UNFCCC en anglais-) le système d'observation globale du climat (« Global Climate Observing System » -GCOS en anglais-) a mis en place un ensemble d'exigences pour les données satellitaires, afin de répondre aux besoins de la communauté scientifique sur les changements climatiques au cours des dernières décennies (voir GCOS, Satellite Supplement, 2011). Ces exigences sont décomposées en paramètres clés du système climatique, appelés variables climatiques essentielles (ECVs en anglais-). Le but est de fournir aux chercheurs des produits précis et stables issus d`observations spatiales et in situ, sur le long terme. Parmi les 50 ECVs identifiées jusqu'à présent par le GCOS, 26 sont observables depuis l`espace. Le niveau de la mer est l'une d'entre elles.

C'est dans ce contexte que l'ESA a mis en place le projet CCI pour répondre à ce besoin de fournir des séries climatiques de qualité basées sur l'observation spatiale. Le but du CCI est de contribuer significativement aux exigences du GCOS en réalisant des archives mondiales d'ECVs à partir de données satellitaires. Au travers d'une collaboration internationale, les ECVs du projet CCI sont dérivées de plusieurs ensembles de données satellitaires avec des informations spécifiques sur les incertitudes. Ma thèse s'inscrit dans le cadre du projet CCI de l'ESA et vise entre autres, à valider les produits "Sea Level" CCI.

Inter-comparaison des produits GMSL

Chacun des 6 groupes de traitement des données altimétriques a mis en place sa propre approche pour le traitement des données. Certains fournissent non seulement des séries temporelles du niveau de la mer, mais aussi d'autres produits océanographiques (par exemple,

pour l'étude de la méso-échelle océanique). AVISO, CU, NOAA, GSFC et CSIRO produisent des séries temporelles du niveau de la mer basées sur les satellites altimétriques Topex/Poseidon, Jason 1 et 2, en moyennant géographiquement les données entre 66°S et 66°N (les données de CSIRO sont moyennées entre 65°S et 65°N). Les grilles du niveau de la mer du CCI sont moyennées entre 66°S et 66°N et sont obtenues en combinant Topex/Poseidon, Jason 1 et 2 avec les missions altimétriques ERS-1/2 et Envisat (*Ablain et al.* 2015). L'effet du rebond postglaciaire (appelé aussi l'ajustement glaciaire isostatique -GIA en anglais-) de -0.3 mm/an en moyenne globale (*Peltier*, 2004), est pris en compte. Les cycles annuel et semi-annuel sont en général supprimés lorsqu'on s'intéresse à la tendance et à la variabilité interannuelle. Il est important aussi de noter que les séries temporelles de GMSL sont obtenues soit en moyennant directement les données de hauteur de mer le long des traces des satellites (par exemple, CU et GSFC) ou en calculant d'abord des grilles régulières à partir des données inégalement réparties le long des traces, puis de moyenner les grilles sur l'ensemble du domaine considéré (par exemple, AVISO, NOAA et CCI). Pour plus de détail sur ces données voir les articles *Dieng et al.* 2015a, 2015b ci-joints.

La Fig.2.1a décrit l'évolution au cours du temps des 6 différents produits GMSL (cités plus haut) sur la période allant de janvier 1993 à avril 2016. Nous avons prolongé la série temporelle du GMSL CCI, qui s'arrête en décembre 2014, par celle d'AVISO à partir de janvier 2015. En termes de tendance, nous notons un bon accord entre les produits GMSL sur la période 1993-2016 (voir *table.2.1* ci-dessous). La moyenne des séries de GMSL des 6 groupes présente une tendance de 3.36 ± 0.08 mm/an. L'incertitude représente l'erreur à 2-sigma déduite de la dispersion des données GMSL autour de la moyenne. Nous observons que sur des périodes plus courtes (quelques années à une décennie), les tendances du GMSL montrent d'importantes différences (jusqu'à ~0.6 mm/an sur la période 2005-2013, voir *section 2.3.2*). Cette valeur est nettement supérieure à l'erreur de 0.4 mm/an issue de l'étalonnage externe du GMSL avec des données marégraphiques et de l'évaluation de toutes les sources d'erreurs agissant sur le niveau de la mer altimétrique (*Ablain et al.* 2009, 2015, 2016).

A l'échelle de temps interannuelle, les produits GMSL présentent de fortes anomalies notamment durant les épisodes ENSO (voir Fig.2.1b). Les plus grandes anomalies du GMSL atteignant les 10 mm sont observées sur la dernière décennie, durant les événements La Niña de 2010-2011 et El Niño de 2015-2016. Cela indique-t-il une intensification du phénomène ENSO en réponse au changement climatique ? Nous observons aussi des écarts de plusieurs mm entre les différents produits GMSL. CSIRO s'écarte largement des autres produits, principalement sur les périodes 1993-1999 et 2004-2008; de même que NOAA sur la période 1999-2002. Le produit CU

s'accorde mieux avec GSFC sur toute la période à l'exception de quelques dates. Nous notons aussi que le GMSL CCI présente la plus faible variabilité interannuelle en comparaison des autres produits (par exemple durant La Niña de 2010-2011). Cela provient en partie du fait que les données sont moyennées sur 1 mois. De plus, le produit CCI s'accorde assez bien avec AVISO et NOAA. En comparant les moyennes quadratiques (root mean square -rms- en anglais ; voir *table.2.1*) des produits GMSL sans leur tendance linéaire, sur les périodes 1993-2016 et 2005-2013, nous distinguons 2 groupes : *(1)* AVISO, NOAA et CCI qui montrent de faibles fluctuations interannuelles; et *(2)* CU, GSFC qui présentent de plus fortes anomalies interannuelles. Le GMSL CSIRO montre de fortes anomalies du niveau de la mer, mais il est plus proche du groupe 2 en termes de corrélation.

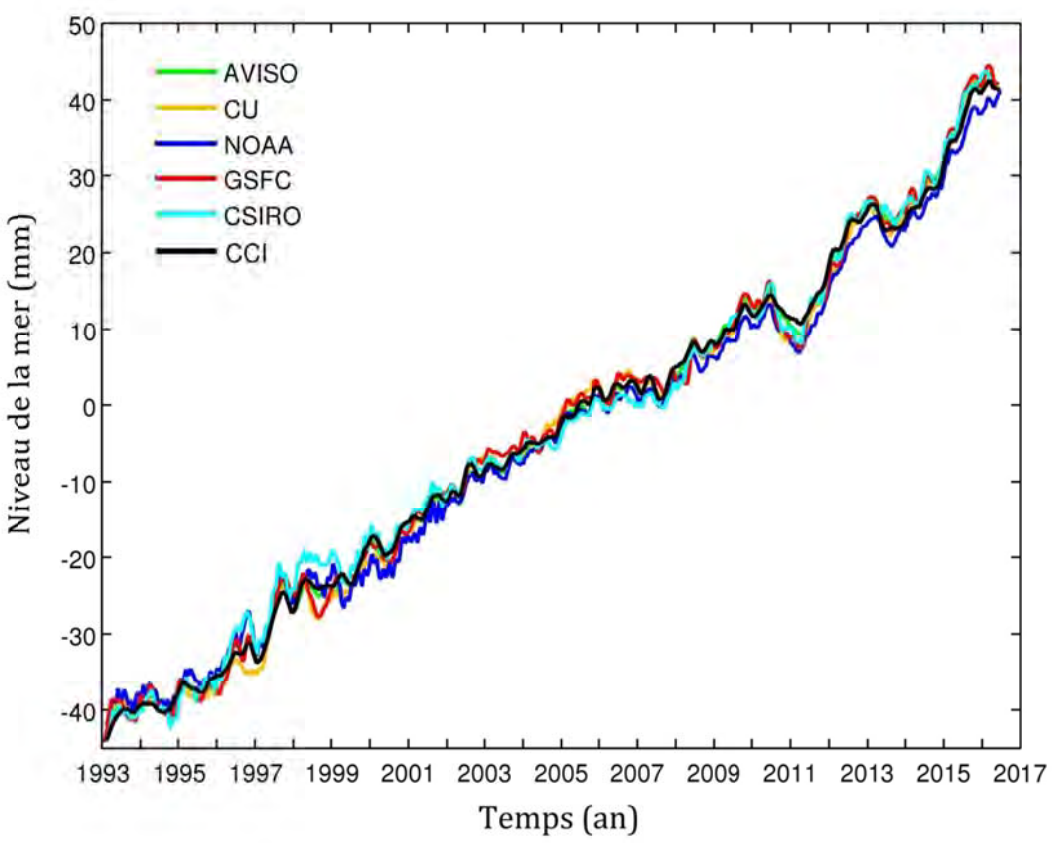

Fig.2.1a : Variations temporelles du niveau moyen global de la mer (GMSL) des 6 groupes de traitement des produits altimétriques : AVISO (courbe verte), CU (courbe jaune), NOAA (courbe bleue), GSFC (courbe rouge), CSIRO (courbe bleue claire) et CCI (courbe noire), sur la période Janvier 1993 - Avril 2016.

Il est important de comprendre les causes des différences entre les produits afin éventuellement d'identifier les données les plus appropriées en fonction de l'application envisagée. Quelques études ont cherché à comprendre les causes des différences entre les produits de GMSL (*Masters et al.* 2012 et *Henry et al.* 2014). Ces études ont identifié les effets respectifs des corrections géophysiques utilisées ainsi que les méthodes de calcul des moyennes

géographiques. Toutefois, ces comparaisons restent incomplètes, et les centres de traitements ne fournissent pas de directives pour les utilisateurs de leurs produits.

Il serait important de mettre en place un exercice de comparaison internationale pour les produits de niveau de la mer comme cela se fait dans la modélisation du climat (par exemple CMIP5). De ce fait, l'étude de bilan du GMSL avec plusieurs estimations de chaque contribution permet de mieux estimer les incertitudes.

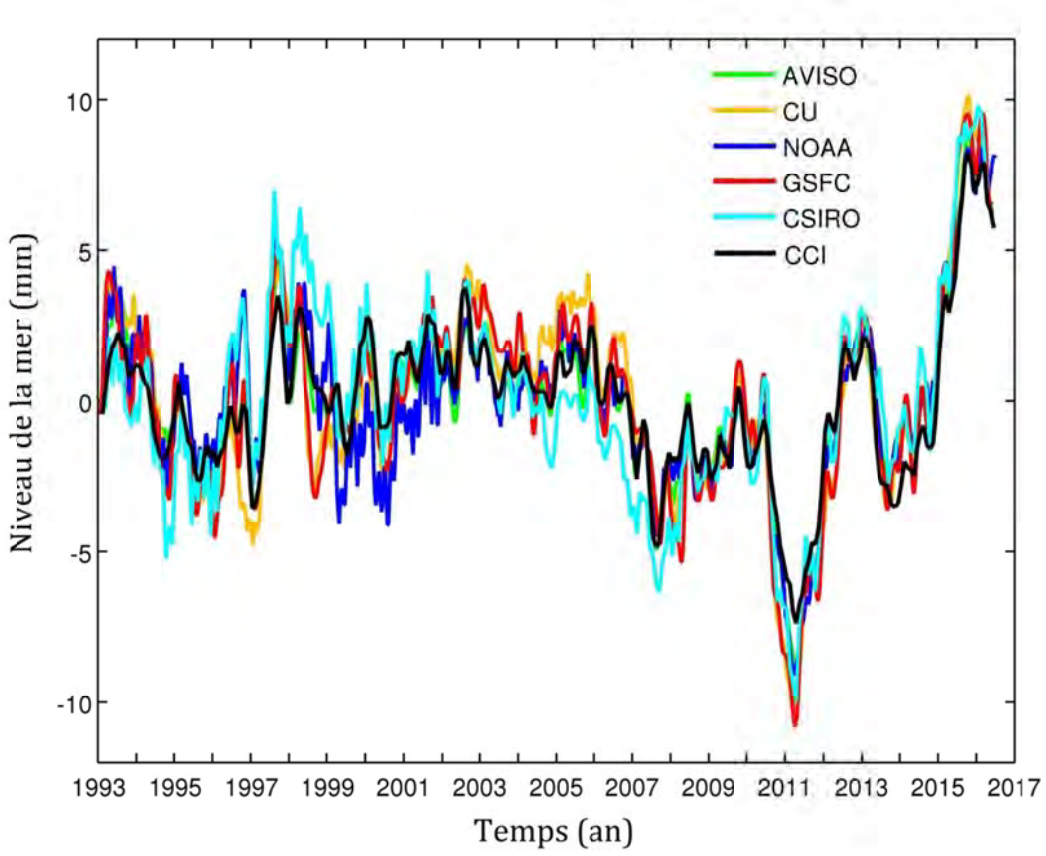

Fig.2.1b : Variabilité interannuelle du GMSL des 6 groupes après retrait des tendances linéaires respectives sur la période Janvier 1993 - Avril 2016 : AVISO (courbe verte), CU (courbe jaune), NOAA (courbe bleue), GSFC (courbe rouge), CSIRO (courbe bleue claire) et CCI (courbe noire).

Table.2.1

Produits GMSL	Janvier 1993 - Avril 2016		Janvier 2005 - Décembre 2013	
	Tendance du GMSL (mm/an)	RMS (mm)	Tendance du GMSL (mm/an)	RMS (mm)
AVISO	3.40	2.53	3.17	2.57
CU	3.39	3.22	2.83	2.96
NOAA	3.23	2.78	3.26	2.52
GSFC	3.40	3.13	2.80	3.01
CSIRO	3.34	3.19	3.35	2.82
CCI	3.39	2.51	3.11	2.16
Moyenne GMSL	3.36 ± 0.08	2.78	3.09 ± 0.17	2.62

2.2 Les contributions climatiques à la hausse du niveau de la mer

2.2.1 Contribution stérique à la hausse du niveau de la mer : données Argo

Avant les années 2000, les navires marchands et de recherche ont fourni à l'aide des XBT (Expandable Bathy Thermographers), des instruments CTD (Conductivity-Temperature-Depth) et des MBT (Mechanical BathyThermograph), des mesures de température et de salinité depuis la surface jusqu'à environ 700 m de profondeur. Ces données ont permis d'estimer la hauteur de mer stérique, décrite par l'équation suivante (*Antonov,* 2002):

$$H(0,z) = \int_0^z \frac{\rho(z) - \rho_{ref}(z)}{\rho_{ref}(z)} dz \qquad (2.4)$$

H (0,z) correspond à l'élévation d'une colonne d'eau de densité $\rho(z)$ (avec $\rho(z)= \rho(T,S,P)$) par rapport à la hauteur qu'aurait une colonne d'eau de densité de référence ρ_{ref} (de température T_{ref} = *0˚C* , de salinité S_{ref} = *35PSU* (Practical Salinity Unit) et de pression P_{ref}). En plus de la température et de la salinité, la densité de l'eau de mer dépend aussi de la pression, donc de la profondeur. La profondeur de référence Z_{ref} (ou P_{ref}) correspond à la profondeur à la quelle l'océan est au repos et où la pression est constante. Dans ce cas Z_{ref} = 700 m. Avec les données Argo utilisées dans la suite, la profondeur de référence est prise à 2000 m.

Les données des navires marchands et de recherche ont une distribution spatiale non homogène et certaines zones géographiques, principalement les hautes latitudes, sont peu couvertes.

Depuis le début des années 2000, le programme international Argo (*Roemmich et al.* 2015) consiste à environ 3900 flotteurs profilants automatiques mesurant la température et la salinité de l'océan de la surface jusqu'à 2000m de profondeur avec une couverture quasi globale et une répétitivité de 10 jours. Comme les produits GMSL, les données Argo sont traitées par différents groupes dans le monde. Nous avons utilisé 4 produits Argo dans cette étude:

1. IFREMER (Institut Français de Recherche pour l'Exploitation de la Mer), données traitées par Karina von Schuckmann (produit appelé par la suite KvS), France
2. IPRC (International Pacific Research Center), USA
3. JAMSTEC (Japan Agency for Marine-Earth Science and Technology), Japon
4. SCRIPPS (Scripps Institution of Oceanography), USA.

IPRC, JAMSTEC et SCRIPPS produisent des profils de température et de salinité sur des grilles temporelles. Nous avons calculé le niveau de la mer stérique en utilisant l'équation 4 ci-dessus, en intégrant les données de température et salinité de la surface jusqu'à 2000m de profondeur. Les séries temporelles du niveau de la mer moyen global stérique IPRC, JAMSTEC et SCRIPPS sont estimées en moyennant géographiquement les données respectivement dans les domaines 62.5°S–

64.5°N, 60.5°S–70.5°N et 61.5°S–64.5°N. Les grilles stériques KvS (0-2000m) sont calculées par von *Schuckmann and Le Traon* (2011) et moyennées entre 60°S et 60°N. Comme pour les produits GMSL, les cycles annuel et semi-annuel sont supprimés. Pour plus de détail sur ces données voir les articles *Dieng et al.* 2015a, 2015b ci-joints.

Comme pour le GMSL, chaque groupe utilise des méthodes de traitement spécifique, en particulier pour le remplissage des 'trous' dans la couverture des données, le contrôle de la qualité, le choix de la climatologie mais aussi les techniques de maillage (*Abraham et al.* 2014). L'inter-comparaison des produits Argo des différents groupes, mais aussi l'étude de bilan du niveau de la mer, nous permet d'évaluer les écarts existants entre les produits Argo.

La Fig.2.2a décrit l'évolution au cours du temps des 4 différents produits du niveau de la mer stérique basées sur Argo (cités plus haut) sur la période janvier 2005 - décembre 2014. Ces produits présentent des différences en tendance pouvant atteindre 2 mm/an sur les périodes 2005-2014 et 2005-2013 (voir *table.2.2*). Ces différences sont du même ordre de grandeur que la contribution stérique de la couche océanique 700-1500m à la hausse du GMSL sur la période 2005-2012 (voir *Dieng et al.* 2015a, résumé à la *section 2.3.1*). Même si les différences de tendance sont faibles en comparaison à celles du GMSL, elles ne sont pas négligeables.

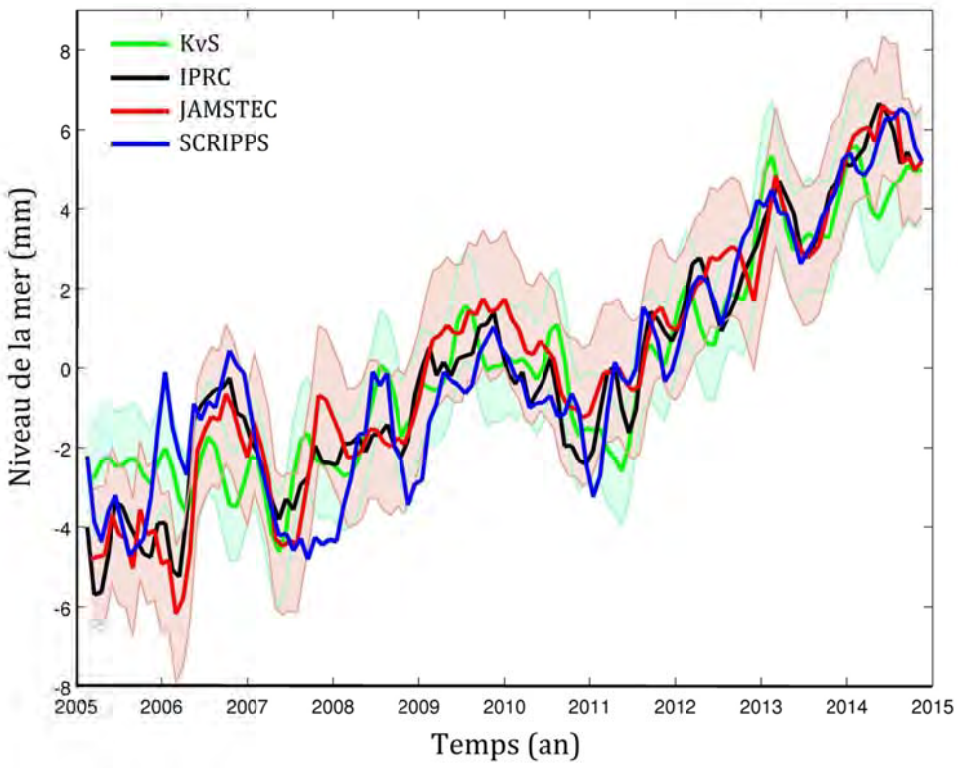

Fig.2.2a : Variations temporelles du niveau moyen global de la mer stérique des 4 produits Argo : KvS (courbe verte), IPRC (courbe noire), JAMSTEC (courbe rouge) et SCRIPPS (courbe bleue), sur la période Janvier 2005 - Décembre 2014. Les erreurs des données KvS et JAMSTEC sont représentées.

La Fig.2.2b montre une importante variabilité interannuelle du niveau de la mer stérique sur la période 2005-2014, principalement durant La Niña de 2010-2011 avec une anomalie négative de ~4mm. Des écarts de plusieurs mm sont observés entre les différents produits Argo. SCRIPPS montre la plus grande variabilité interannuelle (en termes de rms, voir *table.2.2*) et s'écarte légèrement des autres produits en 2006 et durant La Niña de 2007-2008. Nous rappelons que l'anomalie négative du GMSL pendant La Niña de 2007-2008 (voir Fig.2.1b), non observée par les produits de masse de l'océan basés sur GRACE (Gravity Recovery And Climate Experiment) (voir Fig.2.3b), est expliquée, au moins pour une partie, par les données Argo du SCRIPPS. Nous reviendrons plus en détail sur cette question dans le chapitre 4 (sur l'influence d'ENSO sur la variabilité interannuelle du GMSL).

Cependant, même si le programme Argo est un élément essentiel du système d'observation de l'océan global pour comprendre et prévoir le rôle de l'océan sur le climat, il reste incomplet du fait du manque de mesures de température et de salinité en dessous de 2000m de profondeur. Les données sont nécessaires pour estimer le contenu thermique de l'océan profond et comprendre sa contribution dans l'accumulation de la chaleur durant la période de "pause" (discutée plus en détail dans la *section 2.3.1*).

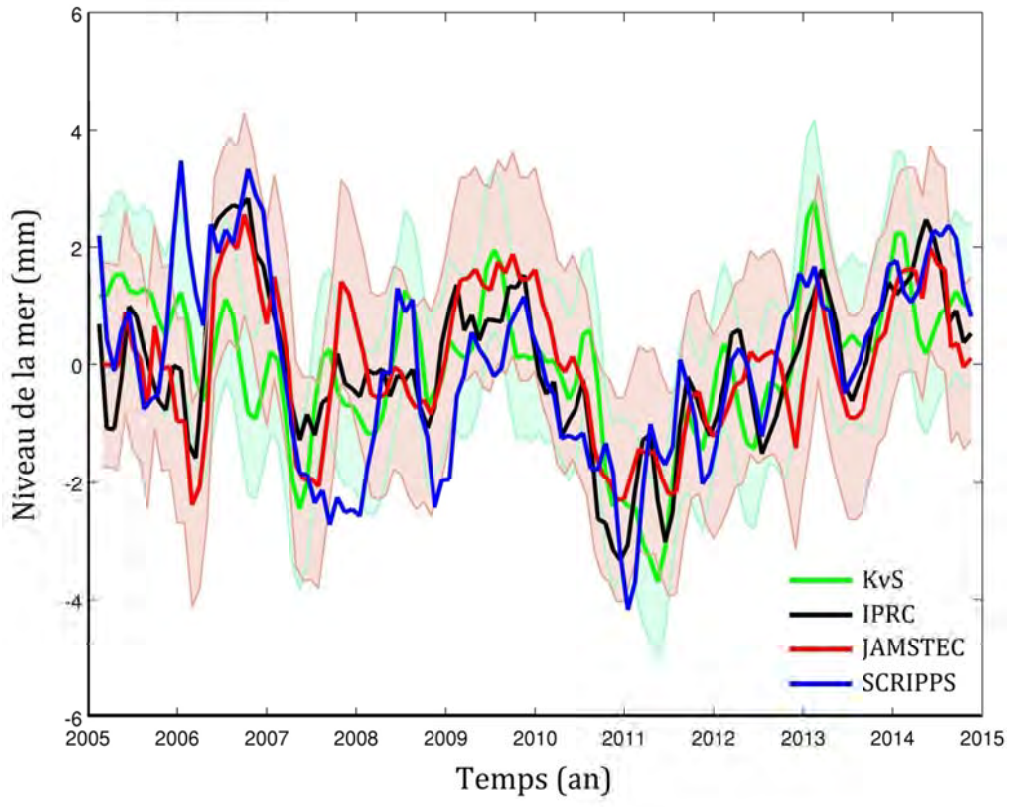

Fig.2.2b: Variations temporelles du niveau moyen global de la mer stérique des 4 produits Argo après retrait des tendances linéaires respectives sur la période Janvier 2005 - Décembre 2014: KvS (courbe verte), IPRC (courbe noire), JAMSTEC (courbe rouge) et SCRIPPS (courbe bleue). Les erreurs des données KvS et JAMSTEC sont représentées.

En plus d'Argo, nous utilisons dans cette étude, d'autres sources de données de température et de salinité : EN4 du Hadley Center (UK), Ishii&Kimoto (Japon), Levitus/NOAA (USA) et la réanalyse océanique ORAS4 de M. Balmaseda (ECMWF). Ces données intègrent, en plus des profils d'Argo, les données XBT, MBT et CTD (principalement avant 2003). Pour plus de détails sur ces données voir *Dieng et al.* (2015a) et *section 2.3.1*.

Table.2.2

Produits stériques du niveau de la mer Argo (0-2000m)	Janvier 2005 - Décembre 2014		Janvier 2005 - Décembre 2013	
	Tendance (mm/an)	RMS (mm)	Tendance (mm/an)	RMS (mm)
KvS	0.82	1.25	0.74 ± 0.13	1.22
IPRC	0.96	1.31	0.76	1.24
JAMSTEC	1.02	1.21	0.94 ± 0.16	1.17
SCRIPPS	0.90	1.58	0.83	1.52
Moyenne stérique	0.92 ± 0.1	1.14	0.82 ± 0.11	1.07

2.2.2 Contribution de masse de l'océan à la hausse du niveau de la mer : en utilisant les satellites de gravimétrie spatiale GRACE

La mission de gravimétrie spatiale GRACE lancée en 2002, a permis pour la première fois de déterminer les redistributions de masse à la surface de la terre (et à l'intérieur) avec un échantillonnage spatial et temporel sans précédent. GRACE fournit de manière très précise les variations temporelles du champ de gravité terrestre jusqu'au degré harmonique sphérique 60 ce qui correspond à une résolution spatiale ~300-400 km (*Tapley et al*. 2004). Avec GRACE a débuté une nouvelle ère dans l'étude des redistributions de masse dans le système Terre, permettant de mesurer par exemple le bilan de masse des calottes polaires et des glaciers de montagne, les variations des stocks d'eau dans les bassins hydrographiques et la masse de l'océan, facteurs qui contribuent à la hausse du GMSL des dernières décennies (*Cazenave and Chen,* 2010 ; *Church et al.* 2013).

Dans cette étude, nous avons utilisé les données de la Release-5 (RL05) de GRACE des 3 centres:
1. CSR (Center for Space Research) de l'Université du Texas, USA
2. GFZ (Deutsches GeoForschungsZentrum), Allemagne
3. JPL (Jet Propulsion Laboratory), USA

Comme indiqué sur le site web de GRACE TELLUS (http://grace.jpl.nasa.gov), les données grillées de GRACE sur l'océan ne peuvent pas être utilisées pour calculer les séries temporelles de masse de l'océan global due à une forte atténuation du signal causée par des traitements destinés à diminuer les erreurs des données (*Swenson and Wahr,* 2006 ; *Chambers and Schröter,* 2011 ;

Chambers and Bonin, 2012). En effet, les produits GRACE sur l'océan souffrent de plusieurs problèmes. Par exemple, l'effet de "leakage" (fuite de signaux près des côtes en raison de la résolution grossière de GRACE) et les "stripes" (erreurs distribuées selon la direction nord-sud causées par des erreurs systématiques dans les données de GRACE). Pour plus de détails sur les erreurs qui affectent les données GRACE, voir *Velicogna and Wahr* (2013).

Pour les applications à l'étude du niveau de la mer, des séries temporelles de masse de l'océan global (moyenne sur le domaine 90°S-90°N) avec les incertitudes associées ont été calculées par *D. Chambers* et ses collaborateurs afin d'atténuer les problèmes évoqués ci-dessus (voir *Johnson and Chambers*, 2013 et *Chambers and Bonin*, 2012). Pour la correction du "leakage", ils ont estimé et corrigé le signal de « fuite » sur l'océan le long des côtes et au large, en utilisant des estimations du signal continental (dû à l'hydrologie ou au bilan de masse des calottes polaires). Pour ce qui est des strippes, un filtre gaussien de 500 km a été appliqué. Cela a amélioré la qualité des données de la RL05 de GRACE sur l'océan par rapport aux versions précédentes (*Chambers and Bonin*, 2012). Ce sont ces données que nous avons utilisées. La contribution du GIA (phénomène contribuant aux variations du champ de gravité) a été calculée par *D. Chambers* (voir *Chambers and Bonin*, 2012) et retirée des séries temporelles de masse de l'océan.

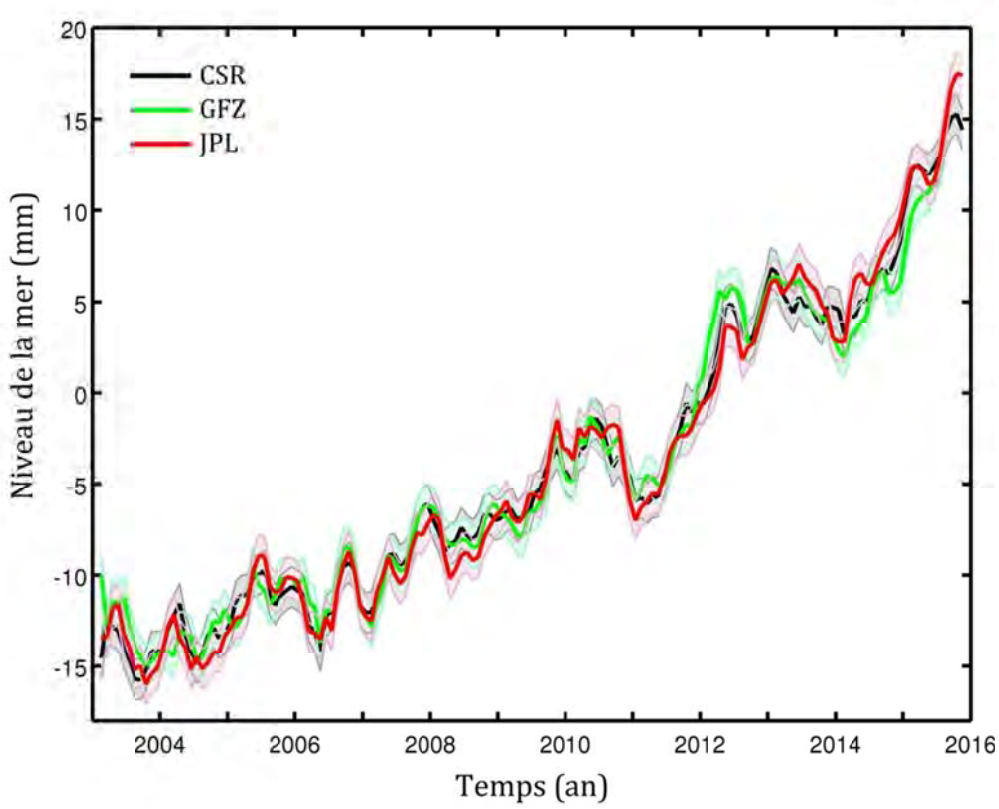

Fig.2.3a: Evolution temporelle de la masse de l'océan de GRACE basée sur des données du CSR (courbe noire), GFZ (courbe verte) et JPL (courbe rouge) sur la période janvier 2003 - décembre 2015. Les erreurs associées sont représentées.

La Fig.2.3a décrit l'évolution au cours du temps des 3 produits de masse de l'océan (cités plus haut) sur la période janvier 2003 - décembre 2015. Nous notons un bon accord entre les produits de masse de l'océan sur la période 2003-2015, en termes de tendance et de variabilité interannuelle (voir Fig.2.3a et Fig.2.3b et *table.2.3* ci-dessous pour les valeurs de tendance et de rms). La Fig.2.3b montre une importante variabilité interannuelle de la masse de l'océan sur la période 2003-2015. Ces fluctuations sont plus marquées (~7 mm) durant les événements La Niña de 2010-2011 et El Niño de 2015-2016. Cela indique-t-il un rôle particulier du cycle de l'eau sur les variations interannuelles du GMSL durant les épisodes ENSO? Cette question sera discutée dans le *chapitre 3*.

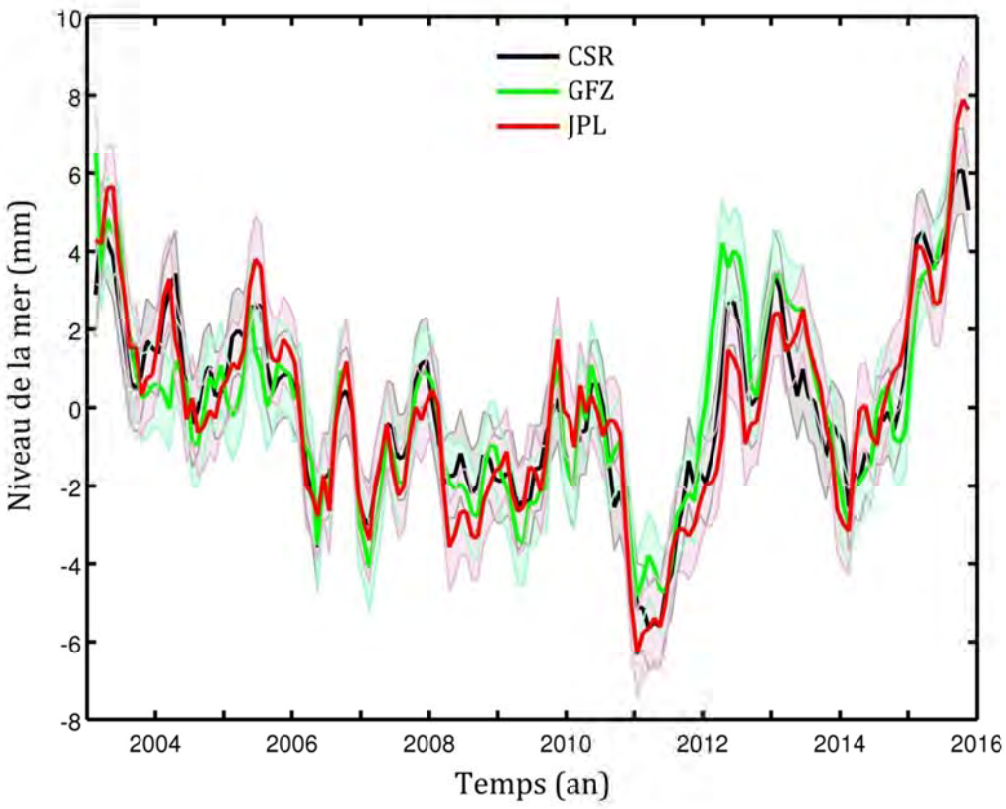

Fig.2.3b : Evolution temporelle de la masse de l'océan de GRACE basée sur des données du CSR (courbe noire), GFZ (courbe verte) et JPL (courbe rouge), après retrait de leurs tendances linéaires respectives sur la période janvier 2003 - décembre 2015. Les erreurs associées sont représentées.

Table.2.3

Produits de masse de l'océan basée sur GRACE RL05	Janvier 2003 - Décembre 2015		Janvier 2005 - Décembre 2013	
	Tendance (mm/an)	RMS (mm)	Tendance (mm/an)	RMS (mm)
CSR	2.10 ± 0.08	2.34	2.01 ± 0.1	1.93
GFZ	2.03 ± 0.08	2.58	2.11 ± 0.1	2.11
JPL	2.16 ± 0.08	2.61	2.00 ± 0.1	2.10
Moyenne Masse	2.10 ± 0.09	2.43	2.04 ± 0.1	1.98

2.3 Bilan du niveau moyen global de la mer (GMSL) : sur la période Argo/GRACE

Dans cette section nous étudions le bilan du GMSL sur la période allant de janvier 2003 à décembre 2013. Nous avons choisi cette période d'étude pour 2 raisons :

- La première est que nous disposons sur cette période, de plusieurs systèmes d'observation de grande précision, indépendants et opérant simultanément : satellites altimétriques, satellites de gravimétrie spatiale GRACE et flotteurs automatiques Argo.
- La deuxième raison est que cette période coïncide avec la période de "pause" où la température moyenne globale de l'air en surface présente une faible augmentation, alors que nous observons un déséquilibre énergétique persistant au sommet de l'atmosphère (*Church et al.* 2011; *Hansen et al. 2011; Trenberth et al. 2014*).

2.3.1 Estimation des contributions manquantes à la hausse du niveau de la mer : contenu thermique de l'océan profond sur la période 2003-2012

L'enjeu lié à la question scientifique majeure, qui est d'estimer la contribution du réchauffement de l'océan profond à la hausse du GMSL sur la dernière décennie, coïncide avec la période dite de "pause", pendant laquelle la température moyenne de l'air en surface augmente peu alors que la Terre continue d'emmagasiner de la chaleur à cause des émissions de gaz à effet de serre (*Peters et al.* 2012; *Trenberth and Fasullo,* 2013 ; *Smith,* 2013) et que des mesures du bilan radiatif net au sommet de l'atmosphère indiquent que la Terre est toujours en état de déséquilibre énergétique de l'ordre de +0.5 à +1 $W.m^{-2}$ (*Church et al.* 2011 ; *Hansen et al.* 2011 ; *Trenberth et al.* 2014). Cette question a fait l'objet d'une attention considérable durant ces dernières années. Des explications différentes ont été proposées, allant d'une réduction du forçage radiatif due à la diminution de l'activité solaire; les aérosols et les nombreuses éruptions volcaniques; les changements de teneur en vapeur d'eau de la stratosphère; l'excédant d'énergie du système utilisé pour fondre les glaciers en particulier les calottes polaires; l'augmentation de l'absorption de chaleur dans l'océan profond, que ce soit dans le Pacifique ou l'Atlantique Nord (voir, *Trenberth and Fasullo,* 2010, 2013 ; *Hansen et al.* 2011 ; *Solomon et al.* 2010 ; *Guemas et al.* 2013 ; *Kosaka and Xie,* 2013 ; *Balmaseda et al.* 2013a ; *Watanabe et al.* 2013 ; *England et al.* 2014 ; *Chen and Tung,* 2014). Bien que l'absorption de la chaleur par l'océan profond soit actuellement l'explication privilégiée du hiatus, le manque de données de température dans l'océan en profondeur n'a permis jusqu'ici de confirmer ou infirmer cette hypothèse. De même, aucun consensus n'existe encore sur le mécanisme par lequel et la région où le réchauffement de l'océan profond peut se produire (voir, *Goddard,* 2014 ; *Trenberth et al.* 2014 ; *Chen and Tung,* 2014).

Pour tenter d'apporter une réponse à cette question, nous avons considéré le bilan du GMSL sur cette période de "pause". La méthode a consisté à comparer le niveau de la mer observé avec la somme des différentes contributions climatiques (niveau de la mer stérique et variations de masse de l'océan). La composante résiduelle issue de la différence entre le GMSL et la somme des composantes connues du niveau de la mer est considérée comme étant principalement due à la composante stérique de l'océan profond (voir équation *2.2*).

Dans cette section, nous n'utilisons pas les données sur les glaces continentales (glaciers et calottes polaires) et le stock d'eau des continents dans le bilan du GMSL. Ces données seront utilisées plus tard dans la *section 2.3.3*.

Résumé de l'article : "**The Sea Level Budget Since 2003 : Inference on the Deep Ocean Heat Content**" *(l'article original est inséré à la fin de cette section 2.3.1)*

Dans cette étude, 16 bases de données différentes ont été analysées sur 2 périodes (2003-2012 et 2005-2012 correspondant à une couverture quasi mondiale des données Argo) pour estimer les contributions manquantes au bilan du niveau de la mer, et tout particulièrement celle due au réchauffement de l'océan profond. Nous avons analysé les séries du GMSL des 6 centres (mentionnés plus haut dans la section 3.1) parallèlement aux 3 produits de masse de l'océan d'après GRACE (voir *section 3.2.2*) et des hauteurs de mer stériques (8 produits de température et salinité considérés : 4 produits Argo sur 2005-2012 (voir *section 2.2.1*), plus les données EN4 du Hadley Center (UK), de Ishii&Kimoto (Japon), de Levitus/NOAA (USA) et la réanalyse océanique ORAS4 de Magdalena Balmaseda (ECMWF)).

En analysant les séries temporelles des différents termes de l'équation bilan *(1)* sur les périodes 2003-2012 et 2005-2012, nous avons montré que les produits GMSL et stérique du niveau de la mer (intégrées entre 0 et 1500m) présentent des différences. Pour les séries temporelles du GMSL, nous pouvons identifier 2 groupes : AVISO et NOAA sont très proches en termes de tendance et de variabilité interannuelle (*groupe 1*) ; et CU et GSFC (*groupe 2*). Le GMSL du CSIRO est plus compatible avec le groupe 1. Les différences de tendance peuvent aller jusqu'à 0.35 mm/an sur la période 2003-2012, entre les GMSL des 2 groupes. Le GMSL du CCI (disponible jusqu'en Décembre 2010 lors de la publication de cet article) avec une tendance de 2.75 mm/an sur la période 2003-2010, s'accorde mieux avec la moyenne des 5 produits altimétriques (AVISO, CU, NOAA, GSFC et CSIRO). La moyenne des 5 GMSL indique une hausse de 2.71 mm/an sur la période 2003-2010. Comme noté par *Masters et al.* (2012) et *Henry et al.* (2014) l'essentiel de ces différences résultent du processus de calcul de la moyenne globale adoptée par les différents groupes. Plusieurs études (voir, *Abraham et al.* 2013; *Lyman and*

Johnson, 2014 ; *von Schuckmann and Le Traon*, 2011) ont montré que les différences entre produits stériques proviennent de plusieurs facteurs : le contrôle de la qualité, le remplissage des lacunes dans la couverture des données, le choix de la climatologie mais aussi les techniques de maillage. Cependant, jusqu'à présent aucune méthode de traitement préférentielle n'est proposée. En ce qui concerne les produits GRACE, le bon accord entre les séries temporelles de masse de l'océan ne signifie rien sur leur précision absolue, vu qu'elles sont toutes traitées par la même méthode décrite dans *Johnson and Chambers* (2013).

En comparant la composante stérique du niveau de la mer des couches 0-700m et 0-1500m de profondeur, nous avons montré une augmentation régulière du réchauffement de la couche océanique 700-1500m depuis 2005, et ceci pour tous les produits Argo analysés. Le réchauffement de la couche 700-1500m sur la période 2005-2012 entraîne une élévation moyenne de 0.2 mm/an de la composante stérique en équivalent niveau de la mer (soit +0.15 $W.m^{-2}$ en énergie par unité de surface de l'océan ; voir *Levitus et al.* (2012) pour la conversion mm/an en $W.m^{-2}$). Ce résultat est très fiable et peut répondre à la question scientifique majeure qui est de savoir: où va l'énergie qui continue à s'accumuler dans le système climatique, alors même qu'elle ne sert plus à réchauffer l'atmosphère? Il est possible que la chaleur 'anthropique' non utilisée pour réchauffer l'atmosphère en surface soit stockée dans ces couches profondes de l'océan. Nos résultats vont dans ce sens.

En analysant le résidu du GMSL « *GMSL observé moins masse de l'océan moins contribution stérique de l'océan entre 0-1500m* », on obtient une estimation de la composante stérique de l'océan profond (en dessous de 1500m), donc du contenu thermique de l'océan profond. Ce signal résiduel de 0.3 ± 0.6 mm/an et 0.5 ± 0.6 mm/an (respectivement sur les périodes 2005-2012 et 2003-2012) avec une forte variabilité interannuelle, contient aussi les erreurs des données. Les valeurs de la tendance de la composante stérique de fond (en dessous de 1500m) selon les 120 combinaisons possibles entre les différents produits utilisés sont comprises dans l'intervalle de confiance [-0.3 0.9] mm/an sur la période 2005-2012. En utilisant les données de la réanalyse océanique ORAS4 (disponible jusqu'en décembre 2009 lors de la publication de l'article), nous avons trouvé une très faible contribution stérique de la couche océanique 1500-6000m, avec une tendance de 0.1 mm/an sur la période janvier 2003 - décembre 2009. En faisant les mises à jour du produit ORAS4 jusqu'en décembre 2012 (voir Fig.2.4 : mise à jour de la Fig.9 de cet article joint), la contribution stérique de cette couche profonde de l'océan avec une tendance de 0.2 mm/an sur la période 2003-2012, présente une légère hausse en comparaison de la période 2003-2009.

En comparant le réchauffement en dessous de 1500m à partir des données ORAS4, nous montrons qu'il est peu probable que le signal résiduel estimé dans cette étude soit attribué au réchauffement de l'océan profond (au-dessous de 1500 m), même si la valeur de la tendance est contenue dans la barre d'incertitude des données. Il est possible que cela reflète peut-être, au moins en partie, la signature d'un signal manquant dans la composante stérique dans les régions non couvertes par le système Argo (par exemple la région Indonésienne, la mer de Chine méridionale, le Golfe du Mexique, ...). Comme les tendances régionales du niveau de la mer sont principalement d'origine stérique (voir *Stammer et al.* 2013), nous avons calculé à partir des grilles altimétriques AVISO la tendance du niveau de la mer de la région indonésienne. Cette région contribue à 0.3 mm/an à la hausse du GMSL sur la période 2003-2012. En utilisant aussi les données ORAS4, la contribution stérique de cette région à la hausse du GMSL est estimée à 0.29 mm/an sur la période 2003-2009 (après mise à jour des données ORAS4, elle est estimée à 0.25 mm/an sur la période 2003-2012). Étant donné que cette région est prise en compte dans les produits GMSL (ainsi que dans les produits de masse de l'océan), mais pas sur les données stériques, nous concluons que la tendance stérique (0-1500m) a été sous-estimée en raison de ces données manquantes. En tenant compte de la région Indonésienne, le signal résiduel moyen (contribution stérique de l'océan en dessous de 1500 m) présente une tendance de ~0.05 ± 0.6 mm/an et ~0.25 ± 0.6 mm/an, respectivement sur les périodes 2005-2012 et 2003-2012. Ces nouvelles tendances sont du même ordre de grandeur que celle de la contribution stérique de l'océan en dessous de 1500m estimée par ORAS4 sur la période 2003-2012 (de 0.2 mm/an).

Dans cette étude, nous mettons en évidence qu'estimer le réchauffement de l'océan en dessous de 1500m à partir de l'étude de bilan du niveau de la mer s'avère difficile pour l'instant vu la dispersion des valeurs de tendance de chaque composante du niveau de la mer.

En conclusion, le résultat le plus fiable de cette étude est la preuve d'un réchauffement continu de la couche océanique 700-1500m au cours des années 2000. Il permet de répondre à la question : où va l'énergie qui continue à s'accumuler dans le système climatique, alors même qu'elle ne sert plus à réchauffer l'atmosphère? Bien que suggéré précédemment par *Levitus et al.* (2012), *von Schuckmann et al.* (2014) et *Balmaseda et al.* (2013a) en utilisant respectivement les ensembles de données stériques NOAA, KvS et la réanalyse ORAS4, ici nous observons un comportement similaire pour chacun des 8 ensembles de données stériques considérées sur les périodes 2003-2012 et 2005-2012. Ceci indique que le résultat est robuste. Cependant, l'incertitude de ±0.6 mm/an du signal résiduel du bilan du niveau de la mer nous empêche encore d'obtenir des résultats définitifs concernant le réchauffement de l'océan en dessous de 1500m. De

plus les lacunes dans la couverture régionale des données stériques, par exemple la région indonésienne, compliquent d'avantage l'approche budgétaire du niveau des mers.

Il est donc important d'identifier les sources d'erreurs des produits de chaque composante du bilan du niveau de la mer, mais aussi d'améliorer le traitement des données de chaque système d'observation. L'identification des sources d'erreurs est traitée dans une autre publication discutée dans la *section 2.3.2* suivante.

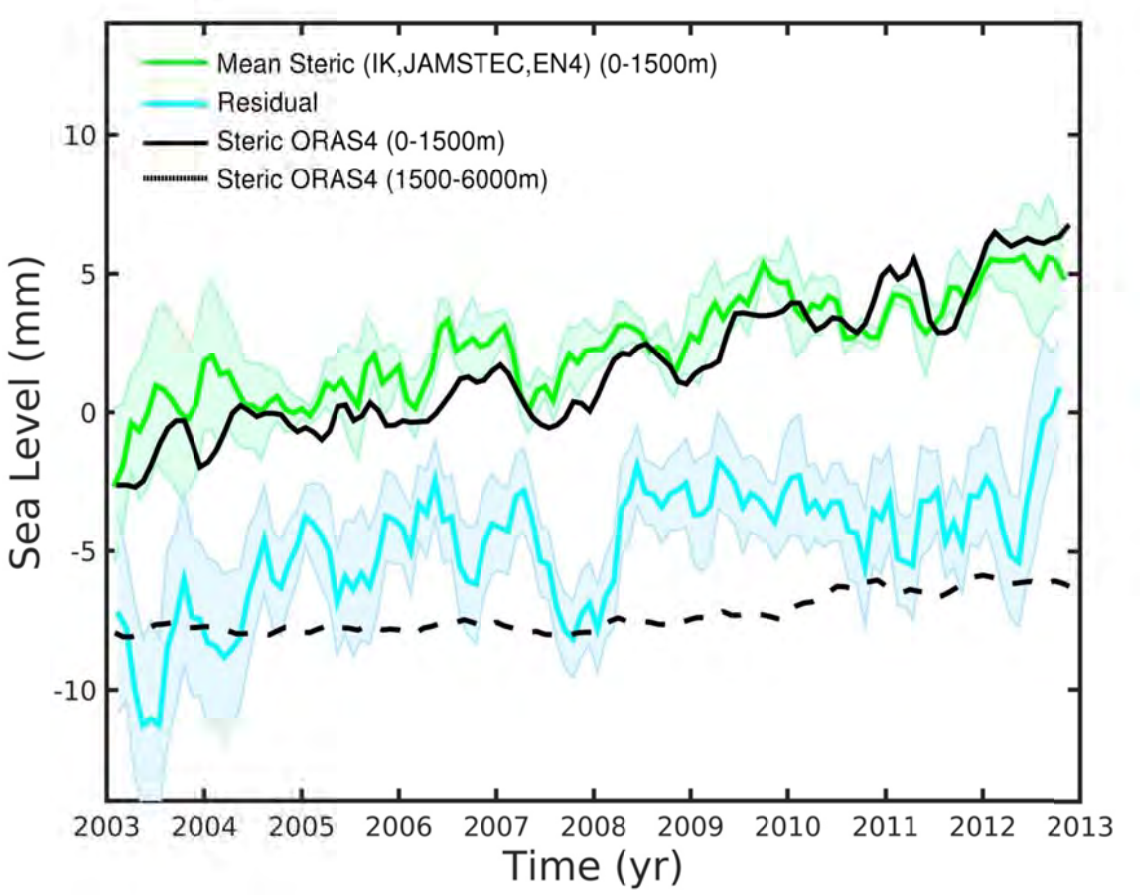

Fig.2.4 : mises à jour de la Fig.9 de l'article *Dieng et al.* 2015a inséré ci-après

The Sea Level Budget Since 2003: Inference on the Deep Ocean Heat Content

Habib B. Dieng, Hindumathi Palanisamy, Anny Cazenave, Benoit Meyssignac & Karina von Schuckmann

Surveys in Geophysics
An International Review Journal
Covering the Entire Field of Geosciences and Related Areas

ISSN 0169-3298

Surv Geophys
DOI 10.1007/s10712-015-9314-6

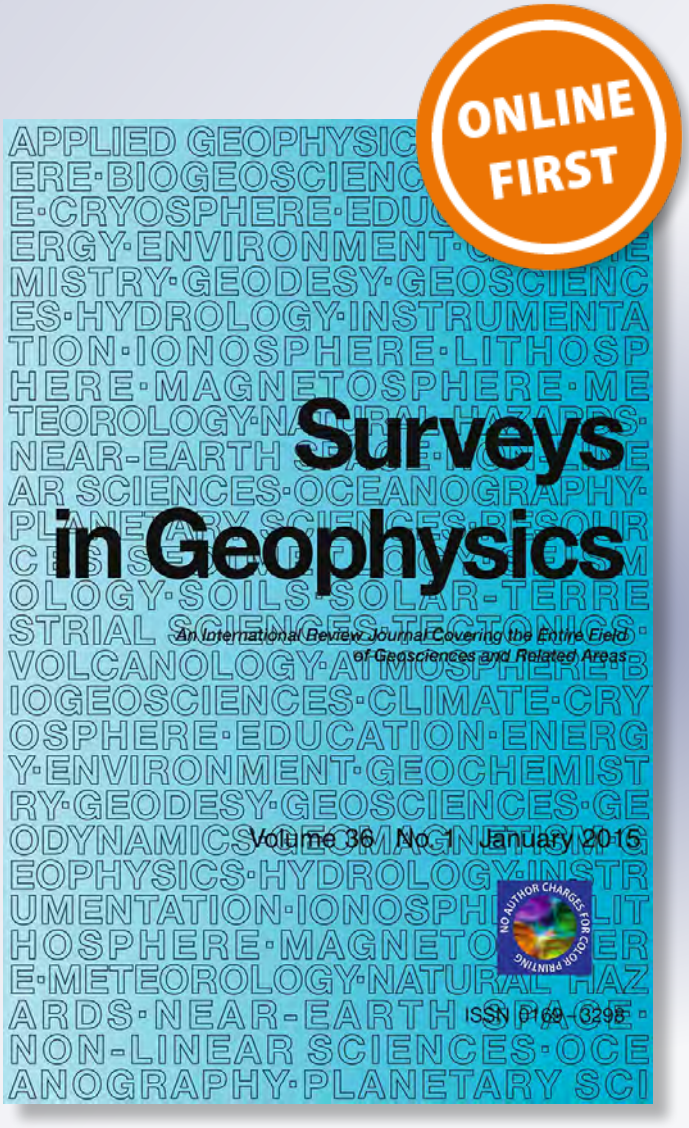

Springer

Surv Geophys
DOI 10.1007/s10712-015-9314-6

The Sea Level Budget Since 2003: Inference on the Deep Ocean Heat Content

Habib B. Dieng · Hindumathi Palanisamy · Anny Cazenave · Benoit Meyssignac · Karina von Schuckmann

Received: 26 September 2014 / Accepted: 2 January 2015

Abstract This study provides an overview of the various components of the global mean sea level evolution over two time spans: (1) 2005–2012 (corresponding to the full deployment of the Argo program) and (2) 2003–2012. Using a sea level budget approach, we compare altimetry-based global mean sea level, global ocean mass from GRACE space gravimetry and steric sea level from Argo and other in situ measurements. One goal of this study is to investigate whether it is possible to constrain the deep ocean contribution to the global mean sea level rise over the last decade. This question is particularly relevant, considering the current debate about the 'hiatus,' i.e., the observed recent pause of the global mean air and sea surface temperature evolution while the planet is still in thermal imbalance. We consider a total of 16 different data sets. Differences are noticed between data sets related to each variable (sea level, ocean mass and steric sea level), mostly due to data processing issues. Therefore, we perform the analysis using averages of the available data sets. For each period, we find that, when removing from the global mean sea level, the contributions of the global mean ocean mass and steric sea level (estimated for the 0–1,500 m ocean layer), there remains a residual signal displaying a positive slope of 0.3 ± 0.6 and 0.55 ± 0.6 mm/year over 2005–2012 and 2003–2012, respectively. Comparing with an ocean reanalysis and according to direct (but sparse) ocean temperature measurements below 1,500 m, it seems unlikely that the observed residual signal can be attributed to deep (below 1,500 m) ocean warming, in agreement with other recently published results. We estimate that it possibly reflects, at least partly, the signature of a missing upper ocean steric signal in regions uncovered by current observing systems. Our study also shows a steady warming increase since 2003 of the 700–1,500 m ocean layer (amounting ~ 0.2 mm/year in steric sea level equivalent), confirming previous findings, but seen in our study in each of the eight different steric data sets considered.

H. B. Dieng · H. Palanisamy · A. Cazenave (✉) · B. Meyssignac
LEGOS-CNES, 18 Avenue E. Belin, 31401 Toulouse Cedex 9, France
e-mail: anny.cazenave@legos.obs-mip.fr

K. von Schuckmann
Mediterranean Institute for Oceanography, University of Toulon, Toulon, France

Published online: 28 January 2015

Keywords Sea level rise · Thermal expansion · Ocean mass · Deep ocean warming

1 Introduction

Sea level is an interesting quantity in Earth sciences research as it integrates variations from different climatic and non-climatic variables. For example, in terms of global mean, current sea level rise mostly results from thermal expansion of seawater due to ocean temperature changes and water mass addition into ocean basins due to glacier melting, ice sheet mass loss and land water storage changes of anthropogenic origin (e.g., Leuliette and Willis 2011; Chen et al. 2013; Church et al. 2013). At interannual timescales, in particular during ENSO (El Nino–Southern Oscillation) events, global mean sea level fluctuations are largely due to land–ocean asymmetry in precipitation, causing temporary ocean mass excess (during El Nino) or deficit (during La Nina) (Boening et al. 2012; Cazenave et al. 2012, 2014; Fasullo et al. 2013). While regional variations in absolute sea level mostly result from ocean temperature and salinity variations (and to a lesser extent from direct atmospheric forcing on the sea surface) (Stammer et al. 2013), non-climatic factors also play a role. In effect, the viscous/elastic response of the solid Earth to past (i.e., last deglaciation) and ongoing land ice melt causes complex deformations of ocean basins and changes in the mutual attraction of ice-water bodies, and hence of sea level (e.g., Stammer et al. 2013). Finally, along coastlines, relative sea level changes occur because of a combination of absolute sea level changes and vertical movements of the Earth's crust (Woppelmann et al. 2009).

In the 5th Assessment Report (AR5) of the Intergovernmental Panel on Climate Change (IPCC), it was reported that over the 1993–2010 time span (corresponding to the high-precision satellite altimetry era), the rate of global mean sea level (GMSL) rise is due to the combined effects of land ice melt (50 %), ocean thermal expansion (37 %) and anthropogenic land water storage decrease (13 %) (Church et al. 2013). The sum of these contributions amounts to 2.8 ± 0.5 mm/year, a value only slightly lower than the rate of sea level rise observed by altimeter satellites, of 3.2 ± 0.4 mm/year. Although of the same order of magnitude as associated uncertainties, the difference may also reflect other contributions either not or incompletely accounted for, e.g., the deep ocean (below 700–1,000 m depth where the coverage of available data is poor or non-existent).

In the IPCC 4th Assessment Report (AR4), the sea level budget was estimated over the 1993–2003 time span (Bindoff et al. 2007). Over that decade, the thermal expansion contribution was $\sim$50 % the rate of sea level rise, i.e., significantly larger than the 1993–2010 average (note, however, that in AR4, thermal expansion estimates were contaminated by Expandable Bathy Thermographers—XBT biases). In fact, the sea level components are not constant through time. During the last 10–15 years, the land ice (mostly the ice sheets) component has accelerated (i.e., Shepherd et al. 2012; see also IPCC AR5 and references herein) while the upper ocean thermal expansion has increased less rapidly than during the 1993–2003 decade (Lyman et al. 2010). This recent slower rate in thermal expansion of the upper ocean coincides with the pause (also called the 'hiatus,' e.g., Held 2013) in global mean air and sea surface temperature evolution observed since the early 2000s (e.g., Trenberth and Fasullo 2013; Smith 2013). The current global warming hiatus is puzzling because greenhouse gases have

continued to accumulate at an increased rate (Peters et al. 2012) and the Earth's energy imbalance at the top of the atmosphere is estimated to still be positive, on the order of 0.5–1 Wm^{-2} (e.g., Hansen et al. 2011; Trenberth et al. 2014). This issue has been the object of considerable attention in the very recent years, and different explanations have been proposed, ranging from reduced radiative forcing due to prolonged solar minimum, increased aerosols and numerous volcanic eruptions, changes in stratospheric water vapor, enhanced heat uptake in the deep ocean, either in the Pacific or Atlantic regions (e.g., Trenberth and Fasullo 2010, 2013; Hansen et al. 2011; Solomon et al. 2010; Guemas et al. 2013; Kosaka and Xie 2013 Balmaseda et al. 2013a; Watanabe et al. 2013; England et al. 2014; Chen and Tung 2014). While deep ocean heat uptake is currently the favored explanation of the hiatus, no consensus yet exists on the exact mechanism at work and on the place where deep ocean warming may occur (e.g., Goddard 2014; Trenberth et al. 2014; Chen and Tung 2014).

Accurate observations of sea level rise and its components (ocean thermal expansion and ocean mass change) can, in principle, help to constrain the problem (e.g., von Schuckmann et al. 2014). In particular satellite altimetry-based GMSL rise corrected for ocean mass change (e.g., using GRACE space gravimetry data over the oceans) provides an estimate of the total (full depth integrated) ocean thermal expansion (or equivalently ocean heat content). Comparison with observed Argo-based ocean thermal expansion (down to $\sim$1,500 m depth) may help to quantify any deep ocean contribution (below 1,500 m) and geographically localize any ocean warming. The first issue is addressed in the present study. Our analysis focusses on the 2003–2012 decade which corresponds to the hiatus period and the availability of new observing systems for estimating thermal expansion and ocean mass (nearly full ocean temperature and salinity coverage down to 2,000 m from Argo floats and direct ocean mass measurements from GRACE space gravimetry). Time series of satellite altimetry-based sea level, thermal expansion and ocean mass components are currently constructed by different groups (see Sect. 2) so that several data sets of each variable are available. But as we will see below, for some of them, in particular ocean thermal expansion, significant discrepancies are noticed between the data sets. Thus, part of our study consists of discussing the differences observed between the different records and estimate the uncertainty of each component. We further address the question: Can we close the sea level budget with available data sets for sea level and components or, if not, can we extract a significant residual possibly related to the deep ocean contribution? The present study deals with global mean time series. Contributions from oceanic regions will be presented in another study. Inside the 2003–2012 time span, two subperiods are considered: period P1 covering January 2005 to December 2012, corresponding to quasi global coverage of Argo data (before 2005, the Argo coverage is incomplete, e.g., von Schuckmann and Le Traon 2011), and period P2 covering January 2003 to December 2012 where GRACE data are available, as well as several steric data sets and ocean reanalyses products (in general available over a longer time span, e.g., 1950–present). In the following, we study periods P1 (2005–2012) and P2 (2003–2012).

While our manuscript was under review, another study by Llovel et al. (2014) was published on the same issue. Llovel et al. (2014) consider the 2005–2013 time span, and not as many data sets as in the present study, but their conclusion is not at odds with ours. In the last section, we discuss their results and compare them with ours.

2 Data

2.1 Sea Level Data

We used five different products from five processing groups for the altimetry-based sea level data:

1. Archiving Validation and Interpretation Satellite Oceanographic Center (AVISO; http://www.aviso.altimetry.fr/en/data/products/ocean-indicators-products/actualitesindicateurs-des-oceansniveau-moyen-des-mersindexhtml.html)
2. Colorado University (CU Release 3; http://sealevel.colorado.edu/)
3. Goddard Space Flight Center (GSFC version 2; http://podaac-ftp.jpl.nasa.gov/dataset/MERGED_TP_J1_OSTM_OST_GMSL_ASCII_V2)
4. National Oceanographic and Atmospheric Administration (NOAA; http://www.star.nesdis.noaa.gov/sod/lsa/SeaLevelRise/LSA_SLR_timeseries_global.php)
5. Commonwealth Scientific and Industrial Research Organization (CSIRO; www.cmar.csiro.au/sealevel/sl_data_cmar.html).

All five sea level data sets are based on Topex/Poseidon, Jason-1 and Jason-2 data averaged over the 66°S–66°N domain, except for the CSIRO data averaged between 65°S and 65°N. For each product, a set of instrumental and geophysical corrections is applied (details are given on the websites of each data set). In addition, the effect of glacial isostatic adjustment (GIA, i.e., a small correction of −0.3 mm/year, Peltier 2004) is accounted for in each sea level time series except in the NOAA data set. We thus corrected the latter sea level data for the GIA effect, using the −0.3 mm/year value. The five sea level time series (AVISO, CU, GSFC, NOAA and CSIRO) are obtained either by directly averaging the along-track sea surface height data (e.g., CU) or by firstly gridding the unevenly distributed along-track data and then performing grid averaging (e.g., AVISO and NOAA). In all cases, an area weighting is applied. In addition to the geographical averaging method, other differences exist between the GMSL data sets because of the applied geophysical and instrumental corrections and the number of satellites considered (discussion on these differences can be found in Masters et al. 2012 and Henry et al. 2014). The sea level time series used in this study cover the period January 2003–December 2012.

Recently, in the context of the European Space Agency (ESA) Climate Change Initiative (CCI) 'Sea Level' project (ftp.esa-sealevel-cci.org/Products/SeaLevel-ECV/V1_11092012/), a new, improved product, combining the Topex/Poseidon and Jason-1/2 with the ERS-1/2 and Envisat missions, has been computed (Ablain et al. 2014). However, at the date of writing it is available until December 2010 only. Even if, for the sea level budget, we will not use the CCI data set as it does not yet extend to 2012, we will compare the CCI-based GMSL with the other data sets during their overlapping time span (January 2003–December 2010) (see Sect. 3.1).

2.2 Ocean Mass Data

For estimating the ocean mass component, we used three different data sets: The GRACE Release 05 products from the Center for Space Research from Texas University (CSR RL05), the German GeoForschungsZentrum (GFZ RL05) and the Jet Propulsion Laboratory (JPL RL05). To study the ocean mass evolution, a specific processing has been carried out by D. Chambers, using the GRACE Release 05 data sets over the oceans. In effect, as warned on the http://grace.jp.nasa.gov Web site, gridded Release 05 data cannot be used to

compute ocean mass changes because they have the global mean removed. In this study, we used the Chambers' ocean data. They are provided as global mean (averaged over the 90°S–90°N domain) time series with associated uncertainty. They are publicly available from https://dl.dropboxusercontent.com/u/31563267/ocean_mass_orig.txt. The processing methodology is described in Johnson and Chambers (2013) (see also Chambers and Schroeter 2011; Chambers and Bonin 2012). The GIA component has been subtracted from each GRACE ocean mass time series using the GIA correction computed in Chambers et al. (2010).

2.3 Steric Data

The steric component is estimated using in situ ocean temperature and salinity data sets. We considered seven different datasets, including four Argo products, plus an ocean reanalysis.

2.3.1 Period P1: Argo Data

We used Argo temperature and salinity data sets provided by four different groups:

- the International Pacific Research Center (IPRC),
- the Japan Agency for Marine-Earth Science and Technology (Jamstec),
- the Scripps Institution of Oceanography (SCRIPPS).

These data sets are available at monthly intervals on a global $1° \times 1°$ grid down to 2,000 m, over the period January 2005–December 2012. They can be downloaded from the http://www.argo.ucsd.edu/Gridded_fields Web site.

Using these data sets, we computed the steric sea level time series (and associated uncertainty; but note that only Jamstec provides errors), integrating the data over the 0–1,500 m depth range. The gridded steric time series from IPRC, Jamstec and SCRIPPS are estimated over the 62.5°S–64.5°N, 60.5°S–70.5°N and 61.5°S–64.5°N domains, respectively (i.e., corresponding to the data availability). An area weighting is applied when computing the global mean time series.

We also used an updated version of the global mean steric time series computed by von Schuckmann and Le Traon (2011) (0–1,500 m ocean layer). This monthly time series is based on a weighted box averaging scheme of Argo data, within the 60°S–60°N domain. In the following, this data set is called KvS.

Therefore, a total of four steric data sets are considered over period P1.

2.3.2 Period P2

In addition to the Jamstec data set, we also used other steric data sets to study the sea level budget over period P2 (since 2003): an updated version of Ishii and Kimoto (2009), the NOAA data set from Levitus et al. (2012) and the EN4 data set (Good et al. 2013). In addition, we also used the ORAS4 reanalysis from Balmaseda et al. (2013b). Over the recent years, these data sets integrate Argo data. Prior to Argo, most data are based on XBT devices and other in situ measurements (see Abraham et al. 2013). A few details on these data sets are given below:

- Ishii and Kimoto (2009) data set (called IK hereinafter): We used the updated 6.13 version available at http://rda.ucar.edu/datasets/ds285.3/. It is based on the World

Ocean Database 2005 and World Ocean Atlas 2005 (WOD05 and WOA05), the Global Temperature-Salinity dataset in the tropical Pacific from the Institut de Recherche pour le Development (IRD, France) and the Centennial in situ Observation Based Estimates (COBE) sea surface temperature. The XBT depth bias correction is applied in the current version. The temperature and salinity data are available at monthly intervals over 24 depth levels ranging from the ocean surface down to 1,500 m depth, on a global 1° × 1° grid from January 1945 to December 2012 (see Ishii and Kimoto 2009 for details).

- NOAA data set: Available at https://www.nodc.noaa.gov/OC5/3M_HEAT_CONTENT. As described in Levitus et al. (2012), this 1° × 1° data set uses the World Ocean Database 2009 (WOD09) plus additional data processed since 2009. Bias corrections are applied to the MBT (Mechanical BathyThermographs) and XBT data as described by Levitus et al. (2009). The temperature and salinity grids below 700 m are not available prior to January 2005. Thus, for the P2 time span, we computed the NOAA steric time series considering data down to 700 m only. Data are given at 3-month interval. Therefore, we interpolated the NOAA time series at monthly intervals to be consistent with the other steric time series.
- EN4 data set: We used the EN4.0.2 version from the Met Office Hadley Centre (http://www.metoffice.gov.uk/hadobs/en4/download-en4-0-2.html). This data set is based on the quality controlled subsurface ocean temperature and salinity profiles and objective analyses. The EN4.0.2 data set is an incremental development of the previous EN2 and EN3 versions. Data sources include the WOD09, Global Temperature and Salinity Profile Program (GTSPP) and Argo data from Argo Global Data Assembly Centres (GDACs). The EN4.0.2 temperature and salinity data are corrected for the XBT and MBT bias. The temperature and salinity data are available at monthly intervals over 40 depth levels ranging from the ocean surface down to 5,350 m depth, on a global 1° × 1° grid from January 1900 to December 2013. Details on the data processing are given in Good et al. (2013).
- The ORAS4 reanalysis from Balmaseda et al. (2013b) (https://icdc.zmaw.de/easy_init_ocean.html?&L=1#c2231). It is based on the Nucleus for European Modelling of the Ocean (NEMO) ocean circulation model (version 3.0) with data assimilation. Assimilated data include temperature and salinity profiles from EN3 version 2a (1958–2009), along-track altimetry-based sea level anomalies and global sea level trend from AVISO, sea surface temperature and sea ice from the ERA-40 archive (prior to November 1981), from NCEP (National Centers for Environmental Prediction) OI version 2 (1981 until December 2009) and from OSTIA (Operational Sea Surface Temperature and Sea Ice Analysis; January 2010 onwards). The ORAS4 temperature and salinity data are available at monthly intervals over 42 depth levels ranging from the ocean surface down to 5,350 m depth, on a global 1° × 1° grid from January 1958 to December 2009. Details on the data processing are given in Balmaseda et al. (2013b).

Except for NOAA for which steric sea level grids are directly available, we computed the steric sea level time series and associated errors for the P2 period, integrating the data over the 0–1,500 m depth range. The global mean steric time series were further estimated by geographically averaging the gridded data (area weighting applied).

For the whole set of time series, annual and semiannual cycles were removed and residual time series were smoothed using a 3-month moving window.

3 Data Analysis

3.1 Global Mean Sea Level and Ocean Mass Time Series

Figure 1a shows plots of the GMSL time series without the CCI data over 2003–2012. We note that the CU and GSFC sea level curves are very close, as are the NOAA and AVISO curves. The CSIRO curve agrees better with NOAA and AVISO than with the other two, at least for the second part of the study time span. Some differences are observed between the time series on short time spans (<2–3 years). In terms of trends, differences up to $\sim$0.35 mm/year are noticed between the AVISO, CSIRO, NOAA groups on the one hand, and CU and GSFC on the other hand, the latter groups giving slower rates. As shown in Masters et al. (2012) and Henry et al. (2014), most of these differences (for both interannual fluctuations and trends) result from the mapping process adopted by the different groups. Table 1 gives the GMSL trend estimates for the five time series and their means, over P1 and P2 periods.

Figure 1b plots the same five GMSL time series as in Fig. 1a, together with the CCI GMSL over January 2003–December 2010 time span. Slight differences are observed between the CCI and other GMSL time series at interannual timescales. Table 1 also gives the GMSL trends over January 2003–December 2010. We note that the CCI trend (2.75 mm/year) is equal to the mean trend of the other five time series (2.71 mm/year) over this time span. In the following, we will only consider the mean GMSL time series based on averaging the AVISO, CU, NOAA, GSFC and CSIRO time series.

Figure 1c shows the three ocean mass time series over 2003–2012. The global ocean mass (GOM) curves agree well, both in terms of trend and interannual variability. The year-to-year discrepancies between the three curves remain within the error bars of each time series. GOM trends for each data set and means, over P1 and P2 periods are given in Table 1.

Note that the reasonably good agreement among the GMSL and GOM products does not imply anything on their absolute accuracy. However, for the GMSL, external calibration with tide gauge data and assessment of all sources of errors acting on the satellite altimetry system allows us to estimate the GMSL trend and the year-to-year mean sea level anomalies accurate to $\sim$0.4 mm/year and 1–2 mm (Ablain et al. 2009, 2014). For the ocean mass component, it is not possible to do external calibration. Although the GRACE-based ocean mass could be compared to the sum of individual mass components (glacier melting, ice sheet mass loss, land water storage change, atmospheric water vapor change), the latter are still too uncertain to perform any reliable calibration at a global scale. The GRACE-based ocean mass precision has been estimated to 1.5 mm for individual monthly gridded values (Wahr et al. 2006; Chambers and Bonin 2012). In terms of trend, the main uncertainty comes from the GIA correction (estimated at the 0.3 mm/year level, Chambers et al. 2010).

Figure 2 plots mean GMSL (average of the five products), mean GOM (average of the three products) and difference 'GMSL minus GOM' (based on the above averaged curves) with associated uncertainty. For the mean GMSL, the uncertainty is based on the dispersion of each time series with respect to the mean. For the mean GOM, it is based on the quadratic sum of individual errors. Estimating the uncertainty of the mean GOM curve from the dispersion of individual curves gives exactly the same result.

Over P2 (2003–2012), the linear trends amount to 2.82 $\pm$ 0.10 mm/year for the mean GMSL, 1.70 $\pm$ 0.10 mm/year for the mean GOM and 1.12 $\pm$ 0.13 mm/year for the difference. Uncertainties quoted here are formal errors (1 standard deviation, SD). More realistic errors are discussed below (Sect. 4). The GMSL minus GOM time series

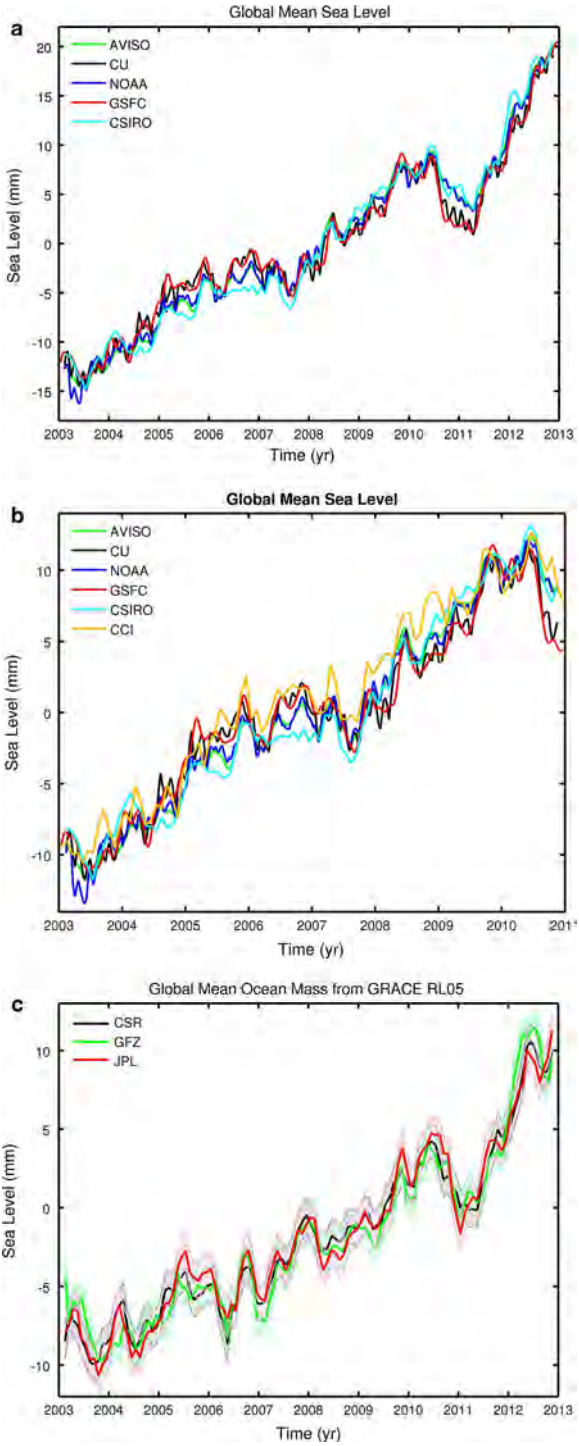

Fig. 1 **a** Global mean sea level (GMSL) time series (January 2003–December 2012) from the five satellite altimetry processing groups (AVISO, CU, CSIRO, GSFC and NOAA). **b** Global mean sea level (GMSL) time series (January 2003–December 2010) from the five satellite altimetry processing groups (AVISO, CU, CSIRO, GSFC and NOAA) and CCI. **c** Global mean ocean mass time series (January 2003–December 2012) from GRACE based on the data from CSR, GFZ and JPL (data provided by D. Chambers)

>**Table 1** Estimated trends for individual GMSL, ocean mass and steric sea level (for 700 and 1,500 m integration depth) time series, as well as their mean over the P1 and P2 periods

Trend estimates	January 2003–December 2010	P1: January 2005–December 2012		P2: January 2003–December 2012	
GMSL (mm/year)					
AVISO	2.90	2.97		2.97	
CU	2.55	2.57		2.66	
NOAA	2.85	2.89		2.91	
GSFC	2.46	2.51		2.61	
CSIRO	2.81	3.18		2.99	
MEAN	2.71 ± 0.10	2.81 ± 0.10		2.82 ± 0.10	
CCI	2.75	–		–	
Ocean mass (OM) (mm/year)					
CSR		1.85 ± 0.12		1.71 ± 0.08	
GFZ		1.94 ± 0.12		1.68 ± 0.08	
JPL		1.81 ± 0.12		1.72 ± 0.08	
MEAN		1.87 ± 0.11		1.70 ± 0.10	
Mean GMSL minus mean OM		0.94 ± 0.16		1.12 ± 0.13	
		0–700 m	0–1,500 m	0–700 m	0–1,500 m
Steric sea level Argo (mm/year)					
KvS		–	0.51 ± 0.15	–	–
IPRC		0.42	0.62	–	–
JAMSTEC		0.53 ± 0.13	0.77 ± 0.16	0.65 ± 0.14	0.92 ± 0.17
SCRIPPS		0.41	0.63	–	–
MEAN		–	0.63 ± 0.12	–	–
Residual (mean GMSL − mean OM mean − steric sea level)		–	0.29 ± 0.21	–	–
Steric sea level (mm/year)					
IK		0.40 ± 0.13	0.67 ± 0.14	0.39 ± 0.11	0.61 ± 0.16
EN4		–	–	0.00 ± 0.14	0.15 ± 0.17
NOAA		–		0.29	–
MEAN		–	–	0.32 ± 0.11	0.56 ± 0.14
Residual (mean GMSL − mean OM mean − steric sea level)		–	–	–	0.55 ± 0.19
ORAS4 Reanalysis (mm/year)	ORAS4 (Jan. 2003–Dec. 2009): 0–1,500 m = 0.65; 1,500–6,000 m = 0.07				

Uncertainties of mean trends correspond to 1 SD. Residual (mean GMSL − mean ocean mass − mean steric sea level) trends are also provided. ORAS4-based steric trends are also given over 2003–2009

displayed in Fig. 2 shows a positive slope between 2003 and 2007, followed by a temporary negative anomaly of several mm (coinciding with the 2007–2008 La Nina). Since mid-2008, the residual trend is lower than during 2003–2007 but still slightly positive. In addition to systematic errors of each observing system, the residual curve represents in principle the total (full depth) steric component.

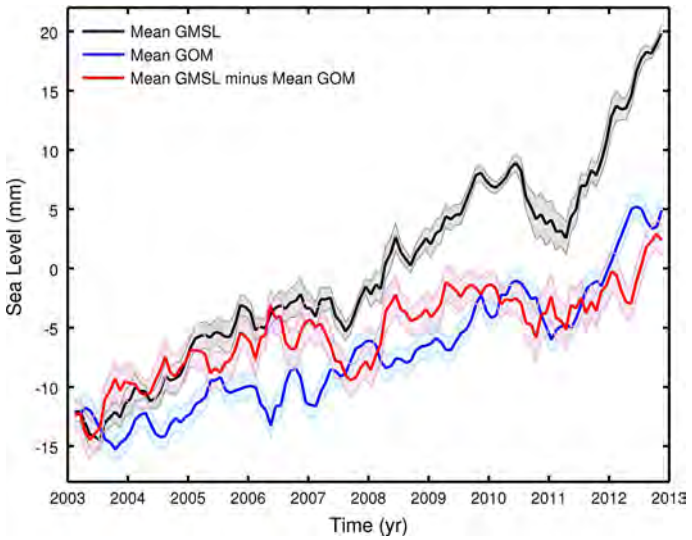

Fig. 2 Averaged GMSL, averaged global mean ocean mass (GOM) and difference time series (January 2003–December 2012)

3.2 Steric Sea Level Time Series: Comparison Between the 'GMSL Minus GOM' Residual Time Series and Steric Sea Level

3.2.1 Period P1 (2005–2012; Argo Time Series)

Figure 3 shows the four Argo steric time series over 2005–2012 for the 0–1,500 depth range. Uncertainties (available only for the KvS and Jamstec data sets) are also shown. Important discrepancies of several mm are noticed at interannual timescales between the four curves. As discussed in detail in Abraham et al. 2013 (see also Lyman and Johnson 2014; von Schuckmann and Le Traon 2011), these differences come from several factors, i.e., quality control, infilling gaps in data coverage, choice of the climatology, gridding process. So far no best processing method can be proposed, and we continue here with a mean Argo time series (as shown in Fig. 4), i.e., the average of the four time series shown in Fig. 3 (called 'mean steric' in the following) and its associated uncertainty (based on the dispersion of individual time series with respect to the mean). We then compare then 'mean steric' curve to the 'GMSL minus GOM' curve (Fig. 4). The mean steric curve displays significant interannual variability that roughly follows that of the 'GMSL minus GOM' curve. Superimposed on the interannual fluctuations, there is positive steric trend amounting to 0.29 ± 0.21 mm/year. Figure 4 also shows the residual 'GMSL minus GOM' minus mean steric curve (called 'residual' hereinafter; with a downward offset of 7.5 mm, for clarity). The residual curve reflects errors affecting all data sets (altimetry-based sea level, GRACE-based ocean mass, GIA, Argo data). It also includes the effect of gaps in Argo data coverage (e.g., in the Indonesian region) as well as a potential contribution from the deep ocean below 1,500 m. Interpretation of this residual curve is not straightforward. The early part of the record is characterized by year-to-year oscillations of about 2–4 mm (peak to peak) amplitude, followed by a strong negative anomaly late 2007. Then, from early 2008 to early 2012, the residual curve is rather flat.

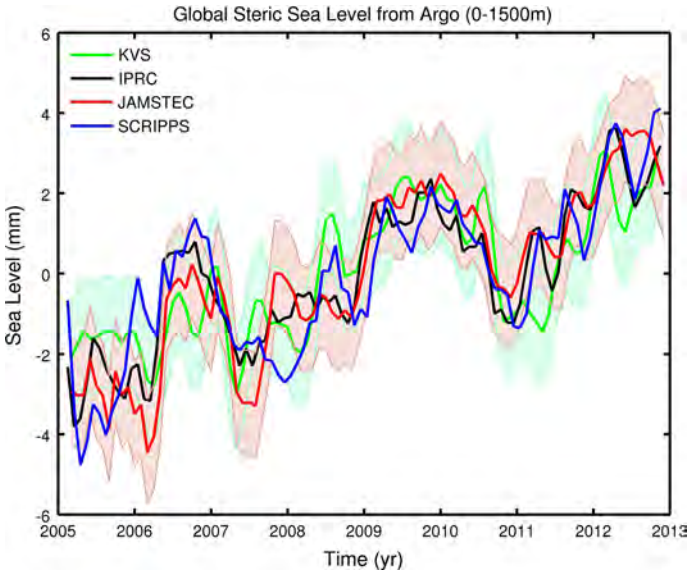

Fig. 3 Argo-based global mean steric sea level from four processing groups (KvS, IPRC, Jamstec and SCRIPPS; January 2005–December 2012)

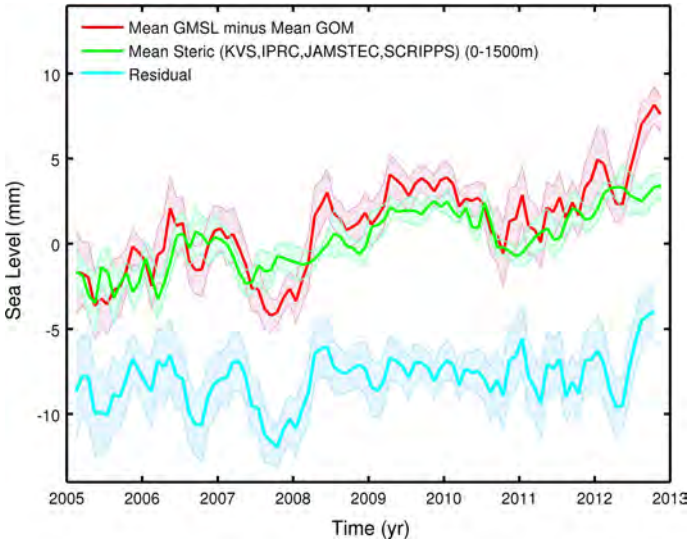

Fig. 4 Difference time series 'GMSL minus GOM' (based on the averaged curves), mean steric sea level (average of KvS, IPRC, Jamstec and SCRIPPS) and residual curve ('GMSL minus GOM' minus mean steric sea level, with downward offset of 7.5 mm for clarity; January 2005–December 2012)

After mid-2012, the 'GMSL minus GOM' curve increases abruptly, unlike the mean steric curve, causing a steep increase in the residual. Overall, what this residual shows is some step-like rise (around early 2008) preceded and followed by a plateau. Another step-like rise is suggested at the end of the period.

Table 1 gives the steric trends estimated over the P1 period for each Argo time series (integration down to 1,500 m) and mean steric trend. Trends of 'mean GMSL minus mean GOM' and residual time series over P1 are also given.

3.2.2 Period P2 (2003–2012; Other Steric Products)

Over the 2003–2005 time span, only the IK, Jamstec and EN4 data sets provide data over the 0–1,500 m depth range (however, we must keep in mind the limited raw data available below 700 m over this time span). So we present below the steric curves for the 0–700 and 0–1,500 m depth ranges separately.

Figure 5a shows the IK, Jamstec, NOAA and EN4 steric curves for the 0–700 m depth range, with associated uncertainties for IK, Jamstec and EN4. Very large errors affect the early part of the time span (2003–2005), and strong discrepancies are noticed between the four curves. These differences predominantly occur from data processing methodologies, in particular different gap filling methods. Moreover, prior to 2005—where the data source is mostly based on XBT measurements—differences in the XBT bias correction add to the discrepancies (see Lyman et al. 2010; Abraham et al. 2013; Lyman and Johnson 2014). Figure 5b shows the IK, Jamstec and EN4 steric curves for the 1,500 m depth range. Similar comments apply as for the 0–700 m depth range. In both cases, the EN4 curve is almost flat over the whole time span (its trend over 2003–2012 is 0.0 ± 0.14 and 0.15 ± 0.17 mm/year for 700 and 1,500 m integration depths, respectively). This is unlike the IK and Jamstec curves that display larger positive trends. Over P2, the IK trend amounts 0.39 ± 0.11 and 0.61 ± 0.16 mm/year down to 700 and 1,500 m, respectively, while the Jamstec trend amounts 0.65 ± 0.14 and 0.92 ± 0.17 mm/year for the same two integration depth. The behavior of the EN4 time series is puzzling and needs further investigation. However, we still consider this data set in our analysis.

Figure 6 shows the mean of IK, Jamstec, NOAA and EN4 for 0–700 m and mean of IK, Jamstec and EN4 for 0–1,500 m depth range (the NOAA data down to 1,500 m are available only as of 2005) for the 2003–2012 time span (P2 period). Interannual variability is very similar for the 700 and 1,500 m cases, as expected since it is essentially due to the upper ocean layers. The main difference between the two curves is a 0.24 mm/year short-term trend increase, from 700 to 1,500 m.

Steric trends estimated over P2 for each time series (0–700 and 0–1,500 m depth ranges) and means are given in Table 1. Trends of 'mean GMSL minus mean GOM' and residual time series over P2 are also given.

Figure 7 shows the 'GMSL minus GOM' curve and mean steric curve (average of IK, Jamstec and EN4) for the 0–1,500 m depth, as well as the residual curve ('GMSL minus GOM' minus mean steric curve; with a downward offset of 7.5 mm, for clarity). Over 2005–2012, the residual curve is very similar to that shown in Fig. 4 when using Argo data, with similar behavior though time. Over 2003–2012 (P2 period), the residual curve displays a positive trend of 0.55 ± 0.19 mm/year.

4 Mid-Ocean and Deep Ocean Contribution

Comparing the upper 700 and 1,500 m steric contributions and their evolution through time shows an interesting behavior. As expected, the 1,500 m steric contribution is larger than the 700 m steric one. But, more interestingly, the difference seems to increase linearly with time. This implies that more and more heat reaches the ocean below 700 m. This is

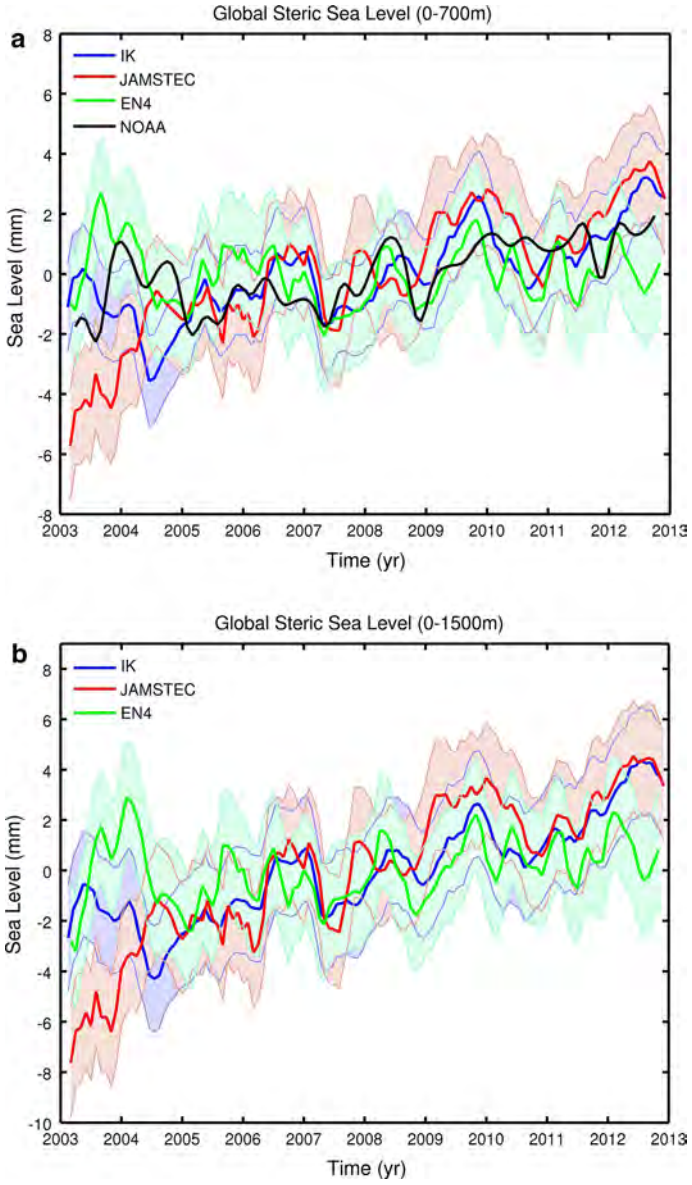

Fig. 5 **a** Global mean steric sea level time series (January 2003–December 2012; 0–700 m); data from IK, NOAA, Jamstec and EN4. **b** Global mean steric sea level time series (January 2003–December 2012; 0–1,500 m); data from IK, Jamstec and EN4

observed for all data sets, although not exactly with the same intensity (ranging from 0.15 to 0.27 mm/year). This is illustrated in Fig. 8, showing the evolution over 2005–2012 of the steric sea level for a few data sets (IPRC, Jamstec, and IK) as well as for their mean (the NOAA and EN4—not shown—show similar behavior). To highlight this time-increasing difference, the 700 and 1,500 m curves start from the same (arbitrary) value.

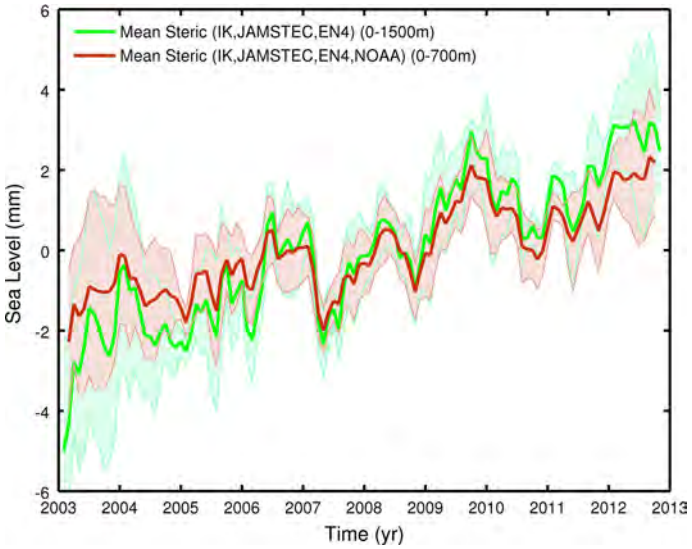

Fig. 6 Averaged steric sea level time series (January 2003–December 2012) for 0–700 m (average of IK, NOAA, Jamstec and EN4) and 0–1,500 m (average of IK, Jamstec and EN4)

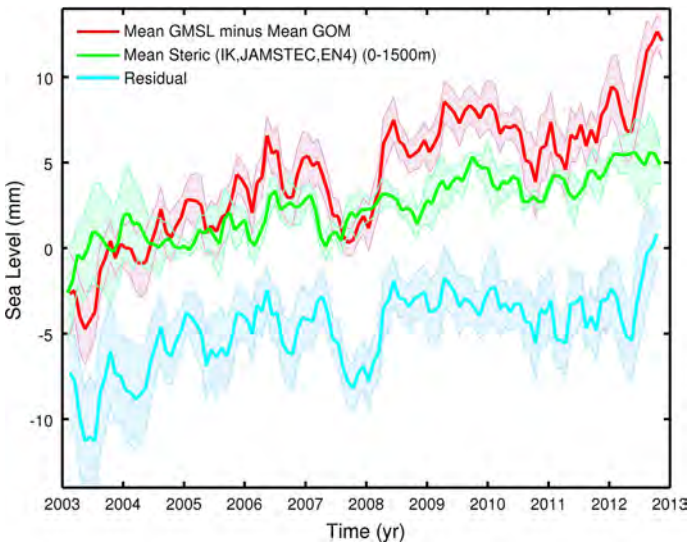

Fig. 7 Difference time series 'GMSL minus GOM' (based on the averaged curves), mean steric sea level for 0–1,500 m (average of IK, Jamstec and EN4) and residual curve ('GMSL minus GOM' minus mean steric sea level, with downward offset of 7.5 mm for clarity; January 2003–December 2012)

Figure 8 clearly shows that the layers below 700 m have gained heat over the last few years. This observation is in agreement with previous results from Levitus et al. (2012) based on the NOAA data set, and Balmaseda et al. (2013a) based on the ORAS4 reanalysis. The latter study showed an increasing warming trend below 700 m. However, it did not

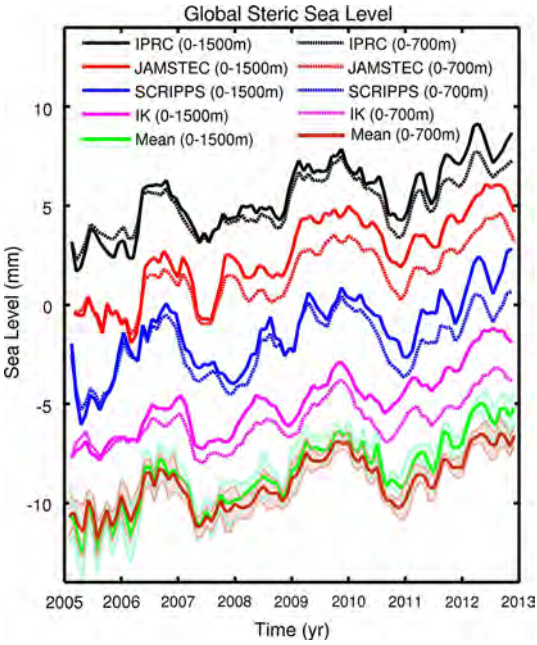

Fig. 8 Steric sea level curves for 0–700 and 0–1,500 m for IK, IPRC, Jamstec and SCRIPPS (January 2005–December 2012)

specify in which layers (likely, it is in the 700–1,500 m depth range; see discussion below). A similar behavior was found by Llovel et al. (2014) between 700 and 2,000 m with Argo data.

The residual curves shown in Figs. 4 and 7, i.e., the 'mean GMSL minus mean GOM' minus mean steric down to 1,500 m, reflect errors of all data sets plus missing contributions. For the latter, one candidate is the steric contribution from the deep ocean (below 1,500 m). Direct steric observations below 1,500 m are very sparse (e.g., Purkey and Johnson 2010; Kouketsu et al. 2011) and not available over the P1 and P2 time spans. However, we can use the ORAS4 reanalysis to compare the deep ocean contribution based on the residual "'GMSL minus GOM' minus steric down to 1,500 m" estimated from observations and the ORAS4 reanalysis (Fig. 9). The ORAS4 data set available to us ends in December 2009. So the comparison is performed over 2003–2009 only. Figure 9 superimposes the mean steric and ORAS4 for 0–1,500 m depth range (upper curves). Very good agreement is found between the two curves. The bottom curves of Fig. 9 correspond to the residual "'GMSL minus GOM' minus steric down to 1,500 m" and the ORAS4 steric contribution for the 1,500–6,000 m depth range. Over the 2003–2009 time span, the ORAS4 steric signal below 1,500 is very small, with a trend of <0.1 mm/year. This is unlike the residual curve "'GMSL minus GOM' minus steric down to 1,500 m" that displays important variability and a large positive trend of 0.55 ± 0.19 mm/year (over 2003–2012). The question whether this trend is significant or not is a difficult one. To the ~ 0.2 mm/year formal error, we must add systematic errors associated with each observing system. We can assume systematic errors of 0.4 mm/year for the GMSL (Ablain et al. 2009, 2014), 0.3 mm/year for GOM (Chambers and Bonin 2012) and 0.3 mm/year for the steric sea level. The latter estimate is likely an upper bound, since summing quadratically the total trend errors given for the steric data gives 0.28 mm/year. Therefore, the resulting (more realistic) error of the residual trend based on the quadratic sum of individual errors is

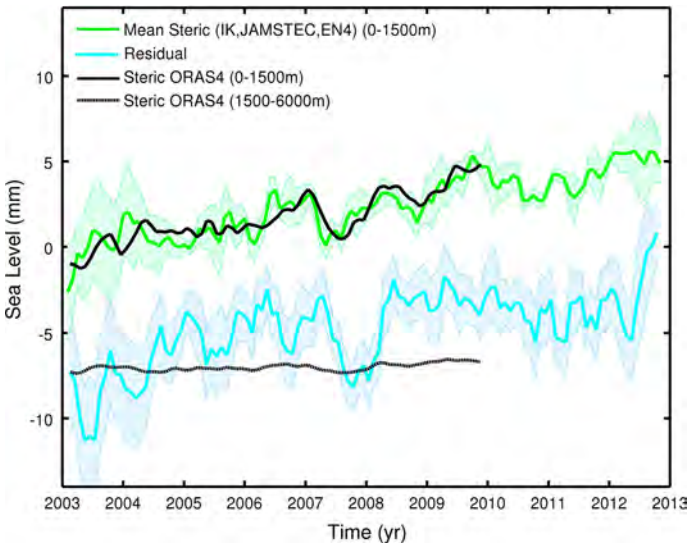

Fig. 9 *Upper curves* averaged steric sea level for 0–1,500 m (average of IK, Jamstec and EN4; January 2003–December 2012) with steric sea level (0–1,500 m) from ORAS4 superimposed. *Lower curves* residual curve ('GMSL minus GOM' minus mean steric sea level)—same as in Fig. 7—with the steric sea level (1,500–6,000 m) from ORAS4 superimposed

0.58 mm/year. So the residual trend (of 0.55 mm/year) is barely significant (the large negative anomalies seen in the residual curve prior to mid-2004 are suspect and likely due to data errors).

5 Discussion and Conclusions

In this study, we have considered 16 different data sets (5 for the GMSL, 3 for the ocean mass and 8 for the steric sea level) to compare the observed GMSL to the sum of components (ocean mass plus steric sea level) and tried to derive constraints on the deep ocean contribution through a sea level closure budget approach. This large number of different data sets would allow 120 different combinations to study the sea level budget. With such an approach, it would always be possible to find some combinations allowing closure of the sea level budget, or inversely leading to nonzero deep ocean contribution. Instead, we used averages of each type of data (GMSL, ocean mass, steric sea level) and estimated their dispersion range. This gives insight into the precision of the different estimates and provides an uncertainty range due to the variants in processing approaches developed by the different groups. On top of this, systematic errors of each observing system have also to be considered.

The main result of our study is that, for the limited time span considered here, the total uncertainty on the "'GMSL minus GOM' minus steric 0–1,500 m" is quite large (0.58 mm/year), preventing us from bringing a realistic constraint on the deep (below 1,500 m) ocean contribution (as previously noticed in von Schuckmann et al. 2014).

In addition, over both P1 (2005–2012) and P2 (2003–2012) periods, the residual curves (Figs. 4, 7) display important interannual variability that is totally unrealistic in the deep

ocean. Very likely, it reflects errors at interannual timescales in one of the components (GMSL, ocean mass or steric sea level) or in all of them. Previous studies (e.g., Cazenave et al. 2012; Masters et al. 2012; Henry et al. 2014; Ablain et al. 2014) showed that at interannual timescales, the (detrended) GMSL time series displays 2–4 mm differences from one data set to another. Thus, it is quite possible that the year-to-year fluctuations seen here in the residual curves are at least partly due to errors in the GMSL. Current efforts conducted in the context of the ESA Climate Change Initiative 'sea level' project already provide improved sea level data (Ablain et al. 2014), but assessment of this new product is still an ongoing work. Moreover, gaps in coverage in the steric data, in particular Argo data (e.g., in the Indonesian region), and the associated missing steric signal very likely impact the residual time series at interannual timescales.

The short-term trends displayed by the residual curves for both P1 and P2 periods are also very likely contaminated by uncertainties in interannual variability as well as by longer-term systematic errors. As shown in Cazenave et al. (2014), ENSO events cause temporary positive or negative sea level anomalies (mostly of mass origin, but also in the steric component) that significantly alter estimates of the rate of sea level rise. However, even if the short-term variability is removed, the trend estimated from the filtered residual curves (not shown) remain unrealistically large to be attributed to the deep ocean (>1,500 m) contribution. As shown in Fig. 9, the ORAS4 reanalysis estimates the 1,500–6,000 m steric trend to $\sim$0.1 mm/year. Such a magnitude is in line with estimates based on sparse, but direct observations. For example, Purkey and Johnson (2010) report a (non uniform) deep ocean contribution of the order of 0.1 mm/year for the 1990–2000 decade. For the same time span, Kouketsu et al. (2011) also find observational support for a deep ocean warming, but not larger than 0.1 mm/year (in steric sea level equivalent) for layers below 3,000 m. Such values agree well with the ORAS4 reanalysis (the ORAS4 steric sea level trend amounts to 0.17 mm/year for the 1993–2003 decade and 1,500–6,000 m depth range). Although it can be expected that more heat has reached the deep ocean since the early 2000s, the residual values reported here for the P1 and P2 periods appear anomalously large.

We suspect that gaps in steric data coverage, like in the Indonesian region, and the associated missing signal, contribute to the residual curves over the P1 and P2 periods. For example, in the oceanic region covering the China Sea, Indonesian region and north of Australia, satellite altimetry shows strong positive spatial trends over these two time spans (also observed over the whole altimetry era). As regional sea level trends are mainly of steric origin (e.g., Stammer et al. 2013), it is possible that the residual curves shown in Figs. 4 and 7 reflect at least partly the missing steric signal. To check this, we computed the altimetry-based sea level trend associated with the Indonesian region over the P1 and P2 periods and found that it contributes by $\sim$0.3 mm/year, hence about 10 % the total sea level trend. Since this region has been considered in the GMSL (as well as in the ocean mass; but a rough estimate indicates a very small mass contribution to the residual trend, less than 0.05 mm/year), but not is the steric data due to the gap in data coverage (since 2005 but also earlier), we conclude that the steric trend has been underestimated because of these missing data. To investigate this issue somewhat further, we computed the steric contribution of the Indonesian region (considering an area covering the Indonesian region, the Timor Sea plus the South China Sea; see Fig. 10) using the ORAS4 data. The steric contribution of this area to the residual trend is estimated to 0.29 and 0.31 mm/year over 2003–2009 and 2005–2009, respectively (after weighting by the ratio of the area to the total ocean surface between 66°S and 66°N). Assuming that the Indonesian steric trend remains more or less constant over the whole P1 and P2 periods and subtracting it (using a

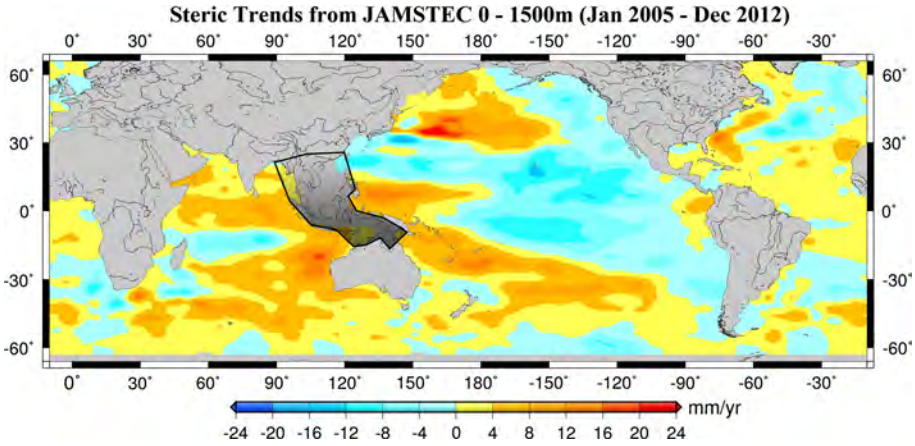

Fig. 10 Steric trend map based on Jamstec data over January 2005–December 2012 showing the Argo data gap in the Indonesian region and the contours (*black line*) of the area considered in this study to estimate—using the ORAS4 reanalysis—its contribution to the global mean steric trend

value of 0.3 mm/year) from the above estimated residual trends, we find new residual trends of $\sim$0 and 0.25 mm/year for P1 and P2, respectively. We consider such a range (0–0.25 mm/year) as an upper limit for the deep ocean contribution to recent years sea level rise.

The recently published study by Llovel et al. (2014) uses different data sets (Colorado University/CU altimetry and CSR GRACE data) for the GMSL and ocean mass. They also integrate Argo data down to 2,000 m (instead of 1,500 m in our study) and consider the January 2005–December 2013 time span. They come up with a residual trend (GMSL rise corrected for GRACE ocean mass and 0–2,000 m Argo steric trends) of -0.13 ± 0.72 mm/year. That their residual trend is lower than ours (amounting 0.29 mm/year over 2005–2012; see Table 1) is largely due to the fact that the CU GMSL trend over P1 is lower by $\sim$0.25 mm/year than the mean GMSL trend used in our study (see Table 1). The remaining difference (on the order of 0.15 mm/year) arises because of differences in the integration depth and study period. Llovel et al. (2014) further consider the upper value of the $\pm$0.72 mm/year uncertainty range to derive an upper bound for the GMSL rise due to deep ocean warming below 2,000 m. Doing this, they estimate at 0.59 mm/year the maximum contribution of the deep ocean warming for the period from 2005 to 2013. This is more than twice our estimate after correcting for the data gap effect. Clearly, more investigations are needed on this important issue.

Probably, the most reliable result of our study is the evidence of a continuing warming of the 700–1,500 m ocean layer. While reported earlier by Levitus et al. (2012) and von Schuckmann et al. (2014) using the NOAA and KvS steric data sets, respectively, Balmaseda et al. (2013a) using the ORAS4 reanalysis, as well as Llovel et al. (2014) using Argo data since 2005, here we observe a similar behavior for each of the eight steric data sets considered over the P1 and P2 periods, indicating that the result is most probably robust. Expressed in steric sea level equivalent, the trend contribution of the 700–1,500 m layer is on the order of 0.2 mm/year.

As discussed in the introduction, the favored candidate for explaining the current hiatus in global warming is deep ocean heat uptake. In the absence of direct deep ocean

temperature measurements, the sea level budget approach may in principle help to constrain the problem. But as shown here and in previous studies (e.g., Abraham et al. 2013; von Schuckmann et al. 2014), uncertainties due to data processing approaches and systematic errors of the different observing systems still prevent us from obtaining accurate enough results, even when using almost all available data sets—as done here, instead of just a selection of them. Besides, regional gaps in the steric coverage of the upper ocean, like in the Indonesian region, complicate the sea level budget approach.

Priority for future work is to improve the data processing of each observing system. Systematic intercomparisons of observational products (i.e., sea level, ocean mass and steric sea level—including ocean reanalyses) should be implemented in an international context in order to better understand the causes of the reported differences and define a best processing methodology (if possible). The following step should be a global reprocessing of all data sets, following the approach of the ESA Climate Change Initiative program. In parallel, implementation of new observing systems (e.g., deep Argo) should be a sustained goal of the scientific community and institutional organizations.

Priority in terms of observing systems is definitely the development of a deep Argo program and improved coverage of the upper ocean temperature and salinity measurements, as advocated in a number of recent articles (e.g., Abraham et al. 2013).

Acknowledgments We thank Don Chambers and two anonymous referees for their constructive reviews. We also thank William Llovel for interesting discussions about our respective studies. H.B.D. PhD is funded by the European Space Agency in the context of the Climate Change Initiative Sea Level Project. H.P. is supported by a joint CNES-CLS PhD grant.

References

Ablain M, Cazenave A, Valladeau G, Guinehut S (2009) A new assessment of the error budget of global mean sea level rate estimated by satellite altimetry over 1993–2008. Ocean Sci 5(2):193–201

Ablain M et al (2014) Improved Sea Level record over the satellite altimetry era 1 (1993–2010) from the Climate Change Initiative project. *Ocean Sci* (in press)

Abraham JP et al (2013) A review of global ocean temperature observations: implications for ocean heat content estimates and climate change. Rev Geophys 51:450 2013RG000432

Balmaseda MA, Trenberth K, Kallen E (2013a) Distinctive climate signals in reanalysis of global ocean heat content. Geophys Res Lett 40:1–6. doi:10.1002/grl.50382

Balmaseda MA, Mogensen K, Weaver A (2013b) Evaluation of the ECMWF ocean reanalysis ORAS4. Q J R Meteorol Soc. doi:10.1002/qj.2063

Bindoff N, Willebrand J, Artale V, Cazenave A, Gregory J, Gulev S, Hanawa K, Le Quéré C, Levitus S, Nojiri Y, Shum CK, Talley L, Unnikrishnan A (2007) Observations: oceanic climate and sea level. In: Solomon S, Qin D, Manning M, Chen Z, Marquis M, Averyt KB, Tignor M, Miller HL (eds) Climate change 2007: the physical science basis. Contribution of Working Group I to the fourth assessment report of the intergovernmental panel on climate change. Cambridge University Press, Cambridge and New York

Boening C, Willis JK, Landerer FW, Nerem RS (2012) The 2011 La Nina: so strong, the oceans fell. Geophys Res Lett 39:L19602. doi:10.1029/2012GL053055

Cazenave A, Henry O, Munier S, Meyssignac B, Delcroix T, Llovel W, Palanisamy H, Becker M (2012) ENSO influence on the global mean sea level over 1993–2010. Mar Geod 35(S1):82–97

Cazenave A, Dieng H, Meyssignac B, von Schuckmann K, Decharme B, Berthier E (2014) The rate of sea level rise. Nat Clim Change. doi:10.1038/NCLIMATE2159

Chambers DP, Bonin JA (2012) Evaluation of Release-05 GRACE time variable gravity coefficients over the ocean. Ocean Sci 8:859–868. doi:10.5194/os-8-859-2012
Chambers DP, Schroeter J (2011) Measuring ocean mass variations from satellite gravimetry. J Geodyn 52:333–343
Chambers DP, Wahr J, Tamisiea ME, Nerem RS (2010) Ocean mass from GRACE and glacial isostatic adjustment. J Geophys Res 115:B11415. doi:10.1029/2010JB007530
Chen X, Tung K-K (2014) Varying planetary heat sink led to global warming slowdown and acceleration. Science 345:897–903
Chen JL, Wilson CR, Tapley BD (2013) Contribution of ice sheet and mountain glacier melt to recent sea level rise. Nat Geosci 6:549–552
Church JA, Clark PU, Cazenave A, Gregory JM, Jevrejeva S, Levermann A, Merrifield MA, Milne GA, Nerem RS, Nunn PD, Payne AJ, Pfeffer WT, Stammer D, Unnikrishnan AS (2013) Sea Level Change. In: Stocker TF, Qin D, Plattner G-K, Tignor M, Allen SK, Boschung J, Nauels A, Xia Y, Bex V, Midgley PM (eds) Climate change 2013: the physical science basis. Contribution of Working Group I to the fifth assessment report of the intergovernmental panel on climate change. Cambridge University Press, Cambridge and New York
England MH et al (2014) Recent intensification of wind-driven circulation in the pacific and the ongoing warming hiatus. Nat Clim Change 4:222–227
Fasullo JT, Boening C, Landerer FW, Nerem RS (2013) Australia's unique influence on global mean sea level in 2010–2011. Geophys Res Lett 40(16):4368–4373. doi:10.1002/grl.50834
Goddard L (2014) Heat hide and seek. Nat Clim Change 4:158161
Good SA, Martin MJ, Rayner NA (2013) EN4: quality controlled ocean temperature and salinity profiles and monthly objective analyses with uncertainty estimates. J Geophys Res Oceans 118:6704–6716. doi:10.1002/2013JC009067
Guemas V, Doblas-Reyes FJ, Andreu-Burillo I, Asif M (2013) Retrospective prediction of global warming slowdown in the past decade. Nat Clim Change 3:649–653
Hansen J, Sato M, Kharecha P, von Schuckmann K (2011) Earth's energy imbalance and implications. Atmos Chem Phys 11:13421–13449. doi:10.5194/acp-11-13421-2011
Held IM (2013) The cause of the pause. Nature 501:318–319
Henry O, Ablain M, Meyssignac B, Cazenave A, Masters D, Nerem S, Leuliette E, Garric G (2014) Investigating and reducing differences between the satellite altimetry-based global mean sea level time series provided by different processing groups. J Geod 88:351–361. doi:10.1007/s00190-013-0687-3
Ishii M, Kimoto M (2009) Reevaluation of historical ocean heat content variations with time-varying XBT and MBT depth bias corrections. J Oceanogr 65(3):287–299. doi:10.1007/s10872-009-0027-7
Johnson GC, Chambers DP (2013) Ocean bottom pressure seasonal cycles and decadal trends from GRACE Release-05: ocean circulation implications. J Geophys Res Oceans 118:4228–4240. doi:10.1002/jgrc.20307
Kosaka Y, Xie S-P (2013) Recent global warming hiatus tied to equatorial Pacific surface cooling. Nature 501:403–407
Kouketsu S et al (2011) Deep ocean heat content changes estimated from observation and reanalysis product and their influence on sea level change. J Geophys Res 116:C03012
Leuliette EW, Willis JK (2011) Balancing the sea level budget. Oceanography 24:122–129
Levitus S et al (2009) Global ocean heat content 1955–2008 in light of recently revealed instrumentation problems. Geophys Res Lett 36:L07608. doi:10.1029/2008GL037155
Levitus S, Antonov JI, Boyer TP, Baranova OK, Garcia HE, Locarnini RA, Mishonov AV, Reagan JR, Seidov D, Yarosh ES, Zweng MM (2012) World ocean heat content and thermosteric sea level change (0–2000 m), 1955–2010. Geophys Res Lett 39:L10603. doi:10.1019/2012GL051106
Llovel W, Willis JK, Landerer FW, Fukumori I (2014) Deep-ocean contribution to sea level and energy budget not detectable over the past decade. Nat Clim Change. doi:10.1038/NCLIMATE2387
Lyman JM, Johnson GC (2014) Estimating global ocean heat content changes in the upper 1800 m since 1950 and the influence of climatology choice. J Clim. doi:10.1175/JCLIM-D-12-00752.1
Lyman JM, Godd SA, Gouretski VV, Ishii M, Johnson GC, Palmer MD, Smith DM, Willis JK (2010) Robust warming of the global upper ocean. Nature 465:334–337. doi:10.1038/nature09043
Masters D, Nerem RS, Choe C, Leuliette E, Beckley B, White N, Ablain M (2012) Comparison of global mean sea level time series from TOPEX/Poseidon, Jason-1, and Jason-2. Mar Geod 35:20–41
Peltier WR (2004) Global glacial isostasy and the surface of the ice-age Earth: the ICE-5G (VM2) model and GRACE. Annu Rev Earth Planet Sci 32:111–149
Peters GP, Marland G, Le Queré C, Boden T, Canadell JG, Raupach MR (2012) Rapid growth in CO2 emissions after the 2008–2009 global financial crisis. Nat Clim Change 2:2–4

Purkey S, Johnson GC (2010) Warming of global abyssal and deep southern ocean waters between the 1990s and 2000s: contributions to global heat and sea level rise budget. J Clim 23:6336–6351

Shepherd A et al (2012) A reconciled estimate of ice sheet mass balance. Science 338(6111):1183–1189. doi:10.1126/science.1228102

Smith D (2013) Has global warming stalled? Nat Clim Change 3:618–6919

Solomon S, Rosenlof K, Portmann R, Daniel J, Davis S, Sanford T, Plattner G-K (2010) Contributions of stratospheric water vapour to decadal changes in the rate of global warming. Science. doi:10.1126/science.1182488

Stammer D, Cazenave A, Ponte RM, Tamisiea ME (2013) Causes for contemporary regional sea level changes. Annu Rev Mar Sci 5:21–46. doi:10.1146/annurev-marine-121211-172406

Trenberth KE, Fasullo JT (2010) Tracking Earth's energy. Science 328:316–317

Trenberth KE, Fasullo JT (2013) An apparent hiatus in global warming? Earth's Future. doi:10.102/2013EF000165

Trenberth KE, Fasullo JT, Balmaseda MA (2014) Earth's energy imbalance. J Clim 27:3129–3144. doi:10.1175/JCLI-D-13-00294.1

Von Schuckmann K, Le Traon PY (2011) How well can we derive Global Ocean Indicators from Argo data? Ocean Sci 7(6):783–791. doi:10.5194/os-7-783-2011

Von Schuckmann K, Sallée JB, Chambers D, Le Traon PY, Cabanes C, Gaillard C, Speich S, Hamon M (2014) Consistency of the current global ocean observing systems from an Argo perspective. Ocean Sci 10:547–557. doi:10.5194/os-10-547-2014

Wahr J, Swenson S, Velicogna I (2006) Accuracy of GRACE mass estimates. Geophys Res Lett 33:L06401. doi:10.1029/2005GL025305

Watanabe M, Kamae Y, Yoshimori M, Oka A, Sato M, Ishii M, Mochizuki T, Kimoto M (2013) Strengthening of ocean heat uptake efficiency associated with the recent climate hiatus. Geophys Res Lett 40:3175–3179. doi:10.1002/grl.50541

Woppelmann G, Letetrel C, Santamaria A, Bouin MN, Collilieux X, Altamimi Z, Williams SDP, Miguez BM (2009) Rates of sea-level change over the past century in a geocentric reference frame. Geophys Res Lett. doi:10.1029/2009gl038720

2.3.2 Analyse des incertitudes des termes de l'équation bilan du niveau de la mer

Nous avions montré qu'il est difficile d'estimer le contenu thermique de l'océan profond (qui présente une grande incertitude) par une étude de bilan du GMSL sur la dernière décennie même si nous disposons sur cette période, de plusieurs systèmes d'observation de grande précision, indépendants et opérant simultanément (satellites altimétriques, gravimétrie spatiale GRACE, flotteurs automatiques Argo). Comme nous l'avons indiqué précédemment dans la *section 2.3.1*, il est important d'identifier les sources d'erreurs des produits de chaque composante du bilan du niveau de la mer. Ceci permet d'améliorer le traitement des données de chaque système d'observation et obtenir des résultats suffisamment précis pour contraindre le contenu thermique de l'océan profond.

Les résultats sur les incertitudes des données sont présentés dans l'article *Dieng et al.* (2015b) que nous résumons ci-dessous.

Résumé de l'article : "Sea level budget over 2005-2013 : missing contributions and data errors" *(l'article original est inséré à la fin de cette section 2.3.2)*

Cette étude porte sur la période 2005-2013 avec davantage de données (prise en compte du produit CCI du niveau de la mer disponible jusqu'à décembre 2013, intégration de la composante stérique du niveau de la mer des données Argo jusqu'à 2000m de profondeur, extension de la série jusqu'à fin 2013, etc.). Pour améliorer l'estimation du contenu thermique de l'océan profond en dessous de 2000m de profondeur, nous ne commençons qu'en 2005 car les données Argo ne couvrent pas l'ensemble de l'océan avant 2005 (*von Schuckmann et al.* 2014; *Roemmich et al.* 2015).

Rappelons que l'objectif principal de la présente étude est de déterminer si le signal temporel résiduel du bilan du GMSL (voir *Eq.2.2*) sur la période Janvier 2005 - Décembre 2013, peut être attribué, tant en termes de tendance que de variabilité interannuelle, à des erreurs associées aux composantes du niveau de la mer (GMSL, masse de l'océan, niveau de la mer stérique) ou non. Un autre objectif est de valider le produit GMSL du CCI. Pour cela, nous avons utilisé plusieurs ensembles de données, traités par différents groupes : six produits altimétriques pour le GMSL dont le CCI, quatre produits Argo plus la réanalyse océanique ORAS4 pour estimer le niveau de la mer stérique et trois produits de masse de l'océan basés sur GRACE. Les mêmes produits sont utilisés dans la *section 2.3.1*, mais en revanche les produits stériques à partir d'Argo sont intégrés jusqu'à 2000m de profondeur.

En analysant les séries temporelles du GMSL sur la période 2005-2013, les deux groupes de GMSL identifiés précédemment s'affichent clairement (groupe1 : CCI, AVISO, NOAA et CSIRO ; groupe2 : CU et GSFC). Nous notons des écarts en tendance importants entre les deux groupes de GMSL (par exemple 0.55 mm/an entre GSFC et CSIRO), nettement supérieurs à l'erreur de l'altimétrie de 0.4 mm/an issue de l'étalonnage externe du GMSL avec des données marégraphiques et de l'évaluation de toutes les sources d'erreurs qui agissent sur le système d'altimétrie par satellite (*Ablain et al.* 2009, 2015). Des écarts interannuels de plusieurs mm sont aussi observés entre les produits GMSL des deux groupes, par exemple de 4 mm durant La Niña de 2010-2011. Cet écart est le double de l'erreur de l'altimétrie en termes de variabilité interannuelle estimée à +2mm par *Ablain et al.* (2009, 2015). Comme montré dans nos travaux antérieurs et dans d'autres publications (*Masters et al.* 2012 ; *Henry et al.* 2014), en plus des processus de moyennage adoptés par les différents groupes, les différences notées entre les produits GMSL résultent des erreurs sur les corrections géophysiques, les biais instrumentaux, le raccordement des missions, etc. Les produits stériques (intégrés entre 0 et 2000m) présentent aussi des différences dues au contrôle de qualité, les méthodes de remplissage des lacunes dans la couverture des données, le choix de la climatologie mais aussi les techniques de maillage (*Abraham et al.* 2013 ; *Lyman and Johnson,* 2014 ; *von Schuckmann and Le Traon,* 2011).

En analysant le signal résiduel estimé en utilisant plusieurs combinaisons de produits des diverses composantes de l'équation bilan du niveau de la mer sur la période 2005-2013, nous observons des différences de tendance allant jusqu'à 0.55 mm/an soit 17% de la hausse du GMSL observé. Notre étude a montré que ces écarts sont essentiellement dus aux produits 'niveau de la mer altimétrique'. La question est alors de savoir quel produit 'niveau de la mer' est le plus réaliste. Pour tenter de répondre à cette question, nous avons utilisé la réanalyse océanique ORAS4 qui fournit des données stériques intégrées jusqu'à 5350 m de profondeur avec une couverture géographique complète, ce qui n'est pas le cas pour les données Argo. En effet, il n'y a aucune donnée Argo dans la région indonésienne ni dans le Golfe du Mexique. C'est dans la région indonésienne que l'on trouve les plus fortes hausses du niveau de la mer sur la période altimétrique (jusqu'à 4 fois la hausse moyenne globale). Le manque de données Argo dans cette région conduit donc à sous-estimer la composante stérique. L'utilisation d'ORAS4 sur la période 2005-2013 montre que la contribution de cette région est de l'ordre de 0.3 mm/an, soit 10% de la hausse du GMSL. Nous montrons ainsi que le manque de données Argo dans la région indonésienne conduit à une surestimation de la valeur absolue de la tendance résiduelle d'environ 0.3 mm/an. La prise en compte de cette contribution nous a conduit à montrer que l'on arrive à parfaitement fermer le bilan du niveau de la mer (en termes de tendance) avec les produits CCI et AVISO mais pas avec les produits CU et GSFC. Une illustration, sur la période janvier 2005 -

décembre 2014, du bilan du GMSL CCI avec la somme des composantes du niveau de la mer "stérique Argo (2000m) + masse océan" est proposée sur la Fig.2.5 ci dessous. Ainsi en tenant compte de l'estimation de la région Indonésienne par ORAS4 sur cette même période, la tendance de la composante résiduelle devient quasi nulle (-0.02 mm/an), ainsi le bilan du GMSL se ferme avec le CCI.

L'étude a aussi montré que les résidus de l'équation de bilan présentent d'importantes fluctuations interannuelles, incompatibles avec une origine profonde. Une analyse statistique, indiquant que les anomalies résiduelles du bilan du niveau de la mer sont significativement corrélées avec les fluctuations interannuelles de la masse de l'océan et de la composante stérique du niveau de la mer, nous conduit à conclure que ces erreurs interannuelles résultent principalement des produits GRACE et Argo.

Un autre résultat de notre étude est qu'en plus de la fermeture du bilan du niveau de la mer avec le GMSL CCI, le signal résiduel présente les plus faibles fluctuations interannuelles (en comparaison avec les signaux résiduels calculés à partir des 5 autres produits GMSL). Il faut noter que plusieurs améliorations on été apportées sur les corrections du produit niveau de la mer du CCI, principalement la réduction des erreurs d'orbite et de correction troposphérique (humide et sèche), la réduction des dérives et des biais instrumentaux et un meilleur inter-étalonnage entre les missions altimétriques. Le produit niveau de la mer du CCI a été validé en utilisant des approches différentes, y compris une comparaison avec les données marégraphiques ainsi que des réanalyses océaniques et des sorties de modèles climatiques (pour plus de détails, voir *Ablain et al.* 2015, 2016). Cependant, même avec ces améliorations, la fermeture du bilan du GMSL en termes de variabilité interannuelle est loin d'être parfaite. Cela est illustré sur la figure Fig.2.6 ci-dessous, représentant la variabilité du GMSL CCI avec la somme des composantes du niveau de la mer "stérique Argo (2000m) + masse océan" après retrait de leurs tendances linéaires respectives sur la période janvier 2005 - décembre 2014.

En conclusion, notre étude a montré que les erreurs du signal résiduel de l'équation bilan du niveau de la mer (*Eq.2.2*) proviennent essentiellement, en termes de tendance des produits GMSL et des lacunes de la couverture géographique des données Argo dans la région Indonésienne. En termes de variabilité interannuelle, les erreurs sont attribuées aux produits GRACE et Argo. Ces résultats et la méthode utilisée montrent que le GMSL et ses composantes sont encore entachés d'erreurs importantes.

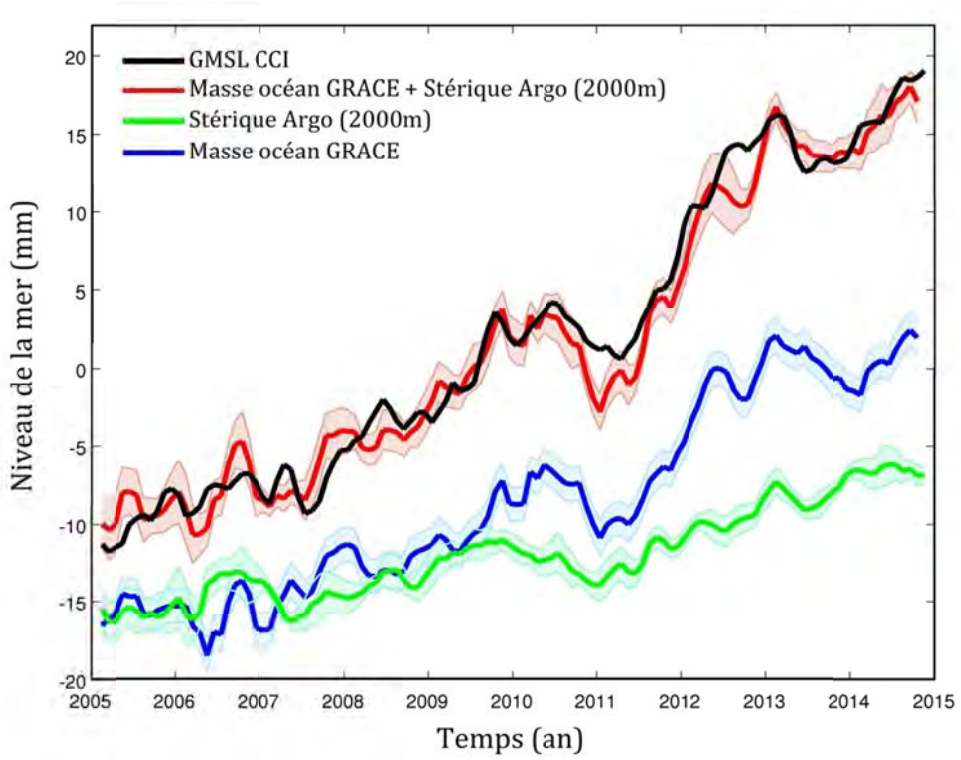

Fig.2.5 : Evolutions temporelles du niveau moyen global de la mer du CCI (noire) superposé à la somme "stérique Argo (2000m) + masse océan GRACE" (rouge ; avec erreurs associées), sur la période janvier 2005 - décembre 2014. La moyenne des 3 séries temporelles de la masse de l'océan basée sur GRACE (bleue). La moyenne des 4 produits stériques Argo (0-2000m ; verte). Les erreurs de dispersion autour de la moyenne de la masse de l'océan et du stérique sont représentées.

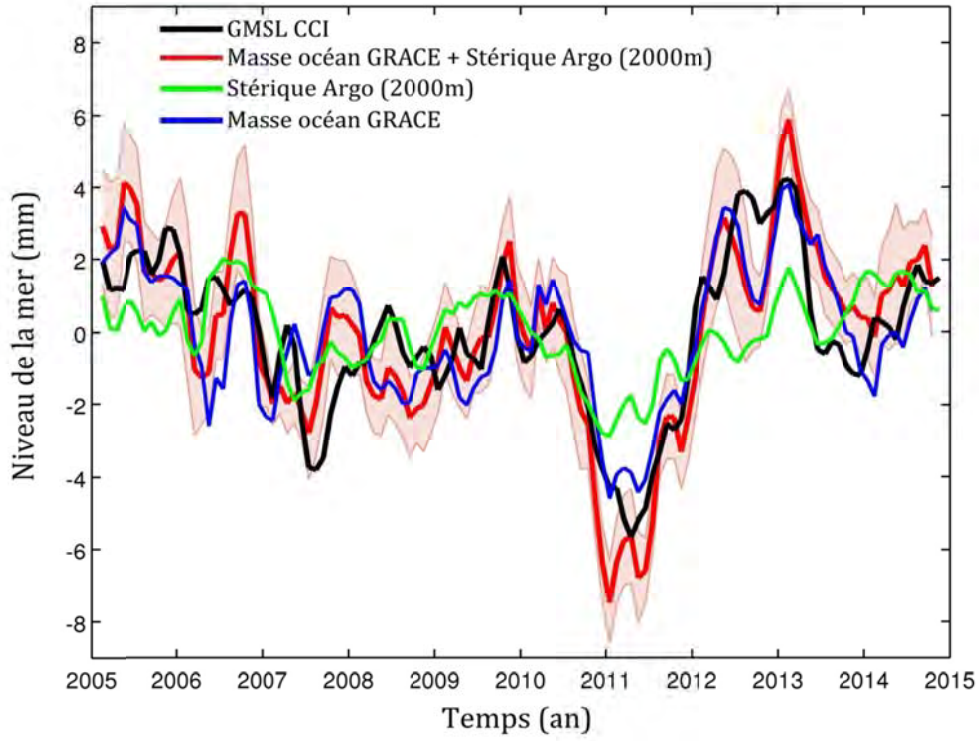

Fig.2.6 : Evolutions temporelles du GMSL du CCI (courbe noire), de la masse de l'océan basée sur GRACE (courbe bleue), du niveau de la mer stérique Argo (0-2000m ; courbe verte) et de la somme "stérique Argo (2000m) + masse océan GRACE" (courbe rouge ; avec erreurs associées), après retrait de leurs tendances linéaires respectives sur la période janvier 2005 - décembre 2014.

Ocean Sci., 11, 789–802, 2015
www.ocean-sci.net/11/789/2015/
doi:10.5194/os-11-789-2015

Ocean Science
Open Access

Sea level budget over 2005–2013: missing contributions and data errors

H. B. Dieng[1], A. Cazenave[1,2], K. von Schuckmann[3], M. Ablain[4], and B. Meyssignac[1]

[1]Laboratoire d'Etudes en Géophysique et Océanographie Spatiales – Centre National d'Etudes Spatiales (LEGOS-CNES), Toulouse, France
[2]International Space Science Institute (ISSI), Bern, Switzerland
[3]Mediterranean Institute of Oceanography (MIO), Université de Toulon, Toulon, France
[4]Collecte Localisation Satellites (CLS), Ramonville, France

Correspondence to: A. Cazenave (anny.cazenave@legos.obs-mip.fr)

Received: 7 April 2015 – Published in Ocean Sci. Discuss.: 13 May 2015
Revised: 27 July 2015 – Accepted: 30 July 2015 – Published: 6 October 2015

Abstract. Based on the sea level budget closure approach, this study investigates the residuals between observed global mean sea level (GMSL) and the sum of components (steric sea level and ocean mass) for the period January 2005 to December 2013. The objective is to identify the impact of errors in one or several components of the sea level budget on the residual time series. This is a key issue if we want to constrain missing contributions such as the contribution to sea level rise from the deep ocean (depths not covered by observations). For that purpose, we use several data sets as processed by different groups: six altimetry products for the GMSL, four Argo products plus the ORAS4 ocean reanalysis for the steric sea level and three GRACE-based ocean mass products. We find that over the study time span, the observed differences in trend of the residuals of the sea level budget equation can be as large as $\sim 0.55\,\mathrm{mm\,yr^{-1}}$ (i.e., $\sim 17\,\%$ of the observed GMSL rate of rise). These trend differences essentially result from differences in trends of the GMSL time series. Using the ORAS4 reanalysis (providing complete geographical coverage of the steric sea level component), we also show that lack of Argo data in the Indonesian region leads to an overestimate of the absolute value of the residual trend by about $0.25\,\mathrm{mm\,yr^{-1}}$. Accounting for this regional contribution leads to closure of the sea level budget, at least for some GMSL products. At short timescales (from subseasonal to interannual), residual anomalies are significantly correlated with ocean mass and steric sea level anomalies (depending on the time span), suggesting that the residual anomalies are related to errors in both GRACE-based ocean mass and Argo-based steric data. Efforts are needed to reduce these various sources of errors before using the sea level budget approach to estimate missing contributions such as the deep ocean heat content.

1 Introduction

For the 1993–2010 time span of the high-precision satellite altimetry era, the Fifth Assessment Report (AR5) of the Intergovernmental Panel on Climate Change (IPCC) reported that the rate of global mean sea level (GMSL) rise could be explained by the combined effects of land ice melt (42 %), ocean thermal expansion (34 %) and anthropogenic land water storage decrease (12 %) (Church et al., 2013). Over this period, GMSL rise observed by altimeter satellites amounted to $3.2 \pm 0.4\,\mathrm{mm\,yr^{-1}}$, a value only slightly higher than the sum of the contributions (amounting to $2.8 \pm 0.5\,\mathrm{mm\,yr^{-1}}$). Although of the same order of magnitude as associated uncertainties, the $0.4\,\mathrm{mm\,yr^{-1}}$ difference may also reflect missing contributions, e.g., the deep ocean contribution below 700 m depth where the coverage of ocean temperature data before the Argo era was poor. Estimating the deep ocean warming is an important issue in the context of the current hiatus reported since the early 2000s in global mean air and sea surface temperature evolution (e.g., Held, 2013; Trenberth and Fasullo, 2013; Smith, 2013). Different explanations have been proposed to explain the hiatus, ranging from reduced radiative forcing due to prolonged solar minimum,

increased aerosol emissions and small numerous volcanic eruptions, changes in stratospheric water vapor, enhanced heat uptake by the deep ocean, either in the Pacific or Atlantic regions (e.g., Trenberth and Fasullo, 2010, 2013; Hansen et al., 2011; Solomon et al., 2010; Guemas et al., 2013; Kosaka and Xie, 2013; Balmaseda et al., 2013a; Watanabe et al., 2013; England et al., 2014; Chen and Tung, 2014), to redistribution of heat in the Indo-Pacific region (Nieves et al., 2015). The deep ocean heat uptake has so far been the favored explanation of the hiatus considering that greenhouse gases continue to accumulate in the atmosphere at an increasing rate (Peters et al., 2012) and the Earth's energy imbalance at the top of the atmosphere is still in the range 0.5–1 Wm^{-2} (e.g., Hansen et al., 2011; Loeb et al., 2012; Trenberth et al., 2014). A recent study by Karl et al. (2015) based on reprocessing of ocean and land surface temperature data claims that there is no evidence of a hiatus during the last decade. While the hiatus is still a matter of debate, attempts to estimate whether and how much the deep ocean is warming remains an important issue. Accurate observations of sea level rise and its components (ocean thermal expansion and ocean mass change) can, in principle, help in constraining the deep ocean contribution, hence its amount of warming (e.g., von Schuckmann et al., 2014). In particular, satellite altimetry-based GMSL rise corrected for ocean mass change (for example, using GRACE space gravimetry data over the oceans) provides an estimate of the total (full depth-integrated) ocean thermal expansion (or equivalently ocean heat content). Since the year 2005, comparison with observed Argo-based ocean thermal expansion (down to $\sim$ 2000 m depth) may help to quantify any deep ocean contribution (below 2000 m). In effect, the sea level budget equation is described as follows:

$$\begin{aligned}\mathrm{GMSL} &= \text{Ocean Mass} + \text{Steric sea level (0–2000 m)} \\ &\quad + \text{Steric sea level (} > \text{2000 m)} + \text{data errors.} \end{aligned} \quad (1)$$

The residual term defined as the difference between observed GMSL and observed estimates of ocean mass and steric sea level down to 2000 m depth (see Eq. 2 below) includes the deep ocean contribution (called "Steric sea level > 2000 m") and data errors:

$$\begin{aligned}\text{Residual} &= \mathrm{GMSL} - \text{Ocean mass} - \text{Steric sea level (0–2000 m)} \\ &= \text{Steric sea level (} > \text{2000 m)} + \text{data errors.} \end{aligned} \quad (2)$$

Attempts to estimate the deep ocean contribution from the sea level budget approach were performed in two recent studies (Llovel et al., 2014; Dieng et al., 2015). Dieng et al. (2015) considered two periods (2005–2012 and 2003–2012) that correspond to the availability of new observing systems for estimating thermal expansion and ocean mass (nearly full ocean temperature and salinity coverage down to 2000 m from Argo floats and direct ocean mass measurements from GRACE space gravimetry, respectively). In Dieng et al. (2015), time series of satellite altimetry-based sea level (five different data sets), thermal expansion (eight different products; integration down to 1500 m) and ocean mass (three products) components were analyzed in order to estimate the residual term of Eq. (2). Llovel et al. (2014) performed a similar study over the 2005–2013 time span but with fewer data sets. Another attempt concerning this issue is by von Schuckmann et al. (2014). These studies came to the same conclusion; i.e., the residual term in Eq. (2) is contaminated by overly large data errors to provide any robust deep ocean contribution estimate. Here we build upon these previous studies, in particular that from Dieng et al. (2015). We focus on the 2005–2013 time span corresponding to maximized Argo coverage and compute the steric sea level component integrating the data down to 2000 m. We also include in our analysis the new sea level product from the European Space Agency (ESA) Climate Change Initiative (CCI) project (www.esa-sealevel-cci.org), available up to December 2013. The main objective of the present study is to investigate whether the residual time series of the sea level budget (Eq. 2) may be attributed to errors associated with the components (GMSL, ocean mass, steric sea level) or not. This is an important issue to be addressed before trying to estimate any missing contribution.

2 Data and method

2.1 Sea level data

We used six different products from six processing groups for the altimetry-based sea level data:

1. Validation and Interpretation of Satellite Oceanographic (AVISO; http://www.aviso.altimetry.fr/en/data/products/ocean-indicators-products/actualitesindicateurs-des-oceansniveau-moyen-des-mersindexhtml.html);
2. University of Colorado (CU Release 5; http://sealevel.colorado.edu/);
3. National Oceanographic and Atmospheric Administration (NOAA; http://www.star.nesdis.noaa.gov/sod/lsa/SeaLevelRise/LSA_SLR_timeseries_global.php);
4. Goddard Space Flight Center (GSFC version 2; http://podaac-ftp.jpl.nasa.gov/dataset/MERGED_TP_J1_OSTM_OST_GMSL_ASCII_V2);
5. Commonwealth Scientific and Industrial Research Organization (CSIRO; www.cmar.csiro.au/sealevel/sl_data_cmar.html); and
6. the CCI sea level data (http://www.esa-sealevel-cci.org/products).

The first five sea level data sets are based on Topex/Poseidon, Jason-1 and Jason-2 data averaged over the 66° S–66° N domain, except for the CSIRO data averaged over 65° S to

Table 1. Trends estimated over January 2005–December 2013 for the GMSL, global ocean mass, Argo-based steric sea level, and residuals. Errors associated with "mean global ocean mass" and "mean Argo-based steric sea level" are estimated from the dispersion around the mean.

Global mean sea level (GMSL) product	GMSL trends ($mm\,yr^{-1}$)	Residual trends ($mm\,yr^{-1}$) (residual computed with mean global ocean mass and mean Argo-based steric sea level)
AVISO	3.17	0.3
CU	2.83	−0.03
NOAA	3.26	0.42
GSFC	2.80	−0.07
CSIRO	3.35	0.49
CCI	3.11	0.26
Global ocean mass	**Global ocean mass trends ($mm\,yr^{-1}$)**	**CCI residual trends ($mm\,yr^{-1}$)**
CSR	2.01	0.28
GFZ	2.11	0.18
JPL	2.00	0.29
Mean	2.04 ± 0.08	
Argo-based steric sea level	**Argo-based steric sea level trends ($mm\,yr^{-1}$)**	**CCI residual trends ($mm\,yr^{-1}$)**
KVS	0.74 ± 0.13	0.33
IPRC	0.76	0.31
JAMSTEC	0.94 ± 0.16	0.14
SCRIPPS	0.83	0.24
Mean	0.82 ± 0.08	
ORAS4 (0–5350 m)	1.14	−0.06

65° N. For each product, a set of instrumental and geophysical corrections is applied (details are given on the websites of each data set). In addition, the effect of glacial isostatic adjustment (GIA, i.e., a small correction of $-0.3\,mm\,yr^{-1}$; Peltier, 2004) is accounted for in each sea level time series except for the NOAA data set. Thus we corrected the latter for the GIA effect, using the $-0.3\,mm\,yr^{-1}$ value (i.e., resulting in an addition of $0.3\,mm\,yr^{-1}$ to the GMSL time series). The sea level time series used in this study cover the period January 1993–December 2013. The five sea level time series (AVISO, CU, GSFC, NOAA and CSIRO) are obtained either by directly averaging the along-track sea surface height data (e.g., CU) or by firstly gridding the unevenly distributed along-track data and then performing grid averaging (e.g., AVISO and NOAA). In all cases, an area weighting is applied. In addition to the geographical averaging method, other differences exist between the GMSL data sets because of the applied geophysical and instrumental corrections and the number of satellites considered (discussion on these differences can be found in Masters et al., 2012, and Henry et al., 2014).

In the context of the ESA CCI Sea Level project, a new, improved product has been computed. It combines data from Topex/Poseidon, Jason-1 and Jason-2 with the ERS-1 and ERS-2 and Envisat missions, and is based on a new processing system with dedicated algorithms and adapted data processing strategies (Ablain et al., 2015). The main improvements include reduction of errors in the orbit solutions and wet/dry atmospheric corrections, reduction of instrumental drifts and biases, improved inter-calibration between satellite altimetry missions and optimized combination of the different sea level data sets. The CCI sea level products have been validated using different approaches, including a comparison with tide gauge records as well as with ocean re-analysis and climate model outputs (see Ablain et al., 2015, for more details). The CCI sea level data set is freely available over January 1993–December 2013.

Figure 1a shows the GMSL time series from January 2005 to December 2013 for the six products presented above. Trend values estimated over this time span are given in Table 1. We first note important trend differences between all GMSL time series, up to $0.55\,mm\,yr^{-1}$ between GFSC and CSIRO data. The lowest trends (around $2.8\,mm\,yr^{-1}$) are obtained for the CU and GSFC data sets. Higher trends (from 3.11 to $3.35\,mm\,yr^{-1}$) are obtained for CCI, AVISO, NOAA and CSIRO GMSL time series. At shorter timescales (from sub-seasonal to multi-annual), significant discrepancies of several mm are observed between the different GMSLs, especially between 2005 and 2008, and between mid-2010 and mid-2011. The latter period coincides with a strong La Niña event.

2.2 Ocean mass data

We use three different data sets for estimating the ocean mass component: the GRACE Release 05 products from the Center for Space Research of the University of Texas (CSR RL05), the Deutsches GeoForschungsZentrum (GFZ RL05) and the Jet Propulsion Laboratory (JPL RL05). The GRACE Release 05 ocean mass data have been specifically processed by D. Chambers to study the ocean mass temporal evolution (data available at http://grace.jpl.nasa.gov). In effect, gridded Release 05 data cannot be used to compute ocean mass changes because the area-weighted global mean is set to zero (as warned on the http://grace.jpl.nasa.gov/data/get-data/monthly-mass-grids-ocean website). The Chambers RL05 GRACE ocean data are publicly available from https://dl.dropboxusercontent.com/u/31563267/ocean_mass_orig.txt. They are provided as global mean (averaged over the 90° S–90° N domain) time series with associated uncertainties. The data processing is described in Johnson and Chambers (2013) (see also Chambers and Schroeter, 2011, and Chambers and Bonin, 2012). The GIA component has been subtracted from each GRACE ocean mass time series using the GIA correction computed as described in Chambers et al. (2010). Figure 1b shows the global ocean mass (called GOM hereafter) time series and associated uncertainties over 2005–2013 for the CSR, GFZ and JPL products (see also Table 1 for trend values and associated uncertainties; note that mean value uncertainties quoted in Table 1 are estimated from the dispersion between available products. These represent lower bounds of errors). All three GOM products

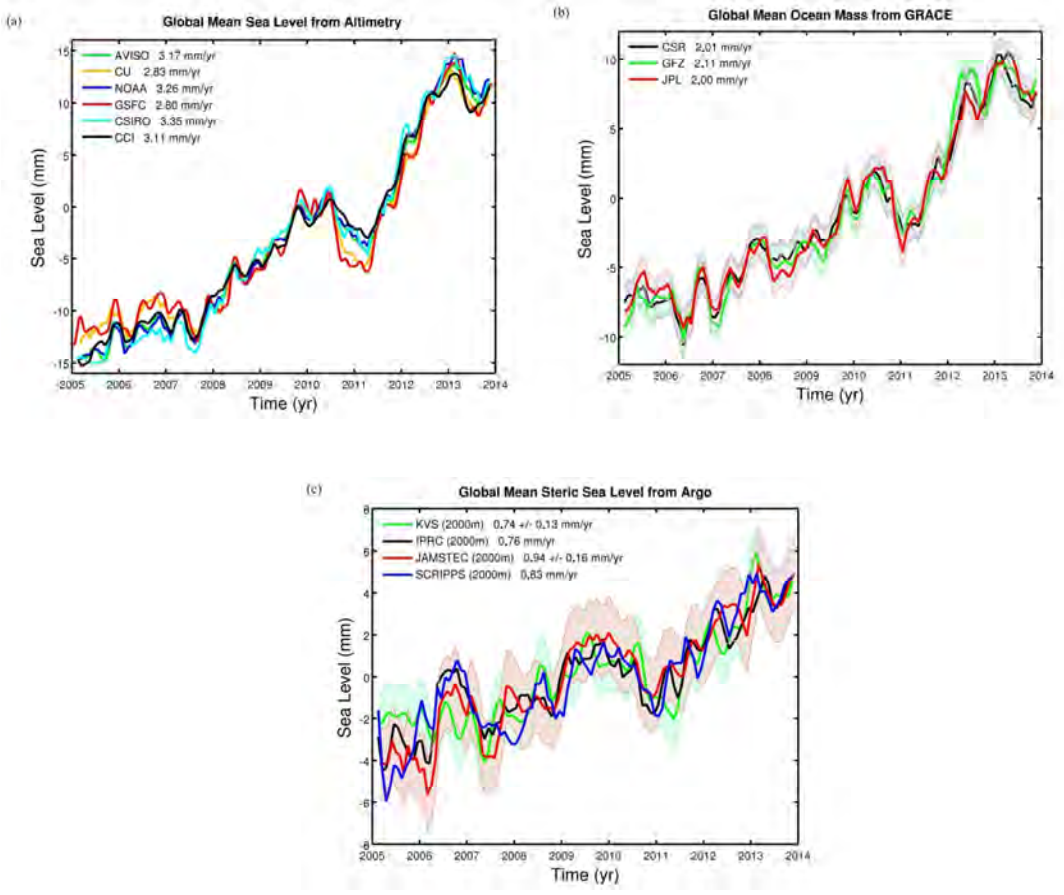

Figure 1. (a) Global mean sea level (GMSL) time series (January 2005–December 2013) from the five satellite altimetry processing groups (AVISO, CU, NOAA, GSFC and CSIRO) and CCI. **(b)** Global ocean mass (GOM) time series and associated uncertainty (shaded area) (January 2005–December 2013) from GRACE, based on the data from CSR (black curve), GFZ (green curve) and JPL (red curve). **(c)** Argo-based monthly global mean steric sea level time series (January 2005–December 2013) (integration down to 2000 m) from four processing groups (KVS, IPRC, JAMSTEC and SCRIPPS). Shaded areas represent uncertainties of the JAMSTEC and KVS steric sea level data.

are quite close to each other, in terms of both trend and short-term fluctuations.

2.3 Steric data

We used four Argo temperature and salinity data sets.

Three gridded data sets are provided by the following groups:

- the International Pacific Research Center (IPRC; http://apdrc.soest.hawaii.edu/projects/Argo/data/gridded/On_standard_levels/index-1.html);
- the Japan Agency for Marine-Earth Science and Technology (JAMSTEC; ftp://ftp2.jamstec.go.jp/pub/argo/MOAA_GPV/Glb_PRS/OI/); and
- the SCRIPPS Institution of Oceanography (SCRIPPS; http://sio-argo.ucsd.edu/RG_Climatology.html).

These data sets are available at monthly intervals on a global $1° \times 1°$ grid down to 2000 m, over the period January 2005 to December 2013, January 2001 to August 2014, and January 2004 to December 2013, respectively.

Argo data sets do not cover the whole ocean before 2005 (von Schuckmann et al., 2014; Roemmich et al., 2015). The study by Chen and Tung (2014) provides a depth coverage map of in situ temperature and salinity measurements, and we note that as of 2005, there are data up to at least 1500 m (e.g., almost full coverage down to 1200 m and 50 % coverage between 1200 and 1500 m). Thus we computed the steric sea level time series (and associated uncertainty; but note that only JAMSTEC provides errors), over January 2005–December 2013, integrating the data over the 0–2000 m depth range. The global mean steric sea level time series from IPRC, JAMSTEC and SCRIPPS are estimated over the 62.5° S–64.5° N, 60.5° S–66° N and 61.5° S–64.5° N domains, respectively.

We also used an updated version of the steric data set processed by von Schuckmann and Le Traon (2011). This data set provides steric sea level and associated uncertainty based

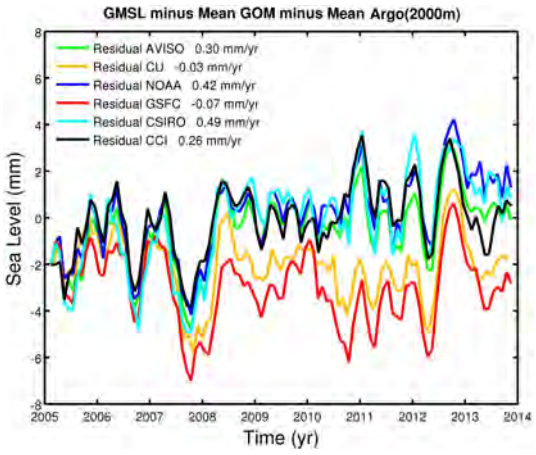

Figure 2. Residual curves (January 2005–December 2013) computed for each of the six GMSL products (AVISO, CU, NOAA, GSFC, CSIRO and CCI). Mean global ocean mass (GOM) and mean Argo-based steric sea level are used. (For example: "Residual AVISO" = "GMSL from AVISO minus Mean GOM minus Mean Argo".)

on quality-controlled Argo-based temperature and salinity data from IFREMER (http://wwz.ifremer.fr/lpo_eng/content/view/full/83074), with integration down to 2000 m depth and averaged on a $5° \times 10°$ grid. The method to derive the gridded products is described in detail in von Schuckmann and Le Traon (2011). In the following, we call this data set "KVS". The KVS data set covers the 60° S–60° N domain. Area weighting is applied to all data sets when averaging.

Figure 1c presents the four steric sea level time series and associated uncertainties (except for IPRC and SCRIPPS, for which errors are not provided) over 2005–2013. Trend values over the study time span can be found in Table 1. Figure 1c shows significant discrepancies of several mm from one time series to another at sub-seasonal to interannual timescales, in particular in the early part of the record (e.g., in 2005) and late 2007 to early 2008. Between 2005 and early 2008, the KVS time series is rather flat, unlike the other steric time series. In terms of trends, we note differences of up to $0.2\,\mathrm{mm\,yr^{-1}}$, the KVS data giving a lower steric trend than the other three (this is actually due to the rather flat start of the KVS curve in 2005).

Finally, we include the ORAS4 reanalysis from Balmaseda et al. (2013b) (https://icdc.zmaw.de/easy_init_ocean.html?&L=1#c2231). This reanalysis is based on the Nucleus for European Modelling of the Ocean (NEMO) circulation model (version 3.0) with data assimilation. Assimilated data include temperature and salinity profiles over 1958–2009 from the v2a version of the EN3 database constructed by the Met Office Hadley Centre (Good et al., 2013), along-track altimetry-based sea level anomalies and global sea level trend from AVISO, sea surface temperature and sea ice from the ERA-40 archive (prior to November 1981), from NCEP (National Centers for Environmental Prediction) OI version 2 (1981 until December 2009) and from OSTIA (Operational Sea Surface Temperature and Sea Ice Analysis; January 2010 onwards). The ORAS4 temperature and salinity data are available at monthly intervals over 42 depth levels ranging from the ocean surface down to 5350 m depth, on a global $1° \times 1°$ grid from January 1958 to December 2014 (see Balmaseda, 2013b, for more details). To estimate the ORAS4 global mean steric sea level, the data are averaged over the 66° S–66° N domain.

Steric sea level trends and associated uncertainties are gathered in Table 1.

3 Residual time series (GMSL minus ocean mass minus steric sea level)

In the following, we present the residual time series (Eq. 2, called "residuals" hereinafter) over January 2005–December 2013. The main objective is to check whether the residual anomalies are correlated – or not – with one or several components of the sea level budget (GMSL, ocean mass, steric sea level; see Eq. 1). In a first step (Sect. 4), we look at residual trends, focusing on the trend differences between the residual time series obtained with different components (and different products for each component). These differences only inform on the residual trend obtained from a given combination of products, relative to other residual trends. They say nothing about the absolute residual trend values. In Sect. 8, we also estimate uncertainty of the absolute trend of the residuals.

In a second step (Sect. 5), we try to explain the short-term (from sub-seasonal to interannual) anomalies in the detrended residual time series and investigate whether these are real signals or errors in one or several components of the sea level budget equation. For that purpose, we correlate the detrended residual with each detrended component, successively. A significant correlation of the residuals with one component of the budget equation (GMSL, ocean mass, steric sea level) may indicate that this particular component is in error. In effect, if one (or more than one) component is error free, one may expect no correlation between the short-term anomalies of the residual time series and that particular component, since in that case this component should be compensated for by the sum of the other two components of the budget equation (Eq. 1).

4 Residuals with trends

Figure 2 shows residual time series computed for each GMSL estimate (i.e., AVISO, CU, NOAA, GSFC, CSIRO and CCI), using mean values of the three GOM and four Argo-based steric sea level products. For the comparison, all curves start at the same (arbitrary) value in January 2005. Table 1 gathers the trend values over January 2005–December 2013 of the residual time series for the different data com-

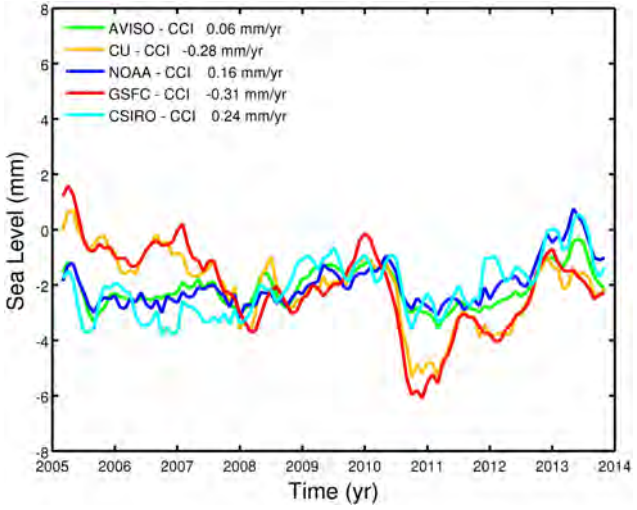

Figure 3. Time series of GMSL differences with respect to the CCI GMSL (January 2005–December 2013).

binations. Figure 2 indicates that over the January 2005–February 2007 time span, the residuals are in fairly good agreement. In late 2007 (a period coinciding with the 2007–2008 La Niña), all residuals are strongly negative. By mid-2008, we observe a step-like increase in the residuals associated with some GMSL time series (AVISO, NOAA, CSIRO and CCI), while a decrease is noticed for the CU and GSFC residuals until mid-to-late 2011. The residual trends seem to fall into two groups (see Table 1): (1) AVISO, NOAA, CSIRO and CCI, and (2) CU and GSFC, with large trend differences, $>0.5\,\mathrm{mm\,yr^{-1}}$, between them. The positive residual trends in Table 1 correspond to group 1, whereas residual trends of group 2 are negative.

Because the same "mean" ocean mass and "mean" steric sea level data are used when computing the residuals shown in Fig. 2, differences in residual trends necessarily result from trend differences in the GMSL time series. To investigate this further, we show in Fig. 3 difference time series between GMSL products, using the CCI GMSL as a reference.

The two groups of GMSL products mentioned above appear much more clearly in Fig. 3. We note that the AVISO, NOAA and CSIRO curves (corresponding to group 1) follow a different trajectory compared to the CU and GSFC curves (group 2), except during 2008–2010. This is particularly clear during 2005–2008 and to a lesser extent beyond 2010. The sources of these differences have been investigated in two recent papers by Masters et al. (2012) and Henry et al. (2014). These studies showed that the choice of the geophysical corrections applied to the data and the averaging method to calculate the GMSL from along-track data are the two main causes of differences between the GMSL time series. For example, AVISO and CU apply different averaging methods that significantly impact the GMSL products (Henry et al., 2014). Moreover, from 2005 to mid-2008, a time span corresponding to the use of Jason-1 satellite data, these groups use different orbit solutions and different corrections for ocean tides and sea surface bias, while beyond mid-2008, they use exactly the same orbit solution and same sea surface bias correction (see the respective websites for more details). Thus, differences between AVISO and CU GMSL time series are to be expected over 2005 to mid-2008. This is indeed what Fig. 3 shows over this time span. To check the CU and GSFC residual drop somewhat further, we computed the residuals trends between January 2005 and June 2008 for all GMSL time series. We find highly negative related residual trends for CU and GFSC (of -0.67 and $-0.91\,\mathrm{mm\,yr^{-1}}$, respectively), while for all other GMSL time series the residual trends are in the range -0.05 to $0.08\,\mathrm{mm\,yr^{-1}}$. Other differences noticed in Fig. 3 beyond 2010 are less clear but may be related to the averaging method with a stronger impact during the 2011 La Niña. More investigation and collaborative work between the different processing groups are needed to fully understand and reduce the reported differences in the GMSL time series.

In a next step, we examine the contribution of the ocean mass and steric components to the residual trend for each GMSL product. Figure 4a and b shows residual curves for the CCI GMSL computed with each ocean product and each steric sea level product. Results show that the different ocean mass products show almost similar residual trends (up to $\sim 0.1\,\mathrm{mm\,yr^{-1}}$ trend differences are noted; see Fig. 4a). For the Argo products, their effect on the trend differences is $<0.2\,\mathrm{mm\,yr^{-1}}$ (see Fig. 4b). We do not show similar figures for other GMSL products because the differences in the residual trends computed between all Argo products (and all ocean mass products as well) are similar to those computed with the CCI GMSL.

From this section, we conclude that trend differences observed in the residual time series (Fig. 2) are dominated by differences in the altimetry-based GMSL products.

5 Detrended residuals

Figure 2 shows that the residual time series also display important high-frequency (sub-seasonal to interannual) anomalies of up to 4 mm amplitude. These anomalies are highly correlated for all GMSL products, in particular for AVISO, NOAA, CSIRO and CCI data sets. In the following, we analyze the detrended residual time series. Only three GMSL data sets are considered: the AVISO, CU and CCI GMSL data (AVISO and CU being representative of group 1 and group 2, respectively). In order to understand whether a given variable (GMSL, ocean mass or steric sea level) is responsible for all – or part – of the observed short-term (from sub-seasonal to interannual) residuals, we correlate this variable (trend removed) with its associated (detrended) residual. What we would expect, if all data sets were error free, is to see no correlation between the detrended variable and its

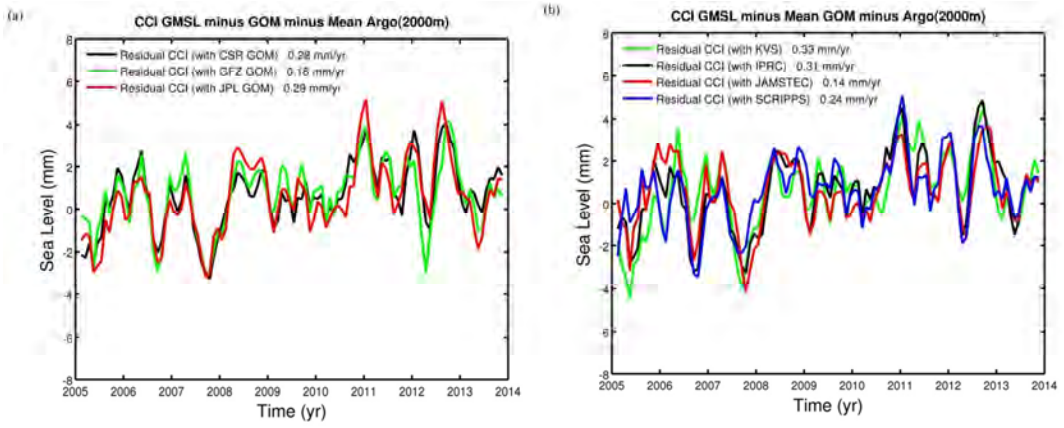

Figure 4. Residual sea level time series (January 2005–December 2013) computed with the CCI GMSL. (**a**) Mean of the four Argo products and each GOM product; (**b**) mean of the three global ocean mass (GOM) data sets and each Argo product.

Table 2. Correlations estimated between detrended residual time series and the associated detrended component. Estimated rms of the corresponding detrended residual time series.

Global mean sea level (GMSL) product	The rms of the residual computed with mean global ocean mass and mean Argo-based steric sea level (mm)	Correlation (detrended GMSL and associated detrended residual)
CCI	1.38	0.02
AVISO	1.32	0.26
CU	1.36	0.55
GRACE-based global ocean mass product	**The rms of the CCI residual computed with mean Argo-based steric sea level (mm)**	**Correlation (detrended global ocean mass and associated detrended residual)**
CSR	1.37	0.46
GFZ	1.46	0.55
JPL	1.56	0.57
Argo-based steric sea level (0–2000 m)	**The rms of the CCI residual computed with mean global ocean mass (mm)**	**Correlation (detrended steric sea level and associated detrended residual)**
KVS	1.59	0.53
IPRC	1.56	0.51
JAMSTEC	1.56	0.51
SCRIPPS	1.45	0.50

associated (detrended) residual. Therefore, a low correlation may be interpreted as a "good result", i.e., little contamination by errors of the associated variable. Such an interpretation may not be unique however. Limitations of this approach are discussed in Sect. 6.

5.1 GMSL short-term (from sub-seasonal to interannual) errors

To analyze the impact of the short-term GMSL errors on the residuals, we simply superimpose the detrended GMSL with its associated residual (also detrended). Figure 5a–c shows, for AVISO, CU and CCI data, the detrended residual curves and associated detrended GMSL. In Table 2 are given the correlation between the detrended residual curve and its associated detrended GMSL as well as the root-mean squares (rms) of the residual time series. On sub-seasonal to interannual timescales, most of the observed GMSL anomalies have been reduced after subtracting the ocean mass and steric sea level components from the GMSL data. Nevertheless, some anomalies still remain (see Fig. 5a–c). This is particularly striking for the 2007–2008.5 time span. This period corresponds to a La Niña event. While the 2011 La Niña is well explained by the mass plus steric components (see Boening et al., 2012, and Cazenave et al., 2014), it is surprising that the same data sets do not explain the negative GMSL anomaly related to the 2007–2008 La Niña. During the period February 2007 to June 2008, the correlation computed between the CCI, AVISO and CU residual curves and associated detrended GMSL amounts to 0.79, 0.89 and 0.92, respectively. This high correlation and amplitude comparison suggests that the residual anomaly during this particular time span at least partly comes from the GMSL data. We cannot rule out however that the steric or ocean mass components also contribute. We will indeed see below that the observed discrepancy at this particular date also partly arises from errors in the GRACE and Argo data.

Over the whole time span (2005–2013), the correlations are 0.02, 0.26 and 0.55 for the CCI, AVISO and CU GMSL, respectively (see Table 2). The lowest correlation is obtained for the CCI data, indicating that the CCI residuals contain fewer GMSL short-term errors than the other two data sets.

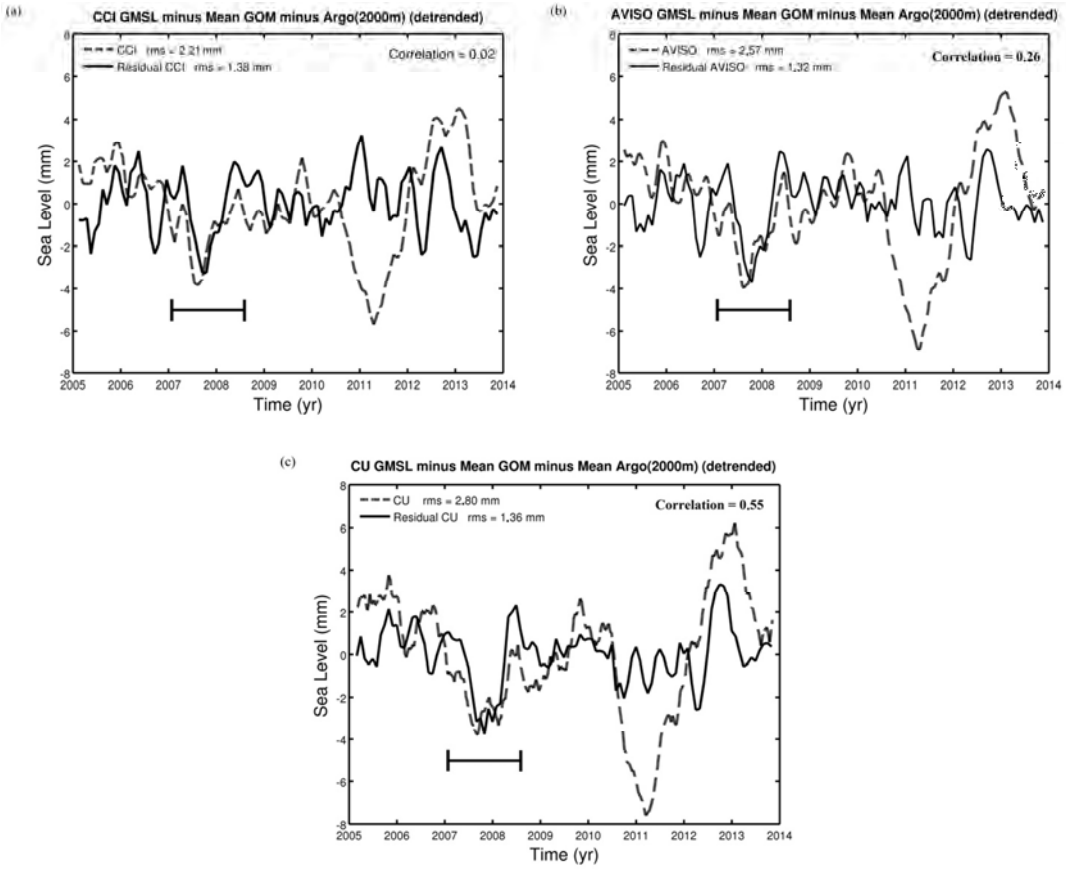

Figure 5. Detrended residual time series (January 2005–December 2013) (mean global ocean mass (GOM) and mean Argo-based steric sea level are used to compute the residual) for CCI (**a**), AVISO (**b**), and CU (**c**). The detrended GMSL from CCI, AVISO and CU are superimposed on each residual, respectively.

5.2 Short-term (from sub-seasonal to interannual) errors in the global ocean mass

We perform a similar comparison with the GRACE-based ocean mass products. For that purpose we only consider a single GMSL data set (i.e., CCI) and superimpose the detrended CCI residual time series computed separately for each ocean mass product with the corresponding detrended GRACE data set. These are shown in Fig. 6a–c. In Table 2 are given the correlation between the detrended residual curve and its associated detrended ocean mass component. The rms of the residual time series are also given.

The correlation is relatively high in all three cases, 0.46, 0.55 and 0.57 for the CSR, GFZ and JPL data, respectively. The detrended global ocean mass and residual time series coincide almost perfectly between mid-2006 and mid-2007 and between mid-2009 and early 2012 (Fig. 6). This indicates that the short-term residual errors are largely affected by errors in GRACE-based ocean mass products. During the 2007–2008 La Niña, we also observe a significant correlation between the detrended ocean mass and associated residual of 0.57, 0.69 and 0.69, respectively, for the CSR, GFZ and JPL data.

5.3 Short-term (from sub-seasonal to interannual) Argo-based steric sea level errors

The rms of the residual time series based on the IPRC, JAMSTEC, SCRIPPS and KVS Argo data (linear trend removed from each time series) are in the range 1.3–1.6 mm (see Fig. 7 and Table 2). The lowest rms are obtained with SCRIPPS data when using the CCI and CU GMSL. For AVISO, the lowest rms are obtained with the KVS steric sea level. Overall, no best Argo product emerges, rms differences being small.

As mentioned previously, in the early part of the time series (2005–2006), we note larger dispersion between all Argo products compared to the subsequent years. These differences can be explained by a still incomplete global coverage of Argo data during this period (Lyman and Johnson, 2014; Roemmich et al., 2015). We note that the negative anomaly coinciding with the 2007–2008 La Niña is still present in the residual curves, with almost the same amplitude as in the

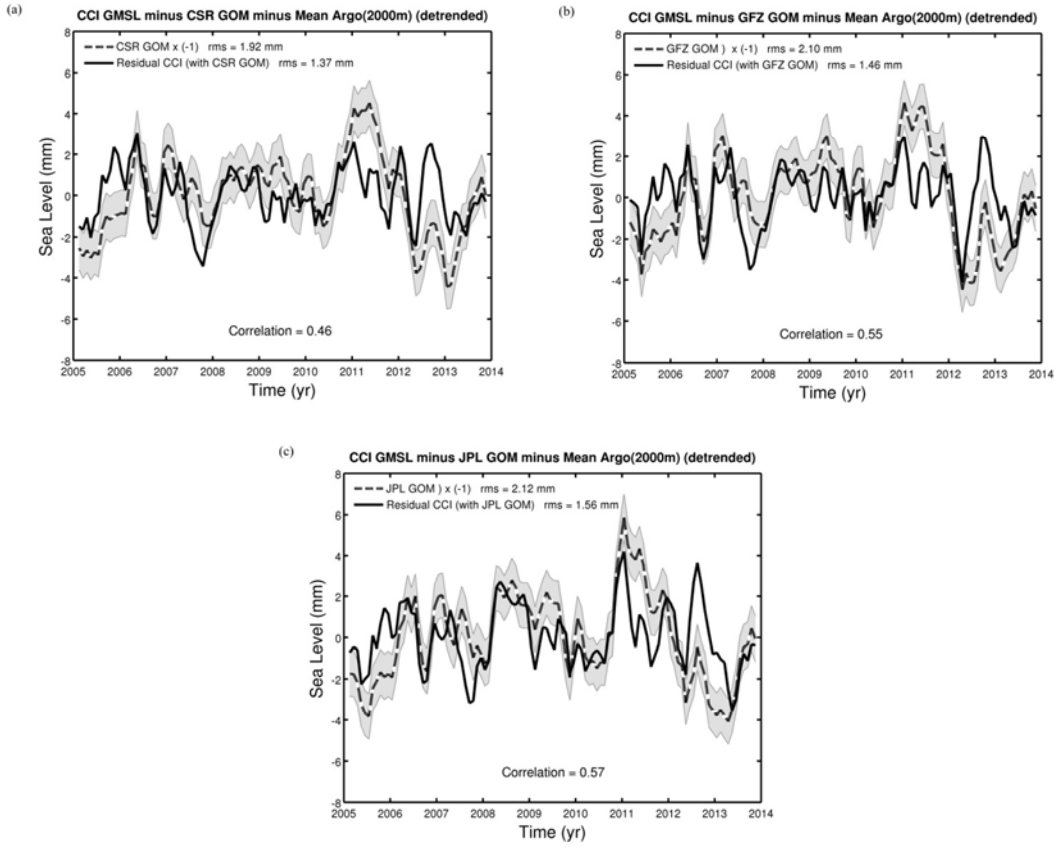

Figure 6. Detrended residual time series (January 2005–December 2013) computed with the CCI GMSL, mean Argo-based steric sea level and different ocean mass products. Associated detrended global ocean mass (GOM) time series superimposed. (**a**) CSR; (**b**) GFZ; (**c**) JPL.

GMSL data, indicating that the GMSL, or the mass or the Argo-based steric components (or all of them), are in error at that particular date.

We next examine the correlation between the residual time series and the detrended steric sea level, considering each Argo product successively. Figure 8a–d shows the detrended residual time series computed with the CCI GMSL superimposed on the detrended steric sea level time series. Each of the four steric products (SCRIPPS, IPRC, JAMSTEC and KVS) is considered. In each case the mean global ocean mass is used for computing the residual.

Examination of Fig. 8 shows that lowest residual rms are obtained with the SCRIPPS time series, but the rms difference with other Argo products is small. We also note that the short-term residual fluctuations are significantly correlated with the associated (detrended) Argo-based steric sea level time series at some periods, for example between mid-2010 and mid-2013, and especially when using the IPRC data. This indicates that the short-term fluctuations of the residuals partly reflect Argo-based steric sea level errors during this period.

5.4 Sea level budget using the ORAS4 ocean reanalysis

Errors in Argo-based steric sea level estimates arise from different sources (gaps in some regions, data editing, mapping techniques, etc.; Abraham et al., 2013; Lyman and Johnson, 2014; von Schuckmann et al., 2014). To investigate further the effect of Argo sampling, as well as other Argo data processing errors, on the residual time series, we recomputed the residuals using steric data from the ORAS4 ocean reanalysis (Balmaseda et al., 2013b). The integration is performed over the whole ocean depth range (0–5350 m) and between 66° S and 66° N. Figure 9 shows the residual time series computed with the CCI GMSL and the mean of the four Argo products (black curve) and ORAS4 data (dotted curve). The detrended CCI GMSL is superimposed. Differences in residuals shown in Fig. 9 directly result from differences in the steric time series (all other parameters being the same). In terms of residual rms, we see little difference between the considered steric sea level products, even if at some periods (e.g., between mid-2010 and mid-2011) the steric curves do not agree very well with each other. For most of the time span, there is good coherence between the mean of the four Argo time series and ORAS4. However, the correlation be-

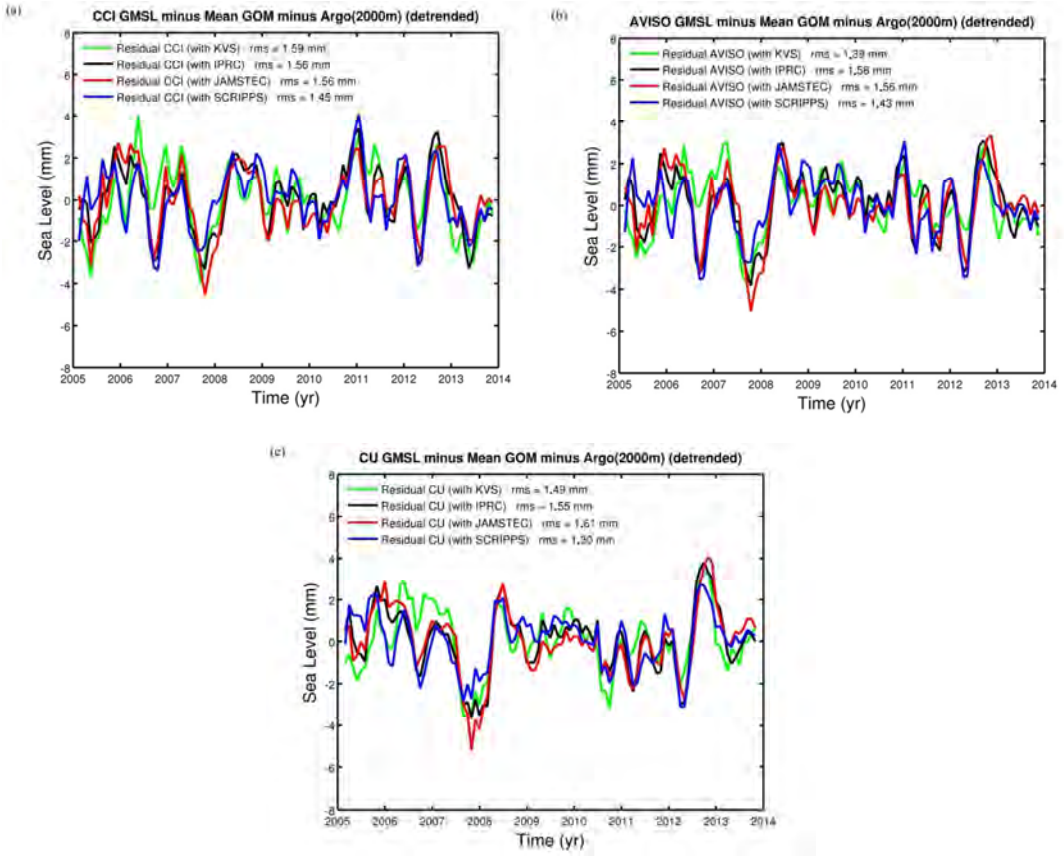

Figure 7. Residual time series (January 2005–December 2013) computed for each of the three GMSL: CCI (**a**), AVISO (**b**), and CU (**c**). Mean global ocean mass (GOM) and each of the four steric sea level products (IPRC, JAMSTEC, SCRIPPS and KVS) are used for computing the residuals.

tween the residuals and the detrended CCI GMSL is slightly lower when using the mean of the four Argo products than when using the reanalysis.

6 Limitation of the approach presented in Sect. 5 (detrended analysis)

One important objection that can be made to our approach is the following: suppose for example that only the GMSL and steric time series are in error (e.g., affected by white noise) and that the ocean mass data are perfect. Then, corresponding residuals and ocean mass time series would be correlated. Following the logic of our approach, one may thus conclude that it is the ocean mass that is in error. To investigate this potential drawback, we did the following test.

1. We first computed a "perfect" ocean mass time series from the difference between (observed) mean GMSL and mean Argo-based steric sea level.

2. Next, we applied a random noise to the mean GMSL and mean steric time series. Two cases have been considered: case 1 corresponds to a random error between -2 and $+2$ mm; case 2 corresponds to a random error between -4 and $+4$ mm (corresponding to typical data uncertainties at interannual timescales). One-hundred drawings of lots have been performed for each case.

3. Then, we computed the corresponding residual time series (i.e., noisy GMSL minus noisy steric sea level minus perfect ocean mass), and correlated these with the "perfect" ocean mass time series.

Figure 10 shows a plot of these new correlations for the two cases. We note that most correlations fall below those of the nominal case (as described in Sect. 5.2). For case 1, in 82 % of the simulations, the correlation worsens. For case 2, this number increases to 92 %. We conclude that if the ocean mass time series is perfect and the GMSL and steric sea level data are noisy, the residuals appear poorly correlated with the ocean mass time series. Thus, a high correlation very likely reflects errors in the mass component.

In Sect. 5 (detrended residuals), we investigated temporally correlated errors between the three data sets (GMSL, steric sea level, ocean mass). This was the motivation for applying a correlation approach. The test described above

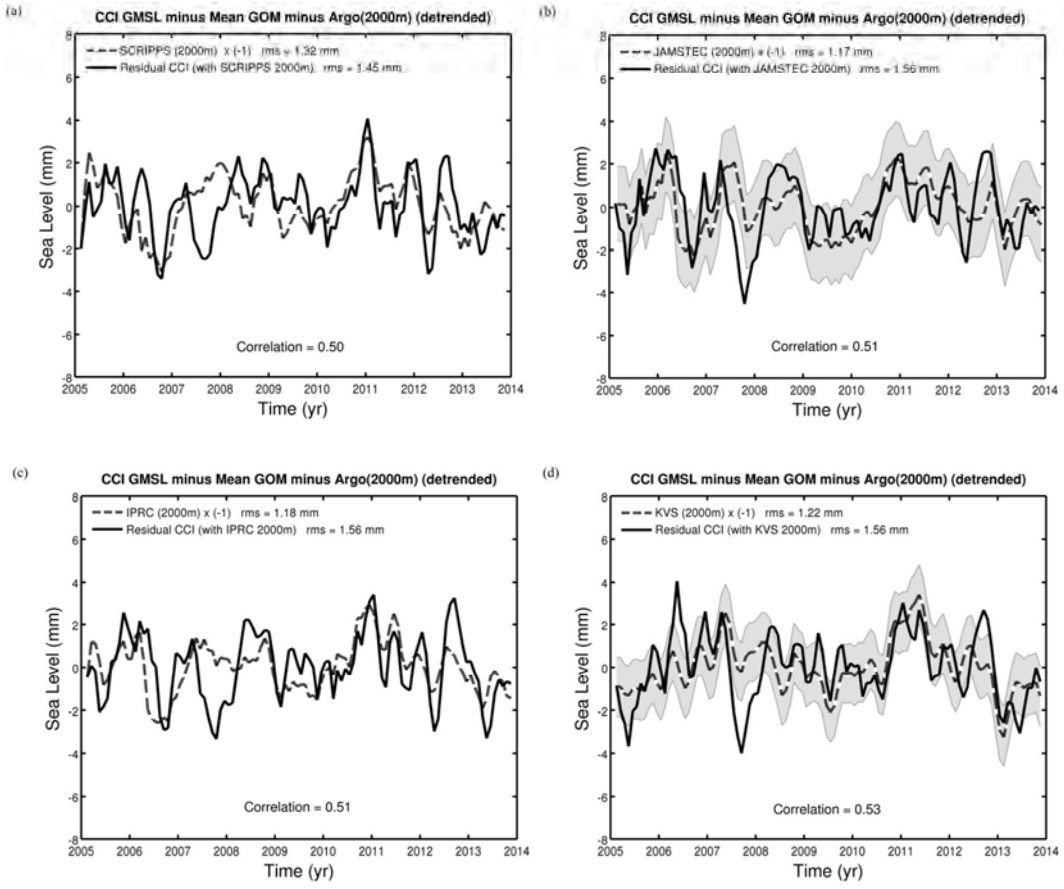

Figure 8. Detrended residual time series of CCI GMSL (January 2005–December 2013) computed with the mean global ocean mass (GOM) and each of the four steric sea level products: SCRIPPS (**a**), JAMSTEC (**b**), IPRC (**c**), and KVS **(d)**; superimposed, the corresponding detrended steric sea level time series.

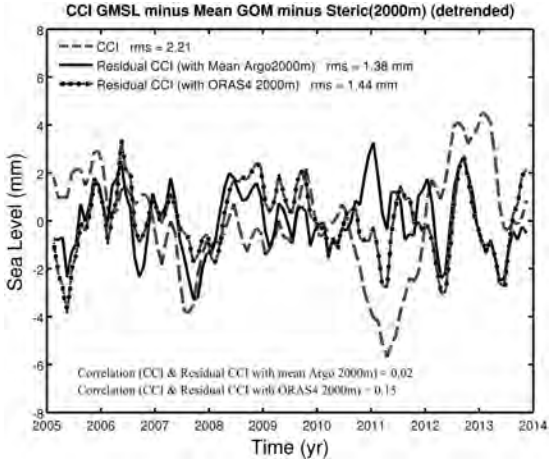

Figure 9. Residual time series (January 2005–December 2013) computed with the CCI GMSL, and the mean of the four Argo products (black curve) and ORAS4 data (dotted curve). The detrended CCI GMSL is superimposed (dashed curve).

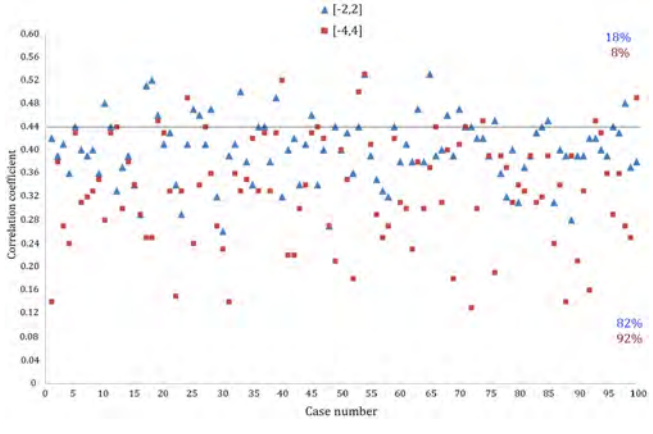

Figure 10. Correlation coefficient between residuals computed from noisy GMSL, noisy steric sea level and perfect ocean mass for 100 drawings of lots. Blue and red points correspond to cases 1 and 2, respectively (see text). The horizontal black line is the correlation of the nominal case (as described in Sect. 5.2).

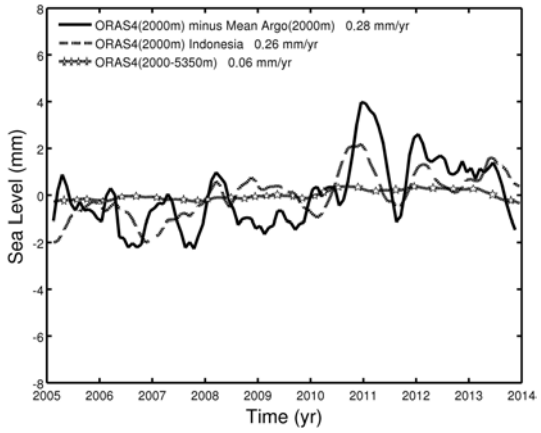

Figure 11. Steric sea level difference ORAS4 minus mean Argo time series (trend not removed) (black curve) (January 2005–December 2013) up to 2000 m depth. The dashed curve is the Indonesian steric sea level time series estimated from ORAS4 up to 2000 m depth. The starry curve is the steric sea level time series from ORAS4 below 2000 m depth.

shows that the proposed method is meaningful and that the conclusions drawn in Sect. 5 are largely valid.

7 Contribution of the Indonesian region and other areas not covered by Argo; uncertainty in the absolute residual trend

The ORAS4 minus mean Argo time series (integration down to 2000 m; trend not removed) is shown in Fig. 11. It displays significant short-term fluctuations, up to 4 mm, and a trend of 0.28 mm yr^{-1} (the ORAS4 steric trend being larger than the mean Argo trend). The ORAS4 reanalysis provides gridded steric data with no gaps, unlike the Argo products. In effect, the coverage of Argo data is not fully global, some regions (e.g., the Indonesian region and the Gulf of Mexico) not being covered. In Fig. 11, the ORAS4 contribution for the 2000–5350 m depth layer is also shown. It only explains the 0.06 mm yr^{-1} sea level trend and (as expected) shows no short-term anomalies, as seen in the residual curve when using Argo. It is likely that both trend difference and short-term anomalies seen in ORAS4 minus Argo time series result from gaps in the Argo geographical coverage (von Schuckmann et al., 2014). This is illustrated also in Fig. 11, which shows the steric sea level contribution from the Indonesian region (0–2000 m layer) computed with ORAS4. Part of the short-term anomalies of the difference curve is due to the lack of Argo data in this region (e.g., in 2011, coinciding with the La Niña event). Moreover, in terms of trend, the Indonesian region explains about the whole trend difference between Argo-based and ORAS4-based steric sea level. This suggests that the steric sea level trend estimated when using Argo is underestimated by ~ 0.25 mm yr^{-1}. Hence, the residual (GMSL minus steric sea level minus ocean mass) trend may be in error (i.e., overestimated) by about this amount. This has important implications for the missing contributions derived from the sea level budget approach.

8 Conclusion

In this study, we estimated the sea level budget over the 2005–2013 time span using a large set of different observational products for the satellite altimetry-based sea level (six products), GRACE-based ocean mass (three products) and steric sea level (five data sets). We analyzed the residual time series (i.e., observed GMSL minus the sum of mass plus steric components) and attempted to attribute an error source to the residual trends and short-term residual anomalies. We found that errors in the GMSL products have a large impact on the residual trends. Trend differences of up to 0.55 mm yr^{-1} between the different GMSL time series are reported. Such trend differences actually prevent one from accurately constraining missing contributions. These trend differences largely arise from differences in processing the Jason-1 satellite data (e.g., choice of the averaging method and geophysical corrections), as previously discussed by Masters et al. (2012) and Henry et al. (2014). While trying to identify the outliers and select the best corrections to be used is beyond the scope of the present study, we stress that this is definitely an important goal to pursue in the future.

In terms of absolute residual trends, we identified the contribution of the Indonesian region, not covered by Argo, as contributing about 0.25 mm yr^{-1} (the computed residual trends being overestimated by about this amount). Contributions from other regional gaps in the Argo coverage (e.g., the Gulf of Mexico) estimated using ORAS4 data are found to be negligible as far as absolute residual trends are concerned. Thus, if we account for the residual trend overestimate due to lack of Argo data in the Indonesian region, the residuals computed with the CCI, AVISO and NOAA GMSL data (using Argo) become close to zero (i.e., 0.00 mm yr^{-1}, 0.04 mm yr^{-1} and 0.16 mm yr^{-1}, respectively), while residual trends computed with the CU and GSFC data become negative (-0.29 mm yr^{-1} and -0.33 mm yr^{-1}, respectively).

This suggests that the sea level budget can be closed when using the CCI, AVISO and NOAA data. Hence, in these cases, the deep ocean (below 2000 m) contribution appears negligible. It is worth mentioning that the residual trend (with the CCI GMSL) amounts to about zero (exactly 0.00 mm yr^{-1}) when using ORAS4 (0–2000 m; Indonesian region accounted for), in agreement with the above statements. Moreover, as mentioned above, the ORAS4 steric sea level trend for the 2000–5350 m depth range amounts to 0.06 mm yr^{-1}. However, further investigation is needed on that issue before drawing any definitive conclusion.

Another result from our study is the attribution of the short-term (from sub-seasonal to interannual) anomalies of the residual time series to errors in both Argo-based steric sea level and GRACE-based ocean mass. Short-term errors

in these two components sometimes act in concert (thus amplifying the residual errors, e.g., during the 2007–2008 La Niña) or affect the residuals at different periods (e.g., over 2011–2014 for Argo, or in 2006 for GRACE).

To summarize the findings of this study, the main source of differences reported in the residual trends appears to be related to altimetry-based sea level data processing. In terms of absolute residual trends, missing Argo data in the Indonesian region contribute as much as $0.25\,\mathrm{mm\,yr^{-1}}$. Accounting for this value leads to closure of the sea level budget, at least with the CCI, AVISO and NOAA GMSLs. At subseasonal to interannual timescales, the main source of uncertainty arises from short-term errors in GRACE and Argo data. More work is required by the different communities involved in either satellite altimetry or GRACE and Argo data processing, to clearly identify the causes of these errors and reduce/eliminate them. This is a challenge of primary importance if we want to precisely address a number of key issues, like the deep ocean heat uptake and its role in the current "hiatus".

Acknowledgements. We thank M. Balmaseda for providing us with the ORAS4 reanalysis data set. We also thank J. François Legeais and L. Zawadski for helpful discussions about errors in altimetry data processing. H. B. Dieng is supported by a PhD grant from the European Space Agency in the context of the Climate Change Initiative Programme.

Edited by: J. M. Huthnance

References

Ablain, M., Cazenave, A., Larnicol, G., Balmaseda, M., Cipollini, P., Faugère, Y., Fernandes, M. J., Henry, O., Johannessen, J. A., Knudsen, P., Andersen, O., Legeais, J., Meyssignac, B., Picot, N., Roca, M., Rudenko, S., Scharffenberg, M. G., Stammer, D., Timms, G., and Benveniste, J.: Improved sea level record over the satellite altimetry era (1993–2010) from the Climate Change Initiative project, Ocean Sci., 11, 67–82, doi:10.5194/os-11-67-2015, 2015.

Abraham, J. P., Baringer, M., Bindoff, N. L., Boyer, T., Cheng, L. J., Church, J. A., Conroy, J. L., Domingues, C. M., Fasullo, J. T., Gilson, J., Goni, G., Good, S. A., Gorman, J. M., Gouretski, V., Ishii, M., Johnson, G. C., Kizu, S., Lyman, J. M., Macdonald, A. M., Minkowycz, W. J., Moffitt, S. E., Palmer, M. D., Piola, A. R., Reseghetti, F., Schuckmann, K., Trenberth, K. E., Velicogna, I., and Willis, J. K.: A review of global ocean temperature observations: implications for ocean heat content estimates and climate change, Rev. Geophys., 51, 450–483, doi:10.1002/rog.20022, 2013.

Balmaseda, M. A., Trenberth, K., and Kallen, E.: Distinctive climate signals in reanalysis of global ocean heat content, Geophys. Res. Lett., 40, 1–6, doi:10.1002/grl.50382, 2013a.

Balmaseda, M. A., Mogensen, K., and Weaver, A. T.: Evaluation of the ECMWF ocean reanalysis system ORAS4, Q. J. Roy. Meteorol. Soc., 139, 1132–1161, doi:10.1002/qj.2063, 2013b.

Boening, C., Willis, J. K., Landerer, F. W., and Nerem, R. S.: The 2011 La Niña: so strong, the oceans fell, Geophys. Res. Lett., 39, L19602, doi:10.1029/2012GL053055, 2012.

Cazenave, A., Dieng, H., Meyssignac, B., von Schuckmann, K., Decharme, B., and Berthier, E.: The rate of sea level rise, Nature Climate Change, 4, 358–361, doi:10.1038/NCLIMATE2159, 2014.

Chambers, D. P. and Bonin, J. A.: Evaluation of Release-05 GRACE time-variable gravity coefficients over the ocean, Ocean Sci., 8, 859–868, doi:10.5194/os-8-859-2012, 2012.

Chambers, D. P. and Schroeter, J.: Measuring ocean mass variations from satellite gravimetry, J. Geodyn., 52, 333–343, 2011.

Chambers, D. P., Wahr, J., Tamisiea, M. E., and Nerem, R. S.: Ocean mass from GRACE and glacial isostatic adjustment, J. Geophys. Res., 115, B11415, doi:10.1029/2010JB007530, 2010.

Chen, X. and Tung, K.-K.: Varying planetary heat sink led to global warming slowdown and acceleration, Science, 345, 897–903, 2014.

Church, J. A., Clark, P. U., Cazenave, A., Gregory, J. M., Jevrejeva, S., Levermann, A., Merrifield, M. A., Milne, G. A., Nerem, R. S., Nunn, P. D., Payne, A. J., Pfeffer, W. T., Stammer, D., and Unnikrishnan, A. S.: Sea level change, in: Climate Change 2013: The Physical Science Basis. Contribution of Working Group I to the Fifth Assessment Report of the Intergovernmental Panel on Climate Change, edited by: Stocker, T. F., Qin, D., Plattner, G.-K., Tignor, M., Allen, S. K., Boschung, J., Nauels, A., Xia, Y., Bex, V., and Midgley, P. M., Cambridge University Press, Cambridge, UK and New York, NY, USA, 2013.

Dieng, H. B., Palanisamy, H., Cazenave, A., Meyssignac, B., and von Schuckmann, K.: The sea level budget since 2003: inference on the deep ocean heat content, Surv. Geophys., 36, 209–229, doi:10.1007/s10712-015-9314-6, 2015.

England, M. H., McGregor, S., Spence, P., Meehl, G. A., Timmermann, A., Cai, W., Gupta, A. S., McPhaden, M. J., Purich, A., and Santoso, A.: Recent intensification of wind-driven circulation in the pacific and the ongoing warming hiatus, Nature Climate Change, 4, 222–227, 2014.

Good, S. A., Martin, M. J., and Rayner, N. A.: EN4: quality controlled ocean temperature and salinity profiles and monthly objective analyses with uncertainty estimates, J. Geophys. Res.-Oceans, 118, 6704–6716, doi:10.1002/2013JC009067, 2013.

Guemas, V., Doblas-Reyes, F. J., Andreu-Burillo, I., and Asif, M.: Retrospective prediction of the global warming slowdown in the past decade, Nature Climate Change, 3, 649–653, doi:10.1038/nclimate1863, 2013.

Hansen, J., Sato, M., Kharecha, P., and von Schuckmann, K.: Earth's energy imbalance and implications, Atmos. Chem. Phys., 11, 13421–13449, doi:10.5194/acp-11-13421-2011, 2011.

Held, I. M.: The cause of the pause, Nature, 501, 318–319, 2013.

Henry, O., Ablain, M., Meyssignac, B., Cazenave, A., Masters, D., Nerem, S., Leuliette, E., and Garric, G.: Investigating and reducing differences between the satellite altimetry-based global mean sea level time series provided by different processing groups, J. Geodesy, 88, 351–361, doi:10.1007/s00190-013-0687-3, 2014.

Johnson, G. C. and Chambers, D. P.: Ocean bottom pressure seasonal cycles and decadal trends from GRACE Release-05: Ocean circulation implications, J. Geophys. Res.-Oceans, 118, 4228–4240, doi:10.1002/jgrc.20307, 2013.

Karl, T. R., Arguez, A., Huang, B., Lawrimore, J. H., McMahon, J. R., Menne, M. J., Peterson, T. C., Vose, R. S., and Zhang, H.: Possible artifacts of data biases in the recent global surface warming hiatus, Science, 348, 1469–1472, doi:10.1126/science.aaa5632, 2015.

Kosaka, Y. and Xie, S.-P.: Recent global warming hiatus tied to equatorial Pacific surface cooling, Nature, 501, 403–407, 2013.

Llovel, W., Willis, J. K., Landerer, F. W., and Fukumori, I.: Deep-ocean contribution to sea level and energy budget not detectable over the past decade, Nature Climate Change, 4, 1031–1035, doi:10.1038/NCLIMATE2387, 2014.

Loeb, N. G., Kato, S., Su, W. Y., Wong, T. M., Rose, F. G., Doelling, D. R., and Huang, X. L.: Advances in understanding top-of-atmosphere radiation variability from satellite observations, Surv. Geophys., 33, 359–385, doi:10.1007/s10712-012-9175-1, 2012.

Lyman, J. M. and Johnson, G. C.: Estimating global ocean heat content changes in the upper 1800 m since 1950 and the influence of climatology choice, J. Climate, 27, 1945–1957, doi:10.1175/JCLIM-D-12-00752.1, 2014.

Masters, D., Nerem, R. S., Choe, C., Leuliette, E., Beckley, B., White, N., and Ablain, M.: Comparison of global mean sea level time series from TOPEX/Poseidon, Jason-1, and Jason-2, Mar. Geod., 35, 20–41, 2012.

Nieves V., Willis J. K., and Patzert W. C.: Recent hiatus caused by decadal shift in Indo-Pacific heating, Science, 1, 532–535, doi:10.1126/science.aaa4521, 2015.

Peltier, W. R.: Global glacial isostasy and the surface of the ice-age Earth: the ICE-5G (VM2) model and GRACE, Annu. Rev. Earth Pl. Sc., 32, 111–149, 2004.

Peters, G. P., Marland, G., Le Queré, C., Boden, T., Canadell, J. G., and Raupach, M. R.: Rapid growth in CO_2 emissions after the 2008–2009 global financial crisis, Nature Climate Change, 2, 2–4, 2012.

Roemmich, D., Church, J., Gilson, J., Monselesan, D., Sutton, P., and Wijffels, S.: Unabated planetary warming and its ocean structure since 2006, Nature Climate Change, 5, 240–245, doi:10.1038/NCLIMATE2513, 2015.

Smith, D.: Has global warming stalled?, Nature Climate Change, 3, 618–619, doi:10.1038/nclimate1938, 2013.

Solomon, S., Rosenlof, K., Portmann, R., Daniel, J., Davis, S., Sanford, T., and Plattner, G.-K.: Contributions of stratospheric water vapour to decadal changes in the rate of global warming, Science, 327, 1219–1223, doi:10.1126/science.1182488, 2010.

Trenberth, K. E. and Fasullo, J. T.: Tracking Earth's energy, Science, 328, 316–317, 2010.

Trenberth, K. E. and Fasullo, J. T.: An apparent hiatus in global warming?, Earth's Future, 1, 19–32, doi:10.1002/2013EF000165, 2013.

Trenberth, K. E., Fasullo, J. T., and Balmaseda, M. A.: Earth's Energy imbalance, J. Climate, 27, 3129–3144, doi:10.1175/JCLI-D-13-00294.1, 2014.

von Schuckmann, K. and Le Traon, P.-Y.: How well can we derive Global Ocean Indicators from Argo data?, Ocean Sci., 7, 783–791, doi:10.5194/os-7-783-2011, 2011.

von Schuckmann, K., Sallée, J.-B., Chambers, D., Le Traon, P.-Y., Cabanes, C., Gaillard, F., Speich, S., and Hamon, M.: Consistency of the current global ocean observing systems from an Argo perspective, Ocean Sci., 10, 547–557, doi:10.5194/os-10-547-2014, 2014.

Watanabe, M., Kamae, Y., Yoshimori, M., Oka, A., Sato, M., Ishii, M., Mochizuki, T., and Kimoto, M.: Strengthening of ocean heat uptake efficiency associated with the recent climate hiatus, Geophys. Res. Lett., 40, 3175–3179, doi:10.1002/grl.50541, 2013.

2.3.3 Cycle global de l'eau : estimation de la contribution totale des eaux continentales à la hausse du niveau moyen global de la mer

Les réservoirs terrestres (rivières, lacs, réservoirs artificiels, zones humides et inondées, aquifères réservoirs d'eau souterraine, ...) échangent en permanence de l'eau avec l'atmosphère et les océans, par le biais des précipitations, de l'évaporation, de la transpiration de la végétation, des eaux de ruissellement et de l'écoulement souterrain. Cependant, le stockage d'eau dans les réservoirs terrestres présente des variations temporelles dues aux activités humaines (pompage de l'eau dans les nappes, construction de barrages sur les cours d'eau, l'urbanisation, le drainage des zones humides, l'utilisation des terres et les changements de la couverture terrestre, la déforestation) (*Wada et al.* 2012, 2016), ainsi qu'à la variabilité climatique naturelle (principalement durant les épisodes ENSO via des échanges d'eau entre l'océan, les continents et l'atmosphère) (*Boening et al.* 2012 ; *Cazenave et al.* 2012, 2014 ; *Fasullo et al.* 2013 ; *Dieng et al.* 2014). A cause de la conservation de la masse d'eau dans le système climatique, les échanges d'eau continent-océan influent de façon importante sur le niveau de la mer (*Boening et al.* 2012 ; *Cazenave et al.* 2012 ; *Church et al.* 2013 ; *Dieng et al.* 2014).

Des études basées sur la modélisation hydrologique n'ont montré aucune tendance à long terme du stock d'eau total des continents (TLWS) due à la variabilité naturelle du climat au cours des 60 dernières années, mais seulement une forte variabilité interannuelle (*Ngo-Duc et al.* 2005). Par contre, les facteurs anthropiques, tels que la construction de barrages et l'extraction d'eau souterraine, présentent un bilan net responsable d'une tendance positive significative, au moins pour les dernières décennies (*Pokhrel et al.* 2012 ; *Wada et al.* 2012 ; *Wada,* 2015). Il faut noter que les barrages contribuent négativement à la hausse du GMSL (*Chao et al.* 2008), par contre le pompage d'eau souterraine a une contribution positive. Les autres facteurs anthropiques influent moins sur la hausse du GMSL (*Konikow,* 2011 ; *Wada et al.* 2012, 2016).

En se basant sur les résultats de *Konikow* (2011) et *Wada et al.* (2012), le dernier rapport du GIEC (AR5 ; *Church et al.* 2013) a estimé que le TLWS (l'effet net des barrages et "le pompage moins la recharge" des eaux souterraines) a contribué pour 0.38 ± 0.12 mm/an (soit ~12%) à la hausse du GMSL observée par altimétrie sur la période 1993-2010. Cette estimation est du même ordre de grandeur que la perte de masse de l'Antarctique en équivalent niveau de la mer sur cette même période (voir *table 13.1* dans *Church et al.* 2013). En raison d'une telle contribution à la hausse du GMSL, cela vaut la peine d'examiner cette composante plus en détail, compte tenu de l'importante incertitude associée.

Plusieurs méthodes on été proposées pour estimer les différents facteurs anthropiques qui influent sur la variation du TLWS. *Chao et al.* (2008) ont estimé l'effet des barrages et des réservoirs artificiels. Ils ont montré que ce facteur contribue pour -0.55 mm/an au GMSL, au cours du dernier demi-siècle, avec une stabilisation durant ces dernières années. Cette étude est basée sur une reconstruction historique de la retenue d'eau de près de 30 000 réservoirs construits au cours du 20^{éme} siècle. Pour l'estimation des eaux souterraines, trois méthodes sont utilisées (voir *Wada,* 2015 ; *Wada et al.* 2016) : *(1)* les variations de volume d'eau, *(2)* les flux d'eau et *(3)* les observations de la mission GRACE. Chacune de ces méthodes à ses avantages et ses inconvénients. Par exemple, GRACE donne une estimation verticalement intégrée du changement total de masse d'eau, mais les eaux de surface et l'humidité du sol doivent être connues et soustraites pour estimer la contribution de l'eau souterraine. Pour les méthodes de volume et de flux, celles-ci manquent énormément d'information à l'échelle globale. Ainsi, l'estimation des eaux souterraines reste très difficile, de même que la contribution globale des barrages.

D'autres études plus récentes ont été réalisées pour estimer la contribution du TLWS à la hausse du GMSL sur la dernière décennie en utilisant GRACE sur les continents. Par exemple *Yi et al.* (2015) et *Schrama et al.* (2014) estiment respectivement une contribution de +0.07 ± 0.04 mm/an et -0.06 ± 0.09 mm/an du TLWS à la hausse du GMSL sur la période 2003-2013. Cependant, étant donné la résolution de GRACE (~300-400 km) la séparation des masses de régions voisines peut être problématique (par exemple, entre les bassins fluviaux et des glaciers ; à cause de l'effet de leakage) (*Longuevergne et al.* 2010 ; *Landerer and Swenson,* 2012). Cela est particulièrement vrai dans la région du bassin du Gange impactée par les glaciers de l'Himalaya. Enfin, des études basées sur GRACE, tenant compte d'un nombre limité de bassins fluviaux (*Llovel et al.* 2010) manquent une partie du signal des eaux terrestres. De plus la correction du GIA qu'il faut appliquer à GRACE, importante dans les hautes latitudes, ajoute une incertitude significative à ces estimations.

Nous avons développé une approche différente basée sur le bilan de masse d'eau global. Elle consiste à comparer la variation de masse de l'océan estimée par GRACE à la somme de toutes les contributions de masse (calottes polaires, glaciers, vapeur d'eau atmosphérique, eaux continentales) et d'en déduire la composante "eaux continentales".

Résumé de l'article : "Total land water storage change over 2003-2013 estimated from a global mass budget approach" *(l'article original est inséré à la fin de cette section 2.3.3)*

Pour quantifier la contribution du TLWS sur la période janvier 2003 - décembre 2013, nous développons une approche basée sur le bilan global de la masse d'eau du système climatique en utilisant l'équation ci-dessous (déduite de l'équation *2.3*).

$$\Delta M_{Eaux\_continents} \pm Erreurs = \Delta M_{Ocean} - [\Delta M_{Glaciers} + \Delta M_{Groenland} + \Delta M_{Antarctique} + \Delta M_{Atmosphere}] \quad (2.5)$$

Cette équation de bilan de masse consiste à soustraire à la composante de masse de l'océan la somme des contributions de masse terrestre (glaciers, Groenland et Antarctique) et atmosphérique (vapeur d'eau). Nous négligeons d'autres composantes telles que le pergélisol (pas de données), la couverture neigeuse (négligeable en termes de contribution au GMSL sur la période altimétrique ; *Biancamaria et al.* 2011).
Le terme "$\Delta M_{Eaux\_continents} \pm Erreurs$", appelé "composante résiduelle de masse", représente la contribution du TLWS à la hausse du GMSL plus les erreurs des données combinées.

Pour plus de clarté, nous mentionnons que toutes les contributions sont exprimées en équivalent niveau de la mer (SLE). Par conséquent, si la valeur de la tendance du résidu est positive, cela correspond à une hausse du GMSL et inversement.

Dans cette approche, nous utilisons différentes sources de données combinant la gravimétrie, l'altimétrie, les mesures in-situ, des ré-analyses océaniques et atmosphériques et des modèles hydrologiques. Pour la composante de masse de l'océan, nous avons utilisé les données GRACE traitées par D. Chambers (voir section 2.3.1 et 2.3.2). Celles-ci montrent une tendance de 1.85 ± 0.1 mm/an en SLE et une accélération de 0.29 ± 0.04 mm/yr^2 sur la période 2003-2013. Pour valider nos résultats, nous avons estimé sur la même période la masse de l'océan (avec une tendance de 2.03 ± 0.11 mm/an et une accélération quasi nulle) en utilisant le GMSL moyen des 6 groupes de traitement des produits altimétriques (voir section 2.1), corrigé des effets stériques du niveau de la mer (de la couche 0-5350m de profondeur) à partir des données de la réanalyse océanique ORAS4 (voir *section 2.3.1* et *2.3.2*). Pour la vapeur d'eau atmosphérique, avec une contribution en tendance presque nulle estimée à -0.04 ± 0.04 mm/an en SLE, nous avons utilisé les données de la réanalyse atmosphérique d'ERA-Interim (voir *Dieng et al.* 2015c inséré ci dessous). Concernant les estimations du bilan de masse des glaciers, nous avons utilisé la moyenne des tendances issues de plusieurs publications scientifiques. La même démarche à été utilisée pour les bilans de masse du Groenland et de l'Antarctique. Pour le Groenland, l'Antarctique et les glaciers, 52, 24 et 4 valeurs de tendance de diverses publications ont été considérées. Les valeurs de tendance moyenne de ces trois composantes sont respectivement 0.77 ± 0.1 mm/an, 0.34 ± 0.12 mm/an et 0.58 ± 0.1 mm/an en SLE sur la période 2003-2013.

Les estimations du bilan de masse des glaciers sont basées sur une combinaison de mesures in-situ et de plusieurs systèmes d'observation par télédétection, indépendants et opérant simultanément. Les mesures in-situ régulières sur le terrain, sur les bilans de masse des glaciers prises individuellement, sont fournies par le service de surveillance mondial des glaciers (-

WGMS- World Glacier Monitoring Service). Depuis 2011, une basse de données de 40000 observations sur plus de 2000 glaciers est mise en place par le WGMS avec des mises à jour régulières (*Zemp et al.* 2011, 2015). Dans les régions difficiles d'accès, des techniques de mesures par télédétection de haute précision fournissant la topographie des glaciers, ont été appliquées (exemples, LIDAR et drones, *Bhardwaj et al.* 2016a, 2016b) pour affiner les techniques d'observation in-situ, ainsi que la fréquence et la qualité des mesures in-situ. Les images photographiques des glaciers faites par les avions de ligne et de recherche ont été aussi utilisées. Pour avoir une estimation plus globale du bilan de masse total des glaciers, les données des satellites sont utilisées pour compléter la couverture spatiale et temporelle principalement des régions éloignées (*Barandun et al.* 2015). Une diversité de satellites (altimétriques comme ICESat et Cryosat2 ; de gravimétrie spatiale GRACE) a permis d'estimer les variations de volume, d'élévation et de masse des glaciers. Cet ensemble de données sur le bilan des glaciers, dérivé d'une combinaison de différentes méthodes avec une couverture mondiale (récemment mis en place sous la forme de l'inventaire des glaciers Randolph (-RGI- Randolph Glacier Inventory) ; voir *Pfeffer et al.* 2014), est désormais largement appliqué par la communauté glaciologique (*Gardner et al.* 2013 ; *Marzeion et al.* 2016). La combinaison de ces différentes méthodes est considérée comme un atout majeur pour estimer le bilan de masse global des glaciers (*Gardner et al.* 2013 ; *Pfeffer et al.* 2014 ; *Marzeion et al.* 2016).

En utilisant tous les jeux de données, nous trouvons une contribution positive du TLWS sur la période 2003-2013, estimée à 0.30 ± 0.18 mm/an en SLE. Ceci correspond à ~17% de l'augmentation de la masse de l'océan observée par GRACE et ~10% de l'élévation du GMSL observée par altimétrie. Cette estimation du TLWS correspond à une diminution de -108 ± 63 km^3/an du stock total d'eaux continentales. Notons que cette quantité représente les effets combinés de la variabilité naturelle du climat, du changement climatique anthropique mais aussi les effets directs des activités humaines sur l'hydrologie.

Pour aller plus loin et vérifier la robustesse de notre estimation du TLWS basée sur une moyenne des bilans de masse publiés, nous utilisons les estimations du bilan de masse du Groenland et de l'Antarctique de *Velicogna et al.* (2014) ainsi que celles du projet CCI "Ice Sheets". Avec ces estimations, les contributions du TLWS à la hausse du GMSL sont estimées respectivement à 0.44 ± 0.24 mm/an et 0.50 ± 0.20 mm/an en SLE. Nos résultats sont aussi en accord avec l'estimation faite par *Wada et al.* (2012) à partir du bilan des masses d'eaux dues aux activités humaines correspondant à *(1)* la somme "pompage d'eaux souterraines + eaux stockées derrière des barrages", estimée à 0.39 ± 0.11 mm/an en SLE ; et *(2)* la somme "pompage d'eaux

souterraines + eaux stockées derrière des barrages + effets de déforestation + drainage des zones humides", estimée à 0.54 ± 0.12 mm/an en SLE.

En termes de tendance, tous les résidus calculés apparaissent plutôt cohérents malgré les différents ensembles de données utilisés, suggérant la contribution positive des eaux continentales à la hausse du niveau de la mer.

Dans cette étude, nous avons aussi estimé les accélérations de chaque composante de l'équation bilan de masse et trouvé que contrairement aux glaciers et à la vapeur d'eau, les bilans de masse du Groenland et de l'Antarctique affichent clairement une accélération. L'accélération du signal résiduel de masse est de +0.17 ± 0.04 mm/an^2 et -0.08 ± 0.05 mm/an^2 calculé à partir de la masse de l'océan respectivement basée sur GRACE et la différence "GMSL - ORAS4". Au final, nous constatons que les données actuellement disponibles ne semblent pas permettre d'estimer une accélération significative du TLWS. Ces données ne permettent pas non plus d'identifier quel terme de l'équation du bilan de masse compense l'accélération du bilan de masse des calottes polaires. En outre, les accélérations des masses d'eaux dues aux activités humaines estimées par *Wada et al.* (2012) sont très petites et non significatives (0.008 ± 0.010 mm/an^2). Nos résultats suggèrent néanmoins que l'accélération du TLWS n'est pas significativement différente de zéro sur la période 2003-2013.

A l'échelle de temps interannuelle, notre étude (en utilisant 3 différents modèles hydrologiques (voir article inséré ci dessous) confirme que les fluctuations interannuelles du TLWS sont principalement causées par les événements ENSO (variabilité naturelle du climat). Un autre résultat est que le TLWS estimé par *Wada et al.* (2012) (c'est à dire le bilan net du pompage et des barrages) répond également à des événements ENSO, probablement par l'intermédiaire de la recharge des aquifères.

En conclusion, les résultats obtenus indiquent que le TLWS contribue à hauteur de +0.3 ± 0.18 mm/an soit 10% à la hausse actuelle du GMSL, et est dominé par le pompage de l'eau dans les nappes pour l'irrigation des cultures. Notre étude repose sur une importante diversité de données combinant l'altimétrie, la gravimétrie, les mesures in-situ, les ré-analyses océaniques et atmosphériques, mais aussi les modèles hydrologiques.
Toutefois, une étude récente publiée en 2016 (*Reager et al.* 2016), basée sur les données "mascons" de GRACE du JPL, fournit une contribution négative de -0.32 mm/an du TLWS à la hausse du GMSL. Ce résultat est contraire au nôtre. Comme indiqué précédemment et dans la *section 2.2.2*, les données GRACE (que ce soit sur l'océan ou sur les continents) souffrent de plusieurs problèmes. Nous pouvons citer en particulier, la séparation des masses des bassins

fluviaux et des glaciers (*Longuevergne et al.* 2010 ; *Landerer and Swenson,* 2012) due au problème du leakage et le bruit de mesures GRACE "stripes" (*Swenson and Wahr,* 2006; *Chambers and Schröter,* 2011 ; *Chambers and Bonin,* 2012). Utiliser les données GRACE sans appliquer des traitements spécifiques apporte beaucoup d'incertitude à l'estimation des variations de masse principalement dans l'océan. Une analyse rapide a montré que la différence de résultat entre notre étude et celle de *Reager et al.* (2016) vient essentiellement de l'incertitude sur les données GRACE. Des études plus approfondies doivent être menées sur ce sujet afin de mieux comprendre les causes des différences observées sur l'estimation du TLWS.

Environmental Research Letters

LETTER

Total land water storage change over 2003–2013 estimated from a global mass budget approach

H B Dieng[1], N Champollion[2], A Cazenave[1,2], Y Wada[3,4,5], E Schrama[6] and B Meyssignac[1]

[1] LEGOS, 18 avenue E. Belin, F-31400 Toulouse, France
[2] ISSI, Hallerstrasse 6, CH-3012 Bern, Switzerland
[3] Department of Physical Geography, Utrecht University, Heidelberglaan 2, 3584 CS Utrecht, The Netherlands
[4] NASA Goddard Institute for Space Studies, 2880 Broadway, New York, NY 10025, USA
[5] Center for Climate Systems Research, Columbia University, 2880 Broadway, New York, NY 10025, USA
[6] Faculty of Aerospace Engineering, Kluyverweg 1, 2629HS Delft, The Netherlands

E-mail: habib.dieng@legos.obs-mip.fr

Keywords: land waters, sea level rise, global water mass budget

Supplementary material for this article is available online

OPEN ACCESS

RECEIVED
20 August 2015

REVISED
28 October 2015

ACCEPTED FOR PUBLICATION
10 November 2015

PUBLISHED
8 December 2015

Abstract

We estimate the total land water storage (LWS) change between 2003 and 2013 using a global water mass budget approach. Hereby we compare the ocean mass change (estimated from GRACE space gravimetry on the one hand, and from the satellite altimetry-based global mean sea level corrected for steric effects on the other hand) to the sum of the main water mass components of the climate system: glaciers, Greenland and Antarctica ice sheets, atmospheric water and LWS (the latter being the unknown quantity to be estimated). For glaciers and ice sheets, we use published estimates of ice mass trends based on various types of observations covering different time spans between 2003 and 2013. From the mass budget equation, we derive a net LWS trend over the study period. The mean trend amounts to $+0.30 \pm 0.18$ mm yr^{-1} in sea level equivalent. This corresponds to a net decrease of -108 ± 64 km^3 yr^{-1} in LWS over the 2003–2013 decade. We also estimate the rate of change in LWS and find no significant acceleration over the study period. The computed mean global LWS trend over the study period is shown to be explained mainly by direct anthropogenic effects on land hydrology, i.e. the net effect of groundwater depletion and impoundment of water in man-made reservoirs, and to a lesser extent the effect of naturally-forced land hydrology variability. Our results compare well with independent estimates of human-induced changes in global land hydrology.

1. Introduction

Liquid fresh water on land is stored in various reservoirs: rivers, lakes, man-made reservoirs, wetlands and inundated areas, root zone (upper few meters of the soil) and aquifers (groundwater reservoirs). Terrestrial reservoirs continuously exchange with the atmosphere, oceans and land, through vertical and horizontal mass fluxes (precipitation, evaporation, transpiration of the vegetation, surface runoff and underground flow). Land water storage (LWS) varies with change in mean climate and climate variability. Human activities also directly affect LWS through water extraction from aquifers, building of dams along rivers, urbanization, wetland drainage, land use and land cover changes, and deforestation. All these effects modify the water budget in river basins, and because of water mass conservation in the climate system, cause sea level changes. Studies based on hydrological modeling have not reported any clear long-term trend in global LWS over the past 60 years but only interannual variability (e.g., Ngo-Duc *et al* 2005). This is unlike human-induced factors such as dam building (Chao *et al* 2008) and groundwater extraction (Konikow 2011, Pokhrel *et al* 2012, Wada *et al* 2012, Wada 2015). Although their contributions to the global mean sea level (GMSL) are of opposite sign (<0 for dams, >0 for groundwater pumping), their net effect is responsible for a significant long-term positive trend at least for the recent decades

(other human-induced factors have negligible contributions to the GMSL). Building on the results from Konikow (2011) and Wada *et al* (2012), Church *et al* (2013) estimated that the net effect of dams and groundwater depletion (i.e., groundwater abstraction minus recharge; e.g., Wada 2015) on the GMSL amounted 0.38 ± 12 mm yr^{-1} over 1993–2010. This represents 12% of the observed GMSL rate of rise over this time span, an amount of the same order of magnitude as the Antarctic ice mass loss (see table 13.1 in Church *et al* 2013). Because of such a significant contribution to sea level, it is worth to examine this component in more detail. In addition, uncertainty of this component has direct impact on our capability to close the sea level budget, thus constrain missing contributions (due to lack of data) such as the deep ocean thermal expansion (see discussions on that topic in Llovel *et al* 2014, Dieng *et al* 2015a).

The effect of dams and man-made reservoirs has been estimated by Chao *et al* (2008). They reconstructed the history of water impoundment in the nearly 30 000 reservoirs built during the twentieth century and estimated the contribution to sea level by dams and artificial reservoirs (including seepage) at −0.55 ± 0.08 mm yr^{-1} in sea level equivalent (SLE) during the last half-century, with a stabilization in recent years. Estimates of groundwater depletion are based on three methods (see Wada 2015): (1) volume-based method, (2) flux-based method, and (3) satellite observations from the GRACE space gravimetry mission. Each method has strengths and weaknesses. For example, GRACE gives a vertically integrated estimate of the water mass change; thus surface waters and soil moisture must be known and removed to estimate the ground water contribution. In addition, GRACE-based estimates do not yet have full global coverage for the estimation of groundwater depletion (Famiglietti 2014, Wada 2015). The volume- and flux-based methods lack global information and suffer from model uncertainties. Thus estimating groundwater depletion remains very challenging, as is the global dam contribution.

In this study, we develop another approach based on the global water mass budget of the climate system to estimate the total LWS change. Focusing on the January 2003–December 2013 time span (for which GRACE data are available), we compare the GRACE-based ocean mass change to the sum of mass components (glaciers, Greenland and Antarctica ice sheets, atmospheric water vapor and LWS). We neglect other mass components such as permafrost because global data are lacking, as well as change in the snow pack, previously shown to give negligible contribution to the GMSL beyond time spans larger than 1 year (Biancamaria *et al* 2011). In this mass budget approach, we use estimates of each component from different observational data sets, except for the net total LWS, the unknown quantity to be estimated. A mean LWS trend is first estimated over 2003–2013. Then, accounting for increasing rate of change (acceleration) of several components (ocean mass, ice sheet mass balances) over the study time span, we investigate whether the LWS rate varies with time. To validate our results, we perform a similar analysis but instead of using GRACE, we estimate the ocean mass term from the satellite altimetry-based GMSL corrected for steric effects (i.e., effects of ocean temperature and salinity).

All results are expressed in terms of SLE change. Units are given in mm yr^{-1} and mm yr^{-2} for trend and acceleration respectively.

2. Method

To estimate the contribution of LWS change to sea level, we can simply consider the conservation of water mass in the Earth's system (e.g., Llovel *et al* 2010). Of course, LWS change could be derived from GRACE data over the continents, as done previously in a number of studies. However, considering that the GRACE resolution (∼300–500 km) may be problematic in separating nearby masses (e.g., river basins and glaciers), our objective here is to use a different approach.

On time scales of years to decades, water mass changes inside the solid Earth (e.g., in the crust) can be neglected, so that only changes in land reservoirs, ocean and atmosphere need to be considered, with the mass conservation equation written as follows:

$$\begin{aligned}\Delta M_{\mathrm{Ocean}}(t) + \Delta M_{\mathrm{Glaciers}}(t) + \Delta M_{\mathrm{Greenland}}(t) \\ +\Delta M_{\mathrm{Antarct.}}(t) + \Delta M_{\mathrm{Atm}}(t) \\ +\Delta M_{\mathrm{LWS}}(t) = 0,\end{aligned} \tag{1}$$

where $\Delta M(t)$ represents changes with time t of water mass in the different reservoirs: ocean, glaciers (including small ice caps), Greenland ice sheet, Antarctica ice sheet, atmosphere and land water stores. Note that ΔM(t) may be either positive or negative. Using equation (1), we deduce the LWS component by simple rewriting as:

$$\begin{aligned}\Delta M_{\mathrm{LWS}}(t) = -\Big[\Delta M_{\mathrm{Ocean}}(t) + \Delta M_{\mathrm{Glaciers}}(t) \\ +\Delta M_{\mathrm{Greenland}}(t) + \Delta \mathrm{M}_{\mathrm{Antarct.}}(t) \\ +\Delta M_{\mathrm{Atm}}(t)\Big].\end{aligned} \tag{2}$$

As mentioned above, all contributions are expressed in terms of SLE.

3. Data

3.1. Ocean mass

For estimating the ocean mass component, we apply two approaches : (1) use of GRACE space gravimetry data over the oceans, and (2) estimate of the GMSL corrected for steric effects.

3.1.1. GRACE-based ocean mass

Three different data sets of the GRACE Release 05 products have been considered:

(1) from the Texas University (CSR RL05),

(2) from the German GeoForschungsZentrum (GFZ RL05)

(3) from the Jet Propulsion Laboratory (JPL RL05).

To study the ocean mass evolution, a specific processing has been carried out by D. Chambers (described in Johnson and Chambers 2013; geocenter terms included; data available at https://dl.dropboxusercontent.com/u/31563267/ocean_mass_orig.txt). The data are provided as global mean (averaged over the 90°S–90°N° domain) time series at monthly interval with associated uncertainty. The GIA (Glacial Isostatic Adjustment) effect is corrected for using the GIA correction computed in Chambers *et al* (2010). In the following, we consider the mean of the three data sets.

3.1.2. Ocean mass estimated from the GMSL corrected for steric effects

Changes in the GMSL result from steric effects plus ocean mass changes. Thus, the ocean mass component can be also derived from the difference 'GMSL minus steric effects'. For that purpose we used the mean of six different satellite altimetry-based GMSL data sets: (1) Validation and Interpretation of Satellite Oceanographic (AVISO; http://aviso.altimetry.fr/en/data/products/ocean-indicators-products/actualitesindicateurs-des-oceansniveau-moyen-des-mersindexhtml.html); (2) University of Colorado (CU Release 5; http://sealevel.colorado.edu/); (3) National Oceanographic and Atmospheric Administration (NOAA; http://star.nesdis.noaa.gov/sod/lsa/SeaLevelRise/LSA_SLR_timeseries_global.php); (4) Goddard Space Flight Center (GSFC version 2; http://podaac-ftp.jpl.nasa.gov/dataset/MERGED_TP_J1_OSTM_OST_GMSL_ASCII_V2); (5) Commonwealth Scientific and Industrial Research Organization (CSIRO; http://cmar.csiro.au/sealevel/sl_data_cmar.html); (6) The European Space Agency/ESA Climate Change Initiative/CCI sea level data (http://esa-sealevel-cci.org/). Details on these data sets can be found in Dieng *et al* (2015a, 2015b).

For the steric component, instead of using Argo that suffer from gaps in the data coverage (e.g., in the Indonesian region; Dieng *et al* 2015b), we make use of the ORAS4 reanalysis (Balmaseda *et al* 2013) that provides ocean temperature and salinity down to 5350 m and global coverage. Note that over their common geographical and depth coverage, Argo-based and ORAS4-based steric sea level are in good agreement (see Dieng *et al* 2015b for a discussion).

Using the mean of the six GMSL products, we compute the ocean mass component by subtracting the ORAS4 steric component. It is simply called below 'GMSL minus ORAS4'.

3.2. Atmospheric water vapor mass

To estimate change in atmospheric water vapor mass, we used the vertically integrated water vapor grids from the ERA Interim reanalysis performed by the European Center for Medium Range Weather Forecast/ECMWF (Dee *et al* 2011). The data are provided as 1.5° × 1.5° grids at monthly interval. We compute a globally averaged water vapor time series and express it in terms of SLE (see Dieng *et al* 2014 for details).

3.3. Greenland and Antarctica mass

For the ice sheet mass balances, we used two approaches: (1) time series given by Velicogna *et al* (2014) and from the ESA CCI Ice Sheet project (http://esa-icesheets-cci.org; see also Forsberg *et al* 2014), (2) published estimates of mass balance trends from the literature. For Greenland, we considered 52 published trend values based on 30 articles. For Antarctica, we used 24 published trend values based on 13 articles. Corresponding list of the 43 articles used in this study, as well as associated trend values are given in the supporting information (SI).

3.4. Glaciers mass

For the glaciers, we considered 4 published estimates of mass balance trends from the literature (Gardner *et al* 2013, Schrama *et al* 2014, Yi *et al* 2015). The Gardner *et al* data are a compilation of a large number of glacier mass balance estimates from different methods (these estimates are in terms of trends over the 2003–2009 time span). Global glacier mass trends from Schrama *et al* and Yi *et al* are based on GRACE and are given over different time intervals: January 2003–December 2013 (Schrama *et al* 2014); January 2005–December 2009 and January 2010–March 2014 (Yi *et al* 2015).

Note that the four glaciers estimates considered in this study do not include Greenland and Antarctica peripheral glaciers. Trend values are given in the SI.

4. Data analysis

When time series are used to estimate trends and accelerations, the annual & semi annual signals are removed by fitting 12-month and 6-month sinusoids.

Figure 1 shows the GRACE-based ocean mass (called GOM) time series over 2003–2013. This time series is an update of that previously used by Dieng *et al* (2015a, 2015b) to examine the closure of the sea level budget. A mean trend of 1.85 ± 0.1 mm yr^{-1} is estimated over the study time span. We fitted a degree 2 polynomial to the data, from which we deduce an acceleration of 0.29 ± 0.04 mm yr^{-2}. The

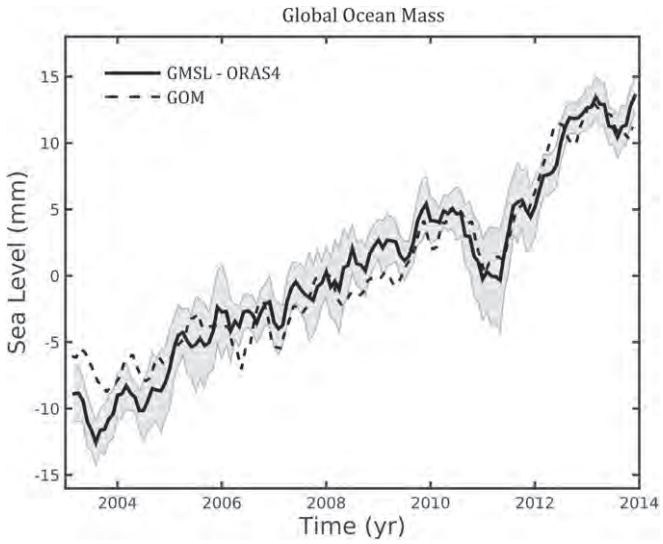

Figure 1. Ocean mass time series over January 2003–December 2013 estimated from GRACE (GOM; mean of CSR, GFZ and JPL products) (dashed black curve), and from 'GMSL minus ORAS4' (solid black curve) with associated uncertainty (shaded area). Unit : mm yr^{-1} SLE.

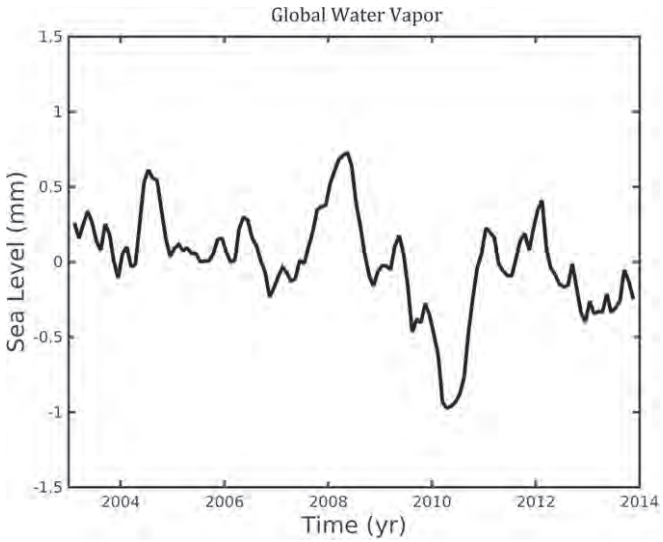

Figure 2. Global water vapor (in sea level equivalent) time series from ERA-Interim, over January 2003–December 2013. Unit: mm yr^{-1} SLE.

acceleration is defined as 2 times the adjusted coefficient of the polynomial t^2 term. The quoted uncertainties represent 1 sigma errors estimated from the least-squares fit and accounting for the time series errors. In figure 1 is superimposed the 'GMSL minus ORAS4'ocean mass time series and associated uncertainty (note that the GOM uncertainty is not shown because smaller than the latter). The mean 'GMSL minus ORAS4' trend over 2003–2013 amounts to 2.03 ± 0.11 mm yr^{-1}. Besides, the acceleration is found to be almost zero over the study time span.

Similarly, figure 2 shows the global atmospheric water vapor time series. The mean trend estimated from the time series is slightly negative (equal to -0.04 ± 0.04 mm yr^{-1} SLE), indicating a small but not significant increase in atmospheric water vapor content. Dieng *et al* (2014) considered other water vapor datasets and found little differences in terms of interannual variability and trend. As for the ocean mass data, we fitted a degree 2 polynomial but found zero acceleration.

Figure 3 shows a plot of the 52 published trend values of the Greenland mass balance (in mm yr^{-1} SLE). Horizontal lines represent the time span covered by each analysis. Note that several values are superimposed and are not visible on the figure. Averaging all published values provides a mean trend of 0.76 ± 0.1 mm yr^{-1} over 2003–2013 (this 1 sigma error is that obtained from the regression, accounting for errors provided with each estimate). This value can

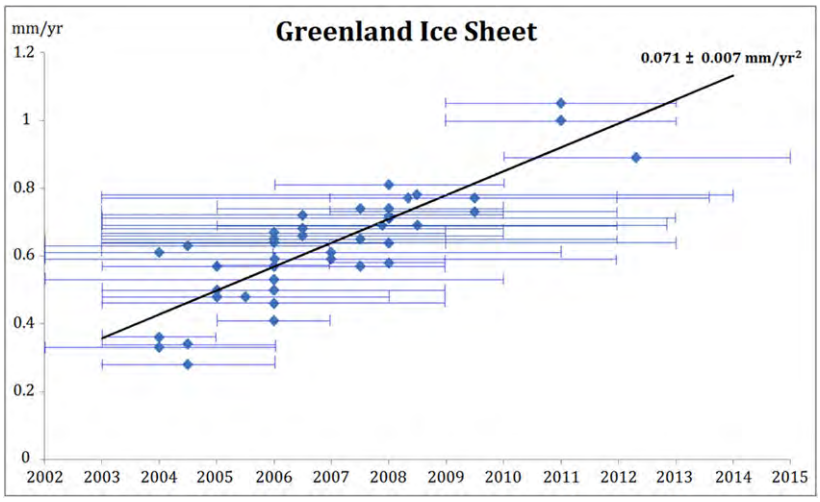

Figure 3. Trends (over different periods) of Greenland ice mass loss from published literature (see SI). Unit: mm yr^{-1} SLE. The black line is the linear trend increase (acceleration).

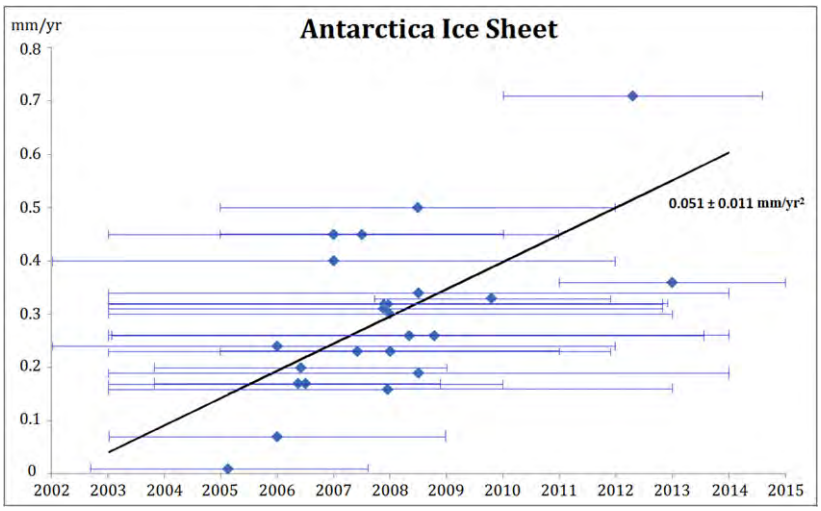

Figure 4. Trends (over different periods) of Antarctica ice mass loss from published literature (see SI). Unit: mm yr^{-1} SLE. Black line is the linear trend increase (acceleration).

be compared with other mean trend estimates over the same time span (2003–2013): 0.77 ± 0.16 mm yr^{-1} (Velicogna *et al* 2014), 0.63 ± 0.1 mm yr^{-1} (CCI data set), and 0.77 ± 0.05 mm yr^{-1} (Schrama *et al* 2014). All trends agree well within their respective error bars. We next performed a linear regression of the trend data shown in figure 3 to estimate the acceleration term (identified in figure 3 by the black line). The computed acceleration of the Greenland ice sheet mass loss amounts to 0.071 ± 0.007 mm yr^{-2}. The acceleration provided by Velicogna *et al* (2014) equals 0.071 ± 0.004 mm yr^{-2}, in perfect agreement with our estimate based on the 52 published values. The acceleration estimated from the CCI data amounts to 0.060 ± 0.007 mm yr^{-2}, slightly less than the other two values.

Figure 4 is a plot similar to figure 3 but for the Antarctica ice sheet. The black straight line has also the same meaning. Unlike Greenland, results for the Antarctica mass trends are much more scattered, even though there is indication of an acceleration (as reported in the literature; see also Church *et al* 2013). The mean trend over 2003–2013 based on all individual trends amounts to 0.34 ± 0.12 mm yr^{-1}, a value slightly larger than those from Velicogna *et al* (2014) (0.19 ± 0.12 mm yr^{-1}), Schrama *et al* (2014) (0.26 ± 0.08 mm yr^{-1}), and the CCI data (0.27 ± 0.10 mm yr^{-1}). Such differences may be partly attributed to the considered GIA correction, highly important for Antarctica (see Schrama *et al* 2014 for a discussion). The acceleration adjusted on the 24 published trends considered in our study amounts to 0.051 ± 0.011 mm yr^{-2}. This value is slightly larger than the Velicogna *et al* (2014) and CCI estimates (of 0.031 ± 0.010 mm yr^{-2} and 0.042 ± 0.010 mm yr^{-1}, respectively).

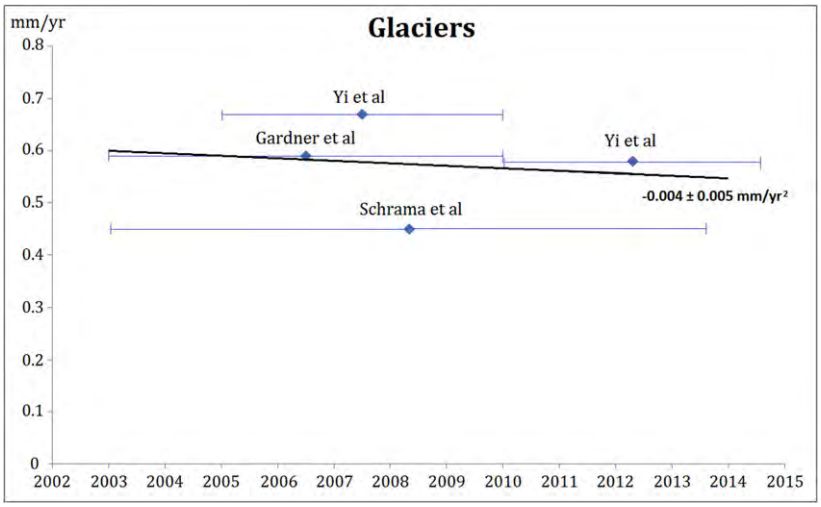

Figure 5. Trends (over different periods) of glaciers mass balance from published literature (see SI). Unit: mm yr^{-1} SLE. The black line represents the acceleration term.

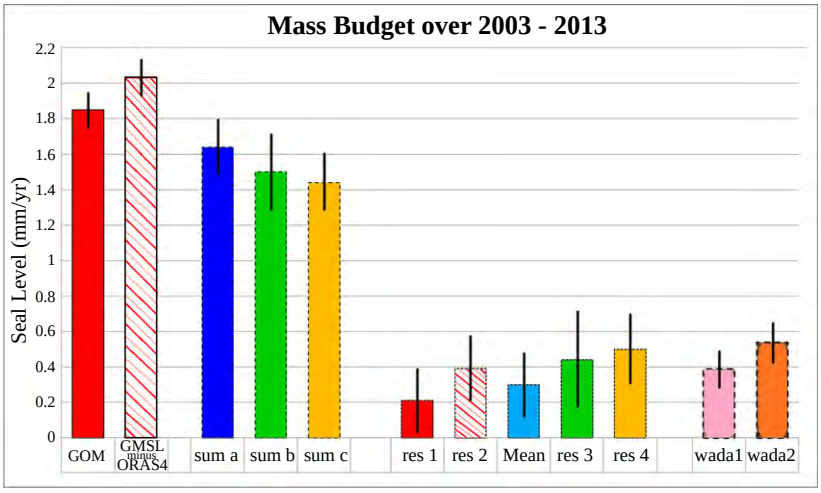

Figure 6. Chart of mean trends over 2003–2013 for different components of the mass budget : ocean mass from GRACE (GOM; red bar) and 'GMSL minus ORAS4' (dashed red bar), sums of mass components (sum a, sum b, sum c—see text) (blue, green and yellow bars), residuals (res1, res2, mean of res1 plus res2, res3 and res4; red, dashed red, light blue, green and yellow bars), and LWS trends from Wada *et al* (2012) (Wada1 and Wada2; pink and light orange bars). Unit: mm yr^{-1} SLE.

A treatment similar to that applied for the ice sheets was performed for the glaciers mean trend and acceleration (see figure 5, with the black straight line representing the acceleration). The mean trend and acceleration over 2003–2013 are estimated to 0.58 ± 0.1 mm yr^{-1} and -0.004 ± 0.005 mm yr^{-2}. The acceleration is not significantly different from zero. Using GRACE only, Schrama *et al* (2014) estimated the mean trend of the glacier contribution over 2003–2013 to 0.44 ± 0.03 mm yr^{-1}. The difference cannot be attributed to peripheral glaciers of Greenland and Antarctica ice sheets, not considered in either case. However, the GRACE only glacier estimate may be contaminated by land hydrology because of the poor GRACE resolution.

We are also aware that the estimated acceleration needs to be used with caution due to the few available glacier observation-based data sets.

5. Results

5.1. LWS trend over 2003–2013

In figure 6, we present a chart of the mean trends over 2003–2013 for $\Delta M_{\mathrm{Ocean}}$ (from GRACE and from 'GMSL minus ORAS4'), the sum of ΔM (atmospheric water vapor plus glaciers plus ice sheets) and the residuals ($\Delta M_{\mathrm{Ocean}}$—sum of ΔM). For the sums (and residuals as well), 3 trend values are considered. Sums a, b and c correspond to: (a) the average trend estimated with the published results (i.e., sum of mean Greenland

plus mean Antarctica plus mean glacier plus water vapor trends—values given in section 4 above-), (b) the Velicogna *et al* (2014)'s trends for Greenland and Antarctica, and (c) the CCI trends also for Greenland and Antarctica. For sums b and c, we consider for glaciers and water vapor trends, the same values as in sum a. All residuals are interpreted in terms of LWS trends over 2003–2013, and are expressed in SLE.

Residuals 1 and 2 (called res1 and res2) in figure 6 are based on $\Delta M_{\mathrm{Ocean}}$ from GRACE and from 'GMSL minus ORAS4', to which 'sum a' is subtracted. We also compute the mean of res1 and res2. Corresponding trends amount to 0.21 ± 0.18 mm yr^{-1} (res1), 0.39 ± 19 mm yr^{-1} (res2) and 0.30 ± 0.18 mm yr^{-1} (mean). Residuals 3 and 4 (called res3 and res4) are based on sums b and c respectively, using the mean value of $\Delta M_{\mathrm{Ocean}}$ from GRACE and 'GMSL minus ORAS4'. These are also plotted in figure 6 as well as LWS trends estimated by Wada *et al* (2012)—based on the flux method- for 2 cases: (1) only dams and groundwater depletion are accounted for, and (2) in addition to dams and ground waters, account of deforestation and wetland drainage (called Wada1 and Wada2 hereinafter). Trends over 2003–2013 for res3, res4, Wada1 and Wada2 amount to 0.44 ± 24 mm yr^{-1}, 0.50 ± 0.20 mm yr^{-1}, 0.39 ± 0.11 mm yr^{-1} and 0.54 ± 0.12 mm yr^{-1}, respectively.

All computed residuals appear rather consistent in spite of the quite different data sets used. They also compare rather well with Wada1 & 2. Trend values are gathered in the SI.

5.2. LWS acceleration over 2003–2013

As mentioned above, figures 3 and 4 show clear acceleration for the Greenland and Antarctica mass balances (unlike the glacier and water vapor components). The $\Delta M_{\mathrm{Ocean}}$ based on GRACE also displays important acceleration over the study time span. Using the mass budget equation, we can deduce the acceleration of the LWS residuals for this case. For res1, it amounts to $+0.17 \pm 0.04$ mm yr^{-2}. However if we consider $\Delta M_{\mathrm{Ocean}}$ based on 'GMSL minus ORAS4', acceleration of the residual time series (res2) becomes negative (and equal to -0.08 ± 0.05 mm yr^{-2}). Besides accelerations of Wada 1 and 2 are very small and non significant (of 0.008 ± 0.010 mm yr^{-2}). With the data currently available, it does not seem possible to estimate any reliable LWS acceleration, nor to identify which term of the mass budget equation compensates the ice sheet mass balance acceleration. Our results suggest nevertheless that the LWS acceleration is not significantly different from zero over the 2003–2013 time span.

5.3. Interannual variability in LWS trends over 2003–2013

We computed short-term trends of the $\Delta M_{\mathrm{Ocean}}$ time series based on GRACE and 'GMSL minus ORAS4', over successive 2-year time spans (with 1 year overlap). To these short-term trends, we removed the acceleration term of sum a (i.e., the combined acceleration of glaciers, ice sheets and water vapor). The corresponding curves are shown in figure 7 (labeled res1 and res2). In figure 7 are superimposed four additional LWS 2-year trend curves (also with 1-year overlap) using: (1) LWS determined by Yi *et al* (2015) using GRACE over continental river basins, (2) LWS based on the ISBA/TRIP global hydrological model (Alkama *et al* 2010), (3) LWS based on the Water Gap Hydrological Model (WGHM, Döll *et al* 2014a), and (4) LWS based on the Modern Era Retrospective-analysis for Research and Applications (MERRA) Reanalysis (Mantas *et al* 2015). The ISBA/TRIP and WGHM land surface schemes calculate time variations of surface energy and water budgets in different soil layers. ISBA/TRIP only considers upper soil layers while WGHM accounts for groundwater and man-made reservoirs (Döll *et al* 2014a, 2014b). The MERRA dataset is the version 5.2.0 of the GEOS-5 data service. We used the total water storage in land reservoirs product that includes the groundwater component. As for ISBA/TRIP and WGHM, it is available as gridded time series at monthly interval over the 2003–2013 time span. We computed geographical averages, applying a cosine latitude weighting.

All six curves (expressed in SLE trends) exhibit large interannual variability, mostly related to El Nino-Southern Oscillation (ENSO) events (note for example the minimum corresponding to the 2011 La Nina). On average, a good correlation at interannual time scale is noticed between these six curves. But we note closer agreement between 2-year trend curves from res1 and Yi *et al* LWS on the one hand, and ISBA/TRIP and MERRA LWS on the other hand. The Wada 1 and Wada 2 short-term trends are also shown in figure 7 (bottom curves; signal amplified by a factor of 10). It is interesting to note that these also display a minimum in 2011. Although the latter only represent the direct anthropogenic components, the 2011 minimum likely reflects increased groundwater recharge during this La Nina episode.

All trends and accelerations estimates presented above are gathered in the SI.

6. Discussion

The mean trend in LWS estimated by the global mass budget approach developed in this study is found to be positive in terms of SLE over the 2003–2013 time span. The mean of the two estimates based on two different values of $\Delta M_{\mathrm{Ocean}}$ is 0.30 ± 0.18 mm yr^{-1} SLE. This corresponds to an annual decrease in net LWS of -108 ± 64 km^3 yr^{-1}. This quantity represents the combined effects of natural climate variability, anthropogenic climate change and direct anthropogenic factors. The uncertainty of this estimate directly relies

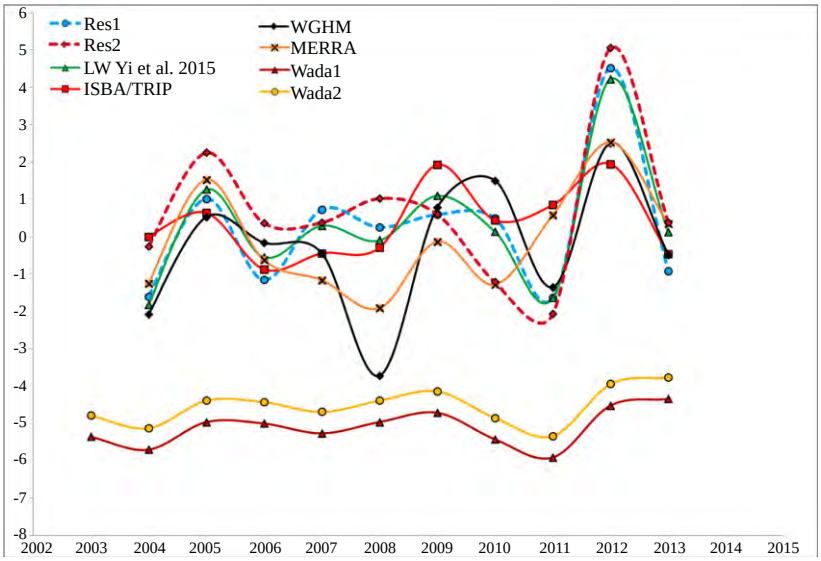

Figure 7. Upper curves: 2-year trends (with 1-year overlap) (expressed in mm yr^{-1} SLE) computed over 2003–2013 for res1 (dashed blue curve), res2 (dashed red curve), global mean LWS rate estimated by Yi *et al* (2015) (green curve), ISBA/TRIP hydrological model (red curve), WGHM hydrological model (black curve) and MERRA reanalysis (orange curve) . Bottom curves: 2-year trends (with 1-year overlap) of Wada1 (red curve) and Wada 2 (yellow curve) (multiplied by 10; expressed in mm yr^{-1} SLE). An arbitrary downward vertical offset has been applied to the bottom curves for clarity.

on the ocean mass trend uncertainty. Here we used two independent methods to estimate $\Delta M_{\mathrm{Ocean}}$ and associated uncertainty, with quite consistent results. Wada *et al* (2012)'s results for the direct anthropogenic LWS components are only slightly larger (of $+0.39 \pm 0.11$ mm yr^{-1} SLE or -140 ± 40 km^3 yr^{-1} LWS trend) for the net effect of dams and ground water depletion. While the rate of reservoir impoundment exceeded groundwater depletion over most of the 20th century, for the recent years, groundwater depletion exceeds impoundment, thus the net effect leads to a positive contribution to the GMSL. In addition to Wada *et al* (2012), other estimates of the groundwater component have been published in the recent years: Konikow (2011) estimated that human-induced groundwater depletion contributed 0.34 ± 0.07 mm yr^{-1} to the GMSL rise over 1993–2008 (based mostly on observational methods). Pokhrel *et al* (2012) estimated much larger groundwater depletion over 1981–2007, amounting 1.0 ± 0.16 mm yr^{-1} SLE (or 0.8 ± 0.25 mm yr^{-1} when accounting for dams and natural climate variability). A recent study by Döll *et al* (2014b) based on the WGHM model combined with GRACE data finds a groundwater contribution to GMSL rise of 0.31 ± 0.06 mm yr^{-1} for the 2003–2009 time span. Thus, these estimates (except for Pokhrel *et al* 2012) agree well with our results.

Other studies based on GRACE have provided estimates of the total (natural plus anthropogenic) LWS change over different time spans. Considering the 33 largest river basins, Llovel *et al* (2010) and Jensen *et al* (2013) estimated to -0.22 ± 0.05 mm yr^{-1} and -0.20 ± 0.04 mm yr^{-1} the LWS contribution to GMSL over 2002–2009. Two LWS trend estimates by Yi *et al* (2015) for 2005–2009 and 2010–2014 give -0.27 ± 0.25 mm yr^{-1} and 0.38 ± 0.48 mm yr^{-1} respectively. Note that over the 2003–2013 period, the Yi *et al* (2015) and Schrama *et al* (2014) LWS trends (both based on GRACE data processing on land) are respectively slightly positive and negative ($+0.07 \pm 0.04$ mm yr^{-1} and -0.06 ± 0.09 mm yr^{-1} respectively). This dispersion of LWS values and large associated uncertainties based on GRACE is not totally surprising. The GRACE LWS rate estimates are much dependent on the study period, considering the importance of the interannual variability (see figure 7), as discussed in Jensen *et al* (2013). Besides, the GRACE resolution does not allow unambiguous separation between nearby sources (Longuevergne *et al* 2010). This is particularly true in the region of the Ganges basin and Himalayan glaciers. Finally, studies considering a limited number of river basins (e.g., Llovel *et al* 2010) miss part of the signal, and the GIA correction, important in high latitudes, adds significant uncertainty. All together, the GRACE LWS estimates remain uncertain, in particular if study time spans are short (Landerer and Swenson 2012).

In this study, we proposed a different approach to estimate the net LWS contribution to GMSL change over a 10 year time span. Using a large number of different data sets for the mass components, we came up to a positive value for the LWS trend over 2003–2013 (in terms of SLE; i.e., decrease of total water storage on land) that likely reflects the net anthropogenic component, i.e., the dominant contribution of groundwater depletion versus dams, in good agreement with the Wada *et al* (2012) estimates.

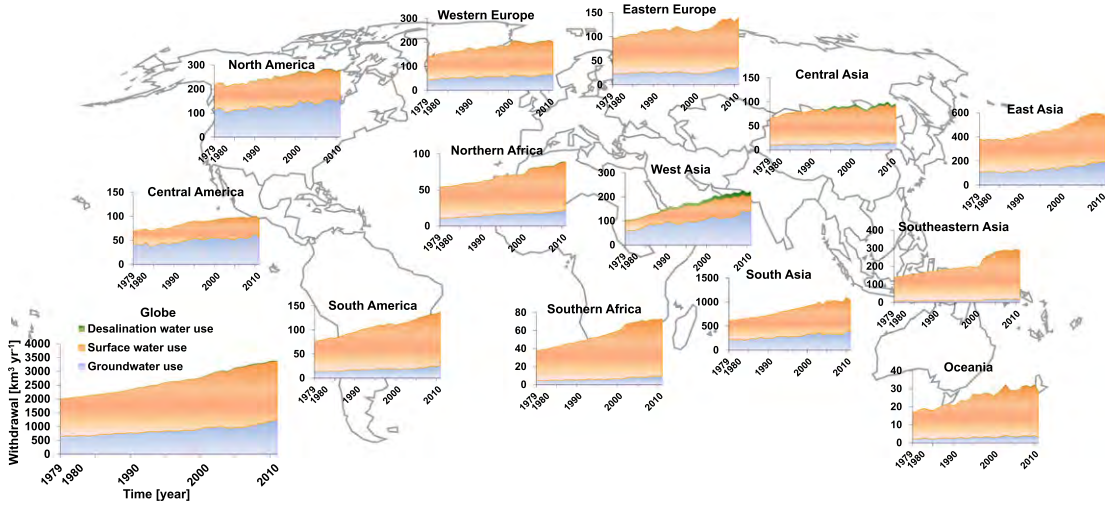

Figure 8. Global and regional trends in surface water and groundwater use (adapted from Wada *et al* 2014).

As far as the acceleration is concerned, results from this study remain inconclusive. But they suggest that there is no significant acceleration in LWS change over the 2003–2013 decade, in agreement with Wada *et al* (2012)'s results. Over the 2000s, Jung *et al* (2010) suggest higher soil moisture and large water availability, which reduce the amount of irrigation needs and thus groundwater pumping. Figure 8 shows the global and regional trends in surface water and groundwater use. For South Asia (India, Pakistan), North America (USA), and Western Europe (Spain, Greece, Italy) where the sum of regional groundwater depletion accounts for more than half of the global total, the increase in groundwater pumping is low over the period. This substantially slowed down the increase in groundwater contribution to sea level rise. At the same time, negative contribution due to reservoir impoundment is also rather constant over the same period, with a sharp increase due to the Three Gorges Dams only over a few years. Considering the two terms being almost constant, the net contribution also became rather constant with negligible acceleration over the 2000s. This explains the results obtained in this study.

Finally, our study confirms that total LWS rate is highly variable on the short-term (interannual time scale) and much impacted by ENSO events. The net LWS rate due to direct anthropogenic forcing (Wada *et al* 2012) also responds to ENSO events, likely via aquifer recharge.

Acknowledgments

H B Dieng is supported by an ESA (European Space Agency) grant in the context of the Climate Change Initiative (CCI) project. Y Wada is supported by Japan Society for the Promotion of Science (JSPS) Oversea Research Fellowship (grant no. JSPS-2014-878). We thank S Yi for providing us with his GRACE-based land water time series, as well as B Decharme for making available to us the outputs of the ISBA/TRIP hydrological model.

References

Alkama R *et al* 2010 Global evaluation of the ISBA-TRIP continental hydrological system I. Comparison to GRACE terrestrial water storage estimates and *in situ* river discharges *J. Hydromet.* **11** 583–600

Balmaseda M A, Mogensen K and Weaver A 2013 Evaluation of the ECMWF ocean reanalysis ORAS4 *Q. J. R. Meteorol. Soc.* **139** 1132–61

Biancamaria S, Cazanave A, Mognard N, Llovel W and Frappart F 2011 Satellite-based high latitudes snow volume trend, variability and contribution to sea level over 1989/2006 *Glob. Planet. Change* **75** 99–107

Chambers D P, Wahr J, Tamisiea M E and Nerem R S 2010 Ocean mass from GRACE and glacial isostatic adjustment *J. Geophys. Res.* **115** B11415

Chao B F, Wu Y H and Li Y S 2008 Impact of artificial reservoir water impoundment on global sea level *Science* **320** 212–4

Church J A *et al* 2013 Sea level change *Climate Change 2013: The Physical Science Basis. Contribution of Working Group I to the Fifth Assessment Report of the Intergovernmental Panel on Climate Change* ed T F Stocker *et al* (Cambridge: Cambridge University Press)

Dee D P *et al* 2011 The ERA-Interim reanalysis: configuration and performance of the data assimilation system *Q. J. R. Meteorol. Soc.* **137** 553–97

Dieng H B, Cazenave A, Messignac B, Henry O, von Schuckmann K and Lemoine J M 2014 Effect of La Niña on the global mean sea level and north Pacific ocean mass over 2005–2011 *J. Geodetic Sci.* **4** 19–27

Dieng H B, Palanisamy H, Cazenave A, Meyssignac B and von Schuckmann K 2015a The sea level budget since 2003: inference on the deep ocean heat content *Surv. Geophys.* **36** 209–29

Dieng H, Cazenave A, von Shuckmann K, Ablain M and Meyssignac B 2015b Sea level budget over 2005–2013: missing contributions and data errors *Ocean Sci.* **11** 1–14

Döll P, Fritsche M, Eicker A and Mueller Schmied H 2014a Seasonal water storage variations as impacted by water abstractions: comparing the output of a global hydrological model with GRACE and GPS observations *Surv. Geophys.* **35** 1311–31

Döll P, Mueller S H, Schuh C, Portmann F T and Eicker A 2014b Global-scale assessment of groundwater depletion and related groundwater abstractions: combining hydrological

modeling with information from well observations and GRACE satellites *Water Resour. Res.* **50** 5698–720
Famiglietti J S 2014 The global groundwater crisis *Nat. Clim. Change* **4** 945–8
Forsberg R *et al* 2014 Mass balance of Greenland from combined GRACE and satellite altimetry inversion, 2014 *AGU fall meeting*
Gardner A S *et al* 2013 A reconciled estimate of glacier contributions to sea level rise, 2003–2009 *Science* **340** 852–7
Jensen L, Rietbroek R and Kusche J 2013 Land water contribution to sea level and Jason-1 measurements *J. Geophys. Res: Oceans* **118** 212–26
Johnson G C and Chambers D P 2013 Ocean bottom pressure seasonal cycles and decadal trends from GRACE Release-05: Ocean circulation implications *J. Geophys. Res. Oceans* **118** 4228–40
Jung M *et al* 2010 Recent decline in the global land evapotranspiration trend due to limited moisture supply *Nature* **467** 951–4
Konikow L F 2011 Contribution of global groundwater depletion since 1900 to sea-level rise *Geophys. Res. Lett.* **38** L17401
Landerer F W and Swenson S C 2012 Accuracy of scaled GRACE terrestrial water storage estimates *Water Resour. Res.* **48** W04531
Llovel W, Becker M, Cazenave A and Crétaux J F 2010 Contribution of land water storage change to global mean sea level from GRACE and satellite altimetry *C.R. Geosci.* **342** 179–88
Llovel W, Willis J K, Landerer F W and Fukumori I 2014 Deep-ocean contribution to sea level and energy budget not detectable over the past decade *Nat. Clim. Change* **4** 1031–5
Longuevergne L, Scanlon B R and Wilson C R 2010 GRACE Hydrological estimates for small basins: evaluating processing approaches on the High Plains Aquifer, USA *Water Resour. Res.* **46** W11517
Mantas V M, Liu Z and Pereira A J S C 2015 A Web service and android application for the distribution of rainfall estimates and Earth observation data *Comput. Geosci.* **77** 66–76
Ngo-Duc T, Laval K, Polcher J, Lombard A and Cazenave A 2005 Effects of land water storage on global mean sea level over the past 50 years *Geophys. Res. Lett.* **32** L09704
Pokhrel Y N, Hanasaki N, Yeh P J-F, Yamada T, Kanae S and Oki T 2012 Model estimates of sea level change due to anthropogenic impacts on terrestrial water storage *Nat. Geosci.* **5** 389–92
Schrama E J O, Wouters B and Rietbroek R 2014 A mascon approach to assess ice shett and glacier mass balance and their uncertainties from GRACE data *J. Geophys. Res. Solid Earth* **119** 6048–66
Velicogna I, Sutterley T C and van den Broeke M R 2014 Regional acceleration in ice mass loss from Greenland and Antarctica using grace time variable gravity data *Geophys. Res. Lett.* **41** 8130–7
Wada Y 2015 Modelling groundwater depletion at regional and global scales: present state and future prospects *Surv. Geophys.* in press (doi:10.1007/s10712-015-9347-x)
Wada Y, van Beek L P H, Weiland F C S, Chao B F, Wu Y-H and Bierkens M F P 2012 Past and future contribution of global groundwater depletion to sea-level rise *Geophys. Res. Lett.* **39** L09402
Wada Y, Wisser D and Bierkens M F P 2014 Global modeling of withdrawal, allocation and consumptive use of surface water and groundwater resources *Earth Syst. Dyn.* **5** 15–40
Yi S, Sun W, Heki K and Qian A 2015 An increase in the rate of global mean sea level rise since 2010 *Geophys. Res. Lett.* **42** 3998–4006

Supporting Information

1. Publications used for the Greenland, Antarctica and Glaciers mass balance trends

Greenland Ice Sheet (GrIS)

Barletta V R, Sørensen L S and Forsberg R 2013 Scatter of mass changes estimates at basin scale for Greenland and Antarctica Cryosphere 7 1411–32.

Chen J L, Wilson C R and Tapley B D 2006 Satellite gravity measurements confirm accelerated melting of Greenland ice sheet Science 313 1958–60.

Chen J L, Wilson C R and Tapley B D 2013 Contribution of ice sheet and mountain glacier melt to recent sea level rise Nature Geoscience 6 549-552.

Csatho B M, Schenk A F, van der Veen C J, Babonisa G, Duncan K, Rezvanbehbahani S, van den Broeke M R, Simonsen S B, Nagarajan S and van Angelen J H 2014 Laser altimetry reveals complex pattern of Greenland Ice Sheet dynamics P NATL ACAD SCI 111 18478–18483

Enderlin E M, Howat I M, Jeong S, Noh M-J, van Angelen J H and van den Broeke M R 2014 An improved mass budget for the Greenland ice sheet Geophys. Res. Lett. 41 866–72.

Ewert H, Groh A and Dietrich R 2012 Volume and mass changes of the Greenland ice sheet inferred from ICESat and GRACE J. Geodyn. 59–60 111–23

Groh A, Ewert H, Fritsche M, Rülke A, Rosenau R, Scheinert M and Dietrich R 2014 Assessing the current evolution of the Greenland ice sheet by means of satellite and ground-based observations Surv. Geophys. 35 1459–80

Helm V, Humbert A and Miller H 2014 Elevation and elevation change of Greenland and Antarctica derived from CryoSat-2, Cryosphere 8 1539–59

Hurkmans R T W L, Bamber J L, Davis C H, Joughin I R, Khvorostovsky K S, Smith B S and Schoen N 2014 Time-evolving mass loss of the Greenland ice sheet from satellite altimetry Cryosphere 8 1725–40

Jacob T, Wahr J, Pfeffer W T and Swenson S 2012 Recent contributions of glaciers and ice caps to sea-level rise Nature 482 514–8

Khan Shfaqat A, Aschwanden A., Bjørk A. A. , Wahr J., Kjeldsen K. K. and Kjær K. H., 2015 Greenland ice sheet mass balance, Rep. Prog. Phys. 78 046801 (26pp), doi:10.1088/0034-4885/78/4/046801

Luthke S B, Zwally H J, Abdalati W, Rowlands D D, Ray R D, Nerem R S, Lemoine F G, McCarthy J J and Chinn D S 2006 Recent Greenland ice mass loss by drainage system from satellite gravity observations Science 314 1286–9

Ramillien G, Lombard A, Cazenave A, Ivins E R, Llubes M, Remy F and Biancale R 2006 Interannual variations of the mass balance of the Antarctica and Greenland ice sheets from GRACE Glob. Planet. Change 53 198–208

Rignot E, Box J E, Burgess E and Hanna E 2008 Mass balance of the Greenland ice sheet from 1958 to 2007 Geophys. Res. Lett. 35 L20502

Rignot E and Kanagaratnam P 2006 Changes in the velocity structure of the Greenland ice sheet Science 311 986–90

Rignot E, Velicogna I, van den Broeke M R, Monaghan A and Lenaerts J 2011 Acceleration of the contribution of the Greenland and Antarctic ice sheets to sea level rise Geophys. Res. Lett. 38 L05503

Sasgen I, van den Broeke M, Bamber J L, Rignot E, Sørensen L S, Wouters B, Martinec Z, Velicogna I and Simonsen S B 2012 Timing and origin of recent regional ice-mass loss in Greenland Earth Planet. Sci. Lett. 333–334 293–303

Schrama, E. J. O., B. Wouters, and R. Rietbroek 2014 A mascon approach to assess ice sheet and glacier mass balances and their uncertainties from GRACE data, J. Geophys. Res. Solid Earth, 119, 6048–6066, doi:10.1002/2013JB010923.

Shepherd A et al 2012 A reconciled estimate of ice-sheet mass balance Science 338 1183–9

Siemes C, Ditmar P, Riva R E M, Slobbe D C, Liu X L and Farahani H H 2013 Estimation of mass change trends in the Earth's system on the basis of GRACE satellite data, with application to Greenland J Geod. 87 69–87

Slobbe D C, Ditmar P and Lindenbergh R C 2009 Estimating the rates of mass change, ice volume change and snow volume change in Greenland from ICESat and GRACE data Geophys. J. Int. 176 95–106

Sørensen L S, Simonsen S B, Nielsen K, Lucas-Picher P, Spada G, Adalgeirs-dottir G, Forsberg R and Hvidberg C S 2011 Mass balance of the Greenland ice sheet (2003–2008) from ICESat data—the impact of interpolation, sampling and firn density Cryosphere 5 173–86

van den Broeke M, Bamber J, Ettema J, Rignot E, Schrama E, van de Berg W J, van Meijgaard E, Velicogna I and Wouters B 2009 Partitioning recent Greenland mass loss Science 326 984–6

Velicogna I 2009 Increasing rates of ice mass loss from the Greenland and Antarctic ice sheets revealed by GRACE Geophys. Res. Lett. 36 L19503

Velicogna I, Sutterley T C and van den Broeke M R 2014 Regional acceleration in ice mass loss from Greenland and Antarctica using GRACE time-variable gravity data Geophys. Res. Lett. 41 8130–7

Velicogna I and Wahr J 2006 Acceleration of Greenland ice mass loss in spring 2004 Nature 443 328–31

Velicogna I and Wahr J 2013 Time-variable gravity observations of ice sheet mass balance: precision and limitations of the GRACE satellite data Geophys. Res. Lett. 40 3055–63

Wouters B, Chanbers D and Schrama E J O 2008 GRACE observes small-scale mass loss in Greenland Geophys. Res. Lett. 35 L20501

Wouters B, Bamber J L, van den Broeke M R, Lenaerts J T M and Sasgen I 2013 Limits in detecting acceleration of ice sheet mass loss due to climate variability Nat. Geosci. 6 613–6

Yi S, Sun W, Heki K and Qian A 2015 An increase in the rate of global mean sea level rise since 2010. *Geophys. Res. Lett.*, doi :10.1002/2015GL063902.

Zwally H J et al 2011 Greenland ice sheet mass balance: distribution of increased mass loss with climate warming; 2003–07 versus 1992–2002 J. Glaciol. 57 88–102

Antarctica Ice Sheet (AIS)

Barletta V R, Sørensen L S and Forsberg R 2013 Scatter of mass changes estimates at basin scale for Greenland and Antarctica Cryosphere 7 1411–32.

Chen J L, Wilson C R and Tapley B D 2013 Contribution of ice sheet and mountain glacier melt to recent sea level rise Nature Geoscience 6 549-552.

GAO Chun-Chun, LU Yang, ZHANG Zi-Zhan, SHI Hong-Ling, ZHU Chuan-Dong, 2015 Ice sheet mass balance in Antarctica measured by GRACE and its uncertainty, Chinese journal of geophysics, Vol. 58, No. 3.

Groh, A., H. Ewert , R. Rosenau, E. Fagiolini, C. Gruber, D. Floricioiu, W. Abdel Jaber, S. Linow, F. Flechtner, M. Eineder, W. Dierking, R. Dietrich, 2014 Mass, Volume and Velocity of the Antarctic Ice Sheet: Present-Day Changes and Error Effects, Survey in Geophys. 35:1481–1505 DOI 10.1007/s10712-014-9286-y

Harig C and Simons F J 2015 Accelerated West Antarctic ice mass loss continues to outpace East Antarctic gains, Earth and Planetary Science Letters 415 134–141

Helm V, Humbert A and Miller H 2014 Elevation and elevation change of Greenland and Antarctica derived from CryoSat-2 Cryosphere 8 1539–59

Jacob Thomas, John Wahr, W. Tad Pfeffer & Sean Swenson 2012 Recent contributions of glaciers and ice caps to sea level rise, doi:10.1038/nature10847

Sasgen I., H. Konrad ,E. R. Ivins ,M. R. Van den Broeke ,J. L. Bamber ,Z. Martinec ,and V. Klemann 2013 Antarctic ice-mass balance 2003 to 2012: regional reanalysis of GRACE satellite gravimetry measurements with improved estimate of glacial-isostatic adjustment based on GPS uplift rates, Cryosphere, 7, 1499–1512

Schrama, E. J. O., B. Wouters, and R. Rietbroek 2014 A mascon approach to assess ice sheet and glacier mass balances and their uncertainties from GRACE data, J. Geophys. Res. Solid Earth, 119, 6048–6066, doi:10.1002/2013JB010923.

Shepherd A et al 2012 A reconciled estimate of ice-sheet mass balance Science 338 1183–9

Velicogna I, Sutterley T C and van den Broeke M R 2014 Regional acceleration in ice mass loss from Greenland and Antarctica using GRACE time-variable gravity data Geophys. Res. Lett. 41 8130–7

Velicogna I and Wahr J 2013 Time-variable gravity observations of ice sheet mass balance: precision and limitations of the GRACE satellite data Geophys. Res. Lett. 40 3055–63

Williams S D P, Moore P, King M A, Whitehouse P L 2014 Revisiting GRACE Antarctic ice mass trends and accelerations considering autocorrelation, Earth Planet.Science Lett. 385 12–21

Wouters B, Bamber J L, van den Broeke M R, Lenaerts J T M and Sasgen I 2013 Limits in detecting acceleration of ice sheet mass loss due to climate variability Nat. Geosci. 6 613–6

Yi S, Sun W, Heki K and Qian A 2015 An increase in the rate of global mean sea level rise since 2010. *Geophys. Res. Lett.,* doi :10.1002/2015GL063902.

Glaciers

Gardner, A. S., et al. (2013), A reconciled estimate of glacier contributions to sea level rise: 2003 to 2009, Science, 340, 852–857, doi:10.1126/science.1234532.

Schrama, E. J. O., B. Wouters, and R. Rietbroek (2014), A mascon approach to assess ice sheet and glacier mass balances and their uncertainties from GRACE data, J. Geophys. Res. Solid Earth, 119, 6048–6066, doi:10.1002/2013JB010923.

Yi S, Sun W, Heki K and Qian A 2015 An increase in the rate of global mean sea level rise since 2010. *Geophys. Res. Lett.,* doi :10.1002/2015GL063902.

2. Table SI1: Published trend values for the Greenland Ice Sheet

Period	Mid-period	Trends (mm/yr)	Errors (mm/yr)	References
2003-2007	2005,495	0,48	0,01	Zwally et al. 2011
2003-2008	2005,995	0,65	0,08	Sorensen et al. 2011
2003-2008	2005,995	0,53	0,06	Sorensen et al. 2011
2003-2008	2005,995	0,67	0,08	Sorensen et al. 2011
2003-2008	2005,995	0,5	0,08	Ewert et al. 2012
2003-2009	2006,495	0,68	0,08	Sasgen et al. 2012
2003-2006	2004,995	0,48	0,06	Khan et al. 2015
2006-2009	2007,995	0,81	0,06	Khan et al. 2015
2009-2012	2010,995	1	0,08	Khan et al. 2015
2003-2008	2005,995	0,65	0,13	Hurkmans et al. 2014
2005-2006	2005,995	0,57	0,11	Rignot and Kanagaratnam 2006
2003-2008	2005,995	0,67	0,06	van den Broeke et al. 2009
2003-2009	2006,495	0,72	0,16	Sasgen et al. 2012
2005-2009	2007,495	0,74	0,05	Enderlin et al. 2014
2009-2012	2010,995	1,05	0,14	Enderlin et al. 2014
2007-2011	2009,495	0,73	0,06	Khan et al. 2015
2002-2005	2003,995	0,61	0,06	Chen et al. 2006
2003-2005	2004,495	0,28	0,04	Luthke et al. 2006
2002-2006	2004,495	0,63	0,09	Velicogna and Wahr 2006
2002-2005	2003,995	0,33	0,04	Ramillien et al. 2006
2003-2008	2005,995	0,5	0,07	Wouters et al. 2008
2003-2005	2004,495	0,34	0,08	Wouters et al. 2008
2006-2008	2007,495	0,57	0,07	Wouters et al. 2008
2002-2007	2004,995	0,48	0,13	Slobbe et al. 2009
2002-2009	2005,995	0,64	0,09	Velicogna 2009
2002-2009	2005,995	0,53	0,06	Ewert et al. 2012

2003-2009	2006,495	0,66	0,08	Sasgen et al. 2012
2003-2004	2003,995	0,36	0,04	Siemes et al. 2013
2005-2006	2005,995	0,41	0,05	Siemes et al. 2013
2007-2008	2007,995	0,58	0,08	Siemes et al. 2013
2003-2008	2005,995	0,46	0,04	Siemes et al. 2013
2003-2011	2007,495	0,65	0,06	Barletta et al. 2013
2003-2008	2005,995	0,59	0,06	Barletta et al. 2013
2002-2007	2004,995	0,5	0,06	Barletta et al. 2013
2007-2011	2009,495	0,77	0,08	Barletta et al. 2013
2003-2012	2007,995	0,72	0,11	Velicogna and Wahr 2013
2003-2006	2004,995	0,57	0,06	Khan et al. 2015
2006-2009	2007,995	0,71	0,06	Khan et al. 2015
2009-2012	2010,995	1	0,06	Khan et al. 2015
2000-2011	2005,995	0,59	0,1	Shepherd et al. 2012
2005-2010	2007,995	0,73	0,08	Shepherd et al. 2012
2003-2008	2005,995	0,64	0,06	Shepherd et al. 2012
Fev 2003-June2013	2008,33	0,77	0,05	Schrama et al. 2014
Jan2003-Dec2010	2006,995	0,61	0,03	Jacob et al. 2012
Jan2003-Sept2012	2007,875	0,69	0,06	Wouters et al. 2013
Jan2003-Dec2012	2007,995	0,64	0,07	Groh et al. 2014
Jan2005-Dec2011	2008,495	0,69	0,07	Chen et al. 2013
2003-2009	2006,495	0,68	0,05	Csatho et al. 2014
2002-2011	2006,995	0,59	0,08	Velicogna et al. 2014
2003-2013	2008,495	0,77	0,16	Velicogna et al. 2014
Jan2005-Dec2009	2007,495	0,57	0,09	Yi et al. 2015
Jan2010-July2014	2012,3	0,89	0,09	Yi et al. 2015

3. Table SI2: Published trends for the Antarctica Ice Sheet

Period	Mid-period	Trends (mm/yr)	Errors (mm/yr)	References
Jan2003-Sept2012	2007,875	0,32	0,06	Sasgen et al. 2013
Aug2002-Jul2007	2005,13	0,01	0,12	Barletta et al. 2013
Oct2003-Nov2008	2006,375	0,17	0,12	Barletta et al. 2013
Jan2003-Nov2011	2007,42	0,23	0,1	Barletta et al. 2013
Aug2007-Nov2011	2009,79	0,33	0,14	Barletta et al. 2013
Oct2003-Dec2008	2006,42	0,2	0,12	Shepherd et al. 2012
2000-2011	2005,995	0,24	0,12	Shepherd et al. 2012
2005-2010	2007,995	0,23	0,1	Shepherd et al. 2012

2003-2013	2008,495	0,19	0,12	Velicogna et al. 2014
2002-2011	2006,995	0,4	0,01	Velicogna et al. 2014
Fev2003--Jun2013	2008,33	0,26	0,08	Schrama et al. 2014
Jan2003-Dec2010	2006,995	0,45	0,2	Jacob et al. 2012
Jan2003-Sept2012	2007,875	0,31	0,06	Wouters et al. 2013
Jan2003-Dec2012	2007,995	0,3	0,08	Groh et al. 2014
Jan2005-Dec2011	2008,495	0,5	0,26	Chen et al. 2013
2003-2008	2005,995	0,07	0,03	Helm et al. 2014
2003-2009	2006,495	0,17	0,12	Helm et al. 2014
2011-2014	2012,995	0,36	0,23	Helm et al. 2014
Jan2003-Nov2012	2007,96	0,32	0,18	Velicogna and Wahr 2013
2003-2012	2007,95	0,16	0,12	Williams et al. 2014
2003-2013	2008,79	0,26	0,03	Harig et al. 2015
Jan2003-Dec2013	2008,495	0,34	0,11	GAO et al. 2015
Jan2005-Dec2009	2007,495	0,45	0,23	Yi et al. 2015
Jan2010-Jul2014	2012,3	0,71	0,25	Yi et al. 2015

4. Table SI3: Published trend values for glaciers

Period	Mid-period	Trends (mm/yr)	Errors (mm/yr)	References
Fev2003-Jun2013	2008,33	0,45	0,03	Schrama et al. 2014
Jan2003-Dec2009	2006,495	0,59	0,07	Gardner et al. 2013
Jan2005-Dec2009	2007,495	0,67	0,05	Yi et al. 2015
Jan2010-Jul2014	2012,3	0,58	0,08	Yi et al. 2015

5. Table SI4: Trends and accelerations estimated in the main text of this study

	Trends (mm/yr)	Acceleration (mm/yr^2)
Global Ocean Mass from GRACE (GOM1)	1.85 ± 0.10	0.29 ± 0.04
Global Ocean Mass from 'GMSL minus ORAS4'	2.03 ± 0.11	0.04 ± 0.05
Water Vapor	-0.04 ± 0.04	0
Mean GrIS	0.76 ± 0.10	0.071 ± 0.007
GrIS from Velicogna et al. 2014	0.77 ± 0.16	0.071 ± 0.004
CCI GrIS	0.63 ± 0.10	0.060 ± 0.007
GrIS from Schrama et al. 2014	0.77 ± 0.05	-
Mean AIS	0.34 ± 0.12	0.051 ± 0.011
AIS from Velicogna et al. 2014	0.19 ± 0.12	0.031 ± 0.010
CCI AIS	0.27 ± 0.10	0.042 ± 0.010
AIS from Schrama et al. 2014	0.26 ± 0.08	-
Mean Glaciers	0.58 ± 0.10	-0.004 ± 0.005

AIS from Schrama et al. 2014	0.44 ± 0.03	-
Residual1 (res1)	0.21 ± 0.18	0.17 ± 0.04
Residual2 (res2)	0.39 ± 0.19	-0.08 ± 0.05
Mean of (res1 + res2)	0.30 ± 0.21	-
Residual3 (res3)	0.44 ± 0.24	-
Residual4 (res4)	0.50 ± 0.20	-
Wada et al. 2012 case1 (Wada1)	0.39 ± 0.11	0.008 ± 0.010
Wada et al. 2012 case2 (Wada2)	0.54 ± 0.12	0.008 ± 0.011

2.4 Bilan du GMSL sur la période altimétrique (1993-2014)

Dans cette section nous étudions le bilan du GMSL sur toute la période altimétrique. L'objectif principal est d'estimer toutes les composantes climatiques contribuant à la hausse du GMSL en termes de tendance sur la période allant de Janvier 1993 à Décembre 2014.

Résumé de l'article : "Evaluation of the Global Mean Sea Level Budget between 1993 and 2014" *(joint à la fin de cette section 2.4)*

Cet article constitue une synthèse sur le bilan du niveau de la mer sur la période altimétrique (1993-2014) et la période GRACE/Argo (2005-2014) en utilisant de nombreux jeux de données altimétriques, stériques et de masse. Cet article se focalise sur la période altimétrique, la période GRACE/Argo étant déjà traitée dans *Dieng et al.* (2015a, 2015b et 2015c) à la *section 2.3*.

En premier lieu nous notons que les résultats de cette étude sont en accord avec les estimations précédentes sur le bilan du niveau de la mer (par exemple, *Church et al.* 2011, 2013 ; *Llovel et al.* 2014 ; *Von Schuckmann et al.* 2014 ; *Dieng et al.* 2015a, b, c). Les principales différences concernent la période d'étude légèrement différente (avec une extension de la série altimétrique jusqu'à fin 2014) et les estimations d'incertitude que nous considérons plus robustes. Pour toutes les séries temporelles du niveau de la mer et de ses composantes, nous avons combiné les biais d'instruments et de corrections en utilisant les moindres carrés pour estimer les barres d'incertitude. Nous montrons que la dilatation thermique constitue environ 40% du signal de la hausse du GMSL sur la période altimétrique, avec une grande contribution de la couche océanique 0-700 m. Nous notons aussi que l'océan profond contribue encore de manière non négligeable à la hausse du niveau de la mer. Sur les 60% restants, la contribution des glaciers de montagne et les glaciers périphériques aux calottes polaires est estimée à ~25% de la hausse totale du GMSL. Les calottes polaires du Groenland et de l'Antarctique et l'hydrologie continentale contribuent respectivement pour 19% et ~15%. Au cours de la dernière décennie, les contributions du Groenland et de l'Antarctique ont considérablement augmenté. Depuis 2005, le Groenland contribue pour 21% à la hausse du GMSL, tandis que l'Antarctique contribue pour 11%. Ensemble, cela constitue presque un tiers de la hausse du GMSL, et une augmentation de près de 68% par rapport à la tendance de 20 ans.

La conclusion générale est que le bilan du GMSL se ferme à la fois sur la période plus longue (1993-2014) et plus courte (2005-2014) dans les barres d'incertitude. Cependant, comme indiqué dans la section précédente, nous sommes encore limités par les erreurs systématiques

potentielles dans les systèmes d'observation et les corrections appliquées. Ainsi, des efforts concertés et continus sont nécessaires pour comprendre et mesurer l'incertitude systématique dans toutes les composantes du système d'observation.

Surv Geophys
DOI 10.1007/s10712-016-9381-3

Evaluation of the Global Mean Sea Level Budget between 1993 and 2014

Don P. Chambers[1] · Anny Cazenave[2,3] · Nicolas Champollion[3] · Habib Dieng[2] · William Llovel[4] · Rene Forsberg[5] · Karina von Schuckmann[6] · Yoshihide Wada[7]

Received: 21 December 2015 / Accepted: 22 July 2016

Abstract Evaluating global mean sea level (GMSL) in terms of its components—mass and steric—is useful for both quantifying the accuracy of the measurements and understanding the processes that contribute to GMSL rise. In this paper, we review the GMSL budget over two periods—1993 to 2014 and 2005 to 2014—using multiple data sets of both total GMSL and the components (mass and steric). In addition to comparing linear trends, we also compare the level of agreement of the time series. For the longer period (1993–2014), we find closure in terms of the long-term trend but not for year-to-year variations, consistent with other studies. This is due to the lack of sufficient estimates of the amount of natural water mass cycling between the oceans and hydrosphere. For the more recent period (2005–2014), we find closure in both the long-term trend and for month-to-month variations. This is also consistent with previous studies.

Keywords Sea level · Ocean mass · Steric sea level · Climate change

✉ Don P. Chambers
donc@usf.edu

[1] College of Marine Science, University of South Florida, 140 7th Ave. S, MSL119, St. Petersburg, FL 33701, USA

[2] Laboratoire d'Etudes en Géophysique et Océanographie Spatiales (LEGOS), 18 avenue Edouard BELIN, 31401 Toulouse Cedex 9, France

[3] International Space Science Institute (ISSI), Hallerstrasse 6, 3012 Bern, Switzerland

[4] Centre Européen de Recherche et de Formation Avancée en Calcul Scientifique (CERFACS), URA1875, 42 Avenue Gaspard Coriolis, 31057 Toulouse Cedex 1, France

[5] Division of Geodynamics, Technical University of Denmark, Elektrovej Building 327, room 022, 2800 Kgs., Lyngby, Denmark

[6] MERCATOR-Ocean, 10 Rue Hermès, 31520 Ramonville-Saint-Agne, France

[7] Department of Physical Geography, Utrecht University, P.O. Box 80115, 3508, TC, Utrecht, The Netherlands

Published online: 17 August 2016

1 Introduction

Sea level varies on a variety of spatial and temporal scales. Regionally, fluctuations in wind and currents can cause large deviations in sea level away from the global mean for periods of years to decades (e.g., Miller and Douglas 2007; Sturges and Douglas 2011; Chambers et al. 2012; Calafat and Chambers 2013; Palanisamy et al. 2015). One example of regional sea level change, from the tide gauge at Key West, Florida, is shown in Fig. 1, compared with an estimate of global mean sea level (GMSL) reconstructed from tide gauge records.

These large regional fluctuations, however, reflect mainly dynamical redistributions of heat and mass in the ocean and thus should average to zero when integrated over the global ocean. While the tide gauge network before the 1960s might not be sufficient to completely average these effects (see Fig. 8 in Calafat et al. 2014), satellite observations of sea surface height allow us to almost completely average out these internal variations and detect the smaller GMSL signal. These records show that GMSL has been rising at a rate between 2.8 and 3.6 mm year^{-1} between January 1993 and December 2014 (90 % confidence bands), with significant low-frequency variability superimposed (e.g., Nerem et al. 2010; Church et al. 2013; Ablain et al. 2015).

However, in order to predict future sea level rise, it is not sufficient to just determine the rate of rise of GMSL. One also needs to understand the mechanisms driving GMSL variability, and how they are changing in time. The primary mechanisms leading to current GMSL rise are: (1) water mass lost from ice sheets, glaciers, and ice caps that is gained by the oceans (e.g., Shepherd et al. 2012; Gardner et al. 2013), (2) volume (density) change due to thermal expansion as the oceans warm (e.g., Domingues et al. 2008; Levitus et al. 2012), and (3) changes in land water storage (e.g., Wada et al. 2012). Salinity changes due to land ice melt, river runoff, and changes in evaporation/precipitation increase have only second-order effects on the GMSL (e.g., Gregory and Lowe 2000). But in practice, as observations are not exactly global, salinity changes to density should also be accounted for when data are available. The combined effect of ocean temperature and salinity is

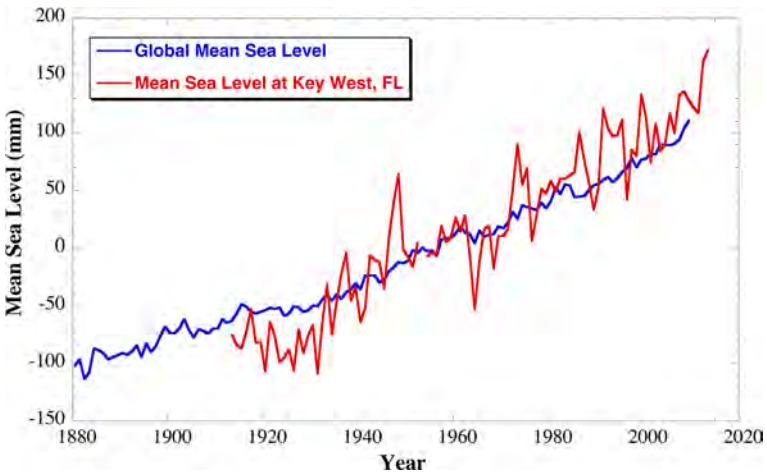

Fig. 1 Yearly averaged sea level change recorded by tide gauges at Key West, Florida compared to GMSL estimate from Church and White (2011). Tide gauge is from the Permanent Service for Mean Sea Level in Liverpool, UK

called the *steric* component, with the thermal contribution denoted *thermosteric*, and salinity contribution *halosteric*.

Because GMSL and estimates of the steric and mass components have different uncertainties and the potential for systematic errors, one often investigates the sea level budget to see how well it closes:

$$\mathrm{GMSL}(t) = \mathrm{GMSL}_{\mathrm{mass}}(t) + \mathrm{GMSL}_{\mathrm{steric}}(t). \quad (1)$$

At any particular time, t, the residual $(\mathrm{GMSL}(t) - \mathrm{GMSL}_{\mathrm{mass}}(t) - \mathrm{GMSL}_{\mathrm{steric}}(t))$ is unlikely to be exactly zero due to random and short-period errors. However, over the long-term, the residual differences should be small. When they are not, it indicates a problem in one or more of the terms in Eq. (1).

In addition, the mass and steric components are often subdivided into the various contributors. For mass, this includes separate estimates for contributions from the Greenland and Antarctica ice sheets, as well as from glaciers and ice caps. Exchanges of water mass between the oceans and the continents related to natural variability contribute significantly to seasonal and interannual contributions (e.g., Chambers et al. 2004; Llovel et al. 2011; Fasullo et al. 2013; Cazenave et al. 2014, Dieng et al. 2015a; Reager et al. 2016; Rietbroek et al. 2016), while storing water behind dams and extracting water from aquifers lead to non-negligible trends in GMSL (Chao et al. 2008; Konikow 2011; Pokhrel et al. 2012; Wada et al. 2012; Wada 2015; Dieng et al. 2015a).

Thermosteric changes are often separated into the upper ocean above 700 m, the layer between 700 and 1000 m, and the deeper ocean (e.g., Domingues et al. 2008; Purkey and Johnson 2010; Levitus et al. 2012). This is mainly an artifact of the older observing system, with substantially more observations in the upper ocean so that yearly averages could be obtained, whereas for the deeper layers, more temporal averaging is needed to extract the trend in the thermosteric component of GMSL. The halosteric component due to salinity changes is poorly known before the advent of the Argo observing system in the early 2000s (e.g., Durack et al. 2013), so typically, the halosteric contribution is neglected in sea level budget studies that include data from the 1990s (e.g., Domingues et al. 2008; Church et al. 2011). For this study, we also only consider the thermosteric sea level for the longer time period (1993–2015) and the steric sea level for the shorter time period (2005–2014).

One way to quantify the closure of the sea level budget is computing trends in GMSL and the various components over various periods of time, and summing these up to see if they match within the uncertainty (e.g., Church et al. 2011, 2013). However, with the advent of global measurements of ocean mass from the GRACE satellite mission (e.g., Johnson and Chambers 2013; Llovel et al. 2014) and ocean temperatures and salinity above 2000 m depth from Argo autonomous profiling floats (Llovel et al. 2014; von Schuckmann et al. 2014), one can now look at the closure on monthly time scales since 2005 (e.g., Dieng et al. 2015b, c for a recent review).

In this paper, we will review the closure of the sea level budget not only in terms of trends, but also in terms of the temporal variability of GMSL and its components. We utilize numerous estimates of GMSL from altimetry, as well as several estimates of the mass components and thermosteric change. These data sets have slightly different temporal sampling and filtering applied. To be consistent, we will utilize a common sampling and filtering scheme to all data. Trends are computed over the same time periods, and uncertainty is computed accounting for correlated signals in the residuals. We assess the closure of the sea level budget on two different time periods: January 1993 to December

2014 (a mixture of all measurements), and January 2005 to December 2014 (GRACE/Argo/altimetry only).

Section 2 will discuss the specific datasets used, filtering applied, and methods used to compute trends and uncertainty. Section 3 will summarize the level of closure of the sea level budget for the three time periods, and Sect. 4 will discuss the results.

2 Data and Methods

2.1 Satellite Altimetry

Products from six processing groups are available for the altimetry-based sea level time series:

1. Validation and Interpretation of Satellite Oceanographic (AVISO; http://www.aviso.altimetry.fr/en/data/products/ocean-indicators-products/actualitesindicateurs-des-oceansniveau-moyen-des-mersindexhtml.html);
2. University of Colorado (CU Release 5; http://sealevel.colorado.edu/).
3. National Oceanographic and Atmospheric Administration (NOAA; http://www.star.nesdis.noaa.gov/sod/lsa/SeaLevelRise/LSA_SLR_timeseries_global.php).
4. Goddard Space Flight Center (GSFC version 2; http://podaac-ftp.jpl.nasa.gov/dataset/MERGED_TP_J1_OSTM_OST_GMSL_ASCII_V2)
5. Commonwealth Scientific and Industrial Research Organization (CSIRO; www.cmar.csiro.au/sealevel/sl_data_cmar.html).
6. The CCI sea level data (ftp.esa-sealevel-cci.org/Products/SeaLevel-ECV/V1_11092012/), Ablain et al. (2015).

The first five sea level data sets are based on TOPEX/Poseidon, Jason-1 and Jason-2 data averaged over the 66°S–66°N domain, except for the CSIRO data averaged over 65°S–65°N. The CCI dataset is based primarily on TOPEX/Poseidon, Jason-1 and Jason-2, but also includes data from the Envisat, ERS-1, and ERS-2 altimeter missions after they have been adjusted to remove orbit error and biases relative to TOPEX/Poseidon, Jason-1 and Jason-2. For each product, a set of instrumental and geophysical corrections is applied (details are given on the websites of each data set). In addition, the effect of glacial isostatic adjustment (GIA) using the estimate proposed by Peltier (2004) is accounted for in each sea level time series except for the NOAA data set. Thus, we corrected the latter for the GIA effect, by adding 0.3 mm year^{-1} to the GMSL time series (Peltier 2004).

The sea level time series are obtained either by directly averaging the along-track sea surface height data (e.g., CU) or by first gridding the unevenly distributed along-track data and then performing grid averaging (e.g., AVISO and NOAA). In all cases, an area weighting is applied. In addition to the geographical averaging method, other differences exist between the GMSL data sets because of the applied geophysical and instrumental corrections and the number of satellites considered. Discussion on these differences can be found in Masters et al. (2012), Henry et al. (2014), and Ablain et al. (2015). Details on the exact corrections applied to the altimetry data are detailed on the webpages of each group.

Five of the time series used in this study cover the period January 1993–December 2014, but one (the CCI product) ends in December 2013. Figure 2 shows the GMSL time series, after removing an annual and semiannual sinusoids and smoothing with a 3-month running mean to reduce a 60-day erroneous signal (e.g., Masters et al. 2012). At shorter time scales (from sub-seasonal to multi-annual) significant discrepancies of several mm are

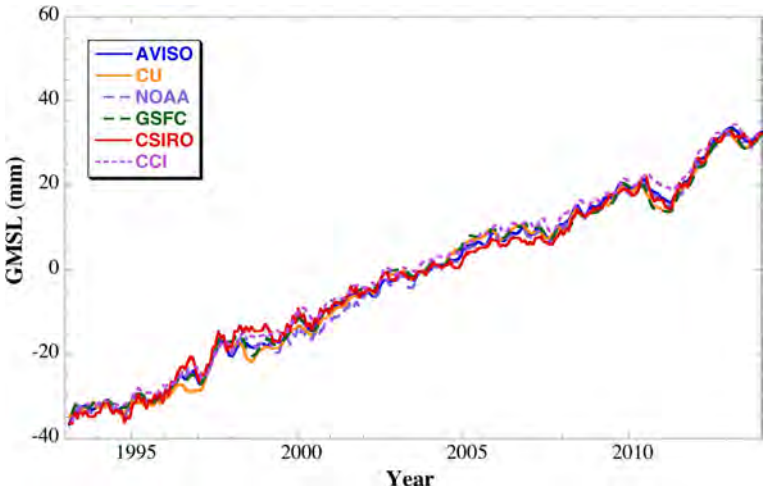

Fig. 2 GMSL from altimetry calculated by six different centers. Annual and semi-annual sinusoids have been estimated and removed, and a 3-month running mean filter has been applied

observed between the different GMSLs, especially between 2005 and 2008, and between mid-2010 and mid-2011, when there was a significant drop in GMSL related to changes in water storage over Australia and South America (Fasullo et al. 2013).

2.2 Steric Sea Level

Before the early 2000s, information on the steric sea level component comes from temperature data, due to the lack of global salinity data, coming primarily from expendable bathythermographs (XBTs), some mechanical bathythermographs (MBTs) and a much smaller number of conductivity-temperature-depth casts (CTDs) (e.g., Levitus et al. 2012; Abraham et al. 2013). The depth ranges of these instruments are very different, with XBTs mostly going only as deep as 700 m (although some go as deep as 1000–1500 m), while CTDs often make measurements to the sea floor. In the beginning of the 2000s, with the advent of the Argo program of autonomous floats (Roemmich et al. 2009), more measurements are available at more regular time intervals and also more globally. The current average density is approximately 1 float for every $3° \times 3°$ grid over the ocean. However, the depth to which Argo floats reach has also changed over time, starting at 1000 m, but now extending to 2000 m.

Computing steric sea level anomalies from these disparate data is not a trivial matter, but many groups have done so, using different interpolation and mapping methods, as well as different corrections for the XBT fall rate biases that have only recently been discovered (e.g., Gouretski and Koltermann 2007; Wijffels et al. 2008). Some groups use all available temperature data, while others restrict the estimate to only Argo data.

To quantify the steric component of GMSL change, we will consider different datasets. For the longer period (1993–2015), we will use two that merge XBTs, MBTs, CTDs, and Argo data, and provide the thermosteric sea level anomalies as a time series. They are:

1. NOAA data set, at https://www.nodc.noaa.gov/OC5/3M_HEAT_CONTENT (Levitus et al. 2012). The data are available as yearly averages of global mean thermosteric sea

level anomalies from the surface to 700 m depth, and 5-year running averages from the surface to 2000 m depth.

2. Domingues et al. (2008) version 3.1 dataset available from http://www.cmar.csiro.au/sealevel/thermal_expansion_ocean_heat_timeseries.html. The data are available as global mean thermosteric sea level anomalies from the surface to 700 m depth at yearly time steps but with a 3-year running mean filter applied.

To compare the two time series, we have applied a 3-year running mean to the NOAA time series (Fig. 3). Although the two estimates have similar long-term trends, there are substantial differences outside the authors' estimated standard errors at interannual periods. The biggest differences occur between 2000 and 2006, when the observing system is transitioning from mainly XBTs to mainly Argo floats. It has been shown that the different mapping techniques are highly sensitive to the mixture of the XBT/Argo data during this transition, partly due to small, unknown biases between different instrument types (Lyman and Johnson 2008; Lyman et al. 2010).

We use the Levitus et al. (2012) estimate of thermosteric sea level to 2000 m, available as 5-year running means, to estimate the thermosteric component between 700 and 2000 m depth. We reconstruct the signal between 700 and 2000 m by subtracting 5-year averages of the Levitus et al. (2012) 0–700 m time series. Uncertainty is that reported by the authors (after subtracting the uncertainty from 0 to 700 m assuming no correlation).

The only observations of deep thermosteric contributions are trends computed from deep hydrographic sections (Purkey and Johnson 2010; Kouketsu et al. 2011), estimated to be 0.11 ± 0.10 mm year^{-1} [uncertainty 95 % as reported by Purkey and Johnson (2010)] between approximately 1995–2005. We assume this value represents the trend for the entire period between 1993.0 and 2015.0.

After 2005, sufficient Argo floats are available to compute steric sea level anomalies from only these data (von Schuckmann et al. 2014; Roemmich et al. 2015). For this study, we utilize four different gridded datasets, providing temperature and salinity down to 2000 m depth at monthly intervals. They are:

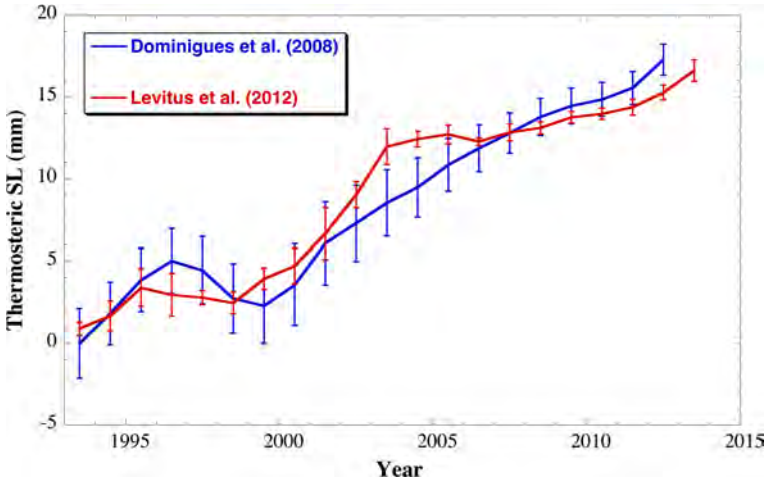

Fig. 3 Global mean thermosteric sea level contribution for upper ocean (0–700 m) from two analyses along with one standard error bars as computed by authors (Domingues et al. 2008; Levitus et al. 2012)

1. The International Pacific Research Center (IPRC; http://apdrc.soest.hawaii.edu/projects/Argo/data/Documentation/gridded-var.pdfhttp://apdrc.soest.hawaii.edu/projects/Argo/data/gridded/On_standard_levels/index-1.html)
2. The Japan Agency for Marine-Earth Science and Technology (JAMSTEC; ftp://ftp2.jamstec.go.jp/pub/argo/MOAA_GPV/Glb_PRS/OI/). Updated from Hosoda et al. (2008).
3. The SCRIPPS Institution of Oceanography (SCRIPPS; http://sio-argo.ucsd.edu/RG_Climatology.html). Updated from Roemmich et al. (2009).
4. The estimate from Karina von Schuckmann (KvS). Updated from Von Schuckmann and Le Traon (2011).

For the IPRC, JAMSTEC, and SCRIPPS data, we computed steric sea level time series from the surface down to 2000 m at monthly interval on a 1° × 1° grid for the period of January 2005 to December 2014 by integrating the density anomalies (defined as differences between the density estimate and a reference density at 0 °C and 35.16504 absolute salinity using the equation of state of seawater TEOS10 (http://www.teos-10.org/index.htm) at each standard depth. The KvS time series was computed using a similar methodology more fully described in von Schuckmann et al. (2009).

The Argo-based estimates of steric sea level since 2005 show similar decadal trends, but significantly different monthly and interannual variations (Fig. 4). Differences are of the order of 5 mm over some periods (2005 and 2010–2011, for example), but closer to 3 mm over other periods. The standard deviation of the differences ranges from a low of 1.5 mm between IPRC and JAMSTEC, to 2.9 mm between Scripps and JAMSTEC. IPRC and JAMSTEC also have the highest correlation of 0.92, while the correlation between Scripps and JAMSTEC, while still significant, is only 0.63. See Dieng et al. (2015b, c) for a detailed discussion on these differences.

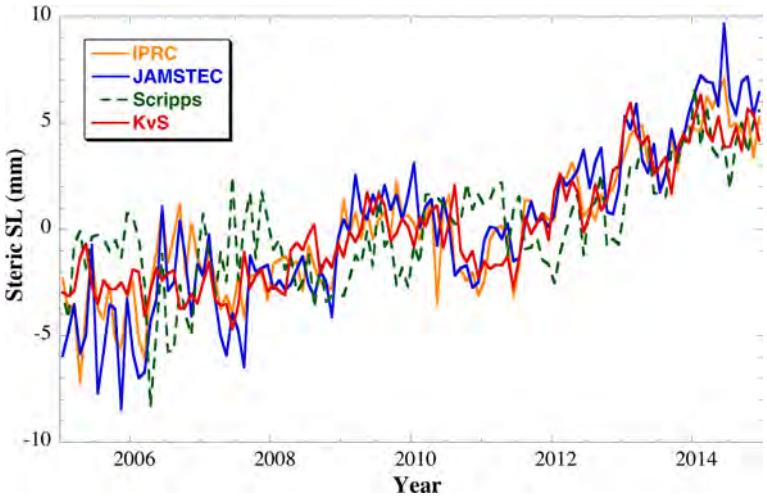

Fig. 4 Monthly estimates of global mean steric sea level anomalies (seasonal sinusoids removed) computed from Argo data from four processing centers

2.3 Satellite Gravity

The GRACE mission measures the Earth gravity field every month, generally released in terms of normalized spherical harmonic coefficients (Tapley et al. 2004), or more recently as gridded mass concentrations, or mascons (Watkins et al. 2015). One can convert the spherical harmonics into ocean mass variations in terms of an equivalent water thickness using either an averaging kernel approach (e.g., Chambers et al. 2004; Johnson and Chambers 2013), or more recently, by simply averaging the gridded mascons over the ocean domain (Watkins et al. 2015).

We utilize both approaches in this study and also use data from the three main processing centers—the Center for Space Research (CSR), the Helmholtz Centre Potsdam, German Research Centre for Geosciences (GFZ), and the Jet Propulsion Laboratory (JPL). JPL produces both spherical harmonics (SH) and mascons. Each center uses slightly different processing and analysis strategies, but many models and methods are similar. Thus, while comparison of the ocean mass from the various centers is instructive for quantifying a level of uncertainty, any systematic errors will not be obvious.

The data utilized are:

1. Averaging kernels from CSR, GFZ and JPL SH coefficients using the method described in Johnson and Chambers (2013), available from https://dl.dropboxusercontent.com/u/31563267/ocean_mass_orig.txt.
2. Averaging the JPL mascons (Watkins et al. 2015) over the global oceans, using an ocean mask that extends to the coastlines. The data are available from: http://grace.jpl.nasa.gov. Note that these data include a small signal from the global mean atmospheric pressure over the ocean, as explained in Johnson and Chambers (2013). This has been estimated and removed using the atmosphere model used to dealias the GRACE gravity data.

The differences between global mean ocean mass from the three centers and between spherical harmonics and mascons are small (Fig. 5). The biggest differences of order 5 mm

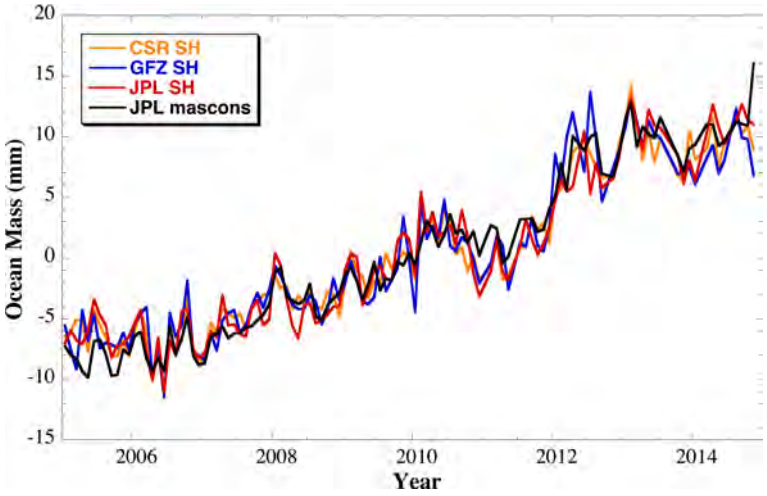

Fig. 5 Monthly estimate of global mean ocean mass anomalies (seasonal sinusoids removed) from GRACE computed by three different processing centers based on spherical harmonics (SH) and mascons

occur at the end and beginning of the records. The overall standard deviation of monthly differences is 1.6 mm.

2.4 Contributions from Ice Sheets and Glaciers

We consider contributions from the largest ice sheets (Greenland and Antarctica) separately from the glaciers and ice caps (GICs). The time series for Greenland and Antarctic mass balance comes from, for the longer period back to 1993, the synthesis of Shepherd et al (2012), based on surface mass balance models, synthetic aperture radar data, altimetry, and gravimetry (available from http://imbie.org/data-downloads/). For the shorter period since 2003, we use the estimates based only on GRACE computed by the group at the Technical University of Denmark (Sørensen and Forsberg 2010; Barletta et al. 2013).

GIC data come from an analysis of global glacier models driven by gridded climate observations, which has been shown to be consistent with extrapolations of in situ mass balance measurements (Marzeion et al. 2015).

2.5 Contributions from Land Hydrology

Ignoring the contribution from glaciers on continents, which is treated separately (Sect. 2.3), the land water contribution to sea level variation includes groundwater depletion, water impoundments behind dams, storage loss of endorheic lakes and wetlands, deforestation, and changes in soil moisture, permafrost and snow (i.e., natural water stores) (Church et al. 2011). Natural water storage change mostly varies with decadal climate variation and with insignificant trend on time periods greater than several decades (Ngo-Duc et al. 2005; Llovel et al. 2011), but can contribute to the trend on shorter periods (Cazenave et al. 2014). However, decomposing this signal is still a matter of significant research and fraught with uncertainties before GRACE observations are available starting in 2002, so we do not consider it for this study for the longer period 1993–2015.

Instead, we consider only estimates of groundwater depletion, water impoundment, deforestation, and the loss from large endorheic lakes. The contribution of groundwater depletion to GMSL is estimated using a flux-based method, i.e., calculating the difference between grid-based groundwater recharge (natural recharge and return flow from irrigation as additional recharge) and groundwater pumping (Wada et al. 2012; Wada 2015). This method, however, overestimates groundwater depletion for humid regions of the world. In order to correct the estimate, a global multiplicative correction factor is applied to the original estimate. The correction factor is based on a comparison between regionally reported groundwater depletion rates and simulated groundwater depletion rates (over 30 regions; Wada et al. 2012). An uncertainty analysis is performed with a Monte Carlo simulation, generating 100 equiprobable realizations of groundwater recharge and 100 equiprobable realizations of groundwater pumping, thus resulting in 10,000 possible realizations of groundwater depletion (assuming errors in groundwater recharge and groundwater abstraction to be independent) (Wada et al. 2012).

Water impoundment behind dams including additional storage in surrounding groundwater (through seepage) is based on the dataset of Chao et al. (2008). As this dataset only covers the period 1900–2007, it has been updated to include recently built dams including the Three Gorges dam and 250 other large dams up to the year 2011 (Wada et al. 2012). After the year 2011, the data are extrapolated. Deforestation rates are estimated from three different sources, averaged, and converted into a contribution to GMSL (Wada

et al. 2012). Wetland loss rate is estimated for USA where reported data are available, and then extrapolated the rate to rest of the world (Wada et al. 2012). Storage loss from endorheic basins is estimated only for the Aral and Caspian Seas (Wada et al. 2012).

2.6 Temporal Filtering and Combining Similar Data

The datasets previously discussed are provided with a range of temporal sampling, from monthly to yearly. Moreover, some have been filtered over longer times than they are sampled. For instance, the upper ocean thermosteric sea level estimate from Domingues et al. (2008) is provided at yearly time steps, but has had a 3-year running mean applied. The upper ocean thermosteric estimates from Levitus et al. (2012), on the other hand, are yearly averages. Thus, direct averaging of the two will lead to spurious differences related to the different smoothing applied.

Since one cannot unfilter a dataset, we are forced to utilize the longest filtering period among the datasets in order to make the time series as uniform as possible, and reduce the effect of unfiltered higher-frequency variability in some data. This means that yearly sampling and a 3-year running mean filter is applied to the time series that extend back to 1993, including the altimetry (Sect. 2.1), thermosteric (Sect. 2.2), ice contributions (Sect. 2.3), and hydrology components (Sect. 2.4). For the period 2005–2015, a monthly average is used, but the seasonal variation is estimated and removed by fitting a sinusoid term with annual (1 cycle per year, cpy) and semi-annual (2 cpy) frequencies using ordinary least squares in order to focus on only the interannual and longer variations. A 3-month running mean is also applied to be consistent with the smoothing used with the altimetry time series (Sect. 2.1).

When multiple datasets are available (e.g., altimetry GMSL, Argo thermosteric variations, GRACE ocean mass) the time series is averaged to compute an ensemble mean. Uncertainty is computed from the standard deviation of the residuals of the individual time series with the ensemble mean. This is assumed to be the standard error at each time step. For time series without multiple estimates, the uncertainty from the authors of the data is used. The total thermosteric signal is reconstructed from the ensemble average of the upper ocean time series (Fig. 3), the estimate from 700 to 2000 m based on Levitus et al. (2012), and the deep warming trend from Purkey and Johnson (2010). Standard errors in each component are added assuming they are uncorrelated by using a root-sum-square (RSS).

The satellite altimetry and GRACE observations also have a likelihood of unknown systematic errors that will affect the trend estimate. For altimetry, this arises from drifts and biases in the different instruments and the difficulty of detecting it through calibration with tide gauges, which also have vertical land motion that is often poorly measured (Mitchum 2000; Ablain et al. 2015; Watson et al. 2015). The full range of possible drift errors has previously been estimated to be between ± 0.4 mm year^{-1} (Mitchum 2000) and ± 0.5 mm year^{-1} (Ablain et al. 2015). More recently, Watson et al. (2015) found a higher possible change of 0.6 mm year^{-1} for the combined record. Here we use the value of ± 0.6 mm year^{-1} to be most conservative. This uncertainty is used for all time periods, even though Watson et al. (2015) argue it is considerably less for the Jason-1 and Jason-2 altimeters (post 2002). For GRACE, the uncertainty arises from uncertainty in the glacial isostatic adjustment (GIA) correction and has been estimated to be ± 0.3 mm year^{-1} (Chambers et al. 2010). These uncertainty values are added to those determined from the internal statistics (Sect. 2.6) using an RSS.

2.7 Fitting Trends and Computing Uncertainty

While trends do not give a complete picture of the sea level budget closure, they are a useful tool to detect imbalance and have been frequently used as a measure of the sea level budget closure (e.g., Church et al. 2011, 2013). We will fit a bias plus a trend ($a_0 + a_1 t$) model to each time series using ordinary least squares (OLS). Uncertainty estimates from ordinary least squares, however, assumes: (1) The uncertainty is proportional to the standard deviation of the residuals about the fit, (2) the uncertainty is proportional to 1/sqrt(N), where N is the number of points, and (3) the N points are statistically uncorrelated. In practice, these assumptions are rarely all true. For example, by temporally smoothing data, the points are not uncorrelated, and assumption (3) is violated. Assumption (1) is based on uncertainty arising from internal, unmodeled variability. But if this is smaller than the standard error of the estimate, the uncertainty in the trend will be underestimated.

There are several ways to deal with this issue and account for uncertainty properly. For small numbers of points (<20 or so), using Monte Carlo estimates with a colored noise model is not preferred, as it is difficult to compute the autocovariance of the data with such limited samples. This is the case for the longer time span when we have applied a 3-year mean filter. Instead, it is better to estimate the effective degrees of freedom (eDOF), which is the number of statistically independent observations minus the number of model parameters estimated (in the case of the 3-year smoothed data, it is only a bias + trend, so 2). In the case of the 3-year smoothed data between 1993 and 2015, we assume the points are uncorrelated after three years. The effective degrees of freedom for each data set are given in Table 1, noting they vary because the time lengths are slightly different.

Once the eDOF is known, it is straightforward to estimate the corrected uncertainty by

$$\sigma_{\text{corr}} = \sigma_{\text{OLS}} \sqrt{\frac{N}{e\text{DOF}}}, \tag{2}$$

Table 1 Estimated trends in GMSL and components between approximately January 1993 and December 2015

Quantity	Period	Trend (mm year^{-1})	Temporal averaging	Effective DOF
GMSL	1993–2015	3.19 ± 0.63[a]	3-year running means	5
Thermosteric				
0–700 m	1992.0–2014.0	0.85 ± 0.2	3-years	5
700–2000 m	1992.0–2014.0	0.24 ± 0.07	5-years	3
Below 2000 m	~1995–2005	0.11 ± 0.1	Trend only	N/A
Total thermosteric	~1992–~2014	1.20 ± 0.23	Sum of component trends	N/A
Antarctica	1992.0–2011.0	0.22 ± 0.14	3-years	4
Greenland	1992.0–2011.0	0.37 ± 0.28	3-years	4
Glaciers/ice caps	1992.0–2013.0	0.76 ± 0.30	3-years	5
Hydrology	1992.0–2013.0	0.45 ± 0.16	3-years	5
Total mass	~1992–~2013	1.8 ± 0.46		
Sum of components		3.00 ± 0.52		

Exact time period for each representative time series is given. Uncertainty is 90 % confidence except for the thermosteric below 2000 m, which is 95 % as estimated by Purkey and Johnson (2010)

[a] Includes uncertainty in knowing systematic drifts of ±0.6 mm year^{-1} (added as RSS)

where σ_{OLS} is the standard error from OLS based on the residuals and assuming N uncorrelated observations, and σ_{corr} is the corrected uncertainty by accounting for the smaller number of independent observations. However, the corrected uncertainty may still be too small, if the standard deviation of the residuals about the fit (used to scale the covariance matrix in OLS) is smaller than the prescribed standard errors for each observation (σ_{obs}). In this case, scaling the covariance matrix using the observation errors such as in weighted least squares (WLS) is better. Thus, to fully compute the most conservative uncertainty, we calculate both σ_{OLS} (based on the residuals to the fit) and σ_{WLS} (based on the observation errors) and derive σ_{corr} based on the greater of the two:

$$\sigma_{\mathrm{corr}} = \begin{bmatrix} \sigma_{\mathrm{OLS}}\sqrt{\dfrac{N}{e\mathrm{DOF}}}, & \text{if } \sigma_{\mathrm{OLS}} > \sigma_{\mathrm{WLS}} \\ \sigma_{WLS}\sqrt{\dfrac{N}{e\mathrm{DOF}}}, & \text{if } \sigma_{\mathrm{WLS}} > \sigma_{\mathrm{OLS}} \end{bmatrix}. \tag{3}$$

For the monthly sampled datasets between 2005 and 2015, we will use instead a Monte Carlo simulation based on a set of 10,000 simulated time series residuals that have an autocovariance similar to the true residuals. To do this, we use an auto-regression (AR) model to impose correlations to an initial random time series. An AR(p) model estimates values (y) at some time, t, based on p earlier times scaled by coefficients that had correlation:

$$y(t) = a_1 y(t-1) + a_2 y(t-2) + a_3 y(t-3) + \cdots + a_p y(t-p) + \varepsilon(t) \tag{4}$$

where $\varepsilon(t)$ is random noise with a prescribed variance.

The coefficients (a) are determined using the Yule-Walker algorithm, based on the one-sided autocovariance (i.e., where negative lags are treated the same as positive lags in the computation, assuming symmetry):

$$\begin{bmatrix} a_1 \\ a_2 \\ a_3 \\ \vdots \\ a_p \end{bmatrix} = \begin{bmatrix} R_0 & R_1 & \cdots & R_{p-1} \\ R_1 & R_0 & \cdots & R_{p-2} \\ \vdots & \vdots & \ddots & \vdots \\ R_{p-1} & R_{p-2} & \cdots & R_0 \end{bmatrix}^{-1} \begin{bmatrix} R_1 \\ R_2 \\ R_3 \\ \vdots \\ R_p \end{bmatrix} \tag{5}$$

$$\sigma_\varepsilon^2 = R_0 - \sum_{k=1}^{p} a_k R_k$$

R_0 is the autocovariance at lag=0, R_1 is the autocovariance at lag = 1, etc., and σ_ε is the standard deviation of the random noise needed to match the covariance at lag = 0.

Starting from 10,000 random time series with a standard deviation equal to that of the residuals, we derive and use the coefficients of an AR(3) model and create a 10,000 different colored noise models so that the covariance to lag-3 matches that of the original residuals. For the monthly sampled time series from 2005 to 2015, we do not consider the uncertainty of the observations, as the standard deviation of the residuals is higher than the observation error for all time series (altimetry, GRACE, Argo). We then fit trends to these simulated residuals, and the standard deviation of the 10,000 sample trends is used as one standard error for the trend uncertainty. This will properly inflate the uncertainty to account

for correlation in the time series. The degrees of freedom are computed from the autocorrelation of the time series, based on dividing the full time length in months by the decorrelation time, and rounding down. The decorrelation time is computed as twice the lag at which the autocorrelation drops below 0.5. The effective degrees of freedom are reduced by 6 (bias + trend, plus the previously estimated annual/semi-annual sinusoid).

All uncertainties are scaled to 90 % confidence, assuming a two-tailed *t*-distribution and accounting for the eDOF.

3 Results and Analysis

3.1 1993 to 2013

Figure 6 and Table 1 summarize the results of our assessment of the sea level budget from January 1993 to approximately December 2013. The end date is approximate, because several of the time series end earlier (notably the estimated from the Greenland and Antarctica ice sheets). The majority of the data have end dates in 2013.

Based on assessment of the trends over the 20-year interval (Table 1), the sea level budget closes within the uncertainty. The trend in GMSL is 3.19 ± 0.63 mm year^{-1}, while the trend in the sum of the components is 3.00 ± 0.52 mm year^{-1}. Thus, we have confidence that we understand the various contributors to GMSL rise over the last 20 years, at least within our current ability to measure them. The largest single contributor has been thermal expansion, explaining about 40 % of the trend (comparing relative to the sum of all components). The upper ocean alone explains about 28 % of the trend, with about 8 % coming from the middle layers, and 4 % from the deep ocean below 2000 m.

The contributors that combine to increase ocean mass, however, explain 60 % of the trend. Thus, the mass component of sea level rise between 1993 and 2014 was roughly 50 % greater than thermal expansion. Of the contributors, the glaciers and ice caps outside of Greenland and Antarctica had the largest effect (~25 % of total GMSL), hydrology the

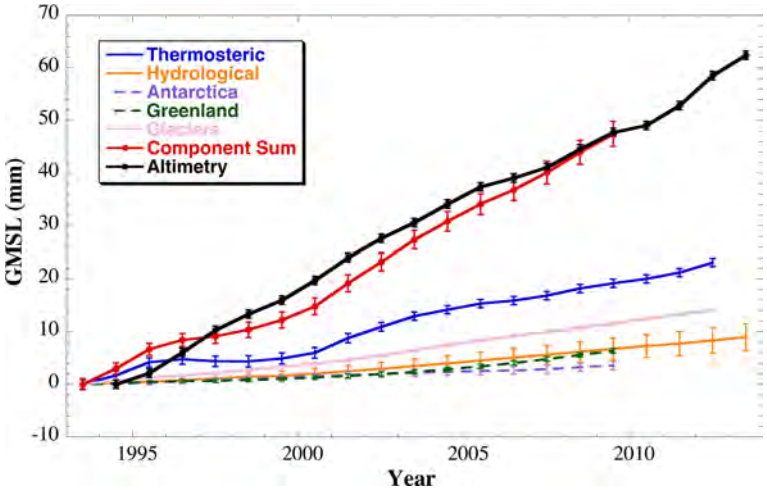

Fig. 6 Three-year running means of GMSL from altimetry, its components, and the sum of the components from 1993.0 to 2014.0. Uncertainty bars are one standard error as described in text

next (~15 %), then Greenland (~12 %), and finally Antarctica (~7 %). However, the contribution from Greenland has accelerated in recent years, as shown by several recent studies (e.g., Shepherd et al. 2012; Schrama et al. 2014; Velicogna et al. 2014; Yi et al. 2015). This is evidenced in Fig. 6 by the increasing separation between Greenland and Antarctica contributions. By 2010, the contribution to GMSL from Greenland has equaled the amount estimated from hydrological sources.

Although trends agree well, the time series of GMSL from altimetry and the sum of the components do not agree that well (Fig. 6). They disagree significantly at low frequencies. This is likely because our hydrological estimate does not include natural climate fluctuations in water cycling between the oceans and continents (Sect. 2.4). It is known that these signals on interannual (3- to 5-year time scales) can be of order 10 mm or so (e.g., Fasullo et al. 2013; Cazenave et al. 2014). These variations will be reflected in the GMSL estimate from altimetry, but not in the sum of the components.

3.2 2005 to 2014

Our ability to balance the sea level budget improves significantly after 2005 (Fig. 7; Table 2). Now, by measuring ocean mass directly from the satellite gravity measurements, we can observe similar low-frequency variability, for example, the significant drop of approximately 5 mm in 2011, followed by a subsequent rise of 16 mm between 2011 and 2013, followed by another 5 mm drop in late 2013 (Fig. 7). These are all related to exchanges of water mass between the oceans and continents and have only small steric sea level signatures. The perturbation in 2011 has been linked to anomalous rainfall over mainly Australia, with a lesser contribution from South America (Fasullo et al. 2013).

As with the 20-year period, the sea level budget over the last 10 years closes to within the uncertainty (Table 2). The rate in GMSL from altimetry is nearly unchanged from the 20-year estimate (3.17 ± 0.67 vs. 3.19 ± 0.63 mm year^{-1}). Although a few recent studies have found lower rates of GMSL over the last 10 years or so, these are affected by the

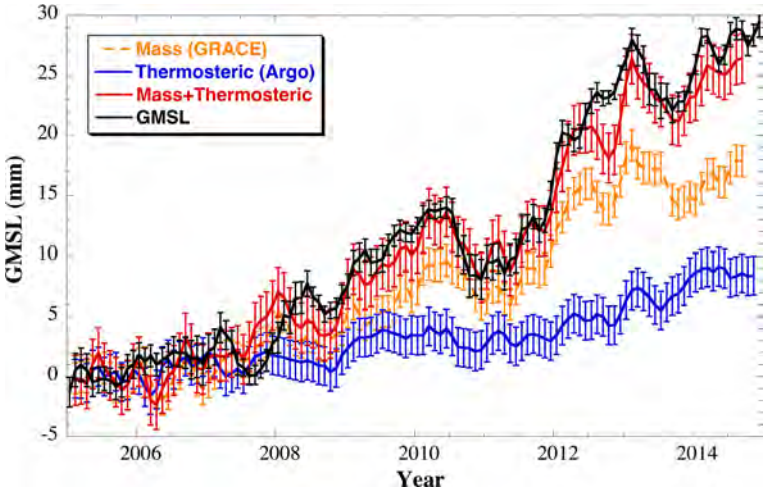

Fig. 7 Three-month running means of GMSL from altimetry, ocean mass from GRACE, and the thermosteric component from Argo for 2005.0–2015.0 (seasonal sinusoids removed). Time series are ensemble means and uncertainty *bars* are one standard error as described in text

Table 2 Estimated trends in GMSL and components between approximately January 2005 and December 2014 and from the representative time series

Quantity	Period	Trend (mm year^{-1})	Temporal averaging	Effective DOF
GMSL	2005.0–2015.0	3.17 ± 0.67[a]	3-month running mean	10
Thermosteric				
0–2000 m	2005.0–2015.0	0.86 ± 0.11	3-month running mean	10
Below 2000 m	~1995–2005	0.11 ± 0.1	Trend only	N/A
Total thermosteric	~2005–~2015	0.97 ± 0.15	Sum of component trends	N/A
Mass	2005.0–2015.0	2.11 ± 0.36[b]	3-month running mean	10
Sum of components		3.08 ± 0.39		

Exact time period for each representative time series is given. Uncertainty is 90 % confidence except for the thermosteric below 2000 m, which is 95 % as estimated by Purkey and Johnson (2010)

[a] Includes uncertainty in knowing systematic drifts of ±0.6 mm year^{-1} (added as RSS)

[b] Includes uncertainty in GIA of ±0.3 mm year^{-1} (added as RSS)

large interannual variability since 2011 (Cazenave et al. 2014). Earlier studies based on a scaling of El Niño indices suggested at least 15 years of data are necessary to distinguish longer term GMSL rise from that related to internal, natural variability (Nerem et al. 1999). Thus, one needs to be cautious of over-interpreting small changes in trends with short records.

The total steric contribution to GMSL is slightly smaller in the last decade than over the 20 years, while the mass component is slightly higher, although the means agree within uncertainty. Although we do not partition the ocean mass component into individual components from 2005 to 2014 due to limited degrees of freedom in the glacier and hydrology data, we do compare the relative contribution of Greenland and Antarctica mass loss (as measured by GRACE) to mean ocean mass (Fig. 8).

Over the last decade, the trend in Antarctica mass loss accounts for 3–27 % (central value 16 %) of the trend in global ocean mass, while Greenland accounts for 21–40 % (central value 32 %), when uncertainty is included in the possible spread. Greenland and Antarctica now account for about for 18–43 % (central value 28 %) of total GMSL rise, approximately the same amount as thermal expansion (25–56 %, central value 37 %). The contribution from glaciers and hydrology make up the remaining 35 %. Compare that to the period that includes the 1990s before the ice sheets began losing mass at an accelerated rate, when Greenland and Antarctica accounted for only ~20 % of the GMSL rate, while glaciers and hydrology accounted for ~40 %, based on the central values.

4 Conclusions

The results of this study are in agreement with previous estimates of the sea level budget (e.g., Church et al. 2011, 2013; Llovel et al. 2014; von Schuckmann et al. 2014; Dieng et al. 2015a, b, c). The main differences are in the slightly different time periods we study, along with what we consider more robust uncertainty estimates. The overall conclusion is that the sea level budget closes on both the longer (1993–2014) and shorter period (2005–2014) within the uncertainty. This gives us high confidence in the disparate measurements that go into the budget calculation. It also gives us increasing confidence that we

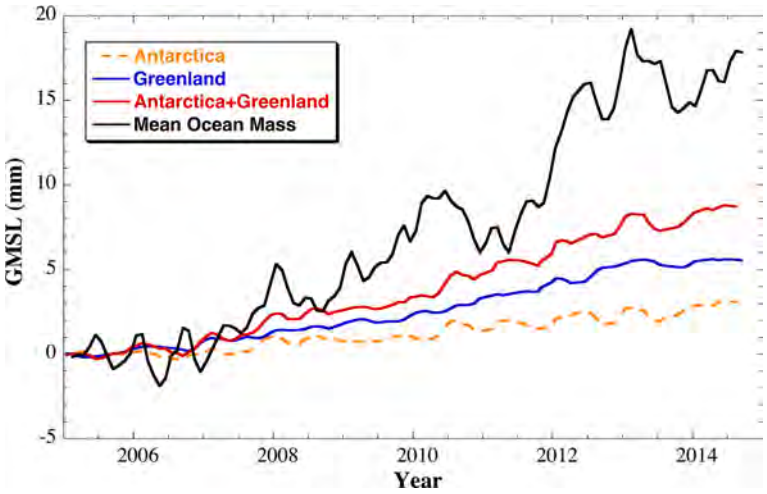

Fig. 8 Three-month running means of global mean ocean mass from GRACE, and the contributions from Greenland and Antarctica, also measured by GRACE

can partition the sources driving the observed rise in GMSL of $\sim$3.2 mm year^{-1}. From the sea level budget exercise, we know that thermal expansion drives about 40 % of the signal, with the majority of the expansion in the upper 700 m of the water column. Temperature changes in the deeper ocean, while smaller, still contribute significantly. Of the remaining 60 %, glaciers and ice caps outside of Greenland and Antarctica contribute the most ($\sim$25 % of total GMSL), Greenland and Antarctica ice sheets the next most (19 %), and hydrology the next ($\sim$15 %).

Over the last decade, the contributions from Greenland and Antarctica have accelerated considerably. Since 2005, Greenland has contributed 21 % of GMSL rise, while Antarctica has contributed 11 %. Combined, this is nearly a third of GMSL rise, and increase of nearly 68 % compared to the 20-year trend. The trend in GMSL over the two time intervals is roughly the same value ($\sim$3.2 mm year^{-1}). Thus, only by measuring the components of GMSL separately are we able to deduce changes in the mechanisms responsible for GMSL change, which allows us to better understand the processes.

These estimates, however, are based on the center of the possible spread of the trends. Unfortunately, we are still limited in reducing the spread due to potential systematic error in the observing system. The two largest uncertainties that have been documented are the inability to constrain the drift in altimeters to better than $\pm$0.6 mm year^{-1} and the GIA uncertainty on gravimetry estimates of ocean mass ($\pm$0.3 mm year^{-1}). As these are systematic, they will not be reduced by longer time series, unlike the error arising from unmodeled internal variability, which is reduced by a factor of 1/sqrt(n). Thus, concerted and continued efforts are needed to understand, measure, and correct systematic uncertainty in all portions of the observing system. Although the sea level budget closes to less than 0.2 mm year^{-1} (Tables 1, 2), this is just as likely to be a fortuitous cancellation of systematic errors as a real indication of accuracy.

Finally, it is vital to continue the observations of not only GMSL, but also the steric and mass components. Greenland and Antarctica contributions can be most directly observed via space-based gravimetry measurements, which provide an important constraint on other types of measurements (altimetry measurements of topography or input–output methods).

The independent Argo measurements confirm a slightly lower steric contribution, leaving no significant change in GMSL. In addition, expansion of the Argo measurements below 2000-m depth is important, as the only information we have from the deeper ocean are from more limited CTD casts. Although these are highly precise instruments, and deep ocean temperature/salinity are more correlated over larger regions, the low data availability results in uncertainty of order 50 %. Although the deep ocean is only a small contributor to sea level rise, as more heat is sequestered into the deeper ocean due to deep water formation, it may play an increasing role, considering that the volume of the deep ocean (below 2000 m) is nearly half that of the total ocean.

Acknowledgments This paper is the outcome of an International Space Science Institute Workshop (ISSI) "Integrative Study of Sea Level", and ISSI provided travel funding for the authors to attend the workshop. The Argo data were collected and made freely available by the International Argo Program and the national programs that contribute to it (http://www.argo.ucsd.edu and http://argo.jcommops.org). The Argo Program is part of the Global Ocean Observing System. DPC was supported by NASA Grant NNX12AL28G and internal funding from the University of South Florida. WL was supported by a CNES post-doctoral fellowship carried out at CERFACS. HD is supported by a doctoral fellowship of the European Space Agency within the Climate Change Initiative (CCI) Programme.

References

Ablain M, Cazenave A et al (2015) Improved sea level record over the satellite altimetry era (1993–2010) from the Climate Change Initiative Project. Ocean Sci 11:67–82. doi:10.5194/os-11-67-2015

Abraham JP et al (2013) A review of global ocean temperature observations: implications for ocean heat content estimates and climate change. Rev Geophys 51:450–483. doi:10.1002/rog.20022

Barletta VR, Sørensen LS, Forsberg R (2013) Scatter of mass changes estimates at basin scale for Greenland and Antarctica. Cryosphere 7:1411–1432. doi:10.5194/tc-7-1411-2013

Calafat FM, Chambers DP (2013) Quantifying recent acceleration in sea level unrelated to internal climate variability. Geophys Res Lett. doi:10.1002/grl.50731

Calafat FM, Chambers DP, Tsimplis MN (2014) On the ability of global sea level reconstructions to determine trends and variability. J Geophys Res Oceans 119:1572–1592. doi:10.1002/2013JC009298

Cazenave A, Dieng H, Meyssignac B, von Schuckmann K, Decharme B, Berthier E (2014) The rate of sea level rise. Nat Clim Chang 4:358–361. doi:10.1038/NCLIMATE2159

Chambers DP, Merrifield MA, Nerem RS (2012) Is there a 60-year oscillation in global mean sea level? Geophys Res Lett 39:L18607. doi:10.1029/2012GL052885

Chambers DP, Wahr J, Nerem RS (2004) Preliminary observations of global ocean mass variations with GRACE. Geophys Res Ltrs 31:L13310. doi:10.1029/2004GL020461

Chao BF, Wu YH, Li YS (2008) Impact of artificial reservoir water impoundment on global sea level. Science 320:212–214. doi:10.1126/science.1154580

Church JA, White NJ (2011) Sea-level rise from the late 19th to the early 21st century. Surv Geophys 32(4–5):585–602. doi:10.1007/s10712-011-9119-1

Church JA, White NJ, Konikow LF, Domingues CM, Cogley JG, Rignot E, Gregory JM, van den Broeke MR, Monaghan AJ, Velicogna I (2011) Revisiting the Earth's sea-level and energy budgets from 1961 to 2008. Geophys Res Lett 38:L18601. doi:10.1029/2011GL048794

Church JA, Clark PU, Cazenave A, Gregory JM, Jevrejeva S, Levermann A, Merrifield MA, Milne GA, Nerem RS, Nunn PD, Payne AJ, Pfeffer WT, Stammer D, Unnikrishnan AS (2013) Sea level change. In: Stocker TF, Qin D, Plattner G-K, Tignor M, Allen SK, Boschung J, Nauels A, Xia Y, Bex V, Midgley PM (eds) Climate Change 2013: The Physical Science Basis. Contribution of Working Group I to the Fifth Assessment Report of the Intergovernmental Panel on Climate Change. Cambridge University Press, Cambridge, UK and New York, NY, USA

Dieng H, Champollion N, Cazenave A, Wada Y, Schrama E, Meyssignac B (2015a) Total land water storage change over 2003–2013 estimated from a global mass budget approach. Environ Res Lett **(in press)**

Dieng H, Palanisamy H, Cazenave A, Meyssignac B, von Schuckmann K (2015b) The sea level budget since 2003: inference on the deep ocean heat content. Surv Geophys 36:1. doi:10.1007/s10712-015-9314-6

Dieng H, Cazenave A, von Shuckmann K, Ablain M, Meyssignac B (2015c) Sea level budget over 2005–2013: missing contributions and data errors. Ocean Sci 11:789–802. doi:10.5194/os-11-789-2015

Domingues CM, Church JA, White NJ, Gleckler PJ, Wijffels SE, Barker PM, Dunn JR (2008) Improved estimates of upper-ocean warming and multi-decadal sea-level rise. Nature 453:1090–1093
Durack PJ, Wijffels SE, Boyer TP (2013) Long-term salinity changes and implications for the global water cycle. In: Siedler G, Griffies SM, Gould J, Church JA (eds) Ocean circulation and climate, a 21st century perspective, 2nd edn. International Geophysics, Academic, Elsevier, Oxford, pp 727–757
Fasullo JT, Boening C, Landerer FW, Nerem RS (2013) Australia's unique influence on global mean sea level in 2010–2011. Geophys Res Lett 40(16):4368–4373. doi:10.1002/grl.50834
Gardner AS, Moholdt G, Cogley JG, Wouters B, Arendt AA, Wahr J, Berthier E, Hock R, Pfeffer WT, Kaser G, Ligtenberg SRM, Bolch T, Sharp MJ, Hagen JO, van den Broeke MR, Paul F (2013) A reconciled estimate of glacier contributions to sea level rise: 2003 to 2009. Science 340:852–857
Gouretski VV, Koltermann KP (2007) How much is the ocean really warming? Geophys Res Lett. doi:10.1029/2006GL027834
Gregory JM, Lowe JA (2000) Predictions of global and regional sea-level rise using AOGCMs with and without flux adjustment. Geophys Res Lett 27:3069–3072
Henry O, Ablain M, Meyssignac B, Cazenave A, Masters D, Nerem S, Leuliette E, Garric G (2014) Investigating and reducing differences between the satellite altimetry-based global mean sea level time series provided by different processing groups. J Geod 88:351–361. doi:10.1007/s00190-013-0687-3
Hosoda S et al (2008) A monthly mean dataset of global oceanic temperature and salinity derived 344 from Argo float observations. JAMSTEC Rep Res Dev 8:47–59
Johnson GF, Chambers DP (2013) Ocean bottom pressure seasonal cycles and decadal trends from GRACE release-05: ocean circulation implications. J Geophys Res Oceans. doi:10.1002/jgrc.20307
Konikow LF (2011) Contribution of global groundwater depletion since 1900 to sea-level rise. Geophys Res Lett 38:L17401. doi:10.1029/2011GL048604
Kouketsu S et al (2011) Deep ocean heat content changes estimated from observation and reanalysis product and their influence on sea level change. J Geophys Res Oceans 116:C03012
Levitus S, Antonov JI, Boyer TP, Baranova OK, Garcia HE, Locarnini RA, Mishonov AV, Reagan JR, Seidov D, Yarosh ES, Zweng MM (2012) World ocean heat content and thermosteric sea level change (0–2000 m), 1955–2010. Geophys Res Lett 39:L10603. doi:10.1019/2012GL051106
Llovel W, Becker M, Cazenave A, Jevrejeva S, Alkama R, Decharme B, Douville H, Ablain M, Beckley B (2011) Terrestrial waters and sea level variations on interannual time scale. Glob Planet Chang 75:76–82. doi:10.1016/j.gloplacha.2010.10.008
Llovel W, Willis JK, Landerer FW, Fukumori I (2014) Deep-ocean contribution to sea level and energy budget not detectable over the past decade. Nat Clim Chang. doi:10.1038/NCLIMATE2387
Lyman JM, Johnson GC (2008) Estimating annual global upper-ocean heat content anomalies despite irregular in situ ocean sampling. J Clim 21:5629–5641
Lyman JM, Good SA, Gouretski VV, Ishii M, Johnson GC, Palmer MD, Smith DA, Willis JK (2010) Robust warming of the global upper ocean. Nature 465:334–337. doi:10.1038/nature09043
Marzeion B, Leciercq PW, Cogley JG, Jarosch AH (2015) Brief communication: global glacier mass loss reconstructions during the 20th century are consistent. Cryosphere Discuss 9:3807–3820. doi:10.5194/tcd-9-3807-2015. www.the-cryosphere-discuss.net/9/3807/2015/
Masters D, Nerem RS, Choe C, Leuliette E, Beckley B, White N, Ablain M (2012) Comparison of global mean sea level time series from TOPEX/Poseidon, Jason-1, and Jason-2. Mar Geod 35:20–41
Miller L, Douglas BC (2007) Gyre-scale atmospheric pressure variations and their relation to 19th and 20th century sea level rise. Geophys Res Lett 34:L16602. doi:10.1029/2007GL030862
Mitchum GT (2000) An improved calibration of satellite altimetric heights using tide gauge sea levels with adjustment for land motion. Marine Geodesy 23:145–166
Nerem RS, Chambers DP, Choe C, Mitchum GT (2010) Estimating mean sea level change from the TOPEX and Jason altimeter missions. Mar Geod 33(Supplement 1):435–446. doi:10.1080/01490419.2010.491031
Nerem RS, Chambers DP, Leuliette E, Mitchum GT, Giese BS (1999) Variations in global mean sea level during the 1997–98 ENSO event. Geophys Res Ltrs 26:3005–3008
Ngo-Duc T, Laval K, Polcher J, Lombard A, Cazenave A (2005) Effects of land water storage on global mean sea level over the past 50 years. Geophys Res Lett 32:L09704. doi:10.1029/2005GL022719
Palanisamy H, Cazenave A, Delcroix T, Meyssignac B (2015) Spatial trend patterns in Pacific Ocean sea level during the altimetry era : the contribution of thermocline depth change and internal climate variability. Ocean Dyn. doi:10.1007/s10236-014-0805-7
Peltier WR (2004) Global glacial isostasy and the surface of the ice-age Earth: the ICE-5G (VM2) model and GRACE. Annu Rev Earth Planet Sci 32:111–149

Pokhrel YN, Hanasaki N, Yeh PJ-F, Yamada T, Kanae S, Oki T (2012) Model estimates of sea level change due to anthropogenic impacts on terrestrial water storage. Nat Geosci 5:389–392. doi:10.1038/ngeo1476

Purkey SG, Johnson GC (2010) Warming of global abyssal and deep Southern Ocean waters between the 1990 s and 2000 s: contributions to global heat and sea level rise budgets. J Clim 23:6336–6351

Reager JT, Gardner AS, Famiglietti JS, Wiese DN, Eicker A, Lo M-H (2016) A decade of sea level rise slowed by climate driven hydrology. Science 351:699–703. doi:10.1126/science.aad8386

Rietbroek R, Brunnabend SE, Kushche J, Schröter J, Dahle C (2016) Revisiting the contemporary sea-level budget on global and regional scales. Proc Natl Acad Sci 113:1504–1509. doi:10.1073/pnas.1519132113

Roemmich D, Johnson GC, Riser S, Davis R, Gilson J, Owens WB, Garzoli SL, Schmid C, Ignaszewski M (2009) The Argo program: observing the global ocean with profiling floats. Oceanography 22(2):34–43. doi:10.5670/oceanog.2009.36

Roemmich D, Church J, Gilson J, Monselesan D, Sutton P, Wijffels S (2015) Unabated planetary warming and its ocean structure since 2006. Nat Clim Chang 5:240–245

Schrama EJO, Wouters B, Rietbroek R (2014) A mascon approach to assess ice shett and glacier mass balance and their uncertainties from GRACE data. J Geophys Res Solid Earth 119:6048–6066. doi:10.1002/2013JB010923

Shepherd A et al (2012) A reconciled estimate of ice-sheet mass balance. Sci 338(6111):1183–1189

Sørensen LS, Forsberg R (2010) Greenland ice sheet mass loss from GRACE monthly models. In: Gravity, Geoid and Earth Observation. Springer. (International Association of Geodesy Symposia; No. 135), pp 527–532. doi:10.1007/978-3-642-10634-7_70

Sturges W, Douglas BC (2011) Wind effects on estimates of sea level rise. J Geophys Res 116:C06008. doi:10.1029/2010JC006492

Tapley BD, Bettadpur S, Watkins M, Reigber C (2004) The gravity recovery and climate experiment: mission overview and early results. Geophys Res Lett 31:L09607. doi:10.1029/2004GL019920

Velicogna I, Sutterley TC, van den Broeke MR (2014) Regional acceleration in ice mass loss from Greenland and Antarctica using Grace time variable gravity data. Res Lett Geophys. doi:10.1002/2014GL061052

Von Schuckmann K, Le Traon PY (2011) How well can we derive Global Ocean indicators from Argo data? Ocean Sci 7(6):783–791. doi:10.5194/os-7-783-2011

Von Schuckmann K, Gaillard F, Le Traon P-Y (2009) Global hydrographic variability patterns during 2003–2008. J Geophys Res 114:C09007. doi:10.1029/2008JC005237

Von Schuckmann K, Sallée JB, Chambers D, Le Traon PY, Cabanes C, Gaillard C, Speich S, Hamon M (2014) Consistency of the current global ocean observing systems from an Argo perspective. Ocean Sci 10:547–557. doi:10.5194/os-10-547-2014

Wada Y (2015) Modelling groundwater depletion at regional and global scales: Present state and future prospects. Surv Geophys. doi:10.1007/s10712-015-9347-x, Special Issue: ISSI Workshop on Remote Sensing and Water Resources

Wada Y, van Beek LPH, Sperna-Weiland FC, Chao BF, Wu Y-H, Bierkens MFP (2012) Past and future contribution of global groundwater depletion to sea-level rise. Geophys Res Lett 39:L09402. doi:10.1029/2012GL051230

Watkins MM, Wiese DN, Yuan D-N, Boening C, Landerer FW (2015) Improved methods for observing Earth's time variable mass distribution with GRACE. J Geophys Res Solid Earth. doi:10.1002/2014JB011547

Watson CS, White NJ, Church JA, King MA, Burgette RJ, Legresy B (2015) Unabated global mean sea-level rise over the satellite altimeter era. Nat Clim Chang 5(6):565. doi:10.1038/nclimate2635

Wijffels SE, Willis J, Domingues CM, Barker P, White NJ, Gronell A, Ridgway K, Church JA (2008) Changing expendable bathythermograph fall rates and their impact on estimates of thermosteric sea level rise. J Clim 21:56575672. doi:10.1175/2008JCLI2290.1

Yi S, Sun W, Heki K, Qian A (2015) An increase in the rate of global mean sea level rise since 2010. Geophys Res Lett. doi:10.1002/2015GL063902

2.5 Amélioration des données niveau de la mer altimétrique du CCI

Dans cette section nous étudions les améliorations apportées aux corrections des données niveau de la mer du CCI en global et en régional.

Résumé de l'article : "Altimetry-based Sea Level at Global and Regional Scales" *(joint à la fin de cette section 2.5)*

Cet article examine les processus altimétriques pour mieux caractériser les erreurs en global et en régional du produit niveau de la mer du CCI sur la période altimétrique. Le but de cet article est de présenter le produit CCI et sa précision. En comparaison des autres produits altimétriques cités dans la *section 2.1*, l'article montre que grâce à l'amélioration des différentes étapes du traitement des données, la précision s'approche des exigences du GCOS (voir la *section 2.1* et pour plus de détails sur le projet CCI). Deux objectifs principaux caractérisent l'étude : *(1)* l'utilisation des missions de l'ESA (ERS-1 & 2 et Envisat) en plus des missions dites «de référence» comme TOPEX/Poseidon et Jason 1, 2 dans le calcul de la série temporelle du niveau de la mer et *(2)* l'amélioration de toutes les étapes de traitement des données altimétriques.

Les nouvelles améliorations sur les corrections géophysiques, les algorithmes de traitement dédiés, la réduction des biais et dérives instrumentales et les raccordements entre les missions nous a conduit à des produits de niveau de la mer avec une plus grande précision. En termes de tendance à long terme, l'incertitude du niveau moyen global de la mer (< 0.5 mm/an) se rapproche maintenant des exigences du GCOS (de ~0.3 mm/an). L'incertitude de la tendance régionale a été réduite d'un facteur de ~2, mais les corrections de la troposphère humide et les erreurs d'orbites empêchent encore d'atteindre pleinement le niveau de précision requis. A l'échelle interannuelle, le niveau moyen global de la mer affiche toujours des erreurs de 2 à 4 mm, qui ne sont pas encore bien comprises. Un effort particulier a été consacré à la région Arctique où l'évolution du niveau de la mer était jusqu'à présent mal connue.

Malgré les efforts importants investis à ce jour, les produits niveau de la mer du projet CCI nécessitent encore des améliorations. Le lancement récent de nouvelles missions altimétriques (Sentinel-3, Jason-3) et la prise en compte des données provenant d'autres missions récemment lancées (par exemple, CryoSat, SARAL/Altika) peuvent fournir de nouvelles améliorations sur la précision de cet indicateur climatique important qu'est le niveau de la mer.

Satellite Altimetry-Based Sea Level at Global and Regional Scales

M. Ablain, J. F. Legeais, P. Prandi, M. Marcos, L. Fenoglio-Marc, H. B. Dieng, J. Benveniste & A. Cazenave

Surveys in Geophysics
An International Review Journal
Covering the Entire Field of Geosciences
and Related Areas

ISSN 0169-3298
Volume 38
Number 1

Surv Geophys (2017) 38:7-31
DOI 10.1007/s10712-016-9389-8

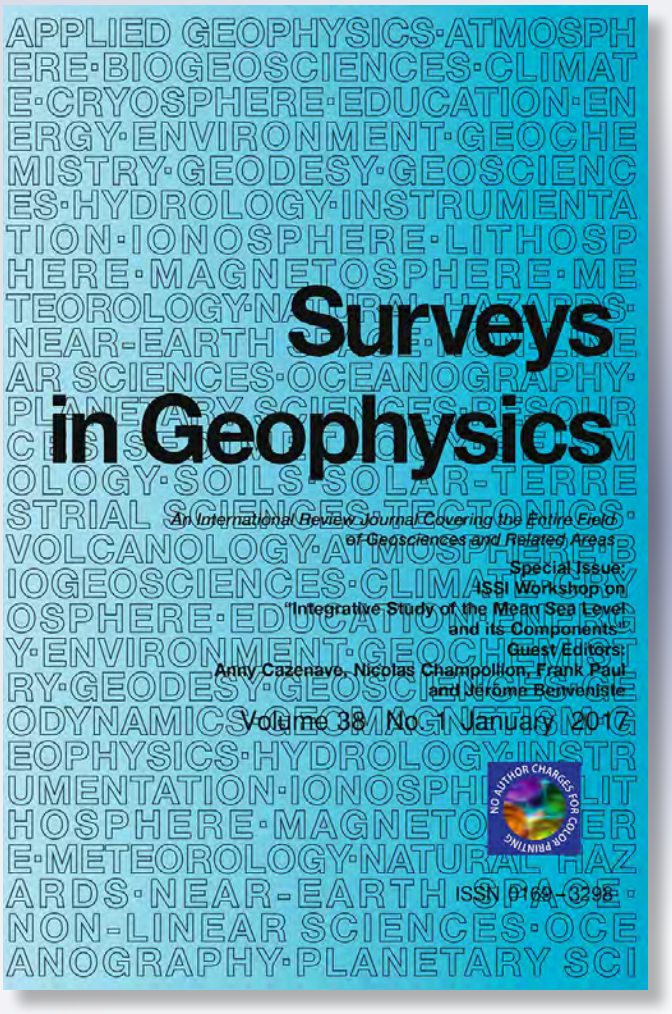

Springer

Surv Geophys (2017) 38:7–31
DOI 10.1007/s10712-016-9389-8

Satellite Altimetry-Based Sea Level at Global and Regional Scales

M. Ablain[1] · J. F. Legeais[1] · P. Prandi[1] · M. Marcos[2] · L. Fenoglio-Marc[3,4] · H. B. Dieng[5] · J. Benveniste[6] · A. Cazenave[5,7]

Received: 19 May 2016 / Accepted: 8 October 2016 / Published online: 16 November 2016

Abstract Since the beginning of the 1990s, sea level is routinely measured using high-precision satellite altimetry. Over the past ~25 years, several groups worldwide involved in processing the satellite altimetry data regularly provide updates of sea level time series at global and regional scales. Here we present an ongoing effort supported by the European Space Agency (ESA) Climate Change Initiative Programme for improving the altimetry-based sea level products. Two main objectives characterize this enterprise: (1) to make use of ESA missions (ERS-1 and 2 and Envisat) in addition to the so-called 'reference' missions like TOPEX/Poseidon and the Jason series in the computation of the sea level time series, and (2) to improve all processing steps in order to meet the Global Climate Observing System (GCOS) accuracy requirements defined for a set of 50 Essential Climate Variables, sea level being one of them. We show that improved geophysical corrections, dedicated processing algorithms, reduction of instrumental bias and drifts, and careful linkage between missions led to improved sea level products. Regarding the long-term trend, the new global mean sea level record accuracy now approaches the GCOS requirements (of ~0.3 mm/year). Regional trend uncertainty has been reduced by a factor of ~2, but orbital and wet tropospheric corrections errors still prevent fully reaching the GCOS accuracy requirement.

This paper is an outcome of the workshop on "Integrative Study of Sea Level Budget", International Space Science Institute Workshop, Bern, 2–6 February 2015.

✉ A. Cazenave
anny.cazenave@issibern.ch

[1] CLS, Toulouse, France

[2] IMEDEA (UIB-CSIC), Esporles, Spain

[3] Technical University Darmstadt, Darmstadt, Germany

[4] University of Bonn, Bonn, Germany

[5] LEGOS, Toulouse, France

[6] ESA-ESRIN, Frascati, Italy

[7] ISSI, Bern, Switzerland

Similarly at the interannual time scale, the global mean sea level still displays 2–4 mm errors that are not yet fully understood. The recent launch of new altimetry missions (Sentinel-3, Jason-3) and the inclusion of data from currently flying missions (e.g., CryoSat, SARAL/AltiKa) may provide further improvements to this important climate record.

Keywords Satellite altimetry · Sea level · Climate Change Initiative

1 Introduction

Sea level is one of the key indicators of climate change because it integrates changes of several components of the climate system in response to anthropogenic forcing as well as natural forcing factors related to natural sources and internal climate variability. Since the beginning of the twentieth century, the global mean sea level (GMSL) has been rising at a mean rate of 1.7 ± 0.3 mm/year as recorded by in situ tide gauges (e.g., Church et al. 2011, 2013; Woppelmann et al. 2009; Jevrejeva et al. 2008). However, values in the range 1.2 to 1.9 mm/year have also been proposed (Hay et al. 2015; Jevrejeva et al. 2014). Since the early 1990s, sea level variations are routinely measured by high-precision satellite altimetry. In terms of global mean, sea level rise over 1993–2014 amounts to 3.4 ± 0.4 mm/year (e.g., Nerem et al. 2010; Cazenave et al. 2014; Ablain et al. 2015). This value is two times larger than that of the previous decades, suggesting an acceleration of the GMSL rise. Present-day GMSL rise primarily reflects ocean warming (through thermal expansion of sea water) and land ice melting, two processes which result from anthropogenic global warming (Church et al. 2013). The Earth is currently in a state of thermal imbalance because of concentrations of anthropogenic greenhouse gases (GHG) in the atmosphere (Von Schukmann et al. 2016). Most of this heat excess is accumulated in the ocean (93 %); the remaining 7 % being used to warm the atmosphere and continents, and melt sea and land ice. GMSL rise is a direct consequence of these processes. Over the course of its five assessments, the Intergovernmental Panel on Climate Change (IPCC) has reported a significant improvement in our understanding of the sources and impacts of GMSL rise. Over the altimetry era, observed sea level rise and sum of contributions (ocean thermal expansion, land ice melt, land water storage change) concur, allowing the closure of the sea level budget for this period within estimated uncertainties (Church et al. 2013). Confidence in projections of future sea level rise has increased, thanks to improved physical understanding and closer agreement between model hinscasts and observations. However, significant problems still remain. The IPCC 5th assessment report—AR5—(Church et al. 2013) reported a 0.4 mm/year difference between the observed GMSL rate and the sum of contributions over the 1993–2010 time span. Yet uncertainties of components of the sea level budget equation (including sea level) are still large, in the order of 1 mm/year (2-sigma) (Church et al. 2013). The challenge is thus to reduce the components' errors, in order to check the statistical significance of the difference between observed sea level and sum of contributions. The satellite altimetry-based sea level record is affected by errors due to the imperfect altimeter corrections applied to the data (with the orbit solution and the wet tropospheric correction displaying the largest uncertainties), geographical averaging process and imperfect linkage between successive altimetry missions. In terms of long-term (decadal) trends, such factors contribute to the 0.4 mm/year difference quoted above (Ablain et al. 2009, 2015). At the interannual time scale, errors in the GMSL record are also significant and amount to 2–4 mm (Ablain et al. 2009; Dieng et al. 2015a, b). Secondly, as

far as the contributions are concerned, current estimates of ice sheet and glacier mass balances also display significant uncertainty (Church et al. 2013; Clark et al. 2015). Another issue concerns the land water contribution due to human activities (e.g., ground water depletion and dam building), its quantification being very difficult due to lack of global data (Church et al. 2013; Dieng et al. 2015c). Finally, although the steric contribution (effects of ocean thermal expansion and salinity) was considerably improved since the advent of the Argo project in the early 2000s. But the contribution of the deep ocean (below 2000 m) remains unknown, and prior to Argo, the steric component is quite uncertain due to the poor and heterogeneous distribution of historical hydrographic observations.

A precise estimation of the influence of these factors is crucial to understand processes at work under current climate change and to validate the climate models used for future projections. Over the last decade, the Global Climate Observing System (GCOS), in support of the United Nations Framework Convention on Climate Change (UNFCCC), has put together a set of requirements for satellite data to meet the needs of the climate change community (see GCOS 2011, for the satellite supplement). These requirements are broken down into key parameters of the Earth system, called Essential Climate Variables (ECVs). The goal is to provide accurate and stable values on the long-term, satellite-based ECV data products for researchers. Among the 50 ECVs identified so far by GCOS, 26 are observable from space. Sea level is one of these.

To respond to this need for climate-quality satellite data, the European Space Agency (ESA) has set up a programme, known as the ESA Climate Change Initiative (CCI). The aim of the programme is to realize the full potential of the long-term global Earth Observation archives from satellites as a significant and timely contribution to the ECV databases required by the UNFCCC. The ECVs are derived from multiple satellite data sets via international collaboration and include specific information on the possible biases and uncertainties of the data set. The CCI provides a unique opportunity to set up dialogue and cooperation between Earth observation and climate research communities.

In this overview article, we focus on the sea level record computed in the context of the ESA CCI project. Contributions and sea level budget issues are discussed in other papers in this Special Issue. Section 2 summarizes the high-precision satellite altimetry missions and their characteristics. Section 3 briefly presents the CCI sea level (SL_cci) project. In Sects. 4 and 5, we discuss how multi-mission altimetry-based sea level products are built and what the current level of uncertainties of the global and regional products are. Validation procedures are discussed in Sect. 6. Section 7 provides a summary of the main accomplishments. Conclusions are presented in Sect. 8.

2 Brief History of Satellite Altimetry Missions

Satellite altimetry has revolutionized the research in ocean dynamics by providing high-precision, high-resolution measurements of the ocean surface topography with global coverage and a revisit time of a few days or weeks. The concept of (nadir) satellite altimetry measurement is rather straightforward. The onboard radar altimeter transmits a short pulse of microwave radiation with known power towards the nadir. Part of the incident radiation reflects back to the altimeter. Measurement of the round-trip travel time provides the height of the satellite above the instantaneous sea surface (called altimeter range R). The quantity of interest in oceanography is the height of the instantaneous sea surface above a fixed reference surface (typically a conventional reference ellipsoid). This

quantity (called SSH) is simply the difference between the height H of the satellite above the reference ellipsoid and the altimeter range R: SSH = H-R. H is computed through precise orbit determination, a long-tested approach in space geodesy, which combines accurate modelling of the dynamics of the satellite motion and tracking measurements (Global Positioning System-GPS, Doppler Orbitography and Radiopositioning Integrated by Satellite—DORIS, or Satellite Laser Ranging) between the satellite and observing stations on Earth or on other observing satellites (Rudenko et al. 2012; Couhert et al. 2015). The range from the satellite to the sea, R, must be corrected for various components of the atmospheric refraction as well as for biases between the mean electromagnetic scattering surface and mean sea surface at the air–sea interface in the footprint of the radar. Other corrections due to a number of geophysical effects must also be applied. Chelton et al. (2001) describe the principle of satellite radar altimetry and details of the estimation of the SSH. They also discuss all corrections to be applied to the SSH measurements, including drifts and bias from onboard instruments.

Satellite altimetry was envisaged in the 1960s, was recognized as a high priority measurement at the Williamstown Symposium in 1969 (Kaula 1970), and the first objective was to measure the shape of the Earth. The development was pursued during the 1970s with an experiment onboard Skylab III, which in 1973 produced the first measurements of undulations in the marine geoid. GEOS3 (NASA) was the very first altimetry mission, launched in 1975 and providing data until 1979 (Agreen 1982). It was followed by Seasat (1978; NASA) and Geosat (1985; US Navy). These pioneering missions led to important discoveries (e.g., Lillibridge et al. 2006). They revealed, in particular, that the mean sea surface is not flat but mimics the oceanfloor topography (Fig. 1). In effect, the sea surface consists of two parts: (1) a static (i.e. time invariable) component that coincides with the geoid, an equipotential surface of the Earth's gravity field, and (2) a time-variable component due to ocean dynamics (e.g., ocean tides, currents, waves). At short and medium wavelengths ($\sim$<1000 km), the mean sea surface reflects the topographic features of the ocean floor.

The amplitude of the static component anomalies ranges from a few decimetres to several tens of meters. This explains why the first altimetry missions easily detected these features in spite of their lesser SSH measurement accuracy (uncertainty of several

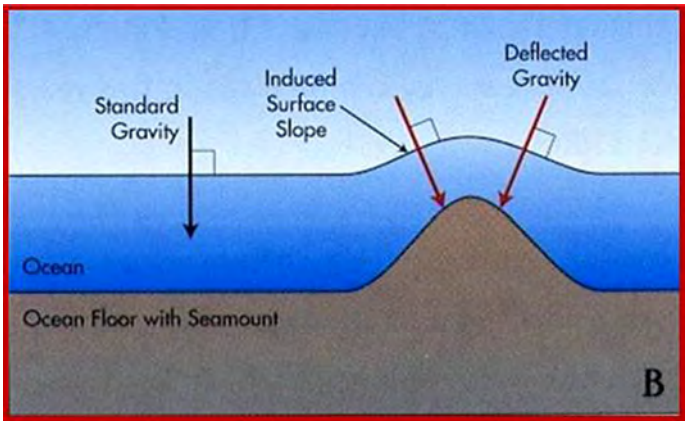

Fig. 1 Sketch of the mean sea surface deformations in response to the gravitational attraction of the sea floor topography

decimetres, mostly due to the orbit error, e.g., Fu and Cazenave 2001) and high instrumental noise.

Nevertheless, these early missions clearly demonstrated the high potential of satellite altimetry to study the dynamics of the world ocean.

The launch of the ERS-1 and TOPEX/Poseidon satellites in 1991 and 1992 opened the era of high-precision altimetry, allowing mapping of the SSH for the first time within a few centimetre accuracy for a single measurement. TOPEX/Poseidon was particularly precise at ocean basin scale and was used as the reference mission while ERS-1 provided the chance to explore the mesoscale variability. They have been followed by several other high-precision altimetry missions with different instrumental characteristics leading to an ever-increasing precision in the SSH measurement. Jason-1, -2, and -3 continued on the tracks of TOPEX/Poseidon, to be succeeded by Sentinel-6/Jason-CS in 2020. Meanwhile ERS-2, Envisat, CryoSat, SARAL/AltiKa and Sentinel-3 supplied and are supplying complementary observations. CryoSat was designed to reveal changing ice fields, but turned out to be an excellent oceanographic mission (Labroue et al. 2012). We now have at our disposal a 25-year-long multi-mission altimetry data set of very high value for studying ocean circulation (because of geostrophy, SSH measurements can be translated in terms of ocean circulation), ocean dynamics and sea level variations.

3 The ESA Climate Change Initiative and the Sea Level ECV

As noted in the introduction, sea level has been identified as a key marine ECV within the CCI programme. Indeed, precise monitoring of changes in the mean level of the oceans is crucial for understanding not just the climate, but also the socio-economic consequences of any rise in sea level.

The sea level project conducted in the CCI programme (SL_cci) gathers a consortium of 15 European partners including experts on altimeter standards as well as a climate research group dedicated to the quality assessment of the products. The first phase of the project (2011–2013) was the opportunity to involve the climate research community and define the user requirements for climate applications. The estimation of the SSH requires not only the knowledge of the altimeter range, but also the instrumental corrections, the satellite orbit and different geophysical corrections to the altimeter range (tides, troposphere and ionosphere corrections, sea state bias, dynamic atmospheric correction; see Table 1) that have to be selected for each altimeter mission. Note that in the following, terms sea level, SSH and SL_cci ECV are used interchangeably.

From the perspective of the production of a sea level ECV, evolutions of these altimeter standards and algorithms were central to the project since they affect the physical content of the SL_cci ECV. The strategy was thus to focus on the improvement of the altimeter corrections which constitute the most important sources of errors at climate scales. Following this strategy, new altimeter algorithms have been developed and tested for all altimeter missions within the phase 1 of the project. Other algorithms from external projects have also been included in the process. A formal validation protocol has been developed (Round Robin approach) for the estimation and the validation of their performances. The evaluation of these standards has been performed, distinguishing different spatial (global and regional) and temporal (long-term, interannual and seasonal) scales. All validation reports are available at www.sea-level-cci.org. A panel of international experts contributed to the selection of the best algorithms for climate

Table 1 Altimeter standards selected for the sea level calculation for the SL_cci products (release 1.1): the choice of these corrections can change with time or from a project to another

Corrections	ERS-1	ERS-2	Envisat	Jason-1	Jason-2	T/P	GFO
Orbit	Reaper combined orbit (Rudenko et al. 2015)		CNES POE-D (Couhert et al. 2015)			GSFC POE (09/2008)	GSFC POE
Sea state bias	BM3 (Gaspar and Ogor 1994)	Nonparametric SSB (Mertz et al. 2005)	Nonparametric SSB V2.1 release	Nonparametric SSB (Tran et al. 2012)	Nonparametric SSB GDR-D release	Nonparametric SSB (Tran et al. 2010)	Nonparametric SSB (Tran et al. 2010)
Ionosphere	NIC09	BENT + GIM	From dual frequency altimeter range measurements (cycles 1–64) and GIM afterwards	From dual frequency altimeter range measurements	From dual frequency altimeter range measurements	From dual frequency altimeter range measurements (TOPEX) and DORIS (Poseidon)	GIM model
Wet troposphere	GPD corrections (Fernandes et al. 2015)						
Dry troposphere	ERA-interim based (Carrere et al. 2016)						
Dynamical atmospheric corrections	ERA-interim based (Carrere et al. 2016)						
Ocean tide	GOT 4.8 (Ray 2013)						
Mean sea surface	DTU 2010 (Andersen 2010)						
Pole tide	(Wahr 1985)						
Solid earth tide	Elastic response to tidal potential (Cartwright and Tayler 1971; Cartwright and Edden 1973)						
Loading tide	GOT4v8 (Ray 2013)						

applications. This has led to a level 2 altimeter database representing more than 50 years of cumulated data from 7 altimeter missions (TOPEX/Poseidon, Jason-1 and 2, ERS-1 and 2, Envisat, and GFO).

The SL_cci ECV consists of monthly maps of sea level anomalies (SLA), and the multi-mission mapping technique used to produce these maps (optimal interpolation) has been optimized for climate scales. The first version of the SL_cci ECV was disseminated in 2012, and the time series has benefited from regular temporal extensions so that the SL_cci v1.1 ECV covers the period 1993–2014 (DOI:10.5270/esa-sea_level_cci-1993_2014-v_1.1-201512). In addition to the monthly SLA maps, the ECV products also include ocean indicators computed over the total period. This includes the temporal evolution of the GMSL and its trend, regional mean sea level trends, and amplitude and phase of the annual signal. The products are available upon request at info-sealevel@esa-sealevel-cci.org, and the Product User Guide can be found on the project website: www.esa-sealevel-cci.org. A full description of the SL_cci v1.1 ECV is provided in Ablain et al. (2015).

The following section provides a detailed discussion of the sea level processing performed in the SL_cci project.

4 The Sea Level Record from High-Precision Satellite Altimetry Missions

This section reviews the altimeter standards and gridding processes used to build the sea level record. One important output of the CCI Programme is the error characteristics of the ECVs, which are described in this section.

4.1 Geophysical Corrections Applied to the SSH Measurements

In this section, we describe the geophysical corrections that are applied to the SSH measurements (hereinafter called 'altimeter standards'). The processing to provide the mean sea level record depends on the altimeter standards selected to derive the sea level from 1-Hz altimeter measurements, and on the gridding process applied to average the along-track measurements and calculate the GMSL time series. Before describing further this processing, it is worth noting that there are some processing differences between the different groups producing GMSL records. The impact of these differences has been described and quantified in several studies (Masters et al. 2012; Henry et al. 2014). The GMSL trend can be modified by few sub-millimetres per year (0.1–0.2 mm/year) due to these differences.

As briefly described in the previous section, corrections need to be applied to the SSH measurement: propagation corrections as the altimeter radar wave is delayed during atmosphere travel (ionospheric correction, wet tropospheric correction, dry tropospheric correction), ocean surface correction for the sea state which directly affects the radar wave (electromagnetic bias), geophysical corrections for the tides (ocean, solid Earth and polar tides as well as loading effects), and atmospheric corrections for the ocean response to atmospheric dynamics (inverse barometer correction for low frequency, atmospheric dynamics correction for high frequency). Furthermore, SSH is calculated for each altimetric measurement considered as valid according to criteria (e.g., threshold, spline, statistics on the ground track) applied either to the main altimetric parameters, the geophysical corrections or the SSH directly. These criteria may vary from one mission to another depending on the altimeter instrumental characteristics. The precise references for

the corrections and orbits used when calculating the mean sea level are given in Table 1 for the SL_cci project. Most of these corrections are not contained in the altimeter level-2 products (e.g., TOPEX M-GDR, Jason-1/Jason-2 GDR). They have been calculated and updated in a multi-mission altimetry database in order to calculate homogenous sea level for all altimetry missions.

4.2 Gridding Process

The recommended method by the SL_cci project in order to produce mean sea level grids has been developed for the SSALTO DUACS (Segment Sol Multimission Altimetrie et Orbitographie, Data Unification and Altimeter Combination System) System (Dibarboure et al. 2011). The main advantages of this method are, first of all, use of TOPEX/Poseidon, Jason-1, Jason-2 and Jason-3 as reference missions in order to obtain the most accurate long-term stability (Ablain, et al. 2009) and use of all other complementary missions (ERS-1, ERS-2, Envisat, Geosat Follow-On, CryoSat, SARAL/AltiKa and Sentinel-3A/B) to increase the spatial resolution of mean sea level grids.

The gridding process is composed of the following steps:

1. Calculation of the along-track sea level over all the altimeter period (1993–2014) for all the altimeter missions with homogenized corrections (as listed in Table 1), after removing spurious data (e.g., impacted by rain cells, sea ice).
2. Calculation of the mean sea level biases between the reference missions, both at global and regional scales. The verification phases between two consecutive missions (i.e. satellites on the same ground track apart from each other by few seconds; e.g., TOPEX/Jason-1, Jason-1/Jason-2, Jason-2/Jason-3) allow estimates of global biases with an accuracy close to 0.5–1 mm in terms of mean sea level (Zawadzki and Ablain 2016). It is worth noting that the absolute GMSL bias is arbitrarily set to 0 at 1993.
3. Reduction of the orbit errors between all the missions through a global minimization of the crossover differences observed within the reference mission and between reference and complementary missions (Dibarboure et al. 2011).
4. Computation of SSH grids (with a spatial resolution of 0.25° using a rectangular projection and a temporal resolution of 1 month) combining data from all missions using an objective analysis approach (Ducet et al. 2000; Le Traon et al. 2003).

The GMSL time series (Fig. 2) is easily deduced from the sea level grids by a area weighting averaging (taking into account the box area dependence with latitude) over the oceanic domain observed by the altimetry data (82°S to 82°N).

Other research teams (University of Colorado, AVISO, CSIRO, NOAA, NASA) only use the reference missions (TOPEX/Poseidon, Jason-1 and Jason-2) to provide GMSL time series. Their method is more simple since steps (3) and (4) described above are replaced by a simple averaging on a cycle basis of each mission (e.g., 1° along the latitudinal axis, 3° along the longitudinal axis for AVISO). Then all the time series are linked together during the verification phases (TOPEX/Jason-1 and Jason-1/Jason-2). The main advantage of this approach is the reduction of the computing time (fewer altimetry missions and no multi-mission adjustments). On the other hand, the GMSL is only estimated between 66°S and 66°N, and the regional sea level variations are not as well-represented as in the SL_cci. Furthermore, errors in altimetry measurements, such as long wavelength orbit errors or oceanic tide errors, are not removed and can impact the mean sea level estimate up to 1–2 mm at each cycle. However, the differences between these gridding process approaches, which each have their own limitations, only slightly impact

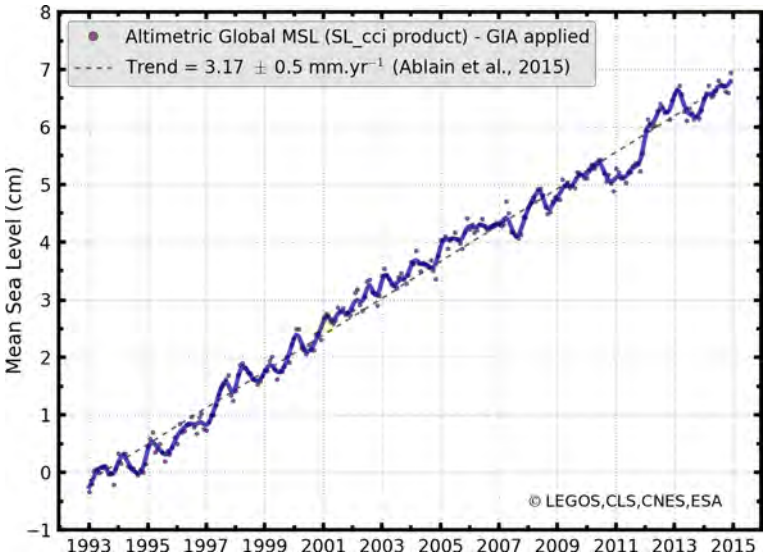

Fig. 2 Global mean sea level evolution over the period 1993–2014 from SL_cci project (DOI:10.5270/esa-sea_level_cci-1993_2014-v_1.1-201512). Annual and semi-annual signals have been removed from the monthly estimates (*red dots*), and a 6-month filter has been applied to produce the *blue curve*

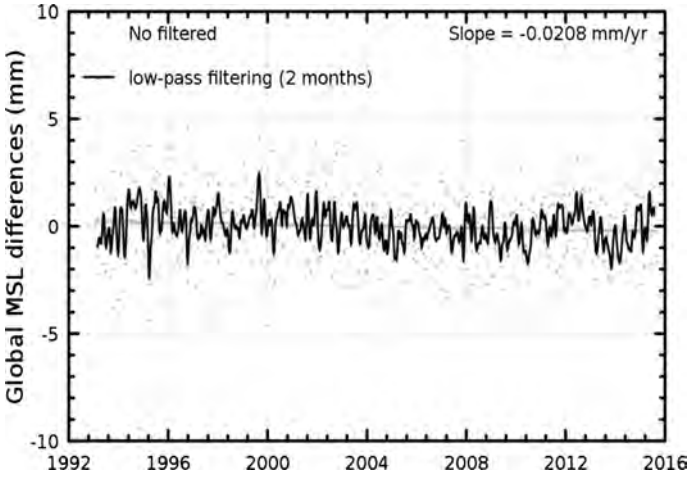

Fig. 3 Global mean sea level differences comparing the method applied to SL_cci products (based on SSALTO/DUACS system) and to AVISO global mean sea level time series. Same altimeter standards are used in both cases

the GMSL trend or the interannual signals (Fig. 3). The differences are lower than 0.05 mm/year over the whole altimetry period for the trend and reach 1–2 mm over shorter periods between 1 and 3 years (Henry et al. 2014).

4.3 Global Mean Sea Level Rise Characteristics

GMSL rises between 3.2 and 3.4 mm/year over the 1993–2014 period, according to the different groups (SL_cci project, AVISO, University of Colorado, NASA, NOAA, CSIRO). Although the global evolution is nearly linear over the period (the linear error adjustment provided by the least squares method is about 0.02 mm/year), interannual variations are also observed. Removing the trend from GMSL time series highlights these variations over a 1-year to 3-year period (Fig. 4). Their magnitudes depend on the period (+3 mm in 1998–1999, -5 mm in 2011–2012, and +10 mm in 2015–2016) and are well-correlated with El Niño Southern Oscillation (ENSO) events. In Fig. 4, the Multivariate ENSO Index (MEI) has been shown to better represent this temporal correlation.

4.4 Global Mean Sea Level Uncertainties

GMSL data contain remaining errors at different time scales. In the SL_cci project, an error budget dedicated to the main temporal scales (i.e. long term—5–10 years or more, inter-annual—<5 years—and seasonal) has been established (see Table 2). Regarding the GMSL trend, an uncertainty of 0.5 mm/year was estimated over the whole altimetry era (1993–2015) within a confidence interval of 95 % (2-sigma). The main source of error is the radiometer wet tropospheric correction with a drift uncertainty in the range of 0.2–0.3 mm/year (Legeais et al. 2014). To a lesser extent, the orbit error (Couhert et al. 2015) and the altimeter parameters (range, sigma-0, significant wave height) instabilities (Ablain et al. 2012) add additional uncertainty, of the order of 0.1 mm/year. It is worth noting that for these two corrections, the uncertainties are higher in the first altimetry decade (1993–2002) when TOPEX/Poseidon, ERS-1 and ERS-2 measurements display larger errors. Furthermore, imperfect links between TOPEX-A and TOPEX-B (February 1999), TOPEX-B and Jason-1 (April 2003), Jason-1 and Jason-2 (October 2008) lead to errors of 2, 1 and 0.5 mm, respectively (Ablain et al. 2009; Zawadzki and Ablain 2016). They cause a GMSL trend uncertainty of about 0.1 mm/year over the 1993–2014 period. It is relevant to

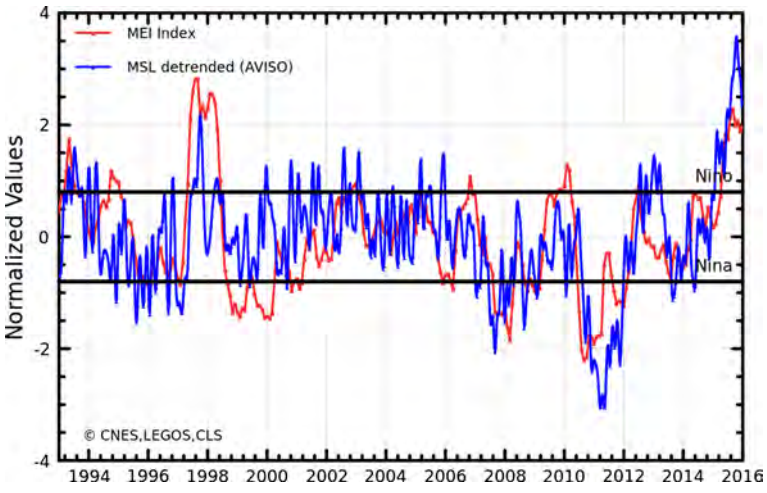

Fig. 4 Comparison of the Multivariate ENSO Index (MEI) and the global mean sea level time series (from AVISO) after removing the global mean trend

Table 2 Mean sea level error budget for the main climate scales (Ablain et al. 2015)

Spatial scales	Temporal scales	Altimetry errors	User requirements
GMSL	Long-term evolution (>10 years)	<0.5 mm/year	0.3 mm/year
	Interannual signals (<5 years)	<2 mm over 1 year	0.5 mm over 1 year
	Annual signals	<1 mm	Not defined
Regional MSL	Long-term evolution (>10 years)	<3 mm/year	1 mm/year
	Annual signals	<1 cm	Not defined

note that the remaining uncertainty of $\sim$0.5 mm/year on the GMSL trend remains 0.2 mm/year higher than the GCOS requirements (of 0.3 mm/year, see GCOS 2011).

All sources of errors described above and the gridding process, already described in Sect. 4.2, also have an impact at interannual time scale (<5 years). The level of error is still 1.5 mm higher than the GCOS requirement of 0.5 mm. This may have consequences on the sea level closure budget studies at interannual time scale. For the annual signal, the amplitude error is estimated lower than 1 mm. Knowing that the annual amplitude of the GMSL is in the order of 9 mm, this error can be considered low.

5 Regional Sea Level

5.1 Spatial Trend Patterns in Sea Level

The regional mean sea level trends (Fig. 5) are directly deduced from the gridded mean sea level time series. As mentioned above, the gridding process applied in the SL_cci project

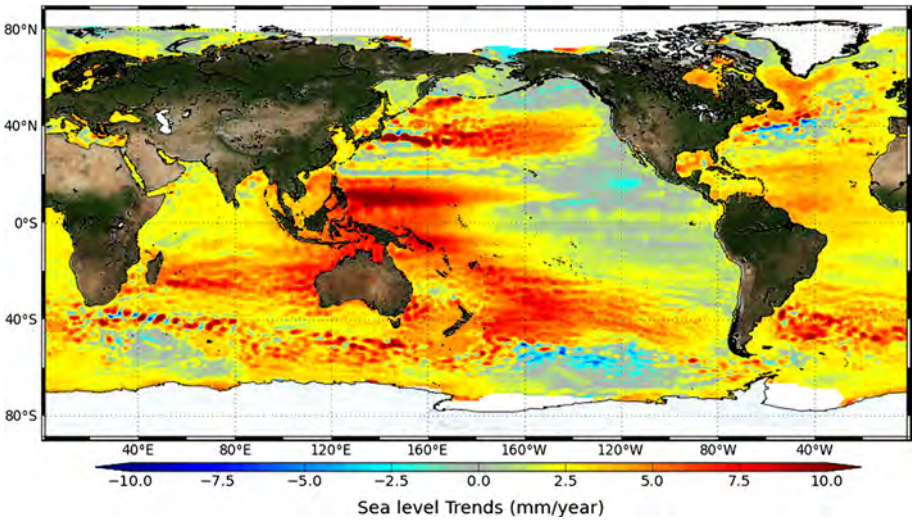

Fig. 5 Regional mean sea level trends over the 1993–2014 period from SL_cci products (release 1.1)

(derived from the SSALTO/DUACS system) provides a spatial resolution of 0.25° between 82°S to 82°N. The results discussed below only apply to the SL_cci products.

5.2 Uncertainties at Regional Scale

At regional scale, trend uncertainty is of the order of 2–3 mm/year (see below). Although the orbit error has been significantly reduced for this spatial scale during the last few years, it remains the main source of uncertainty (in the range of 1–2 mm/year; Couhert et al. 2015) with large spatial patterns at hemispheric scale. The Earth gravity field model errors explain an important part of these uncertainties (Rudenko et al. 2014). Furthermore, errors are higher in the first decade (1993–2002) for which the Earth gravity field models are less accurate due to the unavailability of the Gravity Recovery And Climate Experiment (GRACE) data. Additional errors are still observed, e.g., for the radiometer-based wet tropospheric correction in tropical areas, other atmospheric corrections in high latitudes, and high frequency corrections in coastal areas. The combined errors give rise to an uncertainty of 0.5–1.5 mm/year. Finally, the 2–3 mm/year uncertainty on regional sea level trends remains a significant error compared to the 1 mm/year GCOS requirement, even if this project has led to a 0.5 to 1.5 mm/year error reduction.

In a recent study (Prandi et al., in preparation), uncertainties on sea level trends have been produced. The method to estimate spatial trend uncertainties is based on generalized least-squares (also called inverse method). With this approach, we can separately estimate the errors and the long-term trends, taking into account the natural variability of ocean dynamics (mesoscale circulation, interannual variability). Results (Fig. 6) show that even with no error covariance, trends are not significant in areas of high oceanic variability (Fig. 6, left). When considering measurement errors with 95 % confidence intervals, trend errors generally range from 1 to 3 mm/year (Fig. 6 middle). Adding serial correlation due to natural ocean variability shifts the confidence interval to larger values, from 1 to 4–5 mm/year (Fig. 6, right). In all cases, a large fraction of sea level trends is significant (67 and 52 %, respectively) and cannot be explained by natural variability. It is worth noting that these results rely on numerous assumptions about error covariance shapes and amplitudes.

5.3 New Arctic Products

In this section, a specific focus is performed on the Arctic mean sea level evolution. This is an area of great interest for climate studies with rapid climatic changes, such as the dramatic reduction of sea ice extent. Models also predict that the Arctic Ocean will be

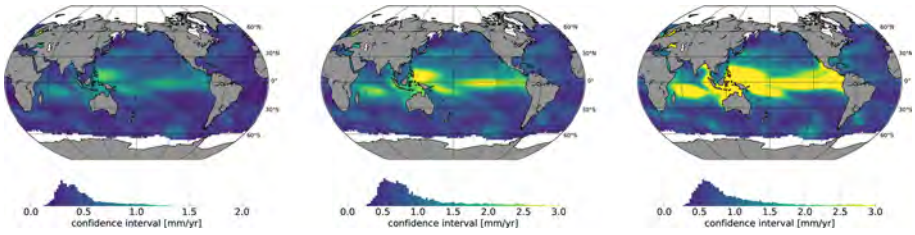

Fig. 6 Uncertainty maps of regional sea level trends. *Left* no error covariance (usual least-squares fit); *middle* measurement error covariance only; *right* measurement error and natural variability error covariance

experiencing large changes in the future (IPCC AR5). However, to date, the Arctic Ocean remains poorly observed by satellite altimetry, mainly due to sea ice cover that prevents accurate sea level measurements.

In recent years, several teams have been working towards a better knowledge of Arctic SSH (e.g., Prandi et al. 2012; Giles et al. 2012; Cheng et al. 2015). Recently, improvements on the processing of altimetry measurements in this area based on a new waveform classification and retracking algorithm (Poisson et al., in preparation) have allowed us to derive improved mean sea level maps with increased data coverage and higher mean sea level accuracy from the ice-covered Arctic (Fig. 7).

6 Validation and Error Assessment of CCI Products at Global and Regional Scales

In situ measurements are used to validate altimeter sea level records. Two types of in situ sensors are generally used: tide gauges and Argo floats. Both provide independent SSH measurements that are very valuable to detect anomalies in the altimeter records.

6.1 Validation with Tide Gauges

Tide gauges are instruments, generally set at the coast, which measure SSH relative to a local datum. There are two methods to compare tide gauges measurements with altimetry data: absolute calibration at dedicated sites, and regional or global comparisons. Absolute calibration requires a carefully monitored tide gauge, along with a precise positioning device (e.g., GPS), placed under or near altimeter ground tracks. There are three such sites in Harvest (Haines et al. 2010), Corsica (Bonnefond et al. 2015) and Bass Strait (Watson et al. 2011), which provide very valuable SSH differences time series from the beginning of the altimeter record. The other approach is to use a much wider network of tide gauges,

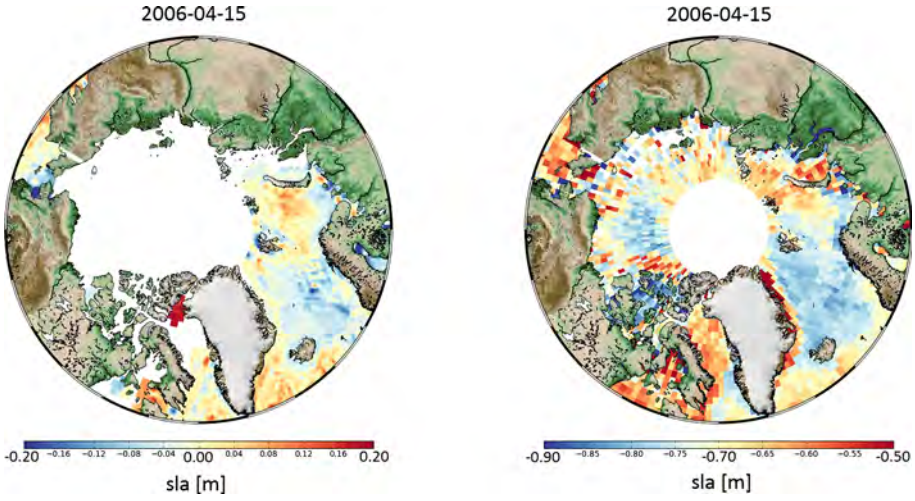

Fig. 7 Maps of sea level anomalies (SLA) in the Arctic Ocean on 15 April 2006. *Left* panel: map derived from global SL_cci products with no specific processing in the Arctic region. *Right* panel: map derived from Envisat data with improved data processing

which are individually less accurate but provide a larger ensemble, to build regional or global biases between an altimetry mission and tide gauges (Nerem et al. 2010; Mitchum et al. 1998, 2010). As the differences between absolute sea level measured by altimetry and relative sea level measured by tide gauges could also partly arise from vertical motion of the land on which the tide gauge is grounded, stations to be used need to be carefully selected and also corrected by vertical land motion if known (Fenoglio-Marc et al. 2004; Santamaría-Gómez et al. 2014).

Tide gauges unevenly sample the global coastlines, and comparisons do not cover the deep open ocean. All comparison methods rely on a similar processing, which is briefly described here. A complete description of the comparison method is available, for example, in Valladeau et al. (2012) and Wöppelmann and Marcos (2016). First, relative SSH measurements from tide gauges are corrected for various effects (tides, atmospheric pressure, vertical land motions) so that the physical content is comparable to absolute SSH measurements from altimetry. Then, altimetry measurements are collocated to tide gauges stations (using different approaches such as bilinear interpolation, area average, etc.), and a time series of altimetry minus tide gauge sea level is extracted at each in situ station. Eventually a global average is estimated from the ensemble of the different times series.

While all groups use similar methods, processing details may vary and result in slightly different estimates of altimeter minus tide gauges biases (Mitchum 1998; Watson et al. 2015). Methods also vary depending on the focus of the comparisons, for example whether it is aimed at obtaining calibrated altimetry records (Watson et al. 2015) or evaluating vertical crustal motions (Wöppelmann and Marcos 2016). But in any case, the advantage of the large number of stations is that a global bias time series can be computed and can then be used to characterize the level of agreement between altimetry and in situ records.

Figure 8 displays two examples of metrics derived from global differences between altimetry and tide gauges. The left panel shows the evolution of global differences between altimetry and tide gauges for the SL_cci and DUACS-DT products (Pujol et al. 2016). In both cases, no significant drift is detected, and differences are generally below 1 cm. The right panel focuses on the residual annual signal observed in the differences. The SL_cci product is found to be in better agreement with tide gauges than the DUACS-DT product regarding the annual signal amplitude.

One objective of such comparisons is to ensure that the altimeter record is not drifting over time. Meanwhile, it is essential to determine the accuracy of tide gauges comparisons. Mitchum (1998) and Watson et al. (2015) claim that the error of the method is about

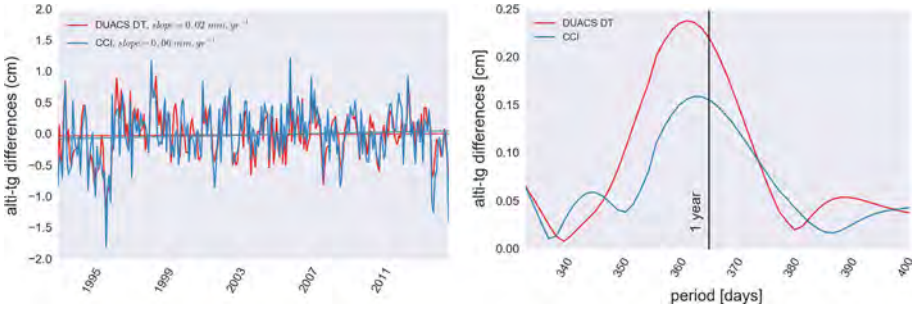

Fig. 8 *Left* time series of global differences between CCI (*red*) or DUACS-DT (*blue*) products and tide gauges. *Right* amplitude of the annual signal in differences between CCI (*red*) or DUACS-DT (*blue*) and tide gauges

0.4 mm/year while Valladeau et al. (2012) provide a 0.7 mm/year estimate and Santamaría-Gómez et al. (2012) found a value of 0.6 mm/year due to vertical land motions. This is actually one important source of error affecting relative SSH measurements by tide gauges. When no precise positioning at the stations exists, these corrections rely on Glacial Isostatic Adjustment (GIA) models (Peltier 2004) that do not account for contemporary vertical land motion sources (present-day ice melt, surface loading, ground water extraction, etc.). Wöppelmann and Marcos (2016) quantified vertical land movements not linked to the GIA process that may reach up to 10 mm/year, although on average they cancel out (0.01 ± 0.27 mm/year) if the number of tide gauge stations used is large enough.

6.2 Validation Using Argo Floats

Data from Argo floats (Roemmich et al. 2009) are another source of in situ information about the state of the ocean. They do not directly measure SSH but vertical profiles of temperature and salinity. These can be converted into density anomalies and integrated over depth to provide dynamic height anomalies (DHA), which can then be compared to altimetry-based SSH data (Valladeau et al. 2012; Legeais et al. 2016). DHA and altimeter SSH do not have consistent physical contents, as DHA are only the steric part of total sea level as measured by altimetry and, unlike tide gauges, cannot be used for absolute calibration of altimeter data but are rather used as a reference to compare two altimeter products or standards. If needed, the mass component can be derived from GRACE measurements. Argo floats are deployed at sea and, since 2005, provide a homogeneous sampling of the upper 2000 m of the global ocean, thus complementing tide gauges stations (Roemmich et al. 2009). Altimeter SSH measurements are interpolated at the time and position of Argo profiles to form an ensemble of SSH minus DHA differences from which various metrics are drawn.

Figure 9 contains a Taylor diagram that compares the CCI and DUACS-DT sea level products to a reference formed by the sum of Argo DHA and GRACE mass component. The diagram visualizes the closeness of altimetry to the reference in terms of correlation and RMS of the differences. Figure 9 shows the total signal separated into different frequencies. The results indicate that at low frequencies the SL_cci product is more consistent with Argo data than DUACS-DT (similar correlation but lower RMS). When all frequencies are considered, differences between the two products are low. A comprehensive review of uncertainty sources for Argo/altimetry comparisons can be found in Legeais et al. (2016).

6.3 Regional Validation

In addition to the global validation described above, a regional validation of the SL_cci products is performed based on the comparison with in situ data for selected regions: North Sea and Mediterranean Sea. These regions have been chosen for the availability of dense and accurate in situ measurements and ocean model data.

Regional closure of the sea level budget was investigated in the Mediterranean Sea. Figure 10 shows the smoothed monthly SL_cci series over January 2003–December 2014 and the sum of the steric and ocean mass components estimated from Argo temperature and salinity data of the EN4 database (Good et al. 2013) and GRACE data (Fenoglio-Marc et al. 2012). The sea level derived from the SL_cci products is in agreement with sea level derived from the sum of steric and mass

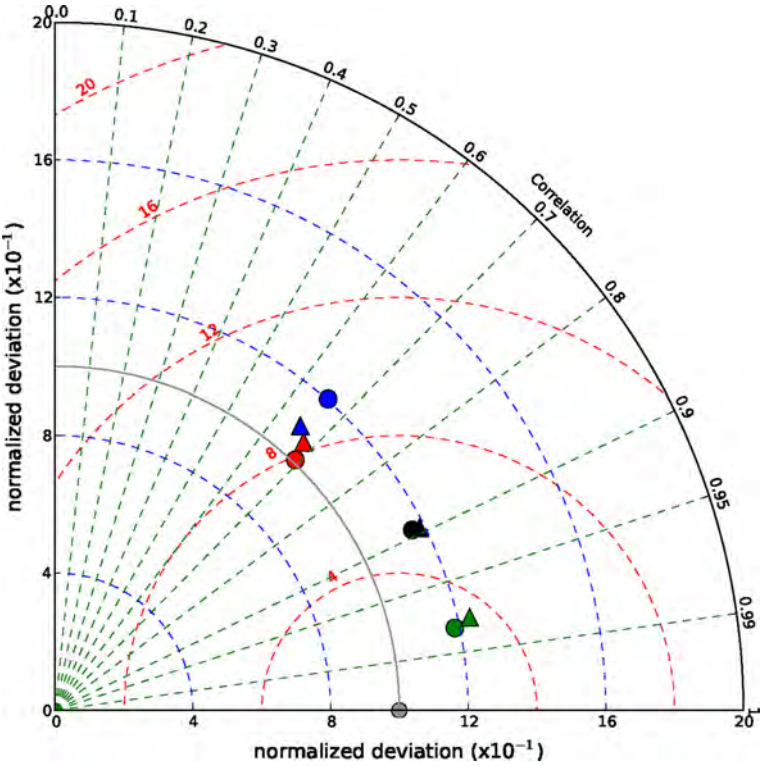

Fig. 9 Taylor diagram of the SL_cci (*triangles*) and SSALTO/DUACS-DT (*circles*) time series compared with the sum of Argo DHA (referenced to 900 dbar) and ocean mass from GRACE GRGS RL03v1 times series (*grey dot*) over 2005–2014. Total time series are in *black* and annual signals in *green*. High (in *red*) and low (in *blue*) frequencies are first adjusted from annual signal and detrended. Taylor diagrams are used to quantify the degree of correspondence between modeled and observed parameters according to 3 variables: correlation coefficient, root-mean-squares error and standard deviation

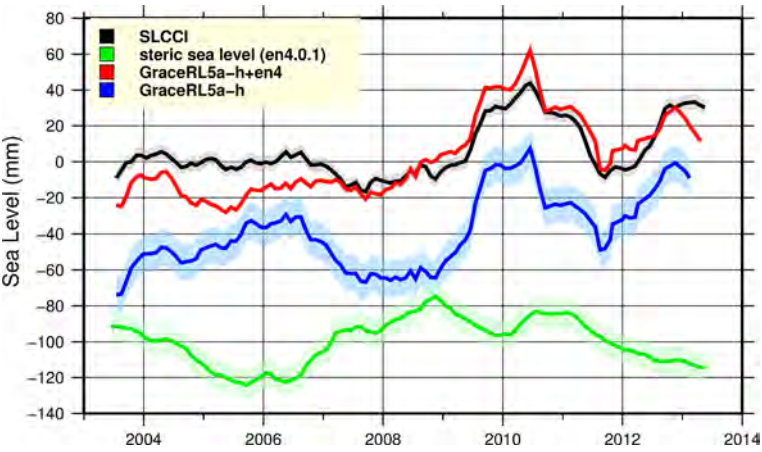

Fig. 10 SL_cci-based regional mean sea level (2004–2014) in the Mediterranean Sea (*black*) and sea level computed as sum of steric and mass components (*red*), with steric (*green*) and mass (*blue*) components

components, with a difference in trend and interannual signals of 0.8 m/year and 10.9 mm, respectively.

In the North Sea, SL_cci data are validated by comparing with tide gauges, quality-controlled with geodetic-referenced data in the German Bight and at a few other stations in the North Sea. In this case, the primary goal is to validate products and estimate errors for the along-track altimetric SSH, to verify their regional mission-long sea level trends and errors, and to compare signals and errors with the gridded sea level solutions. The same analysis has been performed for CryoSat-2 data processed with the SAMOSA model and retracker (Ray et al. 2014) in the ESRIN/GPOD SARvatore service. In the along-track comparison, the uncorrected sea level from tide gauges, expressed in ellipsoidal heights above the reference ellipsoid GRS80, are compared to the SL_cci products corrected as described in Fenoglio-Marc et al. (2015). Figure 11 shows a standard deviation of the differences. It amounts about 7 cm, which reduces to 4 cm when the tidal model TPX08 is used (http://volkov.oce.orst.edu/tides/global.html). The impact of the choice of the improved GNSS Path Delay (GPD+) wet tropospheric correction (Fernandes et al. 2015) in the coastal zone is not significant in this area. We have compared in the same region the monthly time series SL_cci gridded products and tide gauges. They agree well in terms of annual amplitude (differences <1.0 cm) and phase, with statistically significant correlations at all stations. Altimetry and tide gauge sea level trends are not statistically different at any station. The comparison of GPS-derived vertical land motion with the trend of the difference between altimetry and tide gauge shows differences in the order of 1 mm/year, which is within the trend uncertainty (Fig. 12). This uncertainty appears large for an accurate computation of vertical land motion rates from tide gauge and altimetry data. However, we notice a better agreement between altimeter and tide gauge (correlation, standard deviation and difference of trends) when SL_cci data are used, which indicates a higher quality of the SL_cci compared to other altimeter products.

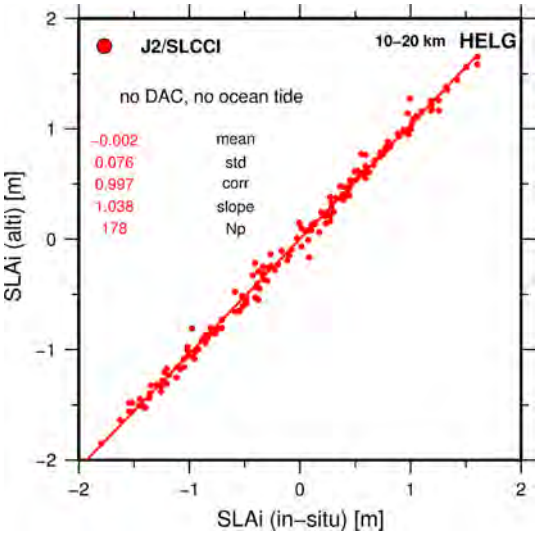

Fig. 11 Scatterplot of instantaneous SLA and statistic of differences for the complete Jason-2 SL_cci along-track data and from in situ data at the Helgoland tide gauge. Data are selected with spatial distance from the station between 10 and 20 km and temporal difference of 30 min. Np is the number of data points

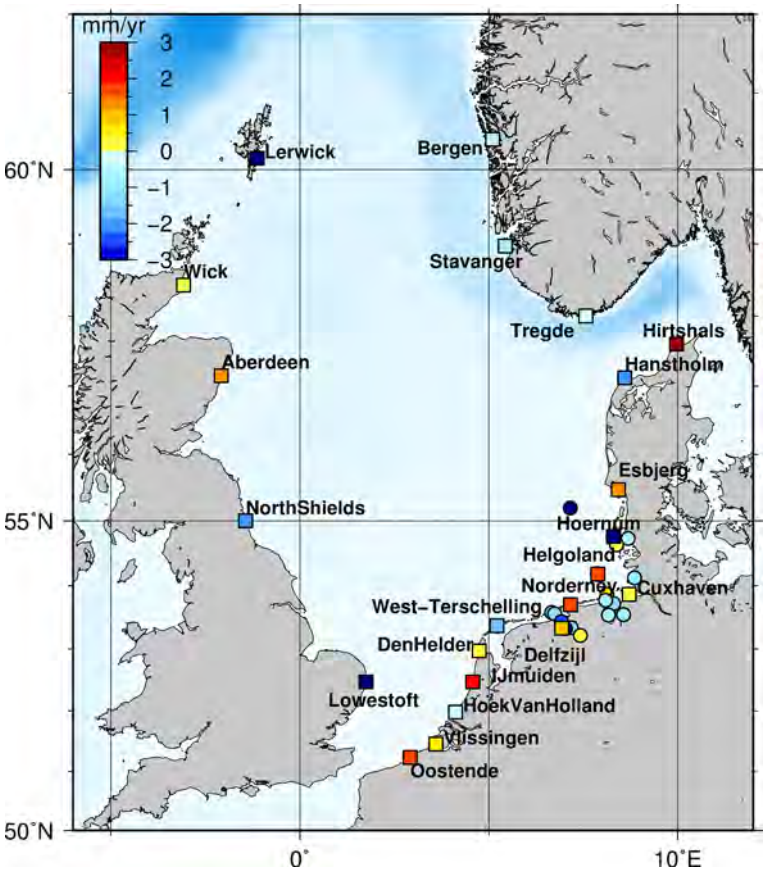

Fig. 12 Vertical land motion from GPS (*circle*) and from SL_cci altimetry minus tide gauges (*square*) in the North Sea, in mm/year

7 The CCI Sea Level Project: A Summary

Compared with previously existing products, the major evolutions of the SL_cci product are related to the following parameters. First, the orbit solutions of the different altimeter missions have been chosen so that the homogeneity of the regional sea level trends has been improved. Secondly, the GPD altimeter wet troposphere correction allows an improved estimation of the wet troposphere path delay in coastal areas. It also improves the sea level estimation in the open ocean, at high latitudes, correcting for invalid observations due to land, ice and rain contamination, and instrument malfunction. This correction exploits the data from various sources, including the Global Navigation Satellite Systems (GNSS). In addition, new dynamic atmospheric corrections computed with the ERA-Interim reanalysis lead to a strong sea level error reduction (Fig. 13) and strong improvement of the regional sea level trends over the early altimetry years.

The most impressive result of the SL_cci project is obtained using a new instrumental correction for the Envisat mission (Garcia and Roca 2010; Thibaut et al. 2012). It is illustrated in Fig. 14 by separating the ERS-1 and 2/Envisat and TOPEX/Jason-1 and 2

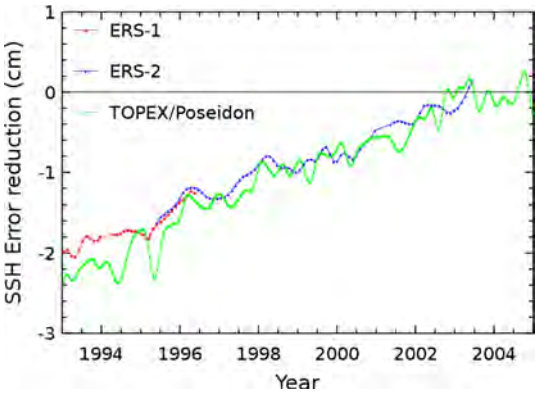

Fig. 13 Sea surface height error reduction for ERS-1 and 2 and TOPEX/Poseidon missions using a dynamic atmospheric correction forced by the ERA-Interim reanalysis compared with the operational ECMWF atmospheric fields

GMSL time series using alternately the old and new altimeter corrections: the trend difference between both time series has been significantly reduced thanks to the new instrumental correction (by 0.9 mm/year). The work performed contributed to better characterize and reduce altimetry errors at climate scales.

New level 2 altimeter algorithms have been developed, focusing on improving the ECV homogeneity and reducing the errors. Compared with the v1.1 SL_cci ECV, the major improvements that can be found in the reprocessed version are associated with the following aspects:

- New GFZ and CNES orbit solutions (Rudenko et al. 2015; Jalabert et al. 2015) have been selected for the SSH calculation of past and present altimeter missions. Compared with the previous POE-D version, the POE-E solution improves the sea level estimation and has a significant impact on the regional sea level trends (Fig. 15, left).
- The FES 2014 ocean tide model (Carrere et al. 2015) is used in the SLA calculation. Compared with other model (GOT 4.8), it leads to a reduced variance of the sea level in many coastal areas and at high latitudes (Fig. 15, right).
- An enhanced radiometer wet troposphere correction, called GPD+ (Fernandes et al. 2015), was selected for the SLA calculation of all altimeter missions. External independent measurements have been used to ensure the stability of this new correction. It significantly impacts the global decadal signals and also the sea level estimation in coastal areas.

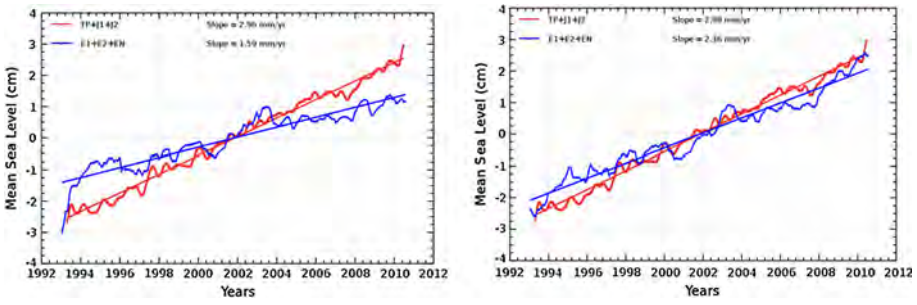

Fig. 14 GMSL evolution and associated trends computed with the TOPEX/Poseidon, Jason 1 and 2 (*red*), and ERS-1, ERS-2 and Envisat (*blue*) altimetry missions

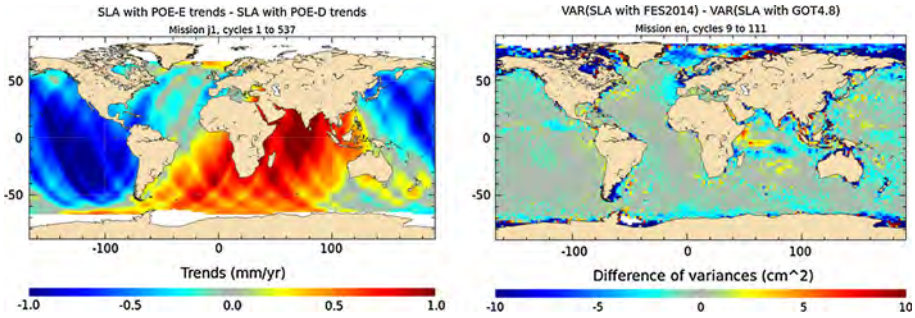

Fig. 15 *Left* map of the difference of Jason-1 (cycles 1–537) mean sea level trends computed successively with POE-D and POE-E orbit solutions. *Right* map of the difference of variance of the SSH computed successively with GOT 4.8 and FES 2014 ocean tide model for the Envisat mission (cycle 9–111)

The SL_cci products benefit from a quality control that includes internal validation, consistency check, and comparison with in situ data. In addition to this validation process, the scientific quality assessment of the ECV is an important ongoing task of the SL_cci project. Two types of assessments are investigated: (1) comparison of ocean model-based sea level with the CCI products and (2) study of the sea level budget. In (1), different methodologies are developed: (a) study of the sensitivity of an ocean reanalysis (the GECCO general ocean circulation model with data assimilation) to the new CCI sea level data via inclusion of these data in the assimilation procedure; (b) comparison with ocean-only simulation at different resolutions and with existing ocean reanalyses, which assimilate subsurface data; (c) assessment of sea level changes at high altitudes and in the Arctic Ocean by comparison of the SL_cci products with simulation runs of the Norwegian Earth System Model (NorESM).

The sea level budget approach consists in computing the sea level components using different observing systems, and comparing their sum to the SL_cci GMSL (Dieng et al. 2015a, b). Figure 16 shows the globally averaged SL_cci time series over January 2003–December 2014 with the sum of the steric and ocean mass components (estimated from Argo temperature and salinity data down to 2000 m depth and GRACE data). Over this time span, there is a very good agreement between the CCI sea level and sum of components, both in terms of trend and interannual variability. Therefore, the SL_cci data lead to quasi-closure of the sea level budget.

Within the second phase of the SL_cci project (2014–2016), updated altimeter standards and corrections are developed in the perspective of a full reprocessing of the sea level ECV (delivered end 2016). By the end of the project, this v2.0 time series will cover the period 1993–2015. Nine altimeter missions will be included, with SARAL/AltiKa and CryoSat-2 missions being new in the dataset.

8 Conclusions

Sea level, a climate variable that integrates changes of several components of the climate system, was identified by GCOS as an ECV and was further selected by ESA to be included in the first phase of the CCI programme. In this paper, we have reported how altimetry-based sea level products from different missions are built, what the current levels of uncertainties of the global and regional products are and how they have been validated.

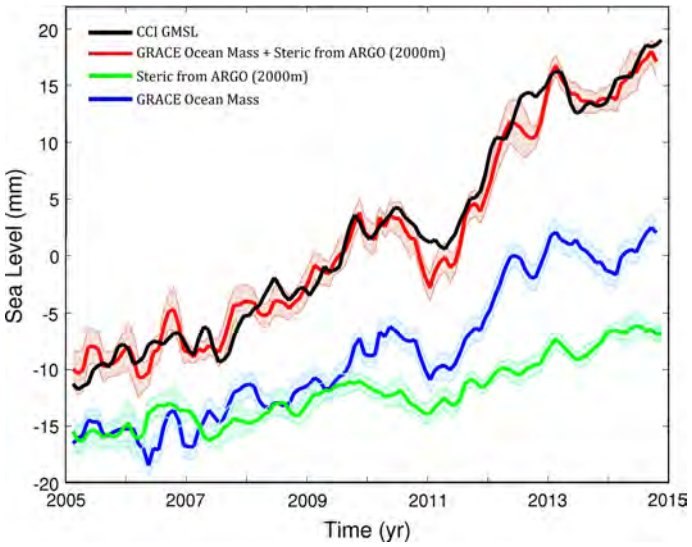

Fig. 16 SL_cci-based GMSL (*black*); Argo-based steric sea level (*green*) GRACE-based ocean mass (in equivalent of sea level, *blue*) over January 2005–December 2014 (update from Dieng et al. 2015b). The *red curve* is the sum of the steric and ocean mass components. An arbitrary vertical offset was applied to the *green* and *blue curves* for clarity

SL_cci products have been significantly improved, revisiting a myriad of instrumental and geophysical corrections. An important outcome of the CCI is that the SL_cci products are now well-characterized in terms of errors. Accounting for the ESA altimetry missions, which have a high-inclination orbit, a specific effort was dedicated to the Arctic region where the sea level evolution was poorly known until recently.

Despite the important effort invested so far, the sea level products provided within the CCI programme still do not fully satisfy the GCOS requirements, in particular at inter-annual time scales. Thus, further improvements of the altimetric standards are needed. The next inclusion of Jason-3 and Sentinel-3A (100 % SAR mode) data to the nearly 25-year-long time series will certainly lead in the near future to more accurate sea level time series, provided that long-term drifts of these new missions are carefully accounted for.

The implementation of the ESA CCI programme has led to the coordination of the Earth Observation and the Climate Research communities. This is a valuable outcome of the programme, and the CCI framework should be sustained in the future, conquering new space-based ECVs, improving existing ECVs, further assimilating ECVs in models and closing imbalances involving climate variables.

Finally, concerning the closure of the sea level budget, efforts are still needed to further improve the accuracy and to characterize the remaining uncertainties of components contributing to sea level, such as glaciers and ice sheet mass balances, ocean heat content and salinity changes, and land water storage changes.

Scientific analysis of the long-term sea level evolution and its societal impacts requires the implementation of an operational and sustainable production of the sea level Climate Data Record (CDR). Regular updates of the time series are also necessary so that the period covered by the dataset is always current. Such challenge has been addressed by the Copernicus Climate Change Service (C3S), which aims at combining observations of the

climate system with the latest science to produce a consistent, comprehensive and credible description of the past and present-day climate in Europe and worldwide. It will become a major contribution from the European Union to the WMO Global Framework for Climate Services and its Climate Monitoring Architecture.

The C3S will ensure the production of the sea level CDR. The sea level record is highly dependent on the altimetry data used as input of the production system. First, the maintenance of the historical altimetry databases is required since the reprocessing of the measurements of past missions will lead to an improved quality of the whole CDR. Secondly, the integration of recent (CryoSat-2, Jason-3, Sentinel-3A) and future (Sentinel-3B, Sentinel-6, SWOT) altimetry missions are of crucial importance to guarantee the future of the sea level record.

Acknowledgments We thank G. Woppelmann and an anonymous reviewer for helpful comments on the original manuscript. M. Ablain, J.F.Legeais, P. Prandi, J. Benveniste, L. Fenoglio-Marc, H.B. Dieng and A. Cazenave acknowledge the support by ESA in the frame of the CCI project. The authors also thank all partners of the SL_cci project. M. Marcos acknowledges a 'Ramon y Cajal' contract funded by the Spanish Ministry of Economy. This work was supported by the research project CLIMPACT (CGL2014-54246-C2-1-R) funded by the Spanish Ministry of Economy.

References

Ablain M, Cazenave A, Valladeau G, Guinehut S (2009) A new assessment of the error budget of global mean sea level rate estimated by satellite altimetry over 1993–2008. Ocean Sci 5:193–201

Ablain M, Philipps S, Urvoy M, Tran N, Picot N (2012) Detection of long-term instabilities on altimeter backscattering coefficient thanks to wind speed data comparisons from altimeters and models. Mar Geod 35(S1):42–60. doi:10.1080/01490419.2012.718675

Ablain M, Cazenave A, Larnicol G, Balmaseda M, Cipollini P, Faugère Y, Fernandes MJ, Henry O, Johannessen JA, Knudsen P, Andersen O, Legeais J, Meyssignac B, Picot N, Roca M, Rudenko S, Scharffenberg MG, Stammer D, Timms G, Benveniste J (2015) Improved sea level record over the satellite altimetry era (1993–2010) from the Climate Change Initiative project. Ocean Sci 11:67–82. doi:10.5194/os-11-67-2015

Agreen RW (1982) The 3.5-year GEOS-3 data set. NOAA Technical Memorandum NOS NGS 33, NOAA, Rockville, MD

Andersen OB (2010) The DTU10 Gravity field and mean sea surface (2010) Second international symposium of the gravity field of the earth (IGFS2), Fairbanks, Alaska, 20–22 September 2010. http://www.space.dtu.dk/english/~/media/Institutter/Space/English/scientific_data_and_models/global_marine_gravity_field/dtu10.ashx. Access 20 June 2014

Bonnefond P, Exertier P, Laurain O, Guillot A, Picot N, Cancet M, Lyard F (2015) SARAL/AltiKa absolute calibration from the multi-mission Corsica facilities. Mar Geod 38(S1):171–192

Carrere L, Lyard F, Cancet M, Guillot A, Picot N, Dupuy S (2015) FES 2014: a new global tidal model. Ocean Surface Topography Science Team, Reston, Virginia, USA, October 2015. http://meetings.aviso.altimetry.fr/fileadmin/user_upload/tx_ausyclsseminar/files/OSTST2015/TIDE-01-Carrere.pdf

Carrere L, Faugère Y, Ablain M (2016) Major improvement of altimetry sea level estimations using pressure derived corrections based on ERA-interim atmospheric reanalysis. Ocean Sci Discuss. doi:10.5194/os-2015-112

Cartwright DE, Tayler RJ (1971) New computations of the tide-generating potential. Geophys J Int 23(1):45–73

Cartwright DE, Edden AC (1973) Corrected tables of tidal harmonics. Geophys J Int 33(3):253–264

Cazenave A, Dieng H, Meyssignac B, von Schuckmann K, Decharme B, Berthier E (2014) The rate of sea level rise. Nat Clim Change 4:358–361. doi:10.1038/NCLIMATE2159

Chelton DB, Ries JC, Haines BJ, Fu LL, Callahan PS (2001) Satellite altimetry. In: Fu L-L, Cazenave A (eds) Satellite altimetry and earth sciences, a handbook of techniques and applications. Academic Press, London. Int Geophys Ser 69:1–131

Cheng Y, Andersen O, Knudsen P (2015) An improved 20-year Arctic Ocean altimetric sea level data record. Mar Geod 38(2):146–162

Church JA, White NJ, Konikow LF, Domingues CM, Cogley JG, Rignot E, Gregory JM, van den Broeke MR, Monaghan AJ, Velicogna I (2011) Revisiting the earth's sea-level and energy budgets from 1961 to 2008. Geophys Res Lett. doi:10.1029/2011gl048794

Church JA, Clark PU, Cazenave A, Gregory JM, Jevrejeva S, Levermann A, Merrifield MA, Milne GA, Nerem RS, Nunn PD, Payne AJ, Pfeffer WT, Stammer D, Unnikrishnan AS (2013) Sea level change. In: Stocker TF, Qin D, Plattner G-K, Tignor M, Allen SK, Boschung J, Nauels A, Xia Y, Bex V, Midgley PM (eds) Climate change 2013: the physical science basis. Contribution of working group I to the fifth assessment report of the intergovernmental panel on climate change. Cambridge University Press, Cambridge

Clark PU et al (2015) Recent progress in understanding and projecting regional and global mean sea level. Curr Clim Change. doi:10.1007/s40641-015-0024-4

Couhert A, Luca Cerri L, Legeais JF, Ablain M, Zelensky NP, Haines BJ, Lemoine FG, Bertiger WI, Desai SD, Michiel Otten M (2015) Towards the 1 mm/y stability of the radial orbit error at regional scales. Adv Space Res 55:2–23

Dibarboure G, Pujol M-I, Briol F, Le Traon PY, Larnicol G, Picot N, Mertz F, Ablain M (2011) Jason-2 in DUACS: updated system description, first tandem results and impact on processing and products. Mar Geod 34(3–4):214–241

Dieng H, Palanisamy H, Cazenave A, Meyssignac B, von Schuckmann K (2015a) The sea level budget since 2003: inference on the deep ocean heat content. Surv Geophys 36:1. doi:10.1007/s10712-015-9314-6

Dieng H, Cazenave A, von Shuckmann K, Ablain M, Meyssignac B (2015b) Sea level budget over 2005–2013: missing contributions and data errors. Ocean Sci 11:789–802. doi:10.5194/os-11-789-2015

Dieng H, Champollion N, Cazenave A, Wada Y, Schrama E, Meyssignac B (2015c) Total land water storage change over 2003–2013 estimated from a global mass budget approach. Environ Res Lett 10:124010. doi:10.1088/1748-9326/10/12/124010

Ducet N, Le Traon PY, Reverdin G (2000) Global high resolution mapping of ocean circulation from the combination of TOPEX/POSEIDON and ERS-1/2. J Geophys Res (Oceans) 105(C8):19477–19498

Fenoglio-Marc L, Groten E, Dietz C (2004) Vertical land motion in the Mediterranean Sea from altimetry and tide gauge stations. Mar Geod 27(3–4):683–701

Fenoglio-Marc L, Becker M, Rietbroeck R, Kusche J, Grayek S, Stanev E (2012) Water mass variation in Mediterranean and Black Sea. J Geodyn. doi:10.1016/j.jog.2012.04.001

Fenoglio-Marc L, Dinardo S, Scharroo R, Roland A, Dutour M, Lucas B, Becker M, Benveniste J, Weiss R (2015) The German Bight: a validation of CryoSat-2 altimeter data in SAR mode. Adv Space Res. doi:10.1016/j.asr.2015.02.014

Fernandes MJ, Lázaro C, Ablain M, Pires N (2015) Improved wet path delays for all ESA and reference altimetric missions. Remote Sens Environ 169(2015):50–74. doi:10.1016/j.rse.2015.07.023

Fu L-L, Cazenave A (2001) Satellite altimetry and earth sciences; a handbook of techniques and applications. Academic Press, San Diego. Int Geophys Ser 69

Garcia P, Roca M (2010) ISARD_ESA_L1B_ESL_CCN_PRO_064, issue 1.b, 1 November 2010, "On-board PTR processing analysis: MSL drift differences"

Gaspar P, Ogor F (1994) Estimation and analysis of the sea state bias of the ers-1 altimeter. Rapport technique, Report of task B1-B2 of IFREMER Contract n° 94/2.426016/C. 84

GCOS (2011) Systematic observation requirements for satellite-based data products for climate (2011 update)—supplemental details to the satellite-based component of the "Implementation plan for the global observing system for climate in support of the UNFCCC (2010 update)". GCOS-154 (WMO, December 2011)

Giles KA, Laxon SW, Ridout AL, Wingham DJ, Bacon S (2012) Western Arctic Ocean freshwater storage increased by wind-driven spin-up of the BeaufortÂ Gyre. Nat Geosci 5(3):194–197

Good SA, Martin MJ, Rayner NA (2013) EN4: quality controlled ocean temperature and salinity profiles and monthly objective analyses with uncertainty estimates. J Geophys Res Oceans 118:6704–6716. doi:10.1002/2013JC009067

Haines BJ, Desai SD, Born GH (2010) The harvest experiment: calibration of the climate data record from TOPEX/Poseidon, Jason-1 and the ocean surface topography mission. Mar Geod 33(S1):91–113

Hay CC et al (2015) Probabilistic reanalysis of twentieth-century sea level rise. Nature 517(7535):481

Henry O, Ablain M, Meyssignac B, Cazenave A, Masters D, Nerem S, Garric G (2014) Effect of the processing methodology on satellite altimetry-based global mean sea level rise over the Jason-1 operating period. J Geod 88:351–361. doi:10.1007/s00190-013-0687-3

Jalabert E, Couhert A, Moyard J, Mercier F, Houry S, Rios-Bergantinos S (2015) Jason-2, SARAL and CryoSat-2 status. Ocean surface topography science team meeting, Reston, Virginia, USA, October 2015. http://meetings.aviso.altimetry.fr/fileadmin/user_upload/tx_ausyclsseminar/files/OSTST2015/POD-01-Jalabert.pdf

Jevrejeva S, Moore JC, Grinsted A, Woodworth PL (2008) Recent global sea level acceleration started over 200 years ago? Geophys Res Lett 35:L08715. doi:10.1029/2008GL033611

Jevrejeva S et al (2014) Trends and acceleration in global and regional sea levels since 1807. Glob Planet Change 113:11–22

Kaula W (1970) The terrestrial environment: solid earth and ocean physics. Williamstown report, M.I.T., Cambridge, MA, NASA CR-1579, April 1970. http://ilrs.gsfc.nasa.gov/docs/williamstown_1968.pdf

Labroue S, Boy F, Picot N, Urvoy M, Ablain M (2012) First quality assessment of the CryoSat-2 altimetric system over ocean. Adv Space Res 50(8):1030–1045. doi:10.1016/j.asr.2011.11.018

Le Traon PY, Faugère Y, Hernandez F, Dorandeu J, Mertz F, Ablain M (2003) Can we merge GEOSAT follow-on with TOPEX/Poseidon and ERS-2 for an improved description of the ocean circulation? J Atmos Ocean Technol 20:889–895. doi:10.1175/1520-0426(2003)020<0889:CWMGFW>2.0.CO;2

Legeais J-F, Ablain M, Thao S (2014) Evaluation of wet troposphere path delays from atmospheric reanalyses and radiometers and their impact on the altimeter sea level. Ocean Sci 10:893–905. doi:10.5194/os-10-893-2014

Legeais J-F, Prandi P, Guinehut S (2016) Analyses of altimetry errors using Argo and GRACE data. Ocean Sci 12:647–662. doi:10.5194/os-12-647-2016

Lillibridge J, Smith WHF, David Sandwell D, Scharroo R, Frank G, Lemoine FG, Zelensky NP (2006) 20 years of improvements to GEOSAT altimetry. Symposium: 15 years of progress in radar altimetry, Venice, Italy, March 13–18, 2006. http://earth.esa.int/workshops/venice06/participants/509/paper_509_lillibridge.pdf

Masters D, Nerem RS, Choe C, Leuliette E, Beckley B, White N, Ablain M (2012) Comparison of global mean sea level time series from TOPEX/Poseidon, Jason-1, and Jason-2. Mar Geod 35(1):20–41

Mertz F, Mercier F, Labroue S, Tran N, Dorandeu J (2005) ERS-2 OPR data quality assessment; long-term monitoring—particular investigation. CLS.DOS.NT-06.001. http://www.aviso.altimetry.fr/fileadmin/documents/calval/validation_report/E2/annual_report_e2_2005.pdf. Access 11 May 2016

Mitchum GT (1998) Monitoring the stability of satellite altimeters with tide gauges. J Atmos Ocean Technol 15(3):721–730

Mitchum GT, Nerem RS, Merrifield MA, Gehrels WR (2010) Modern estimates of sea level changes. In: Church J, Woodworth P, Aarup T, Wilson WS (eds) Understanding sea level rise and variability. Wiley-Blackwell, New York, pp 122–142

Nerem RS, Chambers DP, Choe C, Mitchum GT (2010) Estimating mean sea level change from the TOPEX and Jason altimeter missions. Mar Geod 33(1):435–446

Peltier WR (2004) Global glacial isostasy and the surface of the ice-age earth: the ICE-5G (VM2) model and GRACE. Annu Rev Earth Planet Sci 32:111–149

Prandi P, Ablain M, Cazenave A, Picot N (2012) A new estimation of mean sea level in the arctic ocean from satellite altimetry. Mar Geod 35(1):61–81

Pujol M-I, Faugère Y, Taburet G, Dupuy S, Pelloquin C, Ablain M, Picot N (2016) DUACS DT2014: the new multimission altimeter dataset reprocessed over 20 years. Ocean Sci Discuss. doi:10.5194/os-2015-110 **(in review)**

Ray RD (2013) Precise comparisons of bottom-pressure and altimetric ocean tides. J Geophys Res Oceans 118:4570–4584. doi:10.1002/jgrc.20336

Ray C, Martin-Puig C, Clarizia MP, Ruffini G, Dinardo S, Gommenginger C, Benveniste J (2014) SAR altimeter backscattered waveform model. IEEE Trans Geosci Remote Sens 53(2):911–919. doi:10.1109/TGRS.2014.2330423

Roemmich D, Johnson GC, Riser S, Davis R, Gilson J, Owens WB, Garzoli SL, Schmid C, Ignaszewski M (2009) The Argo program: observing the global ocean with profiling floats. Oceanography 22:34–43

Rudenko S, Otten M, Visser P, Scharroo R, Schöne T, Esselborn S (2012) New improved orbit solutions for the ERS-1 and ERS-2 satellites. Adv Space Res 49(8):1229–1244

Rudenko S, Dettmering D, Esselborn S, Schöne T, Förste Ch, Lemoine J-M, Ablain M, Alexandre D, Neumayer K-H (2014) Influence of time variable geopotential models on precise orbits of altimetry satellites, global and regional mean sea level trends. Adv Space Res 54(1):92–118. doi:10.1016/j.asr.2014.03.010

Rudenko R, Neumayer K-H, Dettmering D, Esselborn S, Schöne T (2015) Improvements in precise orbit determination of altimetry satellites. Ocean Surface Topography Science Team meeting, Reston, Virginia, USA, October 2015. http://meetings.aviso.altimetry.fr/fileadmin/user_upload/tx_ausyclsseminar/files/OSTST2015/POD-04-Rudenko_OSTST2015_20151021new.pdf

Santamaría-Gómez A, Gravelle M, Collilieux X, Guichard M, Martín Míguez B, Tiphaneau P, Wöppelmann G (2012) Mitigating the effects of vertical land motion in tide gauge records using a state-of-the-art GPS velocity field. Glob Planet Change 98–99:6–17

Santamaría-Gómez A, Gravelle M, Wöppelmann G (2014) Long-term vertical land motion from double-differenced tide gauge and satellite altimetry data. J Geod 88:207–222. doi:10.1007/s00190-013-0677-5

Thibaut P, Poisson J-C, Roca M, Nilo Garcia P (2012) WP2100 altimeter instrumental processing: RRDP and validation reports, sea level climate change initiative project, phase I. Algorithm selection meeting, Toulouse, 2 May 2012. http://www.esa-sealevel-cci.org/webfm_send/77

Tran N, Labroue S, Philipps S, Bronner E, Picot N (2010) Overview and update of the sea state bias corrections for the Jason-2, Jason-1 and TOPEX missions. Mar Geod 33(S1):348–362. doi:10.1080/01490419.2010.487788

Tran N, Philipps S, Poisson J-C, Urien S, Bronner E, Picot N (2012) Oral: impact of GDR-D standards on SSB corrections. Aviso, OSTST. http://www.aviso.altimetry.fr/fileadmin/documents/OSTST/2012/oral/02_friday_28/01_instr_processing_I/01_IP1_Tran.pdf

Valladeau G, Legeais JF, Ablain M, Guinehut S, Picot N (2012) Comparing altimetry with tide gauges and argo profiling floats for data quality assessment and mean sea level studies. Mar Geod 35(1):42–60

Von Schukmann K, Palmer MD, Trenberth KE, Cazenave A, Chambers D, Champollion N (2016) An imperative to monitor Earth's energy imbalance. Nat Clim Change 6:138–144

Wahr JM (1985) Deformation induced by polar motion. J Geophys Res 90(B11):9363–9368. doi:10.1029/JB090iB11p09363

Watson C, White N, Church J, Burgette R, Tregoning P, Coleman R (2011) Absolute calibration in bass strait, Australia: TOPEX, Jason-1 and OSTM/Jason-2. Mar Geod 34(3–4):242–260

Watson CS, White NJ, Church JA, King MA, Burgette RJ, Legresy B (2015) Unabated global mean sea-level rise over the satellite altimeter era. Nat Clim Change. doi:10.1038/nclimate2635

Wöppelmann G, Marcos M (2016) Vertical land motion as a key to understanding sea level change and variability. Rev Geophys. doi:10.1002/2015RG000502

Woppelmann G, Letetrel C, Santamaria A, Bouin MN, Collilieux X, Altamimi Z, Williams SDP, Miguez BM (2009) Rates of sea-level change over the past century in a geocentric reference frame. Geophys Res Lett. doi:10.1029/2009gl038720

Zawadzki L, Ablain M (2016) Accuracy of the mean sea level continuous record with future altimetric missions: Jason-3 vs. Sentinel-3a. Ocean Sci 12:9–18. doi:10.5194/os-12-9-2016

Chapitre 3

Influence d'ENSO (El Niño et La Niña) sur la variabilité interannuelle du niveau moyen global de la mer

Comme montré dans le chapitre précédent, le niveau moyen global de la mer (GMSL) mesuré par altimétrie présente une tendance estimée à 3.36 ± 0.4 mm/an sur la période 1993-2016. Après retrait de cette tendance linéaire (et du cycle saisonnier) sur la période altimétrique, le GMSL présente des fluctuations interannuelles qui peuvent atteindre quelques millimètres, dont les plus marquées coïncident avec les épisodes ENSO (El Niño-Southern Oscillation) (*Nerem et al.* 2010; *Llovel et al.* 2010, 2011; *Boening et al.* 2012; *Cazenave et al.* 2012a, b, 2014; *Fasullo et al.* 2013, *Dieng et al.* 2014). Cela est illustré sur la Fig.3.1 qui présente les fluctuations de la moyenne des 6 séries temporelles de GMSL (voir *section 2.1, chapitre 2*) après retrait d'une tendance linéaire moyenne sur la période 1993-2015, superposée aux indices ENSO (MEI -Multivariate ENSO Index-, SOI -Southern Oscillation Index- et Nino3.4). Ces variations interannuelles apparaissent étroitement liées aux événements ENSO, avec des anomalies positives (pendant El Niño) et négatives (durant La Niña) du GMSL (par exemple, lors des événements La Niña de 2007-2008 et de 2010-2011). Il est assez frappant de voir que le GMSL présente une anomalie positive assez marquée lors des 2 grands événements El Niño de l'ère altimétrique (1997-1998 et 2015-2016). Ce dernier est considéré comme le plus intense El Niño depuis 1950 par la NOAA (http://www.cpc.noaa.gov/products/analysis_monitoring/ensostuff/ensoyears.shtml).

Dans ce chapitre, après avoir décrit le phénomène ENSO (El Niño et La Niña), l'objectif sera de répondre à la question suivante: quelle est la (ou les) cause(s) de ces anomalies interannuelles

du GMSL et quel est le lien entre le GMSL et les événements ENSO ? Cela a donné lieu à 2 articles (*Cazenave et al.* 2012b; *Dieng et al.* 2014) résumés et insérés dans la *section 3.2*.

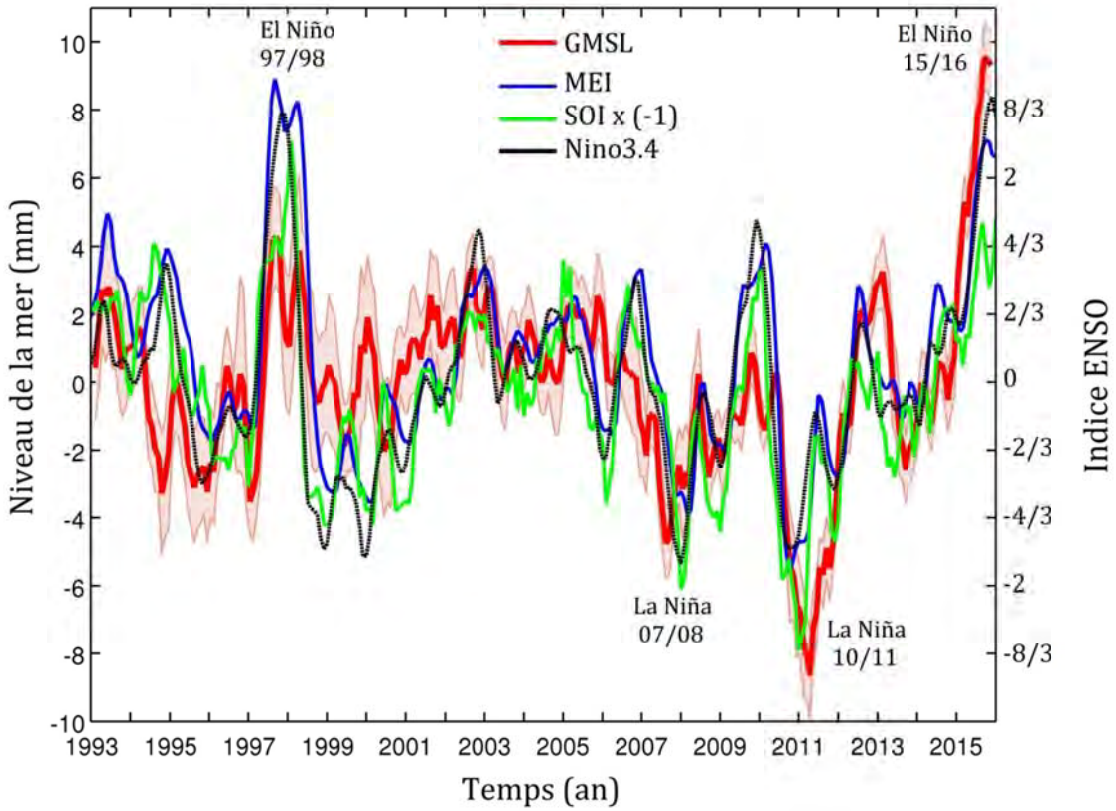

Fig.3.1 : Série temporelle de la moyenne des 6 produits GMSL (voir *section 2.1*) après retrait de la tendance linéaire moyenne sur la période Janvier 1993 - Décembre 2015 (courbe rouge). La surface rouge-grisée représente l'erreur à 2-sigma déduite de la dispersion des données GMSL autour de la moyenne. A ceux-là sont superposés les indices ENSO : MEI (courbe bleue), SOI (multiplié par -1 pour voir la corrélation avec les autres indices; courbe verte) et Nino3.4 (courbe noire) sur la période 1993- 2015.

3.1 Le phénomène ENSO : El Niño & La Niña

L'oscillation australe El Niño (-ENSO- El Niño Southern Oscillation -en anglais-) est un phénomène couplé océan/atmosphère du Pacifique tropical, qui affecte à grande échelle le régime des vents, la température de la mer et les précipitations. Ce phénomène, caractérisé par une anomalie de la température de surface de la mer, présente deux phases opposées : El Niño (chaude) et La Niña (froide). Ces événements (El Niño et La Niña) débutant en général en milieu d'année, apparaissent tous les 2 à 7 ans de manière irrégulière et durent 6 à 18 mois. Les événements ENSO atteignent leur intensité maximale vers Noël.

Dans des ***conditions normales*** (circulation de *Walker)* les alizés de sud-est soufflent vers l'ouest du bassin (de l'Amérique du Sud vers l'Asie), créant des courants marins d'est en ouest le

long de l'équateur dans l'océan Pacifique tropical (*McPhaden,* 1993, 1999). Il en résulte une accumulation des eaux chaudes de surface vers l'ouest du basin. Cela se traduit par une élévation de la surface de la mer de la région tropicale Indonésienne ~0.5 m par rapport aux côtes Est du Pacifique. La température de surface de la mer (SST) est plus chaude au large des côtes d'Asie que dans le Pacifique oriental, en raison d'une remontée des eaux profondes et froides (appelée upwelling) à l'est du Pacifique. Ces eaux froides au large de l'Amérique du Sud sont riches en éléments nutritifs, augmentant la productivité primaire et la diversité des écosystèmes marins. Les précipitations sont localisées à l'Ouest du bassin au dessus de l'eau de surface la plus chaude près de l'Asie, tandis que l'Est du Pacifique est relativement sec.

Pendant ***El Niño***, les alizés s'affaiblissent (voire se renversent selon l'intensité du phénomène) et les masses d'eau chaude de surface s'accumulent au centre et à l'Est du Pacifique tropical. Cela conduit à un enfoncement de la thermocline dans le Pacifique oriental, et une élévation de la thermocline à l'Ouest du bassin (*McPhaden,* 1999). Il en résulte une réduction de l'efficacité de l'upwelling du Pérou-Chili pour refroidir la surface coupée de l'alimentation en eau riche en éléments nutritifs. Les précipitations suivent les eaux chaudes vers l'est du Pacifique, entraînant des inondations au Pérou et la sécheresse en Australie et en Indonésie. Le déplacement de la source de chaleur atmosphérique vers l'est du bassin à des conséquences notables sur les changements globaux de la circulation atmosphérique (*McPhaden,* 2006), ainsi que le cycle de l'eau (*Llovel et al.* 2010, 2011; *Cazenave et al.* 2012a).

Durant ***La Niña***, on assiste à un renforcement des alizés d'Est en comparaison aux conditions normales. Il en résulte une accentuation de l'accumulation des eaux chaudes de surface vers l'ouest du bassin, et une surélévation de la surface de la mer prés des côtes Australiennes et Indonésiennes par rapport à celles du Pacifique Est. La SST est plus chaude au large des côtes d'Asie et plus froide dans l'Est et le centre du Pacifique. Cela implique une montée de l'air entraînant la formation de nuages et de précipitations à l'ouest, et une descente de l'air entraînant des sécheresses à l'Est. Les précipitations sont donc cantonnées à l'ouest du Pacifique équatorial.

Pour caractériser le phénomène ENSO, différents indices sont utilisés. Nous pouvons en citer:

(1) **Nino 3.4** : représente l'anomalie de la température de surface de la mer (SST) (par rapport à la période de référence 1971-2000) dans la région Niño 3.4 (5°S-5°N, 170°W-120°W) du Pacifique équatorial, dans la mesure où cette anomalie est supérieure ou égale à 0.5°C (El Niño), inférieure ou égale à -0.5°C (La Niña) selon une moyenne calculée sur trois mois consécutifs. Pour plus de détails consulter le site (https://www.ncdc.noaa.gov/teleconnections/enso/indicators/sst.php).

(2) **SOI** : basé sur les différences de pression atmosphérique à la surface de la mer observées entre Tahiti et Darwin (en Australie). La phase négative du SOI est caractérisée par la pression d'air inférieure à la normale à Tahiti et au-dessus de la normale à Darwin. Une succession de phases négatives (positives) du SOI coïncident avec l'épisode El Niño (La Niña). Pour plus de détails sur l'indice SOI consulter le site (https://www.ncdc.noaa.gov/teleconnections/enso/indicators/soi/).

(3) **MEI** : caractérisé par les variations des six principales variables observées sur le Pacifique tropical, que sont : la pression de surface de la mer, les composantes du vent de surface (zonale et méridienne), la SST, la température de l'air en surface, et le pourcentage de nébulosité totale du ciel. Le MEI est calculé séparément pour chacune des douze saisons bimensuelles (Dec/Jan, Jan/Fev, ..., Nov/ Dec). Toutes les valeurs saisonnières sont normalisées par rapport à chaque saison et à la période de référence 1950-1993. Les valeurs négatives de l'indice MEI représentent les épisodes La Niña, alors que les valeurs positives représentent les événements El Niño. Pour plus de détails sur l'indice MEI consulter le site (http://www.esrl.noaa.gov/psd/enso/mei/).

Ces 3 indices d'ENSO sont en très bon accord sur la période altimétrique. Cela est illustré sur la Fig.3.1 montrée précédemment.

3.2 L’influence d’El Niño et de La Niña sur le niveau de la mer et la variation de masse du Pacifique tropical Est

Dans le chapitre précédent, nous avons vu que la composante stérique du niveau de la mer et les variations du contenu en eau des océans (causées par les apports d’eau douce issus de la fonte des glaces continentales ou associées à des modifications du stock des eaux continentales) sont les principales causes des variations du GMSL aux échelles de temps interannuelle à multi-décennale. La contribution de chacune des composantes est différente selon qu'il s'agit de la tendance ou de la variabilité interannuelle. Comme le montrent de nombreuses études, l'expansion thermique de l'océan et les glaces continentales (glaciers et calottes polaires) dominent la tendance du GMSL (Church et al. 2013), mais ce n'est pas le cas à l'échelle interannuelle (*Llovel et al.* 2010, 2011; *Cazenave et al.* 2012a; *Boening et al.* 2012). Même si les glaces continentales présentent de petites variations interannuelles, on n’a pas observé de lien net entre leur bilan de masse et ENSO (*Cazenave et al.* 2012a). Il reste donc deux « candidats » pour expliquer les anomalies positives et négatives du niveau moyen global de la mer lors des épisodes El Niño et La Niña : l’expansion thermique de l’océan et la variation du stock d’eau sur les continents.

Résumé des articles : "**L'influence d'El Niño et de La Niña sur le niveau de la mer**" et "**Effect of La Niña on the global mean sea level and north Pacific ocean mass over 2005-2011**" *(les articles originaux sont insérés à la fin de cette section 3.2)*

Durant El Niño de 1997-1998

En se focalisant sur le El Niño de 1997-1998, *Llovel et al.* (2011) ont observé une forte corrélation entre l'anomalie positive du GMSL et le stock total d'eau dans les bassins fluviaux, appelé TLWS (pour -Total Land Water Storage- exprimée en équivalent niveau de la mer: SLE). Nous avons étudié plus en détail cette corrélation entre GMSL et TLWS durant le El Niño de 1997-1998 (*Cazenave et al.* 2012b, inséré à la fin de cette section). Pour cela, nous avons utilisé comme données, le produit niveau de la mer altimétrique AVISO (voir *section 2.1, chapitre 2*), le niveau de la mer thermostérique (intégré jusqu'à 700m de profondeur) d'après la version 6.12 des données de *Ishii and Kimoto*, (2009) (voir *Dieng et al.* 2015a joint à la *section 2.3.1, chapitre 2*), le stock d'eau des continents estimé à partir du modèle hydrologique ISBA-TRIP de Météo-France, et les produits d'ERA-Interim sur les précipitations (P) et l'évaporation (E) dans l'océan. Nous n'avons pas observé d'anomalie significative de l'expansion thermique lors de l'épisode El Niño de 1997-1998. On peut donc écarter l'expansion thermique de l'océan comme cause de l'anomalie positive du niveau de la mer observée à cette date. Nous avons comparé le TLWS (en SLE, c'est à dire en pondérant par le rapport des surfaces entre continents et océans, et en multipliant par -1, pour exprimer le fait qu'un excès d'eau sur les continents correspond à un déficit dans l'océan, et inversement) et la masse de l'océan global (calculée par différence entre le GMSL et l'expansion thermique, après retrait d'une tendance linéaire sur chacune des deux séries temporelles). Cela nous a permis de montrer que, pendant le El Niño de 1997-1998, l'anomalie du GMSL résulte en grande partie d'une augmentation de la masse de l'océan, presque totalement compensée par un déficit du stock d'eau sur les continents (avec une contribution dominante des bassins tropicaux -surtout l'Amazone-). On constate un excès d'eau dans l'océan et un déficit d'eau sur les continents, pendant cet événement. Ceci est lié au fait que lors d'un El Niño, il y a un déficit des précipitations sur les continents et un excès sur les océans tropicaux (principalement l'océan Pacifique, voir *Dai and Wigley*, 2000; *Gu and Adler*, 2011).

Une autre partie de notre étude a porté sur l'emplacement de l'augmentation de la masse de l'océan (uniforme ou localisée ?). Nous avons ainsi analysé les variations spatio-temporelles de la masse de l'océan dans chaque bassin océanique et par bande de latitude de 10°. Nos résultats ont permis de conclure que l'augmentation de la masse de l'océan n'a pas été distribuée de manière uniforme, mais était concentrée sur le nord-est du Pacifique tropical dans une zone délimitée par l'équateur et le parallèle 25°N. Pour expliquer cet excès de masse du Pacifique tropical nord-est

durant El Niño de 1997-1998, plusieurs hypothèses ont été étudiées. Nous avons analysé le bilan d'eau sur la région du Pacifique tropical nord. Pour cela, nous avons calculé la dérivée temporelle de la masse d'eau (dOM/dt), égale à la somme du terme P-E et du terme représentant tous les flux d'eau horizontaux. Ce dernier terme comporte lui-même plusieurs composantes : le ruissellement des fleuves (R ; négligé ici car aucun grand fleuve ne se jette dans l'océan dans la zone considérée) et les transports d'eau horizontaux qui entrent et sortent de la zone (I/O - Inflow/Outflow-). Cela est décrit par l'équation *3.1* ci-dessous.

$$dOM/dt = P - E + I/O \qquad (3.1)$$

Dans un premier temps, nous avons négligé le terme I/O. Nous observons que, si l'on soustrait le terme (P - E) à la dérivée de la masse d'eau du Pacifique tropical Nord, il reste un pic très positif fin 1997 - début 1998. Ce résultat indique que, d'une part, il est nécessaire de faire appel aux transports d'eau horizontaux pour fermer le bilan et que, d'autre part, le flux horizontal net doit être négatif au maximum de l'événement El Niño de 1997-1998 (il sort moins d'eau qu'il n'en rentre dans la zone). Plusieurs études ont montré qu'en période El Niño, le transfert d'eau du Pacifique tropical vers l'océan Indien, via les détroits indonésiens, est réduit d'un facteur 2. Par exemple, *Gordon* (2005) a montré une réduction du débit d'eau entre le Pacifique et l'océan Indien aux détroits indonésiens durant le pic de l'événement El Niño de 1997-1998. Cela conduit à un excès d'eau temporaire du Pacifique. Un bref calcul montre que la réduction du transport d'eau aux détroits indonésiens est du bon ordre de grandeur pour expliquer l'excès de masse (résiduel du bilan de masse) du Pacifique tropical nord. Cependant, on ne peut exclure qu'une diminution des transports méridiens y contribue également, notamment au niveau de l'équateur. Ainsi aucune conclusion définitive n'a été établie et une analyse plus approfondie s'impose donc.

Cette analyse devrait être étendue dans le futur à l'événement El Niño de 2015-2016 lorsqu'on disposera des données. Cependant nous notons une anomalie positive très marquée du niveau de la mer dans le Pacifique tropical Est (10°S-10°N ; 180°E - côtes Américaines) durant le mois de Novembre 2015 (correspondant à El Niño de 2015-2016). Cela est illustré sur la Fig.3.2 ci-dessous qui représente les anomalies du niveau de la mer durant le mois de Novembre 2015 calculées à partir des données altimétriques de Jason-2.

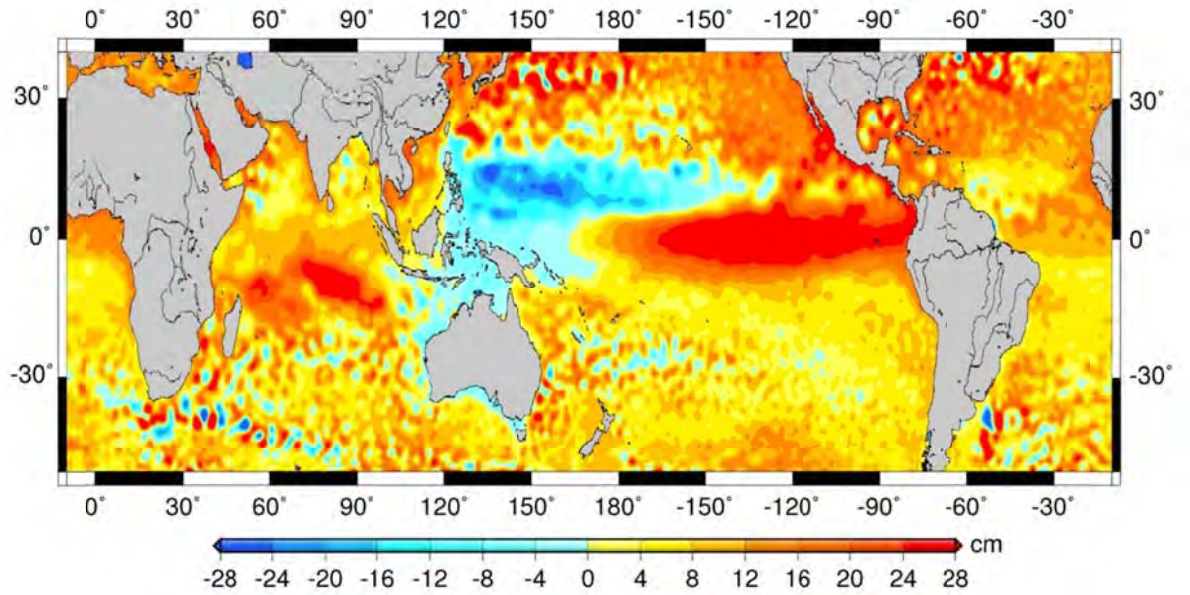

Fig.3.2 : Anomalies du niveau de la mer durant le mois de Novembre 2015 (correspondant à l'événement El Niño de 2015-2016) calculées à partir des données altimétriques de Jason-2.

Durant La Niña de 2010-2011

Dans cette section, nous présentons notre étude (*Dieng et al.* 2014) sur les variations interannuelles du GMSL sur la période 2005-2011, principalement durant l'événement La Niña de 2010-2011. Comme montré précédemment (voir Fig.3.1), la baisse du niveau de la mer durant La Niña de 2010-2011 est la plus marquée de l'ère altimétrique, dépassant de loin le El Niño de 1997-1998 en termes d'amplitude. La même approche, comme pour le El Niño de 1997-1998, a été appliquée, pour comprendre le lien entre l'anomalie du GMSL et le phénomène La Niña de 2010-2011 avec davantage de données (niveau de la mer altimétrique; produit GRACE traité par le GRGS (version RL02); de la vapeur d'eau atmosphérique basée sur les données de la réanalyse d'ERAInterim et des données d'AMSRE (Advanced Microwave Scanning Radiometer-Earth observing system); ainsi que le niveau de la mer thermostérique basé sur les données Argo intégrées jusqu'à 1500m de profondeur). Nous avons tenu compte de la variabilité interannuelle des calottes polaires basée sur GRACE, même si elle est petite et même si on n'a pas observé de lien net entre leur bilan de masse et ENSO (*Cazenave et al.* 2012a). Il faut noter que la tendance linéaire est retirée sur chacune des séries temporelles des produits utilisés. Pour plus de détails sur ces données voir *Dieng et al.* (2014) inséré à la fin de section.

Comme durant El Niño, le régime des précipitations dans les tropiques pendant La Niña est considérablement modifié. Mais, à l'inverse de ce qui se passe pendant El Niño, il pleut plus sur les continents et moins sur l'océan durant La Niña, ce qui se traduit pas un déficit d'eau dans

l'océan. Deux études récentes basées sur les données de gravimétrie spatiale GRACE (*Boeming et al.* 2012; *Fasullo et al.* 2013) ont montré que lors de l'épisode La Niña de 2010-2011, l'excès d'eau sur les continents est dominé par la contribution des bassins hydrologiques australiens, de l'Amazone et de l'Orénoque. Cela est illustré sur la Fig.3.3, représentant les anomalies de hauteur d'eau sur les continents d'après les données GRACE du GRGS, sur une période de 1 an (septembre 2010 – septembre 2011) entourant l'événement La Niña de 2010-2011. Il est assez frappant de voir que le stock d'eau dans la région australienne présente une anomalie positive assez marquée durant cette période. Cela a été aussi montré par *Fasulo et al.* (2013). Nous notons aussi une légère contribution des régions de l'Asie du sud, du sud de l'Amérique du Sud et de l'Afrique de l'ouest et du sud. Nous avons analysé la masse de l'océan par GRACE et le niveau de la mer thermostérique basé sur Argo et les données de *Ishii and Kimoto* V.6.13. Notre étude montre que, contrairement à El Niño de 1997-1998, le déficit de masse de l'océan durant La Niña de 2010-2011 n'explique que partiellement l'anomalie négative du GMSL. Une légère contribution du niveau de la mer thermostérique est observée lors de La Niña 2010-2011. Cela suggère que l'impact de La Niña sur l'océan, sur le niveau de la mer et sur le cycle de l'eau n'est pas l'exact symétrique de celui d'El Niño, comme suggéré par *Okumura and Deser* (2010). La vapeur atmosphérique contribue faiblement (à hauteur de ~0.5 mm) à la baisse du GMSL durant cette période. Nous notons aussi un très bon accord entre le GMSL et les sommes "thermostérique d'Argo + masse de l'océan de GRACE" et "thermostérique d'Argo + vapeur d'eau + calottes polaires", durant La Niña de 2010-2011. Cela signifie la fermeture du bilan du GMSL durant cette période. Cependant la masse de l'océan (inversement le stock d'eau des continents) est la contribution largement dominante de la baisse du GMSL observée durant La Niña de 2010-2011.

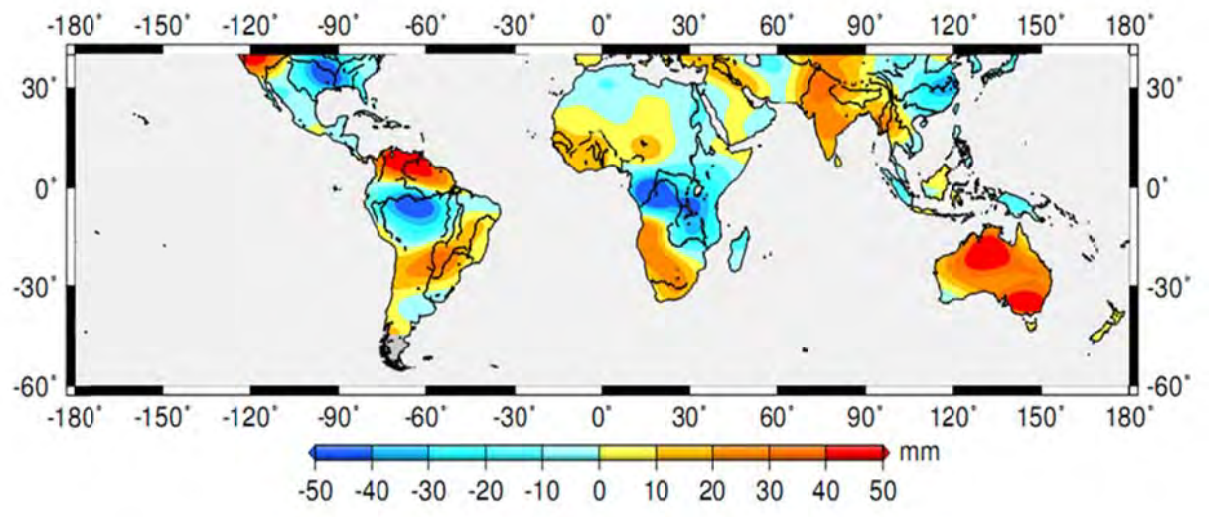

Fig.3.3 : Carte des anomalies de hauteur d'eau (mm) sur les continents mesurées par les satellites de gravimétrie spatiale GRACE (GRGS) sur une période de 1 an (septembre 2010 – septembre 2011) entourant l'événement La Niña de 2010-2011.

Dans cette étude, nous avons aussi étudié la configuration spatiale du GMSL, du niveau de la mer stérique et de la masse de l'océan au cours de La Niña 2010-2011. En effet, nous voulons vérifier si l'anomalie de masse de l'océan, associée à La Niña de 2010-2011 présente une structure spatiale similaire (mais de signe opposé) que celle observée durant El Niño de 1997-1998. Pour cela nous avons analysé plus en détail les variations spatio-temporelles des anomalies de masse de l'océan sur le nord du Pacifique, sur la période 1996-2011. Notre étude montre que, comme pour El Niño de 1997-1998, l'anomalie de masse de l'océan (largement compensée par le stock d'eau total des continents) est localisée dans l'océan Pacifique tropical nord durant La Niña de 2010-2011.

La Niña de 2007-2008 à été aussi analysée dans cette étude. Nous avons vu que l'accord entre le GMSL et la somme des contributions stérique et de masse est moins bonne durant La Niña de 2007-2008, bien que l'utilisation de la somme «stock d'eau des continents + vapeur d'eau + calottes polaires» donne un meilleur résultat que l'utilisation de GRACE. En d'autres termes, l'anomalie négative observée durant La Niña de 2007-2008 n'est ni expliquée par la masse de l'océan, ni par le niveau de la mer stérique. Cela nécessite une enquête plus approfondie afin d'identifier d'autres causes et/où des erreurs potentielles des ensembles de données utilisées.

En conclusion nos résultats montrent le rôle majeur des événements ENSO sur le GMSL, via des modifications importantes du cycle hydrologique global. Plus généralement, ces résultats révèlent que les fluctuations interannuelles du GMSL, associées aux événements El Niño et La Niña, sont essentiellement causées par des changements de la masse de l'océan, localisés au Nord du Pacifique tropical (liés aux fluctuations temporaires des précipitations dans cette zone). La composante stérique de l'océan joue un rôle mineur. Nos résultats ont aussi montré que les plus grandes anomalies du GMSL atteignant les 10mm sont observées sur la dernière décennie, durant les épisodes La Niña de 2010-2011 et El Niño de 2015-2016. Cela montre t-il une intensification des phénomènes ENSO en réponse au changement climatique? Cette question à savoir l'impact du changement climatique sur la périodicité et l'intensité des événements ENSO n'est pas encore résolue.

L'influence d'El Niño et de La Niña sur le niveau de la mer

Anny Cazenave[(1)], **Habib Boubacar Dieng**[(1)], **Simon Munier**[(1)], **Olivier Henry**[(1)], **Benoit Meyssignac**[(1)], **Hindumathi Palanisamy**[(1)] et **William Llovel**[(2)]

(1) Laboratoire d'études en géophysique et océanographie spatiales (LEGOS)
Observatoire Midi-Pyrénées
18 avenue Édouard Belin - 31401 Toulouse Cedex 9, France
(2) Jet Propulsion Laboratory, Pasadena, États-Unis

Résumé

Outre une hausse moyenne de l'ordre de 3 mm par an, le niveau moyen global de la mer présente des fluctuations de quelques millimètres durant les événements El Niño et La Niña. Lors de El Niño, on observe une anomalie positive alors qu'à La Niña correspond une anomalie négative du niveau de la mer. Ces fluctuations du niveau moyen global de la mer sont inversement corrélées aux variations du stock d'eau total sur les continents. Cette observation est en accord avec le fait que, durant El Niño, il pleut davantage sur l'océan que sur les continents, et inversement durant La Niña. Cela suggère que les fluctuations du niveau moyen global de la mer associées aux événements El Niño/La Niña sont plutôt dues à des variations de masse de l'océan qu'à des variations d'origine thermique. Dans cet article, on montre qu'au cours de l'événement El Niño de 1997-1998, l'anomalie positive de masse de l'océan est localisée dans l'océan Pacifique tropical nord. L'excès de masse de cette région compense de manière quasi parfaite le déficit du stock d'eau total des continents à cette période.

L'altimétrie spatiale de haute précision a révélé que le niveau moyen global de la mer a monté assez régulièrement depuis début 1993, à la vitesse moyenne de 3,2 ± 0,4 mm par an (Meyssignac et Cazenave, 2012). Cependant, si l'on y regarde de près, on remarque de petites oscillations interannuelles autour de la tendance linéaire (après retrait du cycle saisonnier), dont l'amplitude est de l'ordre de quelques millimètres. Il est assez frappant que le niveau moyen global de la mer présente une anomalie positive assez marquée lors du grand El Niño de 1997-1998. Cela est illustré sur la figure 1 qui présente les fluctuations du niveau moyen global de la mer entre 1993 et 2011 (après retrait d'une tendance linéaire moyenne sur la période). La figure 1 montre aussi des anomalies négatives du niveau moyen global de la mer lors des événements La Niña de 2007-2008 et de 2010-2011. Quelle est la cause de ces anomalies et quel est le lien entre le niveau moyen de la mer et les événements ENSO (El Niño-Southern Oscillation) ?

Aux échelles de temps interannuelles à multi-décennales, les principaux phénomènes à l'origine des variations du niveau moyen global de la mer sont :
- l'expansion (ou la contraction) thermique des océans, causée par des variations de la température de la mer (lorsque la température augmente, l'eau de mer se dilate et le niveau de la mer s'élève, et inversement) ;
- l'augmentation (ou la diminution) du contenu en eau des

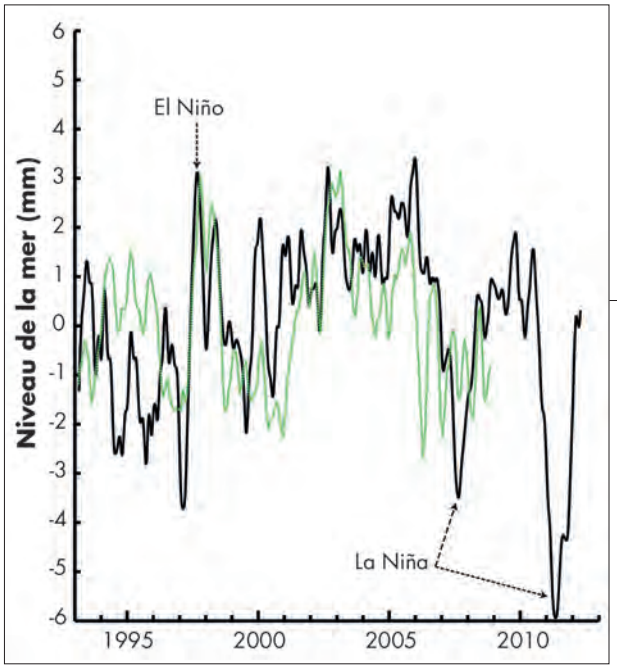

Figure 1 - En noir : niveau moyen global de la mer mesuré par altimétrie spatiale entre janvier 1993 et décembre 2011 (données du site AVISO : www.aviso.oceanobs.com). La tendance linéaire de 3,1 mm/an a été retirée. Les données entre 60° S et 60° N sont considérées.
En vert : stock d'eau continental total, estimé à partir du modèle hydrologique ISBA-TRIP de Météo-France, exprimé en équivalent « niveau de la mer ».

...

Abstract

The influence of El Nino and La Nina on sea level

The detrended global mean sea level displays positive/negative anomalies of a few millimetres amplitude during El Nino/La Nina events that are inversely correlated to total terrestrial water storage variations. This result is in agreement with the observed rainfall deficit/excess over land/oceans during El Nino (and vice versa during La Nina). It suggests that the positive anomaly observed during El Nino in the global mean sea level is likely due to the ocean mass rather than thermal expansion. A detailed analysis over each oceanic region shows that the global mean sea level anomaly observed during the strong 1997-1998 El Nino resulted from an excess of mass of the north tropical Pacific Ocean with almost perfect compensation with the total terrestrial water deficit during this El Nino.

océans, causée par les apports d'eau douce issus de la fonte des glaces continentales ou associés à des modifications du stock des eaux continentales.

Même si les glaces continentales présentent de petites variations interannuelles, on n'a pas observé de lien net entre leur bilan de masse et ENSO, pour le moment. Il reste donc deux « candidats » pour expliquer les anomalies positives et négatives du niveau moyen global de la mer lors des épisodes ENSO : l'expansion thermique de l'océan et la variation du stock d'eau sur les continents.

Expansion thermique et masse de l'océan durant El Niño

Au cours des cinq dernières décennies, des mesures de température de la mer ont été collectées par les bateaux, par les bouées océanographiques et, depuis quelques années, par les flotteurs profilants du projet international Argo. Grâce à ces données, les océanographes peuvent estimer la contribution de l'expansion thermique de l'océan au niveau de la mer en intégrant, jusqu'à 700-1000 m de profondeur, les anomalies de densité de l'eau induites par les variations de température. La figure 2 (courbes du haut) montre l'expansion thermique moyennée sur l'ensemble du domaine océanique, sur la période 1993-2010 (une tendance linéaire moyenne sur la période a été retirée). Le niveau moyen global de la mer (tendance linéaire retirée) y est superposé. On n'observe pas d'anomalie significative de l'expansion thermique lors de l'épisode El Niño de 1997-1998. On peut donc écarter l'expansion thermique de l'océan comme cause de l'anomalie positive du niveau de la mer observée à cette date.

La figure 2 (courbes du bas) présente les variations du niveau moyen global de la mer (tendance linéaire retirée) et de la masse de l'océan global (calculée par différence entre le niveau moyen global de la mer et l'expansion thermique, après retrait d'une tendance linéaire sur chacune des deux séries temporelles). On note une excellente correspondance entre les deux quantités à l'échelle de temps interannuelle, en particulier lors de l'événement El Niño de 1997-1998. Cela suggère que ce sont plutôt les variations de masse de l'océan, et non celles de l'expansion thermique, qui expliquent les fluctuations observées du niveau moyen global de la mer.

Eaux continentales et niveau de la mer durant El Niño

Dans une étude récente (Llovel et al., 2011), une équipe du Laboratoire d'études en géophysique et océanographie spatiales (LEGOS) a observé une forte corrélation quantitative entre la variabilité interannuelle du niveau moyen global de la mer (tendance linéaire retirée) et le stock total d'eau dans les bassins fluviaux, en particulier lors de l'événement El Niño de 1997-1998. Il y a donc

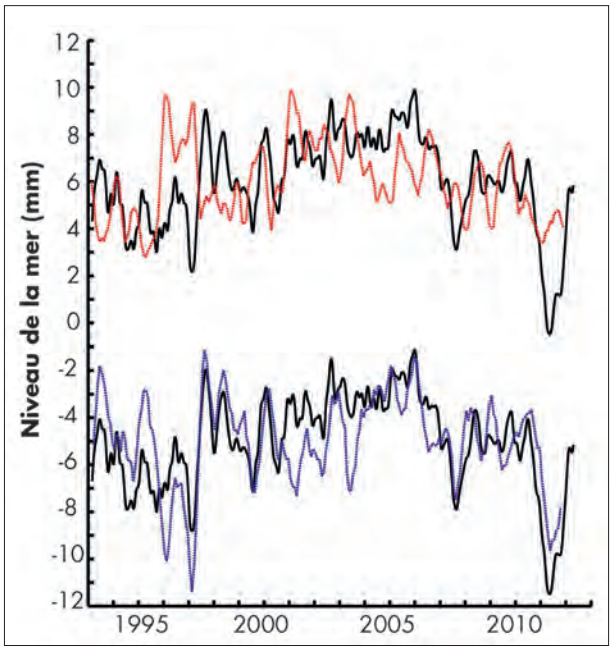

Figure 2 - En haut : en noir, niveau moyen global de la mer mesuré par altimétrie spatiale entre janvier 1993 et décembre 2011, après le retrait de la tendance linéaire (même courbe que sur la figure 1) ; en rouge, expansion thermique moyenne globale, après le retrait de la tendance linéaire (données moyennées entre 60° S et 60° N d'après la version 6.12 des données de Ishii et Kimoto, 2009).
En bas : en noir, niveau moyen global de la mer (même courbe que ci-dessus et sur la figure 1) ; en bleu, composante de masse de l'océan estimée par différence entre niveau moyen global de la mer et expansion thermique (les tendances linéaires ont été retirées).

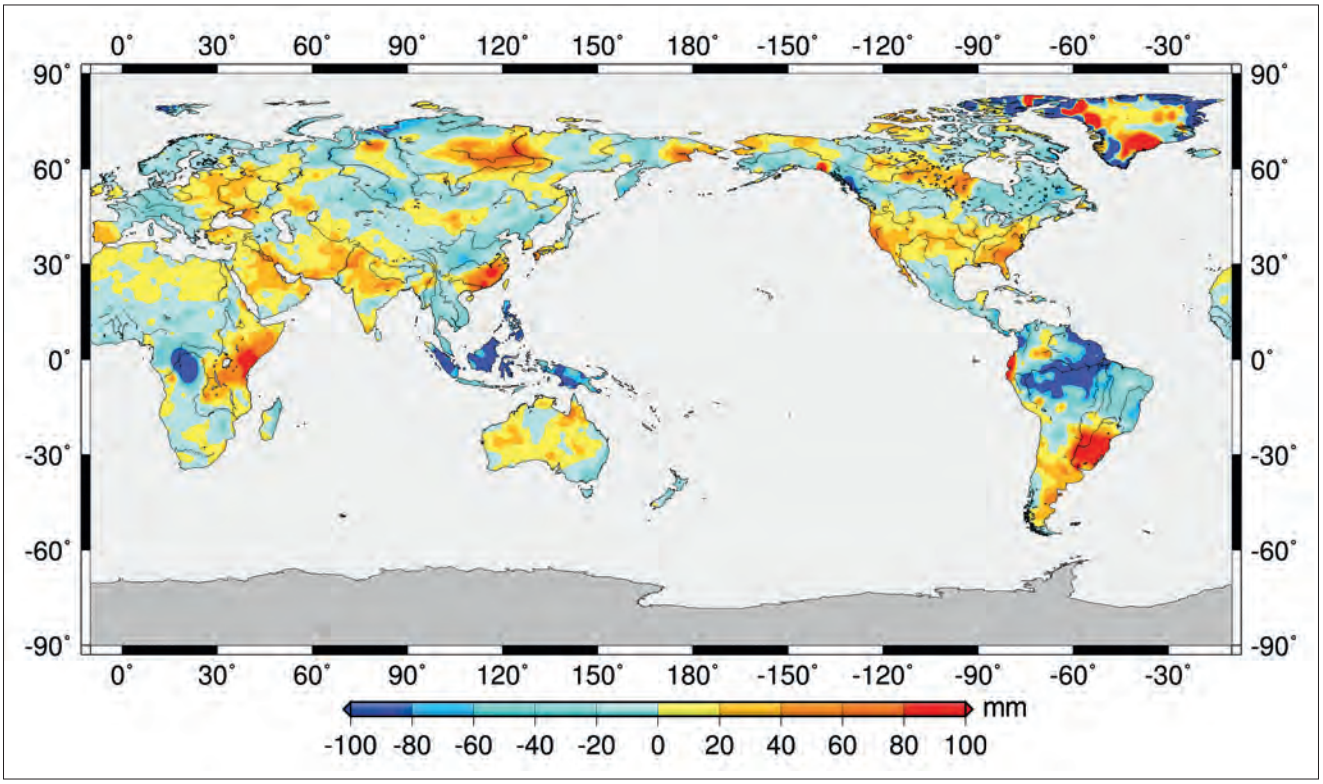

Figure 3 - Carte des anomalies de hauteur d'eau (en mm) sur les terres émergées (d'après le modèle hydrologique ISBA-TRIP de Météo-France). Ces anomalies sont calculées sur une période d'une année (juillet 1997 à juillet 1998) qui coïncide avec l'événement El Niño de 1997-1998.

là une piste pour comprendre le lien entre niveau de la mer et ENSO.

Avec la mission de gravimétrie spatiale *GRACE* lancée en 2002, il est aujourd'hui possible de mesurer, pour la première fois, les variations spatio-temporelles de la gravité de la terre (Cazenave et Chen, 2010). Aux échelles de temps allant de quelques mois à plusieurs années, ces variations temporelles de gravité résultent principalement des variations de la masse de glace des calottes polaires et des glaciers, ainsi que de la masse d'eau sur les continents en réponse à la variabilité climatique ou aux activités humaines (construction de barrages, irrigation, déforestation, urbanisation, etc.). La résolution spatiale de *GRACE* (environ 300 km) permet de cartographier ces différentes sources et les signaux associés, en particulier les variations des stocks d'eau dans les grands bassins fluviaux (Ramillien et al., 2008). Cependant, pour estimer les variations du stock total d'eau sur les continents avant 2002, il faut faire appel à des modèles hydrologiques. C'est ce qu'ont fait Llovel et al. (2011). Ils ont utilisé les sorties du modèle hydrologique global ISBA-TRIP, développé à Météo-France, dans une version utilisant le forçage météorologique de l'université Princeton entre 1950 et 2008, avec un pas de temps d'un mois et une résolution au sol de 1°×1° (voir Alkama et al., 2010). Pour chaque pas de temps, la masse d'eau des différentes couches du sol considérées par le modèle a été moyennée géographiquement sur l'ensemble des terres émergées (à l'exclusion des calottes polaires). Cette masse d'eau a été exprimée en équivalent « niveau de la mer », en pondérant par le rapport des surfaces entre continents et océans, et en multipliant par -1 (pour exprimer le fait qu'un excès d'eau sur les continents correspond à un déficit dans l'océan, et inversement). Sur la figure 1, la série temporelle correspondante est superposée à celle du niveau moyen global de la mer (tendance linéaire retirée). On remarque une correspondance relativement bonne entre les deux quantités lors de l'épisode El Niño de 1997-1998. La corrélation positive entre les deux courbes indique que, pendant cet événement, il y a un excès d'eau dans l'océan et un déficit d'eau sur les continents.

Cela n'est pas vraiment surprenant puisque plusieurs études ont montré que, durant El Niño, il y a davantage de précipitations sur l'océan et moins de pluie sur les continents, en particulier dans les tropiques (Dai et Wigley, 2000 ; Gu et al, 2007 ; Gu et Adler, 2011). L'étude de Llovel et al. (2011) a par ailleurs montré que la contribution dominante au déficit d'eau continental est celle du bassin de l'Amazone, lors de l'événement El Niño de 1997-1998. Cela est illustré par la figure 3 qui montre les anomalies de stock d'eau dans le sol moyennées sur la période juillet 1997-juillet 1998, d'après le modèle ISBA-TRIP de Météo-France (les données sont exprimées en mm d'eau, dans un pixel de 1°×1°). Durant cette période qui correspond au El Niño de 1997-1998, on voit très bien qu'il y a un fort déficit d'eau dans le bassin de l'Amazone.

Augmentation de la masse de l'océan Pacifique tropical nord durant le El Niño de 1997-1998

Ce que traduit la figure 1 est essentiellement la conservation de la masse d'eau dans le système Terre à l'échelle de temps interannuelle (en négligeant le réservoir atmosphérique, ce qui est justifié, en première approximation, compte tenu du court temps de résidence de l'eau dans l'atmosphère). Le déficit d'eau dans les bassins fluviaux lors de l'événement El Niño de 1997-1998 suggère que l'excès d'eau dans l'océan n'est pas causé par le ruissellement des fleuves vers l'océan. Cela est

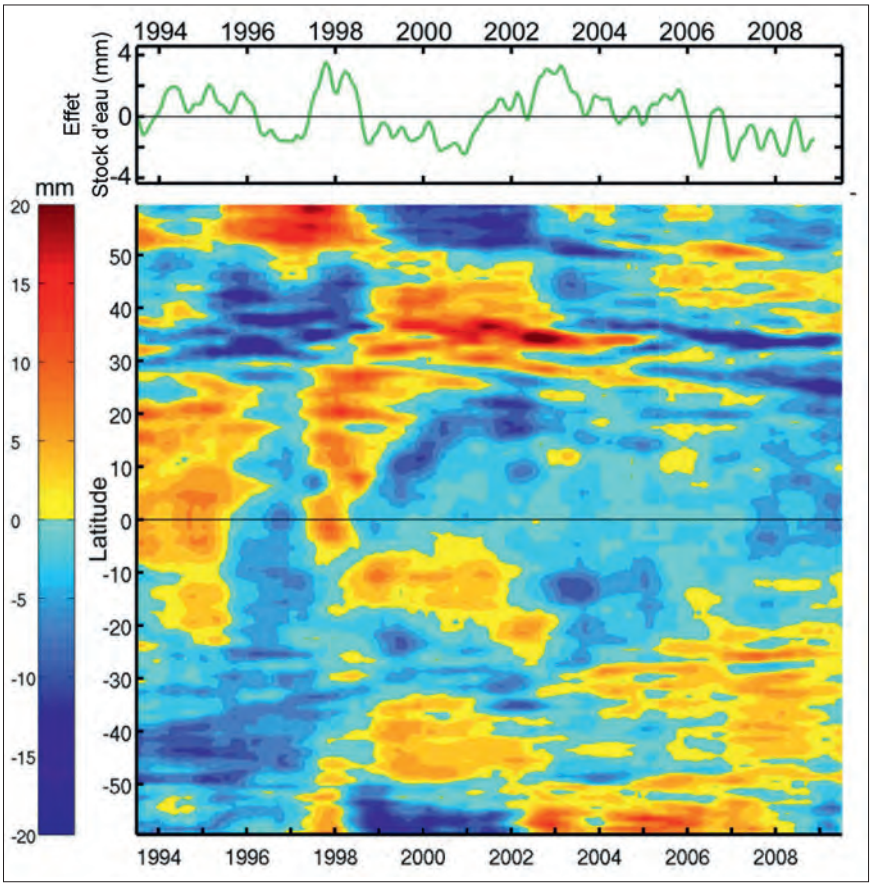

Figure 4 - Diagramme latitude-temps qui représente les variations spatio-temporelles de la masse de l'océan Pacifique moyennée en longitude (entre 120° E et les côtes d'Amérique), en fonction de la latitude et du temps. La courbe du haut (en vert) montre l'évolution, en fonction du temps, du stock d'eau continental exprimé en équivalent « niveau de la mer ».

en accord avec les observations qui indiquent un excès de précipitations sur les océans tropicaux. Mais, l'excès de pluie tombée sur l'océan se répartit uniformément sur le domaine océanique en seulement quelques jours. On pourrait donc s'attendre à ce que l'excès de masse de l'océan qui lui est associé soit uniforme géographiquement. C'est que qu'a cherché à vérifier l'équipe du LEGOS dans une autre étude récemment publiée (Cazenave et al., 2012). L'analyse a consisté à estimer, pour chaque océan, la composante « masse de l'océan » par différence entre le niveau moyen de la mer de cet océan, estimé à partir des données d'altimétrie spatiale, et la composante stérique (après retrait des tendances linéaires). La composante stérique représente la somme de l'expansion thermique et des effets de salinité de l'océan. Cette composante a été calculée en utilisant la base japonaise (mise à jour de Ishii et Kimoto, 2009) de données d'anomalies de température et de salinité de l'océan (alors qu'en moyenne globale, la salinité a une influence négligeable sur le niveau de la mer, ce n'est plus vrai à l'échelle régionale et il faut tenir compte des anomalies de salinité). Pour l'océan Atlantique, l'analyse montre que l'essentiel des variations interannuelles du niveau de la mer est d'origine stérique. La masse de l'océan ne présente aucune anomalie remarquable en 1997-1998. La même observation est faite pour l'océan Indien. En revanche, on voit se dessiner une anomalie positive de la masse de l'océan Pacifique lors de l'événement El Niño de 1997-1998.

Pour cerner plus précisément l'origine géographique de cette anomalie de masse, on a refait la même analyse sur des bandes de latitude de 10° sur tout l'océan Pacifique. On a aussi réalisé un diagramme qui représente les variations spatio-temporelles de la masse de l'océan Pacifique moyennée en longitude (entre 120° E et les côtes d'Amérique) en fonction de la latitude et du temps. Ce diagramme est reproduit sur la figure 4. Il représente également l'évolution, en fonction du temps, du stock d'eau continental exprimé en équivalent « niveau de la mer » (courbe du haut). L'examen de ce diagramme montre bien un excès de masse du Pacifique tropical nord fin 1997-début 1998.

Les deux exercices décrits ci-dessus ont permis de conclure que, durant l'événement El Niño de 1997-1998, l'océan Pacifique présente un excès de masse localisé dans la bande tropicale délimitée par l'équateur et le parallèle 25° N. La figure 5 (courbes du haut) présente le niveau moyen de la mer dans le

▼Figure 5 - En haut : la courbe noire continue représente le niveau moyen de la mer mesuré par altimétrie spatiale sur le Pacifique tropical nord (0-25°N en latitude ; 120° E aux côtes américaines, en longitude) ; la courbe noire en tireté représente la hauteur de la mer stérique moyennée sur la même zone.
En bas : en noir, composante de masse du Pacifique tropical nord (même zone que ci-dessus) ; en vert, stock d'eau continental total, estimé à partir du modèle hydrologique ISBA-TRIP, exprimé en équivalent « niveau de la mer ».

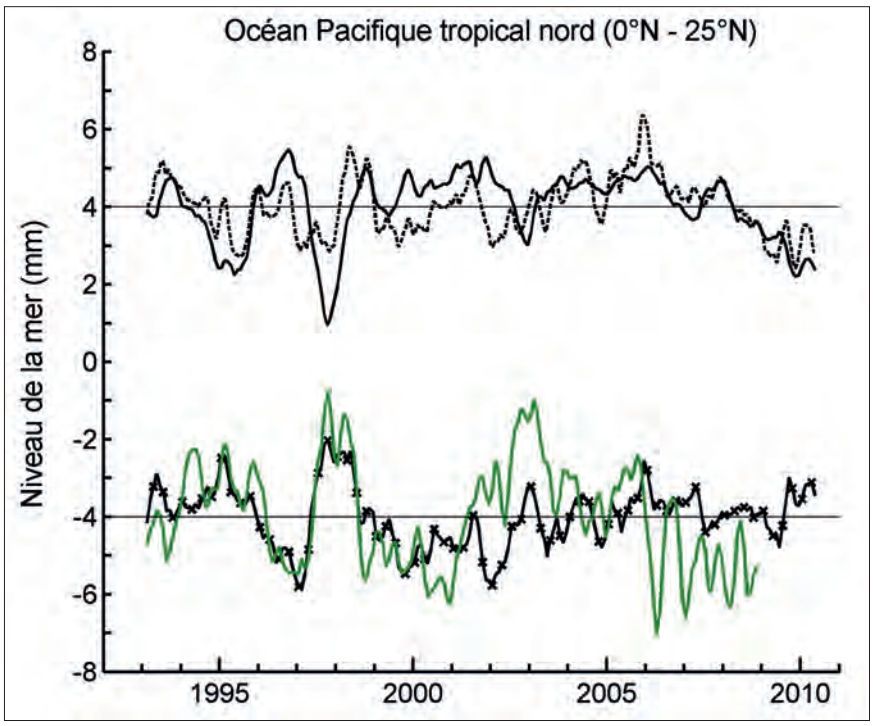

Pacifique tropical nord (0-25° N), superposé à la composante stérique (tendances retirées pour chaque courbe). Les courbes du bas de la figure 5 correspondent à la composante de masse de l'océan Pacifique tropical nord (estimée par la différence entre les deux précédentes quantités) et à la contribution totale des eaux continentales (exprimée en équivalent « niveau de la mer », comme sur la figure 1). On remarque l'excellente correspondance entre la masse du Pacifique tropical nord et la contribution totale des eaux continentales. Cela traduit une compensation quasi parfaite entre l'excès de masse du Pacifique tropical nord et le déficit d'eau sur les continents lors de l'événement El Niño de 1997-1998. Comment expliquer cette observation ?

Bilan d'eau du Pacifique tropical durant El Niño

Une estimation du bilan d'eau sur le Pacifique tropical nord pourrait permettre d'y voir un peu plus clair. Le calcul du bilan d'eau sur la région considérée exprime le fait que la dérivée temporelle de la masse d'eau doit être égale à la somme du terme P-E (précipitation P moins évaporation E) et du terme représentant tous les flux d'eau horizontaux. Ce dernier terme comporte lui-même plusieurs composantes : le ruissellement des fleuves (négligé ici car aucun grand fleuve ne se jette dans l'océan dans la zone considérée) et les transports d'eau horizontaux qui entrent et sortent de la zone. Dans un premier temps, on néglige les transports horizontaux. On observe que, si l'on soustrait le terme (P-E) à la dérivée de la masse d'eau du Pacifique tropical nord, il reste un pic très positif fin 1997-début 1998, comme cela est illustré par la figure 6 (les détails sur les données de précipitation et d'évaporation, utilisées pour ce calcul, se trouvent dans Cazenave et al., 2012). Ce résultat indique que, d'une part, il est nécessaire de faire appel aux transports d'eau horizontaux pour fermer le bilan et que, d'autre part, le flux horizontal net doit être négatif au paroxysme de l'événement El Niño de 1997-1998 (il sort moins d'eau qu'il n'en rentre dans la zone).

Plusieurs études ont montré qu'en période El Niño, le transfert d'eau du Pacifique tropical vers l'océan Indien, via les détroits indonésiens, est réduit

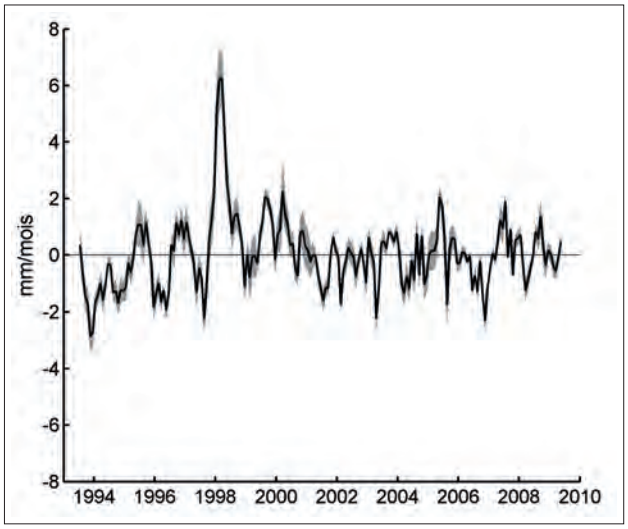

Figure 6 - Différence entre la dérivée de la composante de masse du Pacifique tropical nord et le terme P-E sur la même zone.

d'un facteur 2. Par exemple, Gordon (2005) a montré que, durant le pic de l'événement El Niño de 1997-1998, le transport d'eau au détroit de Makassar (situé entre Bornéo et Sulawasi) est tombé en dessous de 5 Sv, alors que la moyenne est de 8-12 Sv (voir la figure 7 qui montre les échanges d'eau superficiels entre le Pacifique et l'océan Indien, par les détroits indonésiens). L'écoulement de l'eau du Pacifique tropical nord vers l'océan Indien s'est donc ralenti, conduisant à un excès d'eau temporaire dans le Pacifique. Un bref calcul montre que la réduction du transport d'eau aux détroits indonésiens est du bon ordre de grandeur pour expliquer l'excès de masse du Pacifique tropical nord. Cependant, on ne peut exclure qu'une diminution des transports méridiens y contribue également, notamment au niveau de l'équateur. Une analyse plus approfondie s'impose donc.

Figure 7 - Carte représentant les principaux transports océaniques au niveau des détroits indonésiens. (Source : Gordon, 2005.)

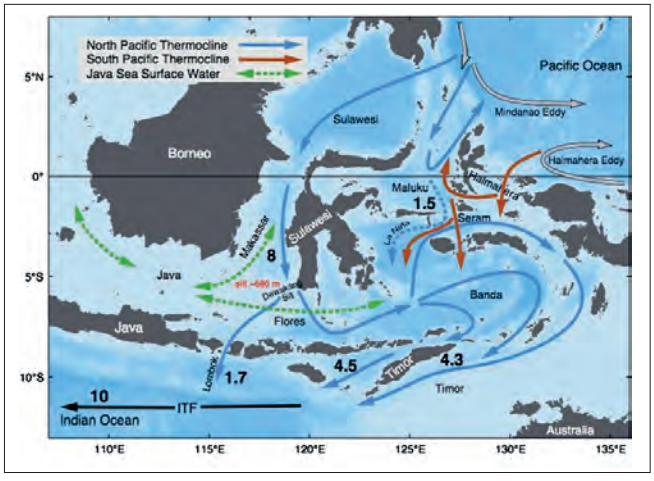

Baisse du niveau de la mer pendant La Niña

Fin 2007-début 2008, ainsi que fin 2010-début 2011, le niveau moyen global de la mer a baissé temporairement de plusieurs millimètres. Ces anomalies négatives coïncident avec deux épisodes La Niña très intenses (voir figure 1). Durant La Niña de 2010-2011, la baisse du niveau de la mer a atteint 5 mm, ce qui représente une perte d'eau (temporaire) de l'océan de 9 000 km^3. Comme durant El Niño, le régime des précipitations dans les tropiques pendant La Niña est considérablement modifié. Mais, à l'inverse de ce qui se passe pendant El Niño, il pleut plus sur les continents et moins sur l'océan durant La Niña, ce qui se traduit pas un déficit d'eau dans l'océan. Dans une étude récente basée sur les données de gravimétrie spatiale *GRACE*, Boeming et al. (2012) ont montré que, lors de l'épisode La Niña de 2010-2011, l'excès d'eau sur les continents est dominé par le bassin de l'Amazone et de l'Orénoque, avec une contribution non négligeable des bassins hydrologiques australiens. Des analyses préliminaires menées au LEGOS semblent indiquer que le déficit d'eau de l'océan se situe principalement dans les océans Pacifique et Indien tropicaux, l'Atlantique ne jouant pratiquement aucun rôle. Mais cela reste à confirmer.

Comme le montre la figure 2 (bas), il faut noter que, durant La Niña de 2010-2011, le déficit de masse de l'océan n'explique que partiellement l'anomalie négative du niveau moyen global de la mer. Il faut donc faire appel à une contribution d'origine thermique lors des phases La Niña. Cela suggère que l'impact de La Niña sur l'océan, sur le niveau de la mer et sur le cycle de

l'eau n'est pas l'exact symétrique de celui d'El Niño, comme suggéré par Okumura et Deser (2010). Des études devront être menées pour clarifier cette question.

Conclusion

Jusqu'à présent, les études sur le niveau de la mer ont principalement concerné les causes de la hausse moyenne globale observée depuis quelques décennies, en lien avec le réchauffement climatique. En revanche, les fluctuations interannuelles ont très peu été analysées. Les résultats récents, mentionnés dans cet article, montrent le rôle majeur des événements ENSO sur le niveau moyen global de la mer, via des modifications importantes du cycle hydrologique global. Plus généralement, ces résultats révèlent que les fluctuations interannuelles du niveau de la mer, associées aux événements El Niño, sont essentiellement causées par des changements de la masse des océans. La composante thermique de l'océan joue un rôle mineur.

Les données globales de niveau de la mer par altimétrie spatiale, ainsi que les données de masse de l'océan par gravimétrie spatiale *GRACE* disponibles depuis 2002, apportent des informations nouvelles et indépendantes des données hydrologiques classiques sur le cycle global de l'eau, en particulier à l'échelle de temps interannuelle.

Bibliographie

Alkama R., B. Decharme, H. Douville, A. Voldoire, S. Tyteca, P. Le Moigne, M. Becker, A. Cazenave et **J. Sheffield**, 2010 : Global evaluation of the ISBA-TRIP continental hydrological system. Part 1: Comparison to GRACE Terrestrial Water Storage estimates and in-situ river discharges. *J. Hydrometeor.*, 11, 583-600, doi:10.1175/2010JHM1211.

Boeming C., J. K. Willis, F. Landerer, S. Nerem et **J. Fasullo**, 2012 : The 2011 La Nina: so strong, the oceans fell. *Geophys. Res. Lett.*, sous presse.

Cazenave A., O. Henry, S. Munier, B. Meyssignac, T. Delcroix, W. Llovel et **H. Palanisamy**, 2012 : ENSO influence on the global mean sea level over 1993-2010. *Marine Geodesy*, doi: 10.1080/01490419.2012.718209, accepté.

Cazenave A. et **J. Chen**, 2010 : Time-variable gravity from space and present-day mass redistribution in the Earth system. *Earth Planet. Sci. Lett.*, 298, 263-274.

Dai A. et **T. M. L. Wigley**, 2000 : Global patterns of ENSO-induced precipitation. *Geophys. Res. Lett.*, 27, 9, 1283-1286.

Gordon A. L., 2005 : Oceanography of the Indonesian seas and their throughflow. *Oceanography*, 18 (4), 14-27.

Gu G. et **R. F. Adler**, 2011 : Precipitation and temperature variations on the interannual time scale: assessing the impact of ENSO and volcanic eruptions. *J. Climate*, 24, 2258-2270.

Gu G., R. F. Adler, G. J.Huffman et **S. Curtis**, 2007 : Tropical rainfall variability on interannual to interdecadal and longer time scales derived from the GPCP monthly products. *J. Climate*, 20, 4033-4046.

Ishii M. et **M. Kimoto**, 2009 : Reevaluation of historical ocean heat content variations with varying XBT and MBT depth bias corrections. *Journal of Oceanography*, 65, 287-299.

Llovel W., M. Becker, A. Cazenave, S. Jevrejeva, R. Alkama, B. Decharme, H. Douville, M. Ablain et **B. Beckley**, 2011 : Terrestrial waters and sea level variations on interannual time scale. *Global and Planetary Change*, 75, 76-82, doi: 10.1016/j.gloplacha.2010.10.008.

Meyssignac B. et **A. Cazenave**, 2012 : Sea level: a review of present-day and recent-past sea level change and variability. *J. Geodyn.*, 58, 96-109.

Okumura Y. et **C. Deser**, 2010 : Asymmetry in the duration of El Nino and La Nina. *J. Climate*, 23, 5826-5843.

Ramillien G., S. Bouhours, A. Lombard, A. Cazenave, F. Flechtner et **R. Schmidt**, 2008 : Land water contributions from GRACE to sea level rise over 2002-2006. *Global and Planetary Change*, 60, 381-392.

Research Article **Open Access**

Habib B. Dieng, Anny Cazenave, Benoit Meyssignac, Olivier Henry, Karina von Schuckmann, Hindumathi Palanisamy, and Jean Michel Lemoine

Effect of La Niña on the global mean sea level and north Pacific ocean mass over 2005-2011

Abstract: Interannual fluctuations of the global mean sea level are highly correlated with El Niño-Southern Oscillation (ENSO) events, with positive/negative anomalies during El Niño/La Niña. In a previous study we showed that during the 1997 – 1998 El Niño, a positive anomaly observed in the global mean sea level was mostly caused by an increase of the ocean mass component rather than by steric (thermal) effects. This result was related to an increase of precipitation over the tropical ocean and a deficit in land water storage. In the present study, we investigate the effect of the recent 2008 and 2011 La Niña events on the satellite altimetry-based global mean sea level. We find that the large global mean sea level drop associated with the 2011 La Niña results from the combined decrease of the steric and ocean mass components, with a slightly dominant contribution from the latter. We show that the ocean mass contribution to the global mean sea level drop is spatially confined over the north eastern tropical Pacific (just as was found previously for the 1997 – 1998 El Niño, but with opposite sign). Corresponding ocean mass spatial pattern is closely correlated to observed sea level and steric spatial patterns over the duration of the La Niña event. This is also observed for previous El Niño and La Niña events. Such a drop in ocean mass during ENSO in the eastern part of the tropical Pacific has not been reported before. It is possibly related to a temporary decrease in the net precipitation over the north eastern Pacific (opposite situation was found during the 1997 – 1998 El Niño).

Habib B. Dieng: LEGOS, OMP, 18 avenue Edouard Belin, 31401 Toulouse Cedex 9
Anny Cazenave: LEGOS, OMP, 18 avenue Edouard Belin, 31401 Toulouse Cedex 9, E-mail: anny.cazenave@legos.obs-mip.fr
Benoit Meyssignac, Olivier Henry: LEGOS, OMP, 18 avenue Edouard Belin, 31401 Toulouse Cedex 9
Karina von Schuckmann: University of Toulon
Hindumathi Palanisamy: LEGOS, OMP, 18 avenue Edouard Belin, 31401 Toulouse Cedex 9
Jean Michel Lemoine: GRGS

1 Introduction

On interannual to decadal time scales, global mean sea level (GMSL) variations mostly result from thermal expansion and mass variations of the oceans. The ocean mass variations themselves result from land ice mass changes (from glaciers and ice sheets), land water storage changes plus a small contribution from atmospheric water vapor. Over the satellite altimetry era (1993-2012), GMSL rise (amounting to 3.1 +/- 0.4 mm/yr) is due to the ocean thermal expansion (by ~30%) and land ice loss (~55%) contributions (e.g., Church et al., 2011, Hansen et al., 2011, Meyssignac and Cazenave, 2012, Hannna et al., 2013, Church et al., 2013). While thermal expansion and land ice dominate the GMSL trend, this is not the case at interannual time scale, as shown by a few recent studies (Llovel et al., 2010, 2011, Cazenave et al., 2012, Boening et al., 2012). These interannual variations appear closely related to ENSO (El Niño-Southern Oscillation) events, with positive/negative sea level anomalies observed during El Niño/La Niña (Nerem et al., 2010). Focusing on the 1997 – 1998 El Niño, Llovel et al. (2010, 2011) showed that GMSL anomalies are inversely related to interannual variations in global land water storage, with a tendency for water deficit on land during El Niño events. This was investigated in more details by Cazenave et al. (2012) who showed that during the 1997 – 1998 El Niño, the GMSL anomaly was largely due to an increase in ocean mass almost fully compensated by water storage deficit on land (with a dominant contribution from tropical river basins –mostly the Amazon-). This is related to the fact that during an El Niño, there is rainfall deficit on land and rainfall excess over tropical oceans (mostly the Pacific Ocean, e.g., Dai and Wigley, 2000, Gu and Adler, 2011). Another result from the Cazenave et al. (2012)' study concerned the location of the ocean mass increase. Counter intuitively, the ocean mass increase was not uniformly distributed over the oceans but concentrated over the northeast tropical Pacific. To explain this ocean mass excess during the 1997 – 1998 El Niño, several hypotheses were investigated (for example, a possible reduced water flow between the Pacific and In-

dian oceans at the Indonesian straits, Gordon et al., 2010) but no definite conclusion has been drawn.

In the present study, we study the interannual variations of the GMSL over 2005-2011, a period with prevailing La Niña events. Over this time span, the interannual GMSL displays negative anomalies of several mm amplitude, coinciding with the 2008 and 2011 La Niña events. As shown by Boening et al. (2012), the GMSL drop during the 2011 La Niña in part results from a temporary decrease in ocean mass (and associated increase in land water storage, Fasullo et al., 2013), as estimated from GRACE space gravimetry data. Here we also compare the interannual GMSL with the sum of the contributions (i.e., the steric and mass components, estimated using different data sets) and explore whether, as for the 1997 – 1998 El Niño, the La Niña-related ocean mass decrease has a particular spatial pattern or not.

2 Method

Interannual variations in GMSL are computed in two ways:

1. Directly from satellite altimetry data after removing, over the study period, the longer-term signal in the GMSL time series,
2. By estimating separately the steric (i.e., due to ocean temperature and salinity) and ocean mass (ΔM_{ocean}) contributions.

The ΔM_{ocean} component can itself be estimated in two ways:

1. By averaging the GRACE space gravimetry data over the oceans to recover the ocean mass variations,
2. By summing up the land water, atmospheric water vapor and land ice components.

In effect, conservation of total water mass in the climate system at interannual time scale leads to:

$$\Delta M_{ocean} = -\Delta M_{LW} - \Delta M_{WV} - \Delta M_{LI} \quad (1)$$

where ΔM_{ocean}, ΔM_{LW} and ΔM_{WV} represent interannual changes of the ocean mass, total land water storage and atmospheric water vapor, respectively. ΔM_{LI} refers to interannual fluctuations in land ice mass.

For regional comparisons with the 1997 – 1998 El Niño (i.e., prior to the GRACE era), we also estimate the ocean mass component by computing the difference between the altimetry-based sea level and steric sea level.

All components are expressed in equivalent sea level (ESL) (see below).

3 Data

3.1 Sea level data

For the altimetry-based sea level data, we use two different products : (1) the GMSL time series from AVISO (Archiving, Validation and Interpretation of Satellite Oceanographic Data,www.aviso.oceanobs.com/en/data/products/sea-surface-height-products/global/msla/, AVISO hereafter) and (2) the Colorado University GMSL (http://sealevel.colorado.edu/, CU hereinafter). Both data sets are based on Topex/Poseidon, Jason-1 and Jason-2 data.

The two GMSL time series (AVISO and Colorado University) are based on different processing approaches, in particular the geographical averaging process. Moreover some of the geophysical corrections applied to the data are slightly different as well as the editing procedure (see Masters et al., 2012 and Henry et al., 2014, for a discussion on these differences). The two GMSL time series cover the period 1993-2013. But for the purpose of the present study that focuses on GRACE and Argo periods, we limit the study time span to January 2005 to December 2011. In the following, we average the two data sets to produce a single GMSL time series, as no preferred product has been identified so far. The corresponding curve and associated uncertainty (based on the dispersion around the mean) is shown in Fig. 1 for the 2005-2011 time span. For the regional analysis presented in section 6, we also use the gridded AVISO data over 1993-2012 (www.aviso.oceanobs.com). The gridded data are based on a larger set of altimetry missions merged together: in addition to the Topex/Poseidon and Jason-1&2- data, ERS-1&2, Envisat and Geosat follow-on data are also used. The gridded data are provided on a 1/4 degree grid at weekly interval.

Both, global mean and gridded sea level data are corrected for the inverted barometer correction. For detailed description of the geophysical corrections, the reader is referred to the AVISO and Colorado University web sites.

3.2 Steric data

Two steric data sets have been considered:

1. Argo data processed as explained in von Schuckmann and Le Traon (2011). The global mean steric time series (data averaged over the 60°N/60°S domain) is based on a weighted box averaging scheme of Argo data. A reference depth of 1500 m is chosen as the number of profiles in the 1500 m-2000 m depth layer is significantly less than within 0-1500 m before year

2009 (Cabanes et al., 2013, their Figure 7). The Argo profiles undergo re-qualified data validation methods using a tool developed by Gaillard et al. (2009) (see also von Schuckmann et al., 2009). Black-listed profiles and platforms are excluded from the data set. Every profile on alert has been checked visually which allows excluding spurious data (e.g. data drift). This procedure minimizes systematic biases in the global Argo data set as discussed by Barker et al. (2011). Error bars represent one standard error, accounting for reduced degrees of freedom in the mapping and uncertainty in the reference climatology as described in von Schuckmann and Le Traon (2011). The Argo based steric sea level time series covers the period 2005-2011. In the following, we consider both the thermosteric and halosteric components.

2. For comparisons between the recent La Niña events and former El Niño events (in particular the 1997 – 1998 El Niño), we also consider the recent update (V6.12) of the Ishii and Kimoto (2009) ocean temperature data (covering the 0-700 m depth range). These data are vertically integrated to estimate the thermosteric sea level from 1993 onwards at monthly interval. This thermosteric product is called IK12.

3.3 GRACE-based space gravimetry data

To estimate the ocean mass variation, we use the GRACE Release 2 products from the Groupe de Recherche en Geodesie Spatiale (GRGS) (http://www.grgs.obs-mip.fr/grace/variable-models-grace-lageos/grace-solutions-release-02). The degree 2 coefficients –poorly determined by GRACE- are those derived from satellite laser ranging to Lageos 1 and 2. These data are provided at 10-day interval on 1°x1° grids. However the real spatial resolution of this data set is coarser, on the order of 400 km (see below). No Gaussian filtering nor destripping are applied to the GRGS data. Such post-processing is developed by other groups for removing the various errors affecting the GRACE data, in particular the north-south noise (stripes) due to systematic correlated errors of GRACE data within a particular spectral order or the leakage of nearby signals onto the study area due to the coarse GRACE resolution (see Velicogna and Wahr, 2013 for a discussion on errors impacting the GRACE data). Such post processing procedure is usually applied to the GRACE products available from the TELLUS website (http://grace.jpl.nasa.gov) that provides gridded ocean data after strong smoothing (due to the application of a destripping filter, a 500 km half-width Gaussian filter and a spherical harmonic cutoff at degree 40). As indicated on this web site, such a data set should not be used for global ocean mass studies due to strong attenuation of the signal (see also Chambers and Schröter, 2011).

A gain factor is sometimes applied to the data in order to compensate for signal attenuation due to the coarse GRACE resolution (the truncation of the GRACE spherical harmonics series at a given degree implies that short-wavelength signal associated with the missing spherical harmonic coefficients, cannot be recovered). In the case of the GRGS data, this truncation is at degree 50, which corresponds to a spatial resolution of 400 km. No gain factor is applied. When computing the ocean mass, we use a mask that ignores data within 400 km of the continents to avoid leakage from continental hydrology and ice sheet mass loss. Finally, as we only consider the interannual variability, we do not correct the GRACE data for Glacial Isostatic Adjustment (i.e., the visco-elastic response of the solid Earth to last deglaciation) because this effect is a purely linear trend.

3.4 Atmospheric water vapor

To estimate change in atmospheric water vapor mass, we used three different products : (1) atmospheric surface pressure grids from the European Centre for Medium-Range Forecast (ECMWF) ERA-Interim data (//data-portal.ecmwf.int/data/d/interim_moda/), (2) the vertically integrated water vapor grids, also from ERA Interim, and (3) vertically integrated water vapor based on AMSRE remote sensing data (kindly provided to us by R. Allan). As shown by Trenberth and Smith (2005), seasonal and interannual variations in atmospheric surface pressure essentially result from changes in atmospheric water vapor content because of dry air mass conservation. Thus atmospheric surface pressure data can be used to estimate change in water mass of the atmosphere. Data from ERA Interim are provided as 1.5°x1.5° grids, at monthly interval. Data from (3) are given as globally averaged water vapor time series at monthly interval.

The atmospheric water vapor contribution is further expressed in ESL by weighting by the ratio of the total Earth's area to the ocean area and multiplied by -1 (to express the fact that more water in the atmosphere leads to lower sea level, and inversely).

3.5 Land water component

To estimate the global land water storage, we use the ISBA-TRIP global hydrological model developed at MétéoFrance. The ISBA (Interaction Soil Biosphere Atmosphere) land surface scheme calculates time variations of surface energy and water budgets. Soil hydrology is represented by three layers: a thin surface layer (1 cm) included in the rooting layer and a third layer to distinguish between the rooting depth and the total soil depth. The soil water content varies with surface infiltration, soil evaporation, plant transpiration and deep drainage. ISBA uses a comprehensive parameterization of sub-grid hydrology to account for heterogeneity of precipitation, topography and vegetation within each grid cell. It is coupled with the TRIP (Total Runoff Integrating Pathways) module (Oki and Sud, 1998). TRIP is a simple river routing model converting daily runoff simulated by ISBA into river discharge on a global river channel network here defined at 1°x 1° resolution. Details on ISBA-TRIP model can be found in Alkama et al. (2010) and Decharme et al. (2010). The outputs of the ISBA-TRIP model cover the period January 1980 to December 2012, with values given at monthly interval on a 0.5°x0.5° grid. They are based on a run in forced mode (global meteorological forcing based on ERA-Interim at 3-hourly time step and 0.25° resolution). The whole land surface has been considered. The land water storage component is further expressed in ESL (after weighting by the land to ocean areas ratio). In the following the land water term refers to the use of the ISBA-TRIP hydrological model.

4 Comparison between the different products

Data between 66°N and 66°S are considered for all products except the Argo-based steric sea level (60°N to 60°S). All time series are re sampled at monthly interval. The seasonal cycle is removed by least-square fitting of a sine function to the data. As we focus here on the interannual variability, we applied a high-pass filter (<7 years) to all data sets over the 2005-2011 time span. Just removing a linear trend over the study time span gives essentially the same result. Finally a 3-month running filter is applied to each time series.

4.1 Differences between the water vapor time series

Fig. 2a shows the water vapor contributions to sea level for the three products as discussed in section 3.4. The integrated water vapor from ERA Interim and AMSRE agree well while the ERA Interim surface pressure curve departs much from the previous two. Differences of 0.5-1 mm ESL are noticed at some periods, in particular in 2007 and 2009/2010.

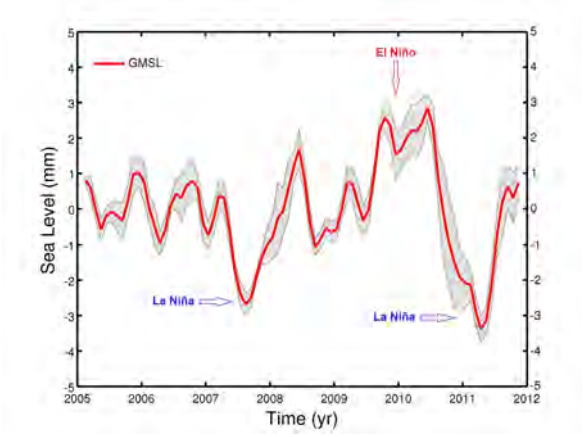

Fig. 1. Interannual GMSL over 2005-2011 based on the mean of the AVISO and Colorado University time series. The gray zone around the red curve represents the uncertainty based on the dispersion of each time series around the mean.

We do not know the source of such differences but it is suspected that the surface pressure curve is less reliable (R. Allan, personal communication). Moreover, global mean water vapor is highly correlated with global mean sea surface temperature (SST). We found a much better correlation between SST and the vertically integrated water vapor than when using the surface pressure data. This is illustrated in Fig. 2b. For that reason, in the following, we use the vertically integrated water vapor time series (from ERA interim).

4.2 Comparison between interannual GMSL and GRACE-based ocean mass & sum of other mass components

In this section we compare the interannual GMSL with the interannual ocean mass component estimated from the GRACE GRGS data as well as with the sum of other mass components (as described by eq. 1): land waters plus water vapor plus land ice. We neglect the interannual variability

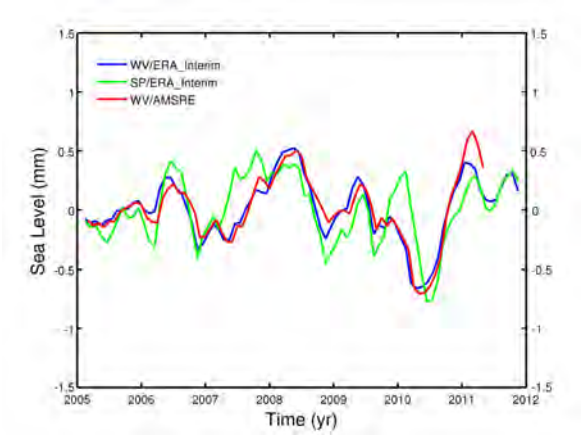

(a)

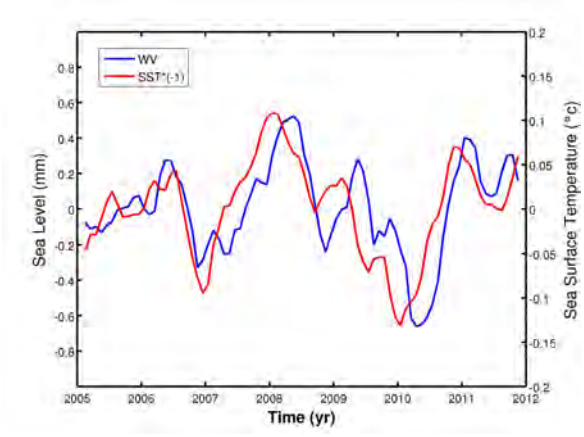

(b)

Fig. 2. a) Interannual global mean water vapor component (expressed in equivalent sea level) from ERA Interim surface pressure (green curve), integrated water vapor from ERA Interim (blue curve) and from AMSRE (red curve); b) Interannual global mean water vapor contribution from ERA Interim (expressed in equivalent sea level, blue curve) and global mean SST (multiplied by -1) (red curve).

of the glaciers as no data are available to estimate it, but account for that of the ice sheets. The latter has been estimated from the GRGS GRACE data averaged over Greenland and Antarctica. It is generally very small, of at most 0.3 – 0.4 mm ESL on interannual time scale (see below).

Fig. 3a compares the interannual GMSL with the GRACE-based ocean mass and the sum of 'land water storage + water vapor + interannual ice sheet component'. Error bars are not shown on this plot. The GRACE GRGS data are not provided with error bars. However from discussions with the GRGS processing group, it comes out that the uncertainty of a single global mean monthly value is on the order of 0.6 mm (1-sigma) (see also Wahr *et. al.*, 2006). Uncertainty of the sum 'land water storage + water vapor + interannual ice sheet component' is also not known. We assume that it is of the same order of magnitude as for the GRACE-based ocean mass. Fig. 3a indicates that the mass component (either from GRACE or from the sum 'land water storage + water vapor + interannual ice sheet component') has a significant contribution to the interannual GMSL, especially during the 2011 La Niña. But clearly not all interannual GMSL signal is of mass origin. In Fig. 3b, we have superimposed the Argo-based steric sea level to the interannual GMSL. The steric signal obviously plays some role at interannual time scale. On Fig. 3b, is also shown the interannual variability of the ice sheets. As mentioned above, this contribution is small, of the same order of magnitude as the water vapor component.

5 Sea level budget at interannual time scale

Fig. 4a,b show the interannual GMSL together with the sum of the steric and mass components (GRACE-based ocean mass for Fig. 4a and sum 'land water storage + water vapor + interannual ice sheet component' for Fig. 4b). From these figures, we clearly see that the negative sea level anomalies coinciding with the 2011 La Niña is almost equally due to a decrease of the ocean mass and steric components. The agreement between the GMSL and the sum of components is less good during the 2008 La Niña, although the use of the sum 'land water storage + water vapor + interannual ice sheet component' (Fig. 4b) gives better result than the use of GRACE (Fig. 4a).

Overall, over the 2005 – 2011 time span, the correlation between interannual GMSL and sum of the contributions amounts to 0.78 in both cases (Fig. 4a and Fig. 4b). We conclude, as previously shown by Boening et al. (2012), that the GMSL drop during the 2011 La Niña event is reasonably well reproduced by the sum of the steric and ocean mass contributions. As indicated above, lesser agreement is noticed for the 2008 La Niña. This calls for further investigation to identify which data set is in error.

6 Spatial patterns of sea level and ocean mass during 2011 La Niña

In this section, we investigate the geographical patterns of the GMSL, steric sea level and ocean mass component during the 2011 La Niña. In particular, we would like to check whether the ocean mass component associated with the 2011 La Niña presents a spatial pattern similar (but with

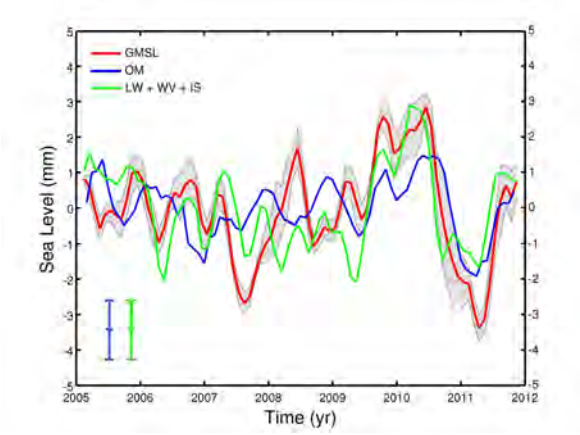

(a)

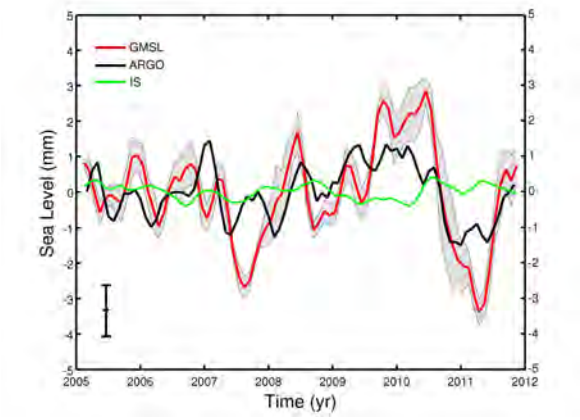

(b)

Fig. 3. a) Interannual GMSL (red curve) on which are superimposed the global mean ocean mass from GRACE (blue curve) and the sum 'land water storage + water vapor + interannual ice sheet, IS, component' (green curve). Vertical bars represent errors on monthly values of GRACE-based ocean mass and sum of mass components; b) Interannual GMSL (red curve) on which are superimposed the steric contribution from Argo (black curve). The interannual ice sheet component is also shown (green curve). The vertical bar represents the error on monthly values of the Argo-based steric sea level.

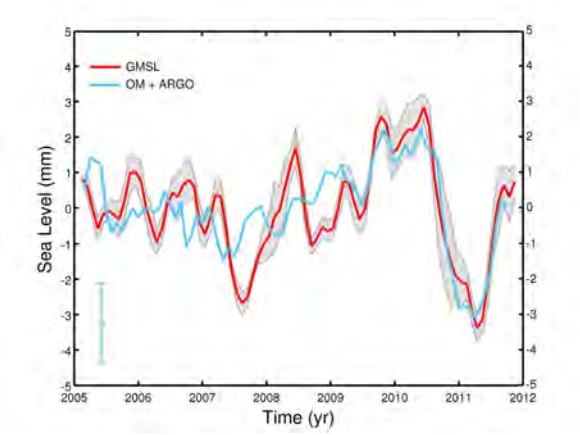

(a)

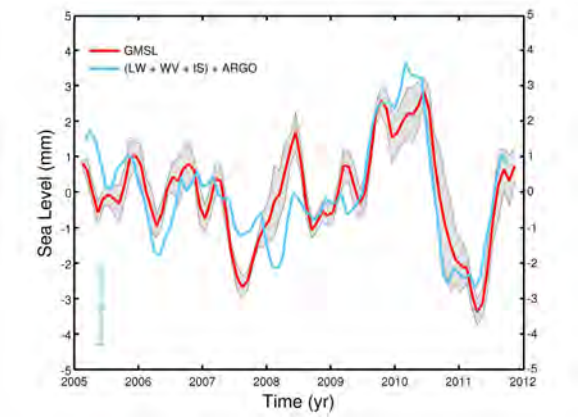

(b)

Fig. 4. a) Interannual GMSL (red curve) on which is superimposed the sum of the mass (from GRACE) and steric contribution from Argo (light blue curve). The vertical bar represents the error on monthly values of the sum of mass and steric contributions; Interannual GMSL (red curve) on which is superimposed the sum of the mass (sum 'land water storage + water vapor + interannual ice sheet component') and steric contribution from Argo. The vertical bar represents the error on monthly values of the sum of mass and steric contributions.

opposite sign) than that observed during the 1997 – 1998 El Niño (Cazenave et al., 2012). As done in Cazenave et al (2012) for El Niño, we first determine the geographical origin of the 2011 ocean mass drop. As for the 1997 – 1998 El Niño, we find that the main contribution comes from the northern tropical Pacific. This is illustrated in Fig. 5 showing the global mean ocean mass from GRACE and north Pacific ocean mass (also estimated from GRACE). The north Pacific area considered here is from 120°E to the coast of America and from the equator to 60°N. While the two curves do not exactly coincide, we find nevertheless good agreement, suggesting that as for El Niño, the La Niña ocean mass anomaly originates in the north Pacific. To investigate in more detail the spatio-temporal variation of the negative ocean mass anomaly during the 2011 La Niña, we constructed a longitude-time diagram of the ocean mass averaging the data in latitude over the north Pacific (same area as indicated above). The diagram is shown in Fig. 6 for the 1996 – 2012 time span (we extended back in time the analysis in order to include the effect of the 1997 – 1998 El Niño). To do this, we computed the ocean mass from the difference between the mean sea level data and IK12 steric data. In effect, for this longer period, neither Argo nor GRACE data can be used (note that

IK12 data cover the 0-700 m depth range only, instead of 0 – 1500 m for Argo). Fig. 6 shows a succession of positive and negative nearly zonal anomalies in the eastern part of the Pacific (west of 180°E). In particular, a strong negative anomaly, amounting –20 to –30 mm and extending east-west, is noticed in 2011. In Fig. 6, we also see the strong positive ocean mass anomaly associated with the 1997 – 1998 El Niño (previously discussed in Cazenave et al., 2012), with the same east-west zonal pattern as the 2011 La Niña anomaly. The results of the present study suggest similar response of the ocean mass during La Niña (but with opposite sign compared to El Niño), likely related to precipitation minus evaporation patterns over the north eastern Pacific characterizing ENSO events (Dai and Wigley, 2000, Gu and Adler, 2011).

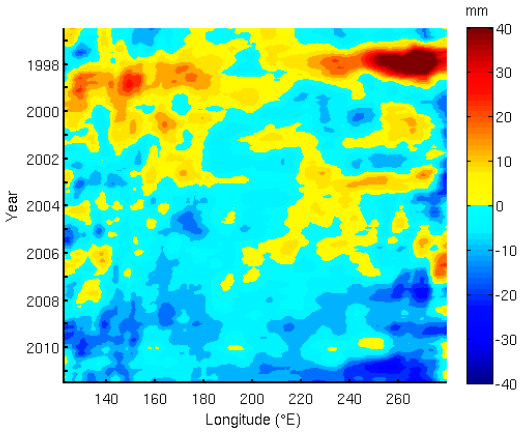

Fig. 6. Longitude/time diagram of the north Pacific (0-60°N) ocean mass from 1996 to 2011 based on the difference between altimetry-based sea level data and IK12 steric data. Units: mm.

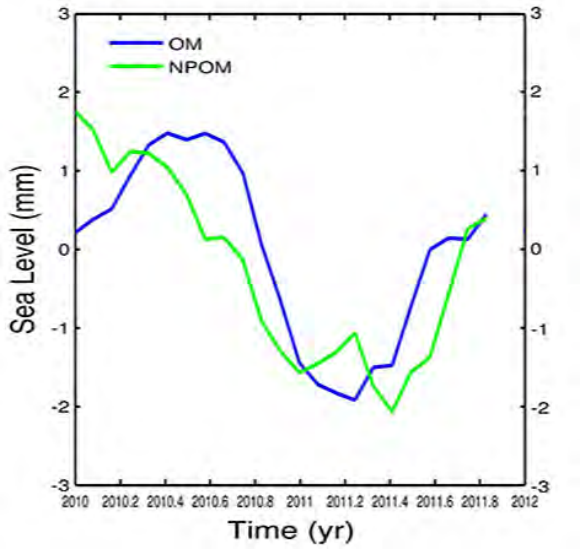

Fig. 5. Interannual global mean ocean mass from GRACE (dark blue curve) and north Pacific ocean mass (also estimated from GRACE) (green curve) during the 2011 La Niña.

We also compared the spatial patterns of the observed, altimetry-based sea level and steric sea level over the north Pacific. A similar treatment was performed on these two data sets (latitude averaging between the equator and 60°N and computation of a longitude/time diagram). These are shown in Fig. 7a and 7b. As expected, the two maps are highly correlated and display clear west-east anomalies during ENSO events. Amplitude of the ENSO-related sea level anomalies is in the range +/–80 mm. Associated ocean mass anomalies shown in Fig. 6 are smaller in amplitude (in the range +/–30-40 mm only) but still significant (local errors in satellite altimetry measurements reach 15 mm –e.g., AVISO website-; they reach 18 mm for IK12 steric data, Llovel et al 2013, which gives a level of local error of 23.4 mm for the mass signal). To confirm that what we interpret as mass anomalies (as shown in Fig. 6) is not a steric contribution not accounted by the IK12 data (i.e., a steric contribution from below 700 m), we computed an ocean mass longitude/time diagram (same procedure as above) by subtracting to the sea level data the Argo data down to 1500 m (but as of 2005 only). Corresponding Argo-based ocean mass diagram is shown in Fig. 8. We note that over their overlapping time span, Fig. 6 and Fig. 8 are very similar. In particular, the west-east negative mass anomalies related to the 2008 and 2011 La Niña events are well reproduced and is still significant when using Argo data down to 1500 instead of IK12 data down to 700 m (local errors in the Argo dataset for the North Pacific reach 15 mm which gives a level of local error of 15 mm for the mass signal). While we cannot exclude that the resulting map contains some steric signal from the deep ocean (below 1500 m), more likely, this results suggests that an ocean mass component is also involved during La Niña, with a very similar geographical pattern as the thermal and sea level anomalies.

7 Conclusions

In this study, we show that the GMSL drop observed during the 2011 La Niña is almost equally due to a decrease in the mass of the ocean and of the steric sea level. This is unlike the positive GMSL anomaly associated with the 1997 – 1998 El Niño that was essentially explained by an increase of the ocean mass due to more rainfall over the tropical Pacific (and associated decrease of water on land)

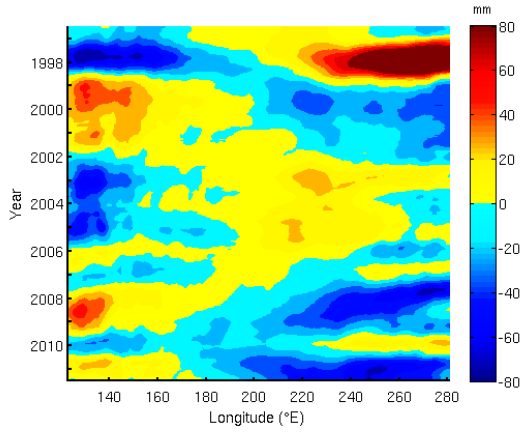

(a)

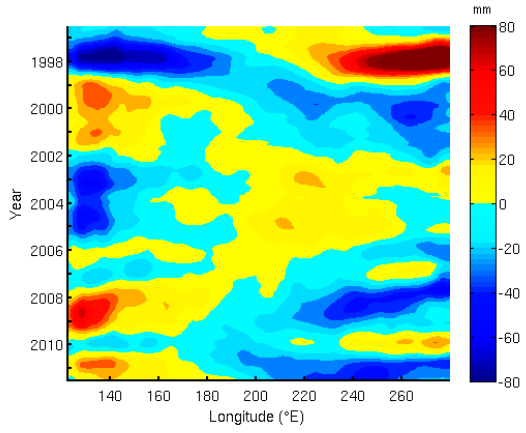

(b)

Fig. 7. Longitude/time diagram of the north Pacific (0-60°N) altimetry-based sea level data from 1996 to 2011. Units: mm; Longitude/time diagram of the north Pacific (0-60°N) steric sea level data from IK12 from 1996 to 2011. Units: mm.

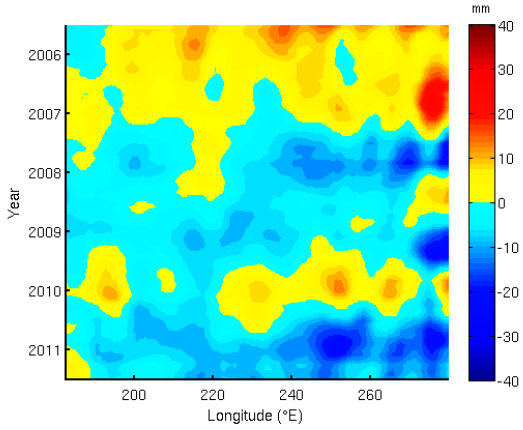

Fig. 8. Longitude/time diagram of the north Pacific ocean (0-60°N) mass sea level data based on the difference between altimetry-based sea level data and Argo steric data (down to 1500 m) over 2005-2011. Units: mm.

(Cazenave et al., 2012). This suggests that the effect of La Niña on the GMSL does not just mirror that of El Niño, as suggested by Okumura and Deser (2010) for other characteristics of these events. This is unlike the spatial patterns in ocean mass anomalies: we find that during the 2011 La Niña, the ocean mass decrease is temporarily confined in the northeastern Pacific, as for 1997 – 1998 El Niño (but with opposite sign).

The origin of this ocean mass decrease during La Niña events is possibly related to the net precipitation over the area, but the exact origin of the observed pattern remains to be investigated. This will be the object of a forthcoming study that should also analyze the relationship between ocean mass anomaly and surface salinity, in particular using data from the SMOS and Aquarius satellite missions. It will be also of interest to investigate whether numerical ocean models are able to reproduce the observed ocean mass decrease and its spatial pattern. This should help better understanding the physical cause of the observed pattern.

Acknowledgement: We thank R. Allan for kindly providing us with water vapor data. H. Palanisamy was supported by a CNES-CLS PhD Grant. K. von Schuckmann was partly supported by the French Lefe/GMMC research programme.

References

Alkama R., Decharme B., Douville H., Becker M., Cazenave A., Sheffield J., Voldoire A., Tyteca S., Le Moigne P. (2010). Global evaluation of the ISBA-TRIP continental hydrologic system; Part 1 : a two-fold constraint using GRACE terrestrial water storage estimates and in situ river discharges J. Hydrometeorology, 11, 583-600, doi:10.1175/2010JHM1211.

Barker P. M., Dunn J. R., Domingues C. M., and Wijffels S. E., (2011) Pressure Sensor Drifts in Argo and Their Impacts, J. Atmos. Ocean. Tech., 28, 1036–1049.

Boening C., Willis J.K., Landerer F.W. and Nerem R.S. (2012). The 2011 La Niña: so strong, the oceans fell, Geophys. Res. Lett., 39, L19602, doi:10.1029/2012GL053055.

Cabanes, C., A. Gourazel, K. von Schuckmann, M. Hamon, V. Turpin, C. Coatanoan, S. Guinehut, C. Boone, N. Ferry, G. Reverdin, S. Pouliquen and P.Y. Le Traon (2013): The CORA dataset: validation and diagnostics of ocean temperature and salinity in situ measurements, Ocean Sci., 9, 1–18, www.ocean-sci.net/9/1/2013/, doi:10.5194/os-9-1-2013.

Cazenave A., O. Henry, S. Munier, B. Meyssignac, T. Delcroix, W. Llovel, H. Palanisamy and M. Becker, (2012). ENSO influence on the global mean sea level over 1993-2010, Marine Geodesy, 35(S1), 82–97.

Chambers D. and J. Schröter (2011). Measuring ocean mass variability from satellite gravimetry, Journal of Geodynamics, 52, 333–

343, doi:10.1016/j.jog.2011.04.004.

Church J.A., N.J. White, L.F. Konikow, C.M. Domingues, J.G. Cogley, E. Rignot, J.M. Gregory, M.R. van den Broeke, A.J. Monaghan, and I. Velicogna (2011). Revisiting the Earth's sea level and energy budgets from 1961 to 2008, Geophys. Res. Lett., 38, L18601, doi:10.1029/2011GL048794.

Church J. A., P. U. Clark, A. Cazenave, J. M. Gregory, S. Jevrejeva, A. Levermann, M. A. Merrifield, G. A. Milne, R. S. Nerem, P. D. Nunn, A. J. Payne, W. T. Pfeffer, D. Stammer and A. S. Unnikrishnan (2013). Sea Level Change. In: Climate Change 2013: The Physical Science Basis. Contribution of Working Group I to the Fifth Assessment Report of the Intergovernmental Panel on Climate Change [Stocker, T. F., D. Qin, G.-K. Plattner, M. Tignor, S. K. Allen, J. Boschung, A. Nauels, Y. Xia, V. Bex and P. M. Midgley (eds.)]. Cambridge University Press, Cambridge, United Kingdom and New York, NY, USA, in press.

Dai A. and Wigley T.M.L (2000), Global patterns of ENSO-induced precipitation, Geophys. Res. Lett., 27, 9, 1283-1286.

Decharme B., Alkama R., Douville H., Becker M., Cazenave A., Sheffield J., Voldoire A., Tyteca S., Le Moigne P. (2010). Global evaluation of the ISBA-TRIP continental hydrologic system using GRACE; Part 2 : results, J. Hydrometeorology, 11, 601- 617.

Fasullo J.T., Boening C. , Landerer F.W. and Nerem R.S. (2013). Australia's unique influence on global mean sea level in 2010-2011, Geophys. Res. Lett., in press.

Gaillard F., Autret E., Thierry V., Galaup P., Coatanoan C., and Loubrieu T. (2009), Quality control of large Argo data sets, J. Atmos. Oceanic Technol., 26, 337–351.

Gordon A.L., Sprintall J., Van Aken H.M., Susanto D., Wijffels S., Molcard R., Ffield A., Pranowo W., Wirasantosa S. (2010) "The Indonesian Throughflow during 2004-2006 as observed by the INSTANT program." "Modeling and Observing the Indonesian Throughflow", Guest Editors: A. L. Gordon and V.M. Kamenkovich, Dynamics of Atmosphere and Oceans, vol(50) 115-128.

Gu G. and Adler R.F. (2011), Precipitation and temperature variations on the interannual time scale : assessing the impact of ENSO and volcanic eruptions, J. Climate, 24, 2258-2270.

Ishii M. and Kimoto M. (2009), Reevaluation of historical ocean heat content variations with varying XBT and MBT depth bias corrections, Journal of Oceanography, 65, 287-299.

Hanna et al. (2013). Ice-sheet mass balance and climate change, Nature, 498, 51-59, doi:10.1038/nature12238.

Henry O., Ablain M., Meyssignac B., Cazenave A., Masters D., Nerem S. and G. Garric (2014). Effect of the processing methodology on satellite altimetry-based global mean sea level rise over the JASON-1 operating period, Journal of Geodesy, in press.

Llovel W., Becker M., Cazenave A. and Crétaux J.F. (2010). Contribution of land water storage change to global mean sea level from GRACE and satellite altimetry, C.R. Geosciences, 342, 179-188.

Llovel W., Becker M., Cazenave A., Jevrejeva S., Alkama R., Decharme B., Douville H., Ablain M. and Beckley B. (2011). Terrestrial waters and sea level variations on interannual time scale, Global Planet. Change, 75, 76-82. doi:10.1016/j.gloplacha.2010.10.008.

Llovel W., Fukumori I. and Meyssignac B. (2013). Depth-dependent temperature change contributions to global mean thermosteric sea level rise from 1960 to 2010, Global Planet. Change, 101, 113-118.

Meyssignac B. and Cazenave A. (2012). Sea level : a review of present-day and recent-past sea level change and variability, J. Geodyn., 58, 96-109.

Nerem R. S., Chambers D. P., Choe C., and Mitchum G. T. (2010), Estimating Mean Sea Level Change from the TOPEX and Jason Altimeter Missions, Marine Geodesy, 33 (1), 435-446.

Oki T. and Sud Y.C. (1998). Design of Total Runoff Integrating Pathways (TRIP), A Global River Channel Network. Earth Inter., Vol. 2., Paper 1.

Okumura Y. and C. Deser (2010). Asymmetry in the duration of El Nino and La Nina. J. Climate, 23, 5826-5843.

Trenberth K. and Smith L. (2005).The Mass of the Atmosphere: A Constraint on Global Analyses, J. Climate, 18, 864-875.

Velicogna I. and Wahr J. (2013), Time variable gravity observations of ice sheet mass balance:precision and limitations of the GRACE satellite data, Geophys. Res. Lett., 40, 1-9, doi:10.1002/grl.50527.

Von Schuckmann K., Gaillard F., and Le Traon P. Y. (2009). Global hydrographic variability patterns during 2003–2008, J. Geophys. Res., 114, C09007, doi:10.1029/2008JC005237.

Von Schuckmann K. and Le Traon P.-Y (2011). How well can we derive Global Ocean Indicators from Argo data?, Ocean Sci., 7, 783–791, doi:10.5194/os-7-783-2011.

Wahr J., Swenson S. and Velicogna I. (2006). Accuracy of GRACE mass estimates, Geophys. Res. Lett., 33, L06401, doi:10.1029/2005GL025305.

Received December 18, 2013 ; accepted February 11, 2013.

Chapitre 4

Evolutions récentes de la température moyenne de la Terre et du niveau de la mer

4.1 Le système climatique au cours des années 2000

La Terre emmagasine de la chaleur à cause des émissions de gaz à effet de serre qui continuent d'augmenter depuis un siècle et demi, avec une nette accélération durant ces dernières décennies (*Myhre et al.* 2013). Cet excès de chaleur a plusieurs conséquences : augmentation de la température moyenne de la Terre, du contenu thermique de l'océan et la fonte des glaces marines et continentales. Mais depuis le début des années 2000, la température moyenne globale de surface de la Terre (GMST pour -global mean surface temperature-) a augmenté moins vite qu'au cours des dernières décennies, alors que les mesures du bilan radiatif net au sommet de l'atmosphère indiquent que la Terre est toujours en état de déséquilibre énergétique de l'ordre de +0.5 à +1 $W.m^{-2}$ (*Church et al.* 2011; *Hansen et al.* 2011; *Peters et al.* 2012; *Trenberth and Fasullo,* 2013; *Smith,* 2013; *Trenberth et al.* 2014). Ce phénomène a été qualifié de "pause" ou "hiatus" ((*Held,* 2013). Comme mentionné dans la *section 2.3.1* du *chapitre 2,* plusieurs hypothèses ont été proposées pour apporter une réponse à la question : où va l'énergie qui continue à s'accumuler dans le système climatique, alors même qu'elle ne sert plus à réchauffer l'atmosphère? Les explications proposées sont :

- une réduction du forçage radiatif due à divers phénomènes (diminution de l'activité solaire, succession d'éruptions volcaniques, changement de teneur en vapeur d'eau de la stratosphère, etc.);
- une partie de la chaleur sert à fondre les glaces, en particulier les calottes polaires, au lieu de réchauffer l'atmosphère;
- l'augmentation de l'absorption de la chaleur par l'océan profond, que ce soit dans le Pacifique ou l'Atlantique Nord ;

(voir, *Trenberth and Fasullo* 2010, 2013; *Hansen et al.* 2011; *Solomon et al.* 2010; *Guemas et al.* 2013; *Kosaka and Xie*, 2013; *Balmaseda et al.* 2013a; *Watanabe et al.* 2013; *England et al.* 2014; *Chen and Tung*, 2014).

4.2 Evolution de la température moyenne globale de surface de la Terre et du contenu thermique des océans, déséquilibre énergétique du système climatique au cours des années 2000

Actuellement l'explication privilégiée de la "pause" du GMST observée depuis 10-12ans est l'absorption de la chaleur par l'océan profond (*Goddard,* 2014; *Trenberth et al.* 2014; *Chen and Tung*, 2014). Nous avions montré dans le *chapitre 2*, une augmentation régulière du contenu thermique de la couche océanique 700-1500m depuis 2005 mais on n'observe pas de réchauffement en dessous de 2000m, pour expliquer le "hiatus". Cependant, aucun consensus n'existe encore sur le mécanisme à l'origine et la région impliquée. Il a été montré que le "hiatus" coïncide avec un refroidissement important de l'océan Pacifique tropical Est, lui-même associé avec une fréquence accrue des épisodes froids La Nina durant les années 2000 (*Nieves et al.* 2015; *England et al.* 2014)**.** Toutefois**,** une étude récente de *Karl et al.* (2015), basée sur le retraitement des données de température à la surface de l'océan et des terres, suggère qu'il n'y a aucune preuve d'une pause au cours de la dernière décennie.

Résumé de l'article : " **Sea and land surface temperatures, ocean heat content, Earth's energy imbalance and net radiative forcing over the recent years** " *(l'article original est inséré à la fin de cette section 4.2)*

Dans une étude récente, nous nous sommes posé les questions suivantes : la pause des années 2000 de la GMST existe-t-elle vraiment ? Si elle existe, est-elle océanique ou continentale, régionale ou globale ? Le refroidissement du Pacifique tropical Est est-il suffisant pour expliquer la hausse moins rapide de la GMST ? Si l'on exclut cette région, la GMST augmente-t-elle comme au cours des précédentes décennies ? Comment évolue le contenu thermique des océans et le bilan radiatif net de la Terre durant la période dite de "pause" ?

Pour répondre à ces questions, 12 bases de données de température de surface ont été analysées sur la période 1950-2014 : 4 produits de température de surface de la mer (SST), 4 produits de température de l'air en surface des continents (LST pour -land surface température-) et 4 produits de GMST. Pour plus de détails sur ces données voir *Dieng et al.* (2017) joint à la fin de cette section. La GMST moyenne présente une tendance de 0.022 ± 0.022 °C/décennie sur la période 2003-2013 contre 0.116 ± 0.007 °C/décennie sur la période 1950-2014. La contribution de la SST globale (GSST) et de la LST globale (GLST) à la tendance du GMST sur la période 2003-2013 reste très faible en comparaison de la période 1950-2014 (voir *table.1* de l'article inséré ci-dessous). En analysant les séries temporelles des produits GMST, GSST et GLST, nous avons montré que le ralentissement de la température de surface est bien réelle, à la fois sur l'océan et les continents, mais qu'il n'y a pas réellement de pause.

Nous avons analysé la SST de chaque bassin océanique et dans 5 bandes de latitude (60°N-90°N, 30°N-60°N, 0-30°N, 30°S-0, 60°S-30°S). Une analyse par bandes de latitudes a été aussi réalisée pour la LST. Notre étude a montré une variabilité interannuelle de la SST et de la LST plus élevée dans les régions tropicales, probablement liée à ENSO. Cette étude confirme bien le refroidissement du Pacifique tropical Est (30°S - 30°N ; 170°E - aux côtes Américaines) sur la période 2003-2013. En soustrayant de la série temporelle de la GMST, celle de la SST de cette zone du Pacifique, la tendance de la température de surface augmente à 0.069 ± 0.024 °C/décennie pour 2003-2013. Mais cette tendance est toujours inférieure à celle de la GMST totale, de 0.116 ± 0.007 °C/décennie sur la période 1950-2014. Nous notons aussi que l'océan Indien, de même que les bandes de latitudes océaniques (60°S-30°S) et continentales (60°N-90°N) se sont réchauffés sur la dernière décennie (voir table1 de *Dieng et al.* 2017 joint ci-dessous). Mais en raison d'une plus grande surface de l'océan dans l'hémisphère sud, les régions correspondantes (par exemple la bande de latitudes océanique 60°S-30°S) contribuent davantage à la tendance de la GSST que l'hémisphère nord.

Nous avons montré que quel que soit l'océan (excepté l'Indien) ou la zone de latitude (excepté 60°S-30°S sur l'océan et 60°N-90°N sur les continents), SST et LST ont augmenté beaucoup moins vite pendant la décennie 2003-2013 qu'auparavant. Ceci indique que la diminution de la hausse du GMST sur la période 2003-2013 ne s'explique pas par le seul refroidissement du Pacifique tropical Est et central, mais est bien un phénomène global.

Dans un second temps, nous avons analysé l'évolution de la dérivée temporelle du contenu thermique total de l'océan (représentant l'essentiel du déséquilibre énergétique net du système climatique; von *Schuckmann et al.* 2016). Trois ensembles de données totalement indépendantes

ont été utilisées pour estimer le contenu thermique de l'océan : *(1)* la réanalyse océanique ORAS4 ; *(2)* différents jeux de données thermostériques ; et *(3)* le niveau de la mer altimétrique corrigé de la masse de l'océan avec les données GRACE. Nous avons aussi utilisé les données du déséquilibre énergétique net au sommet de l'atmosphère (-TOA- Top-of-Atmosphere) du projet CERES (-Clouds and the Earth's Radiant Energy Systems- ; *Loeb et al.* 2012a). Avec ces 4 produits nous estimons à 0.68 ± 0.08 $W.m^{-2}$, 0.50 ± 0.07 $W.m^{-2}$ (sur la période 2003-2010) ; 0.65 ± 0.08 $W.m^{-2}$ et 0.66 ± 0.05 $W.m^{-2}$ le déséquilibre énergétique sur la période 2003-2013. Nous notons un bon accord entre tous ces résultats, surtout en considérant que ces chiffres sont obtenus avec des ensembles de données indépendants. De plus, ces valeurs concordent bien avec les estimations de *Roemmich et al.* (2015) sur la période 2006-2013 basées sur les données Argo. Ces estimations confirment que la planète continue d'être dans un état de déséquilibre énergétique positif (accumulation de chaleur)**.**

Nous avons ensuite estimé le forçage radiatif net (en utilisant l'équation *1* de l'article joint ci-dessous). Aucun signe de diminution n'est observé au cours des dernières années (valeur moyenne de 1.45 ± 0.8 $W.m^{-2}$ sur la période 2000-2014). Au contraire, nous notons une augmentation par rapport aux décennies précédentes. Il faut cependant noter la forte incertitude dans l'estimation du forçage radiatif, due en particulier à notre méconnaissance du paramètre de sensitivité climatique.

En analysant les évolutions de la tendance de la GMST sur des fenêtres glissantes de 1an entre 1950 et 2014, nous observons clairement une diminution de la hausse de la GMST au début des années 2000 en comparaison à la décennie précédente. Pour aller plus loin dans notre analyse, nous avons ainsi calculé la distribution des tendances sur 11ans de la GMST entre 1950 et 2014. Cette distribution des tendances de la GMST (représentée par l'histogramme Fig.4.1) suit une Gaussienne presque parfaite autour de la valeur médiane de 0.106 °C/décennie**.** Cela suggère que la variabilité décennale des tendances résulte de la variabilité interne du climat. Le ralentissement récent (et temporaire) de la GMST s'explique probablement par cette variabilité interne et ne remet pas en cause la tendance à long terme au réchauffement global. La valeur de tendance de la GMST sur la période 2003-2013 est contenue dans la barre grisée de la Fig.4.1. Cet intervalle de tendance de [0 - 0.05°C/décennie] comprend 7 occurrences en comparaison à l'intervalle médian de [0.10 - 0.15°C/décennie] qui comprend 10 occurrences, sur la période 1950-2014. Ceci suggère que la tendance de la GMST observée depuis le début des années 2000 n'est pas exceptionnelle. Cela confirme que le ralentissement de la GMST des années 2000 est plutôt d'origine naturelle.

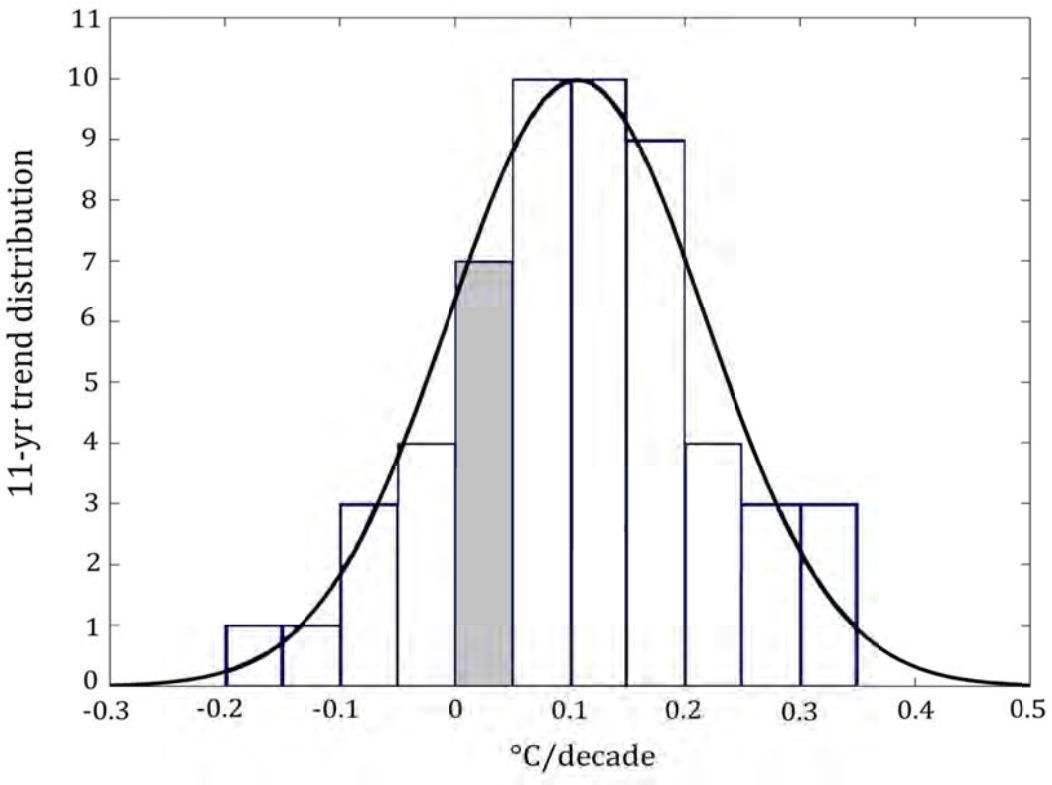

Fig.4.1 : L'histogramme du nombre de valeurs de tendance sur 11 ans (décalé de 1an entre 1950 et 2014) de la GMST. La ligne bleue représente la Gaussienne associée à l'histogramme centré sur la tendance médiane de 0.106 °C/décennie.

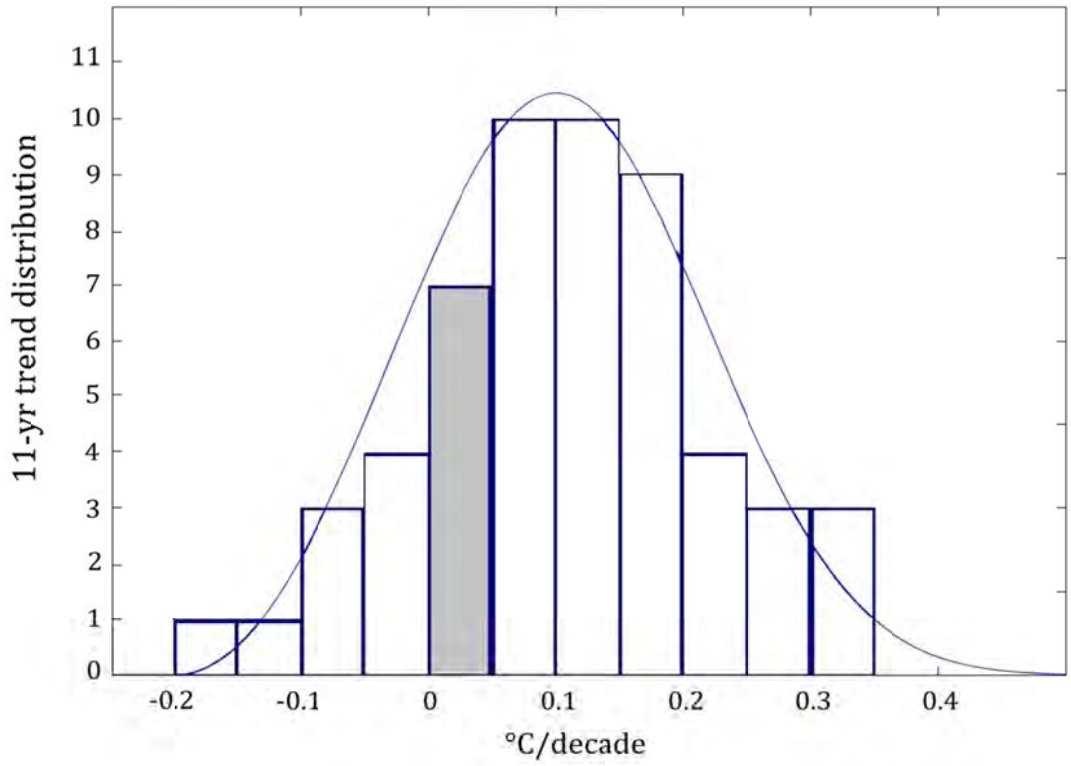

Fig.4.2 : L'histogramme du nombre de valeurs de tendance sur 11 ans (décalé de 1an entre 1950 et 2014) de la GMST. La ligne bleue représente le pdf associé à l'histogramme centré sur la tendance médiane de 0.106 °C/décennie.

Nous avons aussi analysé la courbe de la distribution normale (pdf -normal distribution-) associée à l'histogramme des tendances sur 11 ans de la GMST entre 1950 et 2014. Nous avons observé un étirement de la courbe du pdf vers les tendances croissantes, indiquant une augmentation des tendances positives de la GMST sur la période 1950-2014. Cela est illustré sur la Fig.4.2 ci-dessous. En considérant la période 1970-2014, nous observons une hausse de la tendance médiane de 0.15 °C/décennie.

En conclusion, nous avons montré que le hiatus récent est bien réel. Nous avons aussi montré que ce hiatus est global même si le Pacifique tropical Est s'est fortement refroidi. Nous notons qu'il n'y a pas de diminution du déséquilibre énergétique du système climatique ni du forçage radiatif net au cours de la dernière décennie. Enfin, comme indiqué dans les études précédentes (par exemple, *Llovel et al.* 2014; *von Schuckmann et al.* 2014, 2016), la pause observée dans l'évolution de la GMST n'est en aucun cas le reflet d'une pause dans l'accumulation de chaleur dans le système climatique. Il est de plus en plus clair que la GMST n’est pas le meilleur indicateur du changement climatique. C'est plutôt le contenu thermique de l’océan et/ou le niveau moyen global de la mer.

INTERNATIONAL JOURNAL OF CLIMATOLOGY
Int. J. Climatol. (2017)
Published online in Wiley Online Library
(wileyonlinelibrary.com) DOI: 10.1002/joc.4996

RMetS
Royal Meteorological Society

Sea and land surface temperatures, ocean heat content, Earth's energy imbalance and net radiative forcing over the recent years

H. B. Dieng,[a] A. Cazenave,[a,b]* B. Meyssignac,[a] K. von Schuckmann[c] and H. Palanisamy[a]

[a] *LEGOS, Observatoire Midi-Pyrénées, Toulouse, France*
[b] *International Space Science Institute (ISSI), Bern, Switzerland*
[c] *MERCATOR Océan, Ramonville-St-Agne, France*

ABSTRACT: We investigate the global mean and regional change of sea surface and land surface temperature over 2003–2013, using a large number of different data sets, and compare with changes observed over the past few decades (starting in 1950). We find that over 2003–2013, both global land surface temperature and global sea surface temperature have increased at a rate significantly lower than over the previous decades. While confirming cooling of eastern tropical Pacific during the last decade as reported in several recent studies, our results show that the reduced rate of change of the 2003–2013 time span is a global phenomenon. GMST short-term trends since 1950 computed over successive 11-year windows with 1-year overlap show important decadal variability that highly correlates with 11-year trends of the Atlantic Multidecadal Oscillation index. The GMST 11-year trend distribution is well fitted by a Gaussian function, confirming an unforced origin related to internal climate variability. We evaluate the time derivative of full-depth ocean heat content to determine the planetary energy imbalance with different approaches: in situ measurements, ocean reanalysis and global sea level budget. For 2003–2013, it amounts to 0.5 +/− 0.1 W m^{-2}, 0.68 +/− 0.1 W m^{-2} and 0.65 +/− 0.1 W m^{-2}, respectively for the three approaches. Comparing with the Energy Balanced and Filled (EBAF) data of the Clouds and Earth's Radiant Energy Systems (CERES) project, we find significant agreement at interannual scales. Finally, using 15-year averages of GMST and total ocean heat content rate, we compute the net radiative forcing since 1970 (this start date being constrained by availability of ocean temperature data). Although the uncertainty is quite large because of considerable errors in the climate sensitivity parameter, we find no evidence of decrease in net radiative forcing in the recent years, but rather an increase compared to the previous decades.

KEY WORDS Earth's energy imbalance; Global mean Earth's temperature; Ocean heat content

Received 1 July 2016; Revised 9 December 2016; Accepted 14 December 2016

1. Introduction

Observations of global air surface temperature on land (GLST) and global sea surface temperature (GSST) show that the Earth's global mean surface temperature (GMST) is rising since the beginning of the 20th century but the rate of rise is not steady. In fact, as suggested by Trenberth (2015), the GMST is increasing in a series of staircase steps with period of approximately 10 years of little upward trend, possibly due to the presence of random short-term variability. The first decade of the 21st century is one of these 'flat' periods (Trenberth and Fasullo, 2013; Smith, 2013). Although the reality of a slower trend in GMST during the recent years has been disputed (e.g. Cowtan and Way, 2014; Karl *et al.*, 2015, Cahill *et al.*, 2015; Foster and Abraham, 2015), it is still the object of considerable attention and an abundant literature has been published so far to investigate the reality and potential causes (e.g. Fyfe *et al.*, 2016). Greenhouse gases have continued to accumulate into the atmosphere during the last two decades at an increased rate (Peters *et al.*, 2012; IPCC, 2013) and the Earth's energy imbalance at the top of the atmosphere is estimated on the order of +0.5−1 W m^{-2} (e.g. Hansen *et al.*, 2011; Trenberth *et al.*, 2014, Von Schuckmann *et al.*, 2016), making any recent slower GMST rate even more puzzling. Two classes of explanations have been proposed to explain it: (1) reduced radiative forcing and (2) natural internal variability. The two explanations are not exclusive to each other. Reduced radiative forcing has been proposed because of prolonged last solar minimum, hence slightly lower solar irradiance, increased aerosols, numerous small volcanic eruptions and decrease in stratospheric water vapour (e.g. see Cheng *et al.*, 2015 and Lewandowsky *et al.*, 2015 for reviews). However estimates of these effects indicate that they may not contribute for more than 20% of the recent reduced GMST trend (Trenberth *et al.*, 2014; Trenberth, 2015). The second explanation currently invoked is internal climate variability. The recent slower GMST trend coincides with a negative phase of the Pacific Decadal Variability (PDO) and a succession of La Nina events (cold phase

* Correspondence to: A. Cazenave, LEGOS, UMR5566, Observatoire Midi-Pyrénées, 18 avenue Edouard Belin, 31401 Toulouse, Cedex 9, France. E-mail: anny.cazenave@legos.obs-mip.fr

of El Nino Southern Oscillation, ENSO). Observations and model results suggest that this particular configuration causes wind-driven cooling of eastern Pacific surface waters with large-scale impacts on the global climate, including enhanced heat uptake in the deep ocean and reduced GMST increase (e.g. Trenberth and Fasullo, 2010, 2013, Hansen *et al.*, 2011; Meehl *et al.*, 2011; Kosaka and Xie, 2013; Balmaseda *et al.*, 2013a; Watanabe *et al.*, 2013; Held, 2013; Guemas *et al.*, 2014; England *et al.*, 2014; Goddard, 2014; Trenberth *et al.*, 2014; Chen and Tung, 2014; Nieves *et al.*, 2015; Trenberth, 2015).

Here, we revisit the evolution of surface temperature data, both over the oceans and land during the recent years, with focus on the decade January 2003 to December 2013 (we do not consider year 2014 which is reported as one the hottest years on record, e.g. Cahill *et al.*, 2015) and on a longer time span (January 1950 to December 2014). Using a large number of different data sets for sea and land surface temperature [noted respectively sea surface temperature (SST) and land surface temperature (LST) hereinafter], we examine the contributions of different ocean basins and latitude bands to SST and LST, accounting for the respective weight (in terms of area) of each region with respect to the total Earth' surface. We investigate in particular whether cooling of a particular region (e.g. the eastern tropical Pacific as previously reported in the literature) is sufficient to explain the slower increase in GMST or if all regions have contributed (through reduced surface temperature increase compared to previous decades). Using ocean temperature data and ocean reanalyzes, as well as the global mean sea level corrected for the ocean mass component to estimate the time derivative of the total ocean heat content (OHC), a quantity representing the Earth's radiative imbalance, we further deduce the net radiative forcing and its variations with time, using the radiative budget at the top of the atmosphere (TOA) which relates Earth's radiative imbalance and GMST variation.

2. Data

In this section, we briefly describe the various data sets used in our study. For the SST and LST data, we considered all data sets that provide data over the Arctic region, in order to have data coverage as global as possible.

2.1. Sea surface temperature

For SST, we used four different products from four processing groups:

1. The Extended Reconstructed Sea Surface Temperature, version 4, from National Oceanographic and Atmospheric Administration (NOAA/ERSST4; https://www.ncdc.noaa.gov/data-access/marineocean-data/extended-reconstructed-sea-surface-temperature-ersst-v4). The dataset covering the period January 1854 to June 2015, is a monthly global SST, derived from the International Comprehensive Ocean–Atmosphere Dataset (ICOADS) Release 2.5 (Woodruff *et al.*, 2011). It is provided on a $2^\circ \times 2^\circ$ grid with spatial completeness enhanced using statistical methods. This new version 4 of ERSST is based on optimally tuned parameters using the latest datasets and improved analysis methods compared to methods based on ERSST v3b. It is the most updated version available on the NOAA website. For details of the datasets, see Boyin *et al.* (2015).
2. The COBE SST data from the Japan Meteorological Agency (JMA/COBE SST; http://ds.data.jma.go.jp/tcc/tcc/products/elnino/cobesst/cobe-sst.html) are provided as $1^\circ \times 1^\circ$ grids, at monthly interval over January 1891–May 2015. For details on this product and data analysis, see Ishii *et al.* (2005) and Japan Meteorological Agency (2006).
3. The Cowtan and Way (2014) data set that includes the Arctic region. Except for the Arctic, it is based on the HadSST3 version 3.1.1.0 data set from the Met Office Hadley Centre's (Hadley/HadSST3; http://hadobs.metoffice.com/hadsst3/), and is a monthly SST field covering the January 1850–June 2015 time span. The data are not interpolated and the variance not adjusted. However, the data have been adjusted to minimize the effects of changes in instrumentation throughout the record. For more information, see Kennedy *et al.* (2011). The Cowtan and Way (2014) data set (noted CW herein after) is augmented with satellite-based temperature data over the Arctic region. This data set is provided on a $5^\circ \times 5^\circ$ grid.
4. The Kaplan Extended SST version 2 data set from Kaplan *et al.* (1998) (Kaplan; http://iridl.ldeo.columbia.edu/SOURCES/.KAPLAN/.EXTENDED/.v2/.ssta/) over January 1856–June 2015, is produced by taking the MOHSST5 version of the GOSTA data set from the UK MET office. The data are available as monthly $5^\circ \times 5^\circ$ grids. Several treatments were applied to the data: Optimal Interpolation (OI), Kalman Filter (KF) forecast, KF analysis and an Optimal Smoother (OS). For more description, see the web link above.

The geographically averaged sea surface temperature (hereinafter called GSST – for global SST) time series from NOAA, JMA, CW and Kaplan are estimated over the 88°S–88°N, 89.5°S–89.5°N, 87.5°S–87.5°N and 87.5°S–87.5°N domains, by area weighting the gridded data over their respective latitude coverage.

2.2. Land surface temperature

We used four different products for LST data from four processing groups:

1. The combination of two large individual data sets of station observations collected from the Global Historical Climatology Network version 2 and the Climate Anomaly Monitoring System (GHCN_CAMS; http://www.esrl.noaa.gov/psd/data/gridded/data.ghcncams.html). This monthly data set (from NOAA) is provided on $0.5^\circ \times 0.5^\circ$ grids over January 1948–June 2015. Data processing uses unique interpolation methods,

such as the anomaly interpolation approach with spatially and temporally varying temperature lapse rates derived from the observation-based reanalysis for topographic adjustment (Fan and Van den Dool, 2008).
2. The Cowtan and Way (2014) data that covers the Arctic region. Outside the Arctic, it is based CRUTEM4 version V4.3.0.0 dataset derived from a collaboration between the MetOffice-Hadley Centre and the Climatic Research Unit (CRU) of the University of East Anglia (Hadley_CRU/CRUTEM.4.3.0.0; http://hadobs.metoffice.com/crutem4/). This monthly data set covers the January 1850–June 2015 time span. The data are based on an archive of mean temperatures provided by more than 5500 weather stations distributed around the world. For more information, see Osborn and Jones (2014). This data set is augmented with satellite-based temperatures over the Arctic. It is provided on a $5^\circ \times 5^\circ$ grid.
3. The Goddard Institute for Space Studies (GISS) surface air temperature (no ocean data) with 250 km smoothing (NASA/GISS; http://data.giss.nasa.gov/gistemp/). The dataset is provided on $2^\circ \times 2^\circ$ grids at monthly interval over January 1880–June 2015. For more details, see Hansen *et al.* (2010).
4. The Average Temperature dataset from Berkeley Earth (Berkeley/TAVG; http://berkeleyearth.org/data/), provided on $1^\circ \times 1^\circ$ grids at monthly interval over January 1750–June 2015. For more description, see the web link above.

The geographically averaged land surface temperature (hereinafter called GLST – for global LST) time series from GHCN_CAMS, CW, NASA and Berkeley are estimated over the 89.75°S–89.75°N, 87.5°S–87.5°N, 80°S–89°N and 89.5°S–89.5°N domains, by area weighting the gridded data over their respective latitude coverage.

2.3. Global mean surface temperature

Four different products are used:

1. The Merged Land-Ocean Surface Temperature Analysis (MLOST) version V3.5.4 from NOAA for SST (extended reconstructed sea surface temperature, version 3b including in situ and satellite data) and GHCN version 2 for LST(NOAA_GHNC/MLOST; http://www.esrl.noaa.gov/psd/data/gridded/data.mlost.html). The data are available on $5^\circ \times 5^\circ$ grids at monthly interval between January 1880 and June 2015. For more details, see Smith *et al.* (2008).
2. The Cowtan and Way (2014)/CW data set that includes the Arctic. Outside the Arctic, it is based on the HadCRUT4 version V4.3.0.0 gridded dataset from Met Office Hadley Centre (Hadley/HadCRUT4; http://www.metoffice.gov.uk/hadobs/hadcrut4/), and is a combination of the HadSST3 SST dataset (see section 2.1) and the CRUTEM4 LST dataset. CW data are available on $5^\circ \times 5^\circ$ grids.
3. The GISS surface temperature analysis dataset with 250 km smoothing (NASA/GISTEMP; http://data.giss.nasa.gov/gistemp/), available over January 1880–June 2015, combines three data sets (as described in Hansen *et al.*, 2010): NOAA/ERSST version 4 (ocean areas; see section 2.1), LST GHCN version 3 (meteorological stations on land), and SCAR (Antarctic stations). The data are available on $2^\circ \times 2^\circ$ grids at monthly interval.
4. The monthly Berkeley GMST dataset over January 1850–December 2014, on $1^\circ \times 1^\circ$ grids (Berkeley/TAVG; http://berkeleyearth.org/data/) combines the Berkeley LST data (see section 2.2) with a modified version of the HadSST ocean temperature data set. For more description, see the web link above.

The GMST time series from NOAA_GHNC, CW, NASA and Berkeley are estimated over the 87.5°S–87.5°N, 87.5°S–87.5°N, 89°S–89°N and 89.5°S–89.5°N domains by area weighting the gridded data over their respective latitude coverage.

2.4. Ocean heat content (OHC)

The total ocean heat content (OHC) is computed from the global mean steric sea level (GMSSL) by the relation $\mathrm{OHC} = \mathrm{GMSSL}/\varepsilon$, with ε being the uptake coefficient of the global ocean heat. Here we use for ε a value of 0.12 m Y J^{-1} (Levitus *et al.*, 2005; Kuhlbrodt and Gregory, 2012; Melet and Meyssignac, 2015). This value may have an uncertainty of ∼10% (Kuhlbrodt and Gregory, 2012). Note that OHC could be computed directly using *in situ* ocean temperature data. The choice of computing the steric sea level first arises because we also estimate OHC from the difference between global mean sea level and ocean mass – a quantity representing the steric sea level (see below).

To compute OHC, three different data sets have been used:

1. The temperature and salinity data from the ORAS4 reanalysis, are available at monthly intervals over 42 depth levels ranging from the ocean surface down to 5350 m depth, on a global $1^\circ \times 1^\circ$ grid from January 1958 to December 2014 (see Balmaseda *et al.*, 2013b, for more details). Here we use both temperature and salinity data because the ORAS4 shows sign of compensating errors in the thermosteric and halosteric components that cancel when considering the steric (sum of thermosteric and halosteric terms) component. To estimate the ORAS4 global mean steric sea level, the data are averaged over the 89°S–89°N domain.
2. The annual global mean top-to-bottom thermosteric sea level over 1955–2010 is obtained by combining the 0–700 m depth layer from a mean of Levitus *et al.* (2009); Ishii and Kimoto (2009) and Domingues *et al.* (2008) data sets; data for the 700–2000 m layer are from Levitus *et al.* (2012); and data below 2000 m are based on Purkey and Johnson (2010). This combined

data set was constructed by Melet and Meyssignac (2015).

For 1 and 2, area weighting was performed when averaging.

3. The satellite altimetry-based global mean sea level (GMSL) using an average of six different altimetry products (e.g. Dieng *et al.*, 2015a, 2015b), and an average of 3 GRACE space gravimetry products to estimate the ocean mass (data from Chambers and Bonin, 2012). Details on these data sets can be found in Dieng *et al.*, 2015a, 2015b, 2015c. The global mean steric sea level is estimated by the difference 'GMSL minus ocean mass' over January 2003–December 2013, from which we compute OHC as described above.

We further compute the time derivative of OHC for the three cases and express it in $W\,m^{-2}$.

2.5. Top-of-atmosphere (TOA) energy imbalance (CERES data)

We also used the global mean TOA net flux of Energy Balanced and Filled (EBAF) data product version Edition 2.8, provided by Clouds and the Earth's Radiant Energy System (CERES/TOA; http://ceres.larc.nasa.gov/order_data.php). This global data set is provided on a $1° \times 1°$ grid at monthly interval over March 2000–June 2015. For a more thorough description of the methodology used to produce EBAF, see Loeb *et al.* (2012a).

For all data sets (except for data sets provided at yearly interval), the annual and semi-annual cycles were removed by fitting 12-month and 6-month sinusoids to the original time series over the study period.

3. Results

3.1. Errors calculation

In the following, we use the above described data sets to construct (global or regional) time series. Some data sets are provided with uncertainties while others are not. Thus in the figures, individual time series are plotted with associated errors (two-sigma) when available. When geographical averaging is performed, we combine available time series errors (noted σ_i) with the error estimated from the spread of all data sets with respect to the average (half range of data spread, noted σ_{spread}). We then estimate, at each time step, the total error of the averaged time series from the quadratic sum: $\sqrt{(\sum {\sigma_i}^2 + {\sigma_{spread}}^2)}$.

For estimating trend errors, we use two methods. In method 1, the error is deduced from a generalized (weighted) least-squares adjustment (e.g. Bevington and Robinson, 1969, Kirkup, 1994), accounting for the total error of the average time series (i.e. quadratic sum of the spread error and time series errors, as indicated above). In method 2, we first compute trends of individual weighted time series (accounting for errors in the data), then compute the mean trend and finally estimate the error of the mean trend from the variance of the residuals (individual trends minus mean trend). It appears that for long-term trends (several decade-long), method 2 gives rise to larger errors than method 1. However, for short-term trends (10 to 15-year long), it is the opposite. Trend errors based on both methods are given in Table 1. In the following, we use the largest error estimate (either from method 1 or method 2). This may provide an upper bound of the real trend uncertainty.

3.2. Sea and land surface temperature evolution as a function of regions

Figure 1 presents the monthly time series from January 1950 to December 2014 of GSST and GLST based on the data sets presented in Section 2. The GSST and GLST curves are obtained from the gridded data applying a cosine latitude area weighting. All temperature time series are expressed in terms of anomalies with respect to the mean period 1950–2014. The start values are arbitrary since the quantity of interest here is change with time. The bottom curve represents GMST. Two cases are shown: (1) GMST directly provided by four processing centres (black curve) and (2) GMST based on GSST plus GLST. In the latter case, we first compute the mean of the different GSST and GLST time series. We then compute the global mean (i.e. GMST) by weighting GSST and GLST by the percentage of respective surfaces of ocean and land to the global surface. As shown on Figure 1, both approaches give similar results. The shaded area around the GMST curve based on the sum GSST plus GLST represents the two-sigma error estimated as described in Section 3.1. It agrees well with the estimated GMST error (shown by the thin black line).

The GMST trend over 2003–2013 is much lower than over the longer period. For cases 1 and 2, it amounts 0.010 +/− 0.071 °C/decade and 0.022 +/− 0.050 °C/decade, respectively (compared to 0.116 +/− 0.011 °C/decade for the 1950–2014 time span). We note that for the 2003–2013 time span the GMST trend is not significant.

Figure 2(a) shows SST evolution with time for the Atlantic, Indian and Pacific oceans. The GSST is also shown. In each case, the regional estimate (i.e. ocean basin scale) is weighted by the percentage of the corresponding area relative to the total ocean surface. Over the 1950–2014 time span, the Atlantic and Indian oceans show a clear positive linear trend of 0.024 +/− 0.006 °C/decade in both cases. The weighted Pacific SST time series is rather flat until the mid-1970s. It displays a step increase around that epoch and a slight positive trend since then. On average over the 1950–2014 time span, the Pacific SST trend amounts to 0.035 +/− 0.010 °C/decade. Note that interannual variability is higher in the Pacific compared to other oceans. In terms of un-weighted trends, the Indian Ocean displays the highest heating rate, followed by the Atlantic. The total GSST trend (amounting 0.084+/− 0.023 °C/decade) is simply the sum of the weighted SST trends of each ocean. The interannual variability of the GSST time series is clearly dominated by that of the Pacific Ocean.

Table 1. Trends (in °C/decade) of mean surface temperature data for1950–2014 and 2003–2013. Different area weighting are considered. Trend uncertainties are computed using two methods (see text). Uncertainties in brackets are based on method 2 (variance approach).

Data type *Global area weighting*	Temperature trends 1950–2014 °C/decade	Temperature trends 2003–2013 °C/decade
GSST	0.059 ± 0.008 (+/− 0.016)	−0.006 ± 0.045 (+/− 0.040)
East tropical Pacific SST	0.009 ± 0.003 (+/− 0.005)	−0.047 ± 0.015 (+/− 0.014)
GLST	0.057 ± 0.004 (+/− 0.006)	0.028 ± 0.021 (+/− 0.019)
GMST = GSST + GLST	0.116 ± 0.010 (+/− 0.017)	0.022 ± 0.050 (+/− 0.044)
GMST	0.116 ± 0.011 (+/− 0.017)	0.010 ± 0.071 (+/− 0.042)
GMST minus East tropical Pacific SST	0.107 ± 0.012 (+/− 0.018)	0.069 ± 0.052 (+/− 0.046)
Data type *Ocean area weighting*	Temperature trends 1950–2014 °C/decade	Temperature trends 2003–2013 °C/decade
GSST	0.084 ± 0.010 (+/− 0.023)	−0.009 ± 0.064 (+/− 0.056)
Atlantic SST	0.024 ± 0.005 (+/− 0.006)	0.001 ± 0.032 (+/− 0.016)
Indian SST	0.024 ± 0.005 (+/− 0.005)	0.050 ± 0.030 (+/− 0.018)
Pacific SST	0.035 ± 0.007 (+/− 0.010)	−0.064 ± 0.045 (+/− 0.025)
Tropical Pacific SST	0.022 ± 0.005 (+/− 0.010)	−0.067 ± 0.028 (+/− 0.018)
East tropical Pacific SST	0.012 ± 0.004 (+/− 0.007)	−0.066 ± 0.025 (+/− 0.020)
SST (60°–90°N)	0.006 ± 0.004 (+/− 0.010)	−0.008 ± 0.020 (+/− 0.017)
SST (30°–60°N)	0.011 ± 0.003 (+/− 0.005)	0.016 ± 0.022 (+/− 0.015)
SST (0°–30°N)	0.021 ± 0.004 (+/− 0.007)	−0.039 ± 0.023 (+/− 0.014)
SST (30°S–0°)	0.029 ± 0.004 (+/− 0.007)	−0.026 ± 0.024 (+/− 0.015)
SST (60°–30°S)	0.017 ± 0.004 (+/− 0.012)	0.039 ± 0.022 (+/− 0.022)
Data type *Land area weighting*	Temperature trends 1950–2014 °C/decade	Temperature trends 2003–2013 °C/decade
GLST	0.197 ± 0.012 (+/− 0.021)	0.097 ± 0.072 (+/− 0.066)
LST (60°–90°N)	0.039 ± 0.010 (+/−0.027)	0.081 ± 0.035 (+/− 0.056)
LST (30°–60°N)	0.081 ± 0.005 (+/− 0.033)	0.007 ± 0.040 (+/− 0.019)
LST (0°–30°N)	0.038 ± 0.006 (+/− 0.30)	0.021 ± 0.038 (+/− 0.020)
LST (30°S–0°)	0.030 ± 0.004 (+/− 0.025)	−0.026 ± 0.029 (+/− 0.023)
LST (60°–30°S)	0.006 ± 0.002 (+/− 0.002)	0.008 ± 0.018 (+/− 0.009)

GLST, global air surface temperature; GMST, global mean surface temperature; GSST, global sea surface temperature; SST, sea surface temperature.

The SST evolution with time is also computed as a function of latitude (in five latitude bands: 60°–90°N, 30°–60°N, 0°–30°N, 30°S–0, 60°–30°S) (Figure 2(b)). Each time series is weighted by the ratio of the corresponding latitude band surface over the total ocean surface. Positive trends are noticed for all latitude bands, especially since 1970. The north and south tropical SST curves shows high interannual variability likely dominated by ENSO events in the Pacific (compare Figures 2(a) and (b)). The SST curve north of 60°N is almost flat. This may partly result from incomplete SST data coverage in the Arctic. The mid-latitude (30°–60°N) SST starts to increase in the early 1990s. In the southern hemisphere (30°–60°S), we note a significant positive trend since the mid-1960s.

Focusing on the 2003–2013 period, the recent negative SST trend of the Pacific Ocean can be localized by pointing to contribution of the different sub regions. Figure 2(c) shows area-weighted (with respect to total ocean area) SST time series over 2003–2013 for different regions, including the east tropical Pacific. Figure 2(d) shows a map of regional SST trends over 2003–2013 computed with the NOAA data set. This trend map clearly shows the cooling trend of the equatorial Pacific and important cooling of the northeastern Pacific Ocean. Results here confirm earlier findings (e.g. Nieves *et al.*, 2015), i.e. at least part of the Pacific SST slowdown is due to significant cooling of the eastern tropical Pacific (defined as 30°S–30°N, 170°W–American coast zone).

Figure 3 shows LST evolution with time for the same five latitude bands as in Figure 2(b). Each time series is weighted by the ratio of the corresponding latitude band surface over the total land surface. The GLST is also shown. The 30°–60°N band displays a significant upward trend over 1970–2000 followed by a flattened behaviour later on. On average over the 1950–2014 time span, its trend amounts to 0.081 +/− 0.033 °C/decade. Because of its largest land surface coverage, it contributes to approximately 41% of the GLST trend over 1950–2014 (of 0.197 +/− 0. 021 °C/decade). The tropical and Arctic bands display lower positive trends over this time span (in the range 0.03–0.04 °C/decade). However during the 2003–2013 decade, Arctic warming is quite obvious and explains most of the GLST positive trend. The north and south tropical trends are of opposite sign and cancel out. The mid-latitude LST curves show nearly zero warming.

All trend values for the global and regional cases, and the two time spans are gathered in Table 1. The errors immediately following the trend estimate is based on method 1 while the error in bracket is deduced from method 2.

3.3. Contribution of the eastern tropical Pacific to the recent GMST trend

To consider the cooling impact of the tropical Pacific region on the GMST, we weighted all individual contributions by the percentage of their respective surface with respect to the total Earth' surface. Figure 4 shows for

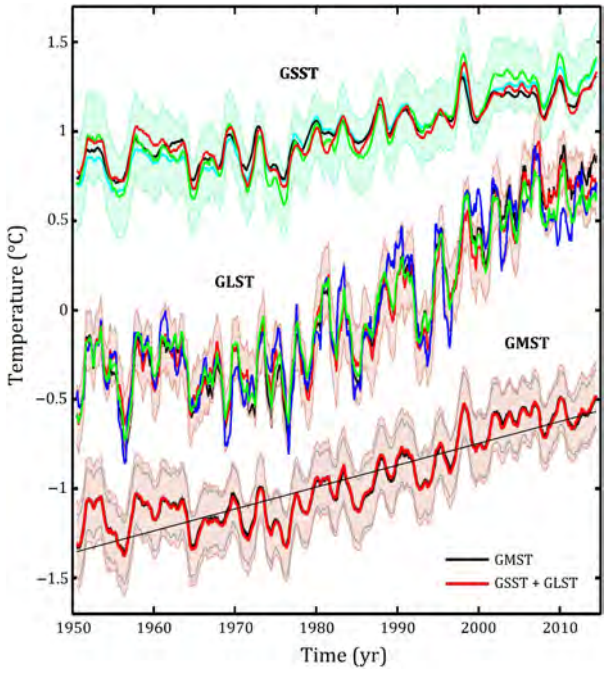

Figure 1. Global sea surface temperature (GSST) time series from January 1950 to December 2014; Average from four datasets: NOAA/ERSST4 (blue), JMA/COBE (black), Cowtan and Way (green) and associated uncertainty (sheded green) and Kaplan (red). Global land surface temperature (GLST) time series from January 1950 to December 2014 derived from four processing groups: GHCN and CAMS (GHCN_CAMS; black), Cowtan and Way (red) and associated uncertainty (shaded red), NASA (GISS; blue) and Berkeley (TAVG; green). Global mean surface temperature (GMST) time series for January 1950 to December 2014 obtained through: (1) average of NOAA_GHNC/MLOST, Cowtan and Way, NASA/GISS and Berkeley/TAVG (black) and associated uncertainty (light black line) and (2) sum of area-weighted 'GSST plus GLST' (red) and associated uncertainty (shaded red) (see text for more details). [Colour figure can be viewed at wileyonlinelibrary.com].

the 2003–2013 time span, time series of GSST, GLST, east tropical Pacific SST (defined as above), GMST and GMST minus east tropical Pacific SST. All curves are area-weighted as mentioned above (i.e. multiplied by the ratio of their respective surfaces to the total Earth' surface). As mentioned above, the GMST trend over the 2003–2013 period amounts to 0.022 +/− 0.050 °C/decade, thus is little significant. When the contribution of the east tropical Pacific is removed, the GMST trend increases by a factor of 3, up to 0.069 +/− 0.052 °C/decade. This results from a departure of the two GMST curves (with and without east tropical Pacific) as of early 2007. However, the GMST trend (east tropical Pacific removed) is still significantly lower than the GMST trend of the 1950–2014 time span (of 0.116 +/− 0.017 °C/decade; Table 1).

3.4. GMST trends evolution since 1950

To further investigate a possible slower GMST trend in the recent years, Figure 5 (upper panel) shows GSST, GLST and GMST trends (the latter estimated as the weighted sum of GSST plus GLST; east tropical Pacific contribution included) computed over successive 11-year intervals with 1-year overlap (estimated at the centre of each 11-year time interval), with 1950–1960 as starting window and 2003–2013 (our focus period) as ending window. Shaded areas represent trend errors (derived as explained in Section 3.1). The 11-year trends are essentially positive, except for some periods where the 11-year GMST trends are negative: between 1960 and 1968 (where both GSST and GLST trends are negative) and in the early 1970s (negative GSST trend). Figure 5 (upper panel) displays significant variability on decadal time scales, possibly caused by internal climate variability. We have computed the 11-year trends, with 1-year overlap, of two climate mode indices: the Atlantic Multidecadal Oscillation (AMO) (Enfield *et al.*, 2001) and the PDO (Barnett *et al.*, 1999). These are shown in Figure 6, superimposed to the GMST 11-year trends. We can note that the correlation between GMST trends and AMO trends is quite high. It amounts 0.88 over the whole time span. At the beginning of the record, the correlation with PDO trends is also high (equal to 0.8) but breaks down after the mid-1980s.

The GMST and AMO trends shown in Figure 6 show a low in the 1960s and high in the 1990s, suggestive of a 60-year oscillation, as reported for the global mean sea level by Chambers *et al.* (2012). Thus the observed temporal evolution of the GMST trends may just reflect a 60-year natural cycle driven by the AMO.

To further investigate the internal variability origin of the GMST trend behaviour, we plotted the distribution (histogram) of the GMST 11-year trends over 1950–2014 (Figure 7). We considered the successive 11-year trends shifted by 1-year, i.e. 55 values in total. The Gaussian function fitted to the 11-year trend values is superimposed. The median trend value (representing the average GMST trend increase over the study period) amounts to 0.11 °C/decade. We note that the histogram is well represented by a Gaussian distribution, with both positive and negative trends around the median value. This result strongly suggests that the trend fluctuations seen in Figure 6 are dominated by the unforced (internal) climate variability rather than by externally forced signal (Hegerl *et al.*, 2007; IPCC, 2013). In Figure 7, the vertical dashed lines define the area around the median, containing 66% of the total population (one standard deviation around the median). Similarly, the solid lines with stars represent the area with 95% of the values (two standard deviations around the median). From Figure 7, we clearly see that the 2003–2013 GMST trend (included in the grey bar) falls within one standard deviation around the median (together with 66% of the total population). Thus it is not statistically unusual, several other 11-year trends with similar amplitude (seven occurrences) being reported over the 1950–2014 time span.

To minimize this interannual variability, GMST trends have also been computed over 15-year long intervals, with 1-year overlap as above (Figure 5, lower panel). Both panels show that during the 2000s, GMST trends have been steadily decreasing, with nearly zero trends over the 2003–2013 time span.

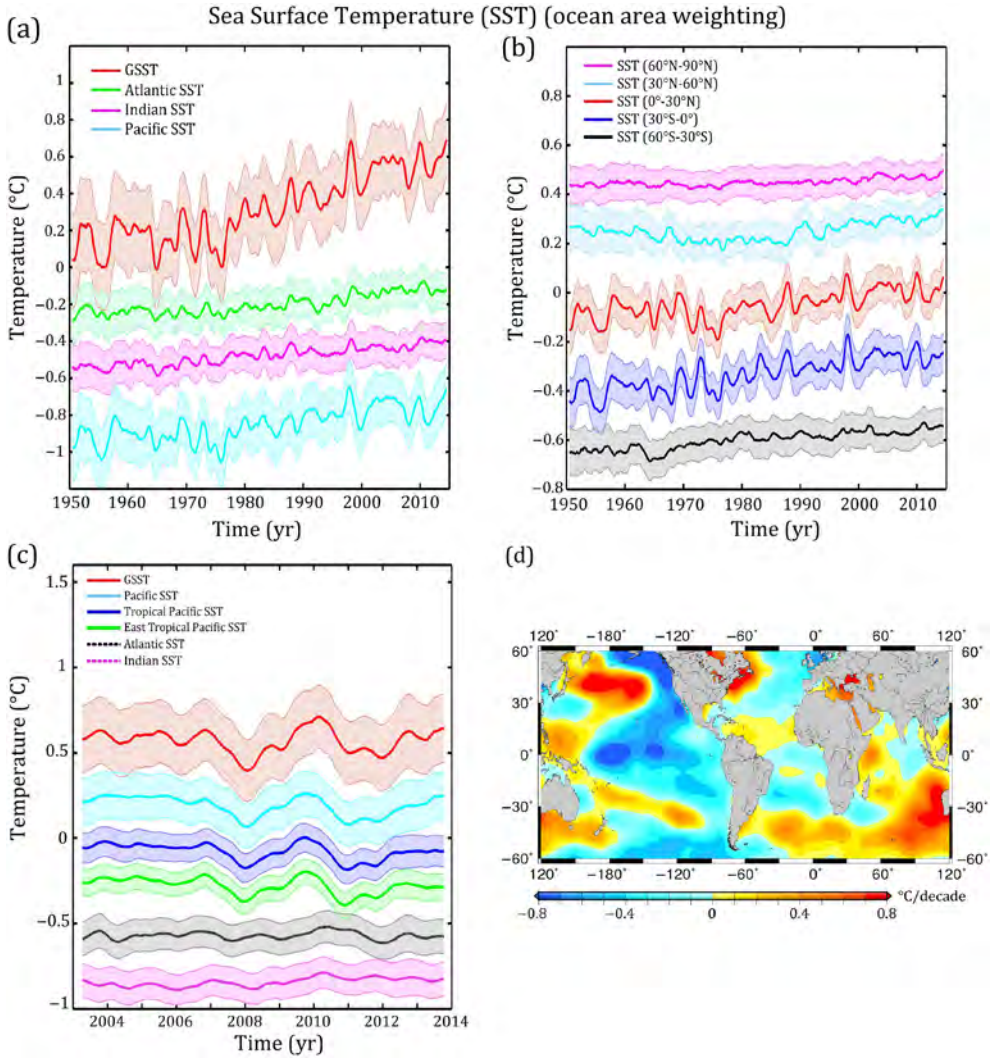

Figure 2. (a) SST time series (average of the four datasets) for January 1950 to December 2014 for the global ocean (GSST; red), Atlantic (green), Indian (magenta) and Pacific (blue) and associated uncertaintes (shaded areas). The Atlantic, Indian and Pacific SST are weighted by the ratio of their area to the total ocean surface; (b) SST time series (average of the four datasets) for January 1950 to December 2014 averaged over different latitude bands with area weighting with respect to the total ocean surface : 60°–90°N (magenta), 30°–60°N (light blue), 0°–30°N (red), 30°S–0° (blue) and 60°–30°S (black), and associated uncertainties (shaded areas); (c) SST time series (average of the four datasets) for January 2003 to December 2013 for the global ocean (GSST; red), Pacific (light blue), tropical Pacific (blue), east tropical Pacific (green), Atlantic (black) and Indian (magenta), and associated uncertainties (shaded areas) (area weighting with respect to the total ocean surface); (d) map of s SST spatial trend patterns over 2003–2013 (NOAA data). [Colour figure can be viewed at wileyonlinelibrary.com].

4. Implication for the Earth's energy imbalance and net radiative forcing of the 2003–2013 and 1970–2014 time spans

In this section, we estimate the net radiative forcing term considering the total Earth's energy imbalance and temperature anomaly change. The Earth's energy imbalance is related to net radiative forcing and global mean Earth's temperature increase by (e.g. Hansen *et al.*, 2011; Melet and Meyssignac, 2015):

$$N(t) = F(t) - \Delta T(t)/S \quad (1)$$

where N is Earth's energy imbalance at the top of the atmosphere, F is net radiative forcing, ΔT is planet surface temperature increase (i.e. response) to an applied forcing, S is the climate sensitivity parameter and t is time. N, F and ΔT are all time-dependent. Note that Equation (1) above is only valid for forced changes in N (e.g. Flato *et al.*, 2013, Brown *et al.*, 2014, Palmer and Mc Neal, 2014).

On a global annual scale, change in TOA net radiation and rate of ocean heat storage should be in phase and of the same magnitude (Loeb *et al.*, 2012b; Palmer and Mc Neal, 2014; Von Schuckmann *et al.*, 2016). This is due to the fact that all other forms of heat storage in the Earth system are factors of 10 smaller than ocean heat storage. Thus in the following, we assume that N(t) can be represented by d(OHC)/dt. For the purpose of computing d(OHC)/dt, we consider three different data sets : (1) the ORAS4 full-depth ocean reanalysis, and (2) a combination of different thermosteric data (full-depth estimate, Melet and Meyssignac, 2015) and (3) the altimetry-based global mean sea level corrected for the GRACE-based ocean mass (see section 2.4 for more details on the data used).

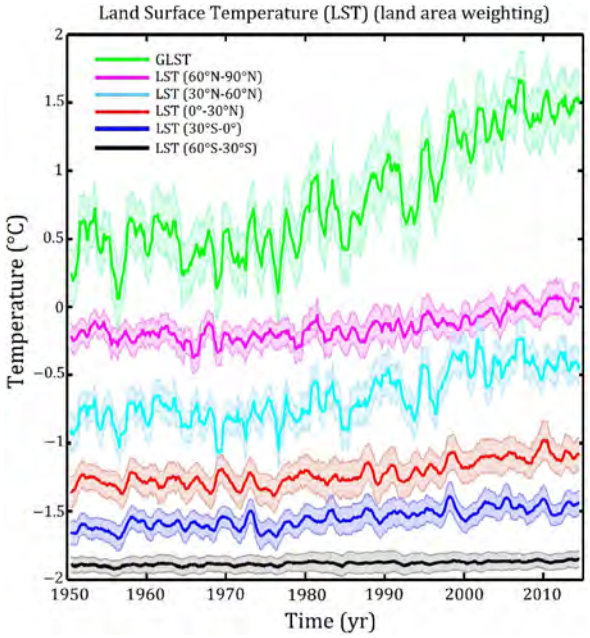

Figure 3. LST time series (average of the four datasets) for January 1950 to December 2014 for global land (GLST; green) and for different latitude bands with area weighting with respect to the total land surface : 60°–90°N (magenta), 30°–60°N (light blue), 0°–30°N (red), 30°S–0° (blue) and 60°–30°S (black), and associated uncertainties(shaded areas). [Colour figure can be viewed at wileyonlinelibrary.com].

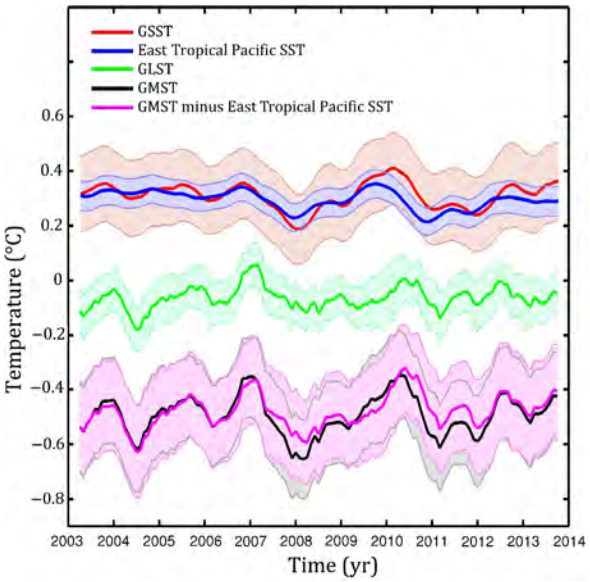

Figure 4. Temperature time series for January 2003 to December 2013 with area weighting with respect to the total Earth' surface. GSST (red), east tropical Pacific SST (blue), GLST (green) and GMST (black) superimposed to 'GMST minus east tropical Pacific SST' (magenta). [Colour figure can be viewed at wileyonlinelibrary.com].

d(OHC)/*dt* data are estimated as yearly averages (by simply averaging over successive years the monthly data) with 1970 as starting year of the time series for (1) and (2) (because of larger in situ ocean temperature data uncertainty prior that date).

Figure 8 shows the Earth's energy imbalance $N(t)$. In the upper panel, *d*(OHC)/*dt* is computed with the ORAS4

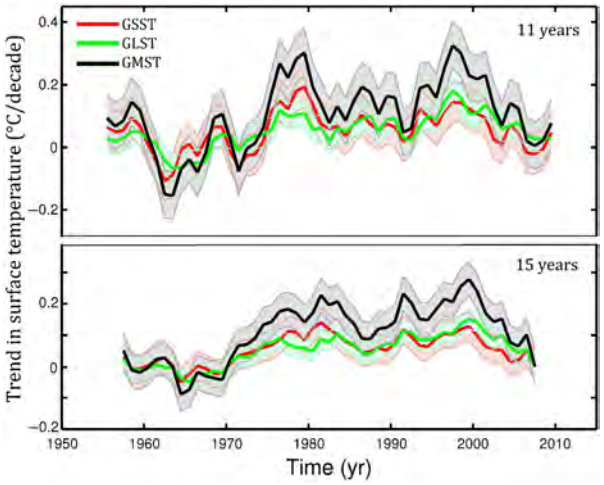

Figure 5. Upper panel: 11-year trends of GMST (black), GSST (green) and GLST (red). GSST and GLST are area weighted with respect to the total Earth' surface. Lower panel: same as for upper panel but for 15-year trends. [Colour figure can be viewed at wileyonlinelibrary.com].

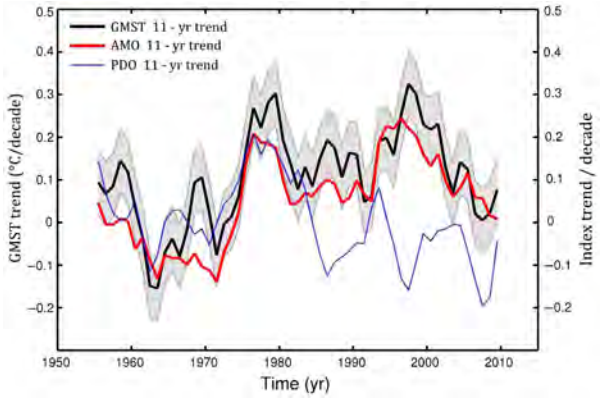

Figure 6. 11-year trends of GMST (black) and associated uncertainty (shaded black); AMO 11-year trends (red) and PDO 11-year trends (dashed blue). [Colour figure can be viewed at wileyonlinelibrary.com].

data while the lower panel uses the combined thermosteric data. It is interesting to see in Figure 7 the visible signature of major volcanic eruptions and ENSO events. Moreover, as previously noted by several authors (e.g. Adams *et al.*, 2003), some El Nino coincide with major volcanic eruptions (e.g. El Chichon in 1982 and Pinatubo in 1991).

In Figure 8 are superimposed the EBAF data at the TOA (noted CERES/TOA, see Section 2.5) as well as *d*(OHC)/*dt* derived from the GMSL minus ocean mass time series. The interannual variability of the CERES/TOA time series agrees rather well with *d*(OHC)/*dt* deduced from the GMSL minus ocean mass . Less agreement is noticed with the other steric data sets, especially around the years 2000–2001 (Smith *et al.*, 2015). Note that the CERES/TOA data are calibrated against Argo-based OHC, explaining why their mean value coincides well with the mean value of the *d*(OHC)/*dt* time series.

Estimating the mean Earth's energy imbalance from all data sets, we find over 2003–2013: 0.66 +/− 0.05 W m^{-2}, 0.68 +/− 0.11 W m^{-2} and 0.65 +/− 0.10 W m^{-2}

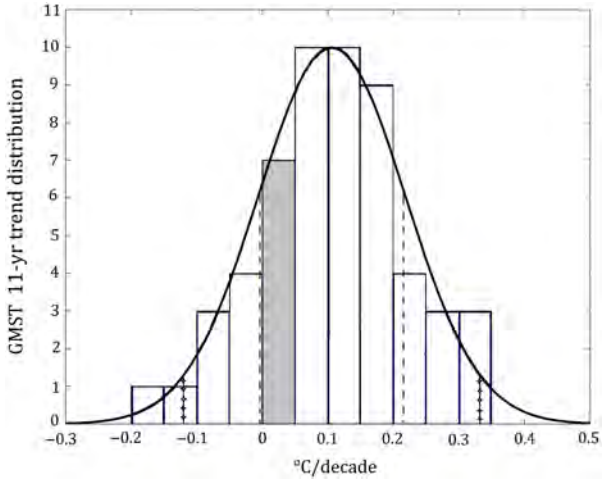

Figure 7. Histogram of GMST 11-year trends over 1950–2014. The solid curve is the Gaussian function fitting the data. The light grey bar includes the trend value of the 2003–2013 window. The vertical dashed/solid with stars lines correspond to one/two standard deviations (respectively 66 and 95% of the population). [Colour figure can be viewed at wileyonlinelibrary.com].

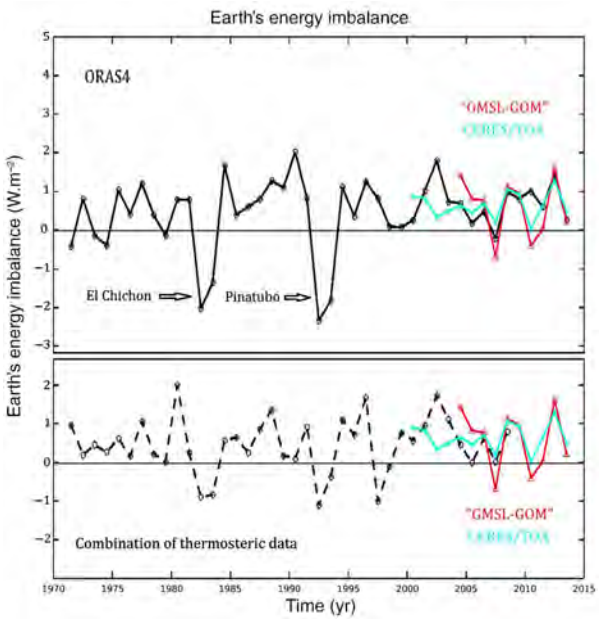

Figure 8. Net Earth's energy imbalance as a function of time computed from total ocean heat content time derivative from ORAS4 (0–5350 m) over 1970–2014 (upper panel; solid curve), and combination of different thermosteric data sets over 1970–2010 (lower panel; dashed curve). Blue and red curves correspond to CERES/TOA and GMSL minus ocean mass (labelled GMSL-GOM) data. [Colour figure can be viewed at wileyonlinelibrary.com].

for CERES/TOA (representing Argo-based $d(\mathrm{OHC})/dt$) and $d(\mathrm{OHC})/dt$ based on ORAS4 and GMSL minus ocean mass, respectively. Note that no errors are provided with the ORAS4 data set. For estimating the corresponding Earth's energy imbalance, we assumed that over 2003–2013, ORAS4 uncertainty can be approximated by Argo errors (see Dieng *et al.*, 2015a,2015b for details). The combined data set leads to a value of 0.5 +/− 0.1 W m^{-2} over 2003–2010. The agreement between all results is quite good, especially considering that these numbers are obtained with independent data sets. The above mean Earth's energy imbalance also agrees well with results reported in the literature (e.g. Allan *et al.*, 2014). Numbers are gathered in Table 2.

Use of Equation (1) assumes that neither $\Delta T(t)$ nor $N(t)$ contain internal variability signals. However as $\Delta T(t)$ is derived from the GMST yearly time series, short-term (interannual) GMST fluctuations likely reflect internal variability. The same comment applies when considering yearly $d(\mathrm{OHC})/dt$ data, thus $N(t)$. To minimize internal variability signals for further estimating the net radiative forcing term $F(t)$ from Equation (1), we apply a 15-year smoothing with 1-year overlap to both GMST and $d(\mathrm{OHC})/dt$ time series. Although this procedure does not fully remove internal variability (some low frequency signals in the unforced variability may remain; e.g. Crowley *et al.*, 2014), considering averages over periods > 10 years will reduce the importance of the unforced variability. In Figure 9 is shown corresponding GMST and $d(\mathrm{OHC})/dt$ (i.e. N) with 15-year smoothing. Only the ORAS4 dataset is shown. The period considered is 1970–2014 as in Figure 7. Thus the first date reported in Figure 9 for these 15-year averages is 1977.5 (middle of the 1970–1985 time span). Over the time span considered, both smoothed GMST and N increase with time. For N, multidecadal fluctuations are superimposed to the positive trend.

In Figure 9 is also plotted the evolution with time of the net radiative forcing term F (computed from Equation (1) above) using GMST and $d(\mathrm{OHC})/dt$ (based on ORAS4 for the latter) with 15-year smoothing. The climate sensitivity parameter S is highly uncertain (IPCC, 2013). Here we consider the whole range of values given in IPCC AR5 for 1/S (called climate feedback parameter): 0.82–2.47 W m^{-2} °C^{-1} (Church *et al.*, 2013). The shaded area around the F curve represents uncertainty on the 1/S parameter (in the calculation, 1/S is taken as the mid-value of the above

Table 2. Estimates of the Earth's energy imbalance in W m^{-2}, using different data sets (ORAS4 reanalysis, net flux at the TOA from CERES, sea level budget approach and combined in situ temperature data sets) (see Section 2 for details on data and methods).

Data type	Earth's energy imbalance (1970–2014) W m^{-2}	Earth's energy imbalance (2003–2013) W m^{-2}
ORAS4	0.45 ± 0.10	0.68 ± 0.11
CERES/TOA	----	0.66 ± 0.05
Sea level budget approach 'GMSL-GOM'	----	0.65 ± 0.10
Combined *in situ* data	0.45 ± 0.08 (1970–2010)	0.50 ± 0.10 (2003–2010)

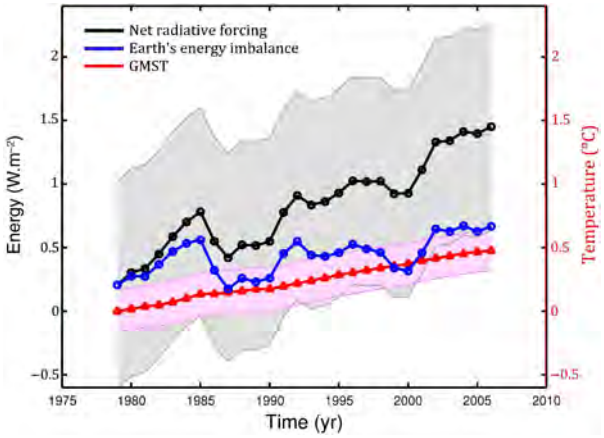

Figure 9. Net Earth's energy imbalance (blue), GMST (red) and net radiative forcing (black) as a function of time computed over successive 15-year long windows with 1-year overlap for the period 1970–2014. The grey shaded area represents net radiative forcing uncertainty. [Colour figure can be viewed at wileyonlinelibrary.com].

range and 2-σ uncertainty as the half range). Note that assumption of a constant climate sensitivity parameter over the whole study time span may not be a valid approach. Such an issue will require further investigation. Figure 9 indicates net radiative forcing increase with time over the last three decades, as expected considering the observed positive trends in both GMST and $d(\mathrm{OHC})/dt$. Besides, Figure 9 shows no evidence of radiative forcing decrease in the recent years.

5. Discussion

In this study, we have investigated the temporal evolution of SST and LST as a function of latitude and region. Our results for SST confirm significant cooling in the Pacific during the last decade. However, removing the tropical Pacific contribution to global mean GSST does not fully explain the recent temperature slowdown. LST variations as a function of latitude, show little positive trend over 2003–2013 in all regions. Our analysis confirms previous studies, i.e. the GMST has increased less rapidly during the years 2000s than during the previous three decades. But what we show here is that this behaviour is not only due to cooling of east the tropical Pacific. Short-term trends in GMST computed since 1950 over successive 11-year windows (with 1-year overlap) display important interannual/decadal fluctuations, highly correlated with 11-year trends of the AMO index. The two trend curves are suggestive of a 60-year periodicity. Besides, the GMST 11-year trends follow a quasi-Gaussian distribution around the median value. These findings strongly suggest that the observed GMST trend fluctuations reflect internal climate variability rather than forced signal. The low GMST trend reported during 2003–2013 is thus likely not exceptional but just a manifestation of the unforced variability, as previously suggested (e.g. Lewandowsky *et al.*, 2016). However, our analysis also shows that GMST is steadily increasing if we filter out most of the internal climate variability signal, in accordance with a positive imbalance and increasing net radiative forcing.

We computed the time derivative of the total OHC from three different data sets, i.e. results from an ocean reanalysis, a combination of full-depth *in situ* ocean temperature data and GMSL corrected for ocean mass. The time derivative of the total OHC was used as a proxy of the net Earth energy imbalance. For the 2003–2013 time span, the Earth energy imbalance amounts to 0.68 +/− 0.08 W m^{-2} when using the ORAS4 reanalysis. Such values agree well with estimates by Roemmich *et al.* (2015) based on Argo data over 2006–2013. A value of 0.65 +/− 0.08 W m^{-2} is found when using the GMSL minus ocean mass. These estimates based on different methods are a robust indication that the planet continues to be in a state of a positive radiative imbalance. Finally, we computed the net radiative forcing over the past three decades after smoothing all data sets over 15-year long windows (with 1-year overlap). Our results reveal no evidence of net radiative forcing decrease in the recent years (Figure 9). On the contrary, years 2000s show the highest values over the studied period. Besides, although the global mean Earth temperature has increased less rapidly during the past decade compared to previous decades, the 15-year GMST average (2000–2014) appears as the highest value since 1980 (Figure 9). Finally, as discussed in previous studies (e.g. Llovel *et al.*, 2014, von Schuckmann *et al.*, 2014, 2016), the so-called pause in global warming or 'hiatus' attributed to a single climate component (the Earth's GMST) by no means reflects a pause in the accumulation of heat in the climate system, implying that GMST may not be the best indicator of global warming.

Acknowledgements

We thank Don Chambers as well as two other anonymous reviewers for their comments that greatly helped us to improve our manuscript.

H.B.D and H. P. are supported respectively by a grant of the European Space Agency in the context of the "Climate Change Initiative" Program and a Centre National d'Etudes Spatiales-Collecte Localisation Satellites (CNES-CLS) PhD grant. We thank A. Melet for providing us with the combined steric data set.

References

Adams JB, Michael E, Mann ME, Ammann CM. 2003. Proxy evidence for an El Niño-like response to volcanic forcing. *Nature* **426**: 274–278.

Allan RP, Liu C, Loeb NG, Palmer MD, Roberts M, Smith D, Vidale PL. 2014. Changes in global net radiative imbalance 1985–2012. *Geophys. Res. Lett.* **41**: 5588–5597.

Balmaseda MA, Trenberth K, Kallen E. 2013a. Distinctive climate signals in reanalysis of global ocean heat content. *Geophys. Res. Lett.* **40**: 1–6.

Balmaseda MA, Mogensen K, Weaver AT. 2013b. Evaluation of the ECMWF ocean reanalysis system ORAS4. *Q. J. R. Meteorol. Soc.* **139**: 1132–1161.

Barnett TP, Pierce DW, Latif M, Dommenget D, Saravanan R. 1999. Interdecadal interactions between the tropics and midlatitudes in the Pacific basin. *Geophys. Res. Lett.* **26**: 615–618.

Bevington PR, Robinson DK. 1969. *Data Reduction and Error Analysis for the Physical Sciences*. McGraw Hill. ISBN: 0-07 247227-8.
Boyin H, Banzon VF, Freeman E, Lawrimore J, Liu W, Peterson TC, Smith TM, Thorne PW, Woodruff SD, Zhang HM. 2015. Extended reconstructed sea surface temperature version 4 (ERSST.v4) part I: upgrades and intercomparisons. *J. Clim.* **28**: 911–930.
Brown PT, Wenhong L, Li L, Ming Y. 2014. Top-of-atmosphere radiative contribution to unforced decadal global temperature variability in climate models. *Geophys. Res. Let.* **41**: 5175–5183, doi: 10.1002/2014GL060625.
Cahill N, Rahmstorf S, Parnell AC. 2015. Change points of global temperature. *Environ. Res. Lett.* **10**(2015): 084002, doi: 10.1088/1748-9326/10/8/084002.
Chambers D, Bonin JA. 2012. Evaluation of Release-05 GRACE time variable gravity coefficients over the ocean. *Ocean Sci.* **8**: 1–10.
Chambers D, Merrifield MA, Nerem RS. 2012. Is there a 60-year oscillation in global mean sea level. *Geophys. Res. Lett.* **39**: L18607.
Chen X, Tung KK. 2014. Varying planetary heat sink led to global warming slowdown and acceleration. *Science* **345**: 897–903.
Cheng L, Zheng F, Zhu J. 2015. Distinctive interior changes during the recent warming slowdown. *Sci. Rep.* **5**: 14346.
Church JA, Clark PU, Cazenave A, Gregory JM, Jevrejeva S, Levermann A, Merrifield MA, Milne GA, Nerem RS, Nunn PD, Payne AJ, Pfeffer WT, Stammer D, Unnikrishnan AS. 2013. Sea level change. In *Climate Change 2013: The Physical Science Basis. Contribution of Working Group I to the Fifth Assessment Report of the Intergovernmental Panel on Climate Change*, Stocker TF, Qin D, Plattner G-K, Tignor M, Allen SK, Boschung J, Nauels A, Xia Y, Bex V, Midgley PM (eds). Cambridge University Press: Cambridge, UK and New York, NY.
Cowtan K, Way RG. 2014. Coverage bias in the HadCRUT4 temperature series and its impact on recent temperature trends. *Q. J. R. Meteorol. Soc.* **140**: 1935–1944.
Crowley TJ, Obrochta SP, Liu J. 2014. Recent global temperature "plateau" in the context of a new proxy reconstruction. *Earths Future* **2**: 281–294.
Dieng HB, Palanisamy H, Cazenave A, Meyssignac B, von Schuckmann K. 2015a. The sea level budget since 2003: inference on the deep ocean heat content. *Surv. Geophys.* **36**: 209–229.
Dieng HB, Cazenave A, von Shuckmann K, Ablain M, Meyssignac B. 2015b. Sea level budget over 2005–2013: missing contributions and data errors. *Ocean Sci.* **11**: 789–802.
Dieng HB, Champollion N, Cazenave A, Wada Y, Schrama E, Meyssignac B. 2015c. Total land water storage change over 2003–2013 estimated from a global mass budget approach. *Environ. Res. Lett.* **10**: 124010, doi: 10.1088/1748-9326/10/12/124010.
Domingues CM, Church JA, White NJ, Gleckler PJ, Wijffels SE, Barker PM, Dunn JR. 2008. *Improved estimates of upper-ocean warming and multi-decadal sea-level rise Nature* **453**: 1090–1093.
Enfield DB, Mestas-Nunez AM, Trimble PJ. 2001. The Atlantic Multidecadal Oscillation and its relationship to rainfall and river flows in the continental U.S. *Geophys. Res. Lett.* **28**: 2077–2080.
England MH, McGregor S, Spence P, Meehl GA, Timmermann A, Cai W, Gupta AS, McPhaden MJ, Purich A, Santoso A. 2014. Recent intensification of wind-driven circulation in the pacific and the ongoing warming hiatus. *Nat. Clim. Change* **4**: 222–227.
Fan Y, van den Dool H. 2008. A global monthly land surface air temperature analysis for 1948-present. *J. Geophys. Res.* **113**: D01103.
Flato GJ, Marotzke B, Abiodun P, Braconnot SC, Chou W, Collins P, Cox F, Driouech S, Emori V, Eyring C, Forest P, Gleckler E, Guilyardi C, Jakob V, Reason C, Rummukainen M. 2013. Evaluation of climate models. In *Climate Change 2013: The Physical Science Basis. Contribution of Working Group I to the Fifth Assessment Report of the Intergovernmental Panel on Climate Change*, Stocker TF, Qin D, Plattner G-K, Tignor M, Allen SK, Boschung J, Nauels A, Xia Y, Bex V, Midgley PM (eds). Cambridge University Press: Cambridge, UK and New York, NY.
Foster G, Abraham J. 2015. *US Clivar Variations* **13**(3): 6–10.
Fyfe JC, Meehl GA, England MH, Mann ME, Santer BD, Flato GM, Hawkins E, Gillett NP, Xie SP, Kosaka Y, Swart NC. 2016. Making sense in the early-2000s warming slowdown. *Nat. Clim. Change* **6**: 224–228.
Goddard L. 2014. Heat hide and seek. *Nat. Clim. Change* **4**: 158161.
Guemas V, Doblas-Reyes FJ, Andreu-Burillo I, Asif M. 2014. Retrospective prediction of global warming slowdown in the past decade. *Nat. Clim. Change* **3**: 649–653.
Hansen J, Ruedy R, Sato M, Lo K. 2010. Global surface temperature change. *Rev. Geophys.* **48**: RG4004.
Hansen J, Sato M, Kharecha P, von Schuckmann K. 2011. Earth's energy imbalance andimplications. *Atmos. Chem. Phys.* **11**: 13421–13449.
Hegerl GC, Zwiers FW, Braconnot P, Gillett NP, Luo Y, Marengo Orsini JA, Nicholls N, Penner JE, Stott PA. 2007. Understanding and Attributing Climate Change. In *Climate Change 2007: The Physical Science Basis. Contribution of Working Group I to the Fourth Assessment Report of the Intergovernmental Panel on Climate Change*, Solomon S, Qin D, Manning M, Chen Z, Marquis M, Averyt KB, Tignor M, Miller HL (eds). Cambridge University Press: Cambridge, UK and New York, NY.
Held IM. 2013. The cause of the pause. *Nature* **501**: 318–319.
IPCC. 2013. *Climate Change 2013: The Physical Science Basis. Contribution of Working Group I to the Fifth Assessment Report of the Intergovernmental Panel on Climate Change*, Stocker TF, Qin D, Plattner G-K, Tignor M, Allen SK, Boschung J, Nauels A, Xia Y, Bex V, Midgley PM (eds). Cambridge University Press: Cambridge, UK and New York, NY.
Ishii M, Kimoto M. 2009. Reevaluation of historical ocean heat content variations with time-varying XBT and MBT depth bias corrections. *J. Oceanogr.* **65**(3): 287–299.
Ishii M, Shouji A, Sugimoto S, Matsumoto T. 2005. Objective analyses of sea-surface temperature and marine meteorological variables for the 20th century using ICOADS and the Kobe collection. *Int. J. Climatol.* **25**: 865–879.
Japan Meteorological Agency 2006. Characteristics of Global Sea Surface Temperature Analysis Data (COBE-SST) for climate use. Monthly Report on Climate System Separated Volume 12, 116pp.
Kaplan A, Cane M, Kushnir Y, Clement A, Blumenthal M, Rajagopalan B. 1998. Analyses of global sea surface temperature 1856–1991. *J. Geophys. Res.* **103**(18): 567–589.
Karl TR, Arguez A, Huang B, Lawrimore JH, McMahon JR, Menne MJ, Peterson TC, Vose RS, Zhang H. 2015. Possible artifacts of data biases in the recent global surface warming hiatus. *Science* **348**(6242): 1469–1472.
Kennedy JJ, Rayner NA, Smith RO, Saunby M, Parker DE. 2011. Reassessing biases and other uncertainties in sea-surface temperature observations since 1850 part 1: measurement and sampling errors. *J. Geophys. Res.* **116**: D14103.
Kirkup L. 1994. *'Experimental Methods. An Introduction to the Analysis and Presentation of Data*. Wiley. ISBN: 978-0-471-33579-5.
Kosaka Y, Xie S-P. 2013. Recent global warming hiatus tied to equatorial Pacific surface cooling. *Nature* **501**: 403–407.
Kuhlbrodt T, Gregory JM. 2012. Ocean heat uptake and its consequence for the magnitude of sea level rise and climate change. *Geophys. Res. Lett.* **39**: L18608.
Levitus S, Antonov J, Boyer T. 2005. Warming of the world ocean, 1955–2003. *Geophys. Res. Lett.* **32**: L02604.
Levitus S et al. 2009. Global ocean heat content 1955–2008 in light of recently revealed instrumentation problems. *Geophys Res. Lett.* **36**: L07608.
Levitus S, Antonov JI, Boyer TP, Baranova OK, Garcia HE, Locarnini RA, Mishonov AV, Reagan JR, Seidov D, Yarosh ES, Zweng MM. 2012. World ocean heat content and thermosteric sea level change (0–2000 m), 1955–2010. *Geophys. Res. Lett.* **39**: L10603.
Lewandowsky S, Risbey JS, Oreskes N. 2015. On the definition and identifiability of the alleged "hiatus" in global warming. *Sci. Rep.* **5**: 16784.
Lewandowsky S, Risbey JS, Oreskes N. 2016. The pause in global warming: Turning a routine fluctuation into a problem for science. *Am. Meteorol. Soc.* **97**(5): 723–733, doi: 10.1175/BAMS-D-14-00106.1.
Llovel W, Willis JK, Landerer FW, Fukumori I. 2014. Deep-ocean contribution to sea level and energy budget not detectable over the past decade. *Nat. Clim. Change* **4**: 1031–1035, doi: 10.1038/NCLIMATE2387.
Loeb NG, Lyman JM, Johnson GC, Allan RP, Doelling DR, Wong T, Soden BJ, Stephens GL. 2012a. Observed changes in top-of-the-atmosphere radiation and upper-ocean heating consistent within uncertainty. *Nat. Geosci.* **5**: 110–113.
Loeb NG, Kato S, Su WY, Wong TM, Rose FG, Doelling DR, Huang XL. 2012b. Advances in understanding top-of-atmosphere radiation variability from satellite observations. *Surv. Geophys.* **33**: 359–385.
Meehl GA, Arblaster JM, Fasullo JT, Hu A, Trenberth KE. 2011. Model based evidence of deep-ocean heat uptake during surface-temperature hiatus periods. *Nat. Clim. Change* **1**: 360–364.
Melet A, Meyssignac B. 2015. Explaining the spread in global mean thermosteric sea level rise. *J. Clim.* **28**: 9918–9940.

Nieves V, Willis JK, Patzert WC. 2015. Recent hiatus caused by decadal shift in Indo-Pacific heating. *Science* **349**(6247): 532–535.
Osborn TJ, Jones PD. 2014. The CRUTEM4 land-surface air temperature dataset: construction, previous versions and dissemination via Google Earth. *Earth System Sci. Data* **6**: 61–68.
Palmer MD, Mc Neal DJ. 2014. Internal variability of Earth's energy budget simulated by CMIP5 climate models. *Environ. Res. Lett.* **9**: 034016.
Peters GP, Marland G, Le Quere´ C, Boden T, Canadell JG, Raupach MR. 2012. Rapid growth in CO2 emissions after the 2008–2009 global financial crisis. *Nat. Clim. Change* **2**: 2–4.
Purkey S, Johnson GC. 2010. Warming of global abyssal and deep southern ocean waters between the 1990s and 2000s: contributions to global heat and sea level rise budget. *J. Clim.* **23**: 6336–6351.
Roemmich D, Church J, Gilson J, Monselesan D, Sutton P, Wijffels S. 2015. Unabated planetary warming and its ocean structure since 2006. *Nat. Clim. Change* **5**: 240–245.
Smith D. 2013. Has global warming stalled? *Nat. Clim. Change* **3**: 618–619.
Smith DM, Reynolds RW, Peterson TC, Lawrimore J. 2008. Improvements to NOAA's historical merged land-ocean surface temperature analysis (1880-2006). *J. Clim.* **21**: 2283–2293.
Smith DM, Allan RP, Coward AC, Eade R, Hyder P, Liu C, Loeb N, Palmer MD, Roberts CD, Scaife AA. 2015. Earth's energy imbalance since 1960 in observations and CMIP5 models. *Geophys. Res. Lett.* **42**: 1205–1213.
Trenberth KE. 2015. Has there been a hiatus? *Science* **349**: 691–692.
Trenberth KE, Fasullo JT. 2010. Tracking Earth's energy. *Science* **328**: 316–317.
Trenberth KE, Fasullo JT. 2013. An apparent hiatus in global warming? *Earths Future* **1**: 19–32.
Trenberth KE, Fasullo JT, Balmaseda MA. 2014. Earth's Energy imbalance. *J. Clim.* **27**: 3129–3144.
Von Schuckmann K, Sallée JB, Chambers D, Le Traon PY, Cabanes C, Gaillard C, Speich S, Hamon M. 2014. Consistency of the current global ocean observing systems from an Argo perspective. *Ocean Sci.* **10**: 547–557.
Von Schuckmann K, Palmer MD, Trenberth KE, Cazenave A, Chambers D, Champollion N et al. 2016. Earth's energy imbalance: an imperative for monitoring. *Nat. Clim. Change* **26**: 138–144.
Watanabe M, Kamae Y, Yoshimori M, Oka A, Sato M, Ishii M, Mochizuki T, Kimoto M. 2013. Strengthening of ocean heat uptake efficiency associated with the recent climate hiatus. *Geophys. Res. Lett.* **40**: 3175–3179.
Woodruff SD, Worley SJ, Sandra J, Lubker SJ, Ji Z, Freeman JE, Berry DI, Brohan P, Kent EC, Reynolds RW, Wilkinson C. 2011. ICOADS Release 2.5: extensions and enhancements to the surface marine meteorological archive. *Int. J. Climatol.* **31**: 951–967.

4.3 La hausse du niveau moyen global de la mer (GMSL) durant les années 2000

Comme montré dans le chapitre 2, le GMSL observé par altimétrie a augmenté à une vitesse de 3.3 mm/an depuis le début des années 1990. Cependant, au cours de la décennie 2001-2011, un ralentissement de ~30% de la vitesse du GMSL a été observé (*Hansen et al.* 2011 ; *Chen et al.* 2013), coïncidant avec la pause de l'évolution de la GMST (voir section précédente). Le niveau de la mer, en plus du réchauffement climatique anthropique répond également à la variabilité naturelle du climat. Dans le *chapitre 3* précédent, nous avions noté des fluctuations interannuelles du GMSL principalement causées par le phénomène ENSO (variabilité climatique naturelle interne) qui impact le cycle de l'eau.

Cette réduction de la vitesse du GMSL sur la dernière décennie a motivé la présente étude : *Cazenave A., Dieng H. B.,* et al. (2014) résumé ci dessous.

Résumé de l'article : " The rate of sea-level rise " *(l'article original est inséré à la fin de cette section 4.3)*

L'objectif principal de cette étude a été d'identifier les causes du ralentissement de la vitesse de hausse du GMSL sur la période 2003-2011, et d'estimer l'impact de la variabilité naturelle du climat (principalement ENSO) sur l'estimation de la tendance du GMSL. Pour cela, nous avons essayé de répondre aux questions suivantes : observe-t-on réellement un ralentissement de la vitesse du GMSL sur la période 2003-2011 ? La succession des épisodes La Niña sur la dernière décennie est-elle suffisante pour expliquer le ralentissement de la vitesse du GMSL si celle-ci est confirmée ? Si l'on soustrait les fluctuations naturelles du niveau de la mer principalement causées par les épisodes La Niña sur la période 2003-2011, le GMSL augmente-t-il comme au cours de la décennie précédente ?

Dans cette étude, nous avons analysé la tendance du GMSL de 5 groupes traitant les données altimétriques (AVISO, CU, NOAA, GSFC et CCI ; voir la *section 2.1* du *chapitre 2*) sur deux périodes distinctes 1994-2002 et 2003-2011. La tendance moyenne des 5 produits de GMSL sur les périodes 1994-2002 et 2003-2011 est estimée à 3.5 ± 0.4 mm/an et 2.4 ± 0.4 mm/an respectivement. Sur la période 2003-2011, la tendance du GMSL est significativement plus faible que durant la période 1994-2002. Ceci est observé avec tous les produits GMSL des 5 groupes ci-dessus. Nous avons aussi analysé l'évolution de la tendance quinquennale des 5 séries temporelles du GMSL (calculée sur les fenêtres mobiles de 5 ans à partir de 1994 et décalées de 1 an ; exemple 1994-1998, 1995-1999, ..., 2007-2011) sur la période 1994-2011. Une diminution de 30% de la tendance est observée à partir de 2003 et ceci avec tous les 5 produits GMSL. Ces

résultats montrent que le ralentissement de la vitesse du GMSL est bien réel, depuis le début des années 2000 en comparaison aux années 1990.

La deuxième partie de l'étude a consisté à soustraire des séries temporelles du GMSL, la variabilité interannuelle de la masse de l'océan et du niveau de la mer stérique sur la période 1994-2011. Pour estimer la variabilité de la masse de l'océan deux approches sont utilisées : *(1)* estimation des fluctuations interannuelles de la somme "stock d'eau total des continents + glace continentale + vapeur d'eau atmosphérique" ; et *(2)* estimation directe de la variabilité interannuelle de la masse océanique globale par GRACE (disponible à partir de 2003). Il faut noter que les glaces continentales affichent également de la variabilité interannuelle (*Church et al.* 2013). Toutefois, les données nécessaires pour la quantifier de manière globale et sur toute la période altimétrique font défaut actuellement. Pour estimer le stock d'eau des continents, la vapeur d'eau atmosphérique et la composante stérique du niveau de la mer (0-700m), nous avons utilisé respectivement les données du modèle hydrologique global ISBA/TRIP développé par Météo-France (*Alkama et al.* 2010), les données de la réanalyse atmosphérique ERAInterim et les données de *Ishii and Kimoto* (2009) version V.6.13. Pour plus de détails sur ces données, voir *Cazenave et al.* (2014) inséré à la fin de cette section. Nous constatons qu'après correction de la variabilité interannuelle (du stock d'eau des continents, de la vapeur d'eau atmosphérique et du niveau de la mer stérique), le ralentissement du GMSL sur la période 2003-2011 disparaît. On estime la hausse du GMSL à 3.3 ± 0.4 mm/an, soit une valeur similaire sur les 2 périodes de l'ère altimétrique (1994-2002 et 2003-2011).

Pour valider nos résultats, nous avons utilisé (dans la partie "Information Supplémentaire") 3 cas pour supprimer la variabilité interannuelle naturelle du GMSL. Pour les données stériques nous avons utilisé les données de Ishii et Kimoto, complétées à partir de 2005 par Argo (0-1500m ; voir *section 2.2.1* du *chapitre 2*). Nous avons remplacé à partir de janvier 2003 la composante de masse "stock d'eau des continents + vapeur d'eau atmosphérique" par la variabilité interannuelle de la masse de l'océan basée sur GRACE : (cas 1) données CSR traitées par *D. Chambers* (voir la *section 2.2.2* dans le *chapitre 2*), (cas 2) données GRGS (voir *Dieng et al. 2014* résumé et inséré dans le *chapitre 3*) et (cas 3) données GRACE sur les continents (fournissant la composante "eaux terrestres"). Les 3 cas confirment bien la disparition du ralentissement de la vitesse du GMSL après correction de la variabilité interannuelle sur la période 2003-2011.

Nous avons ensuite analysé l'évolution de la tendance du GMSL corrigé de la variabilité interannuelle (sur des fenêtres mobiles de cinq ans) comme précédemment. Le ralentissement de la vitesse du GMSL observé au début des années 2000 disparaît dans tous les cas. Ce résultat montre que, lorsque nous retirons de la série temporelle du GMSL, la variabilité interannuelle, il

n'y a pas de différence de hausse du GMSL entre les décennies 1990 et 2000. En d'autres termes, la hausse du GMSL est presque linéaire au cours des 20 dernières années.

Dans le chapitre précédent, nous avions noté une succession d'épisodes La Niña depuis le début des années 2000, ce qui conduit à des anomalies temporaires négatives de plusieurs millimètres dans le GMSL. C'est le cas notamment de La Niña (2010-2011), la plus intense des années récentes.

En conclusion, notre étude montre que le ralentissement du GMSL au cours des années 2000 est dû à la variabilité naturelle interne du climat (principalement des épisodes La Nina) en raison des échanges d'eau entre les océans, l'atmosphère et les continents, avec une moindre contribution du niveau de la mer stérique. Nous mettons en évidence (comme dans la *section 4.2* précédente), le rôle de la variabilité naturelle à court terme sur les changements à plus long terme associés au réchauffement climatique anthropique. Nos résultats confirment la nécessité de quantifier et de retirer la variabilité naturelle interne du climat si l'on veut estimer l'impact du réchauffement climatique sur le niveau de la mer sur une courte période. Bien qu'il ait été suggéré que plusieurs décennies de mesure altimétrique soient nécessaires pour isoler le signal du réchauffement climatique global (*Leuliette and Willis,* 2011), nos résultats montrent également que cela est déjà possible en retirant la variabilité interannuelle (principalement causée par ENSO), une procédure qui améliore le rapport signal-bruit, comme montré par *Foster and Rahmstorf*, (2011) pour l'évolution de la GMST.

nature climate change

LETTERS

PUBLISHED ONLINE: 23 MARCH 2014 | DOI: 10.1038/NCLIMATE2159

The rate of sea-level rise

Anny Cazenave[1]*, Habib-Boubacar Dieng[1], Benoit Meyssignac[1], Karina von Schuckmann[2], Bertrand Decharme[3] and Etienne Berthier[1]

Present-day sea-level rise is a major indicator of climate change[1]. Since the early 1990s, sea level rose at a mean rate of ∼3.1 mm yr^{-1} (refs 2,3). However, over the last decade a slowdown of this rate, of about 30%, has been recorded[4–8]. It coincides with a plateau in Earth's mean surface temperature evolution, known as the recent pause in warming[1,9–12]. Here we present an analysis based on sea-level data from the altimetry record of the past ∼20 years that separates interannual natural variability in sea level from the longer-term change probably related to anthropogenic global warming. The most prominent signature in the global mean sea level interannual variability is caused by El Niño–Southern Oscillation, through its impact on the global water cycle[13–16]. We find that when correcting for interannual variability, the past decade's slowdown of the global mean sea level disappears, leading to a similar rate of sea-level rise (of 3.3 ± 0.4 mm yr^{-1}) during the first and second decade of the altimetry era. Our results confirm the need for quantifying and further removing from the climate records the short-term natural climate variability if one wants to extract the global warming signal[10].

Precisely estimating present-day sea-level rise caused by anthropogenic global warming is a major issue that allows assessment of the process-based models developed for projecting future sea level[1]. Sea-level rise is indeed one of the most threatening consequences of ongoing global warming, in particular for low-lying coastal areas that are expected to become more vulnerable to flooding and land loss. As these areas often have dense populations, important infrastructures and high-value agricultural and bio-diverse land, significant impacts such as increasingly costly flooding or loss of freshwater supply are expected, posing a risk to stability and security[17,18]. However, sea level also responds to natural climate variability, producing noise in the record that hampers detection of the global warming signal. Trends of the satellite altimetry-based global mean sea level (GMSL) are computed over two periods: the period 1994–2002 and the period 2003–2011 of the observed slowdown (Fig. 1a). GMSL time series from five prominent groups processing satellite altimetry data for the global ocean are considered (Methods). During recent years (2003–2011), the GMSL rate was significantly lower than during the 1990s (average of 2.4 mm yr^{-1} versus 3.5 mm yr^{-1}). This is observed by all processing groups (Fig. 1a). The temporal evolution of the GMSL rate (computed over five-year-long moving windows, starting in 1994 and shifted by one year) was nearly constant during the 1990s, whereas the rate clearly decreased by ∼30% after ∼2003 (Fig. 2a). This decreasing GMSL rate coincides with the pause observed over the last decade in the rate of Earth's global mean surface temperature increase[9,10], an observation exploited by climate sceptics to refute global warming and its attribution to a steadily rising rate of greenhouse gases in the atmosphere. It has been suggested that this so-called global warming hiatus[11] results from El Niño–Southern Oscillation- (ENSO-) related natural variability of the climate system[10] and is tied to La Niña-related cooling of the equatorial Pacific surface[11,12]. In effect, following the major El Niño of 1997/1998, the past decade has favoured La Niña episodes (that is, ENSO cold phases, reported as sometimes more frequent and more intensive than the warm El Niño events, a sign of ENSO asymmetry[19]). The interannual (that is, detrended) GMSL record of the altimetry era seems to be closely related to ENSO, with positive/negative sea-level anomalies observed during El Niño/La Niña events[2]. Recent studies have shown that the short-term fluctuations in the altimetry-based GMSL are mainly due to variations in global land water storage (mostly in the tropics), with a tendency for land water deficit (and temporary increase of the GMSL) during El Niño events[13,14] and the opposite during La Niña[15,16]. This directly results from rainfall excess over tropical oceans (mostly the Pacific Ocean) and rainfall deficit over land (mostly the tropics) during an El Niño[20] event. The opposite situation prevails during La Niña. The succession of La Niña episodes during recent years has led to temporary negative anomalies of several millimetres in the GMSL (ref. 15), possibly causing the apparent reduction of the GMSL rate of the past decade. This reduction has motivated the present study. From seasonal to centennial time scales, the two main contributions to GMSL variability and change come from ocean thermal expansion and ocean mass. Owing to water mass conservation in the climate system, sources of global ocean mass variations are land ice masses, land water storage and atmospheric water vapour content. Studies have shown that ENSO-driven interannual variability in the global water cycle strongly impacts land water storage[12–15] and atmospheric water vapour[21], hence ocean mass and GMSL. Here, we quantitatively estimate these interannual water mass contributions and remove them from the altimetry-based GMSL record, to isolate the longer-term signal caused by global warming (here, interannual refers to a temporal window in the range of one to five years, mainly ENSO-related, but not exclusively). To do this, two approaches are possible: estimate interannual land water storage plus atmospheric water vapour contributions; or directly estimate the interannual variability in global ocean mass. The Gravity Recovery and Climate Experiment (GRACE) space mission directly measures ocean mass and land water storage variations but only since ∼2003. Before GRACE, neither ocean mass nor land water storage variations can be directly computed from observations. However, the use of hydrological models developed for climate studies and water resource monitoring[22] allows us to

[1]Laboratoire d'Etudes en Géophysique et Océanographie Spatiales, 18 avenue E. Belin, 31400 Toulouse, France, [2]Mediterranean Institute of Oceanography, avenue de l'Université, 83957 La Grade, France, [3]Centre National de Recherches Météorologiques, MétéoFrance, 42 avenue G. Coriolis, 31100 Toulouse, France. *e-mail: anny.cazenave@legos.obs-mip.fr

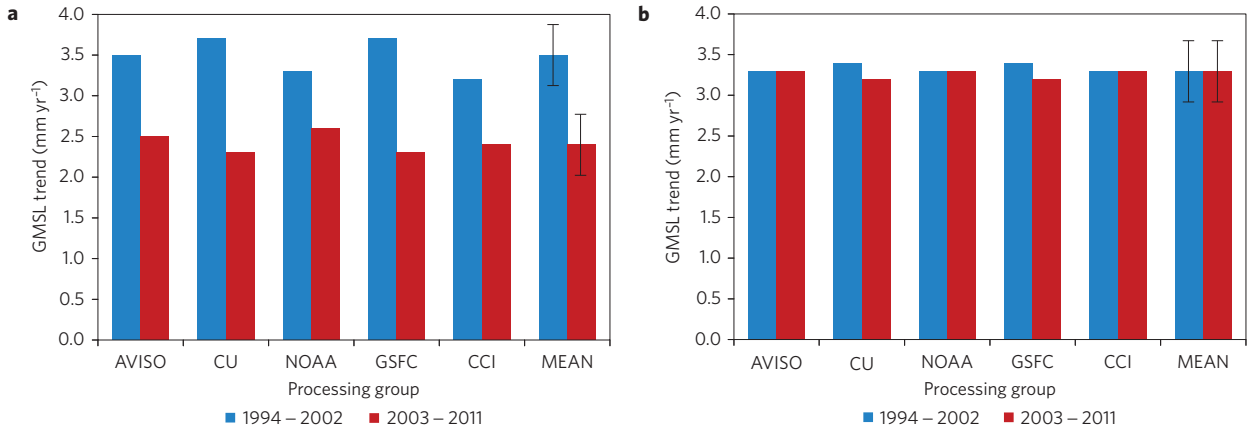

Figure 1 | GMSL trends during the 1994–2002 and 2003–2011 periods. a, GMSL trends computed over two time spans (January 1994–December 2002 and January 2003–December 2011) using satellite altimetry data from five processing groups (see Methods for data sources). The mean GMSL trend (average of the five data sets) is also shown. **b**, Same as **a** but after correcting the GMSL for the mass and thermosteric interannual variability (nominal case). Corrected means that the interannual variability due to the water cycle and thermal expansion are quantitatively removed from each original GMSL time series using data as described in the text. Black vertical bars represent the 0.4 mm yr^{-1} uncertainty (ref. 2).

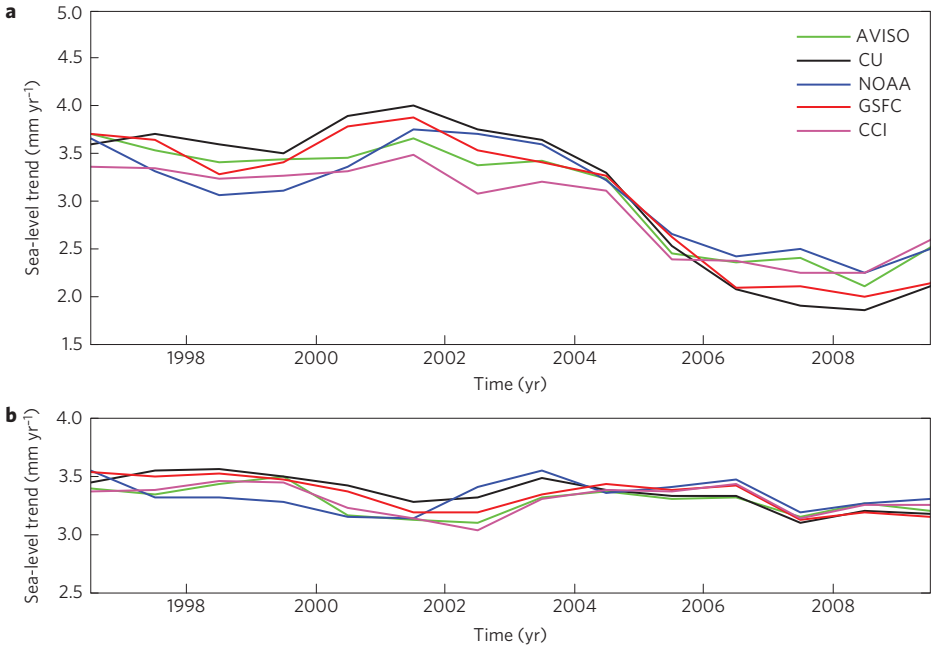

Figure 2 | GMSL rate over five-year-long moving windows. a, Temporal evolution of the GMSL rate computed over five-year-long moving windows shifted by one year (start date: 1994). **b**, Temporal evolution of the corrected GMSL rate (nominal case) computed over five-year-long moving windows shifted by one year (start date: 1994). GMSL data from each of the five processing groups are shown.

estimate the land water contribution since the beginning of the high-precision altimetry record. Both approaches are considered here. As a nominal case, we estimate the interannual land water contribution from a hydrological model (accounting for the atmospheric water vapour component) over the whole analysis time span (1994–2011). We also present as Supplementary Information three hybrid cases where the mass component is estimated as in the nominal case over 1994–2002 but replaced by GRACE data as of 2003. Data and models used to obtain the mass component are presented in the Methods and Supplementary Information. Detrended altimetry-based GMSL records and interannual mass components over the January 1994–December 2011 time span are shown in Fig. 3 (nominal case) and Supplementary Fig. 3 (hybrid case 1; in the following, figures shown as Supplementary Information correspond to hybrid case 1). As illustrated in Fig. 3 and Supplementary Fig. 3, the interannual GMSL signal mainly (but not exclusively) results from ENSO-driven water mass redistributions among the climate system reservoirs, with strong positive and negative GMSL anomalies during the 1997/1998 El Niño and 2011 La Niña, respectively. This raises two questions: what is the impact of ENSO-related (or, more generally, interannual) variability on the estimation of the GMSL trend; and can we separate the interannual natural variability from the longer-term global warming trend in the GMSL record?

To answer these questions we subtracted the interannual mass and thermosteric components from the GMSL record. Although the short-term GMSL fluctuations are mostly related to the global water cycle (Fig. 3 and Supplementary Fig. 3), thermal expansion also slightly contributes. Thus we also removed short-term variations in thermal expansion from the GMSL record (see Methods for information about the ocean temperature data used to

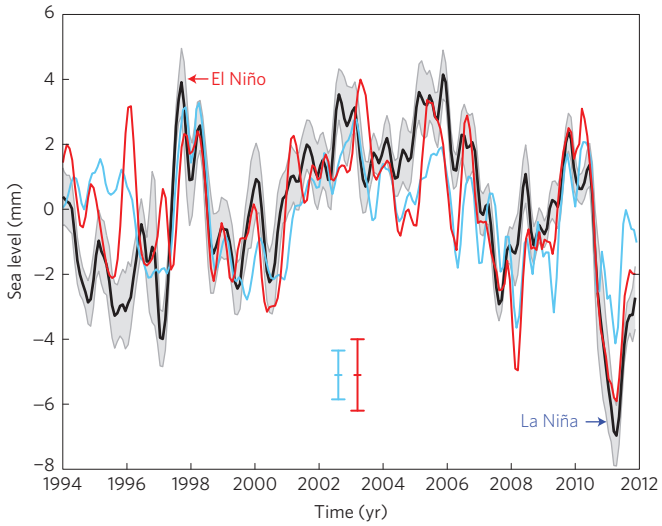

Figure 3 | Detrended GMSL, interannual mass and 'mass plus thermosteric' components. Black curve: mean detrended GMSL time series (average of the five satellite altimetry data sets) from January 1994–December 2011 and associated uncertainty (in grey; based on the dispersion of each time series around the mean). Light blue curve: interannual mass component based on the ISBA/TRIP hydrological model for land water storage plus atmospheric water vapour component over January 1994–December 2011. The red curve is the sum of the interannual mass and thermosteric components. This is the signal removed from the original GMSL time series (nominal case). Vertical bars represent the uncertainty of the monthly mass estimate (of 1.5 mm; refs 22,30; light blue bar) and monthly total contribution (mass plus thermosteric components; of 2.2 mm; refs 22,28–30; red bar).

compute thermal expansion and procedure applied to extract the corresponding interannual signal). Note that land ice also displays interannual mass variability[1]. However, adequate data to quantify it globally and for the whole altimetry period are presently lacking. The sum of interannual mass plus thermosteric components is also shown in Fig. 3 and Supplementary Fig. 3, for both nominal and hybrid case 1. It is this signal that is removed from the GMSL record over the altimetry period. We recomputed the rate of the corrected GMSL time series over the same five-year-long moving windows (shifted by one year) as done previously. The temporal evolution of the corrected GMSL rate is shown in Fig. 2b and Supplementary Fig. 2b. The decreasing rate seen initially over the past decade has disappeared: the rate is now almost constant with time. Fig. 1b and Supplementary Fig. 1b show the corrected GMSL rates for the same two nine-year-long time spans as above, for each of the five altimetry data sets. The mean rate is also shown. The corrected mean rate now amounts to 3.3 ± 0.1 mm yr^{-1} over the two time intervals. The 0.1 mm yr^{-1} uncertainty is the formal error deduced from the dispersion around the mean. A more realistic uncertainty representing systematic errors affecting the altimetry-based GMSL rate (for example, owing to geophysical corrections applied to the altimetry data, and instrumental bias and drifts) would be rather closer to 0.4 mm yr^{-1} (ref. 2). However, this would not change our finding.

The result reported here shows that when removing from the GMSL time series the interannual variability mostly due to exchange of water between oceans, atmosphere and continents, with a smaller contribution from thermal expansion, there is no rate difference between the 1990s and the 2000s: the GMSL has almost linearly increased during the past 20 years. Although no GMSL acceleration is observed over this short time span, our result clearly advocates for no recent slowdown in global warming.

Although it has been suggested that several decades of satellite altimetry-based GMSL would be needed to isolate the long-term global warming signal[6], our result also shows that this may be already achievable by removing the (mainly ENSO-driven) interannual variability, a procedure that enhances the signal-to-noise ratio, as previously shown for the Earth's global mean surface temperature evolution[10]. At present, a persistent positive energy imbalance between the amount of sunlight absorbed by Earth and the thermal radiation back to space is observed[1,8,9,12,23]. The term missing energy[9] is related to an apparent inconsistency between interannual variations in the net radiation imbalance inferred from satellite measurements and upper-ocean heating rate from *in situ* measurements[9]. Although progress has been achieved and inconsistencies reduced[24], the puzzle of the missing energy remains[12], raising the question of where the extra heat absorbed by the Earth is going[9,12]. The results presented here will further encourage this debate as they underline the enigma between the observed plateau in Earth's mean surface temperature and continued rise in the GMSL. The larger GMSL rate calculated during the past decade than previously believed would be compatible with a significant warming contribution from the deep ocean. Such a possibility was raised by recent studies on the ocean heat content, suggesting that ~30% of the ocean warming has occurred below 700 m (ref. 25). This heat may be sequestered into the deep ocean during decades of large ocean–atmosphere natural variability[26], highlighting once more, as shown here, the role of short-term natural variability on longer-term change, probably associated with global warming.

Methods

Since the early 1990s, sea level has been routinely measured with quasi-global coverage and a few days/weeks revisit time by altimeter satellites: Topex/Poseidon (1992–2006), Jason-1 (2001–2013), Jason-2 (2008–), ERS-1 (1991–1996), ERS-2 (1995–2002), Envisat (2002–2011), Cryosat-2 (2010–) and SARAL/AltiKa (2013–). Altimetry-based GMSL time series are routinely produced by five processing groups: Archiving, Validation and Interpretation of Satellite Oceanographic Data (AVISO; www.aviso.oceanobs.com/en/news/ocean-indicators/mean-sea-level), Colorado University (CU; www.sealevel.colorado.edu/), Commonwealth Scientific and Industrial Research Organization (CSIRO; www.cmar.csiro.au/sealevel/sl_data_cmar.html), Goddard Space Flight Center (GSFC; podaac.jpl.nasa.gov/Integrated_Multi-Mission_Ocean_AltimeterData) and National Oceanographic and Atmospheric Administration (NOAA; ibis.grdl.noaa.gov/SAT/SeaLevelRise/LSA_SLR_timeseries_global.php). The GMSL time series from these five groups are based on Topex/Poseidon, Jason-1/2 missions. Recently, in the context of the European Space Agency (ESA) Climate Change Initiative (CCI) Sea Level Project (www.esa-sealevel-cci.org), a new, improved product, combining the Topex/Poseidon, Jason-1/2 with the ERS-1/2 and Envisat missions, has been computed. At present, data up to December 2010 are available. Beyond that date, the CCI GMSL time series has been extended using the AVISO data. All products are considered here except the CSIRO one that uses older geophysical corrections for the Topex/Poseidon data. A small correction of −0.3 mm yr^{-1} is removed to each GMSL time series to account for the glacial isostatic adjustment effect (that is, the visco-elastic response of the solid Earth to the last deglaciation) on absolute sea level[27]. Owing to known errors in the Topex/Poseidon altimetric system in the early part of the mission, we ignore the year 1993 when computing the GMSL trends.

To estimate the mass component due to global land water storage change, we use the Interaction Soil Biosphere Atmosphere (ISBA)/Total Runoff Integrating Pathways (TRIP) global hydrological model developed at MétéoFrance[22]. The ISBA land surface scheme calculates time variations of surface energy and water budgets in three soil layers. The soil water content varies with surface infiltration, soil evaporation, plant transpiration and deep drainage. ISBA is coupled with the TRIP module that converts daily runoff simulated by ISBA into river discharge on a global river channel network of 1° resolution. In its most recent version, ISBA/TRIP uses, as meteorological forcing, data at 0.5° resolution from the ERA Interim reanalysis of the European Centre for Medium-Range Weather Forecast (www.ecmwf.int/products/data/d/finder/parameter). Land water storage outputs from ISBA/TRIP are given at monthly intervals from January 1950 to December 2011 on a 1° grid (see ref. 22 for details). The atmospheric water vapour contribution has been estimated from the ERA Interim reanalysis. The land water storage and atmospheric water vapour contributions are further expressed in

equivalent sea level (ESL) through weighting by the ratio of the total land and Earth areas to the ocean area and multiplied by −1. The land water plus atmospheric water vapour component was estimated over the January 1994–December 2011 time span.

Two thermal expansion data sets were considered: the V6.13 updated version of ocean temperature data down to 700 m, over January 1994–December 2006 (ref. 28) and Argo data down to 1,500 m over January 2007–December 2011 (ref. 29). As we focus on the interannual signal, we applied a high-pass filter (removing all signal >5 years) to the thermosteric time series. For the other data sets, a simple linear trend was removed (the ISBA/TRIP land water and atmospheric water vapour time series essentially display interannual variability; applying the high-pass filter or just removing a linear trend provides essentially the same results). The time series are estimated at monthly time steps. Annual and semi-annual signals are removed by fitting 12- and 6-month period sinusoids to each time series (using a climatology produces similar results). A four-month running mean smoothing is further applied to all time series. Errors in land surface modelling are generally mainly due to uncertainties in atmospheric forcing than in physicals parameterizations such as the representation of groundwater dynamics or not[30]. The global ISBA/TRIP simulation used here was extensively evaluated and the simulated global land water storage was found very close to the GRACE signal over their overlapping time span[22]. Errors of associated monthly mass component are estimated to 1.3–1.5 mm ESL (refs 22,30). Errors on monthly water vapour component are <0.5 mm ESL. Errors on monthly thermosteric values are estimated to ∼1.4 mm ESL (refs 28,29).

In Figs 1–3, the mass component is based on ISBA/TRIP plus water vapour over the whole 1994–2011 time span (nominal case). Supplementary Figs 1, 2 and 3 use ISBA/TRIP outputs plus water vapour over 1994–2002 and GRACE data for 2003–2011 (hybrid case 1). In both cases, thermosteric data are from ref. 28 over 1994–2006 and Argo for 2007–2011.

Received 16 October 2013; accepted 4 February 2014; published online 23 March 2014

References

1. IPCC *Climate Change 2013: The Physical Science Basis* (eds Stocker, T. F. *et al.*) (Cambridge Univ. Press, 2013).
2. Nerem, R. S., Chambers, D. P., Choe, C. & Mitchum, G. T. Estimating mean sea level change from the TOPEX and Jason altimeter missions. *Mar. Geodesy* **33,** 435–446 (2010).
3. Church, J. A. & White, N. J. Sea-level rise from the late 19th to the early 21st century. *Surveys Geophys.* **32,** 585–602 (2011).
4. Willis, J. K., Chambers, D. P. & Nerem, R. S. Assessing the globally averaged sea level budget on seasonal to interannual time scales. *J. Geophys. Res.* http://dx.doi.org/10.1029/2007jc004517 (2008).
5. Leuliette, E. W. & Miller, L. Closing the sea level rise budget with altimetry, Argo and GRACE. *Geophys. Res. Lett.* **36,** L04608 (2009).
6. Leuliette, E. W. & Willis, J. K. Balancing the sea level budget. *Oceanography* **24,** 122–129 (2011).
7. Chen, J. L., Wilson, C. R. & Tapley, B. D. Contribution of ice sheet and mountain glacier melt to recent sea level rise. *Nature Geosci.* **6,** 549–552 (2013).
8. Hansen, J., Sato, M., Kharecha, P. & von Schuckmann, K. Earth's energy imbalance andimplications. *Atmos. Chem. Phys.* **11,** 13421–13449 (2011).
9. Trenberth, K. E. & Fasullo, J. T. Tracking Earth's energy. *Science* **328,** 316–317 (2010).
10. Foster, G. & Rahmstorf, S. Global temperature evolution 1979–2010. *Environ. Res. Lett.* **6,** 044022 (2011).
11. Kosaka, Y. & Xie, S-P. Recent global warming hiatus tied to equatorial Pacific surface cooling. *Nature* **501,** 403–407 (2013).
12. Trenberth, K. E. & Fasullo, J. T. An apparent hiatus in global warming? *Earth's Future* http://dx.doi.org/10.1002/2013EF000165 (2013).
13. Llovel, W. *et al.* Terrestrial waters and sea level variations on interannual time scale. *Glob. Planet. Change* **75,** 76–82 (2011).
14. Cazenave, A. *et al.* ENSO influence on the global mean sea level over 1993–2010. *Mar. Geodesy* **35,** 82–97 (2012).
15. Boening, C., Willis, J. K., Landerer, F. W. & Nerem, R. S. The 2011 La Niña: So strong, the oceans fell. *Geophys. Res. Lett.* **39,** L19602 (2012).
16. Fasullo, J. T., Boening, C., Landerer, F. W. & Nerem, R. S. Australia's unique influence on global sea level in 2010–2011. *Geophys. Res. Lett.* **40,** 4368–4373 (2013).
17. Nicholls, R. J. & Cazenave, A. Sea-level rise and its impact on coastal zones. *Science* **328,** 1517–1520 (2010).
18. Hallegate, S., Green, C., Nicholls, R. J. & Corfee-Morlot, J. Future flood losses in major coastal cities. *Nature Clim. Change* **3,** 802–806 (2013).
19. Gergis, J. L. & Fowler, A. M. A history of ENSO events since A.D. 1525: Implications for future climate change. *Climatic Change* **92,** 343–387 (2009).
20. Gu, G. & Adler, R. F. Precipitation and temperature variations on the interannual time scale: Assessing the impact of ENSO and volcanic eruptions. *J. Climate* **24,** 2258–2270 (2011).
21. Trenberth, K., Fasullo, J. & Smith, L. Trends and variability in column-integrated atmospheric water vapor. *Clim. Dynam.* **24,** 741–758 (2005).
22. Alkama, R. *et al.* Global evaluation of the ISBA-TRIP continental hydrological system. Part 1: Comparison to GRACE Terrestrial Water Storage estimates and in-situ river discharges. *J. Hydromet.* **11,** 583–600 (2010).
23. Church, J. A. *et al.* Revisiting the Earth's sea-level and energy budgets from 1961 to 2008. *Geophys. Res. Lett.* http://dx.doi.org/10.1029/2011gl048794 (2011).
24. Loeb, G. N. *et al.* Observed changes in top-of-the-atmosphere radiation and upper-ocean heating consistent within uncertainty. *Nature Geosci.* **5,** 110–113 (2012).
25. Balmaseda, M. A., Trenberth, K. & Kallen, E. Distinctive climate signals in reanalysis of global ocean heat content. *Geophys. Res. Lett.* **40,** 1–6 (2013).
26. Meehl, G. A., Arblaster, J. M., Fasullo, J. T., Hu, A. & Trenberth, K. E. Model based evidence of deep-ocean heat uptake during surface-temperature hiatus periods. *Nature Clim. Change* **1,** 360–364 (2011).
27. Peltier, W. R. Global glacial isostasy and the surface of the ice-age Earth: The ICE-5G (VM2 model and GRACE). *Annu. Rev. Earth Planet. Sci.* **32,** 111–149 (2004).
28. Ishii, M. & Kimoto, M. Reevaluation of historical ocean heat content variations with time-varying XBT and MBT depth bias corrections. *J. Oceanogr.* **65,** 287–299 (2009).
29. Von Schuckmann, K. & Le Traon, P. Y. How well can we derive global ocean indicators from Argo data? *Ocean Sci.* **7,** 783–791 (2011).
30. Vergnes, J-P. & Decharme, B. A simple groundwater scheme in the TRIP river routing model: Global off-line evaluation against GRACE terrestrial water storage estimates and observed river discharges. *Hydrol. Earth Syst. Sci.* **16,** 3889–3908 (2012).

Acknowledgements

This work was supported by CNES, CNRS, MétéoFrance, The University of Toulon and the ESA CCI project.

Author contributions

A.C. conceived the study and wrote the article. H-B.D. conducted the calculations. B.D. and K.v.S. provided the ISBA/TRIP and Argo data, respectively. B.M. and E.B. contributed to the interpretation and discussion.

Additional information

Supplementary information is available in the online version of the paper. Reprints and permissions information is available online at www.nature.com/reprints. Correspondence and requests for materials should be addressed to A.C.

Competing financial interests

The authors declare no competing financial interests.

nature climate change

SUPPLEMENTARY INFORMATION

DOI: 10.1038/NCLIMATE2159

The rate of sea-level rise

In this Supplementary Information, we test the robustness of our results using different data to compute the mass component. In the main text, we used the ISBA/TRIP hydrological model (Ref. 22) to estimate the mass contribution due to land water storage change because there are no global observations available over the whole period 1994-2011 to estimate it. However with the launch of the GRACE mission that measures the time-varying gravity field, we can directly estimate the mass component since early 2003. In a new computation, we used the same data as in the main text (nominal case) between January 1994 and December 2002, but over the January 2003 to December 2011 time span, we replaced the model-based land water storage component by GRACE data. Two different GRACE products were used: (1) the U. Texas Center for Space Research -CSR RL05- ocean data (unfiltered global mean ocean mass time series processed by Don P. Chambers -ref. S1 & S2-, and available at http//xena.marine.usf.edu/~chambers/SatLab/home.html), and (2) the Release 2 products from the Groupe de Recherches en Geodesie Spatiale/GRGS (www.grgs.obs-mip.fr/grace/variable-models-grace-lageos/grace-solutions-release-02).

We separately estimated from the GRACE/GRGS data, the ocean mass and land water components (in the latter case, we also accounted for atmospheric water vapour, as for the nominal case), by averaging the data over ocean and land, respectively (ignoring the Greenland and Antarctica ice sheets, and masking the Alaska and Patagonia glacier areas for land data). A number of post-processing corrections were applied to the GRACE/GRGS data to improve the signal to noise ratio (details in Dieng et al., Effect of La Niña on the global mean sea level and north Pacific ocean mass over 2005-2011, *J. Geodetic Sci.*, in press, 2014). Note that for the CSR RL05 global mean ocean mass time series, post-processing corrections are already applied by D.P. Chambers. As we focus on the interannual variability, the mass time series were detrended.

The mass component was computed by replacing over January 2003-December 2011, the ISBA/TRIP plus atmospheric water vapour data by GRACE ocean mass, using CSR RL05 and GRGS products (called hybrid cases 1 and 2, respectively). We also considered a case where the ISBA/TRIP land water data were replaced by GRACE/GRGS land water data over January 2003-December 2011) (hybrid case 3). We performed the same analysis as for the nominal case, i.e., removing from the GMSL time series the interannual mass plus

thermosteric component, and re computing the GMSL trends. Fig. S1, S2 and S3 present similar plots as Fig.1, 2 and 3, but for hybrid case 1. Uncertainty of monthly GRACE mass values is estimated to 1.5 mm (ref. S1, S3). Figures for hybrid cases 2 and 3 are not shown as they are quite similar to those of hybrid case 1. Table 1 presents corrected GMSL trends computed over 1994-2002 and 2003-2011 for the 3 hybrid cases. Values for the nominal case are also shown. From this additional analysis that provides hybrid cases combining GRACE data with outputs from the ISBA/TRIP hydrological model, we come up to the same conclusion as for the nominal case, i.e. removing the interannual mass plus thermosteric contribution to the GMSL time series increases the GMSL rate of the 2003-2011 time span to 3.2-3.3 mm yr^{-1}, a value similar to that of the 1994-2002 time span.

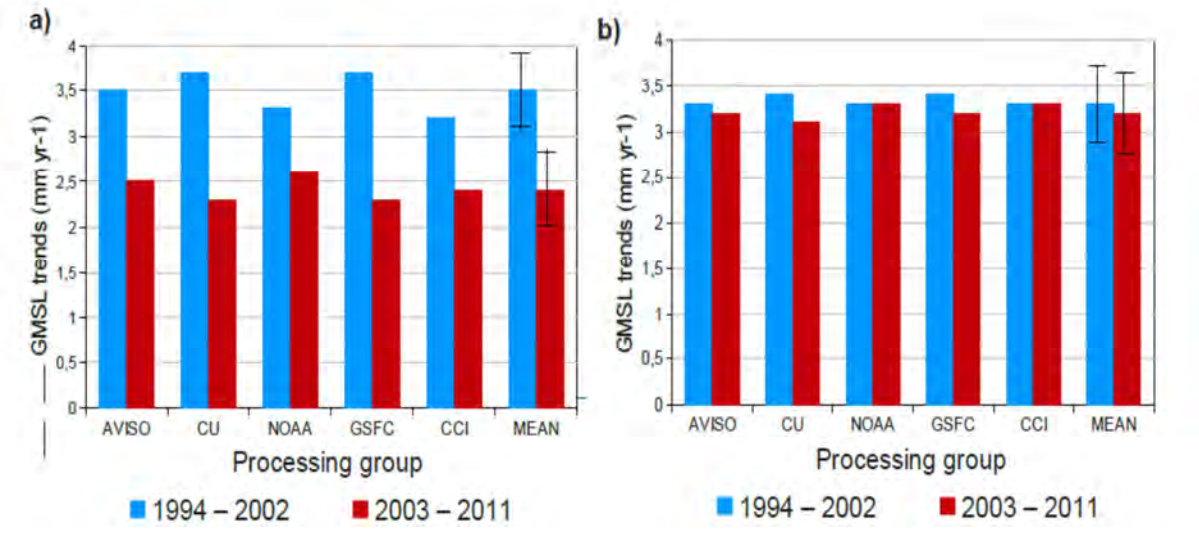

Figure S1: (a) GMSL trends computed over two time spans (January 1994 to December 2002, and January 2003 to December 2011) using satellite altimetry data from five processing groups (see Method for data sources). The mean GMSL trend (average of the five data sets) is also shown. (b) Same as (a) but after correcting the GMSL for the mass and thermosteric interannual variability (hybrid case 1). 'Corrected' means that the interannual variability due to the water cycle and thermal expansion are quantitatively removed from each original GMSL time series using data as described in the main text, Method and Supplementary Information. In hybrid case 1, the mass component used to correct for interannual variability is based on the ISBA/TRIP hydrological model for land water storage plus atmospheric water vapour component over January 1994 to December 2002 and GRACE CSR RL05 ocean mass over January 2003 to December 2011. Black vertical bars represent the 0.4 mm yr^{-1} uncertainty (ref.2). Units: mm yr^{-1}.

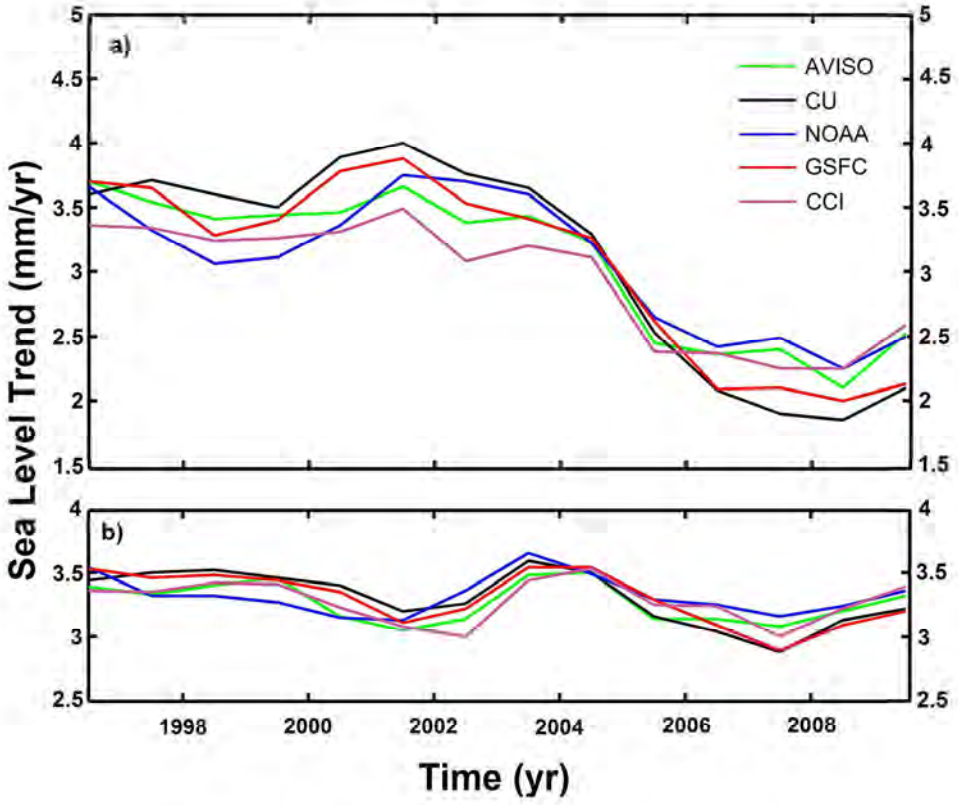

Figure S2: (a) Temporal evolution of the GMSL rate computed over 5-year-long moving windows shifted by 1-year (start date: 1994). (b) Temporal evolution of the corrected GMSL rate computed over 5-year-long moving windows shifted by 1-year (start date: 1994). GMSL data from each of the five processing groups are shown. The mass component is based on the ISBA/TRIP hydrological model for land water storage plus atmospheric water vapour component over January 1994 to December 2002 and GRACE CSR RL05 ocean mass over January 2003 to December 2011 (hybrid case 1). Units: mm yr^{-1}.

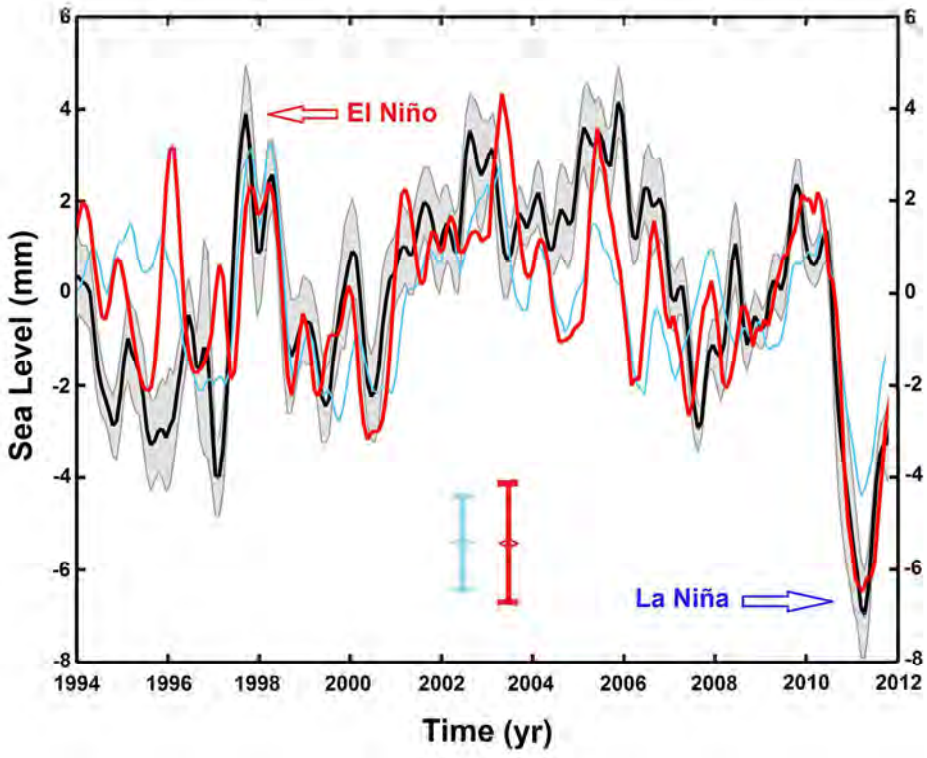

Figure S3: Black curve: mean detrended GMSL time series (average of the five satellite altimetry data sets) from January 1994 to December 2011, and associated uncertainty (in grey; based on the dispersion of each time series around the mean). Light blue curve: interannual mass component based on the ISBA/TRIP hydrological model for land water storage plus atmospheric water vapour component over January 1994 to December 2002 and GRACE CSR RL05 ocean mass for January 2003 to December 2011 (hybrid case 1). The red curve is the sum of the interannual mass plus thermosteric components. This is the signal removed to the original GMSL time series. Vertical bars represent the uncertainty of the monthly mass estimate (of 1.5 mm[22, 30, S1, S3]; light blue bar) and of the monthly total contribution (mass plus thermosteric component) (of 2.2 mm, ref. 22, 30, 28, 29, S1, S3; red bar). Units : mm.

Table S1: Trends of the corrected GMSL time series computed over two time spans (January 1994 to December 2002, and January 2003 to December 2011) for the nominal case and three hybrid cases. Satellite altimetry-based GMSL data from five processing groups, as well as mean (i.e., average of the five data sets) are considered. The mass component used to correct for interannual variability is based on the ISBA/TRIP hydrological model for land water storage plus atmospheric water vapour component over January 1994 to December 2011 in the nominal case, whereas GRACE data are used between January 2003 to December 2011 in the three hybrid cases (see above). Units: mm yr^{-1}.

GMSL rate	Case	AVISO	CU	NOAA	GSFC	CCI	Mean
1994-2002	Nominal	3.3	3.4	3.3	3.4	3.3	3.3
2003-2011	Nominal	3.3	3.2	3.3	3.2	3.3	3.3
2003-2011	Hybrid 1	3.2	3.1	3.3	3.2	3.3	3.2
2003-2011	Hybrid 2	3.2	3.1	3.3	3.1	3.2	3.2
2003-2011	Hybrid 3	3.2	3.1	3.2	3.1	3.2	3.2

References

S1: Chambers D.P., and Bonin J.A. Evaluation of Release-05 GRACE time variable gravity coefficients over the ocean, *Ocean Sci*., 8, 859-868, doi:10.5194/os-8-859-2012 (2012).

S2: Chambers D.P. & Schroeter, J. Measuring ocean mass variations from satellite gravimetry, *J. Geodynamics*, 52, 333-343 (2011).

S3: Wahr, J., Swenson, S. & Velicogna, I. Accuracy of GRACE mass estimates, *Geophys. Res. Lett*., 33, L06401, doi:10.1029/2005GL025305 (2006).

Acknowledgement

CRS RL05 GRACE ocean data were processed by Don P. Chambers, supported by the NASA measures Program, and are available at http://grace.jpl.nasa.gov.

Conclusion : Résumé de la thèse et quelques perspectives (indiquées en caractères gras)

Alors que le niveau des océans s'était stabilisé il y a environ 3000 ans à la fin de la déglaciation associée au dernier cycle glaciaire, les observations marégraphiques indiquent que la mer a recommencé à monter au cours du 20ème siècle. Durant ces deux dernières décennies, à l'aide des observations des satellites altimétriques de grande précision, la vitesse d'élévation a presque doublé par rapport aux décennies précédentes et atteint aujourd'hui en moyenne 3.4 mm/an. Il n'y a plus guère de doute que la hausse actuelle du niveau de la mer résulte du réchauffement de la planète en raison des émissions de gaz à effet de serre (*Church et al.* 2013). Cette hausse qui résulte de deux causes principales (l'expansion thermique des océans et la fonte des glaces continentales) constitue une menace sérieuse pour de nombreuses régions côtières basses, souvent très peuplées. D'après le dernière rapport du GIEC (AR5, *Church et al.* 2013), en utilisant des modèles de prévision climatique, on s'attend à une hausse accrue du niveau moyen global de la mer de l'ordre de 50 cm à 1 m au cours du 21ème siècle (avec cependant de fortes variations régionales) à cause de la dilatation thermique de l'océan qui se poursuivra et surtout à cause de la fonte des glaces continentales. Cependant, les incertitudes des projections du niveau de la mer demeurent encore grandes (±25 cm en moyenne globale et de fortes différences de variabilités régionales entre les différents modèles de climat). Ceci est liée à la diversité des scénarios d'émissions futures de gaz à effet de serre et d'aérosols et à l'occupation future des sols, mais aussi à l'incapacité des modèles climatiques actuelle à modéliser de manière réaliste les différentes composantes de la hausse du niveau de la mer (principalement la fonte des glaciers et des calottes polaires).

L'objectif principal de ma thèse était de valider les produits niveau de la mer du projet CCI (Climate Change Initiative) de l'Agence Spatiale Européenne (ESA) en utilisant différentes approches, en particulier par l'étude du bilan (comparaison du GMSL observé avec la somme des différentes contributions –composante stérique, fonte des glaces continentales et transferts d'eau depuis les terres émergées–).

Durant notre thèse, nous avons inter-comparé tous les produits du niveau de la mer disponibles au niveau international (AVISO, Colorado University, NOAA, GSFC, CSIRO et

CCI). En termes de tendance, nous avons montré un bon accord entre les produits GMSL sur la période 1993-2016, contrairement sur des périodes plus courtes (quelques années à une décennie) où les tendances du GMSL présentent d'importantes différences (jusqu'à ~0.6 mm/an sur la période 2005-2013). Nous avons montré que ces différences peuvent être nettement supérieures à l'erreur de 0.4 mm/an issue de l'étalonnage externe du GMSL avec des données marégraphiques et de l'évaluation de toutes les sources d'erreurs agissant sur le niveau de la mer altimétrique. Il en résulte aussi des écarts de plusieurs mm entre les différents produits niveau de la mer en termes de variabilité interannuelle. Nous avons identifié 2 groupes de produits niveau de la mer : *(1)* AVISO, NOAA et CCI qui montrent de faibles fluctuations interannuelles et des tendances plus élevées; et *(2)* CU, GSFC qui présentent de plus fortes anomalies interannuelles et des tendances plus faibles. Le produit CSIRO montre de fortes anomalies du niveau de la mer, mais il est plus proche du groupe 1 en termes de tendance. Quelques études ont cherché à comprendre les causes des différences entre les produits de GMSL (*Masters et al.* 2012 et *Henry et al.* 2014). Ces études ont identifié les effets respectifs des corrections géophysiques utilisées ainsi que les méthodes de calcul des moyennes géographiques. Toutefois, ces comparaisons restent incomplètes, et les centres de traitements ne fournissent pas de directives pour les utilisateurs de leurs produits.

Nous avons calculé les différentes contributions climatiques à la hausse du niveau moyen global de la mer (composante stérique et variation de masse de l'océan) sur la dernière décennie pour laquelle nous disposons de plusieurs systèmes d'observation de grande précision, indépendants et opérant simultanément (satellites altimétriques, gravimétrie spatiale GRACE, flotteurs ARGO). Comme les produits niveau de la mer altimétrique, différents groupes dans le monde traitent et fournissent les données masse de l'océan et stérique. Les produits Argo présentent des différences en tendance (jusqu'à 2 mm/an sur la période 2005-2014) et en variabilité interannuelle. Ces différences sont en particulier dues au remplissage des "trous" dans la couverture des données, le contrôle de la qualité, le choix de la climatologie mais aussi les techniques de maillage (*Abraham et al.* 2014). Même si les différences de tendance sont faibles en comparaison à celles du niveau de la mer altimétrique, nous avons montré qu'elles ne sont pas négligeables.

Cependant, jusqu'à présent aucune méthode de traitement de produits niveau de la mer altimétrique et stérique préférentielle n'est proposée. En ce qui concerne les produits GRACE, le bon accord entre les séries temporelles de masse de l'océan ne signifie rien sur leur précision absolue, vu qu'elles sont toutes traitées par la même méthode décrite dans *Johnson and Chambers* (2013). **Pour les utilisateurs intéressés par les produits altimétriques, stériques et de masse de l'océan, mais ne participant pas à la phase de traitement, il est important de comprendre**

les causes des différences entre les produits et d'être guidé vers l'ensemble des données les plus appropriées en fonction de l'application envisagée. Il serait important de mettre en place un exercice de comparaison internationale pour les produits niveau de la mer comme cela se fait dans la modélisation du climat (par exemple CMIP5).

Au cours de cette thèse, nous nous somme particulièrement intéressés à l'étude du bilan du niveau moyen global de la mer, qui nous a permis d'estimer les contributions manquantes, et tout particulièrement celle due au réchauffement de l'océan profond non mesurable par le système Argo. Nous avons estimé le résidu du bilan global de la mer (niveau moyen global observé moins composante stérique moins composante "masse de l'océan"), en utilisant plusieurs jeux de données différents sur la dernière décennie (période appelée 'hiatus', pendant laquelle la température moyenne de l'air en surface n'augmente pas alors que la Terre continue d'emmagasiner de la chaleur à cause des émissions de gaz à effet de serre). Nous avons obtenu un signal résiduel (considéré comme étant le signal stérique de l'océan profond) de l'ordre de 0.3 ± 0.6 mm/an avec une forte variabilité interannuelle. Mais ce résidu contient aussi les erreurs des données. L'étude a montré que la contribution de l'océan profond en dessous de 1500 m est très faible et contenue dans la barre d'incertitude des données. Nous avons aussi pu montrer une augmentation régulière du réchauffement de la couche océanique 700-1500m, entraînant une élévation stérique de 0.2 mm/an du niveau de la mer sur la période 2005-2012. Il est possible que la chaleur "anthropique" non utilisée pour réchauffer l'atmosphère en surface durant la période de "hiatus" soit stockée dans les couches profondes de l'océan. Nos résultats vont dans ce sens. De plus nous avons noté que, même si le programme Argo est un élément essentiel du système d'observation de l'océan global, il reste incomplet du fait du manque de mesures de température et de salinité en dessous de 2000m de profondeur. Ces données sont nécessaires pour mieux estimer le contenu thermique de l'océan profond.

Par ailleurs, nous avons analysé les différentes sources d'erreur des composantes du bilan du niveau de la mer. Pour cela, nous avons utilisé plusieurs ensembles de données altimétriques, stériques et de masse de l'océan, traitées par différents groupes. Nous avons montré que les erreurs du signal résiduel de l'équation bilan du niveau de la mer sur la période 2005-2013 proviennent essentiellement, en termes de tendance des produits niveau de la mer altimétrique et des lacunes de la couverture géographique des données Argo dans la région Indonésienne. La prise en compte de cette région en utilisant les données ORAS4, nous a permis de montrer qu'on arrive à fermer le bilan du niveau de la mer, en termes de tendance, avec les produits altimétriques CCI et AVISO mais pas avec les produits CU et GSFC. En termes de variabilité interannuelle, les erreurs sont attribuées aux produits GRACE et Argo. Ces résultats et la méthode utilisée montrent que le

niveau de la mer et ses composantes sont encore entachés d'erreurs importantes. **Dans le futur, il faudra la mise en œuvre de nouveaux systèmes d'observation (par exemple, Argo dans l'océan profond en dessous de 2000m, actuellement en phase expérimentale) et une meilleure couverture géographique des mesures de température et de salinité dans l'océan supérieur, comme le préconise un certain nombre d'articles récents (par exemple, *Abraham et al.* 2013). Ceci est un objectif soutenu de la communauté scientifique et des organismes institutionnels.**

Une autre partie de notre thèse a consisté à estimer la contribution des eaux continentales à la hausse du GMSL par une étude de bilan des masses d'eau sur toute la Terre. Nos résultats indiquent que cette contribution est de l'ordre de 10% la hausse actuelle du niveau de la mer et est dominée par le pompage de l'eau dans les nappes pour l'irrigation des cultures. Cette approche permet d'apporter des contraintes aux modèles hydrologiques.

Outre l'étude de bilan, nos travaux ont montré le rôle majeur des événements ENSO sur la variabilité interannuelle du GMSL, via des modifications importantes du cycle hydrologique global. Nous avons montré que lors des évènements La Nina comme celle de 2010-2011, le déficit de précipitations sur l'océan (et l'excès sur les continents) conduit à une baisse temporaire de la masse de l'océan global et donc du niveau de la mer. Plus généralement, nos résultats révèlent que les fluctuations interannuelles du GMSL, associées aux événements El Niño et La Niña, sont essentiellement causées par des changements de la masse de l'océan, localisés au Nord du Pacifique tropical (liés aux fluctuations temporaires des précipitations dans cette zone). Nos résultats ont aussi montré que les plus grandes anomalies du GMSL atteignant 10mm sont observées sur la dernière décennie, durant les épisodes La Niña de 2010-2011 et El Niño de 2015-2016. Cela montre-t-il une intensification des phénomènes ENSO en réponse au changement climatique ? **Cette question à savoir l'impact du changement climatique sur la périodicité et l'intensité des événements ENSO n'est pas encore résolue et devra faire l'objet de recherche dans le futur.**

Nous avons aussi montré au cour de notre thèse que le ralentissement de 30% de la vitesse d'élévation du GMSL au cours des années 2000 (coïncidant avec la période dite de "pause" ou "hiatus") est dû à la variabilité naturelle interne du climat (principalement des épisodes La Nina) en raison des échanges d'eau entre les océans, l'atmosphère et les continents, avec une moindre contribution du niveau de la mer stérique. Nos résultats confirment la nécessité de quantifier et de retirer la variabilité naturelle interne du climat si l'on veut estimer l'impact du réchauffement climatique sur le niveau de la mer sur une courte période. Bien qu'il ait été suggéré que plusieurs décennies de mesure altimétrique soient nécessaires pour isoler le signal du réchauffement climatique global (*Leuliette and Willis*, 2011), nos résultats montrent également que cela est déjà

possible en retirant la variabilité interannuelle (principalement causée par ENSO), une procédure qui améliore le rapport signal-bruit, comme montré par *Foster and Rahmstorf*, (2011) pour l'évolution de la température moyenne globale de surface de la Terre (GMST).

Tout récemment, nous avons étudié l'évolution de la température moyenne de l'air et de l'océan en surface, ainsi que la GMST sur la période du hiatus. Nous avons montré que le ralentissement récent de la GMST est bien réel et de plus il est quasi global même si le Pacifique tropical Est s'est fortement refroidi. Nous avons aussi montré qu'il n'y a pas de diminution du déséquilibre énergétique du système climatique ni du forçage radiatif net au cours de la dernière décennie. Cette "supposée" pause récente s'explique par la variabilité naturelle interne et que la Terre est toujours en état de déséquilibre énergétique dû à l'accumulation de gaz à effet de serre. Comme indiqué dans les études précédentes (par exemple, *Llovel et al.* 2014 ; *von Schuckmann et al.* 2014, 2016), la pause observée dans l'évolution de la GMST n'est en aucun cas le reflet d'une pause dans l'accumulation de chaleur dans le système climatique. Il est de plus en plus clair que la GMST n'est pas le meilleur indicateur du changement climatique. C'est plutôt le contenu thermique de l'océan et/ou le niveau moyen global de la mer. Nous mettons en évidence le rôle de la variabilité naturelle à court terme sur les changements à plus long terme associés au réchauffement climatique anthropique.

En cette fin de thèse, j'ai démarré des études sur les variations régionales et locales du niveau de la mer actuel et futur près des zones côtières de l'Afrique occidentale et en particulier les côtes Sénégalaises. En effet, l'Afrique de l'Ouest, avec un littoral de ~15000 km où plus de la moitié de la population vit à moins de 100 km des côtes, a une très large part de son économie concentrée dans les grandes métropoles côtières comme Nouakchott, Dakar, Banjul, Bissau, Conakry, Freetown, Monrovia, Abidjan, Accra, Lomé, Cotonou, Lagos, etc. L'objectif principal de ces recherches est d'estimer les impacts de la hausse actuelle et future du niveau de la mer dans cette région de l'Afrique peu étudiée et au Sénégal en particulier, en tenant en compte non seulement de l'évolution du climat global et régional mais aussi des facteurs anthropiques directs comme l'urbanisation, l'évolution démographique, etc. Le Sénégal par sa position géographique avec ~800km de côtes, serait pour moi un lieu idéal pour mener des recherches sur les interactions entre l'océan, l'atmosphère et les continents, ainsi que des études d'impact et d'adaptation face au changement climatique et aux effets anthropiques directs sur l'environnement et l'agriculture. Après ma thèse, je compte développer ce thème de recherche, en collaboration avec d'autres chercheurs de l'Afrique de l'Ouest et du LEGOS.

Bibliographie

Ablain M., Cazenave A., Valladeau G. and Guinehut S. : A new assessment of the error budget of global mean sea level rate estimated by satellite altimetry over 1993-2008. *Ocean Science* 5(2), 193–201 (2009).

Ablain M., Philipps S., Urvoy M., Tran N. and Picot N. : Detection of long-term instabilities on altimeter backscattering coefficient thanks to wind speed data comparisons from altimeters and models. *Mar. Geod.* 35(S1):42–60. doi:10.1080/01490419.2012.718675 (2012).

Ablain M., Cazenave A., Larnicol G., Balmaseda M., Cipollini P., Faugère Y., Fernandes M. J., Henry O., Johannessen J. A., Knudsen P., Andersen O., Legeais J., Meyssignac B., Picot N., Roca M., Rudenko S., Scharffenberg M. G., Stammer D., Timms G., and Benveniste J. : Improved sea level record over the satellite altimetry era (1993–2010) from the Climate Change Initiative project, *Ocean Sci.*, 11, 67–82, doi:10.5194/os-11-67-2015 (2015).

Ablain M., Legeais J. F., Prandi P., Marcos M., Fenoglio-Marc L., Dieng H. B., Benveniste J. and Cazenave A. : Altimetry-based sea level at global and regional scales. *Surv. Geophys*. DOI 10.1007/s10712-016-9389-8 (2016).

Abraham J. P., Baringer M., Bindoff N. L., Boyer T., Cheng L. J., Church J. A., Conroy J. L., Domingues C. M., Fasullo J. T., Gilson J., Goni G., Good S. A., Gorman J. M., Gouretski V., Ishii M., Johnson G. C., Kizu S., Lyman J. M., Macdonald A. M., Minkowycz W. J., Moffitt S. E., Palmer M. D., Piola A. R., Reseghetti F., Schuckmann K., Trenberth K. E., Velicogna I. and Willis J. K. : A review of global ocean temperature observations: implications for ocean heat content estimates and climate change. *Rev. Geophys.*, 51, 450–483, doi:10.1002/rog.20022 (2013).

Abraham J. P., Kumar S., Bickmore B. R. and Fasullo J. T. : Issues Related to the Use of One-dimensional Ocean-diffusion Models for Determining Climate Sensitivity. *J Earth Sci Clim Change*, 5: 220. doi:10.4172/2157-7617.1000220 (2014).

Adams J. B., Michael E., Mann M. E. and Ammann C. M. : Proxy evidence for an El Niño-like response to volcanic forcing. *Nature* 426: 274–278 (2013).

Agreen R. W. : The 3.5-year GEOS-3 data set. NOAA Technical Memorandum NOS NGS 33, NOAA, Rockville, MD (1982).

Andersen O. B. : The DTU10 Gravity field and mean sea surface (2010) Second international symposium of the gravity field of the earth (IGFS2), Fairbanks, Alaska, 20–22 September

2010. (2010) http://www.space.dtu.dk/english/*/media/Institutter/Space/English/scientific_data_and_models/global_marine_gravity_field/dtu10.ashx. Access 20 June 2014.

Alkama R. *et al.* : Global evaluation of the ISBA-TRIP continental hydrological system Part 1: Comparison to GRACE Terrestrial Water Storage estimates and in-situ river discharges. *J. of Hydromet*., 583-600, doi:10.1175/2010JHM1211 (2010).

Allan R. P., Liu C., Loeb N. G., Palmer M. D., Roberts M., Smith D. and Vidale P. L. : Changes in global net radiative imbalance 1985–2012. *Geophys. Res. Lett.* 41: 5588–5597 (2014).

Antonov J. I., Levitus S. and Boyer T. P. : Steric sea level variations during 1957-1994 : Importance of salinity. *Journal of Geophysical Research*, *107*, 8 PP., doi :200210.1029/2001JC000964 (2002).

Antonov J. I., Levitus S. and Boyer T. P. : Thermosteric sea level rise, 1955-2003. *Geophysical Research Letters*, *32*, 4 PP., doi :200510.1029/2005GL023112 (2005).

Balmaseda M. A., Trenberth K. and Kallen E. : Distinctive climate signals in reanalysis of global ocean heat content. *Geophys. Res. Lett.,* 40, 1–6, doi:10.1002/grl.50382 (2013a).

Balmaseda M. A., Mogensen K. and Weaver A. T. : Evaluation of the ECMWF ocean reanalysis system ORAS4. *Q. J. R. Meteorol. Soc.*, 139, 1132–1161, doi:10.1002/qj.2063 (2013b).

Barandun M., Huss M., Sold L., Farinotti D., Azisov E., Salzmann N., Usubaliev R., Merkushkin A., Hoelzle M. : Re-analysis of seasonal mass balance at Abramov glacier 1968–2014. *Journal of Glaciology*, 61(230), 1103-1117 (2015).

Bard E., Fairbanks R., Hamelin B., Zindler A. and Hoang C. : U-234 anomalies in corals older than 150,000 years. *Geochimica Et Cosmochimica Acta*, *55* (8), 2385–2390, doi : 10.1016/0016-7037(91)90115-L, WOS :A1991GC43900026 (1991).

Bard E., Hamelin B. and Delanghe-Sabatier D. : Deglacial meltwater pulse 1B and younger dryas sea levels revisited with boreholes at tahiti. *Science*, *327* (5970), 1235–1237, doi : 10.1126/science.1180557, WOS :000275162100033 (2010).

Barker P. M., Dunn J. R., Domingues C. M. and Wijffels S. E. : Pressure Sensor Drifts in Argo and Their Impacts. *J. Atmos. Ocean. Tech.*, 28, 1036–1049 (2011).

Barnett T. P., Pierce D. W., Latif M., Dommenget D. and Saravanan R. : Interdecadal interactions between the tropics and midlatitudes in the Pacific basin. *Geophys. Res. Lett.* 26: 615–618 (1999).

Barletta V. R., Sørensen L. S. and Forsberg R. : Scatter of mass changes estimates at basin scale for Greenland and Antarctica. *Cryosphere*, 7, 1411–1432, doi:10.5194/tc-7-1411-2013 (2013).

Berthier E., Vincent C., Durand G. and Krinner G. : Bilan de masse des glaciers et des calottes polaires. in *Le climat à découvert. Outils et méthodes en recherche climatique*, edited by Jeandel C. and R. Mosseri, CNRS Edition, (2011).

Bevington P. R. and Robinson D. K. : *Data Reduction and Error Analysis for the Physical Sciences*. *McGraw Hill*, ISBN 0-07 247227-8 (1969).

Bhardwaj A., Sam L., Bhardwaj A. and Martín-Torres F. J. : LiDAR remote sensing of the cryosphere: Present applications and future prospects. *Remote Sensing of Environment*, 177: 125-143 (2016a).

Bhardwaj A., Sam L., Martín-Torres F. J. and Kumar R. : UAVs as remote sensing platform in glaciology: Present applications and future prospects. *Remote Sensing of Environment*, 175: 196-204 (2016b).

Bindoff N., Willebrand J., Artale V., Cazenave A., Gregory J., Gulev S., Hanawa K., Le Quéré C., Levitus S., Nojiri Y., Shum C. K., Talley L., Unnikrishnan A. : Observations: oceanic climate and sea level. In: Climate change 2007: The physical Science Basis. Contribution of Working Group I to the Fourth Assessment report of the Intergouvernmental Panel on Climate Change [Solomon S., Qin D., Manning M., Chen Z., Marquis M., Averyt K. B., Tignor M. and Miller H. L. (eds.)]. Cambridge University Press, Cambridge, UK, and New York, USA (2007).

Boening C., Willis J. K., Landerer F. W. and Nerem R. S. : The 2011 La Nina: so strong, the oceans fell, *Geophys. Res. Lett*., 39, L19602, doi:10.1029/2012GL053055 (2012).

Bonnefond P., Exertier P., Laurain O., Guillot A., Picot N., Cancet M. and Lyard F. : SARAL/AltiKa absolute calibration from the multi-mission Corsica facilities. *Mar. Geod*., 38(S1):171–192 (2015).

Boyin H., Banzon V. F., Freeman E., Lawrimore J., Liu W., Peterson T. C., Smith T. M., Thorne P. W., Woodruff S. D. and Zhang H. M. : Extended reconstructed sea surface temperature version 4 (ERSST.v4) part I: upgrades and intercomparisons. *J. Clim.*, 28: 911–930 (2015).

Brown P. T., Wenhong L., Li L. and Ming Y. : Top-of-atmosphere radiative contribution to unforced decadal global temperature variability in climate models. *Geophys. Res. Let.* 41: 5175–5183, doi: 10.1002/2014GL060625 (2014).

Cabanes C., Gourazel A., von Schuckmann K., Hamon M., Turpin V., Coatanoan C., Guinehut S., Boone C., Ferry N., Reverdin G., Pouliquen S. and Le Traon P.Y. : The CORA dataset: validation and diagnostics of ocean temperature and salinity in situ measurements. *Ocean Sci.*, 9, 1–18, www.ocean-sci.net/9/1/2013/, doi:10.5194/os-9-1-2013 (2013).

Cahill N., Rahmstorf S. and Parnell A. C. : Change points of global temperature, *Environ. Res. Lett*. 10 (2015) 084002, doi: 10.1088/1748-9326/10/8/084002 (2015).

Carrere L, Lyard F, Cancet M, Guillot A, Picot N. and Dupuy S. : FES 2014: a new global tidal model. Ocean Surface Topography Science Team, Reston, Virginia, USA, October 2015. (2015). http://meetings.aviso.altimetry.fr/fileadmin/user_upload/tx_ausyclsseminar/files/OSTST2015/TIDE-01-Carrere.pdf

Carrere L., Faugère Y. and Ablain M. : Major improvement of altimetry sea level estimations using pressure derived corrections based on ERA-interim atmospheric reanalysis. Ocean Sci., 12, 825-842, doi:10.5194/os-12-825-2016 (2016).

Cartwright D. E. and Tayler R. J. : New computations of the tide-generating potential. *Geophys J Int* 23(1):45–73 (1971).

Cartwright D. E and Edden A. C. : Corrected tables of tidal harmonics. *Geophys J Int* 33(3):253–264 (1973).

Cazenave A., Guinehut S., Ramillien G., Llovel W., DoMinh K., Ablain M., Larnicol G., Lombard A. : Sea level budget over 2003–2008; a reevaluation from satellite altimetry, GRACE and Argo data. *Global Planet. Change.* doi:10.1016/j/gloplacha.2008.10.004 (2009).

Cazenave A. and Chen J. : Time-variable gravity from space and present-day mass redistribution in the Earth system. *Earth Planet. Sci. Lett.*, 298, 263-274 (2010).

Cazenave A. and Llovel W. : Contemporary sea level rise. *Annu. Rev. Mar. Sci.* 2, 145–173 (2010).

Cazenave A., O. Henry, S. Munier, B. Meyssignac, T. Delcroix, W. Llovel, H. Palanisamy and M. Becker : ENSO influence on the global mean sea level over 1993-2010, *Marine Geodesy*, 35(S1), 82–97 (2012a).

Cazenave Anny, Habib Boubacar Dieng, Simon Munier, Olivier Henry, Benoit Meyssignac, Hindumathi Palanisamy et William Llovel : L'influence d'El Niño et de La Niña sur le niveau de la mer. La Météorologie - n° 79 - novembre (2012b).

Cazenave A., Dieng H. B., Meyssignac B., von Schuckmann K., Decharme B. and Berthier E. : The rate of sea level rise. *Nature Climate Change*, 4, 358–361, doi:10.1038/NCLIMATE2159 (2014).

Chambers D. P., Wahr J., Nerem R. S. : Preliminary observations of global ocean mass variations with GRACE. Geophys. Res. Lett. 31 (424), L13310. doi:10.1029/2004GL020461 (2004).

Chambers D. P. : Evaluation of new GRACE time-variable gravity data over the ocean. *Geophys. Res. Lett.* 33 (17), LI7603 (2006).

Chambers D. P. and Willis J. K. : Low-frequency exchange of mass between ocean basins. *J. Geophys. Res.*, 114, C11008, doi:10.1029/2009JC005518 (2009).

Chambers D. P., Wahr J., Tamisiea M. E. and Nerem R. S. : Ocean mass from GRACE and glacial isostatic adjustment. *J. Geophys. Res.*, 115, B11415, doi:10.1029/2010JB007530 (2010).

Chambers D. P. and Schroeter J. : Measuring ocean mass variations from satellite gravimetry. *J. Geodyn.*, 52, 333–343 (2011).

Chambers D. P. and Schroeter J. : Measuring ocean mass variations from satellite gravimetry. *J. Geodynamics*, 52, 333-343 (2011).

Chambers D. P. and Bonin J. A. : Evaluation of Release-05 GRACE time variable gravity coefficients over the ocean. *Ocean Sci*., 8, 859-868, doi:10.5194/os-8-859-2012 (2012).

Chambers D., Merrifield M. A. and Nerem R. S. : Is there a 60-year oscillation in global mean sea level. *Geophys. Res. Lett.*, 39: L18607 (2012).

Chambers D. P., Cazenave A., Champollion N., Dieng H. B., Llovel W., Forsberg R., von Schuckmann K., and Wada Y. : Evaluation of the Global Mean Sea Level Budget between 1993 and 2014. *Surv. Geophys*, 1–19, doi:10.1007/s10712-016-9381-3 (2016).

Chao B. F., Wu Y. H. and Li Y. S. : Impact of artificial reservoir water impoundment on global sea level, *Science*, doi:10.1126/science.1154580 (2008).

Chelton D. B., Ries J. C., Haines B. J., Fu L. L. and Callahan P. S. : Satellite altimetry. In: Fu L-L, Cazenave A (eds) Satellite altimetry and earth sciences, a handbook of techniques and applications. *Academic Press, London. Int Geophys Ser* 69:1–131 (2001).

Chen J. L., Wilson C. R. and Tapley B. D. : Satellite gravity measurements confirm accelerated melting of Greenland ice sheet. *Science*, 313(5795) : 1958–60 DOI:10.1126/science.1129007 (2006).

Chen J. L., Wilson C. R. and Tapley B. D. : Contribution of ice sheet and mountain glacier melt to recent sea level rise. *Nature Geoscience*, 6, 549-552 (2013).

Chen X. and Tung K. K. : Varying planetary heat sink led to global warming slowdown and acceleration, *Science*, 345, 897-903 (2014).

Chen X., Feng Y. and Huang N. E. : Varying Global sea level trend during 1993–2012, *Science*, Global and Planetary Change 112 (2014) 26–32 (2014).

Cheng L., Zheng F. and Zhu J. : Distinctive interior changes during the recent warming slowdown. *Sci. Rep.* 5: 14346 (2015).

Cheng Y., Andersen O. and Knudsen P. : An improved 20-year Arctic Ocean altimetric sea level data record. Mar Geod 38(2):146–162 (2015).

Church J. A. and White N. J. : A 20th century acceleration in global sea-level rise. *Geophysical Research Letters*, *33* (1), doi :10.1029/2005GL024826, WOS :000234509300010 (2006).

Church J. A., White N. J. and Arblaster J. : Significant decadal-scale impact of volcanic eruptions on sea level and ocean heat content. *Nature*, *438* (7064), 74–77, doi :10.1038/nature04237 (2005).

Church J. A. and White N. J. : Sea-Level Rise from the Late 19th to the Early 21st Century. *Surveys in Geophysics*, *32*(4-5), 585-602, doi:10.1007/s10712-011-9119-1 (2011).

Church J. A., White N. J., Konikow L. F., Domingues C. M., Cogley J. G., Rignot E., Gregory J. M., van den Broeke M. R., Monaghan A. J. and Velicogna I. *:* Revisiting the Earth's sea-

level and energy budgets from 1961 to 2008. *Geophys. Res. Lett.,* 38, *L18601, doi:*10.1029/2011GL048794 (2011).

Church J. A., Clark P. U., Cazenave A., Gregory J. M., Jevrejeva S., Levermann A., Merrifield M. A., Milne G. A., Nerem R. S., Nunn P. D., Payne A. J., Pfeffer W. T., Stammer D. and Unnikrishnan A. S.: Sea level change, in: Climate Change 2013: The Physical Science Basis. Contribution of Working Group I to the Fifth Assessment Report of the Intergovernmental Panel on Climate Change, edited by: Stocker T. F., Qin D., Plattner G.-K., Tignor M., Allen S. K., Boschung J., Nauels A., Xia Y., Bex V. and Midgley P. M., Cambridge University Press, Cambridge, UK and New York, NY, USA (2013).

Clark P. U., Church J., Gregory J. and Payne T. : Recent progress in understanding and projecting regional and global mean sea level. *Curr Clim Change.,* doi:10.1007/s40641-015-0024-4 (2015).

Cogley J. G. : A more complete version of the world glacier inventory. *Annals of Glaciology*, *50* (53), 32–38, doi :10.3189/172756410790595859 (2010).

Cogné J. and Humler E. : Temporal variation of oceanic spreading and crustal production rates during the last 180 my. *Earth and Planetary Science Letters*, 227 (3-4), 427–439, doi :10.1016/j.epsl.2004.09.002 (2004).

Collilieux X. & G. Wöppelmann : Global sea level rise and its relation to the terrestrial reference frame definition. *Journal of Geodesy,* 85, 9-22 (2011).

Couhert A., Luca Cerri L., Legeais J. F., Ablain M., Zelensky N. P., Haines B. J., Lemoine F. G., Bertiger W. I., Desai S. D. and Michiel Otten M. : Towards the 1 mm/y stability of the radial orbit error at regional scales. *Adv Space Res*, 55:2–23 (2015).

Cowtan K. and Way R. G. : Coverage bias in the HadCRUT4 temperature series and its impact on recent temperature trends. *Q. J. R. Meteorol. Soc.,* 140: 1935–1944 (2014).

Cramer B. S., Toggweiler J. R., Wright J. D., Katz M. E. and Miller K. G. : Ocean overturning since the late cretaceous : Inferences from a new benthic foraminiferal isotope compilation. *Paleoceanography*, *24*, 14 PP., doi :200910.1029/2008PA001683 (2009).

Crowley T. J., Obrochta S. P. and Liu J. : Recent global temperature “plateau” in the context of a new proxy reconstruction. *Earths Future,* 2: 281–294 (2014).

Curry R., Dickson B. and Yashayaev I. : A change in the freshwater balance of the Atlantic Ocean over the past four decades. *Nature*, 426(6968), 826–829 (2003).

Dai A. and Wigley T. M. L. : Global patterns of ENSO-induced precipitation. *Geophys. Res. Lett.*, 27, 9, 1283-1286 (2000).

Decharme B., Alkama R., Douville H., Becker M., Cazenave A., Sheffield J., Voldoire A., Tyteca S., Le Moigne P. : Global evaluation of the ISBA-TRIP continental hydrologic system using GRACE; Part 2 : results. *J. Hydrometeorology*, 11, 601- 617 (2010).

Deschamps P., Durand N., Bard E., Hamelin B., Camoin G., Thomas A. L., Henderson G. M., Okuno J. and Yokoyama Y. : Ice-sheet collapse and sea-level rise at the bolling warming 14,600 years ago, *Nature*, *483* (7391), 559–564, doi :10.1038/nature10902, WOS :000302006100031 (2012).

Dibarboure G., Pujol M-I., Briol F., Le Traon P. Y., Larnicol G., Picot N., Mertz F. and Ablain M. : Jason-2 in DUACS: updated system description, first tandem results and impact on processing and products. Mar Geod 34(3–4):214–241 (2011).

Dibarboure G. and Morrow R. : Value of the Jason-1 geodetic phase to study rapid oceanic changes and importance for defining a Jason-2 geodetic orbit. *Journal of Atmospheric and Oceanic Technology*, 33(9) DOI: 10.1175/JTECH-D-16-0015.1 (2016).

Dieng H. B., Cazenave A., Messignac B., Henry O., von Schuckmann K. and Lemoine J. M. : Effect of La Niña on the global mean sea level and north Pacific ocean mass over 2005-2011, *J. Geodetic Sciences*, 4, 19-27 (2014).

Dieng H. B., Palanisamy H., Cazenave A., Meyssignac B. and von Schuckmann K. : The sea level budget since 2003: inference on the deep ocean heat content. *Surv. Geophys.*, 36, 209–229, doi:10.1007/s10712-015-9314-6 (2015a).

Dieng H. B., Cazenave A., von Shuckmann K., Ablain M. and Meyssignac B. : Sea level budget over 2005-2013: missing contributions and data errors. *Ocean Science*, 11, 789-802, doi:10.5194/os-11-789-2015 (2015b).

Dieng H. B., Champollion N., Cazenave A., Wada Y., Schrama E. and Meyssignac B. : Total land water storage change over 2003-2013 estimated from a global mass budget approach. *Environ. Res. Lett.*, 10, 124010, doi:10.1088/1748-9326/10/12/124010 (2015c).

Dieng H. B., Cazenave A., Meyssignac B., von Shuckmann K. and Palanisamy H. : Sea and land surface temperatures, ocean heat content, Earth's energy imbalance and net radiative forcing over the recent years. *Int. J. Climatol.*, DOI: 10.1002/joc.4996 (2017).

Dee D. P. et al. : The ERA-Interim reanalysis: configuration and performance of the data assimilation system, *Q. J. Roy. Meteor. Soc.*, 137, 553-597, doi:10.1002/qj.828 (2011).

Domingues C. M., Church J. A.,White N. J., Gleckler P. J.,Wijffels S. E., Barker P. M. and Dunn J. R. : Improved estimates of upper-ocean warming and multi-decadal sea-level rise. *Nature*, 453: 1090–1093 (2008).

Döll P, Fritsche M, Eicker A, Mueller Schmied H. : Seasonal water storage variations as impacted by water abstractions: comparing the output of a global hydrological model with GRACE and GPS observations. *Surv Geophys*. doi:10.1093/gji/ggt485 (2014a).

Döll P, Mueller Schmied H, Schuh C, Portmann FT, Eicker A. : Global-scale assessment of groundwater depletion and related groundwater abstractions: combining hydrological modeling with information from well observations and GRACE satellites, *Water Resour Res* 50. doi:10.1002/ 2014WR015595 (2014b).

Ducet N., Le Traon P. Y. and Reverdin G. : Global high resolution mapping of ocean circulation from the combination of TOPEX/POSEIDON and ERS-1/2. J Geophys Res (Oceans) 105(C8):19477–19498 (2000).

Dutton A., Bard E., Antonioli F., Esat T. M., Lambeck K. and McCulloch M. T. : Phasing and amplitude of sea-level and climate change during the penultimate interglacial. *Nature Geoscience, 2* (5), 355–359, doi :10.1038/ngeo470 (2009).

Dutton A. and Lambeck K. : Ice volume and sea level during the last interglacial. Science, 337, 216–219 (2012).

Enderlin E. M., Howat I. M., Jeong S., Noh M-J., van Angelen J. H. and van den Broeke M. R. : An improved mass budget for the Greenland ice sheet Geophys. *Res. Lett.* 41, 866–872 doi:10.1002/2013GL059010 (2014).

Enfield D. B., Mestas-Nunez A. M. and Trimble P. J. : The Atlantic Multidecadal Oscillation and its relationship to rainfall and river flows in the continental U.S. *Geophys. Res. Lett.*, 28: 2077–2080 (2001).

England M. H., McGregor S., Spence P., Meehl G. A., Timmermann A., Cai W., Gupta A. S., McPhaden M. J., Purich A. and Santoso A. : Recent intensification of wind-driven circulation in the pacific and the ongoing warming hiatus, Nature Climate Change, 4, 222–227 (2014).

Ewert H., Groh A. and Dietrich R. : Volume and mass changes of the Greenland ice sheet inferred from ICESat and GRACE. *J. Geodyn.*, 59–60, 111–123, DOI: 10.1016/j.jog.2011.06.003 (2012).

Famiglietti J. S. : The global groundwater crisis. *Nature Clim. Change*, 4, 945-948, doi:10.1038/nclimate2425 (2014).

Fan Y. and van den Dool H. : A global monthly land surface air temperature analysis for 1948-present. *J. Geophys. Res.* 113: D01103 (2008).

Fasullo J. T., C. Boening, F. W. Landerer and R. S. Nerem : Australia's unique influence on global mean sea level in 2010-2011, *Geophys.Res. Lett.*, *40*(16), 4368–4373, doi:10.1002/grl.50834 (2013).

Fenoglio-Marc L., Groten E. and Dietz C. : Vertical land motion in the Mediterranean Sea from altimetry and tide gauge stations. *Mar. Geod.*, 27(3–4):683–701 (2004).

Fenoglio-Marc L., Becker M., Rietbroeck R., Kusche J., Grayek S. and Stanev E. : Water mass variation in Mediterranean and Black Sea. *J Geodyn.* doi:10.1016/j.jog.2012.04.001 (2012).

Fenoglio-Marc L., Dinardo S., Scharroo R., Roland A., Dutour M., Lucas B., Becker M., Benveniste J. and Weiss R. : The German Bight: a validation of CryoSat-2 altimeter data in SAR mode. *Adv Space Res.*, doi:10.1016/j.asr.2015.02.014 (2015).

Fernandes M. J., Lazaro C., Ablain M. and Pires N. : Improved wet path delays for all ESA and reference altimetric missions. *Remote. Sens. Environ.,* 169(2015):50–74. doi:10.1016/j.rse.2015.07.023 (2015).

Flato G. J., Marotzke B., Abiodun P., Braconnot S. C., Chou W., Collins P., Cox F., Driouech S., Emori V., Eyring C., Forest P., Gleckler E., Guilyardi C., Jakob V., Reason C. and Rummukainen M. : Evaluation of climate models. In *Climate Change 2013: The Physical Science Basis. Contribution ofWorking Group I to the Fifth Assessment Report of the Intergovernmental Panel on Climate Change*, Stocker TF, Qin D, Plattner G-K, Tignor M, Allen SK, Boschung J, Nauels A, Xia Y, Bex V, Midgley PM (eds). Cambridge University Press: Cambridge, UK and New York, NY (2013).

Forsberg R., Sandberg Sørensen L., Nilsson J. and Simonsen S. B. : Mass balance of Greenland from combined GRACE and satellite altimetry inversion, *2014 AGU fall meeting* (2014).

Foster G. and Rahmstorf S. : Global temperature evolution 1979–2010. *Environmental Research Letters*, 6, 044022, doi:10.1088/1748-9326/6/4/044022 (2011).

Foster G. and Abraham J. : *US Clivar Variations* 13(3): 6–10 (2015).

Fu L. and Cazenave A. : Satellite Altimetry and Earth Sciences : A Handbook of Techniques and Applications. *Academic Press,* 2001.

Fyfe J. C., Meehl G. A., England M. H., Mann M. E., Santer B. D., Flato G. M., Hawkins E., Gillett N. P., Xie S. P., Kosaka Y. and Swart N. C. : Making sense in the early-2000s warming slowdown. *Nat. Clim. Change*, 6: 224–228 (2016).

Gaillard F., Autret E., Thierry V., Galaup P., Coatanoan C. and Loubrieu T. : Quality control of large Argo data sets. *J. Atmos. Oceanic Technol.*, 26, 337–351 (2009).

GAO C. C., LU Y., ZHANG Z. Z., SHI H. L. and ZHU C. D. : Ice sheet mass balance in Antarctica measured by GRACE and its uncertainty. *Chinese journal of geophysics*, Vol. 58, No. 3 (2015).

Garcia P. and Roca M. : ISARD_ESA_L1B_ESL_CCN_PRO_064, issue 1.b, 1 November 2010, ‘‘Onboard PTR processing analysis: MSL drift differences’’ (2010)

Gardner A. S., Moholdt G., Cogley J. G., Wouters B., Arendt A. A., Wahr J., Berthier E., Hock R., Pfeffer W. T., Kaser G., Ligtenberg S. R. M., Bolch T., Sharp M. J., Hagen J. O., van den Broeke M. R. and Paul F. : A reconciled estimate of glacier contributions to sea level rise, 2003-2009. *Science*, American Association for the Advancement of Science, 340 (6134), pp.852-857, DOI :10.1126/science.1234532 (2013).

Gaspar P. and Ogor F. : Estimation and analysis of the sea state bias of the ers-1 altimeter. *Rapport technique, Report of task B1-B2 of IFREMER Contract* n_ 94/2.426016/C. 84 (1994).

GCOS : Systematic observation requirements for satellite-based data products for climate (2011 update)—supplemental details to the satellite-based component of the ‘‘Implementation

plan for the global observing system for climate in support of the UNFCCC (2010 update)''. GCOS-154 (WMO, December 2011) (2011).

Gergis J. L. & Fowler A. M. : A history of ENSO events since A.D. 1525: Implications for future climate change. *Climatic Change***,** 92**,** 343_387 (2009).

Giles K. A., Laxon S. W., Ridout A. L., Wingham D. J. and Bacon S. : Western Arctic Ocean freshwater storage increased by wind-driven spin-up of the BeaufortAˆ Gyre. *Nat. Geosci.*, 5(3):194–197 (2012).

Goddard L. : Heat hide and seek, *Nature Climate Change*, vol 4, 158161 (2014).

Good, S. A., Martin, M. J., and Rayner, N. A.: EN4: quality controlled ocean temperature and salinity profiles and monthly objective analyses with uncertainty estimates. *J. Geophys. Res.Oceans*, 118, 6704–6716, doi:10.1002/2013JC009067 (2013).

Gordon A. L. : Oceanography of the Indonesian seas and their throughflow. *Oceanography*, 18 (4), 14-27 (2005).

Gordon A. L., Sprintall J., Van Aken H. M., Susanto D., Wijffels S., Molcard R., Ffield A., Pranowo W., Wirasantosa S. : "The Indonesian Throughflow during 2004-2006 as observed by the INSTANT program." "Modeling and Observing the Indonesian Throughflow", Guest Editors: A. L. Gordon and V.M. Kamenkovich, *Dynamics of Atmosphere and Oceans,* vol(50) 115-128 (2010).

Gouretski V. and Koltermann K. P. : How much is the ocean really warming ?. *Geophysical Research Letters*, *34*, 5 PP., doi :200710.1029/2006GL027834 (2007).

Gregory J. M., Banks H. T., Stott P. A., Lowe J. A. and Palmer M. D. : Simulated and observed decadal variability in ocean heat content. *Geophysical Research Letters*, *31*, 4 PP., doi :200410.1029/2004GL020258 (2004).

Gregory J. M., Lowe J. A. and Tett S. F. B. : Simulated Global-Mean sea level changes over the last Half-Millennium. *Journal of Climate*, *19* (18), 4576–4591, doi :10.1175/JCLI3881.1 (2006).

Gregory J.M., Church J.A., Clark P.U., Payne A.J., Merrifield M.A., Nerem R.S., Nunn P.D., Pfeffer W.T., Stammer D. : Comment on "Expert assessment of sea-level rise by AD 2100 and AD 2300", by Horton et al. (2014) *Quaternary Science Reviews, Volume 97, 1 August 2014, Pages 193-194* (2014).

Groh A., Ewert H., Rosenau R., Fagiolini E., Gruber C., Floricioiu D., Abdel Jaber W., Linow S., Flechtner F., Eineder M., Dierking W., Dietrich R. : Mass, Volume and Velocity of the Antarctic Ice Sheet: Present-Day Changes and Error Effects. *Surv. Geophys.*, 35, 1481–1505, DOI:10.1007/s10712-014-9286-y (2014a).

Groh A., Ewert H., Fritsche M., Rülke A., Rosenau R., Scheinert M. and Dietrich R. : Assessing the current evolution of the Greenland ice sheet by means of satellite and ground-based observations. *Surv. Geophys.*, 35 1459–80 (2014b).

Gu G., Adler R. F., Huffman G. J. and Curtis S. : Tropical rainfall variability on interannual to interdecadal and longer time scales derived from the GPCP monthly products. *J. Climate*, 20, 4033-4046 (2007).

Gu G. & Adler R. F. : Precipitation and temperature variations on the interannual time scale: Assessing the impact of ENSO and volcanic eruptions. *J. Climate,* 24, 2258_2270 (2011).

Guemas V**.,** Doblas-Reyes F. J., Andreu-Burillo I. and Asif M. : Retrospective prediction of the global warming slowdown in the past decade. *Nature Climate Change,* 3, 649-653, doi : 10.1038/nclimate1863 (2013).

Haines B. J., Desai S. D. and Born G. H. : The harvest experiment: calibration of the climate data record from TOPEX/Poseidon, Jason-1 and the ocean surface topography mission. *Mar. Geod.*, 33(S1):91–113 (2010).

Hallegate S., Green C., Nicholls R. J. & Corfee-Morlot J. : Future flood losses in major coastal cities. *Nature Clim. Change***, 3,** 802_806 (2013).

Hamlington B. D., Thompson P., Hammond W. C., Blewitt G., Ray R. D. : Assessing the impact of vertical land motion on twentieth century global mean sea level estimates. *Journal of Geophysical Research: Oceans, 2016, 121, 7, 4980* (2016).

Hanna et al. : Ice-sheet mass balance and climate change. *Nature,* 498, 51-59, doi:10.1038/nature12238 (2013).

Hansen J., Ruedy R., Sato M. and Lo K. : Global surface temperature change. *Rev. Geophys.,* 48: RG4004 (2010).

Hansen J., Sato M., Kharecha P. &von Schuckmann K. : Earth's energy imbalance andimplications. *Atmos. Chem. Phys.*, 11, 13421-13449, doi: 10.5194/acp-11-13421-2011 (2011).

Haq B. U. and Al-Qahtani A. M. : Phanerozoic cycles of sea-level change on the arabian platform. *Geoarabia, 10* (2), 127–160, WOS :000231694200005 (2005).

Haq B. U. and Schutter S. R. : A chronology of paleozoic sea-level changes. *Science, 322* (5898), 64–68, doi :10.1126/science.1161648, WOS :000259680200036 (2008).

Harig Christopher and Simons Frederik J. : Accelerated West Antarctic ice mass loss continues to outpace East Antarctic gains. *Earth and Planetary Science Letters,* 415, 134–141, doi:10.1016/j.epsl.2015.01.029 (2015).

Hay C. C., Morrow E., Kopp R. E. and Mitrovica J. X. : Estimating the sources of global sea level rise with data assimilation techniques. *Proc. Natl. Acad. Sci. U.S.A.,* 110, 3692–3699 (2013).

Hay C. C., Morrow E., Kopp R. E. & Mitrovica J. X. : Probabilistic reanalysis of twentieth-century sea level rise. *Nature,* 517(7535):481 doi:10.1038/nature14093 (2015).

Hegerl G. C., Zwiers F. W., Braconnot P., Gillett N. P., Luo Y., Marengo Orsini J. A., Nicholls N., Penner J. E. and Stott P. A. : Understanding and Attributing Climate Change. In *Climate Change 2007: The Physical Science Basis. Contribution of Working Group I to the Fourth Assessment Report of the Intergovernmental Panel on Climate Change*, Solomon S, Qin D, Manning M, Chen Z, MarquisM, Averyt KB, Tignor M, Miller HL (eds). Cambridge University Press: Cambridge, UK and New York, NY (2007).

Heiskanen W. A. and Moritz H. : Physical Geodesy, W.H. Freeman and Co., San Francisco (1967).

Held I. M. : The cause of the pause. *Nature*, 501, 318-319 (2013).

Helm V., Humbert A. and Miller H. : Elevation and elevation change of Greenland and Antarctica derived from CryoSat-2. *Cryosphere*, 8, 1539–1559, doi:10.5194/tc-8-1539-2014 (2014).

Henry O., Ablain M., Meyssignac B., Cazenave A., Masters D., Nerem S., Leuliette E. and Garric G. : Investigating and reducing differences between the satellite altimetry-based global mean sea level time series provided by different processing groups. *J. Geodesy*, 88, 351–361, doi:10.1007/s00190-013-0687-3 (2014).

Holgate S. J. : On the decadal rates of sea level change during the twentieth century. *Geophys. Res. Lett.*, 34, L01602 (2007).

IPCC 2013. *Climate Change 2013: The Physical Science Basis. Contribution of Working Group I to the Fifth Assessment Report of the Intergovernmental Panel on Climate Change*, Stocker TF, Qin D, Plattner G-K, Tignor M, Allen SK, Boschung J, Nauels A, Xia Y, Bex V, Midgley PM (eds). Cambridge University Press: Cambridge, UK and New York, NY (2013).

Ishii M., Shouji A., Sugimoto S. and Matsumoto T. : Objective analyses of sea-surface temperature and marine meteorological variables for the 20th century using ICOADS and the Kobe collection. *Int. J. Climatol.*, 25: 865–879 (2005).

Ishii M., Kimoto M., Sakamoto K. and Iwasaki S. : Steric sea level changes estimated from historical ocean subsurface temperature and salinity analyses. *Journal of Oceanography, 62* (2), 155–170, doi :10.1007/s10872-006-0041-y (2006).

Ishii M. and M. Kimoto : Reevaluation of historical ocean heat content variations with time-varying XBT and MBT depth bias corrections, *J. Oceanogr.*, *65*(3), 287–299, doi:10.1007/s10872-009-0027-7 (2009).

Jacob T., Wahr J., Pfeffer W. T. and Swenson S. : Recent contributions of glaciers and ice caps to sea level rise. *Nature, 482* (7386), 514–518, doi :10.1038/nature10847 (2012).

Jalabert E., Couhert A., Moyard J., Mercier F., Houry S. and Rios-Bergantinos S. : Jason-2, SARAL and CryoSat-2 status. Ocean surface topography science team meeting, Reston, Virginia, USA, October 2015. (2015) http://meetings.aviso.altimetry.fr/fileadmin/user_upload/tx_ausyclsseminar/files/OSTST2015/POD-01-Jalabert.pdf

Japan Meteorological Agency : Characteristics of Global Sea Surface Temperature Analysis Data (COBE-SST) for climate use. Monthly Report on Climate System Separated Volume 12, 116pp (2006).

Jensen L., Rietbroek R. and Kusche J. : Land water contribution to sea level and Jason-1 measurements, *J. Geophys. Res. Oceans*, 118, 212-226, doi:10.1002/jgrc.20058 (2013).

Jevrejeva S., Grinsted A., Moore J. C. and Holgate S. : Nonlinear trends and multiyear cycles in sea level records. *J. Geophys. Res. Oceans*, 111, C09012 (2006).

Jevrejeva S., Moore J. C., Grinsted A. and Woodworth P. L. : Recent global sea level acceleration started over 200 years ago? Geophys. Res. Lett., 35, L08715 (2008).

Jevrejeva S., Grinsted A. and Moore J. C. : Anthropogenic forcing dominates sea level rise since 1850. *Geophys. Res. Lett.*, 36, L20706 (2009).

Jevrejeva S., Moore J. C., Grinsted A., Matthews A. P. and Spada G. : Trends and acceleration in global and regional sea levels since 1807. *Global Planet. Change, 113, 11–22* (2014).

Johnson G. C. and Chambers D. P. : Ocean bottom pressure seasonal cycles and decadal trends from GRACE Release-05: Ocean circulation implications. *J. Geophys. Res.-Oceans*, 118, 4228–4240, doi:10.1002/jgrc.20307 (2013).

Jung M., Reichstein M., Ciais P., Seneviratne S. I., Sheffield J., Goulden M. L., Bonan G., Cescatti A., Chen J., de Jeu R., Dolman A. J., Eugster W., Gerten D., Gianelle D., Gobron N., Heinke J., Kimball J., Law B. E., Montagnani L., Mu Q., Mueller B., Oleson K., Papale D., Richardson A. D., Roupsard O., Running S., Tomelleri E., Viovy N., Weber U., Williams C., Wood E., Zaehle S. and Zhang K. : Recent decline in the global land evapotranspiration trend due to limited moisture supply. *Nature*, 467, 951-954, doi:10.1038/nature09396 (2010).

Kaplan A., Cane M., Kushnir Y., Clement A., Blumenthal M. and Rajagopalan B. : Analyses of global sea surface temperature 1856–1991. *J. Geophys. Res.*, 103(18): 567–589 (1998).

Karl T. R., Arguez A., Huang B., Lawrimore J. H., McMahon J. R., Menne M. J., Peterson T. C., Vose R. S. and Zhang H. : Possible artifacts of data biases in the recent global surface warming hiatus. *Science*, 348 (6242): 1469-1472, *DOI:* 10.1126/science.aaa5632 (2015).

Kaula W. : The terrestrial environment: solid earth and ocean physics. Williamstown report, M.I.T., Cambridge, MA, NASA CR-1579, April 1970. http://ilrs.gsfc.nasa.gov/docs/williamstown_1968.pdf (1970).

Kemp A. C., Horton B. P., Donnelly J. P., Mann M. E., Vermeer M. and Rahmstorf S. : Climate related sea-level variations over the past two millennia RID a-8465-2010, *Proceedings of the National Academy of Sciences of the United States of America, 108* (27), 11,017–11,022, doi :10.1073/pnas.1015619108, WOS :000292376700025 (2011).

Kennedy J. J., Rayner N. A., Smith R. O., Saunby M. and Parker D. E. : Reassessing biases and other uncertainties in sea-surface temperature observations since 1850 part 1: measurement and sampling errors. *J. Geophys. Res.*, 116: D14103 (2011).

Khan Shfaqat A, Aschwanden A., Bjørk A. A., Wahr J., Kjeldsen K. K. and Kjær K. H. : Greenland ice sheet mass balance. *Rep. Prog. Phys.*, 78, 046801 (26pp), doi:10.1088/0034-4885/78/4/046801 (2015).

Kirkup L. : *'Experimental Methods. An Introduction to the Analysis and Presentation of Data*. Wiley-VCH pp. 216. ISBN 0-471-33579-7 (1996).

Konikow L. F. : Contribution of global groundwater depletion since 1900 to sea-level rise. *Geophys. Res. Lett.*, 38, L17401, doi:10.1029/2011GL048604 (2011).

Kopp R. E., Simons F. J., Mitrovica J. X., Maloof A. C. and Oppenheimer M. : Probabilistic assessment of sea level during the last interglacial stage. *Nature*, 462, 863–868 (2009).

Kopp R. E., Mitrovica J. X., Griffies S. M., Yin J., Hay C. C. and Stouffer R. J. : The impact of greenland melt on local sea levels : a partially coupled analysis of dynamic and static equilibrium effects in idealized water-hosing experiments. *Climatic Change, 103* (3-4), 619–625, doi :10.1007/s10584-010-9935-1 (2010).

Kopp R. E., Simons F. J., Mitrovica J. X., Maloof A. C. and Oppenheimer M. : A probabilistic assessment of sea level variations within the last interglacial stage. *Geophys. J. Int.*, 193, 711–716 (2013).

Kosaka Y. and Xie S.-P. : Recent global warming hiatus tied to equatorial Pacific surface cooling, Nature, 501, 403–407 (2013).

Kouketsu S., Doi T., Kawano T., Masuda S., Sugiura N., Sasaki Y., Toyoda T., Igarashi H., Kawai Y., Katsumata K., Uchida H., Fukasawa M. and Awaji T. : Deep ocean heat content changes estimated from observation and reanalysis product and their influence on sea level change. *J. Geophys. Res.*, 116, C03012, doi:10.1029/2010JC006464 (2011).

Kuhlbrodt T. and Gregory J. M. : Ocean heat uptake and its consequence for the magnitude of sea level rise and climate change. *Geophys. Res. Lett.* 39: L18608 (2012).

Labroue S., Boy F., Picot N., Urvoy M. and Ablain M. : First quality assessment of the CryoSat-2 altimetric system over ocean. *Adv Space Res*, 50(8):1030–1045. doi:10.1016/j.asr.2011.11.018 (2012).

Lambeck K. : Aristoteles – An ESA Mission to Study the Earth' s Gravity Field. *ESA Journal*, 14, 1-21 (1990).

Lambeck K., Esat T. and Potter E. : Links between climate and sea levels for the past three million years. *Nature, 419* (6903), 199–206, doi :10.1038/nature01089, WOS :000177931200049 (2002).

Lambeck K., Anzidei M., Antonioli F., Benini A. and Esposito A. : Sea level in roman time in the central mediterranean and implications for recent change. *Earth and Planetary Science Letters, 224* (3-4), 563–575, doi :10.1016/j.espal.2004.05.031, WOS :000223582400024 (2004).

Lambeck K., Woodroffe C. D., Antonioli F., Anzidei M., Gehrels W. R., Laborel J. and Wright A. J. : Paleoenvironmental records, geophysical modeling, and reconstruction of Sea-Level trends and variability on centennial and longer timescales, in *Understanding Sea-Level Rise and Variability*, edited by J. A. Church, P. L. Woodworth, T. Aarup, and W. S. Wilson, pp. 61–121, Wiley-Blackwell, (2010).

Lambeck K., Purcell A. and Dutton A. : The anatomy of interglacial sea levels: The relationship between sea levels and ice volumes during the Last Interglacial. Earth Planet. *Sci. Lett.*, 315, 4–11 (2012).

Landerer F. W. and Swenson S. C. : Accuracy of scaled GRACE terrestrial water storage estimates. *Water Resour. Res.*, 48, W04531, doi:10.1029/2011WR011453 (2012).

Le Traon P. Y., Faugère Y., Hernandez F., Dorandeu J., Mertz F. and Ablain M. : Can we merge GEOSAT follow-on with TOPEX/Poseidon and ERS-2 for an improved description of the ocean circulation? *J Atmos Ocean Technol* 20:889–895. doi:10.1175/1520-0426(2003)020\0889:CWMGFW[2.0.CO;2 (2003).

Legeais J-F., Ablain M. and Thao S. : Evaluation of wet troposphere path delays from atmospheric reanalyses and radiometers and their impact on the altimeter sea level. *Ocean Sci*., 10:893–905. doi:10.5194/os-10-893-2014 (2014).

Legeais J-F., Prandi P. and Guinehut S. : Analyses of altimetry errors using Argo and GRACE data. *Ocean Sci.*, 12:647–662. doi:10.5194/os-12-647-2016 (2016).

Leuliette E.W. & Miller L. : Closing the sea level rise budget with altimetry, Argo and GRACE. *Geophys. Res. Lett.* 36, L04608, doi:10.1029/2008GL036010 (2009).

Leuliette E. W. and Willis J. K. : Balancing the sea level budget. *Oceanography*, 24, 122-129 doi:10.5670/oceanog.2011.32 (2011).

Levitus S., Antonov J. and Boyer T. : Warming of the world ocean, 1955-2003. *Geophysical Research Letters*, *32*, 4 PP., doi :200510.1029/2004GL021592 (2005).

Levitus S., Antonov J. I., Boyer T. P., Locarnini R. A., Garcia H. E. and Mishonov A. V. : Global ocean heat content 1955–2008 in light of recently revealed instrumentation problems. *Geophys. Res. Lett.*, 36, L07608, doi:10.1029/2008GL037155 (2009).

Levitus S., Antonov J. I., Boyer T. P., Baranova O. K., Garcia H. E., Locarnini R. A., Mishonov A. V., Reagan J.R., Seidov D., Yarosh E.S. and Zweng M. M. : World ocean heat content and thermosteric sea level change (0-2000 m), 1955-2010. *Geophys. Res. Lett.*, 39, L10603 640, doi:10.1019/2012GL051106 (2012).

Lewandowsky S., Risbey J. S. and Oreskes N. : On the definition and identifiability of the alleged "hiatus" in global warming. *Sci. Rep.* 5: 16784 (2015).

Lewandowsky S., Risbey J. S. and Oreskes N. : The pause in global warming: Turning a routine fluctuation into a problem for science. *American Meteorological Society*, 97(5), 723-733. DOI: 10.1175/BAMS-D-14-00106.1 (2016).

Lillibridge J., Smith W. H. F., David Sandwell D., Scharroo R., Frank G., Lemoine F. G., Zelensky N. P. : 20 years of improvements to GEOSAT altimetry. *Symposium: 15 years of progress in radar altimetry, Venice, Italy, March* 13–18, 2006. (2006) http://earth.esa.int/workshops/venice06/participants/509/paper_ 509_lillibridge.pdf

Llovel W., Becker M., Cazenave A. and Crétaux J. F. : Contribution of land water storage change to global mean sea level from GRACE and satellite altimetry. *C.R. Geosciences*, 342, 179-188 (2010).

Llovel W., Becker M., Cazenave A., Jevrejeva S., Alkama R., Decharme B., Douville H., Ablain M. and Beckley B. : Terrestrial waters and sea level variations on interannual time scale. *Glob. Planet. Change*, **75,** 76_82, doi:10.1016/j.gloplacha.2010.10.008 (2011).

Llovel W., Willis J. K., Landerer F. W. and Fukumori I. : Deep-ocean contribution to sea level and energy budget not detectable over the past decade. *Nature Climate Change*, 4, 1031–1035, doi:10.1038/NCLIMATE2387 (2014).

Loeb N. G., Kato S., Su W. Y., Wong T. M., Rose F. G., Doelling D. R. and Huang X. L. : Advances in understanding top-of-atmosphere radiation variability from satellite observations. *Surv. Geophys.*, 33, 359–385, doi:10.1007/s10712-012-9175-1 (2012a).

Loeb N. G., Lyman J. M., Johnson G. C., Allan R. P., Doelling D. R., Wong T., Soden B. J. and Stephens G. L. : Observed changes in top-of-the-atmosphere radiation and upper-ocean heating consistent within uncertainty. *Nature Geosci.* 5, 110_113 DOI: 10.1038/NGEO1375 (2012b).

Lombard A., Cazenave A., Le Traon P. Y. and Ishii M. : Contribution of thermal expansion to present-day sea-level change revisited. *Global Planet. Change*, 47, 1–16 (2005).

Longuevergne L., Scanlon B. R., and Wilson C. R. : GRACE Hydrological estimates for small basins: Evaluating processing approaches on the High Plains Aquifer, USA, *Water Resour. Res.*, 46, W11517, doi:10.1029/2009WR008564 (2010).

Luthke S. B., Zwally H. J., Abdalati W., Rowlands D. D., Ray R. D., Nerem R. S., Lemoine F. G., McCarthy J. J. and Chinn D. S. : Recent Greenland ice mass loss by drainage system from satellite gravity observations. *Science*, 314, 1286–9 (2006).

Lyman J. M., Godd S. A., Gouretski V. V., Ishii M., Johnson G. C., Palmer M. D., Smith D. M. and Willis J. K. : Robust warming of the global upper ocean. *Nature*, 465, 334–337, doi:10.1038/nature09043 (2010).

Lyman, J. M. and Johnson, G. C.: Estimating global ocean heat content changes in the upper 1800m since 1950 and the influence of climatology choice. *J. Climate*, 27, 1945–1957, doi:10.1175/JCLIM-D-12-00752.1 (2014).

Mantas V. M., Liu Z. and Pereira A. J. S. C. : A Web service and android application for the distribution of rainfall estimates and Earth observation data. *Computers & Geosciences*, **77**, 66-76, doi:10.1016/j.cageo.2015.01.011 (2015).

Marcos M., Puyol B., Calafat F.M., Wöppelmann G., : Sea level changes at Tenerife Island (NE Tropical Atlantic) since 1927. *Journal of Geophysical Research,* 118, 4899-4910, doi:10.1029/2011JC007558 (2013).

Marzeion B., Jarosch A. H. and Hofer M. : Past and future sea-level changes from the surface mass balance of glaciers. *Cryosphere,* 6, 1295–1322 (2012).

Marzeion B., Leclercq P. W., Cogley J. G., Jarosch A. H. : Brief Communication: 1053 Global reconstructions of glacier mass change during the 20th century are 1054 consistent. The Cryosphere 9:2399–2404. doi:10.5194/tc-9-2399-2015 (2015).

Marzeion B., Champollion N., Haeberli W., Langley K., Leclercq P., Paul F. : Observation of glacier mass changes on the global scale and its contribution to sea level change. *Surv. Geophys.,* DOI 10.1007/s10712-016-9394-y (2016).

Masson-Delmotte, V., M. Schulz, A. Abe-Ouchi, J. Beer, A. Ganopolski, J.F. González Rouco, E. Jansen, K. Lambeck, J. Luterbacher, T. Naish, T. Osborn, B. Otto-Bliesner, T. Quinn, R. Ramesh, M. Rojas, X. Shao and A. Timmermann, : Information from Paleoclimate Archives. In: Climate Change 2013: The Physical Science Basis. Contribution of Working Group I to the Fifth Assessment Report of the Intergovernmental Panel on Climate Change [Stocker, T.F., D. Qin, G.-K. Plattner, M. Tignor, S.K. Allen, J. Boschung, A. Nauels, Y. Xia, V. Bex and P.M. Midgley (eds.)]. Cambridge University Press, Cambridge, United Kingdom and New York, NY, USA (2013).

Masters D., Nerem R. S., Choe C., Leuliette E., Beckley B., White N. and Ablain M. : Comparison of global mean sea level time series from TOPEX/Poseidon, Jason-1, and Jason-2. *Mar. Geod.,* 35, 20–41, DOI:10.1080/01490419.2012.717862 (2012).

McGranahan G., Balk D. and Anderson B. : The rising tide: assessing the risks of climate change and human settlements in low elevation coastal zones. Environ Urban 19: 17–37. doi: 10.1177/0956247807076960 (2007).

McPhaden M. J. : TOGA-TAO and the 1991-93 El Niño-Southern Oscillation Event. *Oceanography,* 6, 36-44 (1993).

McPhaden M. J. : Genesis and evolution of the 1997-98 El Niño. *Science,* 283, 950-954 (1999).

McPhaden M. J., Zebiak S. E. and Glantz M. H. : ENSO as an integrating concept in Earth science. *Science,* 314, 1740-1745 (2006).

MEEHL G. A., STOCKER T. F., COLLINS W. D., FRIEDLINGSTEIN P., GAYE A. T., GREGORY, J. M., KITOH R., KNUTTI R., MURPHY J. M., NODA A., RAPER S. C. B., WATTERSON I. G., WEAVER A. J. and ZHAO Z.-C. : Global climate projections. Climate Change 2007: The Physical Science Basis. Contribution of Working Group 1 to the Fourth Assessment Report of the Intergovernmental Panel on Climate Change. [SOLOMON, S., QIN, D., MANNING, M., CHEN, Z., MARQUIS, M., AVERYT, K. B., TIGNOR, M. and MILLER, H. L.] Cambridge, UK and New York, NY, USA; Cambridge University Press. (2007)

Meehl G. A., Arblaster J. M., Fasullo J. T. and Trenberth K. E. : Model-based evidence of deep-ocean heat uptake during surface temperature hiatus periods. *Nature Climate Change*, 1, 360–364, doi:10.1038/NCLIMATE1229 (2011).

Melet A. and Meyssignac B. : Explaining the spread in global mean thermosteric sea level rise. *J. Clim.*, 28: 9918–9940 (2015).

Mertz F., Mercier F., Labroue S., Tran N. and Dorandeu J. : ERS-2 OPR data quality assessment; long-term monitoring—particular investigation. *CLS.DOS.NT-06.001* (2005) http://www.aviso.altimetry.fr/fileadmin/documents/calval/validation_report/E2/annual_report_e2_2005.pdf. Access 11 May 2016

Meyssignac B., Becker M., Llovel W., Cazenave A. : An Assessment of Two-Dimensional Past Sea Level Reconstructions Over 1950–2009 Based on Tide-Gauge Data and Different Input Sea Level Grids. *Surveys in Geophysics*, Volume 33, Issue 5, pp 945-972. doi:"10.1007/s10712-011-9171-x (2012)

Meyssignac B. and Cazenave A. : Sea level: a review of present-day and recent-past sea level change and variability. *J. Geodyn.*, 58, 96-109 (2012).

Miller K. G., Kominz M. A., Browning J. V., Wright J. D., Mountain G. S., Katz M. E., Sugarman P. J., Cramer B. S., Christie-Blick N. and Pekar S. F. : The phanerozoic record of global Sea-Level change. *Science, 310* (5752), 1293–1298, doi :10.1126/science.1116412 (2005).

Miller K. G., Sugarman P. J., Browning J. V., Horton B. P., Stanley A., Kahn A., Uptegrove J. and Aucott M. : Sea-level rise in new jersey over the past 5000 years : Implications to anthropogenic changes. *Global and Planetary Change*, *66* (1-2), 10–18, doi : 10.1016/j.gloplacha.2008.03.008 (2009).

Miller K. G., Mountain G. S., Wright J. D. and Browning J. V. : A 180-Million-Year record of sea level and ice volume variations from continental margin and Deep-Sea isotopic records. *Oceanography*, *24* (2), 40–53, WOS :000292348000008 (2011).

Milne G. and Mitrovica J. : Searching for eustasy in deglacial sea-level histories. *Quaternary Science Reviews, 27* (25-26), 2292–2302, doi :10.1016/j.quascirev.2008.08.018 (2008).

Milne G. A., Gehrels W. R., Hughes C. W. and Tamisiea M. E. : Identifying the causes of sea-level change. *Nature Geoscience*, *2* (7), 471–478, doi :10.1038/ngeo544 (2009).

Mitchum G. T. : Monitoring the stability of satellite altimeters with tide gauges. *J Atmos Ocean Technol* 15(3):721–730 (1998).

Mitchum G. T., Nerem R. S., Merrifield M. A. and Gehrels W. R. : Modern sea level change estimates. in *Understanding Sea-Level Rise and Variability*, edited by J. A. Church, P. L. Woodworth, T. Aarup, and W. S. Wilson, pp. 122–142, Wiley-Blackwell (2010).

Mondal P. and Tatem A. J. : Uncertainties in Measuring Populations Potentially Impacted by Sea Level Rise and Coastal Flooding. *PLoS ONE*, 7(10): e48191. doi:10.1371/journal.pone.0048191 (2012).

Müller R. D., Sdrolias M., Gaina C., Steinberger B. and Heine C. : Long-Term Sea-Level fluctuations driven by ocean basin dynamics. *Science*, *319* (5868), 1357–1362, doi :10. 1126/science.1151540 (2008).

Munk W. : Ocean freshening, sea level rising. *Science*, 300, 2041–2043 DOI: 10.1126/science.1085534 (2003).

Myhre, G., D. Shindell, F.-M. Bréon, W. Collins, J. Fuglestvedt, J. Huang, D. Koch, J.-F. Lamarque, D. Lee, B. Mendoza, T. Nakajima, A. Robock, G. Stephens, T. Takemura and H. Zhang, : Anthropogenic and Natural Radiative Forcing. In: Climate Change 2013: The Physical Science Basis. Contribution of Working Group I to the Fifth Assessment Report of the Intergovernmental Panel on Climate Change [Stocker, T.F., D. Qin, G.-K. Plattner, M. Tignor, S.K. Allen, J. Boschung, A. Nauels, Y. Xia, V. Bex and P.M. Midgley (eds.)]. Cambridge University Press, Cambridge, United Kingdom and New York, NY, USA (2013).

Naish T., Powell R., Levy R., Wilson G., Scherer R., Talarico F., Krissek L., Niessen F., Pompilio M., Wilson T., Carter L., DeConto R., Huybers P., McKay R., Pollard D., Ross J., Winter D., Barrett P., Browne G., Cody R., Cowan E., Crampton J., Dunbar G., Dunbar N., Florindo F., Gebhardt C., Graham I., Hannah M., Hansaraj D., Harwood D., Helling D., Henrys S., Hinnov L., Kuhn G., Kyle P., Läufer A., Maffioli P., Magens D., Mandernack K., McIntosh W., Millan C., Morin R., Ohneiser C., Paulsen T., Persico D., Raine I., Reed J., Riesselman C., Sagnotti L., Schmitt D., Sjunneskog C., Strong P., Taviani M., Vogel S., Wilch T. and T. Williams : Obliquity-paced Pliocene West Antarctic ice sheet oscillations. Nature, 458, 322–328 doi:10.1038/nature07867 (2009).

Nerem R. S., Chambers D. P., Choe C. and Mitchum G. T. : Estimating mean sea level change from the TOPEX and Jason altimeter missions. *Mar. Geodesy*, 33 (1), 435–446 (2010).

Ngo-Duc T., Laval K., Polcher J., Lombard A., Cazenave A. : Effects of land water storage on global mean sea level over the past 50 years. *Geophys. Res. Lett.*, 32, L09704, doi:10.1029/2005GL022719 (2005).

Nicholls R. J., Hanson S., Herweijer C., Patmore N., Hallegatte S., Corfee-Morlot J., Chateau J. and Muir-Wood R. : Ranking port cities with high exposure and vulnerability to climate extremes : Exposure estimates, OECD Environment Working Papers, No. 1, OECD Publishing. http ://dx.doi.org/10.1787/011766488208 (2008).

Nicholls R. J. and Cazenave A. : Sea-level rise and its impact on coastal zones. *Science*, 328, 1517_1520 (2010).

Nicholls R. J., MARINOVA N., LOWE J. A., BROWN S., VELLINGA P., DE GUSMÃO D., HINKEL J. and TOL R. S. J. : Sea-level rise and its possible impacts given a ‘beyond 4 degrees C world’ in the twenty-first century. *Philos. Trans. R. Soc. London A*, 369, 161–181 doi:10.1098/rsta.2010.0291 (2011a).

Nicholls R. J., Hanson S. E., Lowe J. A., Warrick R. A., Lu X., Long A. J. and Carter T. R. : Constructing Sea-Level Scenarios for Impact and Adaptation Assessment of Coastal Area: A Guidance Document. Supporting Material, Intergovernmental Panel on Climate Change

Task Group on Data and Scenario Support for Impact and Climate Analysis (TGICA), 47 pp (2011b).

Nieves V., Willis J. K. and Patzert W. C. : Recent hiatus caused by decadal shift in Indo-Pacific heating. *Science***,** 349(6247): 532–535. *DOI:* 10.1126/science.aaa4521 **(**2015).

Oki T. and Sud Y.C. : Design of Total Runoff Integrating Pathways (TRIP), A Global River Channel Network. *Earth Inter.*, Vol. 2., Paper 1 (1998).

Okumura Y. and Deser C. : Asymmetry in the duration of El Nino and La Nina. *J. Climate*, 23, 5826-5843 (2010).

Osborn T. J., Jones P. D. : The CRUTEM4 land-surface air temperature dataset: construction, previous versions and dissemination via Google Earth. *Earth System Sci. Data* 6: 61–68 (2014).

Palmer M. D. and Mc Neal D. J. : Internal variability of Earth's energy budget simulated by CMIP5 climate models. *Environ. Res. Lett.* 9: 034016 (2014).

Parry M., Canziani O., Palutikof J., van der Linden P. and Hanson C. (Eds.) : *Contribution of Working Group II to the Fourth Assessment Report of the Intergovernmental Panel on Climate Change, 2007*, Cambridge University Press, Cambridge, United Kingdom and New York, NY, USA, (2007).

Passchier S. : Linkages between East Antarctic Ice Sheet extent and Southern Ocean temperatures based on a Pliocene high-resolution record of ice-rafted debris off Prydz Bay, East Antarctica. *Paleoceanography*, 26, Pa4204 (2011).

Peltier W. R. : Global glacial isostatic adjustment and modern instrumental records of relative sea level history. In *Sea Level Rise: History and Consequences*, ed. B. C. Douglas, M. S. Kearney, S. P. Leatherman. pp. 65–95. *San Diego: Academic* (2001).

Peltier W. R. : Global glacial isostasy and the surface of the ice-age Earth: the ICE-5G (VM2) model and GRACE. *Annu. Rev. Earth Pl. Sc.*, 32, 111–149 (2004).

Peltier W. R. : Closure of the budget of global sea level rise over the GRACE era: the importance and magnitudes of the required corrections for global glacial isostatic adjustment. *Quat. Sci. Rev.* 28:1658–74 (2009).

Peltier W. R., Luthcke S. B. : On the origins of Earth rotation anomalies: new insights on the basis of both "paleogeodetic" data and Gravity Recovery and Climate Experiment (GRACE) data. *J. Geophys. Res.* 114:B11405 (2009).

Peters G. P., Marland G., Le Queré C., Boden T., Canadell J. G. and Raupach M. R. : Rapid growth in CO_2 emissions after the 2008–2009 global financial crisis. *Nature Climate Change*, 2, 2–4 (2012).

Pfeffer W. T., Arendt A. A., Bliss A., Bolch T., Cogley J. G., Gardner A. S., Hagen J-O., Hock R., Kaser G., Kienholz C., Miles E. S., Moholdt G., Mölg N., Paul F., Radić V., Rastner P.,

Raup B. H., Rich J. and Sharp M. J. : The Randolph Glacier Inventory: a globally complete inventory of glaciers. Journal of Glaciology 60(221):537-552 (2014)

Pokhrel Y. N., Hanasaki N., Yeh P. J.-F., Yamada T., Kanae S. and Oki T. : Model estimates of sea level change due to anthropogenic impacts on terrestrial water storage. *Nat. Geosci.*, 5, 389–392, doi:10.1038/ngeo1476 (2012).

Prandi P., Ablain M., Cazenave A. and Picot N. : A new estimation of mean sea level in the arctic ocean from satellite altimetry. *Mar. Geod*., 35(1):61–81 (2012).

Pujol M. I., Faugère Y., Taburet G., Dupuy S., Pelloquin C., Ablain M. and Picot N. : DUACS DT2014: the new multimission altimeter dataset reprocessed over 20 years. *Ocean Sci.*, 12, 1067-1090, doi:10.5194/os-12-1067-2016 (2016).

Purkey S. and Johnson G.C. : Warming of global abyssal and deep southern ocean waters between the 1990s and 2000s: contributions to global heat and sea level rise budget. *J. Clim.*, 23:6336-6351 (2010).

Radic V. and Hock R. : Regional and global volumes of glaciers derived from statistical upscaling of glacier inventory data. *Journal of Geophysical Research, 115*, 10 PP., doi : 201010.1029/2009JF001373 (2010).

Ramillien G., Lombard A., Cazenave A., Ivins E. R., Llubes M., Remy F. and Biancale R. : Interannual variations of the mass balance of the Antarctica and Greenland ice sheets from GRACE. *Glob. Planet. Change*, 53, 198–208, DOI: 10.1016/j.gloplacha.2006.06.003 (2006).

Ramillien G., Bouhours S., Lombard A., Cazenave A., Flechtner F. and Schmidt R. : Land water contributions from GRACE to sea level rise over 2002-2006. *Global and Planetary Change*, 60, 381-392 (2008).

Ray C., Martin-Puig C., Clarizia M. P., Ruffini G., Dinardo S., Gommenginger C. and Benveniste J. : SAR altimeter backscattered waveform model. *IEEE Trans Geosci Remote Sens* 53(2):911–919. doi:10.1109/TGRS.2014.2330423 (2014).

Ray R. D. : Precise comparisons of bottom-pressure and altimetric ocean tides. *J Geophys Res Oceans* 118:4570–4584. doi:10.1002/jgrc.20336 (2013).

Ray R. D. and Douglas B. C. : Experiments in reconstructing twentieth-century sea levels. *Prog. Oceanogr.*, 91, 495–515 (2011).

Raymo M. E., Mitrovica J. X., O'Leary M. J., DeConto R. M. and Hearty P. L. : Departures from eustasy in Pliocene sea-level records. *Nature Geosci.*, 4, 328– 332 (2011).

Raymo M. E. and Mitrovica J. X. : Collapse of polar ice sheets during the stage 11 interglacial. *Nature*, 483, 453–456 (2012).

Rhein M., S.R. Rintoul, S. Aoki, E. Campos, D. Chambers, R.A. Feely, S. Gulev, G.C. Johnson, S.A. Josey, A. Kostianoy, C. Mauritzen, D. Roemmich, L.D. Talley and F. Wang, : Observations: Ocean. In: Climate Change 2013: The Physical Science Basis. Contribution

of Working Group I to the Fifth Assessment Report of the Intergovernmental Panel on Climate Change [Stocker, T.F., D. Qin, G.-K. Plattner, M. Tignor, S.K. Allen, J. Boschung, A. Nauels, Y. Xia, V. Bex and P.M. Midgley (eds.)]. Cambridge University Press, Cambridge, United Kingdom and New York, NY, USA (2013).

Rignot E. and Kanagaratnam P. : Changes in the velocity structure of the Greenland ice sheet Science 311 (5763), 986–990, DOI:10.1126/science.1121381 (2006).

Rignot E., Box J. E., Burgess E. and Hanna E. : Mass balance of the Greenland ice sheet from 1958 to 2007. *Geophys. Res. Lett.*, 35, L20502, doi:10.1029/2008GL035417 (2008).

Rignot E., Velicogna I., van den Broeke M. R., Monaghan A. and Lenaerts J. : Acceleration of the contribution of the Greenland and Antarctic ice sheets to sea level rise. *Geophys. Res. Lett.,* 38, L05503, doi:10.1029/2011GL046583 (2011).

Riva R. E. M., Bamber J. L., Lavallée D. A. and Wouters B. : Sea-level fingerprint of continental water and ice mass change from GRACE. *Geophys. Res. Lett.* 37:L19605 (2010).

Roemmich D., Gould W. J. and Gilson J. : 135 years of global ocean warming between the Challenger expedition and the Argo Programme, *Nature Climate Change, 2*(6), 425-428, doi:10.1038/nclimate1461 (2012).

Roemmich D., Church J., Gilson J., Monselesan D., Sutton P. and Wijffels S. : Unabated planetary warming and its ocean structure since 2006. *Nature Climate Change,* 5, 240–245, doi:10.1038/NCLIMATE2513 (2015).

Rohling E. J., Grant K., Hemleben C., Siddall M., Hoogakker B. a. A., Bolshaw M. and Kucera M. : High rates of sea-level rise during the last interglacial period. *Nature Geoscience, 1* (1), 38–42, doi :10.1038/ngeo.2007.28 (2007).

Rohling E. J., Grant K., Bolshaw M., Roberts A. P., Siddall M., Hemleben C. and Kucera M. : Antarctic temperature and global sea level closely coupled over the past five glacial cycles. *Nature Geoscience, 2* (7), 500–504, doi :10.1038/ngeo557 (2009).

Rowley D. B. : Rate of plate creation and destruction : 180 ma to present. *Geological Society of America Bulletin, 114* (8), 927–933, doi:10.1130/0016-7606(2002)114_0927: ROPCAD_2.0.CO;2 (2002).

Rudenko S., Otten M., Visser P., Scharroo R., Schöne T. and Esselborn S. : New improved orbit solutions for the ERS-1 and ERS-2 satellites. *Adv Space Res*, 49(8):1229–1244 (2012).

Rudenko S., Dettmering D, Esselborn S, Schöne T., Fo¨rste Ch., Lemoine J-M., Ablain M., Alexandre D. and Neumayer K-H. : Influence of time variable geopotential models on precise orbits of altimetry satellites, global and regional mean sea level trends. *Adv Space Res*, 54(1):92–118. doi:10.1016/j.asr.2014.03.010 (2014).

Rudenko R., Neumayer K-H., Dettmering D., Esselborn S. and Schöne T. : Improvements in precise orbit determination of altimetry satellites. *Ocean Surface Topography Science Team meeting, Reston, Virginia, USA, October 2015*. (2015)

http://meetings.aviso.altimetry.fr/fileadmin/user_upload/tx_ausyclsseminar/files/OSTST2015/POD-04-Rudenko_OSTST2015_20151021new.pdf

Santamaría-Gómez A., Gravelle M., Collilieux X., Guichard M., Martıín Míguez B., Tiphaneau P. and Wöppelmann G. : Mitigating the effects of vertical land motion in tide gauge records using a state-of-the-art GPS velocity field. *Glob Planet Change* 98–99:6–17 (2012).

Santamaría-Gómez A., Gravelle M., Wöppelmann G., : Long-term vertical land motion from double-differenced tide gauge and satellite altimetry data. Journal of Geodesy, 88, 207-222, doi:10.1007/s00190-013-0677-5 (2014).

Sasgen I., van den Broeke M., Bamber J. L., Rignot E., Sørensen L. S., Wouters B., Martinec Z., Velicogna I. and Simonsen S B. : Timing and origin of recent regional ice-mass loss in Greenland. *Earth Planet. Sci. Lett.*, 333–334, 293–303 (2012).

Sasgen I., Konrad H., Ivins E. R., Van den Broeke M. R., Bamber J. L., Martinec Z. and Klemann V. : Antarctic ice-mass balance 2003 to 2012: regional reanalysis of GRACE satellite gravimetry measurements with improved estimate of glacial-isostatic adjustment based on GPS uplift rates. *Cryosphere*, 7, 1499–1512, doi:10.5194/tc-7-1499-2013 (2013).

Schrama E. J. O., Wouters B. and Rietbroek R. : A mascon approach to assess ice shett and glacier mass balance and their uncertainties from GRACE data. *J. Geophys. Res., Solid Earth*, 119, 6048-6066, doi:10.1002/2013JB010923 (2014).

Shepherd A., Ivins E. R. A. G., Barletta V. R., Bentley M. J., Bettadpur S., Briggs K. H., Bromwich D. H., Forsberg R., Galin N., Horwath M., Jacobs S., Joughin I., King M. A., Lenaerts J. T., Li J., Ligtenberg S. R., Luckman A., Luthcke S. B., McMillan M., Meister R., Milne G., Mouginot J., Muir A., Nicolas J. P., Paden J., Payne A. J., Pritchard H., Rignot E., Rott H., Sørensen L. S., Scambos T. A., Scheuchl B., Schrama E. J., Smith B., Sundal A. V., van Angelen J. H., van de Berg W. J., van den Broeke M. R., Vaughan D. G., Velicogna I., Wahr J., Whitehouse P. L., Wingham D. J., Yi D., Young D., Zwally H. .J. : A reconciled estimate of ice-sheet mass balance. *Science*, 338, 1183–1189, doi: 10.1126/science.1228102 (2012).

Siddall M., Bard E., Rohling E. J. and Hemleben C. : Sea-Level reversal during termination II. *Geology*, *34* (10), 817–820, doi :10.1130/G22705.1 (2006).

Siemes C., Ditmar P., Riva R. E. M., Slobbe D. C., Liu X. L. and Farahani H. H. : Estimation of mass change trends in the Earth's system on the basis of GRACE satellite data, with application to Greenland. *J. Geod.*, 87, 69–87, (2013).

Slangen A. B. A., Katsman C. A., van de Val R. S. W., Vermeersen L. L. A. and Riva REM. : Towards regional projections of twenty-first century sea level change based on IPCC SRES scenarios. *Clim. Dyn.* 38:1191–209 (2011).

Slangen ABA, Carson M, Katsman CA, van de Wal RSW, Koehl A, Vermeersen LLA, Stammer D, Van De Wal RSW (2014) Projecting twenty-first century regional sea-level changes. Clim Change 124:317–332. doi:10.1007/s10584-014-1080-9

Slobbe D. C., Ditmar P. and Lindenbergh R. C. : Estimating the rates of mass change, ice volume change and snow volume change in Greenland from ICESat and GRACE data. *Geophys. J. Int.*, 176, 95–106, (2009).

Smith D. M., REYNOLDS R. W., PETERSON T. C. and LAWRIMORE J. : Improvements to NOAA's Historical Merged Land-Ocean Surface Temperature Analysis (1880-2006). *J. Climate.* 21**:** 2283-2293 (2008).

Smith D. : Has global warming stalled?. *Nature Climate Change,* 3, 618–619, doi:10.1038/nclimate1938 (2013).

Smith D. M., Allan R. P., Coward A. C., Eade R., Hyder P., Liu C., Loeb N., Palmer M. D., Roberts C. D. and Scaife A. A. : Earth's energy imbalance since 1960 in observations and CMIP5 models. *Geophys. Res. Lett.* 42: 1205–1213 (2015).

Solomon S., Qin D., Manning M., Chen Z., Marquis M., Averyt K., Tignor M. and Miller H. (Eds.) : *Contribution of Working Group I to the Fourth Assessment Report of the Intergovernmental Panel on Climate Change, 2007*, Cambridge University Press, Cambridge, United Kingdom and New York, NY, USA (2007).

Solomon S., Rosenlof K., Portmann R., Daniel J., Davis S., Sanford T. and Plattner G.-K. : Contributions of stratospheric water vapour to decadal changes in the rate of global warming. *Science,* 327, 1219–1223, doi:10.1126/science.1182488 (2010).

Sørensen L. S., Simonsen S. B., Nielsen K., Lucas-Picher P., Spada G., Adalgeirs-dottir G., Forsberg R. and Hvidberg C. S. : Mass balance of the Greenland ice sheet (2003–2008) from ICESat data—the impact of interpolation, sampling and firn density. *Cryosphere,* 5, 173–186, doi:10.5194/tc-5-173-2011 (2011).

Spada G. : Glacial Isostatic Adjustment and Contemporary Sea Level Rise: An Overview, *Surv Geophys,* 1–33, doi:10.1007/s10712-016-9379-x (2016).

Stammer D., Cazenave A., Ponte R. M. and Tamisiea M. E. : Causes for contemporary regional sea level changes. In: *Annual Review of Marine Science,* Vol. 5 [C. A. Carlson and S. J. Giovannoni (eds.)]. *Annual Reviews,* Palo Alto, CA, USA, pp. 21–46 (2013).

Swenson S., and Wahr J. : Post-processing removal of correlated errors in GRACE data. *Geophys. Res. Lett.*, 33, L08402, *doi:*10.1029/2005GL025285 (2006).

Tamisiea M. and Mitrovica J. : The moving boundaries of sea level change : Understanding the origins of geographic variability. *Oceanography, 24* (2), 24–39, doi:10.5670/oceanog.2011.25 (2011).

Tapley B. D., Bettadpur S., Watkins M. M. and Reigber C. : The gravity recovery and climate experiment; mission overview and early results. *Geophys. Res. Lett.* 31 (9), L09607. doi:10.1029/2004GL019920 (2004).

Thibaut P., Poisson J-C., Roca M. and Nilo Garcia P. : WP2100 altimeter instrumental processing: RRDP and validation reports, sea level climate change initiative project, phase I. Algorithm selection meeting, *Toulouse, 2 May* (2012) http://www.esa-sealevel-cci.org/webfm_send/77

Thompson W. G., Curran H. A., Wilson M. A. and White B. : Sea-level oscillations during the last interglacial highstand recorded by Bahamas corals. *Nature Geosci.,* 4, 684–687 (2011).

Tran N., Labroue S., Philipps S., Bronner E and Picot N. : Overview and update of the sea state bias corrections for the Jason-2, Jason-1 and TOPEX missions. *Mar Geod* 33(S1):348–362. doi:10.1080/01490419.2010.487788 (2010).

Tran N., Philipps S., Poisson J. C., Urien S., Bronner E. and Picot N. : Oral: impact of GDR-D standards on SSB corrections. Aviso, OSTST. (2012) http://www.aviso.altimetry.fr/fileadmin/documents/OSTST/2012/oral/02_friday_28/01_instr_processing_I/01_IP1_Tran.pdf

Trenberth, K., Fasullo, J. & Smith, L. : Trends and variability in column-integrated atmospheric water vapor. *Clim. Dynam.* 24, 741_758 (2005).

Trenberth K. and Smith L. : The Mass of the Atmosphere: A Constraint on Global Analyses. *J. Climate,* 18, 864-875 (2005).

Trenberth K. E. and Fasullo J. T. : Tracking Earth's energy, Science, 328, 316–317 (2010).

Trenberth K. E. and Fasullo J. T. : An apparent hiatus in global warming?. *Earth's Future,* 1, 19–32, doi:10.1002/2013EF000165 (2013).

Trenberth K. E., Fasullo J. T. and Balmaseda M. A. : Earth's Energy imbalance, *J. Climate,* 27, 3129–3144, doi:10.1175/JCLI-D-13-00294.1 (2014).

Trenberth K. E. : Has there been a hiatus? *Science* 349: 691–692 (2015).

Vail P., Mitchum R. and III S. T. : Seismic stratigraphy and global changes of sea level, part 4 : global cycles of relative changes of sea level. in *Seismic stratigraphy-Applications to Hydrocarbon Exploration*, edited by C. Payton, pp. 83–98, American Association of Petroleum Geologists Memoir, 26, Tulsa, Oklahoma (1977).

van den Broeke M., Bamber J., Ettema J., Rignot E., Schrama E., van de Berg W. J., van Meijgaard E., Velicogna I. and Wouters B. : Partitioning recent Greenland mass loss. *Science,* 326, 984–6, doi: 10.1126/science.1178176 (2009).

Valladeau G., Legeais J. F., Ablain M., Guinehut S. and Picot N. : Comparing altimetry with tide gauges and argo profiling floats for data quality assessment and mean sea level studies. *Mar Geod* 35(1):42–60 (2012).

Vaughan, D.G., J.C. Comiso, I. Allison, J. Carrasco, G. Kaser, R. Kwok, P. Mote, T. Murray, F. Paul, J. Ren, E. Rignot, O. Solomina, K. Steffen and T. Zhang, : Observations: Cryosphere. In: Climate Change 2013: The Physical Science Basis. Contribution of Working Group I to the Fifth Assessment Report of the Intergovernmental Panel on Climate Change [Stocker, T.F., D. Qin, G.-K. Plattner, M. Tignor, S.K. Allen, J. Boschung, A. Nauels, Y. Xia, V. Bex

and P.M. Midgley (eds.)]. Cambridge University Press, Cambridge, United Kingdom and New York, NY, USA (2013).

Velicogna I. and Wahr J. : Acceleration of Greenland ice mass loss in spring 2004. *Nature*, 443, 328–331, doi:10.1038/nature05168 (2006).

Velicogna I. : Increasing rates of ice mass loss from the Greenland and Antarctic ice sheets revealed by GRACE. *Geophys. Res. Lett.*, 36, L19503, doi:10.1029/2009GL040222 (2009).

Velicogna I. and Wahr J. : Time variable gravity observations of ice sheet mass balance : precision and limitations of the GRACE satellite data. *Geophys. Res. Lett.*, 40, 3055–3063, doi:10.1002/grl.50527 (2013).

Velicogna I., Sutterley T. C. and van den Broeke M. R. : Regional acceleration in ice mass loss from Greenland and Antarctica using Grace time variable gravity data. *Geophys. Res. Lett.*, 41, 8130–8137, doi:10.1002/2014GL061052 (2014).

Von Schuckmann K., Gaillard F. and Le Traon P. Y. : Global hydrographic variability patterns during 2003–2008. *J. Geophys. Res.*, 114, C09007, doi:10.1029/2008JC005237 (2009).

von Schuckmann K. and Le Traon P.-Y. : How well can we derive Global Ocean Indicators from Argo data?. *Ocean Sci.*, 7, 783–791, doi:10.5194/os-7-783-2011 (2011).

von Schuckmann, K., Sallée, J.-B., Chambers, D., Le Traon, P.-Y., Cabanes, C., Gaillard, F., Speich, S., and Hamon, M. : Consistency of the current global ocean observing systems from an Argo perspective. Ocean Sci., 10, 547–557, doi:10.5194/os-10-547-2014, (2014).

Von Schukmann K., Palmer M. D., Trenberth K. E., Cazenave A., Chambers D., Champollion N.**,** Hansen J., Josey S., Loeb N., Mathieu P.-P., Meyssignac B. and Wild M. : An imperative to monitor Earth's energy imbalance. *Nature Climate Change*, 6, 138–144, doi:10.1038/nclimate2876 (2016).

Wada Y., Ludovicus P. H. van Beek, Frederiek C. S. W., Benjamin F. C., Yun-Hao W. and Marc F. P. B. : Past and future contribution of global groundwater depletion to sea-level rise. *Geophys. Res. Lett*., 39, L09402, doi:10.1029/2012GL051230 (2012).

Wada Y., Wisser D. and Bierkens M. F. P. : Global modeling of withdrawal, allocation and consumptive use of surface water and groundwater resources. *Earth Syst. Dyn*., 5, 15-40, doi:10.5194/esd-5-15-2014 (2014).

Wada Y. : Modelling groundwater depletion at regional and global scales: Present state and future prospects. *Surveys in Geophysics*, 37, 419-451, doi:10.1007/s10712-015-9347-x (2015).

Wada et al. **:** Fate of water pumped from underground and contributions to sea-level rise. *Nature Climate Change*, 6(8), DOI: 10.1038/nclimate3001 (2016).

Wadhams P. and Munk W. : Ocean freshening, sea level rising, sea ice melting. *Geophys. Res. Lett.*, 31(11), L11311, doi:10.1029/ 2004GL020039 (2004).

Wahr J., Swenson S. and Velicogna I. : Accuracy of GRACE mass estimates. *Geophys. Res. Lett*., 33, L06401, doi:10.1029/2005GL025305 (2006).

Wahr J. M. : Deformation induced by polar motion. *J Geophys Res*, 90(B11):9363–9368. doi:10.1029/JB090iB11p09363 (1985).

Watanabe M., Kamae Y., Yoshimori M., Oka A., Sato M., Ishii M., Mochizuki T. and Kimoto M. : Strengthening of ocean heat uptake efficiency associated with the recent climate hiatus. *Geophys. Res. Lett.*, 40, 3175–3179, doi:10.1002/grl.50541 (2013).

Watson C., White N., Church J., Burgette R., Tregoning P., and Coleman R. : Absolute calibration in bass strait, Australia: TOPEX, Jason-1 and OSTM/Jason-2. *Mar. Geod.*, 34(3–4):242–260 (2011)

Watson C. S., White N. J., Church J. A., King M. A., Burgette R. J. and Legresy B. : Unabated global mean sealevel rise over the satellite altimeter era. *Nat Clim Change,* doi:10.1038/nclimate2635 (2015)

Williams S. D. P., Moore P., King M. A. and Whitehouse P. L. : Revisiting GRACE Antarctic ice mass trends and accelerations considering autocorrelation. *Earth and Planetary Science Letters,* 385, 12–21, doi:10.1016/j.epsl.2013.10.016 (2014).

Willis J. K., Chambers D. P. & Nerem R. S. : Assessing the globally averaged sea level budget on seasonal to interannual timescales. *J. Geophys. Res., 113*(C6), doi:10.1029/2007jc004517 (2008).

Wong A. P. S., Bindoff N. L. and Church J. A. : Large-scale freshening of intermediate waters in the Pacifi c and Indian oceans. *Nature,* 400(6743), 440–443 (1999).

Woodroffe C. D., McGregor H. V., Lambeck K., Smithers S. G., and Fink D. : Mid- Pacific microatolls record sea-level stability over the past 5000 yr. Geology, 40, 951–954 (2012).

Woodruff S. D., Worley S. J., Sandra J., Lubker S. J., Ji Z., Freeman J. E., Berry D. I., Brohan P., Kent E. C., Reynolds R. W. and Wilkinson C. : ICOADS Release 2.5: extensions and enhancements to the surface marine meteorological archive. *Int. J. Climatol.*, 31: 951–967 (2011).

Wöppelmann G., Pouvreau N. and Simon B. : Brest sea level record : a time series construction back to the early eighteenth century. *Ocean Dynamics, 56* (5), 487–497, doi : 10.1007/s10236-005-0044-z (2006).

Wöppelmann G., Martin Miguez B., Bouin M. and Altamimi Z. : Geocentric sea-level trend estimates from GPS analyses at relevant tide gauges world-wide. *Global and Planetary Change, 57* (3-4), 396–406, doi :10.1016/j.gloplacha.2007.02.002 (2007).

Wöppelmann G., Pouvreau N., Coulomb A., Simon B. and Woodworth P. L. : Tide gauge datum continuity at brest since 1711 : France's longest sea-level record. *Geophysical Research Letters, 35*, 5 PP., doi :200810.1029/2008GL035783 (2008).

Wöppelmann G., Letetrel C., Santamaria A., Bouin M. N., Collilieux X., Altamimi Z., Williams S. D. P. and Miguez B. M. : Rates of sea-level change over the past century in a geocentric reference frame. *Geophys. Res. Lett.* 36, doi 10.1029/2009gl038720 (2009).

Wöppelmann G. & M. Marcos : Coastal sea level rise in southern Europe and the nonclimate contribution of vertical land motion. *Journal of Geophysical Research,* 117, C01007, doi:10.1029/2011JC007469 (2012).

Wöppelmann G., Le Cozannet, M. De Michele, *et al.* : Is land subsidence increasing the exposure to sea level rise in Alexandria, Egypt ? *Geophysical Research Letters,* 40, 2953-2957 (2013).

Wöppelmann G., M. Marcos, A. Coulomb, *et al.* : Rescue of the historical sea level record of Marseille (France) from 1885 to 1988, and its extension back to 1849-1851. *Journal of Geodesy,* 88, 869-885 (2014a).

Wöppelmann G., M. Marcos, A. Santamaria-Gomez, *et al.* : Evidence for a differential sea level rise between hemispheres over the twentieth century. *Geophysical Research Letters,* 41, 1639-1643 (2014b).

Wöppelmann G. & M. Marcos : Vertical land motion as a key to understanding sea level change and variability. *Reviews of Geophysics*, 54, doi:10.1002/2015RG000502 (2016).

Wouters B., Chanbers D. and Schrama E. J. O. : GRACE observes small-scale mass loss in Greenland. *Geophys. Res. Lett.,* 35, L20501 (2008).

Wouters B., Bamber J. L., van den Broeke M. R., Lenaerts J. T. M. and Sasgen I. : Limits in detecting acceleration of ice sheet mass loss due to climate variability. *Nat. Geosci.,* 6(8), 613–616, doi:10.1038/ngeo1874 (2013).

Yi S., Sun W., Heki K. and Qian A. : An increase in the rate of global mean sea level rise since 2010. *Geophys. Res. Lett.,* 42, doi :10.1002/2015GL063902 (2015).

Zawadzki L. and Ablain M. : Accuracy of the mean sea level continuous record with future altimetric missions: Jason-3 vs. Sentinel-3a. Ocean Sci 12:9–18. doi:10.5194/os-12-9-2016 (2016).

Zemp M., Zumbühl H. J., Nussbaumer S. U., Masiokas M. H., Espizua L. E., Pitte P. : Extending glacier monitoring into the Little Ice Age and beyond. *PAGES News,* 19(2), 67-69 (2011).

Zemp M., Frey H., Gärtner-Roer I., Nussbaumer S. U., Hoelzle M., Paul F., Haeberli W., Denzinger F., Ahlstrøm A. P., Anderson B., Bajracharya S., Baroni C., Braun L. N., Cáceres B. E., Casassa G., Cobos G., Dávila L. R., Delgado Granados H., Demuth M. N., Espizua L., Fischer A., Fujita K., Gadek B., Ghazanfar A., Hagen J. O., Holmlund P., Karimi N., Li Z., Pelto M., Pitte P., Popovnin V. V., Portocarrero C. A., Prinz R., Sangewar C. V., Severskiy I., Sigurđsson O., Soruco A., Usubaliev R., Vincent C. : Historically unprecedented global glacier decline in the early 21st century. *Journal of Glaciology,* 61(228), 745-762, doi: 10.3189/2015JoG15J017 (2015).

Zwally H. J., LI J., Brenner A. C., Beckley M., Cornejo H. G., DiMarzio J., Giovinetto M. B., Neumann T. A., Robbins J., Saba J. L., Yi D. and Wang W. : Greenland ice sheet mass

balance: distribution of increased mass loss with climate warming; 2003–07 versus 1992–2002. *J. Glaciol.*, 57, 88–102 (2011).

Annexe : Liste des publications

- **Dieng H. B.,** Cazenave A., Messignac B., Henry O., von Schuckmann K., Hindumathi P. and Lemoine J.M.; Effect of La Nina of the global mean sea level and north Pacific ocean mass over 2005-2011, J. Geod. Sci., 4:19–27 DOI10.2478/jogs-2014-0003, **2014**.

- **Dieng H. B.**, Palanisamy H., Cazenave A., Meyssignac B. & von Schuckmann K. ; The Sea Level Budget Since 2003: Inference on the Deep Ocean Heat Content, Surv. Geophys., 36, 209–229, doi:10.1007/s10712-015-9314-6, **2015a**.

- **Dieng H. B.**, Cazenave A., von Shuckmann K., Ablain M. and Meyssignac B. : Sea level budget over 2005-2013: missing contributions and data errors *Ocean Science* 11, 789-802, doi:10.5194/os-11-789-2015, **2015b**.

- **Dieng H. B.**, Champollion N., Cazenave A., Wada Y., Schrama E. and Meyssignac B. : Total land water storage change over 2003-2013 estimated from a global mass budget approach. *Environ. Res. Lett.*, 10, 124010, doi:10.1088/1748-9326/10/12/124010, **2015c.**

- **Dieng H. B.**, Cazenave A., Meyssignac B., von Shuckmann K. and Palanisamy H. : Sea and land surface temperatures, ocean heat content, Earth's energy imbalance and net radiative forcing over the recent years. *Int. J. Climatol.*, DOI: 10.1002/joc.4996, **2017.**

- Anny Cazenave, **Habib Boubacar Dieng**, Simon Munier, Olivier Henry, Benoit Meyssignac, Hindumathi Palanisamy et William Llovel : L'influence d'El Niño et de La Niña sur le niveau de la mer. La Météorologie - n° 79 - novembre **2012**.

- Cazenave A., **Dieng H. B**., Meyssignac B., von Schuckmann K., Decharme B., and Berthier E., The rate of sea-level rise, *Nature Climate Change* 4, 358–361 DOI:10.1038/NCLIMATE2159, **2014**.

- Chambers D. P., Cazenave A., Champollion N., **Dieng H. B.,** Llovel W., Forsberg R., von Schuckmann K., and Wada Y. : Evaluation of the Global Mean Sea Level Budget between 1993 and 2014. *Surv. Geophys*, 1–19, doi:10.1007/s10712-016-9381-3, **2016**

- Ablain M., Legeais J. F., Prandi P., Marcos M., Fenoglio-Marc L., **Dieng H. B.,** Benveniste J. and Cazenave A. : Altimetry-based sea level at global and regional scales. *Surv. Geophys*. DOI 10.1007/s10712-016-9389-8, **2016.**